NATO Science for Peace and Security Series - C:
Environmental Security

Air Pollution Modeling and its Application XXII

Edited by
Douw G. Steyn
Peter J.H. Builtjes
Renske M.A. Timmermans

Springer

NATO OTAN

This publication is supported by:

The NATO Science for Peace and Security Programme

Air Pollution Modeling and its Application XXII

NATO Science for Peace and Security Series

This Series presents the results of scientific meetings supported under the NATO Programme: Science for Peace and Security (SPS).

The NATO SPS Programme supports meetings in the following Key Priority areas: (1) Defence Against Terrorism; (2) Countering other Threats to Security and (3) NATO, Partner and Mediterranean Dialogue Country Priorities. The types of meeting supported are generally “Advanced Study Institutes” and “Advanced Research Workshops”. The NATO SPS Series collects together the results of these meetings. The meetings are co-organized by scientists from NATO countries and scientists from NATO’s “Partner” or “Mediterranean Dialogue” countries. The observations and recommendations made at the meetings, as well as the contents of the volumes in the Series, reflect those of participants and contributors only; they should not necessarily be regarded as reflecting NATO views or policy.

Advanced Study Institutes (ASI) are high-level tutorial courses to convey the latest developments in a subject to an advanced-level audience

Advanced Research Workshops (ARW) are expert meetings where an intense but informal exchange of views at the frontiers of a subject aims at identifying directions for future action

Following a transformation of the programme in 2006 the Series has been re-named and re-organised. Recent volumes on topics not related to security, which result from meetings supported under the programme earlier, may be found in the NATO Science Series.

The Series is published by IOS Press, Amsterdam, and Springer, Dordrecht, in conjunction with the NATO Emerging Security Challenges Division.

Sub-Series

A.	Chemistry and Biology	Springer
B.	Physics and Biophysics	Springer
C.	Environmental Security	Springer
D.	Information and Communication Security	IOS Press
E.	Human and Societal Dynamics	IOS Press

http://www.nato.int/science
http://www.springer.com
http://www.iospress.nl

Series C: Environmental Security

Air Pollution Modeling and its Application XXII

edited by

Douw G. Steyn
The University of British Columbia, Vancouver, BC, Canada

Peter J.H. Builtjes
Netherlands Organisation for Applied Scientific Research TNO, Utrecht, The Netherlands

and

Renske M.A. Timmermans
Netherlands Organisation for Applied Scientific Research TNO, Utrecht, The Netherlands

Published in Cooperation with NATO Emerging Security Challenges Division

Proceedings of the 32nd NATO/SPS International Technical Meeting on Air Pollution Modeling and its Application
Utrecht, The Netherlands
7–11 May 2012

Library of Congress Control Number: 2013942469

ISBN 978-94-007-6096-7 (PB)
ISBN 978-94-007-5576-5 (HB)
ISBN 978-94-007-5577-2 (e-book)
DOI 10.1007/978-94-007-5577-2

Published by Springer,
P.O. Box 17, 3300 AA Dordrecht, The Netherlands.

www.springer.com

Printed on acid-free paper

Previous Volumes in this Mini-Series

Volumes I-XII were included in the NATO Challenges of Modern Society Series

Air Pollution Modeling and its Application I
Edited by C. de Wispelaere

Air Pollution Modeling and its Application II
Edited by C. de Wispelaere

Air Pollution Modeling and its Application III
Edited by C. de Wispelaere

Air Pollution Modeling and its Application IV
Edited by C. de Wispelaere

Air Pollution Modeling and its Application V
Edited by C. de Wispelaere, Francis A. Schiermeier, and Noor V. Gllani

Air Pollution Modeling and its Application VI
Edited by Han van Dop

Air Pollution Modeling and its Application VII
Edited by Han van Dop

Air Pollution Modeling and its Application VIII
Edited by Han van Dop and Douw G. Steyn

Air Pollution Modeling and its Application IX
Edited by Han van Dop and George Kallos

Air Pollution Modeling and its Application X
Edited by Sven-Erik Gryning and Millán M. Millán

Air Pollution Modeling and its Application XI
Edited by Sven-Erik Gryning and Francis A. Schiermeier

Air Pollution Modeling and its Application XII
Edited by Sven-Erik Gryning and Nadine Chaumerliac

Air Pollution Modeling and its Application XIII
Edited by Sven-Erik Gryning and Ekaterina Batchvarova

Air Pollution Modeling and its Application XIV
Edited by Sven-Erik Gryning and Francis A. Schiermeier

Air Pollution Modeling and its Application XV
Edited by Carlos Borrego and Guy Schayes

Air Pollution Modeling and its Application XVI
Edited by Carlos Borrego and Selahattin Incecik

Air Pollution Modeling and its Application XVII
Edited by Carlos Borrego and Ann-Lise Norman

Air Pollution Modeling and its Application XVIII
Edited by Carlos Borrego and Eberhard Renner

Air Pollution Modeling and its Application XIX
Edited by Carlos Borrego and Ana Isabel Miranda

Air Pollution Modeling and its Application XX
Edited by Douw G. Steyn and S. Trivikrama Rao

Air Pollution Modeling and its Application XXI
Edited by Douw G. Steyn and Silvia Trini Castelli

Preface

In 1969, the North Atlantic Treaty Organization (NATO) established the Committee on Challenges of Modern Society (CCMS). From inception, the subject of air pollution was established as one of the priority problems for study within the framework of various pilot studies undertaken by this committee. The main activity relating to air pollution is the periodic organization of a conference series called **International Technical Meeting on Air Pollution Modeling and its Application** (ITM). Pilot countries organizing these meetings have been: United States of America; Federal Republic of Germany; Belgium; The Netherlands; Denmark; Portugal and Canada.

This volume contains the abstracts of papers and posters presented at the 32nd NATO/SPS ITM, held in Utrecht, The Netherlands, from May 7 to 11, 2012. This ITM was organized by TNO (Host Country) in cooperation with VVM and The University of British Columbia (Pilot Country). Key topics presented at this ITM included: Local and urban scale modeling, Regional and intercontinental modeling, Data assimilation and air quality forecasting, Model assessment and verification, Aerosols in the atmosphere, Interactions between climate change and air quality, Air quality and human health.

The ITM was attended by 159 participants representing 35 countries. Invited papers were presented by S.T. Rao, USA (Model assessment and verification); George Kallos, Greece (Aerosols in the atmosphere); David Simpson, Norway (Regional and Intercontinental modeling); and Leendert Hordijk, The Netherlands (Air quality models and policy).

On behalf of the ITM Scientific Committee and as organizers and editors, we would like to thank all the participants who contributed to the success of the meeting. We especially recognize the organizational and support efforts of the chairpersons and rapporteurs, staff at VVM and TNO. Finally, special thanks to the sponsoring institutions: TNO (The Netherlands), both Earth, Environment and Life sciences and Space, The University of British Columbia (Canada), and the sponsoring organizations NATO Science for Peace and Security; Environment

Canada; City of Utrecht and European Association for the Science of Air Pollution (EURASAP). A special grant was given by EURASAP to award prizes to young researchers for the best paper or poster.

The next meeting will be held in August 2013 in Miami, USA.

Utrecht, The Netherlands — Renske Timmermans & Peter Builtjes (Local Conference Organizers)

Vancouver, BC, Canada — Douw G. Steyn (Scientific Committee Chair)

Members of the Scientific Committee for the 32nd NATO/SPS International Technical Meeting (ITM) on Air Pollution Modeling and its Application

Clemens Mensink	Belgium
Ekaterina Batcharova	Bulgaria
Douw G. Steyn	Canada (Chair)
Sven-Erik Gryning	Denmark
Nadine Chaumerliac	France
Eberhard Renner	Germany
George Kallos	Greece
Silvia Trini Castelli	Italy
Trond Iversen	Norway
Ana Isabel Miranda	Portugal
José Baldasano	Spain
Peter Builtjes	The Netherlands
Selahattin Incecik	Turkey
Tony Dore	United Kingdom
S.T. Rao	United States of America
Werner Klug	Germany (honorary member)
Han van Dop	The Netherlands (honorary member)
Frank Schiermeier	United States of America (honorary member)

History of NATO/CCMS (SPS) Air Pollution Pilot Studies

Pilot Studies on Air Pollution

International Technical Meetings (ITM) on Air Pollution Modelling and its Application

Dates and Locations of Completed Pilot Studies:

1969–1974	Air Pollution Pilot Study (*Pilot Country: United States of America)*
1975–1979	Air Pollution Assessment Methodology and Modelling (*Pilot Country: Germany)*
1980–1944	Air Pollution Control strategies and Impact Modelling (*Pilot Country: Germany)*

Dates and Locations of Pilot Follow-Up Meetings:

Pilot Country – United States of America (R.A. McCormick, L.E. Niemeyer)

Feb., 1971	Eindhoven, The Netherlands	First Conference on Low Pollution Power Systems Development
July, 1971	Paris, France	Second Meeting of the Expert Panel on Air Pollution Modelling

All subsequent meetings were supported by the NATO Committee for Challenges to Modern Society, and were designated NATO/CCMS International Technical Meetings (ITM) on Air Pollution Modelling and its Application, until 2007 when the designation changed to NATO/SPS with the creation of the NATO Committee on Science for Peace and Security.

Oct.	1972	Paris, France	3rd	ITM
May	1973	Oberursel, Federal Republic of Germany	4th	ITM
Jun.	1974	Roskilde, Denmark	5th	ITM
		Pilot Country – Germany (Erich Weber)		
Sept.	1975	Frankfurt, Federal Republic of Germany	6th	ITM
Sept.	1976	Airlie House, USA	7th	ITM
Sept.	1977	Louvain-la-Neuve, Belgium	8th	ITM
Aug.	1978	Toronto, Canada	9th	ITM
Oct.	1979	Rome, Italy	10th	ITM
		Pilot Country – Belgium (C. De Wispelaere)		
Nov.	1980	Amsterdam, The Netherlands	11th	ITM
Sept.	1981	Menlo Park, California, USA	12th	ITM
Sept.	1982	Ile des Embiez, France	13th	ITM
Sept.	1983	Copenhagen, Denmark	14th	ITM
Apr.	1985	St. Louis, Missouri, USA	15th	ITM
		Pilot Country – The Netherlands (H. van Dop)		
Apr.	1987	Lindau, Federal Republic of Germany	16th	ITM
Sept.	1988	Cambridge, United Kingdom	17th	ITM
May	1990	Vancouver, BC, Canada	18th	ITM
Sept.	1991	Ierapetra, Greece	19th	ITM
		Pilot Country – Denmark (Sven-Erik Gryning)		
Nov.	1993	Valencia, Spain	20th	ITM
Nov.	1995	Baltimore, Maryland, USA	21st	ITM
May	1997	Clermont-Ferrand, France	22nd	ITM
Sept.	1998	Varna, Bulgaria	23rd	ITM
May	2000	Boulder, Colorado, USA	24th	ITM
		Pilot Country – Portugal (Carlos Borrego)		
Sept.	2001	Louvain-la-Neuve, Belgium	25th	ITM
May	2003	Istanbul, Turkey	26th	ITM
Oct.	2004	Banff, Canada	27th	ITM
May	2006	Leipzig, Germany	28th	ITM
Sept.	2007	Aveiro, Portugal	29th	ITM
		Pilot Country – Canada (Douw G. Steyn)		
May	2009	San Francisco, California, USA	30th	ITM
Sept.	2010	Torino, Italy	31st	ITM
May	2012	Utrecht, The Netherlands	32nd	ITM

List of Participants

Australia

Lee, Sunhee
sunhee.lee@csiro.au
CSIRO
107-121 Station St, Aspendale
Melbourne

Belgium

Adriaenssens, Sandy
adriaenssens@irceline.be
Flemish Environment Agency
Alfons Van De Maelestraat 96
9320 Erembodegem

Ridder, Koen de
koen.deridder@vito.be
VITO
Boeretang 200
2400 Mol

Delcloo, Andy
andy.delcloo@meteo.be
Royal Meteorological Institute of Belgium
Ringlaan 3
B-1180 Brussel

Hordijk, Leendert
leendert.hordijk@ec.europa.eu
Joint Research Center – European Commission
Square de Meeus 8
B-1049 Brussels

Janssen, Stijn
stijn.janssen@vito.be
VITO
Boeretang 200
2400 Mol

Lefebvre, Wouter
wouter.lefebvre@vito.be
VITO
Boeretang 200
2400 Mol

Mensink, Clemens
clemens.mensink@vito.be
VITO
Boeretang 200
2400 Mol

Vanpoucke, Charlotte
vanpoucke@irceline.be
IRCEL – VMM
Kunstlaan 10
1210 Brussel

Brazil

Andrade, Maria
mftandra@model.iag.usp.br
Universidade de Sao Paulo
rua do Matao 1226
05508-090 Sao Paulo

Buske, Daniela
danielabuske@gmail.com
UFPel – Federal University of Pelotas
Rua Francisco Moreira, 142 Areal
CEP: 96077-080 Pelotas/RS

Quadros, Régis
quadros99@gmail.com
UFPel – Federal University of Pelotas
Rua Francisco Moreira, 142 Areal
CEP: 96077-080 Pelotas/RS

Bulgaria

Batchvarova, Ekatarina
Ekaterina.Batchvarova@meteo.bg
National Institute of Meteorology
66 Blvd Tzarigradsko chaussee
1784 Sofia

Gadzhev, Georgi
ggadjev@geophys.bas.bg
National Institute of Geophysics, Geodesy and Geography – BAS
Acad. G. Bonchev 3
1113 Sofia

Miloshev, Nikolay
ggadjev@geophys.bas.bg
National Institute of Geophysics, Geodesy and Geography – BAS
Acad. G. Bonchev 3
1113 Sofia

Prodanova, Maria
maria.prodanova@meteo.bg
Nationl Institute of Meteorology and Hydrology
Tzarigradsko chaussee Bulvd 66
1784 Sofia

Syrakov, Dimiter
dimiter.syrakov@meteo.bg
Nationl Institute of Meteorology and Hydrology
Tzarigradsko chaussee Bulvd 66
1784 Sofia

Canada

Antonopoulos, Stavros
stavros.antonopoulos@ec.gc.ca
Environment Canada
2444 Benny Crescent 316
H4B 2R3 Montreal

Gong, Wanmin
wanmin.gong@ec.gc.ca
Environment Canada
4905 Dufferin Street
M3H 5T4 Toronto

Hakami, Amir
amir_hakami@carleton.ca
Carleton University
1125 Colonel By Drive, ME 2374
K1S 5B6 Ottawa

Makar, Paul
paul.makar@ec.gc.ca
Environment Canada
146 Indian Road Cresent
M6P 263 Toronto

Mesbah, Seyyed Morteza
smesbah@connect.carleton.ca
Carleton University
1125 Colonel By Drive ME 3432
K1S 5B6 Ottawa

Moran, Michael
Mike.Moran@ec.gc.ca
Environment Canada
4905 Dufferin Street
M3H 5T4 Toronto, ON

Pappin, Amanda
apappin@connect.carleton.ca
Carleton University
1125 Colonel By Drive ME 3432
K1S 5B6 Ottawa

Seagram, Annie
aseagram@eos.ubc.ca
UBC Department of Earth and Ocean Sciences
6339 stores Road
V6T1X1 Vancouver

Steyn, Douw G.
dsteyn@eos.ubc.ca
The University of British Columbia
6339 Stores Road
V6T 1Z4 Vancouver, B.C.

China

Chao Ka Man
kmmok@umac.mo
University of Macau
Av. Padre Tomás Pereira Taipa
Macau

Fung, Christopher
cfung@epd.gov.hk
Environmental Protection Department
33/f, Revenue Tower, 5 Gloucester Road, WanChai
Hong Kong

Croatia

Jericevic, Amela
jericevic@cirus.dhz.hr
Croatian Meteorological and Hydrological Service
Gric 3
10000 Zagreb

Cyprus

Astitha, Marina
m.astitha@cyi.ac.cy
The Cyprus Institute
15 Kypranoros Street
1061 Nicosia

Czech Republic

Kukacka, Libor
kukacka@it.cas.cz
Charles University in Prague, Faculty of Mathematics and Physic
Ke Karlovu 3
12116 Praha

Vladimir, Fuka
vladimir.fuka@mff.cuni.cz
Charles University in Prague
Ke Karlovu 3
12116 Prague 2

Denmark

Gryning, Sven-Erik
sveg@dtu.dk
DTU Energy Department, Technical University of Denmark
Frederiksborgvej 399 118
DK-4000 Roskilde

Silver, Jeremy David
jds@dmu.dk
Dept. Environmental Science, Aarhus University
Frederiksborgvej 399
4000 Roskilde

Estonia

Kaasik, Marko
marko.kaasik@ut.ee
University of Tartu, Institute of Physics
Riia 142
51014 Tartu

Ots, Riinu
riinu.ots@ut.ee
University of Tartu, Institute of Physics
Riia 142
51014 Tartu

Finland

Kouznetsov, Rostislav
rostislav.kouznetsov@fmi.fi
Finnish Meteorological Institute
P.O. BOX 503
FI-00101 Helsinki

Prank, Marje
marje.prank@fmi.fi
Finnish Meteorological Institute
Erik Palmenin Aukio 1
00560 Helsinki

Soares, Joana
joana.soares@fmi.fi
Finnish Meteorological Institute
Erik Palmenin Aukio 1
00560 Helsinki

Sofiev, Mikhail
mikhail.sofiev@fmi.fi
Finnish Meteorological Institute
Erik Palmenin Aukio 1
00560 Helsinki

Vira, Julius
julius.vira@fmi.fi
Finnish Meteorological Institute
P.O. BOX 503
FI-00101 Helsinki

France

Barbet, Christelle
c.barbet@opgc.univ-bpclermont.fr
CNRS-LaMP
Université Blaise Pascal-24 av des Landais
63171 Aubière cedex

Carissimo, Bertrand
carissim@cerea.enpc.fr
CEREA
6-8 avenue Blaise Pascal, Cité Descartes Champs-su
77455 Marne la Vallée Cedex 2

Chaumerliac, Nadine
n.chaumerliac@opgc.univ-bpclermont.fr
CNRS-LaMP
Université Blaise Pascal-24 av des Landais
Aubière cedex

Debry, Edouard
edouard.debris@ineris.fr
INERIS
Parc Technologique Alata – BP 7
60550 VERNEUIL EN HALATTE

Foret, Gilles
foret@lisa.u-pec.fr
62 av. de Général de Gaulle
94000 Créteil

Gaubert, Benjamin
gaubert@lisa.u-pec.fr
LISA
61 Avenue de général de Gaulle
94010 Créteil

Jaumouillé, Elodie
elodie.jaumouille@cerfacs.fr
CERFACS
42 avenue Gaspard Coriolis
31057 Toulouse

Malherbe, Laure
laure.malherbe@ineris.fr
INERIS
Parc Technologique Alata – BP 7
60550 VERNEUIL EN HALATTE

Patryl, Luc
luc.patryl@cea.fr
Commissariat à l'Energie Atomique
Centre DAM-Île de France
91297 Arpajon CEDEX Bruyères-le-Chatel

Qu, Yongfeng
yongfeng.qu@cerea.enpc.fr
Ecole des Ponts ParisTech
6-8 avenue Blaise Pascal, Cité Descartes Champs-su
77455 Marne la Vallée

Quérel, Arnaud
arnaud.querel@irsn.fr
IRSN
Aerosol Physics and Metrology Laboratory,
BP68-91192 Gif-sur-Yvette

Régis, Briant
briantr@cerea.enpc.fr
CEREA
6-8 avenue Blaise Pascal, Cité Descartes
77455 Champs-sur-Marne Cedex 2 Marne la Vallée

Turquety, Solene
solene.turquety@lmd.polytechnique.fr
LMD/IPSL
Ecole Polytechnique
91128 Palaiseau Cedex

Zaidi, Hanane
hanane-externe.zaidi@edf.fr
CEREA
6-8 avenue Blaise Pascal, Cité Descartes Champs-su
77455 Marne la Vallée

Germany

Banzhaf, Sabine
sabine.banzhaf@met.fu-berlin.de
University of Berlin
Carl Heinrich Beckerweg 6-10
12165 Berlin

Bieser, Johannes
johannes.bieser@hzg.de
Helmholtz Zentrum Geesthacht
Max-Planck-Strasse 1
21502 Geesthacht

Forkel, Renate
renate.forkel@kit.edu
Karlsruhe Institute for Technology, IMK-IFU
Kreuzeckbahnstr. 19
82467 Garmisch-Partenkirchen

Graff, Arno
arno.graff@uba.de
Federal Environment Agency
Wörlitzer Platz 1
06844 Dessau-Rosslau

Matthias, Volker
volker.matthias@hzg.de
Helmholtz-Zentrum Geesthacht
Max-Planck-Strasse 1
21502 Geesthacht

Mues, Andrea
andrea.mues@met.fu-berlin.de
University of Berlin
Carl Heinrich Beckerweg 6-10
12165 Berlin

Ouwersloot, Huug
huug.ouwersloot@wur.nl
Max Planck Institute for Chemistry
Johann-J.-Becher-Weg 27
D-55128 Mainz

Renner, Eberhard
renner@tropos.de
Inst. for Tropospheric Research
Permoserstraße 15
04318 Leipzig

Scheuschner, Thomas
thomas.scheuschner@oekodata.com
OEKODATA GmbH
Hegermühlenstraße 58
15344 Strausberg

Suppan, Peter
peter.suppan@kit.edu
Karlsruher Institute of Technology (KIT)/IMK-IFU
Kreuzeckbahnstrasse 19
82467 Garmisch-Partenkirchen

Sändig, Beate
saendig@tropos.de
Leibniz Institute for Tropospheric Research (IfT)
Permoserstrasse 15
04318 Leipzig

Wolke, Ralf
wolke@tropos.de
Leibniz Institute for Tropospheric Research
Permoserstrasse 15
04318 Leipzig

Greece

Fountoukis, Christos
cfountoukis@iceht.forth.gr
FORTH
1A Erotokritou Str.
54250 Thessaloniki

Kallos, George
kallos@mg.uoa.gr
University of Athens, School of Physics
University Campus, Bldg PHYS-V
15784 Athens

Megaritis, Thanasis
athmegaritis@chemeng.upatras.gr
FORTH/ICE-HT
Stadiou Str., PlatanI
26504 Patras

Israel

Kishcha, Pavel
pavel@cyclone.tau.ac.il
Tel-Aviv University
Geophysics and planetary sciences, Te-Aviv university, Ramat Aviv
69978 Tel-Aviv

Levitin, Yosef
jlevitin@yahoo.com
Israel Meteorological Service
Research and Development, Israel Meteorological service, P.O. Box 25
52050 Bet Dagan

Reisin, Tamir Gustavo
tgreisin@gmail.com
Tamir Reisin
Carmel 13
48560 Rosh Haayn

Italy

Anfossi, Domenico
d.anfossi@isac.cnr.it
CNR – ISAC
Corso Fiume 4
10133 Torino

Balzarini, Alessandra
alessandra.balzarini@rse-web.it
RSE S.p.A.
Via Rubattino, 54
20134 Milano

Borghi, Sergio
sergio.borghi@meteoduomo.it
Corso Sempione 6
I-20154 Milano

D'Isidoro, Massimo
massimo.disidoro@enea.it
Via Martiri di Monte Sole 4
40129 Bologna

Falabino, Simona
simona.falabino@unito.it
Department of Physics, University of Turin
Via Giuria 1
10125 Torino

Favaron, Maurizio
maurizio@serviziterritorio.it
Maurizio Favaron
Via Dante 7
I23871 Lomagna

Frustaci, Giuseppe
g.frustaci@climateconsulting.it
Corso Sempione 6
I-20154 Milano

Galmarini, Stefano
stefano.galmarini@jrc.ec.europa.eu
Joint Research Center
Via Enrico Fermi 2749 (TP 441)
I-21027 ISPRA (VA)

Riccio, Angelo
angelo.riccio@uniparthenope.it
Università Parthenope
Centro Direzionale
80143 Napoli

Solazzo, Efisio
efisio.solazzo@jrc.ec.europa.eu
Joint Research Centre, European Commission
via E. Fermi 2749
21027 Ispra

Trini Castelli, Silvia
s.trinicastelli@isac.cnr.it
Institute of Atmospheric Sciences and Climate
corso Fiume 4
I-10133 Torino

Tuccella, Paolo
paolo.tuccella@aquila.infn.it
University of L'Aquila-CETEMPS
Department physics, university of l'Aquila, via vetoio, coppito
67010 L'Aquila

Japan

Kitada, Toshihiro
kitada@gifu-nct.ac.jp
Gifu National College of Technology
2236-2, Kami-makuwa
501-0495 Motosu City, Gifu Prefecture

Korea

Choi, Dae Yeon
chleofus@naver.com
Dept. of Environmental Engineering, Anyang University
708-113, 5 Anyang-dong, Manan-gu,
Anyang

Koo, Youn-Seo
koo@anyang.ac.kr
Dept. of Environmental Engineering, Anyang University
708-113, 5 Anyang-dong, Manan-gu,
Anyang

Luxemburg

Aleluia Reis, Lara
laleluia@gmail.com
CRP Henri Tudor
P.O. Box 144
4001 Esch-sur-Alzette

Netherlands

Builtjes, Peter
peter.builtjes@tno.nl
TNO-EELS
P.O. Box 80015
3508 TA Utrecht

Curier, Lyana
lyana.curier@tno.nl
TNO
Postbus 80015
3508 TA Utrecht

Dop, Han van
h.vandop@phys.uu.nl
Universiteit Utrecht
Berlagelaan 97
3723 AC Bilthoven

Erbrink, Hans
hans.erbrink@dnvkema.com
DNVKEMA
Postbus 9035
6800 ET Arnhem

Eskes, Henk
eskes@knmi.nl
KNMI
P.O. Box 201
3730 AE De Bilt

Hendriks, Carlijn
carlijn.hendriks@tno.nl
TNO
Postbus 80015
3508 TA Utrecht

Kok, Arnaud
ko@dgmr.nl
Postbus 370
2501 CJ Den Haag

Kokmeijer, Esther
esther.kokmeijer@dnvkema.com
DNVKEMA
Postbusnummer 9035
6800 ET Arnhem

Kranenburg, Richard
richard.kranenburg@tno.nl
TNO – Climate Air and Sustainability
P.O. BOX 80015
3508 TA Utrecht

Kumar, Ujjwal
ujjwal.kumar@knmi.nl
KNMI – Royal Netherlands Meteorological Institute
P.O. Box 201
NL-3730 AE De Bilt,

Manders, Astrid
astrid.manders@tno.nl
TNO
P.O. Box 80015
3508 TA Utrecht

Mika, Agnes
agnes.mika@bmtargoss.com
BMT ARGOSS
P.O. Box 61
8325 ZH Vollenhove

Nguyen, Lan
Lan.Nguyen@rivm.nl
RIVM
Postbus 1
3720 BA Bilthoven

Schaap, Martijn
martijn.schaap@tno.nl
TNO
P.O. Box 80015
3508 TA Utrecht

Segers, Arjo
Arjo.Segers@tno.nl
TNO
P.O. Box 80015
3508 TA Utrecht

Timmermans, Renske
renske.timmermans@tno.nl
TNO
Princetonlaan 6
3584 CB Utrecht

Swaluw, Eric van der
Eric.van.der.Swaluw@rivm.nl
RIVM-Centre for Environmental Monitoring
Postbus 1
3720 BA Bilthoven

Pul, Addo van
addo.van.pul@rivm.nl
RIVM
P.O. Box 1
3720 BA Bilthoven

Vila-Guerau de Arellano, Jordi
jordi.vila@wur.nl
Wageningen University Research
P.O. Box 47
6700 AA Wageningen

Weijers, Ernie
weijers@ecn.nl
ECN
Postbus1
1755 ZG Petten

Wichink Kruit, Roy
roy.wichinkkruit@tno.nl
TNO
Princetonlaan 6
3584 CB Utrecht

Wijma, Femke
femke.wijma@buroblauw.nl
Buro Blauw
Nude 54
6702 DN Wageningen

Wilde Barbaro, Eduardo
eduardo.wildebarbaro@wur.nl
Wageningen University – Meteorology and Air quality department
Akkermaalsbos 14
6708 PB Wageningen

Norway

Fagerli, Hilde
h.fagerli@met.no
Norwegian Meteorological Institute
Henrik Mohns Plass 1
O313 Oslo

Poland

Kryza, Maciej
maciej.kryza@uni.wroc.pl
University of Wroclaw
pl. Uniwersytecki 1
50-137 Wroclaw

Werner, Malgorzata
malgorzata.werner@uni.wroc.pl
University of Wroclaw
pl. Uniwersytecki 1
50-137 Wroclaw

Portugal

Borrego, Carlos
cborrego@ua.pt
IDAD – Institute for Environment & Development
Campus Universitario
3810-193 Aveiro

Miranda, Ana Isabel
miranda@ua.pt
IDAD – Institute for Environment & Development
Campus Universitario
3810-193 Aveiro

Tchepel, Oxana
oxana@ua.pt
University of Aveiro
Dep. Environment and Planning
3810-193 Aveiro

Saudi Arabia

Alqahtani, Jumaan
JUMAAN.QAHTANI.1@ARAMCO.COM
Saudi Aramco
West Park 2 , Floor 2, -221
31311 Dhahran

Slovenia

Boznar, Marija Zlata
marija.zlata.boznar@meis.si
MEIS d.o.o.
Mali Vrh pri Smarju 78
1293 Smarje-Sap

Mlakar, Primoz
primoz.mlakar@meis.si
MEIS d.o.o.
Mali Vrh pri Smarju 78
1293 Smarje-Sap

Spain

Baldasano, Jose
jose.baldasano@bsc.es
BSC-CNS
Jordi Girona 29
08034 Barcelona

Jimenez-guerrero, Pedro
pedro.jimenezguerrero@um.es
University of Murcia
Ed. CIOyN, Campus de Espinardo
30100 Murcia

Jorba, Oriol
oriol.jorba@bsc.es
Barcelona Supercomputing Center
C.Jordi Girona 29
08034 Barcelona

Rodríguez López, Angel
angel.rodriguez@usc.es
University of Santiago de Compostela
Escola Técnica Superior de Enxeñería,c/Lope Gómez
15782 Santiago de Compostela

Saavedra Vázquez, Santiago
santi.saavedra@usc.es
University of Cantiago de Compostela
Escola Técnica Superior de Enxeñería,c/Lope Gómez
15782 Santiago de Compostela

Sweden

Björnham, Oscar
oscar.björnham@foi.se
Swedish Defence Research Agency
FOI Cementvägen 20
S-901 82 Umeå,

Burman, Jan
jan.burman@foi.se
Swedish Defence Research Agency
FOI Cementvägen 20
S-901 82 Umeå,

Simpson, David
david.simpson@met.no
Dept. Earth and Space Sciences,Chalmers University of Technology
Hörsalsvg. 11
SE-412 96 Gothenburg

Von Schoenberg, Pontus
pontus.von.schoenberg@foi.se
Swedish Defence Research Agency
FOI Cementvägen 20
S-901 82 Umeå,

Switzerland

Aksoyoglu Sloan, Sebnem
sebnem.aksoyoglu@psi.ch
Paul Scherrer Institute
Laboratory of Atmospheric Chemistry, OFLA/012
5232 Villingen PSI

Brunner, Dominik
dominik.brunner@empa.ch
Empa, Swiss Federal Laboratories for Materials Science and Technology
Ueberlandstrasse 129
8600 Dübendorf

Turkey

Incecik, Selahattin
incecik@itu.edu.tr
Department of meteorology, Instanbul Technical University
34469 Sariyer

Ukraine

Biliaev, Mykola
envteam@ukr.net
National University of Railway Engineering
Lazaryana Str. 2 2
49000 Dnepropetrovsk

Kharytonov, Mykola
mykola_kh@yahoo.com
Dnipropetrovsk State Agrarian University
Voroshilov st. 25
49027 Dnipropetrovsk

Nochvai, Volodymyr
volivn@ukr.net
Pukhov Institute of Modelling Problems in Power Engineering National Academy of Sciences of Ukraine
General Naumov str. 15 Department 8
03164 Kiev

Shupranova, V
ecohous@ukr.net
Dnepropetrovsk National University, Biology Institute
Gagarina av.72 72 72
49600 Dnepropetrovsk

United Kingdom

Dore, Anthony
todo@ceh.ac.uk
Centre for Ecology and Hydrology
Bush Estate Penicuik
EH26 OQB Midlothian

Savage, Nicholas
nicholas.savage@metoffice.gov.uk
Met Office
Fitzroy Road
EX1 3PB Exeter

Sutton, Paul
paul.sutton@rwenpower.com
RWE npower
Becky Pearce, RWE npower, Trigonos Building, Windm
SN5 6PB

United States of America

Alapaty, Kiran
alapaty.kiran@epa.gov
USEPA
109 TW Alexander Drive
27711 Research Triangle Park

Arunachalam, Saravanan
sarav@email.unc.edu
University of North Carolina at Chapel Hill
137 E Franklin Street 645 A
27599-6116 Chapel Hill, NC

Garcia, Valerie
garcia.val@epa.gov
US EPA
109 TW Alexander Drive
27711 Research Triangle Park

Hogrefe, Christian
hogrefe.christian@epa.gov
US EPA
109 TW Alexander Drive
27711 Research Triangle Park

Janssen, Mark
janssen@ladco.org
LADCO
9501 W Devon Ave suite 701
60018 Rosemont, Illinois

Mathur, Rohit
mathur.rohit@epa.gov
EPA
T.W. Alexander Drive 109
27711 Durham, North Carolina

Minoura, Hiroaki
hiroaki.minoura@tema.toyota.com
Toyota Motor E&M North America
1555 Woodridge Ave.
48105 Ann Arbor

Napelenok, Sergey
napelenok.sergey@epa.gov
USEPA
109 TW Alexander Drive
27711 Research Triangle Park

Nolte, Chris
nolte.chris@epa.gov
USEPA
109 TW Alexander Drive
27711 Research Triangle Park

Odman, Mehmet
odman@gatech.edu
Georgia Institute of Technology
311 Ferst Drive
30332-0512 Atlanta, Georgia

Ozkaynak, Haluk
ozkaynak.haluk@epa.gov
USEPA
109 TW Alexander Drive
27711 Research Triangle Park

Porter, Steve
porter@if.uidaho.edu
University of Idaho
1776 science center
83402 Idaho falls

Rao, ST
Rao.ST@epamail.epa.gov
2316 Heartley Dr.,
Raleigh, NC 27615

Sarwar, Golam
sarwar.golam@epa.gov
USEPA
109 TW Alexander Drive
27711 Research Triangle Park

Weil, Jeff
weil@ucar.edu
NCAR
3450 Mitchell Lane
80301 Boulder Colorado

Contents

Part I
Climate Change and Air Quality

Chapter 1
Future Air Pollution in Europe from a Multi-physics Ensemble of Climate Change-Air Quality Projections

Pedro Jiménez-Guerrero, Sonia Jerez, Juan J. Gómez Navarro, Raquel Lorente, and Juan P. Montávez

Abstract This work conducts a multi-physics ensemble of air quality projections in order to elucidate the spreads and uncertainties behind the election of the physical parameterizations in the regional climate models. Results indicate that the studied parameterized processes and air pollutants transport and dispersion are closely tied together, and hence the projected changes are strongly affected by the atmospheric variables on the projections for air quality.

Keywords Climate change • Air quality • Ensemble

1.1 Introduction

Climate change alone influences the future concentrations of air pollutants through modifications of gas-phase chemistry, transport, removal, and natural emissions. The impacts of climate change on air quality may affect long-term air quality planning, and can be characterized by the use of chemistry transport models (CTMs). One of the most important components of climate simulation models, especially of regional climate models (RCMs), are the parameterization schemes. When coupled to CTMs, they can constitute an important source of uncertainty for air quality projections. While multi-model ensembles of regional climate simulations have been widely performed and investigated in an attempt to evaluate and overcome intermodel-related uncertainties, few studies deal with similar multi-physics ensembles for elucidating intramodel uncertainties [1]. Therefore, the main objective of this work is to conduct a comparative numerical modelling study of air quality projections from a climatic perspective using a multi-physics

P. Jiménez-Guerrero (✉) • S. Jerez • J.J. Gómez Navarro • R. Lorente • J.P. Montávez
Physics of the Earth, University of Murcia, 30100 Murcia, Spain
e-mail: pedro.jimenezguerrero@um.es

D.G. Steyn et al. (eds.), *Air Pollution Modeling and its Application XXII*,
NATO Science for Peace and Security Series C: Environmental Security,
DOI 10.1007/978-94-007-5577-2_1,

ensemble of MM5-EMEP-CHIMERE simulations. Two aspects will be covered in this contribution: (1) What is the changing signal of future air pollution in Europe and what is the associated spread?; (2) Can we isolate the leading processes causing the largest spreads and therefore the largest uncertainties in regional climate-air quality projections?

1.2 Methods and Models

Experiments span the periods 1971–2000, as a reference, and 2071–2100, as a future enhanced greenhouse gas and aerosol scenario (SRES A2). The atmospheric simulations with MM5-EMEP-CHIMERE have a horizontal resolution of 25 km and 23 vertical layers (up to 100 mb), and were driven by ECHAM5 outputs. The ensemble is the result of combining two of the available options for cumulus (CML, Grell and Kain-Fritsch), microphysics (MIC, Simple Ice and Mixed Phase) and planetary boundary layer (PBL, Eta and MRF) parameterizations within MM5. The analysis presented here, for the sake of brevity, will deal with PM2.5 ground levels. The ensemble spread (maximum difference among all the ensemble members in the projected changes) will characterize the intramodel uncertainty relative to the mean projected changes. In order to isolate the effect of changing the physical option for a particular parameterized process, we propose a methodology based on subensembles (subgroups) of simulations. These subensembles are given by fixing the PBL, the CML or the MIC scheme to one of the two options considered. From here we can identify the leading schemes (LS), defined as the process (PBL, CML or MIC) contributing most to the projected spread of PM2.5.

1.3 Results and Discussions

The results associated to meteorological variables can be found elsewhere [2]. For 2-m temperature, the average rise is about 2.5 K for wintertime and up to 6 K during the summertime over Southwestern Europe. However, it should be highlighted that the spread of these results is up to 50 % of the estimated warming, which is mainly caused by changes in the PBL scheme, with MRF providing the largest temperature increase. The most important change signals for precipitation are, on average, increases of about 40 mm/month in Western Europe in summer (where convective precipitation dominates and thus the CML plays a decisive role) and a generalized reduction in the rest of sites/seasons up to 50 %. Nevertheless, the spread in the precipitation projections involves even disagreement in the change sign among the ensemble members.

Projected PM2.5 changes and spreads depict diverse patterns for different areas of Europe. The largest projected increases of PM2.5 (Fig. 1.1) are mainly located over southern Europe (Iberian Peninsula and the Balkans region) especially during

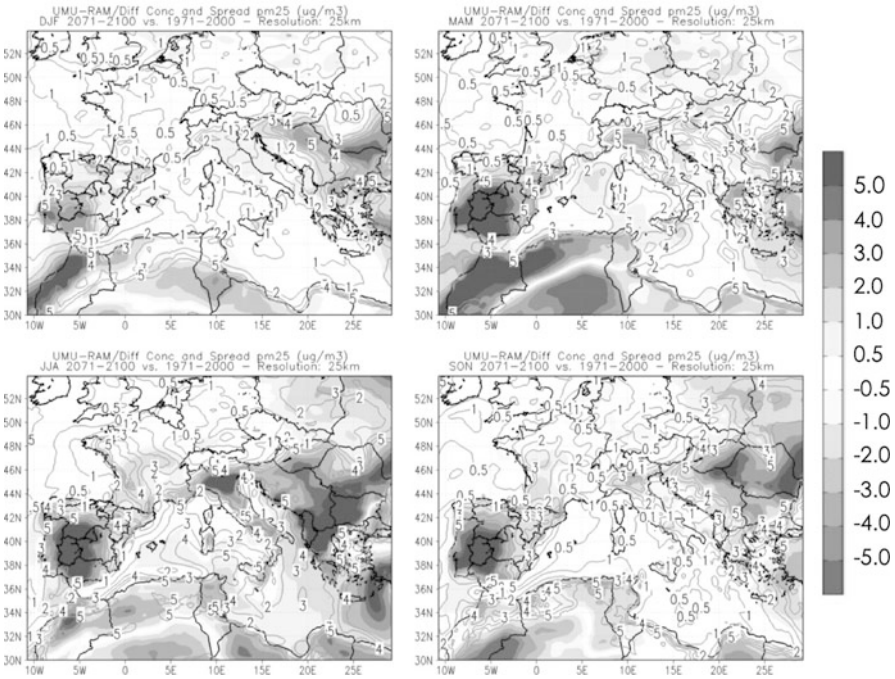

Fig. 1.1 Projected changes (2071–2100 vs. 1991–2000) in PM2.5 concentrations for Europe (*shaded*) and associated spread (*contours*) for DJF (*top*, *left*), MAM (*top*, *right*), JJA (*bottom*, *left*) and SON (*bottom*, *right*)

spring and summertime (up to $+5$ $\mu g\ m^{-3}$) meanwhile more northern areas show even slight decreases during springtime (-2 $\mu g\ m^{-3}$). The largest spreads are not always associated to the most important changing signal; for instance, over the western Mediterranean during JJA there is no noticeable increase in the concentration of aerosols, but the spread is 5 $\mu g\ m^{-3}$, highlighting the strong uncertainty associated to PM2.5 projections in this area (the sign of the changing signal disagrees among simulations). In most parts of the domain, the spread represents above 100 % of the ensemble-mean projected change for PM2.5.

Figure 1.2 depicts the leading schemes (LS defined as those parameterizations whose election presents the largest spread) regarding the uncertainty associated to the seasonal PM2.5 projections presented in Fig. 1.1. If LSs are looked for over the areas showing the largest spreads, some can be easily distinguished. Over land, the CML scheme determines the spread, with the KF scheme leading to the largest variation of the precipitation amount in the future. As well, the large spreads in PM2.5 changes appearing over the Iberian Peninsula and Eastern Europe in all seasons (Fig. 1.1) respond mainly to the change of the CML scheme. The use of the KF scheme combined to the ETA PBL scheme generally leads to the largest projected increases in the concentrations of PM2.5 over all Europe. However, the

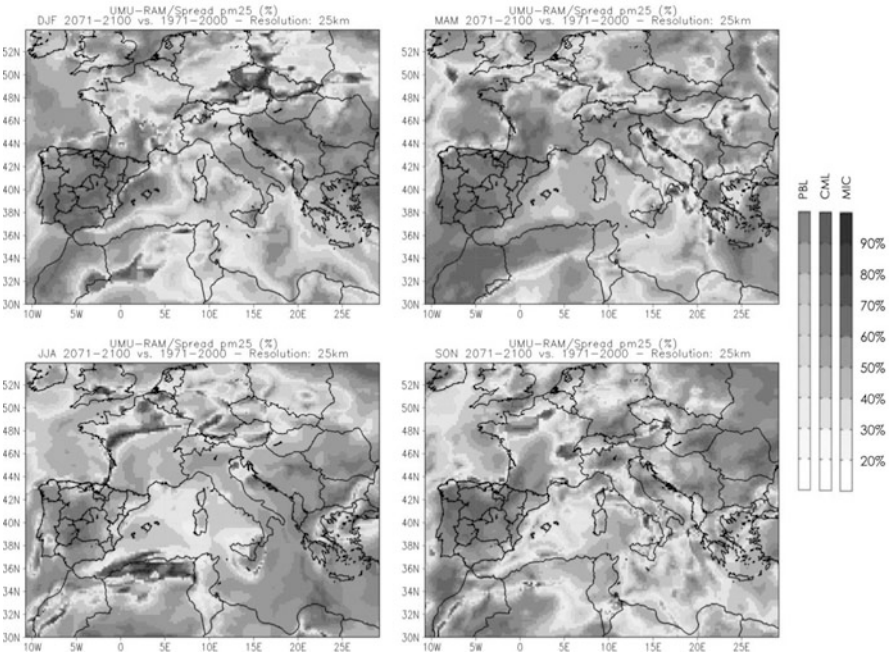

Fig. 1.2 Schemes leading to the largest spread in PM2.5 projections for DJF (*top*, *left*), MAM (*top*, *right*), JJA (*bottom*, *left*) and SON (*bottom*, *right*)

huge spread affecting the positive signals over some Mediterranean coastal areas is controlled by the PBL scheme alone especially in autumn and wintertime. The impacts of temperature on air quality are related to the dependence of gaseous-phase pollution and aerosols on this variable. While temperature uncertainties mostly affects gas-phase pollutants, the spreads in precipitation have a strong effect in the frequency of the washout and therefore in the projected levels and spreads in the concentrations of aerosols.

1.4 Conclusions

A valuable conclusion drawn from this assessment is that uncertainties affecting atmospheric variables also affect the air quality patterns and associated spreads, which show a great sensitivity to the physical configuration of the regional climate model. In the case of PM2.5, the LS for projected spreads and changes is conditioned by the election of the CML scheme (even modifying the sign of projected changes), while the PBL and MIC schemes add importance under future conditions for certain regions. Results further claim for future studies aimed at deepening the knowledge about the processes and reducing uncertainties.

References

1. Jacob D, Barring L, Christensen O, Christensen J, de Castro M, Deque M, Giorgi F, Hagemann S, Lenderink G, Rockel B, Sanchez E, Schaer C, Seneviratne S, Somot S, van Ulden A, van denHurk B (2007) An inter-comparison of regional climate models for Europe: model performance in present-day climate. Clim Change 81:31–52
2. Jerez S, Montávez JP, Gómez-Navarro JJ, Fernández J, Lorente R, García-Valero JA, Jiménez-Guerrero P (2012) A multi-physics ensemble of climate change projections over the Iberian Peninsula: mean changes, uncertainties and leading processes. Clim Dyn, doi: 10.1007/s00382-012-1539-1
3. Jiménez-Guerrero P, Gómez-Navarro JJ, Jerez S, Lorente-Plazas R, García-Valero JA, Montávez JP (2011) Isolating the effects of climate change in the variation of secondary inorganic aerosols (SIA) in Europe for the 21st century (1991–2100). Atmos Environ 45(4):1059–1063

Questions and Answers

Questioner Name: Stefano Galmarini

Q: Is intra-model ensemble spread the same as multi-model ensemble spread? What are the differences, if any?
A: This assessment reveals the great sensitivity of European air quality to future climate changes, yet highlighting the crucial role played by regional climate model (RCM) physics in air quality projections. The results of this contribution point to spreads among various simulations using the same model (intra-model spread) of similar magnitude to the spreads obtained in multi-model ensembles of air pollution. Note that in the multi-model ensemble there is a mixture of domain configurations and resolutions, nesting strategies, dynamic cores and physical configurations. All these factors contribute to the multi-model ensemble spread, while in our multi-physics single-model ensemble the spread is only attributable to the physical configuration of the regional model. Hence, the similar magnitude of the spreads obtained in both cases suggests that a large part of the multi-model spread could derive from the fact that the different models employ different physical configurations.

Q: Special attention should be paid to the use of the concepts "accuracy" versus "uncertainty".
A: The questioner raises an interest concern. This contribution does not cover the topic of accuracy of the simulations (e.g. the biases of the different configurations that are part of the air quality ensemble), since it has been identified elsewhere [3]. This work tries to identify the uncertainty associated to the election of the physics configuration of the RCM. Uncertainty is here defined as the differences among the various ensemble members (*spread*). These differences in the future projections could be considered as a matter of uncertainty in the change signals (as similarly assumed in multi-model studies).

Chapter 2
Influences of Regional Climate Change on Air Quality Across the Continental U.S. Projected from Downscaling IPCC AR5 Simulations

Christopher Nolte, Tanya Otte, Robert Pinder, J. Bowden, J. Herwehe, Greg Faluvegi, and Drew Shindell

Abstract Projecting climate change scenarios to local scales is important for understanding, mitigating, and adapting to the effects of climate change on society and the environment. Many of the global climate models (GCMs) that are participating in the Intergovernmental Panel on Climate Change (IPCC) Fifth Assessment Report (AR5) do not fully resolve regional-scale processes and therefore cannot capture regional-scale changes in temperatures and precipitation. We use a regional climate model (RCM) to dynamically downscale the GCM's large-scale signal to investigate the changes in regional and local extremes of temperature and precipitation that may result from a changing climate. In this paper, we show preliminary results from downscaling the NASA/GISS ModelE IPCC AR5 Representative Concentration Pathway (RCP) 6.0 scenario. We use the Weather Research and Forecasting (WRF) model as the RCM to downscale decadal time slices (1995–2005 and 2025–2035) and illustrate potential changes in regional climate for the continental U.S. that are projected by ModelE and WRF under RCP6.0. The regional climate change scenario is further processed using the Community Multiscale Air Quality modeling system to explore influences of regional climate change on air quality.

Keywords Regional climate modeling • Climate change • Air quality • CMAQ

C. Nolte (✉) • T. Otte • R. Pinder • J. Herwehe
U.S. Environmental Protection Agency, Research Triangle Park, NC 27711, USA
e-mail: nolte.chris@epa.gov

J. Bowden
Institute for the Environment, University of North Carolina, Chapel Hill, NC 27599, USA

G. Faluvegi • D. Shindell
NASA Goddard Institute for Space Studies, New York, NY 10025, USA

D.G. Steyn et al. (eds.), *Air Pollution Modeling and its Application XXII*,
NATO Science for Peace and Security Series C: Environmental Security,
DOI 10.1007/978-94-007-5577-2_2,

2.1 Introduction

Global climate models (GCMs) and, more recently, global earth system models are used to simulate the past and future evolution of the Earth's climate. Because these models are run for centuries and cover the entire globe, computational resource considerations limit them to using relatively coarse spatial resolution (e.g., 1° latitude × 1° longitude). Climate change impacts, however, are experienced at much finer spatial scales. Regional climate models (RCMs) provide one way to bridge the gap between coarse future climate scenarios provided by a GCM and the regional/local scales needed for climate change impact assessments. Previously, Nolte et al. [5, 6] used the Goddard Institute for Space Studies (GISS) II' global climate model as input to the mesoscale meteorological model MM5 and the Community Multiscale Air Quality (CMAQ) Model to examine climate change impacts on regional scale air quality over the continental United States circa 2050. Surface ozone levels were predicted to increase by 2–5 ppb over much of the eastern U.S. However, the interpretation of these results was hampered by biases in the meteorological simulation of current climate.

2.2 Development of Downscaling Methodology

Recognizing the limitations in simulating air quality imposed by errors in downscaling, recent work has focused on development and testing of a regional climate downscaling methodology [1, 2, 7]. The Weather Research and Forecasting (WRF) model was used to downscale the 2.5° × 2.5° Atmospheric Model Intercomparison Project (AMIP-II) Reanalysis data [3] (hereafter, R-2), which emulates the spatial and temporal resolutions of fields provided by a GCM. The R-2 data are the best available representation at coarse spatial scales of the meteorology that occurred, and thus can be regarded as "perfect boundary conditions." During the course of a continuous simulation of the 20-year period 1988–2007, no observational data exogenous to R-2 were assimilated in order to maintain consistency with the scale of data available from a GCM. However, unlike the situation when downscaling a GCM future climate scenario, the downscaled R-2 simulation can be evaluated against finer-scale observations or analyses, such as the 32-km North American Regional Reanalysis (NARR) [4].

The results showed that when forcing WRF only via the lateral boundaries of a large continental modeling domain, substantial biases can exist over large regions [1]. These biases can be significantly reduced by using the large-scale driving fields to constrain or "nudge" the RCM solution. Nudging not only improves the simulation of mean quantities, but also improves the accuracy of simulated extreme temperature and precipitation events [7] and the large-scale atmospheric circulation [2].

2.3 Modeling Application

The downscaling techniques that were tested and evaluated using the historical data sets were applied to simulations from the NASA GISS ModelE [8]. Two 11-year time slices were simulated, one a control run representing current climate around 2000 (nominally 1995–2005) and one following RCP6.0 around 2030 (i.e., 2025–2035). As shown in Fig. 2.1, WRF projects no change in mean 2-m temperature for most of the western U.S. and a warming of up to 2 K in the central U.S. during July, and a much broader warming exceeding 3 K for most of the domain during January.

To examine the implications of this climate scenario for future air quality, the downscaled meteorology was used to drive the CMAQ chemical transport model. Two 1-year simulations were conducted using meteorology downscaled from the current decade GCM simulation (i.e., 1995) and downscaled from the RCP6.0 simulation (i.e., 2025). For both simulations, anthropogenic emissions were based on the U.S. EPA National Emission Inventory for 2005, while biogenic emissions were computed online.

The number of days simulated as exceeding the U.S. 8-h average surface ozone concentration standard of 75 ppb was computed for both annual runs. As shown in Table 2.1, for these 2 years the future meteorology leads to a substantial (∼10 %) increase in the number of ozone exceedances on an annual basis. However, the magnitude and location of the change in ozone levels varies widely over the course of the year, with strong increases in June and July partially offset by decreases in August. These differences, though plausible, are not statistically significant, as more years of model simulations are needed to distinguish the climate change

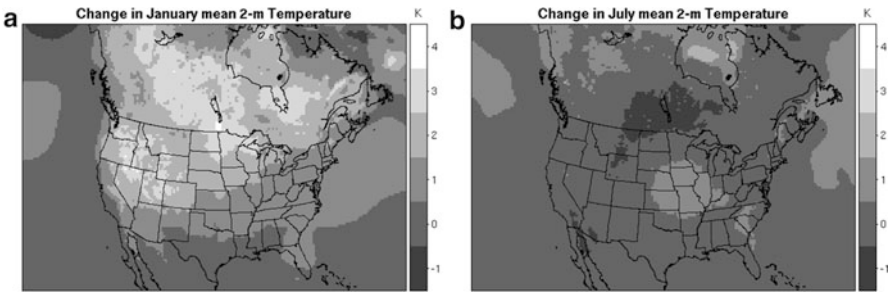

Fig. 2.1 Change in monthly mean 2-m temperatures downscaled from ModelE by WRF for (**a**) January and (**b**) July

Table 2.1 Domain-wide number of grid cells with exceedances of 75 ppb threshold for daily maximum 8-h average surface ozone concentrations

	1995	2025
June	17,921	24,539
July	25,000	27,604
August	26,541	21,528
Annual total	97,905	107,257

signal from the noise of interannual variability. Both simulations will be extended to encompass the entire 11-year period, and the analysis will be repeated to discern the impact of the change in ozone and particulate matter air quality attributable to regional climate change.

Acknowledgments and Disclaimer The United States Environmental Protection Agency through its Office of Research and Development funded and managed the research described here. It has been subjected to the Agency's administrative review and approved for publication.

References

1. Bowden JH, Otte TL, Nolte CG, Otte MJ (2012) Examining interior grid nudging techniques using two-way nesting in the WRF model for regional climate modeling. J Clim 25:2805–2823
2. Bowden JH, Nolte CG, Otte TL (2013) Simulating the impact of the large-scale circulation on the regional 2-m temperature and precipitation climatology. Clim Dyn. doi: 10.1007/s00382-012-1440-y
3. Kanamitsu M, Ebisuzaki W, Woolen J, Yang S-K, Hnilo JJ, Fiorino M, Potter GI (2002) NCEP-DOE AMIP-II Reanalysis (R-2). Bull Am Meteorol Soc 83:1631–1643
4. Mesinger F et al (2006) North American regional reanalysis. Bull Am Meteorol Soc 87:343
5. Nolte C, Gilliland A, Hogrefe C (2007) Linking global and regional models to simulate U.S. air quality in the year 2050. In: Borrego C, Miranda AI (eds) Air pollution modeling and its application XIX. Springer, Dordrecht, pp 633–647
6. Nolte CG, Gilliland AB, Hogrefe C, Mickley LJ (2008) Linking global to regional models to assess future climate impacts on surface ozone levels in the United States. J Geophys Res 113:D14307
7. Otte TL, Nolte CG, Otte MJ, Bowden JH (2012) Does nudging squelch the extremes in regional climate modeling? J Clim 25:7046–7066. doi:10.1175/JCLI-D-12-000048.1
8. Schmidt GA et al (2006) Present day atmospheric simulations using GISS ModelE: comparison to in-situ, satellite and reanalysis data. J Clim 19:153–192

Questions and Answers

Questioner Name: P. Makar

Q: The model results show effects due to nesting/downscaling very well. What would be the impact of running an RCM globally? That is, the computers we use should have reached the state where this is possible. Would you expect similar effects with a global RCM?
A: It is difficult to differentiate effects due to discontinuities at the lateral boundaries from errors in the RCM physics formulations. Though a global version of WRF has been developed, to my knowledge it has not been used for long-term simulations, which could help determine whether WRF is in radiative balance. We are experimenting with using WRF on a hemispheric domain, which may reduce the influence of lateral boundary conditions. It might also be interesting to conduct a global-to-regional "Big Brother Experiment" using the WRF model.

Chapter 3
Projection of Air Quality in Melbourne, Australia in 2030 and 2070 Using a Dynamic Downscaling System

Martin Cope, Sunhee Lee, Sean Walsh, Melanie Middleton, Mark Bannister, Wal Delaney, and Andrew Marshall

Abstract A multi-scale dynamical downscaling system has been set up to investigate future air quality trends in Melbourne, Australia due to climate and/or emission changes. The system consists of a comprehensive air emissions inventory; an ensemble of climate trends, a regional climate model for downscaling from synoptic to regional scale and a meteorological-chemical transport model for downscaling from regional to urban scale. Air quality projections for 2030 and 2070 suggest that, in the absence of emission controls, ozone concentrations will increase, leading to a 20–25 % increase in population exposure. The outcomes for PM2.5 show mixed results depending on season. The air quality trends with three different emission scenarios for 2030 were also modelled under the same climate projection. Some impact measures, such as average ozone concentration, are insensitive to the choice of emission scenarios, while others such as exposure to nitrogen dioxide show significant variations for different scenarios.

Keywords Climate-Air Quality • Downscaling • PM2.5

3.1 Introduction

The first part of this paper presents results from simulations of Melbourne's air quality over three decades, 1996–2005 (Decade 1), 2025–2034 (Decade 2), 2065–2074 (Decade 3) with a fixed 2006 local emission inventory to investigate the

M. Cope • S. Lee (✉)
Centre for Australian Weather and Climate Research, CSIRO Marine and Atmospheric Research, Melbourne, Australia
e-mail: sunhee.lee@csiro.au

S. Walsh • M. Middleton • M. Bannister • W. Delaney • A. Marshall
EPA Victoria, Melbourne, Australia

D.G. Steyn et al. (eds.), *Air Pollution Modeling and its Application XXII*,
NATO Science for Peace and Security Series C: Environmental Security,
DOI 10.1007/978-94-007-5577-2_3,

climate penalty, i.e. the effects of climate change. The climate trends from four global climate models (GCM) were used to drive the regional climate model for these three decades to investigate the climatic effect on air quality in future decades. Apart from these annual runs with one selected GCM, January and February (representing summer) and July and August (winter) of Decade 1 and Decade 3 were simulated with the climate trends of four GCMs. The trends in air quality due to climate change are presented in terms of exceedence rates against National Environment Protection Measure Ambient Air Quality Standards (AAQS) and changes in population exposure.

The second part of this paper presents air quality trends under both climate and emission changes. We have modelled three emission scenarios for 2030 under the same climate projection. The results are also presented in terms exceedence rates and population exposure.

3.2 The Methodology

The climate trends generated by four GCMs have been used- the Geophysical Fluid Dynamics Laboratory Climate Model ver. 2.1; the CSIRO Mk3.5 GCM; the United Kingdom UKMO-HadCM3 GCM; and the German ECHAM5/MPI-OM GCM. These models were selected on the basis of their performance in modelling key meteorological features in the Australian region as part of the Climate Futures for Tasmania project [2]. In that project the climate trends (as represented by the GCM sea surface temperatures) were corrected for biases and used to force the CSIRO Conformal Cubic Atmospheric Model (CCAM; [4]), and generate climate over the Australian region at 60 km grid spacing and then at higher resolution over Tasmania.

The 60 km CCAM meteorological fields have been used to drive high resolution (nesting down to 3 km grid spacing) meteorological and chemical transport modeling over Melbourne using TAPM [3], and the CSIRO Chemical Transport Model (CTM; [1]).

In the first part of this work, the CTM was forced by a 2006 anthropogenic inventory for all modelled decades. Thus the intent is to first investigate the relationship between air pollution and climate without the confounding factor of simultaneous anthropogenic emission changes (other than for sources such as evaporative VOC with meteorological dependency).

3.3 Air Quality Projection Under Climate Change

The projected changes in air quality due to the climate penalty were determined by comparing air pollution metrics for future Decade 2 and Decade 3 with Decade 1. In this paper we present examples for O_3 and $PM_{2.5}$. We quantify these changes using exceedence frequencies of the AAQS and through the use of

Table 3.1 Average annual number of exceedences of the NEPM AAQS for the GFDL v2.1 downscaled projections

	O_3 (1-h)	O_3 (4-h)	NO_2 (1-h)	PM2.5 (24-h)
AAQS	100 ppb	80 ppb	120 ppb	25 $\mu g\ m^{-3}$
Decade 1	1.2	2.8	0	9.7
Decade 2	3.4	5.2	0	10.4
Decade 3	6.5	10.7	0	12.7

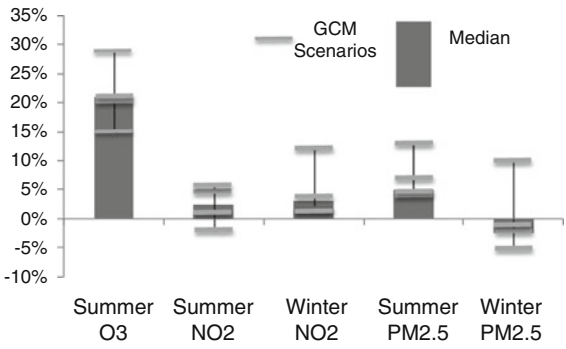

Fig. 3.1 The median and range of the change in population exposure for Decade 3 based on the multi-GCM decadal simulations of summer and winter months

the Residential Population Exposure metric where exposure is calculated as the population weighted concentration once a prescribed threshold has been exceeded.

Table 3.1 shows ozone exceedence rates will increase by 110–275 % while $PM_{2.5}$ shows less significant change in future decades. In this study we have calculated ozone population exposure using 1-h averaged ozone and a threshold of 25 ppb; NO_2 is based on a 1-h concentration and zero threshold; and $PM_{2.5}$ is based on 24-h average concentration and zero threshold. Figure 3.1 shows population exposure to ozone during summer months will increase by 15–30 % for the various GCM simulations. All GCM results show that population exposure to $PM_{2.5}$ increases by 4–13 % in summer while most GCM results show it decreases by 2–5 % in winter due to reduced wood heater usage during warmer winter months.

3.4 Air Quality Projection Under Different Emission Scenarios

In this study three different emission scenarios were devised to investigate the impacts of different emission scenarios on air quality under the same climate projection. We modelled three emission scenarios for 2030, hereafter referred as E1, E2 and E3. These emission scenarios are developed using different assumptions for industrial emissions control, location of population growth, development of vehicle technology, power generation and other categories. E2 is a most likely scenario while E1 and E3 are alternative scenarios. Figure 3.2 shows differences in annual

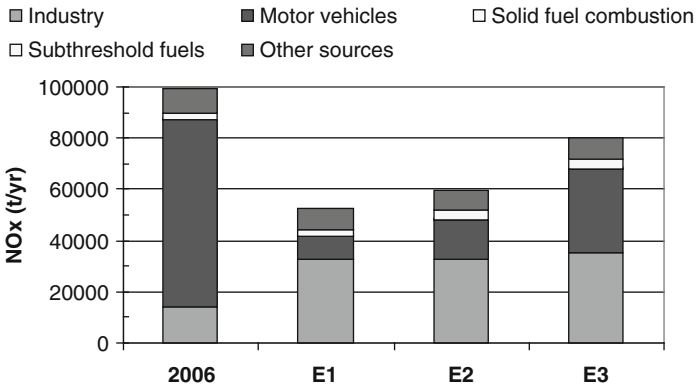

Fig. 3.2 Annual NO_x emission in Melbourne from different emission scenarios

NO_x emission from various sources in Melbourne with current NO_x The model simulations have been carried out with one GCM, CSIRO Mk3.5.

For all three emission scenarios, 1-h ozone and 24-h $PM_{2.5}$ are predicted to breach the AAQS while 1-h NO_2, 8-h CO and 24-h SO_2 are not expected to exceed the AAQS. Some air quality metrics such as average ozone concentration are insensitive to the selection of emission scenarios while others such as exposure to nitrogen dioxide show significant variations for different scenarios.

3.5 Summary

The air quality trends under climate change with the current emission inventory and with three different emission scenarios are modelled for Melbourne with a multi-scale dynamic downscaling system for future decades. The climate penalty simulations show ozone is most sensitive to climate change with projected increase in population exposure of 20–30 % with substantial increase of AAQS exceedence days. Changes in $PM_{2.5}$ exposure and exceedence rates show seasonal differences, likely due to a reduction in wood heater emissions for warmer winter months.

Projections from simulation of the combined effects of climate change and anthropogenic emission change show population exposure to nitrogen dioxide is very sensitive to the choice of emission scenario while others such as ozone concentration are not. Both 1-h ozone and 24-h $PM_{2.5}$ are predicted to exceed AAQS under all three emission scenarios.

Acknowledgments This work was carried out as a cooperative research project between CSIRO Marine and Atmospheric Research and Environment Protection Authority Victoria.

References

1. Cope M, Lee S, Noonan J, Lilley B, Hess D, Azzi M (2010) Chemical transport model technical description. CSIRO, Melbourne. ISBN 978 0 643 09824 4
2. Corney et al (2010) Climate futures for Tasmania. Technical report on climate modelling, p 72
3. Hurley PJ (2009) The Air Pollution Model (TAPM) version 4. Part 1. Technical description. CSIRO Atmospheric Research technical paper 71, Aspendale, 54 p
4. McGregor JL, Dix MR (2005) The conformal-cubic atmospheric model: progress and plans. JSPS international meeting series. JSPS/JAMSTEC, Yokohama, 2 p

Questions and Answers

Questioner Name: Sebnem Aksoyoglu

Q: Do you keep biogenic emissions constant? Do you take changes in land use into account?
A: No, biogenic emissions are calculated on the fly in the chemical transport model, thus it reflects changing meteorological conditions, but we keep surface characteristics such as land use or leaf area index constant for the future decade run.

Questioner Name: Volodymyr Nochvai

Q: What is the relationship between exposure assessment values and health effects?
A: We assess impact of air quality on human health with a metric that represents changes in population exposure for the future decade from the current decade. Population exposure is defined as pollutant concentration multiplied by population. With higher concentrations and larger population, total population exposure in the study region gets higher, thus adverse health impact.

Chapter 4
Investigating Differences in Air Quality Between Urban and Rural Regions Under Current and Future Climate Conditions

Andrea Mues, Astrid Manders, Bert van Ulft, Erik van Meijgaard, Martijn Schaap, and Peter Builtjes

Abstract The differences between air quality in urban and rural regions has been investigated for the current situation using both observations and modeling and also for future climate conditions

Keywords LOTOS-EUROS • PM 10 • Air quality • Climate change

4.1 Introduction

Urban regions are very important in relation to air quality and climate change because they represent the main areas of anthropogenic emissions and a high proportion of the population lives in urbanized regions and is therefore exposed to the resulting air pollution. The concentration gradient between an urban region and its surrounding rural area is mainly caused by different emission density and composition, different land use, as well as by meteorological effects. In this study PM10 measurement data from the AirBase database for the years 2003–2008 are

A. Mues (✉)
Freie Universität Berlin, Berlin, Germany
e-mail: andrea.mues@met.fu-berlin.de

A. Manders • M. Schaap
TNO, Utrecht, The Netherlands
e-mail: astrid.manders@tno.nl; martijn.schaap@tno.nl

B. van Ulft • E. van Meijgaard
KNMI, De Bilt, The Netherlands

P. Builtjes
Freie Universität Berlin, Berlin, Germany

TNO, Utrecht, The Netherlands
e-mail: peter.builtjes@tno.nl

D.G. Steyn et al. (eds.), *Air Pollution Modeling and its Application XXII*,
NATO Science for Peace and Security Series C: Environmental Security,
DOI 10.1007/978-94-007-5577-2_4,

selected in order to determine the gradient between urban and rural background concentrations. To analyse whether a chemistry transport model (CTM) is able to reproduce the observed gradient and to investigate the chemical composition of PM10 in urban and rural regions, simulation runs were performed with the CTM LOTOS-EUROS [3] for 2003–2008 on a $0.5° \times 0.25°$ lon-lat grid covering Europe (LE_eu) with ECMWF input meteorology. A second run for the year 2008 on a $0.25° \times 0.125°$ lon-lat grid covering The Netherlands and Germany (LE_zoom) was performed to investigate the impact of different horizontal grid resolutions on the modeled PM10 concentrations in urban and rural regions.

The air pollution situation in future is expected to change because meteorological conditions are influenced by climate change and the emission intensity is reduced when emission reductions plans are carried out. The effect of meteorological conditions differs for each pollutant (e.g. ozone and PM) and because PM consists of several components with different physical and chemical properties, the effect of meteorology on the individual component varies as well. As a consequence the impact of a changing climate on air pollution levels and the PM composition might differ between an urban and the surrounding rural region and therefore also the concentration gradient might change. In this study a one-way coupled model system consisting of the regional climate model RACMO2 [4] and LOTOS-EUROS is used to investigate the effect of climate change on PM concentrations and composition. Different sets of simulations were produced, for which the output of the GCMs ECHAM5 and MIROC with SRES-A1B for the time period 1970–2060 as well as ERA-interim data for the time period 1989–2009 were dynamically downscaled on a $0.5° \times 0.25°$ grid using RACMO. LOTOS-EUROS runs were then forced with the resulting outputs (LE_ERA, LE_ECHAM, LE_MIROC). Anthropogenic emissions (MACC2005) were kept constant for these runs to focus on the impact of meteorology.

The main focus in this study is on the urban Ruhr area which is located in the west of Germany and characterized by a dense cluster of cities, industries and road networks, surrounded by a rural area with mainly forest and agriculture. For the Ruhr area, four rural stations and four urban stations were selected in this study.

4.2 Results

The two different horizontal grid resolutions had only a small effect on the modeled PM10 concentrations and the gradient between urban and rural regions. Therefore the LE_eu run and the LE_RACMO simulation runs are used to determine a concentration gradient.

For the Ruhr area lowest concentrations but large differences between the stations are found in the surrounding rural area, whereas the concentrations at stations in the urban area are highest and very similar for the average of the years 2003–2008 (Fig. 4.1, left). The average over every urban and over every rural stations results in a concentration gradient of 7.3 $\mu g/m^3$ (34.8 %). The model underestimates

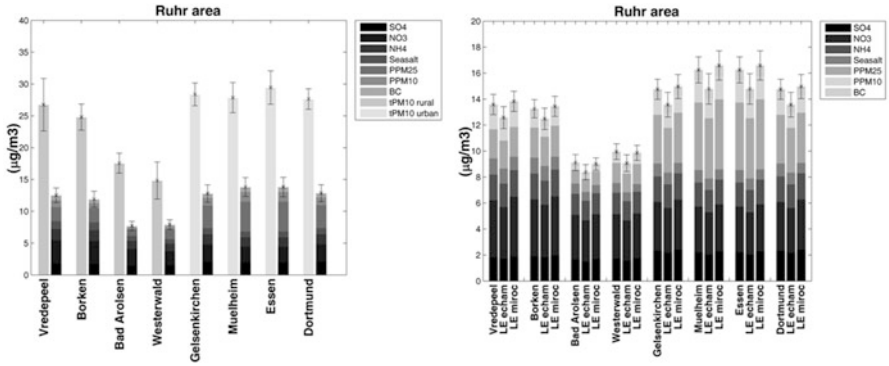

Fig. 4.1 Measured (*grey*) and modeled (LE_eu) (*black*) PM10 concentrations averaged over 2003–2008 (*left*) and modeled PM10 concentrations averaged over the present-day period (1989–2009) (*right*) for LE_ERA, LE_ECHAM and LE_MIROC for different stations in the Ruhr area

the averaged PM10 concentrations but the variability of concentration between the stations is still reproduced (Fig. 4.1, left). This also holds for the gradient, which is underestimated when considering the absolute difference due to the underestimation of PM10. But if the gradient is expressed as a percentage the difference between model results and observation is only small.

Also the simulations with the coupled climate – air quality model system show a gradient for PM between urban and rural stations for the present-day period. But simulated concentrations were different for the run using ECHAM and the one using MIROC boundary conditions and both runs differed significantly from the present-day simulations with ERA-interim forcing with small implications for the gradient (Fig. 4.1, right).

The differences between the concentration of PM10 and its components for the present-day and future period are only between ± 2 % for LE_ECHAM and ± 8 % for LE_MIROC (Fig. 4.2). The differences are smaller than differences between LE_ERA and LE_ECHAM, LE_MIROC respectively. For LE_ECHAM most components (except seasalt) decrease but for LE_MIROC they increase under simulated future climate conditions.

4.3 Discussion

Observations of PM10 showed a concentration gradient between an urban and the surrounding rural region, which was reproduced by the model. LOTOS-EUROS indicated that the gradient was mainly due to higher concentrations of the primary components and elemental carbon in the urban region. The model underestimated the absolute concentrations and the gradient, due to the lack of a good description

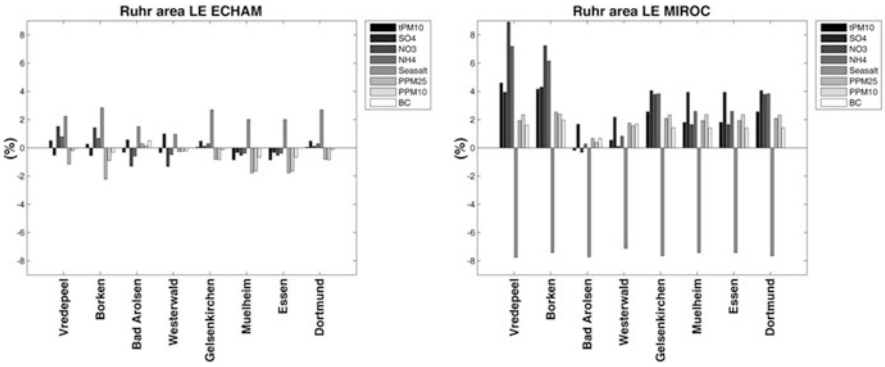

Fig. 4.2 Relative difference between the future and the present-day period for PM10 components for LE_ECHAM (*left*) and LE_MIROC (*right*)

of the formation of secondary organic aerosol and dust emissions, and potentially other processes and species. The finding that the grid resolution hardly affects the gradient allows the conclusion that the RACMO – LOTOS-EUROS runs can be used to investigate the impact of climate change on the concentration gradient from urban areas to rural regions. On average the effect of the future climate runs on PM10 is only small, therefore emission changes could be more important than climate change for air pollution in future. Previous studies showed considerable biases in the climate model results [1] and that the CTM underestimates the variability of PM with meteorology [2]. Therefore uncertainties in the model system for both the climate model and the CTM have to be considered when interpreting the model results.

References

1. Manders AMM, van Meijgaard E, Mues AC, Kranenburg R, van Ulft LH, Schaap M (2012) The impact of differences in large-scale circulation output from climate models on the regional modeling of ozone and PM. Atmos Chem Phys Discuss 12:12245–12285
2. Mues A, Manders A, Schaap M, Kerschbaumer A, Stern R, Builtjes P (2012) Impact of the extreme meteorological conditions during the summer 2003 in Europe on particulate matter concentrations. Atmos Environ 55:377–391
3. Schaap M, Timmermans RMA, Sauter FJ, Roemer M, Velders GJM, Boersen GAC, Beck JP, Builtjes PJH (2008) The LOTOS-EUROS model: description, validation and latest developments. Int J Environ Pollut 32(2):270–289
4. Van Meijgaard E, Van Ulft LH, Van de Berg WJ, Bosveld FC, Van den Hurk BJJM, Lenderink G, Siebesma AP (2008) The KNMI regional atmospheric climate model RACMO version 2.1. KNMI technical report, TR-302

Questions and Answers

Questioner Name: Sebnem Aksoyoglu

Q: Among the modeled species, there was no secondary organic aerosols. Are they not included in the model?
A: The formation of secondary organic aerosols (SOA) is not included in the model version used for this study. Due to the dependency of the formation of SOA on meteorological parameters, SOA is important to consider when discussing the impact of climate change on air quality. And because the precursors of SOA have different emission sources (anthropogenic, biogenic) which are also depending on the location (urban or rural region), SOA might also contribute to the concentration gradient.

Questioner Name: T. Dore

Q: The model under-estimated measurements of PM10. Can this be partly attributed to the water content contained in measurements of particulate matter?
A: The analytical results from the chemical speciation of measured PM10 mass always show a certain percentage of unexplained mass. This unknown part is anticipated to be to a high fraction water. This water content in the measurements of PM is not taken into account in the model and contributes therefore to the underestimation of PM10. But several other important components of PM10 are not yet included in the model as for example SOA and windblown dust, furthermore emissions are uncertain just as the description of some processes in the model. This also contributes significantly to the underestimate of PM10.

Part II
Air Quality and Human Health

Chapter 5
The Role of Aerosol Properties on Cloud Nucleation Processes

Stavros Solomos, George Kallos, Jonilda Kushta, A. Nenes, D. Barahona, and N. Bartsotas

Abstract The clouds that develop in maritime or polluted environments have significant differences in their properties. A number of modeling sensitivity tests have been performed to describe the physical processes related to aerosol – cloud interactions at various stages of cloud development. Precipitation amounts and cloud structure were found to be very sensitive to changes in the size distribution and number concentrations of the aerosols. Certain combinations of CCN/IN properties and atmospheric properties may lead to significant enhancement of convection and precipitation. These interactions are not linear and it is the synergetic effects between meteorology and atmospheric chemistry that are responsible for the variation of precipitation.

Keywords Aerosols • Clouds • CCN • Nucleation

5.1 Introduction

Airborne particles, depending on their size distribution and chemical composition/solubility, may serve as CCN and/or IN. Natural (e.g. sea salt, dust, volcanic ash) and anthropogenic (e.g. sulfates, nitrates), are responsible for the formation of cloud drops and cloud ice particles [2, 3]. For example the effects of particles

S. Solomos • G. Kallos (✉) • J. Kushta • N. Bartsotas
School of Physics, University of Athens, Athens, Greece
e-mail: kallos@mg.uoa.gr

A. Nenes
School of Earth and Atmospheric Sciences, Georgia Institute of Technology, Atlanta, GA, USA

D. Barahona
NASA Goddard Space Flight Center, Greenbelt, MD, USA

D.G. Steyn et al. (eds.), *Air Pollution Modeling and its Application XXII*,
NATO Science for Peace and Security Series C: Environmental Security,
DOI 10.1007/978-94-007-5577-2_5,

on radiative transfer may either enhance cloud formation or invigorate cloud burn off. Also, the aerosols that contain soluble matter can form cloud droplets while insoluble particles such as mineral dust and black carbon act as efficient ice nuclei (IN). In this work, the impact of natural and anthropogenic aerosols and their mixture on cloud formation and precipitation has been investigated. A series of sensitivity runs were performed with the implementation of the recently developed integrated modeling system – RAMS/ICLAMS [4].

5.2 Sensitivity Tests

The model was set up in a 2D configuration for 12 different mixtures of aerosol particles, as seen in Table 5.1. Each run lasted for 6 h and the airborne particles were allowed to act as CCN and/or IN for the formation of clouds. The distribution of the particles in the model was represented by a three-modal lognormal distribution with constant geometric dispersion ($\sigma = 2$), assuming various chemical compositions and concentrations.

Activation of the different aerosol types as CCN resulted in significant variation in the total accumulated precipitation as indicated in Fig. 5.1. The aerosols that consisted of dust particles externally coated with soluble material produced similar precipitation amounts – within the range of 300–350 mm. However, by increasing the percentage of soluble material, the accumulated precipitation was reduced (e.g. Case 3, Case 11). This is due to the increased number of cloud droplets resulting in slower auto-conversion rates of cloud to rain sizes. In Cases 6–8, the particles were assumed to be completely soluble (NaCl) with different size distribution characteristics. A slight reduction in total precipitation was found for the aerosols with the greater particle diameters. Bigger cloud and rain droplets were formed

Table 5.1 Aerosol characteristics for the 12 modeling scenarios

Case	Chemical composition	Soluble fraction	Concentration (cm^{-3})	Mean diameter (fine-accumulated-coarse) (μm)
1	Dust + NaCl	0.2	1,000	0.02-0.2-2
2	Dust + NaCl	0.5	1,000	0.02-0.2-2
3	Dust + NaCl	0.7	1,000	0.02-0.2-2
4	NaCl	1.0	1,000	0.02-0.2-2
5	NaCl	1.0	2,000	0.02-0.2-2
6	NaCl	1.0	1,000	0.05-0.2-2
7	NaCl	1.0	1,000	0.02-0.5-2
8	NaCl	1.0	1,000	0.02-0.2-5
9	Dust + $(NH_4)_2SO_4$	0.2	1,000	0.02-0.2-2
10	Dust + $(NH_4)_2SO_4$	0.5	1,000	0.02-0.2-2
11	Dust + $(NH_4)_2SO_4$	0.7	1,000	0.02-0.2-2
12	$(NH_4)_2SO_4$	1.0	1,000	0.02-0.2-2

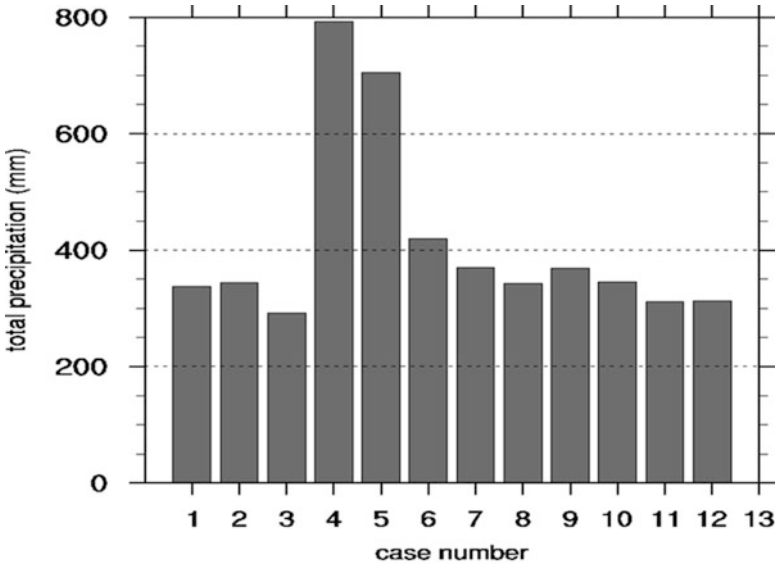

Fig. 5.1 Domain total accumulated (6 h) precipitation (mm) for the 12 aerosol scenarios

and precipitation from the ice phase of the cloud was limited. A comparison of the maximum precipitation rate assuming NaCl (Case 4) and $(NH_4)_2SO_4$ (Case 12) particles is seen in Fig. 5.2. In Case 4, the precipitation rate remained relatively high even during the latest stages of cloud development due to significant contribution of the ice condensates. This resulted in almost 100 % increase in total precipitation compared to the rest of the case studies.

These results imply the crucial role of the chemical composition (Table 5.2) in the temporal evolution of the microphysical processes. For example, as seen in Fig. 5.3, the activation of ammonium sulphate particles as CCN resulted in increased cloud droplet concentrations throughout the modelling period, thus suppressing the formation of precipitable rain droplets. However, the most significant difference between these two runs comes from the ice stage of the cloud. As seen in Fig. 5.4, the cloud updrafts in Case 4 were significantly higher than in Case 12 and more ice was found near the cloud top (Fig. 5.5). Melting and rimming of the frozen elements invigorated the production of graupel and hail at the middle and higher cloud layers and the major part of precipitation during 4–6 h simulation was generated from this stage of the cloud. In order to illustrate the synergetic effects that lead to such severe phenomena, one more run was performed for exactly the same air quality properties as in Case 4. However, in this run the initial dew point temperature profile was reduced by 1 °C. The total accumulated precipitation for this case was 234.41 mm – which is three times lower than the 792.92 mm of Case 4. Such results imply the importance of the synergetic effects between air quality and meteorology since a minor change in any of the two can lead in significant precipitation variability.

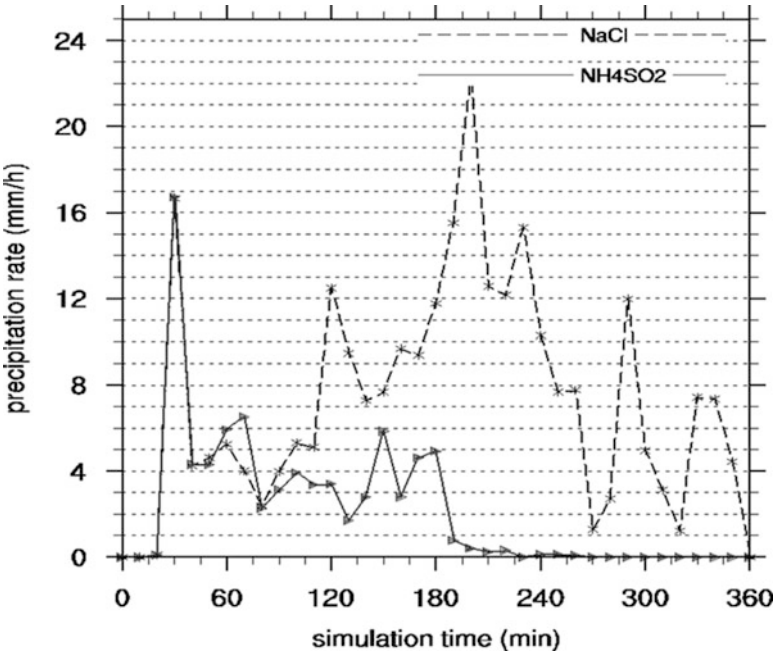

Fig. 5.2 Maximum precipitation rate (mm/h) for Case 4 (NaCl) and Case 12 (NH_4SO_2)

Table 5.2 Chemical properties of the aerosol soluble fraction

	Density (kg m^{-3})	Molar mass (kg mol^{-1})	Van't Hoff factor (ions $molec^{-1}$)
NaCl	2,165	0.058	2
$(NH_4)_2SO_4$	1,760	0.132	3

The interplay between air quality and high clouds has also been tested within the framework of the model, assuming initial conditions that are representative of a cold cloud structure. The amount of ice particles that will activate during cloud formation depends on the IN concentration, atmospheric conditions and also on the competition between homogeneous and heterogeneous ice processes, as seen in Fig. 5.6. For example, by considering 12 different concentrations of dust or soot particles that can be activated as IN, the respective accumulated precipitation performed great variance as seen in Fig. 5.7. In general, the precipitation remained similar for both species until an aerosol concentration of 50 $\mu g\ m^{-3}$. After this threshold, the results varied considerably. Maximum precipitation values were found for the 500 $\mu g\ m^{-3}$ and for the 1,000 $\mu g\ m^{-3}$ of soot and dust particles respectively. A significant amount of precipitation for the 1,000 $\mu g\ m^{-3}$ of soot scenario was hail. Further increase of the aerosol concentrations resulted in less precipitation as these clouds contained great amounts of small ice elements and finally burned off before these condensates managed to grow up to precipitable sizes.

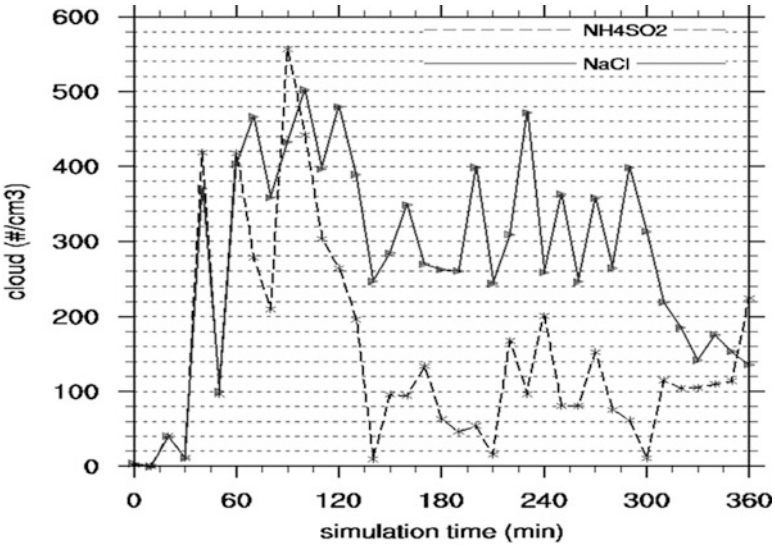

Fig. 5.3 Maximum cloud droplet concentration (cm^{-3})

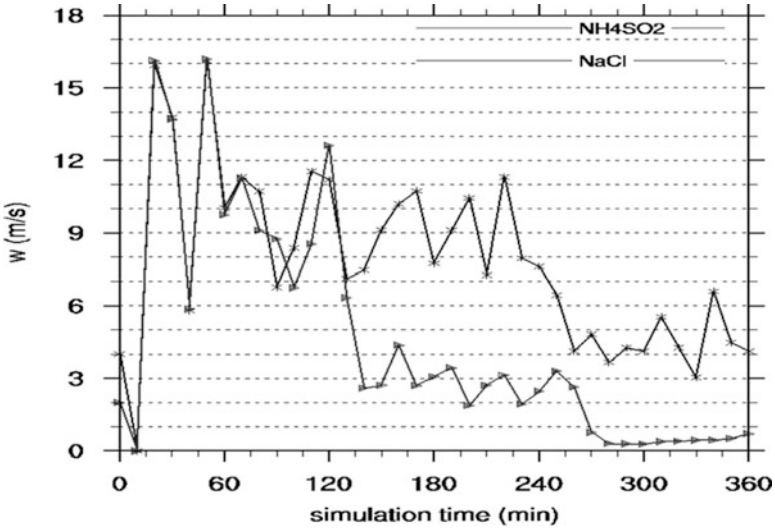

Fig. 5.4 Maximum updrafts (m/s) for NH_4SO_2 (*triangles*) and NaCl (*stars*)

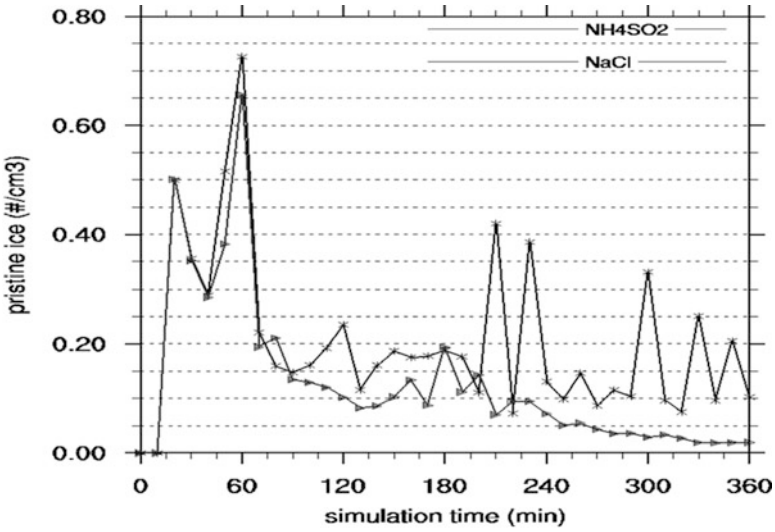

Fig. 5.5 Maximum ice concentration (cm^{-3}) for NH_4SO_2 (*triangles*) and NaCl (*stars*)

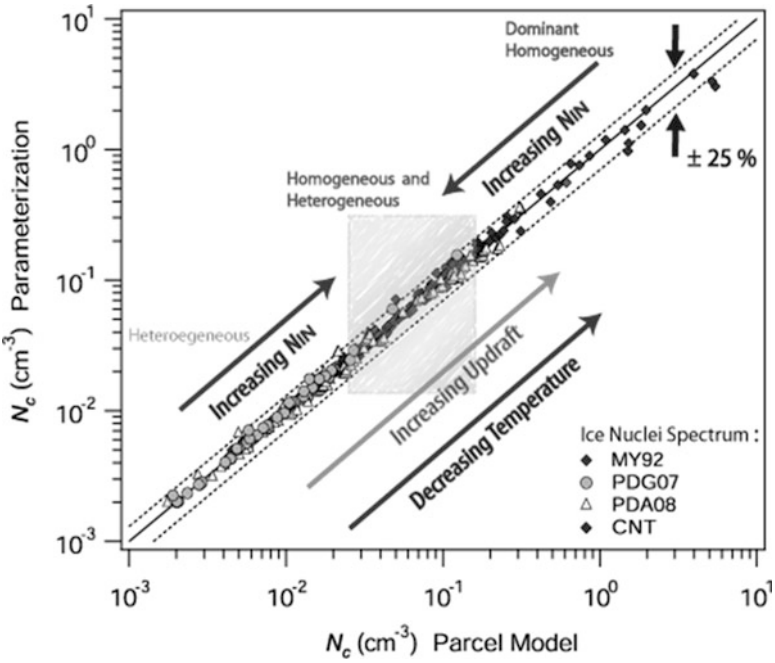

Fig. 5.6 Parameterization of the competition between homogeneous and heterogeneous ice formation processes [1]

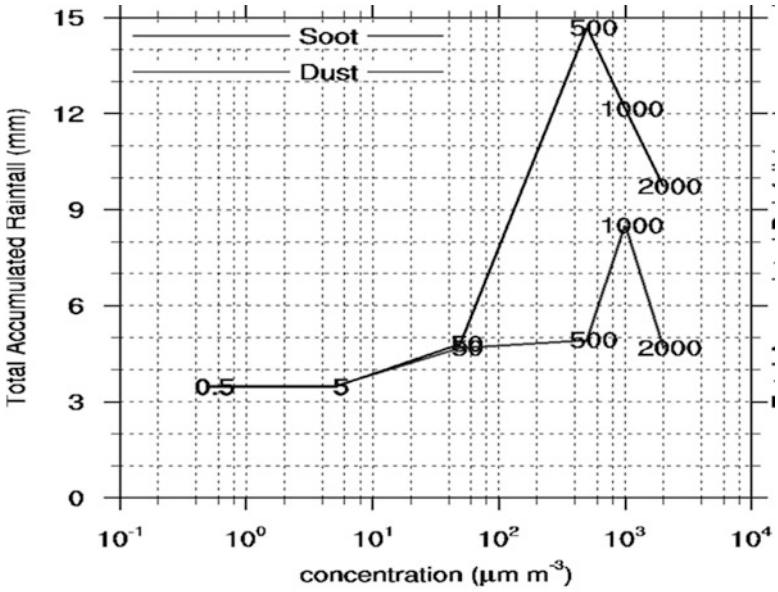

Fig. 5.7 Total accumulated precipitation (mm) for various concentrations of soot and dust (in $\mu g\ m^{-3}$)

5.3 Conclusion

Minor changes in the aerosol field can result in significant modification of precipitation. However the correlation is not linear. Certain combinations of air quality and atmospheric conditions are likely to trigger flood events or, in contrary, to suppress rainfall. These differences are attributed to the complex role of the aerosols in cloud microphysics for both the warm and cold stages of the clouds. Additional model runs and experimental measurements are needed in order to improve our understanding on the role of airborne particles in cloud microphysics.

References

1. Barahona D, Nenes A (2009) Parameterizing the competition between homogeneous and heterogeneous freezing in ice cloud formation – polydisperse ice nuclei. Atmos Chem Phys 9:5933–5948
2. Levin Z, Cotton WR (2009) Aerosol pollution impact on precipitation – a scientific review. Springer, Dordrecht
3. Liu X, Penner JE, Wang M (2009) Influence of anthropogenic sulfate and black carbon on upper tropospheric clouds in the NCAR CAM3 model coupled to the IMPACT global aerosol model. J Geophys Res 114:D03204. doi:10.1029/2008JD010492

4. Solomos S, Kallos G, Kushta J, Astitha M, Tremback C, Nenes A, Levin Z (2011) An integrated modeling study on the effects of mineral dust and sea salt particles on clouds and precipitation. Atmos Chem Phys 11:873–892

Questions and Answers

Questioner Name: ST Rao

Q: You have presented the role of precipitation in enhancing and suppression of precipitation. Is the reversed process (scavenging of pollution) well represented and what are the open points?
A: Scavenging of aerosols occurs through the aqueous phase and not only through nucleation. In aqueous phase the processes involved are not fully understood yet. For example, in water droplets there are several aerosol particles diluted or partially diluted (different size and composition). When the droplets evaporate, the particles left have different physical (size, shape) and chemical (composition, solubility) characteristics. These particles are involved later in nucleation processes and the results are different (e.g. acting rather as GCCN). In general, we need to understand these mechanisms quite well and try to further improve the models.

Questioner Name: Talat Odman

Q: What kind of experimental measurements do you use to evaluate evaluate/validate your models? What data do you need to further improve understanding? Do you have any plans to collect such data?
A: Experimental data sets for such evaluations are always needed. This is especially true in aerosol-radiation-cloud parameterization. Such data sets are not easily found. Measurements related to CCN activation, aerosol characterization (physical and chemical properties) and of course cloud droplet spectra are needed at the most. For ice nucleation (IN) such data are even more difficult to obtain. Most of the experimental data for IN are from cloud chamber experiments. CCN, IN and cloud droplet measurements are usually airborne and difficult to obtain. Satellite data are useful to a certain degree and for some cases. Obviously, conventional observations (e.g. wind, temperature, moisture profiles) are extremely useful. Currently we look for existing data sets from past airborne experimental campaigns. A CCN measurement campaign is organized by my Group in Saudi Arabia next year.

Chapter 6
Targeted NO_x Emissions Control for Improved Environmental Performance

S. Morteza Mesbah, Amir Hakami, and Stephan Schott

Abstract Nitrogen oxides (NO_x) are the main ozone precursors, and NO_x control programs in the US have led to substantial reductions in emissions. However, it is unknown whether these programs have optimally reduced ozone concentrations. Current control programs do not account for spatial and temporal specificities of NO_x emissions. In this paper, this shortcoming in traditional trading systems is addressed and a methodology for identifying optimal NO_x emission control strategies is developed. The proposed method combines an optimization platform with an adjoint (or backward) sensitivity model. Using the proposed method, a 2007 case study of 218 US power plants is examined. The results indicate that differentiating between emissions can significantly enhance environmental performance.

Keywords NO_x • Ozone • Health damage • Abatement cost • Adjoint of CMAQ

6.1 Introduction

Surface ozone is a threat to human health. Ozone is formed in the atmosphere by a series of photochemical reactions in the presence of NO_x, volatile organic compounds, and sunlight. To control the damage caused by ozone, NO_x emissions reduction is often required. The total benefit for a society when emissions are reduced is the same as the total damage (TD) caused by a given amount of emissions.

S.M. Mesbah (✉) • A. Hakami
Department of Civil and Environmental Engineering, Carleton University, Ottawa, ON, Canada
e-mail: smesbah@connect.carleton.ca; amir_hakami@carleton.ca

S. Schott
School of Public Policy and Administration, Carleton University, Ottawa, ON, Canada

D.G. Steyn et al. (eds.), *Air Pollution Modeling and its Application XXII*,
NATO Science for Peace and Security Series C: Environmental Security,
DOI 10.1007/978-94-007-5577-2_6,

To calculate TD, calculation of source-receptor relationships is required. These relationships, which relate emissions to TD, can be calculated using sensitivity analysis methods. Forward and backward (or adjoint) methods for formal sensitivity analysis calculate the derivatives of outputs (i.e., ambient air quality) with respect to inputs (e.g., emissions). In a single simulation run, the adjoint method calculates the influences of all sources on a single receptor (or an integrated metric known as the adjoint cost function), while forward methods calculate the influence of a single source (or uniform change to a collection of sources) on all receptors. Since the concern is to calculate the influences from individual sources, the adjoint method is employed in this work.

6.2 Methodology

The change in damage (ΔD) is based on mortality only and estimated as follows:

$$\Delta D = S\, Y_0\, P\, (1 - e^{-\beta\, \Delta C}) \approx S\, Y_0\, P\, \beta\, \Delta C \tag{6.1}$$

where S is the value of a statistical life and is taken as \$6.8 million in 2007 (US EPA), Y_0 is the baseline non-accidental mortality rate (744.8 per 100,000 people for 2007), P is the population, β is the epidemiological concentration response factor which correlates mortality from air pollution to non-accidental death, and ΔC is the change in concentrations. β in this work is taken as 0.51 % [3] to conform with the averaging time of the current US standard for ozone. To calculate the influences of sources on TD, Eq. (6.1) is used to drive adjoint equations. The adjoint gradient term (λ_i) relates the change in TD to changes in emissions (e_i) at source i ($\lambda_i = \partial D / \partial e_i$). The optimization problem that minimizes the TD in the system is as follow:

$$\textit{Minimize}: \quad \sum\nolimits_{i=1}^{n} D_i(e_i), \quad \textit{Subject to}: \sum\nolimits_{i=1}^{n} e_i \leq TC,\ e_i \in \left[0, e_i^0\right] \tag{6.2}$$

where D_i is the TD caused by source i, e_i is the minimized emission level of source i, e_i^0 is the initial emissions from source i, and TC is the total cap on emissions. The solution of this problem leads to an emissions distribution that minimizes the damage. On the other hand, a cap-and-trade system minimizes total abatement cost (TAC):

$$\textit{Minimize}: \quad \sum\nolimits_{i=1}^{n} c_i \left(e_i^0 - e_i\right), \quad \textit{Subject to}: \sum\nolimits_{i=1}^{n} e_i \leq TC,\ e_i \in \left[0, e_i^0\right] \tag{6.3}$$

where c_i is the abatement costs of source i. The abatement costs used in this paper have a general form of $c_i = \alpha_i \left(e_i^0 - e_i\right)$ which is estimated for short-term using the US EPA's Integrated Planning Model [1].

In this paper, the potential improvement in the current cap-and-trade system is examined using a case study of 218 electric generation coal-fired units that took part in the US NO_x budget trading program in 2007. For air quality simulation and sensitivity analysis, the gas-phase Community Multiscale Air Quality Modeling System (CMAQ) version 4.5.1 and its adjoint are used [2]. The modeling period is from July 1st to July 7th of 2007, and the modeling domain is the continental US with a 36 km grid cell size and 34 vertical layers.

6.3 Results and Discussion

The current US NO_x trading regime does not differentiate emissions based on their contributions to TD. This system leads to an emissions distribution for which TAC is minimized. To investigate the potential improvement in the system performance, three scenarios are considered: command-and-control (CaC), which assumes emissions are at the allocated level; cap-and-trade (CaT), which is the current regime in place in the US that minimizes the TAC (Eq. 6.3); and benefit maximization (BM), which minimizes the TD (Eq. 6.3). For all three scenarios, the total emission cap is the same (i.e., 204,000 tons of NO_x which is the total allocated allowances to the considered units in the ozone season of 2007). The ozone state of the CaC scenario is presented in Fig. 6.1.

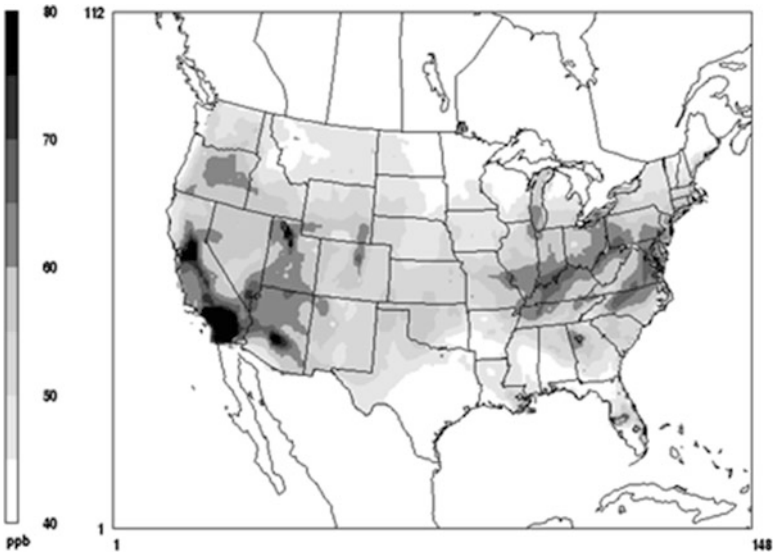

Fig. 6.1 The average of daily maximum 8-h ozone concentration for a 7 day modeling period for CaC

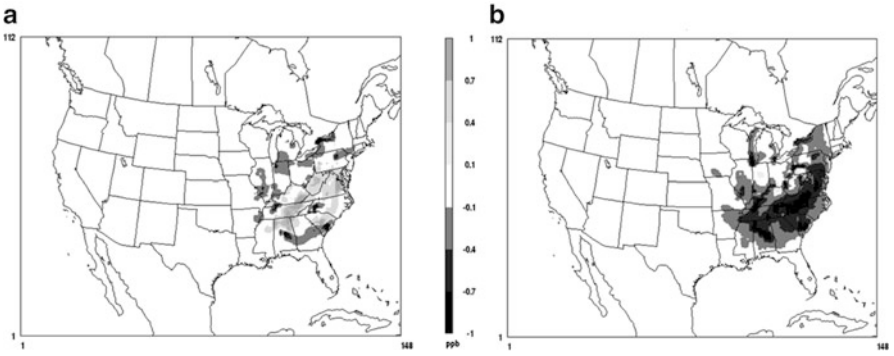

Fig. 6.2 The improvement of average daily maximum 8-h ozone for the 7 day modeling period by switching from CaC to CaT (**a**, *left*), and from CaC to BM (**b**, *right*). The negative values represent improvements and the positive values represent deteriorations in air quality

Table 6.1 Average damage and abatement costs ($/ton) for three scenarios

	CaC	CaT	BM
Average damage	4,218	4,434	2,227
Average abatement cost	1,845	1,306	1,922

The current US ozone standard for ozone (75 ppb) is based on the 4th highest value of daily maximum 8-h ozone over 3 years. All dark gray areas in Fig. 6.1 that represent the weeklong average values greater than 60 ppb are likely to violate the ozone standard. The potential improvement in air quality achieved by switching from CaC to CaT and BM is presented in Fig. 6.2.

The change in air quality under different scenarios occurs only by redistributing emissions while constraining by the same total cap. There is a small improvement in air quality under the CaT (Fig. 6.2a). However, the improvements for the BM are significant and occur in a wide area in the eastern US where ozone issue have not been resolved to this date. It should be noted that the improvements in daily values of maximum 8-h ozone are even larger than the average values reported in Fig. 6.2. The improvements obtained by switching from CaC to BM (maximum of 6 ppb, Fig. 6.2b) indicates a high potential for enhanced air quality. As BM does not account for the abatement costs, it is a more expensive option. To compare the costs and damage of all scenarios, average damages and costs are listed in Table 6.1.

The reported values in Table 6.1 are short-term values, and do not represent long-term costs and benefits. The least costs are realized in the CaT scenario which minimizes the total abatement cost, but minimum damage occurs in the BM scenario which is designed to minimize the total damage. Based on these values, replacing CaT by BM leads to a $616/ton increase in cost, and a $2,207/ton decrease in damages (for a benefit-to-cost ratio of 3.6).

The results presented in this paper are derived from 1 week of simulation, and a longer period of simulation is required for more accurate results. The preliminary short-term cost-benefit analysis indicates, however, that differentiating between emissions can lead to a significant enhancement in the performance of the current US NO_x trading system. Differentiation between emissions can be achieved by exchange rates where traders exchange their emissions based on relative ozone formation potential of NO_x emissions at different locations. Implementation of such emissions differentiated polices would need further investigation.

References

1. EPA (2010) Emission control technologies, Chapter 5. In: Integrated planning model. EPA, Office of Air and Radiation, Washington
2. Hakami A, Henze DK, Seinfeld JH, Singh K, Sandu A, Kim S, Byun D, Li Q (2007) The adjoint of CMAQ. Environ Sci Technol 41(22):7807–7817
3. Zanobetti A, Schwartz J (2008) Mortality displacement in the association of ozone with mortality: an analysis of 48 cities in the United States. Am J Respir Crit Care Med 177(2):184–189

Questions and Answers

Questioner Name: Haluk Ozkaynak

Q: Is the difference between marginal abatement cost and marginal damage driven mostly by where and how many people are exposed to source-specific emissions?
A: The difference in marginal damages is driven by population exposure to pollution and source-receptor relationships for the episode, but the difference in marginal costs depends on the capacity of the plants and their control technologies.
Q: What about uncertainties in the marginal health damage and economic control costs? How can these be incorporated in cost-benefit analyses?
A: Uncertainties are not considered in this study. The most important uncertainties are likely to be in source-receptor coefficients, epidemiological concentration response factors, valuation of damage, and the estimation of abatement costs. Incorporating these uncertainties into the model requires detailed information and could be a computationally costly undertaking.

Questioner Name: Yoledymyr Nochvai

Q: What is the mathematical formulation of the adjoint cost function? Is it the same as sensitivity function?
A: The cost function is not the same as sensitivity function. The sensitivities are the derivatives of the adjoint cost function with respect to model inputs. For this work, the adjoint cost function is defined as the total mortality due to short-term ozone exposure integrated over all grid cells in the US and during the simulation episode.

Questioner Name: Mark Janssen

Q: The EPA's IPM model assumes full economic fluidity in the market. The final implementation of cap-and-trade looked more like economic risk minimization. How would your paper change knowing this?
A: Any change in the estimation of abatement costs will affect cost minimizations for the CaT scenario. Therefore, such change will also affect the pattern of improvements in air quality under the said scenario. However, the significant improvements under BM will remain unaffected since they do not depend on abatement costs.

Chapter 7
Attribution of Ozone Pollution Control Benefits to Individual Sources

Amanda Pappin, Amir Hakami, Jaroslav Resler, Jitka Liczki, and Ondrej Vlcek

Abstract Adjoint sensitivity analysis of numerical models provides a platform for directly linking public health effects with air quality for evaluating emission control policies in a more straightforward manner. We link epidemiological and valuation statistics to the adjoint of CMAQ and calculate sensitivities of short-term mortality-related benefits in Canada, the U.S. and Europe to anthropogenic NO_x and VOC emissions across two continental domains. Our results show significant spatial variability in impacts of NO_x and VOC emissions reduction on short-term mortality. We estimate that sensitivities of mortality-related benefits to 10 % NO_x emissions reductions in major cities reach monetary values in excess of $635K/day in Europe and $355K/day in North America. We find that when the cumulative effects of anthropogenic emissions on O_3 and NO_2 population exposure are considered, NO_x emissions reductions generally yield higher mortality-related benefits than the same relative reductions in VOC emissions.

Keywords Air pollution mortality • Health benefits • CMAQ adjoint

A. Pappin (✉) • A. Hakami
Department of Civil and Environmental Engineering, Carleton University, Ottawa, Canada
e-mail: apappin@connect.carleton.ca; amir_hakami@carleton.ca

J. Resler • J. Liczki
Institute of Computer Science, Academy of Sciences of the Czech Republic, Prague, Czech Republic

O. Vlcek
Czech Hydrometeorological Institute, Prague, Czech Republic

D.G. Steyn et al. (eds.), *Air Pollution Modeling and its Application XXII*,
NATO Science for Peace and Security Series C: Environmental Security,
DOI 10.1007/978-94-007-5577-2_7,

7.1 Introduction

Air pollution decision making becomes more straightforward when public health impacts (e.g. mortality, morbidity) are directly linked to emission sources. Currently, regulatory frameworks use air quality models in a forward or source-oriented manner, where the effectiveness of an emission control strategy is evaluated by projecting a change in emissions forward in time to estimate impacts (e.g. health effects) across all receptors. This type of approach is often scenario-based and unsuitable for estimating the marginal contributions of individual sources towards health benefits or costs as a whole (i.e. source specificity). Adjoint (backward) sensitivity analysis is a complementary approach that allows for calculation of spatiotemporal *contributions* of emission sources (or their reduction) to concentration-based health metrics. In this work, we conduct adjoint sensitivity analysis to estimate the response of national mortality (in terms of a monetary value or "benefit") to anthropogenic NO_x and VOC emissions at each location across Canada, the U.S., and Europe using the Community Multiscale Air Quality Model adjoint (CMAQ-adjoint).

7.2 Methodology

We define our sensitivity metrics, or adjoint cost functions, as the monetary value of the national mortality count for (1) Canada, (2) the U.S. and (3) Europe. Here, we look strictly at gas-phase pollutants correlated with short-term mortality. Mortality calculations for Canada and Europe are performed on the basis that both ozone (O_3) and nitrogen dioxide (NO_2) have been correlated with short-term mortality in Canadian and/or European epidemiological studies. In the U.S., epidemiological evidence suggests a strong correlation between short-term mortality and O_3, but not NO_2. In all cases, we define the cost function using a Taylor series expansion to the exponential epidemiological functions describing the response of mortality to changes in pollutant concentrations (Eq. 7.1).

$$\Delta M = M_0 P \beta \Delta C \tag{7.1}$$

Here, ΔM is the change in mortality count (relative to a baseline), M_0 is the all-age, non-accidental baseline mortality rate (#/population-year), P is the population, β is the pollutant-specific coefficient derived from relevant epidemiological studies, and ΔC is the change in pollutant concentration for a specified averaging period.

This is a proof-of-concept study to demonstrate applicability of the adjoint method in source attribution of health outcomes. Therefore, we use similar β-values of 8.39×10^{-4} ppb^{-1} for daily 1-h maximum O_3 and 7.48×10^{-4} ppb^{-1} for 24-h average NO_2 [2] for Canada and Europe despite the wide range of epidemiological findings for these domains. For the U.S., we use a β-value of 3.9×10^{-4} for daily

1-h maximum O_3 [3]. Finally, we monetize the mortality counts using the value of a statistical life (VSL) for different regions/countries ($5.7M, 2011 PPP for Canada from Health Canada's Air Quality Benefits Assessment Tool; $8.1M, 2011 PPP for the US from the U.S. EPA, and $2.8M, 2011 PPP for Europe from Bell et al. [1]).

Using CMAQ-adjoint, we calculate the derivatives of national mortality valuation due to exposure to O_3 (and NO_2 for Canada and Europe) with respect to emissions of each model species, and average over the modeling period. Our preliminary simulations for Canada and the U.S. are conducted for August 2007, while our European simulation is conducted for a 2-week period from June 15–30, 2009. We calculate sensitivities at horizontal resolutions of 36 and 27 km for the North American and European domains, respectively.

7.3 Results and Discussion

Our adjoint simulations provide the spatiotemporal distribution of sensitivities of the adjoint cost functions (i.e. benefits from avoided mortality) over the domain (Fig. 7.1a–c). These sensitivities are scaled to amount to the monetary amount that a nation would expect to benefit by if anthropogenic emissions of NO_x or VOCs in a given location were reduced by 10 %.

Local and long-range influences of NO_x emissions on national mortality are evident in Fig. 7.1a–c, while VOC emission influences have a tendency to be more localized. Domestic emission patterns are strong drivers of mortality-related costs or benefits (depending on perspective) as a result of demographic trends and regions of concentrated anthropogenic activity.

In Canada, a significant portion of the benefits come from highly populous areas of south-eastern Ontario/Quebec (Fig. 7.1a). The sensitivities of mortality to NO_x emissions in these regions reach peak values of $300K/day (upwind of Toronto, Ontario). That is, if NO_x emissions in that grid cell within the Toronto region were reduced by 10 %, Canada (not necessarily Toronto) would expect to benefit by that daily amount from reduced exposure to O_3 and NO_2. Sensitivities for Canada are positive across the domain due to the inclusion of NO_2 in the cost function. Where O_3 shows a negative sensitivity to NO_x emissions, larger, positive sensitivities related to NO_2 exposure contribute to an overall benefit. Influences coming from locations in the north-eastern U.S. and the western provinces (sensitivities upwards of $65K/day for NO_x) are also notable in Fig. 7.1a. These locations of high influence correspond to areas of high NO_x emissions and/or populous Canadian areas. VOC emissions have significantly lower influences on mortality, with the largest benefit seen around Vancouver, British Columbia, with a gradient of $45K/day for a 10 % reduction.

Contributions of North American NO_x and VOC emissions towards short-term mortality in the U.S. are significantly higher in magnitude as compared to Canada (Fig. 7.1b) due to larger populations and emissions in the U.S. Sensitivities of short-term mortality to NO_x emissions (from O_3 exposure only) reach upwards

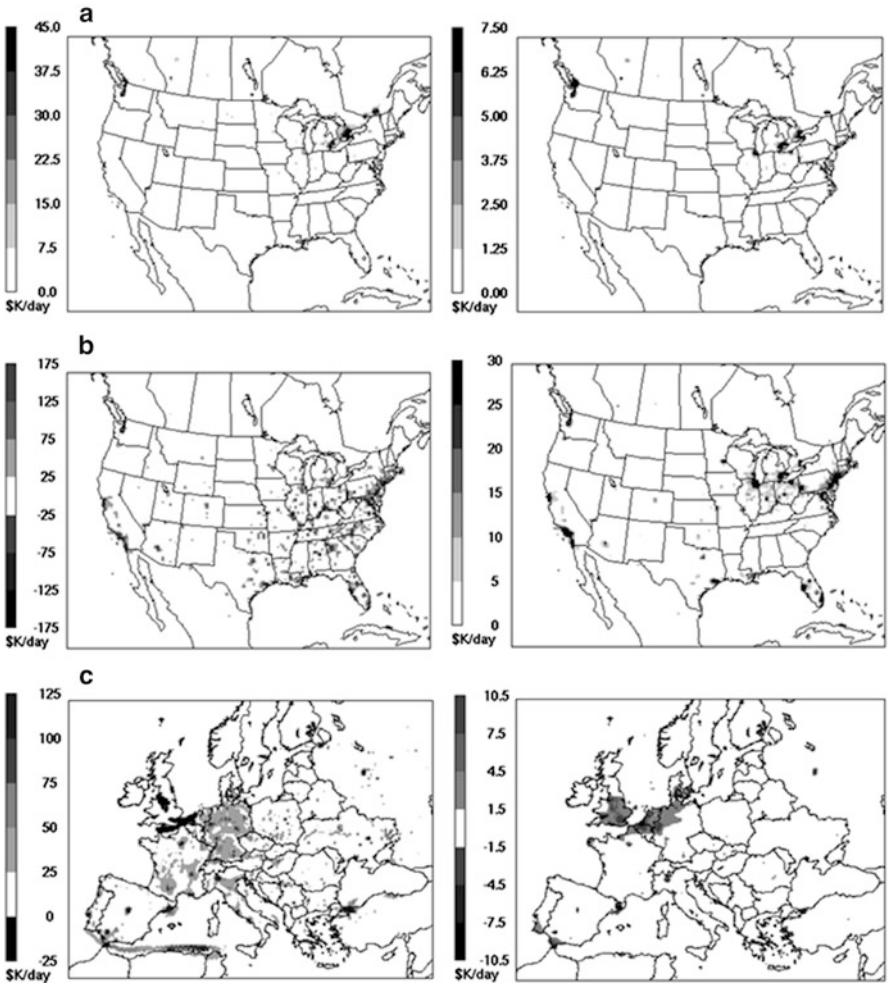

Fig. 7.1 Average daily sensitivities of (**a**) Canadian, (**b**) U.S., and (**c**) European short-term mortality to a 10 % reduction in anthropogenic NO_x (*left*) and VOC (*right*) emissions. Sensitivity values for Canada and Europe are due to exposure to O_3 and NO_2 while values for the U.S. are due to O_3 exposure only

of $355K/day (Atlanta, Georgia). A few locations show negative sensitivities to NO_x, such as Los Angeles, California, whose sensitivity is -$255K/day for that same 10 % reduction in emissions. In other words, reducing emissions in this particular location would increase national exposure to daily 1-h maximum O_3 in the U.S. In Los Angeles, there is a significant, positive sensitivity to VOC emissions reduction ($575K/day), indicating the highly NO_x-inhibited/VOC-limited regime in this metropolitan environment.

Our preliminary results for Europe show sensitivities that are considerably larger than those for North American NO_x emissions reduction, but comparable for VOCs (Fig. 7.1c). Overall, higher population densities generally lead to larger influences over the European domain. Similar to Canada, inclusion of NO_2 in the exposure-based sensitivity metric results in widespread positive sensitivities (benefits) with respect to NO_x emissions reduction (with the exception of the U.K.). The largest benefits are attributed to emissions in Barcelona, Spain, whose sensitivities are \$635K/day for NO_x and \$155K/day for anthropogenic VOCs. Significant contributions are also seen from the Southern Mediterranean shipping routes.

In contrast to the North American domain, spatial heterogeneities observed in European contributions do not simply follow population centres and have a more regional structure (such as areas of influence over Germany and France). Due to complexities over the European domain, delineating regional trends may require longer and higher resolution adjoint simulations.

References

1. Bell ML, Davis DL, Cifuentes LA et al (2008) Ancillary human health benefits of improved air quality resulting from climate change mitigation. Environ Health 7:41
2. Burnett RT, Stieb D, Brook JR et al (2004) Associations between short-term changes in nitrogen dioxide and mortality in Canadian cities. Arch Environ Health 59:228–236
3. Ito K, De Leon SF, Lippmann M (2005) Associations between ozone and daily mortality: analysis and meta-analysis. Epidemiology 16:446–457

Questions and Answers

Questioner Name: Wouter Lefebvre

Q: Would including PM (or its components) in your results change your costs? Would it, in your opinion, eliminate the negative costs per vehicle? If no, would it then be advised to encourage people to drive more?

A: Firstly, our analysis only considers gas-phase pollutant exposure as the adjoint to CMAQ for PM is still under development. Including PM would indeed affect the health benefit sensitivities and hence the transportation cost estimates we calculate. In some cities, dis-benefits (or negative sensitivities) associated with NO_x emissions reduction would be outweighed by the beneficial impacts of reduced national exposure to secondary PM. However, in strongly NO_x-inhibited urban environments where substantial negative sensitivities exist, we expect that the negative costs per vehicle removed might still exist. Reduced mobile emissions of NO_x usually accompany reduction in co-pollutants such as primary PM, so the overall benefit in a multi-pollutant analysis is likely to be positive.

The results of this work do not necessarily suggest that people should be encouraged to drive in locations that show negative sensitivities. Long-term air quality planning would incorporate a combination of local and particularly regional emission controls (e.g. power plants) that would cause urban environments to become less and less NO_x-inhibited. Therefore, these dis-benefits are likely to become smaller as more progressive controls take effect.

Questioner Name: Sergey Napelenok

Q: Do you think your results will change by picking different episode lengths?
A: We have noticed that the temporally-averaged benefit sensitivities do change over various simulation periods due to a strong dependency on meteorology. For long-term air quality planning, it is advised to perform adjoint sensitivity analysis over more than just a single season of 1 year to capture intra-season and intra-annual variability.

Chapter 8
Country-Wide Health Impact Assessment of Airborne Particulate Matter in Estonia

Kaisa Kesanurm, Erik Teinemaa, Marko Kaasik, Tanel Tamm, Taavi Lai, and Hans Orru

Abstract This study is aimed to assess the health impacts of outdoor $PM_{2.5}$ concentrations to entire population of Estonia. As the air quality monitoring network in Estonia is rather sparse (six urban, three rural and a few industrial sites), the exposure assessment was based on long-term modelling, controlled by monitoring data from existing stations. The model runs were performed with IairViro modelling system, including the Eulerian MATCH model for country-wide run with 5 km grid resolution and AirViro urban model with 200 m grid resolution for five major cities. The database of pollution sources includes industrial, transport and domestic heating emissions. The average annual $PM_{2.5}$ concentrations were found 7–9 $\mu g/m^3$ at most of rural and in 9–13 $\mu g/m^3$ typically at urban areas, up to 30 $\mu g/m^3$ in some parts of capital city Tallinn. To estimate the health risks, the base-line national health statistics and exposure-response coefficients from previous epidemiological studies (ACS, APHEIS), were applied. It was found that on average 600 (CI 95 % 155–1,061) premature deaths per year are caused by $PM_{2.5}$ pollution in Estonia, which

K. Kesanurm
Institute of Physics, University of Tartu, Riia 142, 51014 Tartu, Estonia

Estonian Environmental Research Centre, Marja 4d, 10617 Tallinn, Estonia

E. Teinemaa
Estonian Environmental Research Centre, Marja 4d, 10617 Tallinn, Estonia

M. Kaasik (✉)
Institute of Physics, University of Tartu, Riia 142, 51014 Tartu, Estonia
e-mail: marko.kaasik@ut.ee

T. Tamm
Institute of Ecology and Earth Sciences, University of Tartu, Vanemuise 46, 51014 Tartu, Estonia

T. Lai • H. Orru
Department of Public Health, University of Tartu, Ravila 19, 50411 Tartu, Estonia

D.G. Steyn et al. (eds.), *Air Pollution Modeling and its Application XXII*,
NATO Science for Peace and Security Series C: Environmental Security,
DOI 10.1007/978-94-007-5577-2_8,

has population nearly 1.3 million. On average 5 months of life are lost, maximum 14 months in some parts of Tallinn. About 900 additional hospitalizations due to pulmonary and cardiovascular diseases occur per year.

Keywords PM • Health impact • MATCH-model

8.1 Introduction

Urban air pollution poses a significant public health problem. Every year it causes a large number of premature deaths, hospitalizations, and various other types of morbidity. Generally, air pollution contributes to a decrease of up to 1 year of life expectancy in Europe [1]. Particulate matter is one of the most studied and problematic pollutants due to its toxicity and relatively high concentrations. Estonia is an example of a transitional country that regained its independence from the Soviet Union in 1991. Currently, the car fleet and main air pollution sources are relatively similar to other European countries, and especially similar to the Nordic countries. The biggest problems are related to the use of studded tires and the high proportion of population using local heating. Among the pollutants, the main concern is relatively high levels of particulate matter, which is a common problem in other European countries as well.

This study aims to assess the health impacts of $PM_{2.5}$ concentrations to entire population of Estonia, to clarify the main sources and exposures, study their associations with cardiovascular and pulmonary health effects, and estimate the extent of those effects on territorial basis.

8.2 Models and Methods

As the air quality monitoring network in Estonia is rather sparse (six urban, three rural and a few industrial sites), the exposure assessment in this study is based on long-term modelling, controlled by monitoring data from existing stations. The model runs were performed with IairViro system operated by Estonian Environmental Research Centre, including the Eulerian MATCH model [2] for country-wide run with 5 km grid resolution and AirViro urban model with 200 m grid resolution for five major cities: Tallinn, Tartu, Narva, Kohtla-Järve, Pärnu. The national AirViro-based database of pollution sources includes industrial and traffic emissions (over 600 point sources, about 5,000 km of streets and roads).

As roughly a half of Estonian population live in locally heated habitats, an assessment of domestic heating emissions was performed specially for this study. The emissions are based on questionnaire study on locally heated habitats in Tartu [3] and emission factors by Karvosenoja [4]. The emissions are upscaled for entire country, based on census of people and habitats 2001, that enables to distinguish the distant-heated and locally heated dwelling areas and also specific fuel consumption

patterns of two urban types – family houses and old densely built-up areas (mixed fuels) – and rural-type (highly dominating firewood) inhabited areas.

Based on comparison with monitoring results in existing stations, a non-linear empirical correction was made in modelled yearly average concentrations: initial values were systematically overestimated in cities, possibly due to overestimation of street emissions.

To estimate the cardiovascular and pulmonary health risks, the national health statistics and exposure-response coefficients from previous epidemiological studies (ACS [5], APHEIS [6]), were applied. The years of life lost (YLL), decrease of life expectancy and number of additional hospitalisations were calculated for municipalities.

8.3 Results and Discussion

The calculated average annual $PM_{2.5}$ concentrations range from 5 $\mu g/m^3$ at remote islands to 30 $\mu g/m^3$ in some parts of the capital Tallinn, being 7–9 $\mu g/m^3$ at most of rural and in 9–13 $\mu g/m^3$ typically at urban areas (Fig. 8.1) The modeled concentrations in Tallinn are given in Fig. 8.2, rural background is not included. It was found that on average 600 (CI 95 % 155–1,061) premature deaths per year are caused by $PM_{2.5}$ pollution in Estonia, which has population nearly 1.3 million, on average 5 months of life are lost (Fig. 8.3), maximum 14 months in some parts of

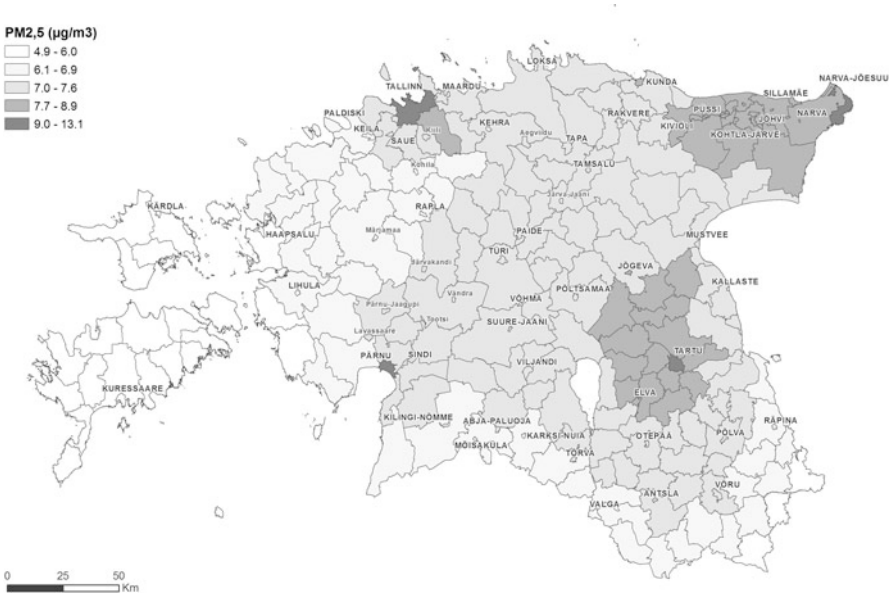

Fig. 8.1 Average concentrations of $PM_{2.5}$ in municipalities

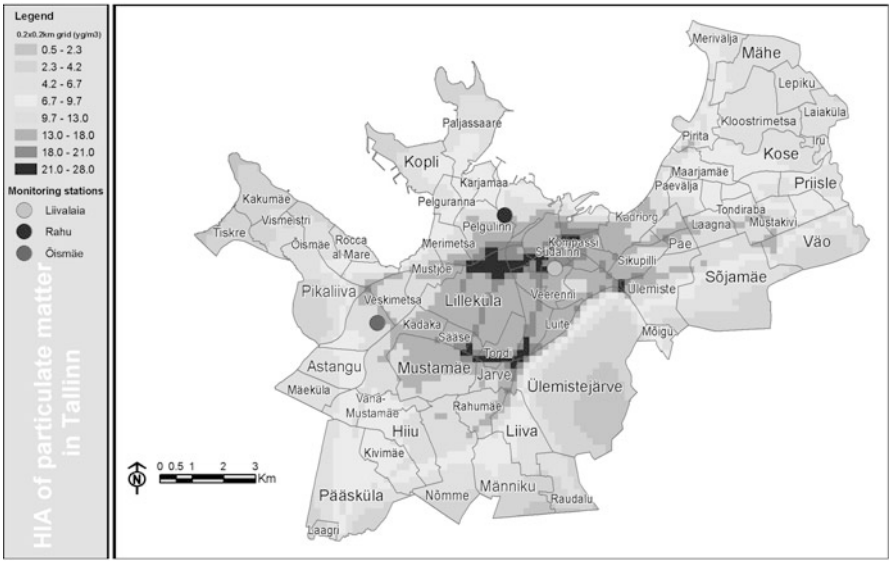

Fig. 8.2 Average concentrations of $PM_{2.5}$ in Tallinn city ($\mu g/m^3$). Bullets indicate positions of monitoring stations: Liivalata – street; Rahu – industrial, Õismäe – urban background

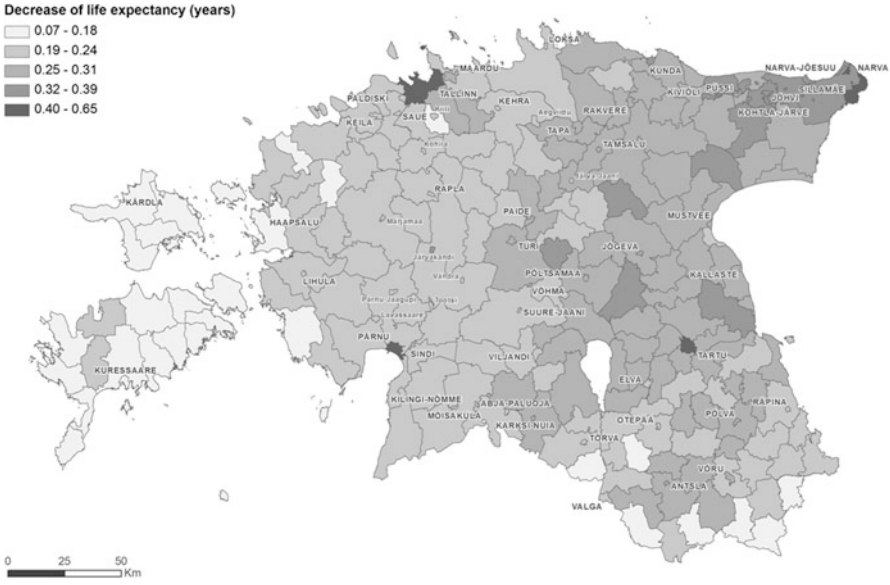

Fig. 8.3 Decrease of life expectancy due to $PM_{2.5}$, years

Tallinn. About 900 additional hospitalisations due to pulmonary and cardiovascular diseases occur per year. These statistics are nearly at European average level.

However, these results are based on exposure estimates for residential areas. Actually, working and socially active people spend about a half of time outside of home: at work, leisure, driving, walking and moving by other means. E.g. a person living in a municipality adjacent to Tallinn and working in the city-center of Tallinn 40 h per week, gets roughly 50 % higher exposition than expected on residential basis. On the other hand, leisure trips of urban people decrease their exposure. And last but not least: indoor effects may change the exposure dramatically.

Nevertheless, this study shows that health effects of ambient particulate matter pollution are not negligible in Estonia, in urban areas in first order.

Acknowledgments This study is funded by Estonian Ministry of Environment, Estonian Centre of Environmental Investments, and Estonian National Targeted Financing Project SF0180038s08.

References

1. Boldo E, Medina S, LeTertre A, Hurley F, Mucke H, Ballester F et al (2006) Apheis: health impact assessment of long-term exposure to PM2.5 in 23 European cities. Eur J Epidemiol 21:449–458
2. Robertson L, Langner J, Engardt M (1998) An Eulerian limited-area atmospheric transport model. J Appl Meteorol 38:190–210
3. Kaasik M, Orru H, Tekkel E, Vals P (2007) Situation and tendencies in air quality in a North European medium-sized town. In: Abstracts of the 6th international conference on urban air quality, University of Hertfordshire, Hatfield, 212
4. Karvosenoja N (2001) Primary particulate emissions from stationary combustion processes in Finland. Finnish Environment Institute, Helsinki, 232, 28 p
5. Pope C, Burnett R, Thun M, Calle E, Krewski D, Ito K et al (2002) Lung cancer, cardiopulmonary mortality, and long-term exposure to fine particulate air pollution. JAMA 287:1132–1141
6. Atkinson RW, Anderson HR, Medina S, Iñiguez C, Forsberg B, Segerstedt B et al (2005) Analysis of all-age respiratory hospital admissions and particulate air pollution within the APHEIS programme. In: Medina S et al (eds) APHEIS health impact assessment of air pollution and communication strategy. Third year report. Institut de Veille Sanitaire, Saint-Maurice, pp 127–133

Questions and Answers

Q: Your map of PM2.5 in Tallinn seems to indicate that the monitoring stations are not optimally located to sense the distribution of PM2.5. Have the monitoring authorities considered using model output to design the monitoring network?
A: All the stations have specific purpose: street, urban background and urban-industrial (incl. marine port). Perhaps we should have some station in relatively clean outskirts, but that depends on finances.

Chapter 9
Temporal Collinearity Amongst Modeled and Measured Pollutant Concentrations and Meteorology

Valerie Garcia, P.S. Porter, Edith Gégo, and S.T. Rao

Abstract The results from epidemiology time series models that relate air quality to human health are often used in determining the need for emission controls in the United States. These epidemiology models, however, can be sensitive to collinearity among co-variates, potentially magnifying biases in the parameter estimates caused by exposure misclassification error or other deficiencies in the time series models by orders of magnitude. As a result, we examined collinearity among several covariates typically used in air quality epidemiology time series studies (ozone, fine particulate matter and its species, and temperature). In addition, we examined the ability of a bias-correction technique applied to estimates simulated by the Community Multi-scale Air Quality (CMAQ) model to "fill-in" for the spatial and temporal limitations of observations for purposes of reducing exposure misclassification. Specifically, we evaluated whether the bias-adjusted CMAQ estimates could replicate the correlation among variables seen in the observations. The results presented are for a domain east of the Rocky Mountains for the entire 2006 year and indicate that collinearity among covariates varies across space.

Keywords Epidemiology • CMAQ

V. Garcia (✉) • S.T. Rao
Atmospheric Modeling Division, U.S. Environmental Protection Agency,
Research Triangle Park, NC, USA
e-mail: garcia.Val@epamail.epa.gov; rao.st@epa.gov

P.S. Porter
Civil Engineering/Environmental Engineering, University of Idaho, Idaho falls, ID, USA
e-mail: porter@if.uidaho.edu

E. Gégo
Porter-Gego and Associates, Idaho Falls, ID, USA
e-mail: e.gego@onewest.net

D.G. Steyn et al. (eds.), *Air Pollution Modeling and its Application XXII*,
NATO Science for Peace and Security Series C: Environmental Security,
DOI 10.1007/978-94-007-5577-2_9,

9.1 Introduction

The United States Environmental Protection Agency (USEPA) relies predominantly on epidemiology time series studies to estimate future health impacts of emission controls [1]. High correlation among explanatory variables used in these studies can result in inaccurate results when applied in health impact assessments. In addition, the assignment of the wrong exposure value differentially (misclassification) can mask the true health effect of a pollutant [2]. To address these two issues, this study examines (1) the collinearity that exists among ozone, particulate matter and its species, and temperature; and (2) whether we can fully represent this natural relationship among covariates in the deterministic, 3-dimensional Community Multiscale Air Quality (CMAQ) model. This latter objective is particularly relevant due to the paucity of measurements for some pollutants (e.g., speciated fine particulate matter) that are typically measured once- in-3-days at relatively few locations in the U.S.

Figure 9.1 shows an example of a typical time series model used in an epidemiology study and the collinearity between ozone and temperature for ten summers (1997–2006) in New York State. Collinearity can also exist between ozone and fine particulate matter. Multicollinearity among covariates can magnify the effect of bias introduced by autocorrelation, misclassification error or other model deficiencies by orders of magnitude. Thus, while it doesn't necessarily reduce the predictive power or reliability of a model when all collinear covariates are included, it can affect calculations regarding individual predictors, such as when the main effects coefficients are used to assess health impacts. If the covariates (and relationship among them) in the new dataset differ from the data that was fitted, it can introduce large errors in predictions [3].

Misclassification (inaccurately assigning exposure across space or time differentially) can also introduce errors in epidemiology time series studies. Air quality models, such as CMAQ, can help fill in missing measurement data but

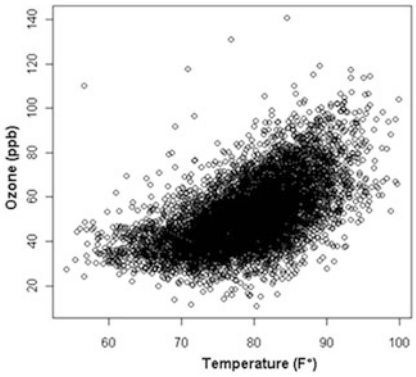

Fig. 9.1 Example of variables used in an epidemiology Poisson regression model. *Scatter plot* shows relationship between ozone and temperature ($R^2 = .58$)

contains some bias due to uncertain emissions and meteorology input data, as well as limited knowledge of the physical and chemical processes governing the formation of ambient pollutants. Hence, CMAQ model estimates were combined with observations [4] to produce bias-adjusted pollutant estimates with the objective of providing more spatially and temporally complete ambient air pollutant data for use in epidemiology studies. As part of this study, we examined the ability of the model alone, and the bias-adjusted model to reproduce the relationships that exist in the observed covariates used in a standard epidemiology study.

The objectives of this study were to (1) examine whether the temporal variability seen intimated by CMAQ and adjusted CMAQ reflect those seen in observations, and (2) understand what pollutants are correlated with each other and with temperature.

9.2 Approach

Maximum daily 8-h averaged ozone (O_3), and 24-h averaged fine particulate matter ($PM_{2.5}$), sulfate (SO_4), nitrate (NO_3), ammonium (NH_4), elemental carbon (EC) and organic carbon (OC) were calculated from measurements obtained from the USEPA's Air Quality System database (http://www.epa.gov/oar/data/aqsdb.html) for 2006. Measurements of O_3 and $PM_{2.5}$ were available for each day, whereas, measurements for $PM_{2.5}$ species were available for 1-in-3 days only. Daily averages were also calculated from the hourly concentrations simulated by the CMAQ model v.4.5 at a 12 km horizontal grid resolution. The meteorology and emissions inputs for this simulation were from the Fifth-Generation NCAR/Penn State Mesoscale Model (MM5) and EPA's 2001 National Emissions Inventory, respectively. The 12-km simulation encompassed most of the Eastern U.S. and was nested within a 36 km $\times$ 36 km horizontal grid simulation covering the contiguous U.S. using the same model configuration as the 12-km nested simulation. Finally, the observations and modeled estimates were combined using a multiplicative adjusted bias approach described in [4] to produce daily averaged estimates as described above. To summarize the process, the ratio of observed to modeled values is calculated for each grid cell containing an observation. These ratios are interpolated using a kriging technique and then applied to the CMAQ estimates to produce a "bias-adjusted" value for each CMAQ grid cell. Pearson correlation coefficient (R) was calculated to measure the temporal dependencies.

9.3 Discussion and Results

Bias-adjusted CMAQ estimates captured the temporal variability seen in observations for most pollutants (objective 1). Challenges, however, still remain in estimating EC because of the high spatial and temporal heterogeneity of this

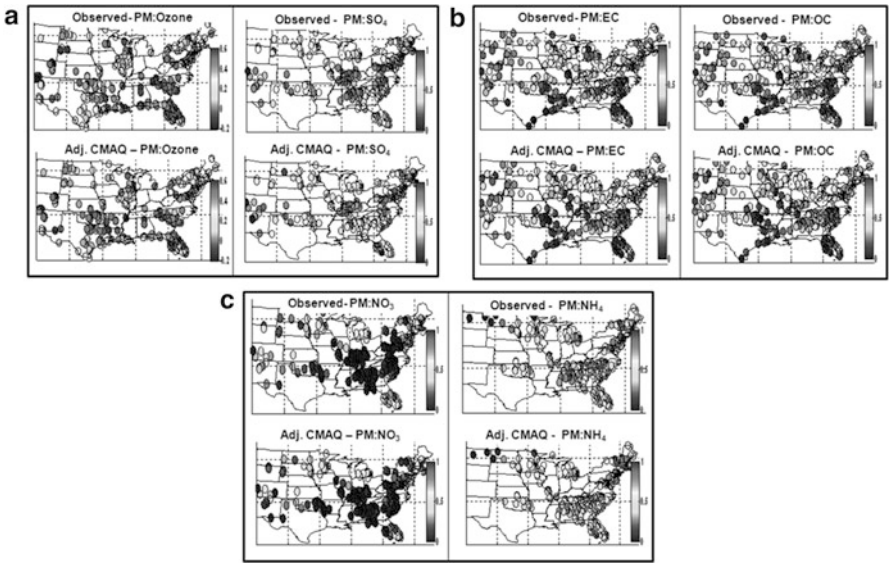

Fig. 9.2 Collinearity between PM2.5, and ozone and SO4 (panel **a**), EC and OC (panel **b**), and NO3 and NH4 (panel **c**). *Second row* of each panel shows ability of bias-adjusted CMAQ to replicate the collinearity among observed pollutant concentrations shown in *first row*. Each *circle* represents Pearson's correlation (R) between the indicated pollutants across 365 days at each monitoring location

pollutant. In addition, spatial differences in capturing the observed temporal variability were seen for OC along the Southern coastline and NO_3 along the Western edge of the domain and in the South. With regard to collinearity among variables (objectives 2 and 3), ozone is positively correlated with $PM_{2.5}$, SO_4 and temperature at most sites, reflecting the dominant SO_4 component of $PM_{2.5}$ mass and its common source with secondarily formed ozone from photolysis. Strong spatial patterns existed for several pollutants, with very strong spatial correlations between ozone and nitrate and ammonium in the Southeastern U.S. (not shown). As expected, $PM_{2.5}$ is highly correlated with most of its constituents (Fig. 9.2), but surprisingly, not as correlated with NO_3, perhaps due to seasonal differences (e.g., high correlation in winter, but relatively low correlation in summer for the domain studied). The correlation between $PM_{2.5}$, and EC and OC is strongest in the upper Northwest portion of the domain, most likely due to wood burning. Correlation between $PM_{2.5}$ and NH_4 is dominant in the Eastern U.S.

Disclaimer The United States Environmental Protection Agency through its Office of Research and Development funded and collaborated in the research described here under EP-D-10-078 to Porter-Gego. It has been subjected to Agency review and approved for publication.

References

1. US Environmental Protection Agency (2010) Our nation's air status and trends through 2008. Report no. EPA-454/R-09-002
2. Rothman KJ (2002) Epidemiology: an introduction. Oxford University Press, New York
3. Farrar DE, Glauber RR (1967) Multicollinearity in regression analysis: the problem revisited. Rev Econ Stat 49:92–107
4. Garcia VC, Foley KL, Gego E, Holland DM, Rao ST (2010) A comparison of statistical techniques for combining modeled and observed concentrations to create high-resolution ozone air quality surfaces. J Air Waste Manage Assoc 60:586–595

Chapter 10
Reconstruction of Past and Prediction of Future Benzo[a]pyrene Concentrations Over Europe

Johannes Bieser, Armin Aulinger, Volker Matthias, and Markus Quante

Abstract Benzo[a]pyrene (BaP) is a highly carcinogenic substance that is created as an unintentional byproduct of combustion processes.

In order to simulate the development of European BaP concentrations between 1980 and 2020 a consistent emission dataset for the time span 1980–2010 was created using the SMOKE-EU emission model. Moreover, a variety of different emission scenarios for the year 2020 was created to estimate the future development of BaP emissions. The emission datasets have been used as input for a modified version of the Chemistry Transport Model (CTM) CMAQ. This CMAQ version is to our knowledge the only regional CTM to include the heterogeneous reaction of particulate BaP with ozone which, besides wet deposition, is the main sink of atmospheric BaP.

It was found that BaP concentrations have been decreasing strongly between 1980 and 2000. This is due to the large reduction of primary BaP emissions from industrial processes, residential wood and coal burning, and vehicle exhausts. Depending on the emission scenario, simulated BaP concentrations over Europe between 2000 and 2020 are changing by -25 to $+5$ %. Because further reduction of industrial BaP emissions is supposed to be low, the future development depends mainly on the amount of wood used for heat production. Also changes of emissions of ozone precursors showed to impact the degradation of BaP.

Finally, several regions were identified in which the annual BaP target value of 1 ng/m^3 was exceeded. In 1980 this was the case for the Po-valley, the Paris

J. Bieser (✉) • M. Quante
Institute for Coastal Research, Helmholtz Zentrum Geesthacht, D-21502 Geesthacht, Germany

Institute of Ecology and Environmental Chemistry, Leuphana University Lüneburg, D-21335 Lüneburg, Germany
e-mail: johannes.bieser@hzg.de

A. Aulinger • V. Matthias
Institute for Coastal Research, Helmholtz Zentrum Geesthacht, D-21502 Geesthacht, Germany
e-mail: volker.matthias@hzg.de

D.G. Steyn et al. (eds.), *Air Pollution Modeling and its Application XXII*,
NATO Science for Peace and Security Series C: Environmental Security,
DOI 10.1007/978-94-007-5577-2_10,

metropolitan area, the Rhine-Ruhr area, Vienna, and Madrid. Predictions for 2020 lead to exceedances in the Po-valley, the Paris metropolitan area, and Vienna.

Keywords Benzo[a]pyrene • Atmospheric concentrations • Chemistry transport modeling • CMAQ • BaP • Scenario's

10.1 Introduction

Benzo[a]pyrene (BaP) is a polycyclic aromatic hydrocarbon. It is almost solely emitted from incomplete combustion processes. Many experimental and epidemiological studies have proven BaP to be toxic and carcinogenic. Therefore, in 1998 BaP was included in the UN/ECE POP-Protocol which commits all ratifying parties to reduce all major sources of BaP. In 2010 the European Union officially established a target value for BaP concentrations in ambient air of 1 ng/m^3 on annual average.

The aim of this study is to quantize the effects of emission reductions of different sources for BaP and emissions of ozone precursors on atmospheric BaP concentrations. For this reason multiple runs of a chemistry transport model (CTM) using different emission scenarios for the years 1980, 2000 and 2020 were performed.

10.2 Methodology

For this model study hourly gridded emissions for the years 1980, 2000, and 2020 were created with the SMOKE for Europe model [1]. The SMOKE for Europe emission model uses national total emissions as input data. For ozone precursors, primary aerosols and aerosol precursors national total emissions from the European Monitoring and Evaluation Program (EMEP) were used.

For BaP, however, a consistent emission inventory for the time range 1980–2020 does not exist. Especially before the year 2000 inventories mostly included total PAH emissions only. Because the percentage of BaP in the total PAH emissions is highly uncertain, only emission inventories which explicitly include BaP were used for this study. Furthermore, the emission factors (EF) of BaP from various sources found in the literature are subject to large uncertainties (e.g. factor of 5–10 for wood combustion) [7]. The usage of different EFs can lead to large differences in the estimated annual total BaP emissions. The officially reported emissions as provided by EMEP show large differences between different countries [5]. It is suggested that these differences are due to different methodologies used by the reporting national authorities.

Because of these findings, only BaP emissions as estimated by experts were used. For the year 1980 national total BaP emissions were taken from Pacyna et al. [6].

Emission data for the year 2000 as well as different estimates for BaP emissions in 2020 were taken from TNO [3]. Finally, the different emission inventories needed to be harmonized in order to create consistent BaP emissions for the time range 1980–2020. This was achieved mainly by adjusting the EFs for wood combustion in the 1980 inventory.

The fate of BaP in the atmosphere was simulated with a modified version of the Community Multiscale Air Quality (CMAQ) modelling system, which is developed under the leadership of the US Environmental Protection Agency.

The original CMAQ model was enhanced to include the atmospheric degradation of BaP. Degradation by OH• and photolysis were implemented as first order reactions. The reaction of BaP with ozone was implemented as a heterogeneous reaction of gaseous ozone with BaP bound to organic aerosols following Kwamena et al. [4] which assume a Langmuir-Hinshelwood type reaction.

10.3 Results and Discussion

To evaluate the simulated atmospheric concentrations of BaP for the year 2000 a comparison to observations has been performed. The modelling system was able to reconstruct the annual average concentrations as well as the inter-annual variability (Fig. 10.1). Because the measurement data at many stations is influenced by local emission peaks, the model results are generally lower than the observations. A more detailed evaluation of the model results can be found in Bieser et al. [2].

Between 1980 and 2000 the annual average concentrations of BaP over Europe decreased from 0.1 to 0.06 ng/m^3. This is mainly caused by large reductions of BaP emissions from industrial production processes due to the political and technical development in the late twentieth century. Depending on the future emission scenario the simulated BaP concentrations over Europe in 2020 vary between 0.042 and 0.064 ng/m^3 (Fig. 10.2). A key finding is that lower total BaP emissions can

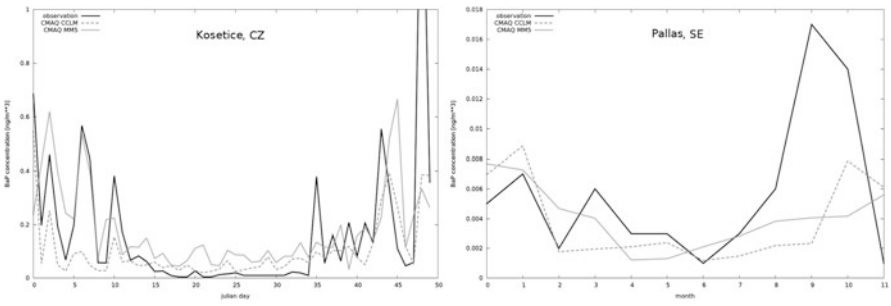

Fig. 10.1 Comparison of simulated and observed (*bold line*) BaP concentrations. The CTM CMAQ has been run using different meteorological fields from COSMO-CLM (*solid thin line*) and MM5 (*dashed*)

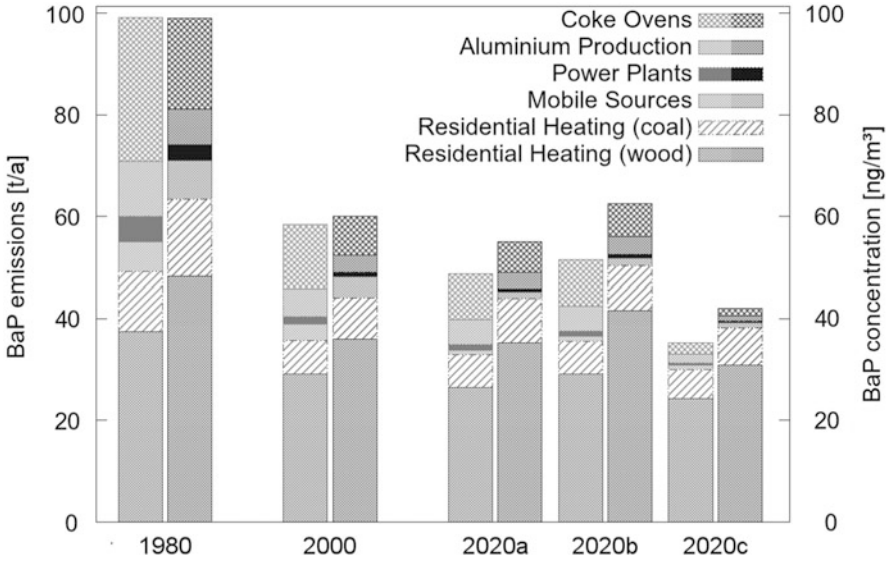

Fig. 10.2 Contribution of BaP emissions from different source types (*light colors*) to near surface atmospheric concentrations of BaP (*dark colors*) for different years

lead to higher atmospheric concentrations. This is caused by the different spatial and temporal distribution of the sources for BaP. The most important factor is that industrial production processes show almost no inter-annual variability while emissions related to heating take place during the cold seasons only. However, due to the high availability of ozone, emissions in summer have only a small impact on annual average BaP concentrations. Figure 10.2 illustrates the BaP emissions and their impact on the atmospheric concentrations for the different model scenarios. Additionally, other species were found to have a large impact on BaP concentrations. Changes of ozone precursors lead to an additional 10 % decrease of BaP concentrations between 2000 and 2020. This can be explained by lower ozone minima during night time due to decreasing NO_X emissions from road traffic.

Finally, four regions were identified in which the annual average BaP concentrations exceeded the European target value of 1 ng/m^3 for all modelled years. These are the metropolitan areas around Paris, Milan, Vienna and Moscow.

References

1. Bieser J, Aulinger A, Matthias V, Quante M, Builtjes P (2011) SMOKE for Europe – adaptation, modification and evaluation of a comprehensive emission model for Europe. Geosci Model Dev 4:1–22. doi:10.5194/gmd-4-1-2011
2. Bieser J, Aulinger A, Matthias V, Quante M (2011) Impact on emission reductions between 1980 and 2020 on atmospheric benzo[a]pyrene concentrations. Water Air Soil 223(3):1393–1414. doi:10.1007./s11270-011-0953-z

3. Denier van der Gon HAC, van het Bolscher M, Visschedijk AJH, Zandveld PYJ (2007) Emissions of persistent organic pollutants and eight candidate POPs from UNECE-Europe in 2000, 2010 and 2020 and the emission reduction resulting from the implementation of the UNECE POP protocol. Atmos Environ 41:9245–9261
4. Kwamena NOA, Thornton JA, Abbatt JPD (2004) Kinetics of surface-bound benzo[a]pyrene and ozone on solid organic and salt aerosols. J Phys Chem A 108:11626–11634
5. Mareckova K, Wankmueller R, Anderl M, Muik B, Poupa S, Wieser M, Inventory Review (2008) Emission data reported under the LRTAP convention and NEC directive, stage 1 and 2 review, status of gridded data. EEA & CEIP, EMEP technical report CEIP 1/2008
6. Pacyna JM, Breivik K, Münch J, Fudala J (2003) European atmospheric emissions of selected persistent organic pollutants, 1970–1995. Atmos Environ 37(Suppl 1):S119–S131
7. Ravindra K, Sokhi R, van Grieken R (2008) Atmospheric polycyclic aromatic hydrocarbons: source attribution, emission factors and regulations. Atmos Environ 42:2895–2921

Questions and Answers

Questioner Name: Stefano Galmarini

Q: Why is BaP not measured regularly and what is the precision of measurements given a target value of 1 ng/m^3?
A: For measurements of particulate atmospheric BaP the coefficient of variation is about 10 % and the detection limit, using a high volume sampler over 24 h, is in the range of 50–100 pg/m^3. Thus, the minimum sampling duration is given by the atmospheric concentrations of BaP. The highest resolution of BaP measurements currently available are 24–72 h averages. However at most stations BaP measurements are not taken continuously. This is because of the fact that the samples need to be analyzed manually in the laboratory and the samples can not be stored because of degradation processes.

Questioner Name: Marina Astitha

Q: Have you tried to run the model on higher resolutions and investigated the impact on comparisons with measurements and the spatial distribution of BaP?
A: So far we have run CMAQ-BaP on a 54×54 km^2 and a 24×24 km^2 grid. Our emission data allow for resolutions up to 5×5 km^2. We have planned to perform nested CMAQ runs with resolutions up to 6×6 km^2. Since we have only compared modelled BaP concentrations with observations from rural background measurement stations we do not expect a significant improvement of model performance using higher resolutions. This is of course not necessarily true for urban areas. However, due to the large spatial and temporal uncertainties of BaP emissions from wood burning it is not clear if the model is able to reproduce local urban observations.

Chapter 11
Evaluating Alternative Exposure Metrics Used for Multipollutant Air Quality and Human Health Studies

Halûk Özkaynak, Vlad Isakov, Lisa Baxter, Stephen E. Graham, Stefanie Ebert Sarnat, Jeremy A. Sarnat, James Mulholland, Barbara Turpin, David Q. Rich, and Melissa Lunden

Abstract Epidemiologic studies of air pollution have traditionally relied upon surrogates of personal pollutant exposures, such as ambient concentration measurements from fixed-site pollutant monitors. This study evaluates the performance of alternative measured and modeled exposure metrics for multiple particulate and gaseous pollutants, in the context of different epidemiologic studies performed by EPA, Rutgers/Rochester/LBNL and Emory/Georgia Tech researchers. Alternative exposure estimation approaches used, included: central site or interpolated monitoring data, regional pollution levels based on measurements or models (CMAQ) and local scale (AERMOD) air quality models, hybrid models, statistically blended modeling and measurement data, concentrations adjusted by home infiltration rates based on LBNL algorithms, and population human exposure (SHEDS and APEX) model predictions. The Emory/Georgia Tech team examined the acute morbidity effects of ambient traffic-related pollutants (CO, NOx, $PM_{2.5}$ and $PM_{2.5}$ EC)

H. Özkaynak (✉) • V. Isakov • L. Baxter
U.S. EPA/ORD/NERL, Research Triangle Park, NC 27711, USA
e-mail: ozkaynak.haluk@epa.gov

S.E. Graham
U.S. EPA/OAR/OAQPS, Research Triangle Park, NC, USA

S.E. Sarnat • J.A. Sarnat
Emory University, Atlanta, GA, USA

J. Mulholland
Georgia Institute of Technology, Atlanta, GA, USA

B. Turpin
Rutgers University, New Brunswick, NJ, USA

D.Q. Rich
University of Rochester School of Medicine and Dentistry, Rochester, NY, USA

M. Lunden
Lawrence Berkeley National Laboratory, Berkeley, CA, USA

D.G. Steyn et al. (eds.), *Air Pollution Modeling and its Application XXII*,
NATO Science for Peace and Security Series C: Environmental Security,
DOI 10.1007/978-94-007-5577-2_11,

and ozone using time series analyses of emergency department (ED) visits and case-crossover analysis of implantable cardioverter defibrillator (ICD) detected ventricular arrhythmias in Atlanta, GA. The Rutgers/Rochester/LBL team examined the associations between $PM_{2.5}$ mass and its species with myocardial infarction (case-crossover study) and adverse birth outcomes (cohort study) in New Jersey. Initially, the various exposure indicators/metrics were compared in terms of their ability to characterize the spatial and temporal variations of multiple ambient air pollutants across the different study areas. These metrics were then used to examine associations between ambient air pollution and adverse health effects. Next, pollutant–specific relative risks (RRs) obtained from epidemiologic analyses of the alternative exposure metrics were evaluated against those obtained from using a conventional approach (i.e., central site data alone). Pollutant and metric dependent exposure prediction differences were found in some cases, indicating a non-uniform exposure prediction error structure across pollutants. Results suggest the need for additional refinements to methods used to estimate exposures in support of different types of air pollution epidemiologic studies.

Keywords Air pollution • Exposure • Air quality modeling • Epidemiologic studies

11.1 Introduction

Numerous air pollution epidemiology studies conducted to-date have used measurements from central site ambient monitors to estimate population exposures to air pollution. However, depending on the epidemiological study design, this approach may introduce exposure prediction errors and misclassification of exposures for pollutants that are spatially heterogeneous, such as those associated with traffic emissions (e.g., carbon monoxide, elemental carbon, nitrogen oxides and fine and ultrafine particulate matter). Moreover, central-site monitors do not account for multitude of factors that influence personal exposures and associated health effects of ambient pollutants such as, elevated concentrations/exposures near localized emissions sources, variations in infiltration of outdoor pollutants indoors either at home or in other microenvironments, demographic human activity and mobility patterns and indoor pollution exposures. Exposure prediction errors resulting from the use of simple surrogates of personal exposure, such as central-site measurements, may in turn influence the strength and significance of the inferences derived from epidemiologic investigations [1, 2].

In order to enhance the results from epidemiologic studies of ambient $PM_{2.5}$, $PM_{2.5}$ components and gaseous air pollution, the U.S. Environmental Protection Agency (EPA) recently sponsored a collaborative agreement research program with three academic institutions: Emory University, Rutgers University and University

of Washington. The investigators from these institutions, along with modelers from EPA's National Exposure Research Laboratory (NERL) developed and evaluated several indicators or tiers of air pollution exposure metrics (ranging from simple to more complex indicators or predictors of exposure) and their influence on epidemiological study finding in several locations in the US. This presentation summarizes the key findings for the Emory/Georgia Tech study conducted in the Atlanta metropolitan area and the Rutgers study conducted in the State of New Jersey.

11.2 Atlanta Study

The Atlanta study area is centered on downtown Atlanta and extends 70 km in all directions. This study examined the spatial and temporal variations of alternative measured and modeled exposure metrics for multiple pollutants: fine particulate matter ($PM_{2.5}$), $PM_{2.5}$ elemental carbon, $PM_{2.5}$ sulfates, nitrogen oxides, carbon monoxide and ozone. Alternative exposure assignment approaches considered various techniques ranging from traditional central site ambient measurements to more sophisticated exposure models, such as the SHEDS (Stochastic Human Exposure and Dose Simulation) and the APEX (Air Pollutants Exposure) models. Six alternative indicators of exposure to ambient traffic and regional pollutants were developed for use in time-series analyses of emergency department (ED) visits and case-crossover analyses of tachyarrhythmic events in patients with implantable cardioverter defibrillators (ICD) in Atlanta, GA, over a 4-year period, 1999–2002 [3]. The exposure metrics included several indicators at varying levels of exposure refinement. Under the first tier of refinement, existing ambient fixed-site monitoring data were used for CO, NO_x, O_3, $PM_{2.5}$, SO_4, and EC (metric i), as well as estimates of the regional background for each of the pollutants obtained by removing local source impacts estimated by an emissions-based air quality model (AERMOD) from ambient monitor observations and then spatially resolving the regional background estimates using a previously developed distance-squared weighting approach (metric ii) [4]. Under the second tier of refinement, an air quality emissions model (AERMOD, metric iii) and hybrid and blended models (metric iv) were used to obtain spatially-resolved estimates of ambient concentrations at 225 zipcode centroids (for the ED study) and over 400 Census Block Group centroids, for the ICD study [1, 5]. Under the final two tiers of exposure refinement in the ED study, spatially- and temporally-resolved estimates of air exchange rates (AER) as an exposure factor (metric v) and outputs from APEX and SHEDS modeling (metric vi) were utilized as estimates of population exposures for each of the pollutants of interest. Health risk estimates from models using the various exposure metrics were then compared and evaluated for each pollutant and health outcome.

11.3 New Jersey Study

Two different epidemiologic heath data sets in New Jersey were chosen: (1) The New Jersey (NJ) Triggering of Myocardial Infarction (MI) Study and (2) The NJ Adverse Birth Outcomes Study. The MI study used a time-stratified case-crossover design, with case periods defined as the 24 h period before emergency room (ER) admission for MI. The Birth study was a cohort study examining associations between fetal growth restriction and trimester-specific mean $PM_{2.5}$ concentrations. Epidemiologic analyses examined the association between the health outcome and $PM_{2.5}$ exposure, using four different exposure surrogates: Tier 1 – central site $PM_{2.5;}$ Tier 2a – exposures estimated using the Stochastic Human Exposure and Dose Simulation (SHEDS) model; Tier 2b – indoor concentrations of ambient $PM_{2.5}$ predicted using a deterministic mass balance model (Aerosol Penetration and Persistence, APP, model) and an air exchange rate model (Lawrence Berkeley National Laboratory Infiltration Model); and Tier 3 – a hybrid approach (SHEDS with modeled AER). Additional analyses were also performed to investigate whether there were differences in the risk of a MI associated with increased ambient $PM_{2.5}$ concentration for communities with high, medium, and low AERs, and whether the $PM_{2.5}$ health effects were modified when the mass fractions of sulfate, nitrate, ammonium, elemental carbon (EC) and organic carbon (OC) on that day were high versus low.

11.4 Results

Exposure metric characteristics in Atlanta confirmed previously reported findings of greater spatiotemporal variability in traffic-related pollutants (i.e., CO, NO_x, and EC) compared to secondary pollutants (i.e., O_3 and SO_4) [5, 6]. Distributions of modeled exposure estimates were found to differ from modeled ambient air pollutant concentrations due to either the influence of infiltration factors or varying times spent in non-ambient microenvironments. Specifically, the $PM_{2.5}$ exposures were lower than the ambient levels, while the NO_x and CO exposures were greater than ambient values mainly, due to the influence of local traffic sources. In comparison to the use of central site monitoring data, we found greater estimated effects on respiratory disease and asthma/wheeze ED visits for the traffic-related pollutants when using the spatiotemporally-refined hybrid and APEX/SHEDS exposure metrics. However, we did not observe similar results for secondary pollutants. These results suggest that the modeled exposure metrics for traffic-related pollutants captured patterns of spatiotemporal variability in air pollution that were not reflected by measurements from the central site. On the other hand, these findings did not hold for cardiovascular disease ED visits, for which observed associations were similar among the various exposure metrics for each pollutant. We did not detect any significant associations in the ICD study.

In both of the New Jersey epidemiological studies, consistent results were obtained across all four exposure surrogates. Namely, the use of refined exposure surrogates did not lead to a change in the predicted risk of MI or "small for gestational age" over that predicted by the central site $PM_{2.5}$ measurements (i.e., added explanatory power). In an alternative MI analysis, the use of air exchange rate was found to be an effect modifier of the PM2.5/MI association. Namely, we found that each interquartile range (10.8 $\mu g/m^3$) increase in $PM_{2.5}$ concentration was associated with a significant 15 % increase in the relative odds of MI for subjects living in zip codes within the medium or high air exchange rate tertile, compared to subjects living in zip codes within the low air exchange rate tertile [7]. Also, acute effects of ambient $PM_{2.5}$ on MI were greatest on days with a larger fraction of secondary PM (sulfate, nitrate and/or secondary OC), using based on bias corrected CMAQ model $PM_{2.5}$ species predictions [7].

11.5 Conclusions

Our results indicate that the type of an epidemiologic study design and the level of detail of available health data can influence the spatio-temporal resolution needs of exposure information used for health effects research. Observed benefits of refined exposure estimates depend on the study design (time-series vs. cohort), health outcome (long vs. short), and spatial and temporal patterns of the pollutant. However, neither a case-crossover study nor a study that involves mid-term (e.g., trimester-long) averages of exposures is an optimal design for detecting whether refined exposure estimates add a significant amount of information beyond the central site monitor mainly due to their design. Epidemiologic study designs most likely to benefit from the use of refined exposure surrogates include those that have individual and/or household level data. We found in general that for time-series studies (e.g., MI or ED studies) ambient concentrations may serve as an appropriate exposure surrogate. However, for cohort studies or better spatio-temporally resolved acute studies (as shown in the Atlanta analysis) the use of more refined exposure surrogates than the conventionally used ambient monitoring data may boost study power, reduce exposure prediction errors, and strengthen the estimated associations between air pollution and health data. We also found that for spatially heterogeneous urban pollutants like CO and NO_x, the associations of asthma ED visits with model-based exposure estimates were higher and more statistically significant than those with central site-based exposure estimates. However, for spatially homogenous pollutants, spatiotemporal models may add little to explaining variability as we found for O_3 in Atlanta. Clearly, it is important to better understand the different sources and factors influencing uncertainties in ambient pollution epidemiology analyses. It is possible that potential compounding errors or uncertainties in exposure model specification could introduce additional errors during the epidemiologic analyses when using modeled exposure metrics. We anticipate that the results of this research will improve exposure assessments in future air pollution epidemiology studies and

help identify situations that might require refined exposure metrics. Overall, these new approaches will help to reduce uncertainty in health risk assessments of ambient air pollution and consequently the effectiveness of federal and state/local air quality management strategies.

Disclaimer This paper has been subjected to Agency review and approved for publication. Approval does not signify that the contents reflect the views of the Agency nor does mention of trade names or commercial products constitute endorsement or recommendation for use.

References

1. Özkaynak H, Isakov V, Sarnat S, Sarnat J, Mulholland J (2011) Examination of different exposure metrics in an epidemiological study. EM Magazine, November 2011
2. Sarnat SE, Klein M, Sarnat JA, Flanders WD, Waller LA, Mulholland JA, Russell AG, Tolbert PE (2010) An examination of exposure measurement error from air pollutant spatial variability in time-series studies. J Expo Sci Environ Epidemiol 20:135–146
3. Sarnat SE, Sarnat J, Klein M, Tolbert PE, Mulholland J (2011) Alternative metrics of ambient air pollution exposure for use in epidemiologic studies in Atlanta, GA. Revised final report prepared for EPA agreement CR-83407301, 28 Dec 2011
4. Ivy D, Mulholland JA, Russell AG (2006) Development of ambient air quality population-weighted metrics for use in time-series health studies. J Air Waste Manage Assoc 58:711–720
5. Isakov V, Touma J, Valari M, Özkaynak H, Sarnat SE, Sarnat S, Kewada P, Mulholland J (2011) Development and evaluation of alternative metrics of ambient air pollution exposure for use in epidemiologic studies. In: Steyn DG, Castelli ST (eds) Air pollution modeling and its applications XXI. Springer, Dordrecht
6. Wade KS, Mulholland JA et al (2006) Effects of instrument precision and spatial variability on the assessment of the temporal variation of ambient air pollution in Atlanta, Georgia. J Air Waste Manage Assoc 56(6):876–888
7. Turpin B, Rich D, Lunden M (2011) Refined exposure surrogates for ambient PM in epidemiologic studies: accounting for temporal/spatial variations in infiltration. Final report prepared for EPA agreement CR-83407201, 30 Nov 2011

Questions and Answers

Questioner Name: Amir Hakami

Q: Based on your results, would you consider higher spatial or higher temporal resolution more beneficial to exposure assessment?
A: This is a very good but complex question to respond. Typically, improved understanding of within vs. between individual variations in exposures is critical for conducting better exposure and health risk assessments, as well as, formulating optimum risk management strategies for many pollutants of health concern. Either higher temporal or spatial resolution can be important, depending on the context how individual or population level exposure information will be used in subsequent analysis. For instance, in predicting exposures to pollutants with short-term

or acute health effects concerns (e.g., supporting epidemiological time-series or case-crossover studies on acute mortality or morbidity effects of air pollution, longitudinal panel studies on limited number of subjects) higher temporal resolution is often more desirable. However, for predicting exposures to pollutants with long-term or chronic health effects implications (e.g., supporting epidemiological cohort studies, cross-sectional studies, spatially resolved health data sets used in daily time-series studies) higher spatial resolution is often more desirable.

Chapter 12
Benefits of Using Enhanced Air Quality Information in Human Health Studies

P.S. Porter, Edith Gégo, Valerie Garcia, and S.T. Rao

Abstract The ability of four (4) enhancements of gridded $PM_{2.5}$ concentrations derived from observations and air quality models to detect the relative risk of long-term exposure to $PM_{2.5}$ are evaluated with a simulation study. The four enhancements include nearest-neighbor (NN or central monitor), ordinary kriging (OK), FUSED (bias-adjusted model output), and direct use of model outputs (CMAQ). The methods are applied to the state of New York. After adjusting for PM estimation bias and range modification, FUSED PM and CMAQ had similar performance and were better than kriged and nearest neighbor PM.

Keywords Human health • PM2.5 • CMAQ

12.1 Introduction

The importance of local spatial variability in exposure estimation has recently been emphasized. Photochemical simulation models such as CMAQ provide continuous gridded estimations of pollution levels but despite continual improvement, are often biased, limiting their use 'as is' in health analyses. Garcia et al. [2] showed that a simple technique to fuse observations and model estimates (FUSED PM) creates unbiased gridded maps of PM that respect observations and fill the area devoid of observations with more detail than provided by kriging.

P.S. Porter (✉)
Civil Engineering/Environmental Engineering, University of Idaho, Idaho Falls, ID, USA
e-mail: porter@if.uidaho.edu

V. Garcia • S.T. Rao
AMAD/NERL, U.S.E.P.A., Research Triangle Park, NC, USA
e-mail: garcia.val@epa.gov; Rao.ST@epamail.epa.gov

E. Gégo
Gego and Associates, Idaho Falls, ID, USA

D.G. Steyn et al. (eds.), *Air Pollution Modeling and its Application XXII*,
NATO Science for Peace and Security Series C: Environmental Security,
DOI 10.1007/978-94-007-5577-2_12,

In this context, we present a simulation based evaluation of four methods for estimating PM concentrations at unmonitored locations then assess the impact of long-term exposure to PM concentrations on adverse human health outcomes [4]. Long-term exposure is assumed to correspond to the average $PM_{2.5}$ concentrations for the year 2006.

12.2 Methods

Simulated 'true' PM25 exposure estimates were generated through sequential gaussian simulation (SGS) of 2006 annual mean $PM_{2.5}$ concentrations measured in the US east of the Rocky Mountains (Phase domain, [5]). Five hundred equally likely maps were generated. A subset of simulated cells in the vicinity of the state of New York was the designated 'monitoring' network (number of monitors equal 50 for this presentation). An additional subset of 863 cells, consisting of the grid cells in the state of New York, was designated the 'cohort'. The number of individuals per cohort cell was varied between 20 and 100. The enhanced exposure estimates, calculated from the SGS maps include (1) ordinary kriging, (2) fusion (Garcia et al.) (FUSED = CMAQ – kriged map of (CMAQ – observations)), (3) nearest neighbor (NN or 'central monitor'), and (4) CMAQ (direct use of model output). Figure 12.1 shows a typical simulation result.

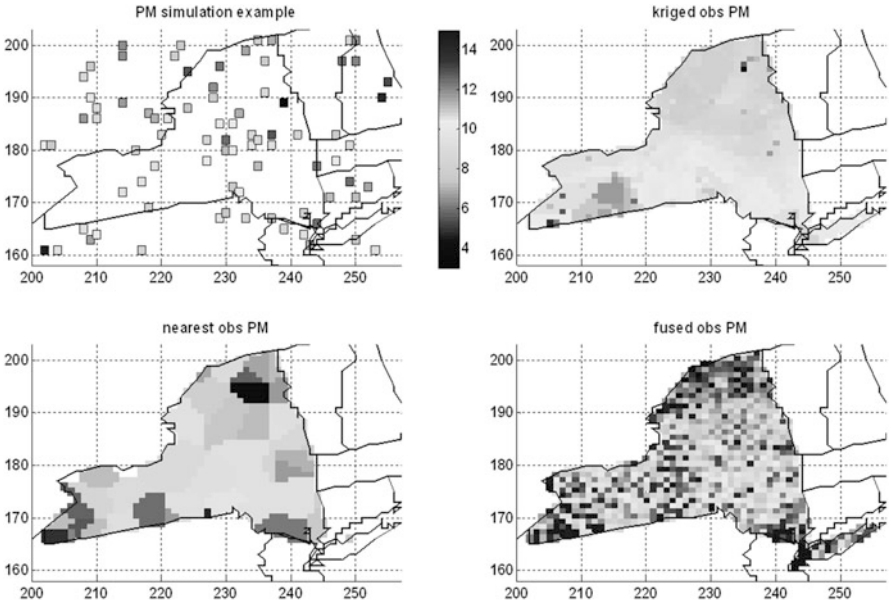

Fig. 12.1 Typical simulation results: *top right* – observed; *top left* – kriged; *lower left* – nearest; *lower right* – FUSED

The link between health affects and air pollution was defined with the Cox proportional hazards model using parameters established by Miller et al. [4] as follows:

$$\gamma = \frac{1}{\lambda_0 \exp\left[\beta\left(PM - \overline{PM}\right)\right]} \tag{12.1}$$

γ = expected survival time (years) of population members
PM = exposure at a particular location (annual average PM concentration)
$\overline{PM}$ = mean regional exposure
λ_o = baseline incidence rate (0.032), β = relative risk (0.0215)

Survival times of individuals, denoted $\hat{\gamma}$, are exponentially distributed with mean γ.

Expected survival times, γ, were calculated from PM values using Eq. (12.1). PM values included 'True' and enhanced (using the four methods listed above). Individual survival times, $\hat{\gamma}$, were generated as exponential random numbers given the expected values from Eq. (12.1). Finally, partial maximum likelihood regression was used to estimate relative risk (β values) from PM and $\hat{\gamma}$. The estimated β values were compared with the known value of 0.0215.

12.3 Results and Discussion

Preliminary results indicated that in terms of bias and root mean squared error, the performance of the four enhanced techniques followed the order OK > (FUSED, nearest neighbor) > CMAQ (OK is best) (Table 12.1; notice that 'TRUE' PM values (row 1), do not lead to perfect β estimates because individual survival times ($\hat{\gamma}$) are exponentially distributed random numbers. Estimation of expected survival times (γ) from 'TRUE' PM values does lead to perfect β estimates).

Table 12.1 Performance of enhanced methods in estimating relative risk (β)

	Relative absolute bias (Individuals/location)			Relative root mean squared error (Individuals/location)		
Method	20	50	100	20	50	100
TRUE	0.162	0.104	0.072	0.203	0.128	0.091
FUSED	0.469	0.462	0.465	0.492	0.473	0.471
OK	0.304	0.229	0.186	0.388	0.294	0.240
NN	0.458	0.442	0.442	0.515	0.477	0.468
CMAQ	0.483	0.476	0.479	0.503	0.486	0.485

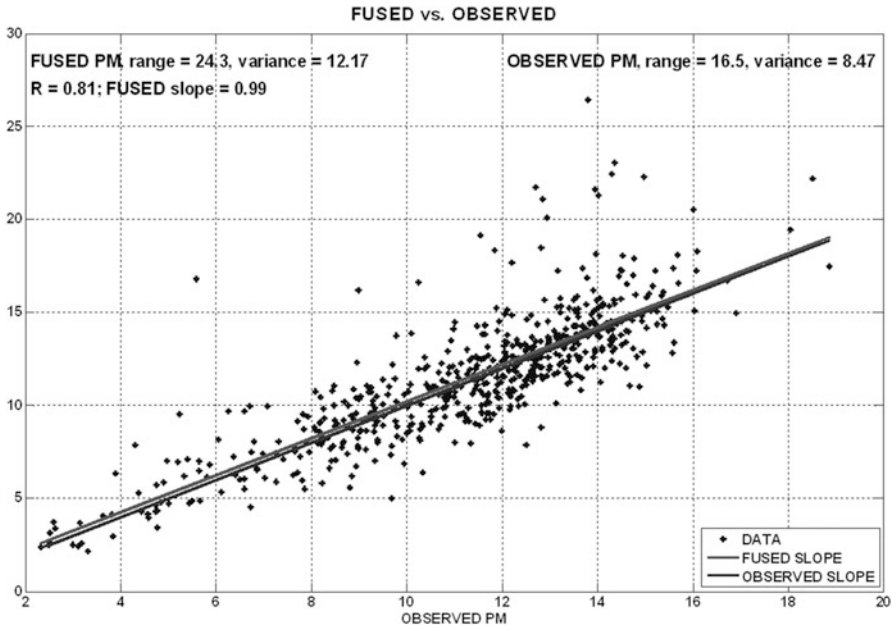

Fig. 12.2 PM FUSED vs. observed: range of FUSED exceeds the observed range

The poor performance of FUSED and CMAQ relative to kriging can be explained by modifications that enhanced techniques impose on the relationship between observed PM and surrogate PM values $\left(\widehat{\boldsymbol{PM}}\right)$. For example, fused PM is unbiased but has a wider range than true PM (Fig. 12.2); the wider range results in a biased $\boldsymbol{\beta}$ estimate (Fig. 12.3). The bias can be eliminated by dividing the initial $\boldsymbol{\beta}$ estimate by the reliability ratio [1]:

$$\boldsymbol{\beta}\,(\textbf{adjusted}) = \boldsymbol{\beta}\,(\textbf{initial})\,/\textbf{reliability ratio} = \boldsymbol{\beta}(\textbf{initial})/\left(\frac{\sigma^2_{PM}}{\sigma^2_{\widehat{PM}}}\right) \tag{12.2}$$

Kriged PM, which is a smoothing of the original PM values, has a reduced range relative to the original PM. Bias caused by the reduced range can be eliminated by multiplying the initial $\boldsymbol{\beta}$ estimate by the slope of PM (true) vs. $\widehat{PM}$ (surrogate PM values).

After applying the reliability ratio and the PM/$\widehat{\boldsymbol{PM}}$ slope to $\boldsymbol{\beta}$, the performance of the four 'enhanced' PM methods followed the order CMAQ > FUSED ≫ KRIGING ≫ NN (CMAQ best). Table 12.2 shows relative root mean squared error for each method as a function of the number of individuals per cohort location.

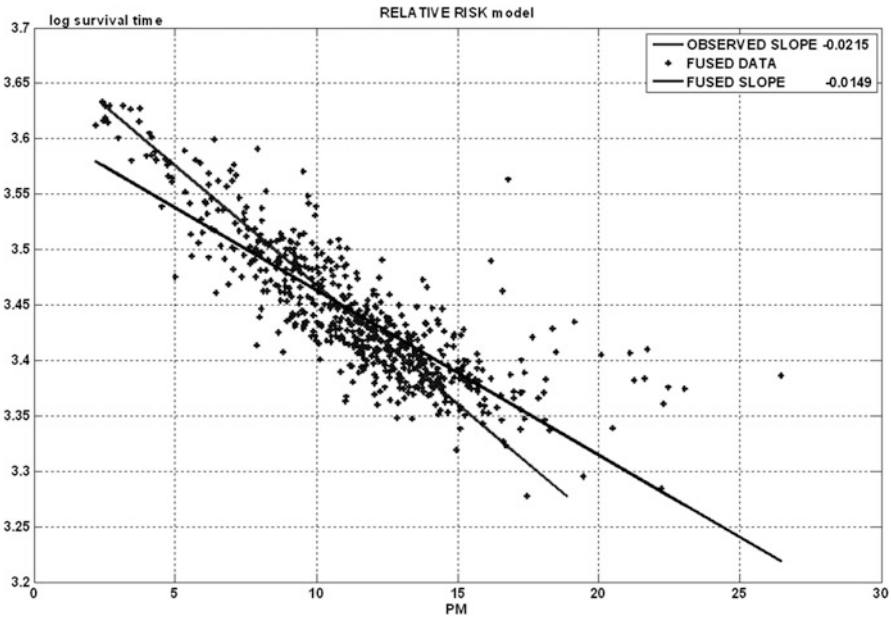

Fig. 12.3 Survival time vs. FUSED PM: to match PM, survival times are rotated counter-clockwise, decreasing the slope (β)

Table 12.2 Application of reliability ratio and slope adjustment: performance of enhanced methods (50 monitors)

	Relative absolute bias (Individuals/location)			Relative root mean squared error (Individuals/location)		
Method	20	50	100	20	50	100
TRUE	0.162	0.104	0.072	0.203	0.128	0.091
FUSED	0.273	0.177	0.151	0.311	0.228	0.194
OK	0.641	0.221	0.186	0.368	0.280	0.235
NN	0.461	0.290	0.252	0.496	0.385	0.334
CMAQ	0.287	0.169	0.145	0.294	0.215	0.184

12.4 Summary

PM estimation bias does not play a role in relative risk estimation, but bias in the variance does, explaining why CMAQ and FUSED maps, though unbiased, perform poorly in relative risk estimation unless adjusted. FUSED map techniques are designed to reduce CMAQ PM bias but could be designed to also reproduce PM variance.

Disclaimer The United States Environmental Protection Agency through its Office of Research and Development collaborated in the research described here. It has been subjected to Agency review and approved for publication.

References

1. Fuller WA (1987) Measurement error models. Wiley, New York
2. Garcia VC, Foley KM, Gego E, Holland DM, Rao ST (2010) A comparison of statistical techniques for combining modeled and observed concentrations to create high-resolution ozone air quality surfaces. J Air Waste Manage Assoc 60:586–595
3. Miller KA, Siscovick DS, Sheppard L, Shepherd K, Sullivan JH, Anderson GL, Kaufman JD (2007) Long-term exposure to air pollution and incidence of cardiovascular events in women. N Engl J Med 356(5):447–459
4. USEPA (2011) Remote Sensing Information Gateway (RSIG). http://badger.epa.gov/rsig/

Question and Answer

Haluk Ozkaynak: How does bias correction methodology influence the confidence interval estimates of the alternative relative risk (β) estimates?
P. Steven Porter: We did not compute β confidence intervals. Methods with smaller mean squared errors should also have smaller confidence intervals.

Chapter 13
Is Driving 1 km to Work Worse for the Environment Than Driving 1 km for Shopping?

Wouter Lefebvre, Bart Degraeuwe, Carolien Beckx, Marlies Vanhulsel, Bruno Kochan, Tom Bellemans, Davy Janssens, Geert Wets, Stijn Janssen, Ina de Vlieger, Stijn Dhondt, and L. Int Panis

Abstract One of the measures that is promoted in order to improve the air quality is the decrease of vehicle mileage. However, there are different reasons to assume that not every kilometer driven by car yields the same impact on air pollution nor on the exposure of people. For instance, some trips are driven at high speeds on highways, while others are driven at relatively low speeds in urban environments. This will have an impact on the resulting emissions. Furthermore, emissions exhausted during the night will have a larger impact on the ground-level concentrations than emissions exhausted during the day, due to the higher atmospheric stability. And another aspect is that emissions produced in cities will affect a larger population than emissions in sparsely populated areas. These and other aspects are examined in this chapter. Analysis of the results per trip purpose shows that driving 1 km to work increases the pollutant concentrations about 1.3–1.4 times more than driving 1 km to go shopping, mainly due, but not confined to, the time of the day at which the activity is performed.

Keywords Car-emissions • Impact studies

W. Lefebvre (✉) • B. Degraeuwe • C. Beckx • M. Vanhulsel • S. Janssen • I. de Vlieger
Flemish Institute for Technological Research (VITO), Boeretang 200, 2400 Mol, Belgium
e-mail: wouter.lefebvre@vito.be; stijn.janssen@vito.be

B. Kochan • T. Bellemans • D. Janssens • G. Wets • L.I. Panis
Transportation Research Institute (IMOB), Faculty of Applied Economics,
Department of Medical Sociology and Health Sciences, Hasselt University,
Wetenschapspark 5 Box 6, B-3590 Diepenbeek, Belgium

S. Dhondt
Faculty of Medicine and Pharmacy, Vrije Universiteit Brussel, Laarbeeklaan 103,
1090 Brussel, Belgium

D.G. Steyn et al. (eds.), *Air Pollution Modeling and its Application XXII*,
NATO Science for Peace and Security Series C: Environmental Security,
DOI 10.1007/978-94-007-5577-2_13,

13.1 Introduction

The importance of source-related measures to reduce the environmental impact of transport is widely acknowledged. Unlike technological measures, source-related measures intervene at an earlier stage of the problem and are therefore considered to be a more efficient solution towards transport related air quality problems.

A longer version of this chapter has been submitted as Lefebvre et al. [2].

13.2 Model Chain

In this chapter, an integrated model chain is applied to assess the environmental impact of trips with different trip purposes. More detailed information on the individual models, the applied coupling procedure and the validation analysis can be found in Lefebvre et al. [1]. The motives for every trip are defined by the activity performed at the trip destination. As a result, going to work (motive work) is assigned a different motive than going home (motive home).

13.3 From Kilometers Travelled to Emissions

The emissions per trip motive (relative to an average passenger car) are presented in Fig. 13.1 (blue bars). Higher emissions per driven kilometer are seen with the heavy duty vehicles, compared to the passenger cars. This is as expected due to their high fuel consumption per kilometer. Comparing different trip motives driven by cars, we see a difference between them. For instance, trips for shopping and services have lower emission values per kilometer than for transit trips. This is closely correlated to the highway use of transit traffic and the almost complete lack of highway use for shopping and services.

13.4 From Emissions to Concentrations

The concentration changes per exhausted emission reflect the marginal impact of an exhaust emission on the resulting concentration. Comparing the concentrations per emission value (calculated by dividing the total concentration change per motive by the total emissions change per motive), we see some differences between the different motives (Fig. 13.1, red bars (relative to an average passenger car)). In contrast to the emission results, where the road type used appeared to be an important factor, the concentration changes are influenced by the moment in the

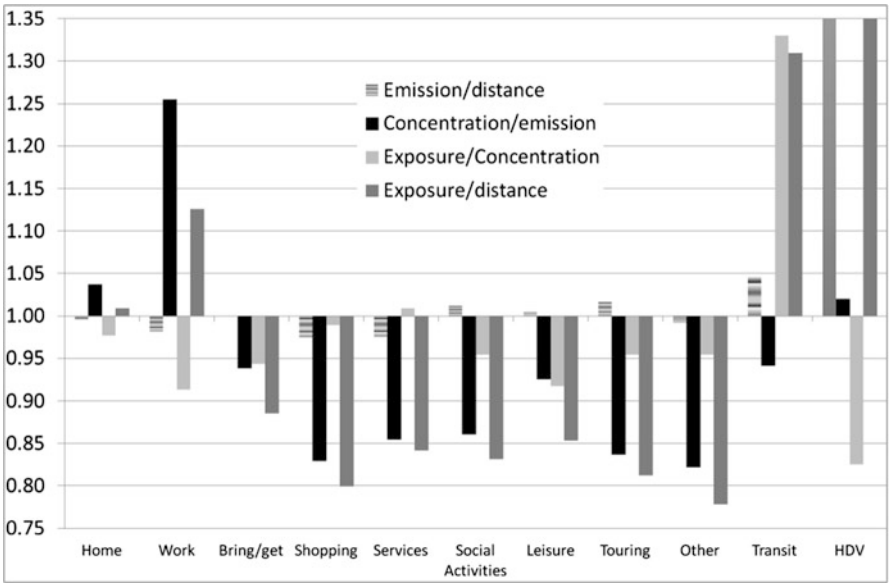

Fig. 13.1 The relative values of the emission per distance, the concentration per emission, the PMF and the EI, relative to an average car trip, per motive for NO_2 (Color figure online)

daily cycle when the emissions are exhausted. For example, the trip motive 'going to work' is generally done in the early morning, when the dispersion is very limited. As a result, an emission produced during a trip to work usually results in larger concentration increases than an emission produced when going home. Shopping, services, social activities and touring are activities that generally take place during the day or in the early evening. As a result, trips with these trip motives occur on average at moments with good dispersion conditions, leading to smaller concentration increases.

13.5 From Concentrations to Exposure

In this chapter, exposure is defined as a simple passive exposure, based on residential address information. More specific exposure aspects like indoor exposure and dynamic exposure are not assessed. The added value of the exposure assessment lies in the high resolution (up to 5 m) habitation data used in this study.

In fact, as there is more traffic in densely populated areas than in non-densely populated areas, the static exposure (i.e. the sum of the multiplication of each person with the corresponding concentration value) will be higher than the multiplication of

the regional averaged concentration with the total population. We call the proportion of both factors the population multiplication factor (PMF) and define it thus as follows:

$PMF = \frac{\sum_{people} \Delta C_l}{N\overline{\Delta C}}$, with ΔC_l the concentration change when eliminating the motive at the location of the home address of person l, N the number of persons and $\overline{\Delta C}$ the average concentration change over the region when eliminating the motive.

As expected, this factor is above 1 for all motives, ranging from 1.75 to 2.55. Indeed, for all motives, more traffic is generated in densely populated areas than in sparsely populated areas. Furthermore, results show that motives which have a larger fraction of highway use have a lower PMF than those which do not have such an abundant highway use (Fig. 13.1, green bars (relative to an average passenger car)). However, the correlation is small, as highways regularly cross densely populated areas in Flanders. The exception is the transit traffic, which has a high highway use fraction but also the highest PMF of all motives. This is due to the specific distribution of the transit fraction over the region.

13.6 Combining All Aspects: From Trip Motives to Population Exposure

The exposure per kilometer driven will be given by the multiplication of the emission per km driven, the concentration per emission and the exposure increase per concentration. We call the exposure per kilometer driven the exposure intensity (EI). As expected, heavy duty vehicles have a much higher EI than cars, but the EI is not so high as could be expected when comparing their respective emission per kilometer (Fig. 13.1, dark yellow bars). This is due to the low PMF for heavy duty vehicles. Furthermore, transit traffic exhibits a high EI, due to their high PMF. Finally, the EI is also high for going to work, but this is due to the stronger atmospheric stability in the morning. This effect is somewhat lowered by the low PMF for going to work.

13.7 Conclusions

In this chapter we have shown that different trip motives, due to their inherent differences in location of the emissions, road type used and time of the day at which they take place, have different influences on concentration and exposure. These differences lead to significantly different exposure estimates per kilometer driven for each motive. We can conclude that the response to the question posed in the title is positive, with a 1.3–1.4 times higher exposure for a kilometer driven to work compared to a kilometer driven for shopping.

Acknowledgments We want to thank the Flemish Environment Agency VMM, for the detailed habitation data that they kindly provided to us for this study. This research has been supported by the Institute for the Promotion of Innovation by Science and Technology in Flanders.

References

1. Lefebvre W, Degraeuwe B, Beckx C, Kochan B, Bellemans T, Janssens D, Wets G, Janssen S, Int Panis L, Dhondt S (2011) Presentation and evaluation of an integrated model chain destined to respond to traffic- and health-related policy questions. Env Mod Softw (submitted)
2. Lefebvre W, Degraeuwe B, Beckx C, Vanhulsel M, Kochan B, Bellemans T, Janssens D, Wets G, Janssen S, de Vlieger I, Dhondt S, Int Panis L (2012) Is driving 1km to work worse for the environment than driving 1km for shopping? (submitted)

Chapter 14
Integrated Assessment of an Emission Trading Scheme to Reduce Emissions from International Shipping and the Related Environmental Impact Over Europe

Stijn Janssen, Felix Deutsch, Nele Veldeman, Kris Vanherle, Pieter Lodewijks, Jan Duerinck, and Paul Campling

Abstract This chapter assesses the use of an Emission Trading Scheme (ETS) for the year 2020 to reduce the emissions from international ships entering European Community ports. Additional costs and benefits of including the maritime sector into a land-based ETS for NO_x and SO_2 are quantified.

Keywords Maritime emissions • Emission trading • Integrated impact assessment

14.1 Introduction

Shipping transports the majority of goods traded internationally and although it is acknowledged as being the most efficient and the most environmentally friendly mode of transport it is also an important contributor to anthropogenic emissions. An integrated assessment is made of the use of an Emission Trading Scheme (ETS) for the year 2020 to reduce the emissions from international ships entering European Community ports.

S. Janssen (✉) • F. Deutsch • N. Veldeman • P. Lodewijks • J. Duerinck • P. Campling
VITO, Boeretang 200, 2400 Mol, Belgium
e-mail: Stijn.janssen@vito.be

K. Vanherle
Transport & Mobility Leuven, Diestsesteenweg 57, 3010 Leuven, Belgium

D.G. Steyn et al. (eds.), *Air Pollution Modeling and its Application XXII*,
NATO Science for Peace and Security Series C: Environmental Security,
DOI 10.1007/978-94-007-5577-2_14,

14.2 Emission Modelling

We use EX-TREMIS and EUROSTAT databases and emission factors from the EMMOSS study to construct a spatially explicit database projections for 2016, 2020, and 2030 that account for activity data and port callings. The database distinguishes between 7 vessel types and 5 size classes. The emission baseline takes into account several recently adopted policy measures. The most recent ones being the additional measures to reduce NO_x and SO_2 from maritime emissions according to the amendments of October 2008 to MARPOL ANNEX VI. The most important conclusions from the emission analysis were as follows:

- Although fuel consumption by shipping is projected to increase from 2016 towards 2030 as a consequence of transport demand, NO_x emissions are more or less constant and SO_2 emissions show a strong decline. This is the direct consequence of the recently adopted IMO legislation on NO_x and SO_2 emissions.
- Container vessels are the largest polluters, followed by tankers and then bulk container ships.
- All vessels show a large decrease in SO_2 emissions between 2016 and 2020 due to the new IMO regulations setting the upper bound of sulphur content of maritime fuel to 0.5 %.
- 70 % of NO_x emissions and 85 % of SO_2 emissions occur outside the EU ports.
- The most important ports are in N-W Europe and the busiest shipping lane is the one taking ships from the N-W European ports to the Suez canal.
- The validation of the developed database by comparing data with the TREMOVE model and IIASA data shows in general a good match.

14.3 Technologies and Cost to Reduce Maritime Emissions

An extensive literature review and expert consultation was carried out to investigate the appropriateness of existing and potential technologies to reduce NO_x and SO_2 emissions from shipping. The abatement cost curves are developed based on "conservative" and "optimistic" scenarios to explore the uncertainty of aggregated abatement cost curves for 2016, 2020 and 2030 (see Fig. 14.1).

14.4 Emission Trading Scenarios

On the basis of aggregated NO_x marginal abatement cost curves for land based (LB), land based + maritime emissions (12 nm zone + ports) and land based + maritime emissions (EU waters) for the conservative (Scen1) and optimistic (Scen2) scenarios, we see that between a trading price of 1 and 3.5 k€/ton the potential for reducing

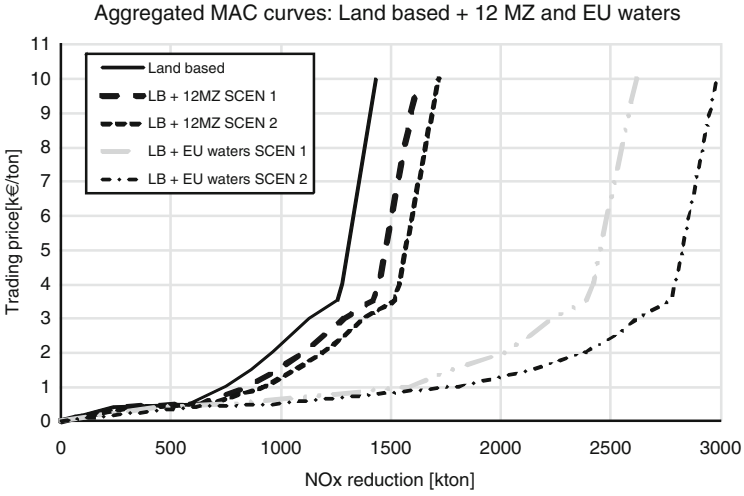

Fig. 14.1 Aggregated MAC curves for land based and Maritime NO_x emissions

more NO_x emissions is higher for the maritime sector (especially emissions in the EU waters). For SO_2 there is very limited reduction potential for SO_2. This is a result of the strengthening of the environmental legislation for SO_2 emissions in the maritime sector which will come into force after 2016. In fact the remaining maritime emissions even at higher trading prices such as 10 k€/ton will be very low compared to land based emissions and so the opportunities to reduce SO_2 further will be very limited.

On the basis of the aggregated marginal abatement cost curves for land based emissions, maritime emissions for 12 nm zone + ports and maritime emissions from EU waters – we could set up different emission trading scenarios. The following trading prices for NO_x and SO_2 were used:

- NO_x trading price 241€/ton, SO_2 trading price 256€/ton ("Low")
- NO_x trading price 1,194€/ton, SO_2 trading price 2,913€/ton ("High")

We considered two fixed price scenarios and fixed volume scenarios. In the fixed price scenarios we keep the trading price at the level of a corresponding IPPC land base scenario. Including emissions of the maritime sector results in additional emissions reduction of maritime emissions and the level of land based IPPC emissions remains the same.

For all scenarios the costs and benefits are evaluated in an integrated impact assessment. The BelEUROS model was used as a dispersion model to evaluated spatially explicit emission reduction scenarios and produce concentrations and deposition maps. The impact assessment took into account a basket of indicators that cover different health and ecosystem effects.

14.5 Conclusion

Based on the integrated impact assessment we conclude that there is an additional benefit of including the maritime sector in a land based ETS, but only if the trading price is sufficiently high. A scenario which sets the NO_x trading price at 1,194€/ton, results in significant improvements – however we view that it would be more effective to restrict the maritime emissions to the 12 nm zone + ports zones in the EU because:

1. the legal analysis indicates all vessels (EC and non-EC) can be required to join an ETS regime in ports (+ internal waters) and territorial seas (i.e. within the 12 nm zone). This means that a cap on maritime emissions can be imposed and the scheme is not voluntary.
2. the effectiveness of emissions abated in the 12 nm zone + ports zones, although much lower in volume, are more effective in terms of reducing environmental impacts than emissions abated in all EU waters.

One practical problem that would have to be resolved is that due to the fact that foreign ships enjoy the "right of innocent passage" in territorial seas no construction, design, equipment and manning (CDEM measures), going beyond the generally accepted international rules and standards, may be involved. To ensure that an ETS is robust and secure requires a full proof monitoring and verification scheme – this means that ships would need to install equipment such as the on-line Continuous Emission Monitoring System (CEMS), which is currently not a standard equipment for all ships.

For this reason the European Commission or Member States might want to consider alternative market based instruments or measures to reduce NO_x emissions from ships, such as differentiated kilometer charges, taxation, port dues and subsidies.

Acknowledgments This project was accomplished under the authority of DG Environment, European Commission, ENV.C.4/SER/2008/0019_Lot2.

Chapter 15
Effects Evaluation and Risk Assessment of Air Pollutants Deposition at European Monitoring Sites of the ICP Forests

Richard Fischer, Thomas Scheuschner, Angela Schlutow, Oliver Granke, Volker Mues, Konstantin Olschofsky, and Hans-Dieter Nagel

Abstract The study presents modelled critical deposition load exceedances for over 4,700 representatively selected forest plots in 21 European countries. It is based on measured soil data, different deposition scenarios and an application of the Simple Mass Balance (SMB) model. Effects of climate change on critical loads and exceedances are presented for 108 intensive monitoring plots in 17 countries. Results suggest hardly any more exceedances of critical loads for acidity in the near future. In contrast, even a maximum feasible emission reduction scenario which will leave 10 % of the forest sites unprotected against nitrogen effects by the year 2020. Full implementation of existing clean air legislation will result in 20 % of unprotected forest sites. Forests are less sensitive compared to other ecosystems as for these areas with exceedances are up to 58 %. Under a climate change scenario, decreasing critical loads suggest increasing sensitivity towards nutrient nitrogen inputs. When comparing critical load exceedances over the period 2020–2100, the share of 'safe' sites is assumed to decrease from 60 % (constant climate) to 50 % (climate change).

Keywords Critical loads • Simple mass balance • Climatic shifts

R. Fischer • O. Granke • V. Mues • K. Olschofsky
vTI-Institute for World Forestry, Leuschnerstrasse 91, 21031 Hamburg, Germany

T. Scheuschner (✉) • A. Schlutow • H.-D. Nagel
German National Focal Center for ICP Modelling and Mapping, OEKO-DATA, Hegermuehlenstr. 58, 15344 Strausberg, Germany
e-mail: thomas.scheuschner@oekodata.com

D.G. Steyn et al. (eds.), *Air Pollution Modeling and its Application XXII*,
NATO Science for Peace and Security Series C: Environmental Security,
DOI 10.1007/978-94-007-5577-2_15,

15.1 Background

Decades of strong increase of reactive nitrogen emissions in Europe have passed. Even if this trend stopped in the 1990s the nitrogen deposition levels stagnate in some areas on a high level. Effects of nitrogen deposition on forests are of specific interest as forests provides a multitude of ecosystem services. Acidifying sulphur deposition, which caused alarming headlines in the 1980s has been drastically reduced in the meantime. Over 25 years ago these depositions led to the creation of the International Cooperative Programme on the Assessment of Air Pollution Effects on Forests (ICP Forests) in 1986. This forest monitoring system has grown into one the largest of its kind worldwide covering more than 180 million hectare of surveyed forest area in Europe with harmonized forest condition assessments and providing the basis for assessing state and effect of air pollutants in European forests. Measurements of ICP Forests have shown that mean annual sulphur deposition decreased between 1998 and 2010 by 30 % including significant reductions on half of the 157 investigated plots. Annual nitrate and ammonium throughfall deposition fluctuated and only 12, resp. 13 % of the plots showed significant improvements [2]. Under LRTAP Convention the calculation of critical loads and exceedances [7] has been proved to be an appropriate instrument for the assessment of atmospheric deposition effects on forest. First results of critical loads for large scale representative forest plots of ICP Forests were presented by de Vries and Erismann [1] and later by Lorenz et al. [5] based on an adapted simple mass balance approach. Based on the data provided by a network of collaborating National Focal Centres and under the assumption of future emission reductions as a consequence of existing EU and national legislation Hettelingh et al. [3] showed that the European area at risk of acidification will decrease from 10 % in 2000 to 4 % by 2020. The computed European area at risk of eutrophication is projected to decrease from 52 % in 2000 to 32 % by 2020.

15.2 SMB Critical Loads and Exceedances

Critical loads for **Level I** and **Level II** plots were calculated according to the manual of ICP Modelling and Mapping using the Simple mass balance approach. These Critical Loads were compared with different deposition scenarios. The threat of **acidification** was widespread in the year 1980 and demonstrates a potential for severe effects of air pollution in central Europe in the past. Thirty-two percent of the **Level I** plots show very high exceedances of critical loads with more than 1,500 eq $ha^{-1}a^{-1}$. The situation improved considerably until 2000 when more than 98 % of the plots had no exceedances. A continued positive future projection is clearly visible. Already with the COB 2020 scenario a low risk of acidification on nearly all **Level-II** plots can be achieved (Fig. 15.1b). The trend for

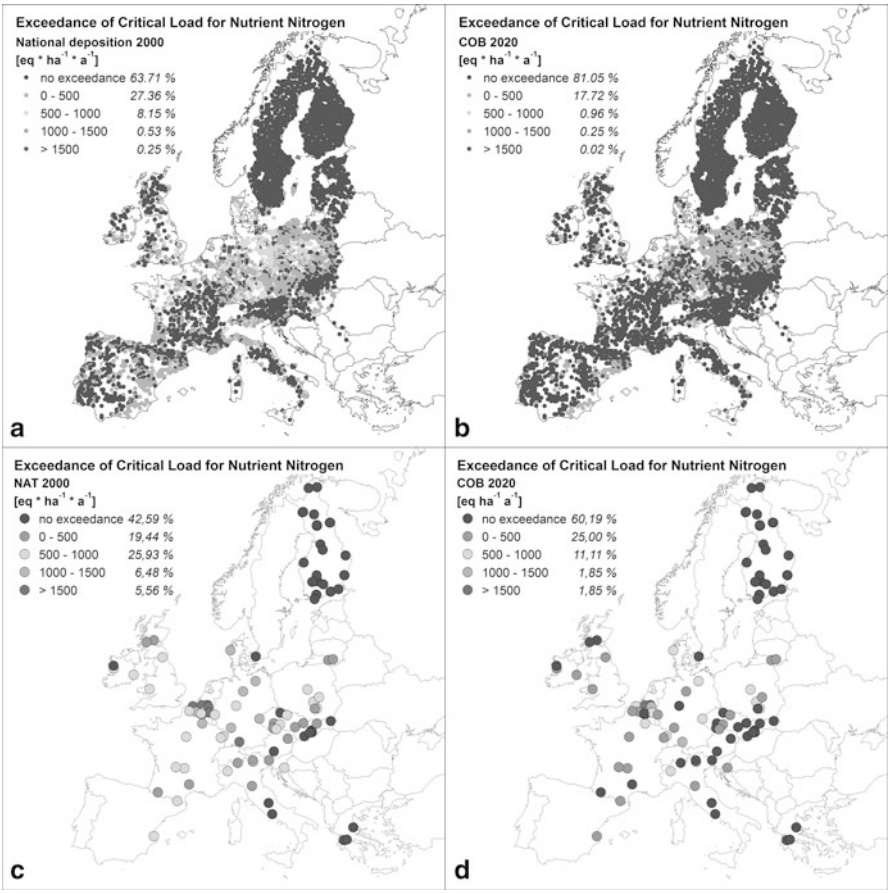

Fig. 15.1 Meteorological data and climate scenarios

the **nutrient nitrogen** shows a less successful progress. In 1980 only 54 % of the plots did not show any exceedance. Even if the deposition rates are mostly lower in 2000 the share of plots with exceedances decreased only by 10 % (Fig. 15.1c). The future scenarios show a further increase of the protected sites to 81 % (COB 2020, Fig. 15.1d) and 89 % of the plots (MFR), but even the maximum (technically) feasible reduction scenario wouldn't protect all sites from the risk of eutrophication.

ICP Forests does not measure meteorological parameters on Level I plots. Therefore, annual mean temperature and annual mean precipitation was extracted from New et al. [6] who offer gridded data of interpolated station means for the period 1961–1990.

For Level II plots A1B and B1 climate scenarios of the Intergovernmental Panel on Climate Change (IPCC) were applied assuming potential economic

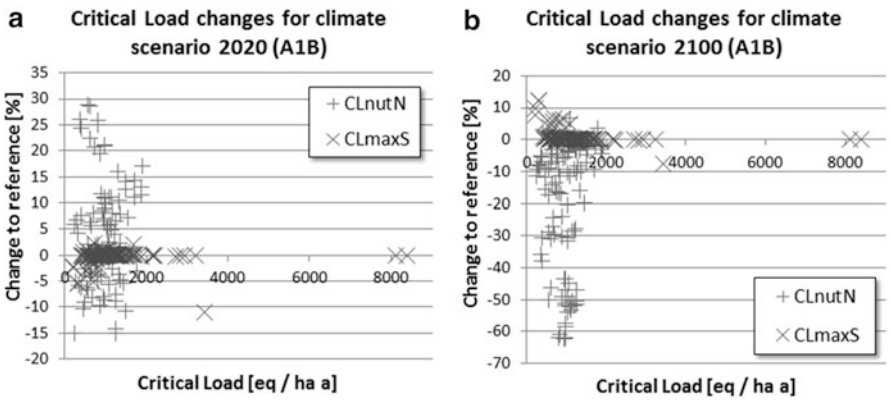

Fig. 15.2 Critical loads for level II for scenario 2020 (*left*) and scenario 2100 (*right*)

and social global development as defined in the Special Report on Emissions Scenarios (SRES). For Europe, the climate projections of the ECHAM5 model are regionalized to a resolution of 0.2° by the CLM model as calculated by Hollweg et al. [4]. Based on these data, further regionalization was carried out for Level II plots by calculating an area weighted mean for each meteorological parameter for a 30 km circular surrounding of each plot. For periods with measured meteorological data at the Level II plot, the mean monthly bias between observed and scenario parameters was calculated. In cases of missing measurements CRU data [8] were taken for bias estimations. Scenario values were corrected for local forest climate conditions applying this empirical bias correction.

Two future climate scenarios were obtained by this method, 2020 (A1B) and 2100 (A1B). Using these scenarios the Critical Loads for Level II plots were calculated again and compared with the reference climate (Fig. 15.2a, b). The Critical Load for acidification ($CL_{max}S$) doesn't show large differences. The variation of the Critical Load for nutrient nitrogen is significant and illustrates the strong effect of precipitation and temperature to the Critical Load.

15.3 Conclusion

The widespread and clear reduction of sulphur deposition starting in the 1980s shows the success of the clean air policies under the UNECE and the EU. For nitrogen inputs, however, the monitoring data and model results reveal less change (for **Level I** see Fig. 15.1a, b, for **Level II** see Fig. 15.3a, b). By relating past, present and future deposition scenarios to present stand and soil condition, critical load exceedances offer an important tool to assess deposition effects and their potential

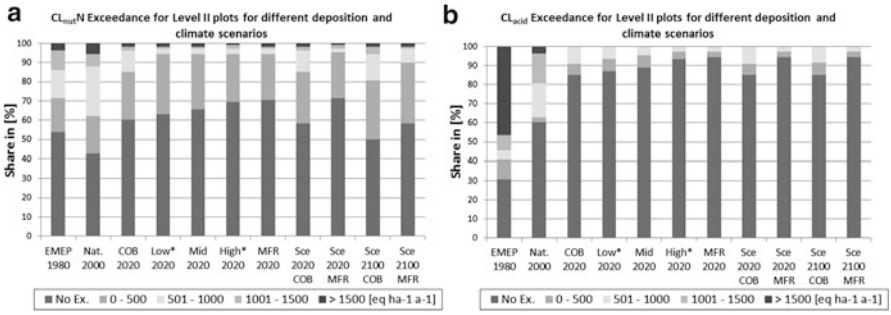

Fig. 15.3 Critical load exceedances for nutrient Nitrogen (*left*) and critical load exceedances for acidification (*right*) for level II plots for different deposition and climate scenarios

for damage to forest ecosystems. We show that on the European scale the rather unchanged nitrogen inputs are very obviously leading to continued exceedances of critical N loads. Even the full implementation of maximally technically feasible reductions will leave 10 % of the forest sites unprotected by the year 2020.

References

1. De Vries W, Erismann JE (eds) (1997) Ten years of monitoring forest condition in Europe. EC-UNECE, Brussels/Geneva
2. Fischer R, Lorenz M, Granke O, Mues V, Iost S, Van Dobben H, Reinds GJ, De Vries W (2010) Forest condition in Europe, 2010 Technical report of ICP forests. Work report of the Institute for World Forestry 2010/1. ICP Forests, Hamburg
3. Hettelingh J-P, Posch M, Slootweg J, Le Gall AC (2010) Analysis of environmental impacts caused by the baseline and maximum feasible reduction scenarios. In: Slootweg J, Posch M, Hettelingh JP (eds) Progress in the modelling of critical thresholds, impacts to plant species diversity and ecosystem services in Europe: CCE status report 2010, RIVM, Bilthoven
4. Hollweg HD, Böhm U, Fast I, Hennemuth B, Keuler K, Keup-Thiel E, Lautenschlager M, Legutke S, Radtke K, Rockel B, Schubert M, Will A, Woldt M, Wunram C (2008) Ensemble simulations over Europe with the regional climate model CLM forced with IPCC AR4 global scenarios. M & D Technical report 3, Max Planck Institut, Hamburg
5. Lorenz M, Nagel HD, Granke O, Kraft P (2008) Critical loads and their exceedances at intensive forest monitoring sites in Europe. Environ Pollut 155:426–435
6. New M, Lister D, Hulme M, Makin I (2002) A high-resolution data set of surface climate over global land areas. Clim Res 21:1–25
7. Nilsson J, Grennfelt P (1988) Critical loads for sulphur and nitrogen. Miljørapport 1988:15. Nordic Council of Ministers, Copenhagen
8. Mitchell TD, Carter TR, Jones PD, Hulme M, New M (2004) A comprehensive set of climate scenarios for Europe and the globe. Tyndall Centre working paper 55. Climatic Research Unit, University of East Anglia

Chapter 16
Application of the 1 km × 1 km Resolution FRAME Model to Poland for the Assessment of Ammonia and Ammonium Concentrations and Exceedance of Critical Levels

Maciej Kryza, Anthony J. Dore, and Małgorzata Werner

Abstract The total mass of ammonia emitted in Poland has dropped in recent years. Despite this decrease, Poland is still one of the European countries with the highest NH_3 emissions. Ammonia and ammonium air concentrations and deposition of reduced nitrogen in Poland were modelled with the Fine Resolution Atmospheric Multi-pollutant Exchange (FRAME) model with an increased resolution of 1 × 1 km for the years 2005 and 2008. The model results were compared with air concentrations measurements made at the EMEP sites. The modelled NH_3 concentrations were further used to calculate the CLEs exceedances for the Natura 2000 sites in Poland.

Keywords Frame-model • NH3

16.1 Introduction

The total mass of ammonia emitted in Poland has dropped in recent years from c.a. 320 Gg NH_3 in year 2005 to 285 Gg NH_3 in 2009. Despite this decrease in emission, Poland is still in a group of European countries with the highest emissions, together with France, Italy Spain and the United Kingdom. High emission of NH_3 in Poland leads to serious environmental problems related to acidification and eutrophication, with further consequences e.g. biodiversity loss [6].

M. Kryza (✉) • M. Werner
Department of Climatology and Atmosphere Protection, Wrocław University, Wrocław, Poland
e-mail: maciej.kryza@uni.wroc.pl

A.J. Dore
Centre for Ecology and Hydrology, Edinburgh, UK

D.G. Steyn et al. (eds.), *Air Pollution Modeling and its Application XXII*,
NATO Science for Peace and Security Series C: Environmental Security,
DOI 10.1007/978-94-007-5577-2_16,

To quantify the ecosystem exposure from the concentration of air pollutants, the critical level (CLE) is defined as the concentration in the atmosphere above which direct adverse effects on receptors, such as plants, ecosystems or materials, may occur according to present knowledge [8]. Recently new values of ammonia CLE for ecosystems protection have been defined by Cape et al. [1], based on up to date scientific background. For lichens and bryophytes, the long term CLE is set at 1 μg NH_3 m^{-3}. For higher plants, the long-term CLE is set at 3 μg NH_3 m^{-3}, with an uncertainty range of 2–4 μg NH_3 m^{-3}.

Ammonia and ammonium air concentrations and deposition of reduced nitrogen in Poland were modelled with the Fine Resolution Atmospheric Multi-pollutant Exchange (FRAME) model, with a 5 km × 5 km grid resolution. However, reports from the UK and Denmark suggest that this resolution may be insufficient for the assessment of NH_3 air concentrations because of the large local gradients in ammonia emissions and changes in vegetation and roughness [5, 9]. This may further lead to the insufficient protection of ecosystems. To address this issue, the FRAME model was applied here with the spatial resolution increased to 1 km × 1 km and used to calculate the NH_3 and NH_4^+ annual average air concentrations for two selected years 2005 and 2008. The model results were compared with air concentrations measurements made at the EMEP sites. The modelled NH_3 concentrations were further used to calculate the CLEs exceedances for the Natura 2000 sites in Poland.

16.2 Data and Methods

16.2.1 FRAME Model Description and Evaluation

FRAME is a statistical trajectory model that describes the main atmospheric processes in a column of air that travels along straight-line trajectories over the model domain. Detailed description of the model and its application for the United Kingdom is provided by Dore et al. [2] and Fournier et al. [4]. Here the model was applied for the area of Poland, with a domain of 800 × 800 grid cells of size 1 km × 1 km [7]. In the vertical, FRAME consists of 33 layers with thickness changing from 1 m at the surface to 100 m at the top of the domain. Boundary conditions for the model run are calculated with the FRAME-Europe model, that runs for the entire Europe with spatial resolution of 50 km × 50 km. The Polish national emission inventory for year 2008 was used in this study [3], and re-gridded onto the model grid [7]. For each year considered in this work, year specific meteorological data were used for modeling.

The FRAME model was run for year 2005 and 2008 and the results compared with $NH_3 + NH_4^+$ air concentrations measurements gathered at EMEP stations operating within the model domain (eight sites). The NH_3 only measurements were not available for model evaluation. The model was found to be in good agreement

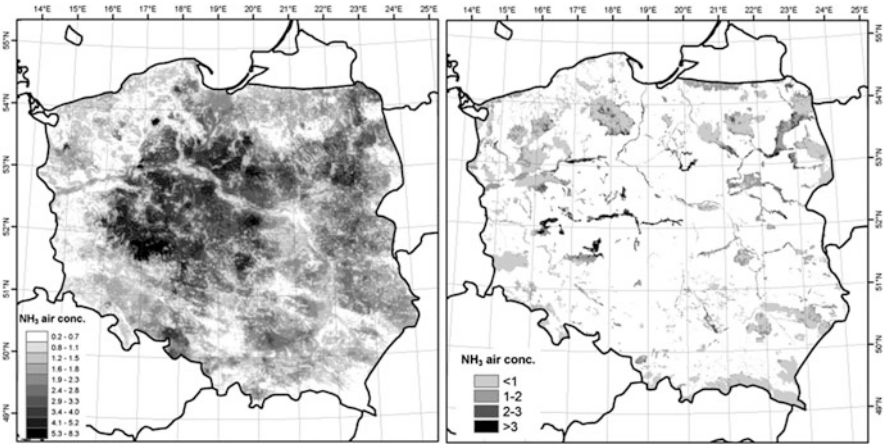

Fig. 16.1 Annual average NH_3 air concentrations for year 2005 (*left*, $\mu g\ m^{-3}$) and Natura 2000 sites in Poland (*right*)

with the measurements, with a Pearson correlation coefficient of 0.62 for year 2005 and 0.72 for 2008. The mean bias was −0.07 for year 2005 and 0.13 for year 2008. The number of modeled values which were within a factor of two of the measured value was 88 % for both years.

16.2.2 Natura 2000 Sites

Natura 2000 is the key instrument to protect biodiversity in the European Union. CLE exceedances were calculated and summarised for the Natura 2000 network. These are both Special Protection Areas, established within the frame of the Birds Directive, and Special Areas of Conservation, which are required by the Habitats Directive. The map of the Natura 2000 was obtained from the European Environment Agency website (Fig. 16.1), and imported into GIS GRASS package for further processing. In this study, the marine Natura 2000 sites were not considered. The total area of the Natura 2000 sites in Poland, calculated with this map is 78,948 km^2, and the total number of sites is 949.

16.2.3 Calculation of the Critical Levels

The method of quantification of the national level CLE exceedances used in this work directly follows the approach applied by Hallsworth et al. [5]. The FRAME modelled NH_3 air concentrations were grouped into three levels: less than 1 μg $NH_3\ m^{-3}$ (no risk to ecosystems), $\geq 1\ \mu g\ NH_3\ m^{-3}$, $\geq 2\ \mu g\ NH_3\ m^{-3}$, and $\geq 3\ \mu g$

Table 16.1 Summary statistics for the Area Weighted Indicator (AWI) and Designation Weighted Indicator (DWI) for Natura 2000 sites in years 2005 and 2008

	AWI (%)		DWI (%)	
CLE	2005	2008	2005	2008
$\geq$1 μg NH_3 m^{-3}	43	47	88	90
$\geq$2 μg NH_3 m^{-3}	11	13	39	44
$\geq$3 μg NH_3 m^{-3}	3	4	18	21

NH_3 m^{-3}, following the newly established CLEs proposed by Cape et al. [1]. Two indicators were applied to summarize these levels at national scale for all Natura 2000 sites at the national level: the Area Weighted Indicator (AWI) and the Designation Weighted Indicator (DWI). AWI quantifies the overall percentage area of the Natura 2000 sites in Poland with the CLE thresholds exceeded. AWI is defined as [5]:

$$AWI_{CLE} = \sum_j area\ exceeded\ site\ (j)_{CLE}$$

Where area exceeded site(j)$_{\mathrm{CLE}} = \sum_i A(i)$ in site (j) and where A(i) is any area in site j with mean concentration above CLE.

DWI is defined as the total number of Natura 2000 sites with any area with annual mean concentration of NH_3 above the CLE.

16.3 Results

FRAME calculated spatial pattern of NH_3 air concentrations are similar for both years considered (Fig. 16.1 – year 2005 as an example). The highest annual average concentrations of ammonia are calculated for central Poland, and exceed 8 μg NH_3 m^{-3}. These are the emission source areas, with the agriculture contributing the most. Natura 2000 sites located in central Poland are therefore in the highest risk due to CLE exceedances. The remote mountainous areas in the south and along the SW and SE country borders are relatively well protected.

The overall AWI and DWI statistics are summarized in Table 16.1. For AWI, almost half of the total area of the Natura 2000 is at risk due to high atmospheric ammonia concentrations. There is a small increase in AWI if years 2005 and 2008 are compared, which seems to be especially large for the $\geq$2 μg NH_3 m^{-3}. Nearly 90 % of Natura 2000 sites have some areas at risk due to the above $\geq$1 μg NH_3 m^{-3} air concentrations, which is described by DWI (Table 16.1). For the year 2008, over 40 % of the sites are at risk for both lichens and higher plants. Only c.a. 10 % of the Natura 2000 sites are not affected by the exceedances of NH_3 CLE.

16.4 Summary and Conclusions

In this chapter the preliminary assessment of the threat of NH_3 to the Natura 2000 sites in Poland was presented. The main findings are:

- The majority of the Natura 2000 sites are not well protected from high ammonia concentrations and the CLE for sensitive plants are exceeded for nearly 50 % of the total area and nearly 90 % of the total number of sites.
- The share of the total area and number of sites at risk is higher if compared with e.g. the United Kingdom [5].
- The areas at risk are closely related to domestic agricultural emissions of NH_3. The Natura 2000 sites along the country borders are relatively well protected.
- There is a tendency for an increase in the area and the number of sites at risk, but this has to be confirmed by the long term study.

References

1. Cape JN, van der Eerden LJ, Sheppard LJ, Leith ID, Sutton MA (2009) Evidence for changing the critical level for ammonia. Environ Pollut 157:1033–1037
2. Dore AJ, Vieno M, Fournier N, Weston KJ, Sutton MA (2006) Development of a new wind-rose for the British Isles using radiosonde data, and application to an atmospheric transport model. Q J R Meteorol Soc 132:2769–2784
3. Dębski B, Olendrzyński K, Cieślińska J, Kargulewicz I, Skośkiewicz I, Olecka A, Kania K (2009) Inwentaryzacja emisji do powietrza SO2, NO2, CO, NH3, pyłów, metali ciężkich, NMZO, TZO w Polsce za rok 2005. Institute of Environmental Protection
4. Fournier N, Dore AJ, Vieno M, Weston KJ, Dragosits U, Sutton MA (2004) Modelling the deposition of atmospheric oxidised nitrogen and sulphur to the United Kingdom using a multi-layer long-range transport model. Atmos Environ 38:683–694
5. Hallsworth S, Dore AJ, Bealey WI, Dragosits U, Vieno M, Hellsten S, Tang YS, Sutton MA (2010) The role of indicator choice in quantifying the threat of atmospheric ammonia to the 'Natura 2000' network. Environ Sci Policy 13:671–687
6. Krupa SV (2003) Effects of atmospheric ammonia (NH3) on terrestrial vegetation: a review. Environ Pollut 124:179–221
7. Kryza M, Werner M, Blas M, Dore AJ, Sobik M (2010) The effect of emission from coal combustion in nonindustrial sources on deposition of sulfur and oxidized nitrogen in Poland. J Air Waste Manage Assoc 60:856–866
8. Posthumus AC (1988) Critical levels for effects of ammonia and ammonium. In: Proceedings of the Bad Harzburg workshop, UBA, Berlin, pp 117–127
9. Skjoth CA, Geels C, Berge H, Gyldenkaerne S, Fagerli H, Ellermann T, Frohn LM, Christensen J, Hansen KM, Hansen K, Hertel O (2011) Spatial and temporal variations in ammonia emissions – a freely accessible model code for Europe. Atmos Chem Phys 11:5221–5236

Chapter 17
Air Pollution Assessment in the Dnepropetrovsk Industrial Megapolice of Ukraine

Larisa V. Shupranova, Valentina M. Khlopova, and Mykola M. Kharytonov

Abstract Extensive studies have been undertaken to assess the influence of industrial and transport emissions on the contents and compositions of storage proteins in the seeds of tree species – acacia (*Robinia pseudoacacia* L.) and horse chestnut (*Aesculus hippocastanum*) – in the Dnepropetrovsk area. These investigations have shown that specificity and variability in the component compositions of proteins in the studied plant varieties as well as the alterations in the types of distribution of their electrophoretic spectra and frequencies of their occurrence depend on the levels and nature of pollution suffered by the urban environment.

Keywords Air pollution • Biological indication • Wood plants seed • Protein markers • SDS-electrophoresis

The territory of the Dnepropetrovsk Region has been exposed to severe anthropogenous influence caused by intensive mineral mining operations and a great number of chemical, metallurgical and mining industries concentrated in the region. Hence, the levels of air and soil pollution in the industrial areas of the Dnepropetrovsk Region remain rather high [1, 2]. Plant species are more susceptible to the influence

L.V. Shupranova (✉)
Institute of Biology, Dnipropetrovsk National University, Dnepropetrovsk 49010, Ukraine
e-mail: ecohous@ukr.net

V.M. Khlopova
Dnepropetrovsk Hydrometeorological Center, Dnipropetrovsk 49600, Ukraine
e-mail: lnza@yandex.ru

M.M. Kharytonov
Ecology Department, Dnepropetrovsk State Agrarian University,
Dnepropetrovsk 49027, Ukraine
e-mail: mykola_kh@yahoo.com

D.G. Steyn et al. (eds.), *Air Pollution Modeling and its Application XXII*,
NATO Science for Peace and Security Series C: Environmental Security,
DOI 10.1007/978-94-007-5577-2_17,

of excessive levels of many dangerous air pollutants even when there are not yet evident signs of intoxication of humans or animals with the same harmful substances. Proteins, being the primary products of gene expression, represent information about genetic systems in the most explicit way. Therefore, an analysis of a protein phenotype provides a direct way for an analysis of a genotype. In this regard, the application of the method of protein markers in investigations of the impacts of pollutants on vegetation organisms seems to be the most appropriate approach in terms of its efficiency, because it provides a reliable assessment of quality of the urbanized areas. With the above in view, the goal of the present research was to apply genetic-environmental approach as a tool for investigating the impacts of industrial and motor transport emissions on woody plants condition in the Dnepropetrovsk Region.

The monitoring of atmospheric air pollution in the environment of the Dnepropetrovsk megalopolis area was carried out in the city of Dnipropetrovsk and its satellite city Dneprodzerzhynsk with use of the network of stationary monitoring stations at the Dnepropetrovsk Regional Center of Hydrometeorology. The initial evaluation of technogenic atmospheric pollution with toxic substances was performed with due to the limit values of so-called maximum permissible concentrations (MPCs) for harmful emissions in the atmosphere as set out in the Ukrainian Air Quality Standards.

The seeds of acacia (*Robinia pseudoacacia* L.) were collected in different locations of the city of Dnepropetrovsk suffering from motor transport emissions, i.e. along the highways with the average traffic activity of 2.360 vehicles per hour (site No. 1) and in the territory of the Botanical Garden at Dnepropetrovsk National University (site No. 2), and also in the proximity of the ore mining operations in the town of Manganetz (site No. 3).

The seeds of horse chestnut were collected in the territory of metallurgical operations in Dneprodzerzhynsk and also along the highways with the average traffic activities of 1.740 and 2.360 vehicles per hour (sites Nos. 1 and 2, respectively). The seeds for the control group of trees were collected in the areas where the concentration of pollutants did not exceed the maximum permissible standard values. Proteins in the seeds constitute multicomponent systems of individual polypeptides, and the patterns of their arrangement were detected by means of SDS-electrophoresis. While analyzing an individual sample set comprising 50–100 seeds, the following parameters were defined: the total number of spectrum types as an inherent characteristic of each level of polymorphism in the seed proteins, a quantitative ratio of spectrum types, and frequencies of occurrence of the most common spectrum types in the plants being studied.

The most crucial factors which determine the quality of the atmosphere in the megalopolice of Dnepropetrovsk are the amounts and compositions of industrial emissions. The range of pollutants depends on the number and types of the industrial enterprises located within the urban area. The values of complex indices of air pollution (CIAPs) in Dnepropetrovsk and Dneprodzerzhinsk for the period of 2009–2011 are presented in Table 17.1.

Table 17.1 The values of complex indices of air pollution (CIAPs) in 2009–2011 in the Dnepropetrovsk megapolice area

	CIAPs, %		
City	2009	2010	2011
Dnipropetrovsk	9.07	10.27	11.70
Dniprodzerzhinsk	14.00	15.40	12.17

Table 17.2 Frequency of spectrum types occurrence of storage proteins of *R .pseudoacacia* L. seeds, selected from areas with different level and composition of pollutants

	Frequency of spectrum types occurrence, %			
Number of spectrum types	Control	Site No. 1	Site No. 2	Site No. 3
β-zone				
1	15.8	10.5	13.2	2.6
2	13.2	–	–	23.7
3	10.5	–	–	7.9
4	15.8	5.3	–	–
5	10.5	–	–	18.4
6	2.6	7.9	7.9	13.2
7	10.5	13.2	2.6	13.1
8	15.8	5.3	–	–
9	5.3	13.2	2.6	–
10	–	–	–	21.1
11	–	36.8	31.6	–
12	–	5.3	15.8	–
13	–	2.5	26.3	–
γ-zone				
1	29.0	15.8	18.4	36.8
2	15.8	–	7.9	7.9
3	18.4	7.9	13.2	2.6
4	18.4	–	–	–
5	10.5	21.0	7.9	47.4
6	7.9	2.6	–	5.3
7	–	39.5	50.0	–
8	–	13.2	2.6	–

The electrophoretic investigations of proteins in individual *Robinia* seeds showed that the widest phenotypic diversity was inherent to the β- and γ-zones, which contained from one to six components and a number of their combinations. It has been found that the *R. pseud i* L. trees from different types of the technogenic environment are distinct from one another by the number of their spectrum types and frequencies of their occurrence (Table 17.2).

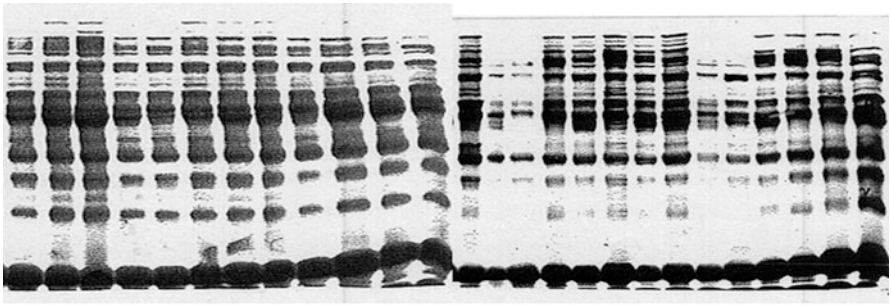

Fig. 17.1 The electrophoretic spectra of storage proteins of individual seeds of *Ae. hippocastanum* L. selected from clean zone (I) and from territories of Metallurgical Works (II)

It was established that majority seeds of *Ae. hippocastanum* L. taken in area neighboring with Metallurgical Plant in Dneprodzerzhinsk city have got more poor composition of protein (Fig. 17.1).

It was shown various reactions of individual seeds that were formed in identical conditions as well.

Using genetic-environmental approach, the impacts of industrial and motor transport emissions on deciduous woody tree species was assessed by testing the seed samples of the plants. Compared to the control samples, the seeds of the deciduous plants from the polluted environment had some disorders in protein metabolism that make themselves evident in altered contents of the storage proteins, their component compositions, the number of the types of electrophoretic spectra and their ratios, and frequencies of their occurrence. The proposed method for investigation of seed protein variability allows to expand the possibility of the assessment of the genetic structure and diversity of deciduous plant species under changing conditions of their existence.

References

1. Kharytonov M, Kroik A, Vinnichenko O et al (2007) Air pollution assessment related with large industrial city activities. In: Barnes I, Kharitonov M (eds) Simulation and assessment of chemical processes in a multiphase environment. NATO science for peace and security – series C: environmental security, Springer, Dordrecht, pp 385–393
2. Vasilyeva T, Duka Y, Kharytonov M (2006) Alleviation of toxic impact of chemical agents on human organism. NATO advanced research workshop on medical treatment of intoxications and decontamination of chemical agents in the area of terrorist attack. Springer, Dordrecht, pp 263–274

Chapter 18
Decision Making Problem Under Uncertainties Relating to Air Quality Management

Volodymyr I. Nochvai

Abstract Air pollution models are still associated with large uncertainties. The accuracy of air pollution models depends on uncertainty in the input parameter values and errors in model formulation. Meteorological parameters are influenced by random factors. Emission parameters are usually estimated rather roughly. These uncertainties have to be taken into account when we solve the decision making problems in air quality management systems. For this purpose the methods of optimization under uncertainty and fuzzy decision-making models are used. The model of multi-objective optimization is developed for fuzzy decision making in information systems for air quality management.

Keywords Multi-objective optimization • Emission parameters • Fuzzy decision making • Air quality management • Uncertainties

18.1 Introduction

Air pollution models are still associated with large uncertainties [1]. Development of methods for quantifying the uncertainty associated with human input needs to be considered in relation to the incorporation of uncertainty in decision-making processes [2].

The accuracy of air pollution models depends on uncertainty in the input parameter values and errors in the models formulation. The basic input data for the models are the meteorological parameters and emission estimates. Details of the meteorological parameters mostly are probabilistic in nature and often appear in the form of statistical characteristics. Emission parameters are usually estimated

V.I. Nochvai (✉)
Pukhov Institute for Modeling in Energy Engineering, National Academy of Science Ukraine, Kyiv, Ukraine
e-mail: volivn@ukr.net

D.G. Steyn et al. (eds.), *Air Pollution Modeling and its Application XXII*,
NATO Science for Peace and Security Series C: Environmental Security,
DOI 10.1007/978-94-007-5577-2_18,

rather roughly. Accurate calculation requires consideration of each emission source separately. As usual, this is not possible for regions with a large number of stationary and mobile sources. But the spatial characteristics of impacts are quite significant for the tasks of urban air quality management. Biogenic emissions are usually underestimated. Recent studies [1] suggest that air quality models produce the degree of uncertainty of results within factor of two. These uncertainties have to be taken into account when we solve the decision making problems in the air quality management systems.

18.2 Multi-objective Optimization Relating to Air Pollution

The usual tasks of multi-objective optimization relating to air pollution are both minimizing of environmental cost functions (air quality damage) and the control cost to ensure quality standards in the most effective way using the technical and economical means [3–6]. This can be expressed using generalized criteria [7] for n_c-cost functions with a given vector of preference $\boldsymbol{\rho}$:

$$F(Q) = \sum_{i=1}^{\mathrm{n_c}} \rho_i w_i(Q) \to min,$$

where $Q = \{{Q_s}^j\}$, $0 \le {Q_s^j}^{\min} \le {Q_s}^j \le {Q_s^j}^{\max}$ is the vector of control variables: emission rates of j-pollutant from s-source, $s = \{1, \ldots, n\}$.

Constraints for j-pollutant concentration (${Y^j}_k$) near surface in an area k: ${Y^j}_k \le \tilde{n}_{kd}^j$

$\tilde{n}_{kd}^j$ denotes the admissible level of air pollution in k-zone.

Diverse cost functions can be brought to comparable form with dimensionless transformation using Ideal point (f_i^o) method:

$$w_i(f_i(Q)) = \begin{cases} \dfrac{f_i^o - f_i(Q)}{f_i^o}, \forall i \in MaxF, \\ \dfrac{f_i(Q) - f_i^o}{f_i^o}, \forall i \in MinF. \end{cases}$$

18.3 Decision Making Under Uncertainties

It is important to assess the risks of elevated air pollution levels that occur in the region during some weather conditions that conducive to this. Meteorological parameters, can be calculated in meteorological models with a certain degree of

accuracy, and are measured only at specific time periods in separate points of the region. It is possible for each atmosphere condition ω_l to estimate the probability of its realization for the given period of time in the region.

Let's impose a condition for safe concentrations for all even unfavorable weather conditions. To minimize the risk of harmful effects on environmentally sensitive areas (kindergartens, schools), it is appropriate to apply the guaranteed estimation of the maximin criterion to eliminate uncertainty.

$$Y(Q,q)_{kj} = \max_{\omega_l \in \omega} Y(Q,q,\omega_l),$$

where q – random parameter that characterizes the error and incompleteness of emissions estimates.

Then, for the case of a pessimistic emission scenario:

$$Y(Q) = \max_{q\in\Omega} Y(Q,q);\ Q^* = \arg\min_{Q\in U} \max_{q\in\Omega} F(Q,q).$$

Whereas for other zones more optimistic criteria can be used, such as Hurwitz criterion that allows to specify a compromise between extreme pessimism and extreme optimism:

$$Y(Q) = \alpha \min_{q\in\Omega} Y(Q,q) + (1-\alpha) \max_{q\in\Omega} Y(Q,q)$$

The weighting factor $\alpha \in [0,1]$ characterizes the degree of risk that is allowed by decision-makers in achieving this criterion.

Also, it is possible to use Maximum Likelihood estimation for emissions $\bar{q}$ using the criterion $Y(Q) = Y(Q,\bar{q})$. For example, business-as-usual emission scenario [8] may be appropriate for this case. Then the solution of the optimization problem is: $Q^* = \arg\min_{Q\in U} F(Q,\bar{q})$

18.4 Fuzzy Decision Making Model

We can give to the decision-makers the ability to set thresholds for possible constraint violations and deviations from the desired target function using fuzzy programming [9]. The optimization task for air quality management can be written in the form of fuzzy decision making model:

$$F(x) = \sum_{i=1}^{n} \rho_i w_i(Q,q) \lesssim z_0,$$

$$Y(Q,q,\omega)_{kj} \lesssim c_{k j \tilde{a} \tilde{a} \tilde{a}},\ \mathrm{j} = 1,\ 2,\ldots,\mathrm{m},\ \mathrm{k} = 1,\ 2,\ldots,\mathrm{n}$$

with fuzzy sets of the objective function and constraints:

$$\mu_F(x) = \begin{cases} 0, if\ F(x) \le z_0; \\ \mu(x,a), if\ z_0 < F(x) < z_0 + a; \\ 1, if\ F(x) \ge z + a; \end{cases}$$

$$\mu_{\tilde{n}}(x) = \begin{cases} 1, if\ c(Q,q,\omega)_{kj} \ge c_{k\,j_{a\tilde{i}\tilde{i}}} + b; \\ \mu(x,b), if\ c_{k\,j_{\tilde{a}\tilde{i}\tilde{i}}} < c\,(Q,q,\omega) < c_{k\,j_{a\tilde{i}\tilde{i}}} + b; \\ 0, if\ c(Q,q,\omega)_{kj} \le c_{k\,j_{\tilde{a}\tilde{i}\tilde{i}}}; \end{cases}$$

where $\mu(x,a)$, $\mu(x,b)$ – the functions $X \to [0;1]$ that are correspondent to inequalities accomplishment degree, in terms of the decision-makers. Decision support system may offer a set of graphs of the membership function to decision maker choice.

z_0 – is some reasonable value of the objective function; b, a – thresholds that are set by decision-makers for constraint violations and deviations from the desired target function.

A compromise settlement can be obtained where the minimum k_0 of weighted loss with all criteria does not exceed: $\rho_i w_i(Q,q) \le k_{0\min}, i = 1..n_c$.

If the number of criteria is not very large and criteria can be arranged through interaction with the decision-makers in the process of a problem solving then the vector of gradient can be calculated:

$$Q_i^{(j+1)} = \max\left\{0; {Q^j}_i + \lambda' \sum_{l=1}^{n} \mu_l \rho_l \frac{\partial w_i(Q)}{\partial Q_i^j} + \lambda \sum_{l=1}^{n} \mu_l \rho_l \partial\left(\frac{C(Q,q)}{C_{\tilde{a}\tilde{i}\tilde{i}}^j}\right)/\partial Q_i^j\right\}$$

18.5 Concluding Remarks

The Fuzzy model enables the decision-makers 'to move' a set of compromise points. This also allows us to formalize in the optimization problem such fuzzy values as "greatly exceed health standards", "slightly exceed" with correspondent risk levels. The interaction with a decision-maker through the user interface is necessary to provide implementation of this in the fuzzy decision support system. Thus, it is desirable to interview experts among specialists of the local sanitary-epidemiological and environmental services for objective determination of the threshold b. Fuzzy decision support system is perspective framework for including different aspects of uncertainties, expert knowledge and the decision-makers preferences to the decision making model.

References

1. Fisher B (2006) Fuzzy approaches to environmental decisions: application to air quality. Environ Sci Policy 9(1):22–31
2. Ascough JC II, Maier HR, Ravalico JK, Strudley MW (2008) Future research challenges for incorporation of uncertainty in environmental and ecological decision-making. Ecol Model 219:383–399
3. Ismael A, Vaz F, Ferreira EC (2009) Air pollution control with semi–infinite programming. Appl Math Model 33:1957–1969
4. Holnicki P (2006) On the real-time emission control – case study application. Control Cybern 235:351–367
5. Carnevale C, Pisoni E, Volta M (2008) A multi-objective nonlinear optimization approach to designing effective air quality control policies. Automatica 44:1632–1641
6. Marchuk GI (1986) Mathematical models in environmental problems. Elsevier Science, Amsterdam
7. Nochvai VI (2012) Multi-objective optimization of emission parameters for air pollution models. In: Steyn DG, Trini Castelli S (eds) NATO science for peace and security series C: environmental security, vol 4, Part 7. Springer, Dordrecht, pp 705–709
8. Cai YP, Guo H, Huang Q, Lin G, Xiang-hui Nie, Tan Q (2009) An optimization-model-based interactive decision support system for regional energy management systems planning under uncertainty. Expert Syst Appl 36(2):3470–3482
9. Zaichenko (2006) Operation research. Kyiv, p 816, (In Ukrainian)

Part III
Aerosols in the Atmosphere

Chapter 19
Impact of Aerosol Radiation Absorption on the Heat Budget and Dynamics of the Atmospheric Boundary Layer

Eduardo Wilde Barbaro, Jordi Vilà-Guerau de Arellano, Maarten C. Krol, and Albert A. M Holtslag

Abstract The impact of aerosol radiation absorption on the heat budget and the dynamics of the PBL has been investigated using a Large Eddy Simulation model.

Keywords LES-model • PBL • Aerosol • Absorption

19.1 Introduction

The aerosol absorption of heat within the atmospheric boundary layer (ABL) can bring modifications on the ABL dynamics and therefore, in the boundary layer height. Briefly, shortwave radiation (SW) is scattered and absorbed by the aerosol layer. This process leads to a decreased surface sensible heat flux, might induce a weaker thermal inversion and an enhanced ABL stratification. Here, we investigate how a characteristic ABL formed in the afternoon hours is perturbed by the aerosols heat absorption.

Following Yu et al. [1] and Gao et al. [2], the effect of aerosols in the ABL dynamics is still a broad open field. Especially studies about how the heat induced by the SW absorption perturbs the vertical structure of the ABL in terms of dynamics of the thermal inversion and the upper mixed layer are still lacking. Angevine et al. [5] proposed that SW absorption translates to a heating of about 3–5 K/day while Raga et al. [6] has found for Mexico City heating rates that can be bigger than 10 K/day depending on the vertical distribution of the aerosols. The main objective of this work is to investigate the disturbances in the heat budget caused by aerosol shortwave radiation absorption with focus on the CBL vertical structure. Numerical simulations are carried out with a large-eddy simulation model (DALES – project

E.W. Barbaro (✉) • J.V.-G. de Arellano • M.C. Krol • A.A. M Holtslag
Meteorology and Air Quality Department, Wageningen University, Wageningen, The Netherlands
e-mail: eduardo.wildebarbaro@wur.nl; Jordi.vila@wur.nl

D.G. Steyn et al. (eds.), *Air Pollution Modeling and its Application XXII*,
NATO Science for Peace and Security Series C: Environmental Security,
DOI 10.1007/978-94-007-5577-2_19,

SH-060-10) in order to study both the CBL vertical structure and time evolution. The latter result is also supported by a 0-order bulk model (MXL). The objective is comparing the results obtained by a complex 3D model with the ones derived from a 0-order model. In order to get a realistic impact of the radiation field, the simulations have the support of a radiative transfer code (TUV).

19.2 Theoretical Background

The starting point is the relation between the divergence of net irradiance (F) and actinic flux (ϕ) in an atmosphere perturbed by absorbing aerosols. Following Madronich [3] and Bierwirth et al. [4], the expression reads:

$$\phi\overline{\sigma_a} = -\frac{dF}{dz} \tag{19.1}$$

where σ_a is the average amount of absorbing particles over a layer (m^{-1}).

Equation 19.1 connects the divergence of net irradiance with the amount of radiation which is absorbed in all directions through the layer by aerosol particles. The heating rate (HR, in Ks^{-1}) can be derived from both sides of the Eq. (19.1) by normalizing it by the air density and the thermal capacity (ρc_p) as it follows:

$$\mathrm{HR} = \frac{1}{\rho c_p}\phi\overline{\sigma_a} = -\frac{1}{\rho c_p}\frac{dF}{dz} \tag{19.2}$$

The physical interpretation of Eq. (19.2) indicates that by calculating the expression based on the actinic flux, we quantify the radiation absorbed in all directions by the amount of particles *inside* the layer (e.g. [2]) whereas the net irradiance considers the divergence *over* the layer (e.g. [5, 6]). Since the actinic flux and net-irradiance are commonly used for different purposes [4], the preferred expression is mainly a matter of convenience.

19.3 Numerical Experiments: Effects of the Aerosol Heat Absorption

A numerical experiment (control) is designed assuming an ABL in steady-state like the ones observed in the afternoon period, i.e. hardly any change on time. This steady ABL can be altered by the presence of an absorbing aerosol layer. In order to evaluate the impact of the aerosols within the ABL, three additional experiments (Table 19.1) are designed, characterized by different aerosol concentrations (τ). The radiation field (net-irradiance and actinic flux) is calculated by the TUV model [3].

Table 19.1 Numerical experiments simulated with DALES and MXL

Case	$\overline{\sigma_a} \times 10^{-6}$ (m^{-1})	τ	$\overline{HR}$ ($Kday^{-1}$)
Control	0	0.0	0.0
AC	25	0.2	3.2
HC	55	0.5	7.0
EC	90	0.8	10.2

The radiation variables are calculated using TUV
AC average aerosol concentration, *HC* high aerosol concentration, *EC* extreme aerosol concentration

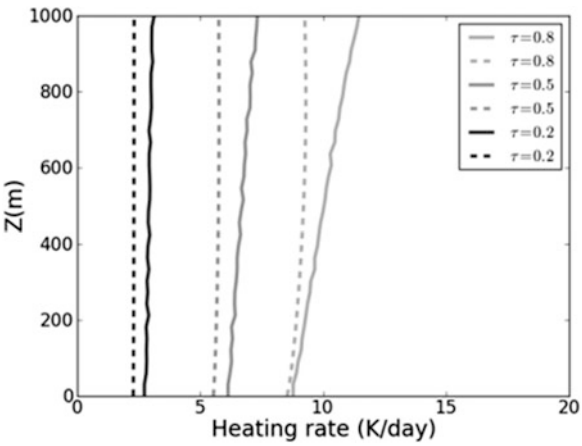

Fig. 19.1 Heating rate vertical profiles calculated by TUV model using actinic flux (*continuous lines*) and the divergence of the net-irradiance (*dotted lines*). The *gray-scale* indicates different aerosol concentrations based on the Table 19.1

In order to keep the experiments energy consistent, the sensible heat flux at the surface is reduced proportionally to the heating induced by the aerosols.

Figure 19.1 shows the heating rate vertical profiles calculated by using Eq. (19.2) for the conditions shown in the Table 19.1. The results indicate a similar HR by using either actinic flux or net-irradiance divergence expressions. The differences between the two approaches are due to the fact that a constant σ_a throughout the CBL is assumed.

19.4 Aerosols Impact on the ABL Evolution and Vertical Structure

Since the AC case is the most representative of an average polluted continental situation (e.g. [5, 6]), it was selected to be further investigated. In addition to the profile obtained by the TUV model (light gray lines), a second experiment (TOP) is designed, where the heating is totally placed at the top of the ABL (dark gray lines in Figs. 19.2 and 19.3). The objective is to analyze the role of the vertical distribution of aerosols within the ABL.

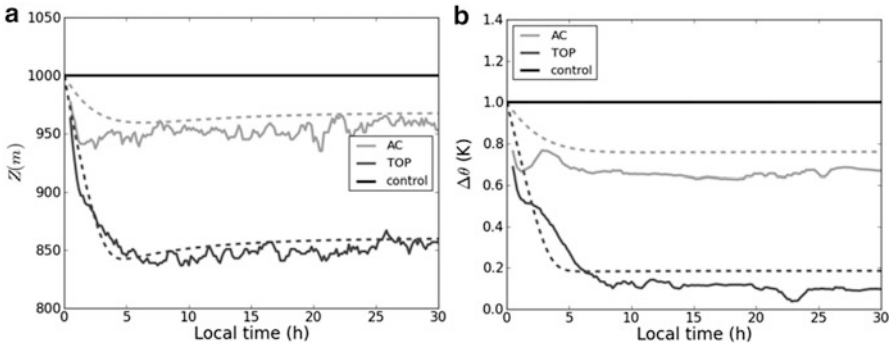

Fig. 19.2 CBL height evolution (**a**) and inversion layer intensity (**b**) for both vertical distributions (*AC* and *top*). The *black line* represents the reference case. The *full lines* indicate DALES results and the *dots* MXL

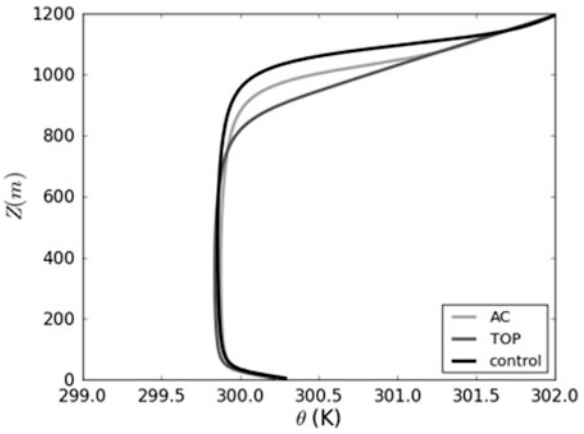

Fig. 19.3 Potential temperature vertical profile (*AC* and *top*). The *black line* represents the reference case

Figure 19.2a shows the evolution of the ABL height for the reference, AC and TOP cases. As expected, in the reference case, the ABL height is constant on time; however, it decreases when the aerosol layer is present. The reduction is even more pronounced when the heating is located all at the top of the ABL (dark gray). The effect of aerosols on the strength of the thermal layer ($\Delta\theta$) is displayed in Fig. 19.2b. The differences on the weakening of the thermal layer are due to the heating at the top of the ABL, since the same surface heat flux is applied to both cases. Note that the MXL model is able to reproduce the DALES results.

Figure 19.3 shows the vertical profile of the potential temperature for the three same cases. It indicates that the aerosol heating leads to a stratification of the ABL below the inversion layer. This stratification is stronger when the aerosols are concentrated at the top of ABL (dark gray). Stabilization of the upper mixed-layer homogenizes the flow and is the responsible physical mechanism for preventing the CBL growth.

Our main findings indicate that the boundary height decreases compared to a clear condition (no aerosols). The thermal inversion diminishes, (positive feedback for the boundary layer growth) however this feedback is counterbalanced by the stratification of the upper mixed layer, due to the aerosol heating absorption.

References

1. Yu H, Liu SC, Dickson RE (2002) Radiative effects of aerosols on the evolution of the evolution of the atmospheric boundary layer. J Geophys Res 107(D12). doi:10.1029/2001JD000754
2. Gao RS et al (2008) Calculations of solar shortwave heating rates due to black carbon and ozone absorption using in situ measurements. J Geophys Res 113(D14203). doi:10.1029/2007JD009358
3. Madronich S (1987) Photodissociation in the atmosphere: actinic flux and effects of ground reflections and clouds. J Geophys Res 92(D8):9740–9752
4. Bierwirth E et al (2010) A new method to retrieve the aerosol absorption coefficient from airborne flux density and actinic radiation measurements. J Geophys Res 115(D14211). doi:10.1029/2009JD013636
5. Angevine WM, Grimsdell AW, McKeen SA, Warnock JM (1998) Entrainment results from the Flatland boundary layer experiments. J Geophys Res 103(12):13689–13701
6. Raga GB, Castro T, Baumgardner D (2001) The impact of megacity pollution on local climate and implications for the regional environment; Mexico city. Atmos Environ 35:1805–1811

Questions and Answers

Questioner Name: Yosef Levitin

Q: What source of surface heat flux of 100 Wm^{-2}?
A: We prescribe during the whole simulation in both mixed-layer and large-eddy simulation models a constant surface sensible heat flux (SH) of 0.1 mKs^{-1} for the REF experiment. For UNI and TOP the SH is reduced to 0.08 mKs^{-1} due to the aerosol shadowing at the surface.

Q: Do you use different models for rural and urban areas?
A: We do not have land-use or surface heterogeneity. We consider a flat and homogeneous surface for all the experiments with a constant and prescribed surface sensible heat flux.

Questioner Name: Peter Buitjes

Q: Is there an explanation why the uniform case height of the ABL goes faster to equilibrium than the aerosol-cases?
A: Since the aerosols initial condition in the UNI is already uniformly distributed in the mixed-layer, the equilibrium is reached around 2 h before than the TOP experiment. In addition, the aerosol layer in the TOP experiment disturbs more the inversion layer jump (Fig. 19.2b) and as a consequence additional time is needed to reach a new equilibrium state.

Chapter 20
Impact of Different Physical Parameterizations on the Global Modeling of Desert Dust – Importance of the Initialization Fields

Marina Astitha, Jos Lelieveld, Alexander de Meij, Astrid Kerkweg, Mohamed Abdel Kader, Andrea Pozzer, and Gregor Gläser

Abstract In this work we use the atmospheric chemistry general circulation model EMAC (ECHAM5/MESSy2 Atmospheric Chemistry) with new physical parameterizations of desert dust emissions. We assess the impact of the different physical parameterization schemes, highlight the importance of several initialization fields, identify the key-input parameters and explore the benefits and/or disadvantages of using a-priori sources of atmospheric dust particles. This presentation will discuss primarily the processes that lead to dust emissions and explore the difficulties that arise from a global parameterization applied to areas with different and heterogeneous soils (e.g. North African versus Asian deserts). The performed case studies and sensitivity tests include comparisons with in-situ measurements of dust concentrations and satellite retrievals of aerosol optical depth. The conclusions from this work include recommendations on selecting the input fields depending on the application, in order to improve the modelling of dust globally.

Keywords ECHAM/Messy – model • Desert dust

M. Astitha (✉) • A. de Meij • M.A. Kader
Energy, Environment and Water Research Centre, The Cyprus Institute, Athalassa Campus, Nicosia, Cyprus
e-mail: m.astitha@cyi.ac.cy

J. Lelieveld
Energy, Environment and Water Research Centre, The Cyprus Institute, Athalassa Campus, Nicosia, Cyprus

Max Planck Institute for Chemistry, Becherweg 27, 55128 Mainz, Germany

A. Kerkweg • G. Gläser
Institute for Atmospheric Physics, University Mainz, 55128 Mainz, Germany

A. Pozzer
Earth System Physics Section, International Centre for Theoretical Physics, Trieste, Italy

D.G. Steyn et al. (eds.), *Air Pollution Modeling and its Application XXII*,
NATO Science for Peace and Security Series C: Environmental Security,
DOI 10.1007/978-94-007-5577-2_20,

20.1 Introduction

Modeling the dust emissions globally has proven a challenging task due to the balance needed between input fields and output accuracy in representing the arid areas of the world. The phenomenon of dust particles emitted in the atmosphere through saltation bombardment is of episodic nature and takes place in small spatial and temporal scales, whereas the multiple effects of dust in the environment are of global interest. The uncertainties that span the dust emission process are indicated by the large variety of global models using different parameterization schemes, input parameters and removal procedures [1, 5–7]. The aim of this presentation is to explore the difficulties of modelling the dust emission using an atmospheric chemistry global model and assess the impact of two different physically-based dust emission parameterizations in the global dust distribution. This is accomplished by performing annual simulations with the different parameterization schemes which are evaluated using in situ measurements and aerosol optical depth retrievals in several locations globally, following the AEROCOM dust benchmark dataset as used in Huneeus et al. [2].

20.2 Dust Production Scheme in the EMAC Model – Differences in the Parameterization Schemes

The ECHAM5/MESSy2.41 Atmospheric Chemistry (EMAC) model is used for the implementation of the new dust production scheme. The EMAC model is a combination of the ECHAM5 general circulation model and the Modular Earth Submodel System [3]. The MESSy system is modular and all sub-models follow strict coding standards to allow easy implementation within other models. The EMAC model was run with a spectral resolution of T106 ($\sim 1.1° \times 1.1°$) and 31 vertical levels up to 10 hPa for the year 2000.

The two physical dust emission parameterization schemes are based on the same principles and methodology, as presented in Marticorena et al. [4] and applied in Zender et al. [7] among others. The main difference between the two schemes (referred to as DU1 and DU2) is the inclusion of an explicit soil size distribution using the Zobler soil texture classification (in DU2), as opposed to assuming an optimal size for saltation at 60 μm particle diameter (DU1). This has an immediate consequence to the calculation of the horizontal and vertical dust flux and to the threshold friction velocity needed for the initiation of the emission process. The impact of these two emission schemes in the global distribution of desert dust is assessed through annual simulations for the year 2000 and through evaluation of the results using dust concentration measurements and aerosol optical depth. A brief discussion on the findings from this work is given in the following section.

20.3 Results and Discussion

The dust emissions produced from the two parameterization schemes DU1 and DU2 are not seasonally different as can be seen in Fig. 20.1.

The discrepancies between the parameterizations do not depend on the seasonality but rather on the soil maps and the assumptions on the source size distribution. The differences are mostly region-sensitive, with N. Africa producing less dust emissions with the DU2 and to a smaller extent so is Australia and S. Africa. Especially for N. Africa, the geographical pattern shows fewer dust emissions with DU2 for more Central African deserts (Sahara, Mauritania, Bodele Depression) and higher emissions for the northern part (Libya, Algeria). This is a direct effect of the size distribution assigned to the soil in DU2, because the parts of Sahara, Bodele depression and Mauritania include mostly coarse particles, while in the northern part we find more medium type particles (according to the Zobler classification).

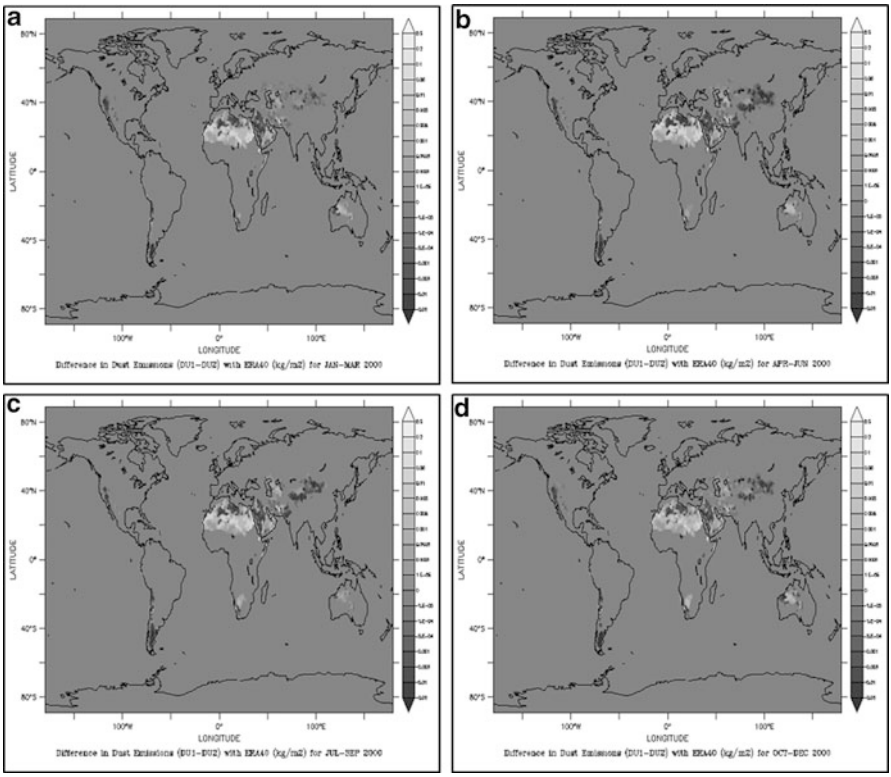

Fig. 20.1 Difference in the seasonal dust emissions (kg/m^2) between the nudged simulations for the year 2000 (DU1-DU2): (**a**) January to March, (**b**) April to June, (**c**) July to September and (**d**) October to December

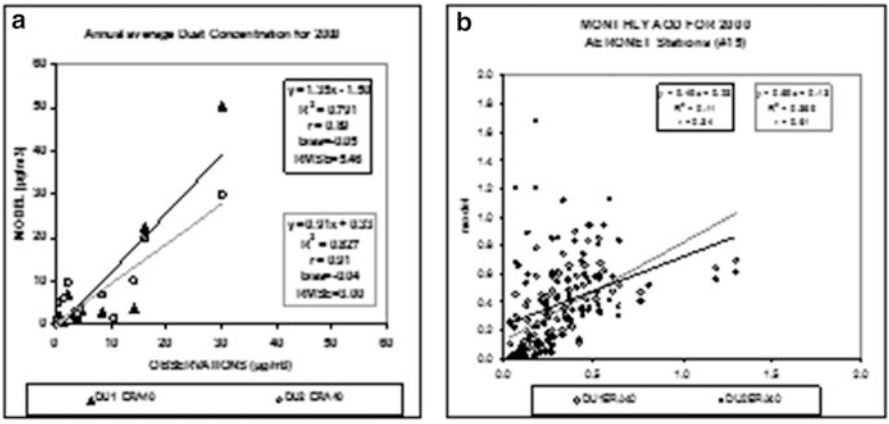

Fig. 20.2 (**a**) Comparison of annual average dust concentration in 24 stations for both emission schemes DU1 and DU2. (**b**) Comparison of monthly AOD from AERONET stations with modeled AOD for both emission schemes

The evaluation of the model's performance with DU1 and DU2 showed a diversity that depends on the type of measurements used for the comparison. For example, when using stations with dust concentration or deposition which are located away from the main dust source areas, the DU2 is performing slightly better than DU1 (Fig. 20.2a). When evaluating the modelled AOD with AERONET data by choosing stations as closer to the dust sources as possible, the DU1 scheme shows a better correlation with the observations than DU2 (Fig. 20.2b). A main conclusion from this work is the necessity to treat each arid region of the world differently, respecting the diversity of the soils releasing dust particles in the atmosphere and trying to resolve the meteorological conditions favoring such processes with a global atmospheric chemistry model.

Acknowledgments The research leading to these results has received funding from the European Research Council under the European Union's Seventh Framework Programme (FP7/2007-2013)/ERC grant agreement n° 226144.

References

1. Ginoux P, Chin M, Tegen I, Prospero JM, Holben B, Dubovik O, Lin S (2001) Sources and distributions of dust aerosols simulated with the GOCART model. J Geophys Res 106:20255–20274. doi:10.1029/2000JD000053
2. Huneeus N et al (2011) Global dust model intercomparison in AeroCom phase I. Atmos Chem Phys 11:7781–7816
3. Jockel P, Kerkweg A, Pozzer A, Sander R, Tost H, Riede H, Baumgaertner A, Gromov S, Kern B (2010) Development cycle 2 of the Modular Earth Submodel System (MESSy2). Geosci Model Dev 3:717–752. doi:10.5194/gmd-3-717-2010

4. Marticorena B, Bergametti G, Aumont B, Callot Y, N'Doumé C, Legrand M (1997) Modeling the atmospheric dust cycle: 2. Simulation of Saharan dust sources. J Geophys Res 102:4387–4404
5. Stier P, Feichter J, Kinne S, Kloster S, Vignati E, Wilson J, Ganzeveld L, Tegen I, Wener M, Balkanski Y, Schulz M, Boucher O (2005) The aerosol-climate model ECHAM5-HAM. Atmos Chem Phys 5:1125–1156, doi:10.5194/acp-5-1125-2005
6. Tegen I, Harrison SP, Kohfeld K, Prentice IC, Coe M, Heimann M (2002) Impact of vegetation and preferential source areas on global dust aerosol: results from a model study. J Geophys Res-Atmos 107(D21):4576. doi:10.1029/2001JD000963
7. Zender CS, Bian H, Newman D (2003) Mineral Dust Entrainment and Deposition (DEAD) model: description and 1990s dust climatology. J Geophys Res 108(D14):4416. doi:10.1029/2002JD002775

Questions and Answers

Questioner Name: Sunhee Lee

Q: Dust mass shown on Australian continent is on Western Australia while major dust sources are in Central Australia. Any explanation why no dust mass shown on dust source region?
A: The major Australian dust sources are located in the central part of the continent and are associated with paleolake beds consisting of fine-grained lacustrine sediments. With the use of an implicit treatment of dust sources based on the global biomes map of Olson, it is not easy to locate the Australian dust sources efficiently. Some models use a-priori definition of these dust sources (also called preferential sources) to overcome this problem. We chose not to use preferential dust sources in our model to explore the efficacy of the system to represent dust sources without external fine tuning. In the case of focusing on the Australian dust production and transport, with our modelling system, the use of a more detailed soil map will be unavoidable and essential.

Questioner Name: Sunhee Lee

Q: Stations shown on map are from fire prone region not dust prone region. Any reason why two other Aeronet stations in the Central Australia are not used?
A: The map showing the 19 Aeronet stations selected for the model evaluation does not include any Australian stations because no data was available for the year 2000 on the AOT Level 2.0 (Quality Assured Data). The map showing the stations providing dust concentration data from multiannual databases included only two stations in Australia (Cape Grim, Jabirun) and we used them in the evaluation procedure.

Chapter 21
Modelling of Particle Number Concentrations with LOTOS-EUROS

Astrid Manders, Antoon Visschedijk, Hugo Denier van der Gon, Bas Henzing, and Martijn Schaap

Abstract Particle number (PN) concentrations over Europe were calculated by the CTM LOTOS-EUROS using aerosol dynamics from M7 and a new particle number emission database. Results were compared with PN observations (EUSAAR). In autumn and winter the correspondence was better than in spring and summer, possibly due to a poor modeling of nucleation and the incomplete contribution of secondary aerosols. In addition, the emission inventory was used under certain assumptions with regard to (amongst others) the hygroscopicity of particles, and the particles properties of wood combustion products. Sensitivity tests were performed to verify the impact of uncertainties in these assumptions.

Keywords LOTOS-EUROS • Particle number concentrations

21.1 Introduction

There is increasing evidence that the composition of aerosol, rather than its total mass, determines the adverse impact of aerosol on health. The smallest particles are thought to protrude deeper into the lungs and are considered potentially more dangerous, despite their small contribution to aerosol mass concentrations. Particle number distributions are therefore gaining attention, both in measurements and modelling. To study the particle number distribution over Europe with the regional CTM LOTOS-EUROS, the model was extended with the aerosol dynamics module M7 which accounts for aerosol ageing effects (condensation, coagulation, hygroscopic growth) in seven lognormal modes [5].

A. Manders (✉) • A. Visschedijk • H.D. van der Gon • B. Henzing • M. Schaap
TNO, PO Box 80015, 3508 TA Utrecht, The Netherlands
e-mail: astrid.manders@tno.nl; martijn.schaap@tno.nl

D.G. Steyn et al. (eds.), *Air Pollution Modeling and its Application XXII*,
NATO Science for Peace and Security Series C: Environmental Security,
DOI 10.1007/978-94-007-5577-2_21,

Traditionally, emission databases consist of mass emissions in size classes, usually PM2.5 and PM10. To be able to use these emissions, a translation has to be made to the species that are used in M7. This requires assumptions on the size distribution of the emitted particles. In addition, particles must be assumed to be externally mixed. Recently, a European particle number emission database was developed, for particles with dry diameters between 5 and 250 nm, divided over 12 size bins. Particles have a specific composition per emission source type, and are internally mixed. But also here assumptions regarding the exact composition have to be made to translate the emissions to M7-species. In addition, part of the traditional mass inventory is by definition not included, since the PN inventory is restricted to the smaller particles.

Model simulations with LOTOS-EUROS were performed for the year 2008 and on-line calculated sea salt emissions in both cases.

Two sets of emissions were used for the base simulations:

1. PN emissions [2]
2. MACC 2005 emissions [3].

Results were compared with EUSAAR SMPS/DMPS data for several European sites [1].

21.2 Results

The MACC simulation in general gives more Aitken mode particles (Fig. 21.1), whereas for the accumulation mode the results are similar. This is mainly the result of attributing all black carbon mass in the PM2.5 category to the Aitken mode and let the molecules age in the model, whereas in the PN inventory part of it was directly emitted in the accumulation mode as combined particles. In addition, the black carbon of the full PM2.5 fraction of the MACC emissions was put into the Aitken mode, so that more mass is put into the system than for the PN database.

When comparing the results to observations, Aitken mode concentrations tend to be underestimated in summer, in particular for the PN inventory. In winter, the PN inventory leads to a better correspondence with observations than the MACC inventory, showing the added value of the PN emission inventory. One has to note that the size classes as defined in LOTOS-EUROS do not correspond one-to-one to the size bins of the observations. Both on the low end of the Aitken mode (<30 nm) and on the high end of the accumulation mode (>250 nm), particles are not included in the harmonized data set. In fall and winter, the PN emission database leads to a better model performance than the MACC emissions. Spring/summer concentrations for which biogenic emissions and nucleation play a role are underestimated. Secondary organic aerosols and the secondary inorganic aerosols based on nitrate and ammonium are not taken into account, and the model needs improvement for these processes.

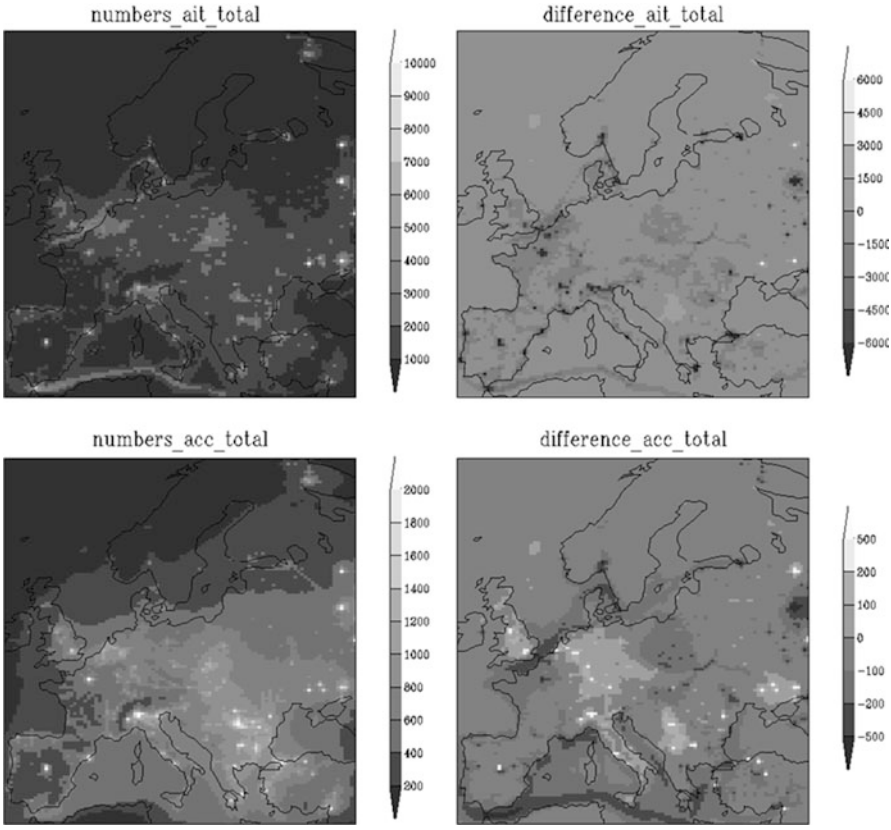

Fig. 21.1 Annual mean concentrations for Aitken and accumulation mode when using the PN emissions (*left*) and the difference with annual mean concentrations using the MACC emissions (PN-MACC)

A sensitivity test regarding the hygroscopicity revealed that increasing the hygroscopicity by 50 % had a minor impact on the concentrations, allowing a faster ageing and a shift from the Aitken to the accumulation mode. For wood burning, part of the co-emitted gases rapidly condense on the particles when the smoke cools down. This process may be not completely accounted for in the emission database, whereas the scale of LOTOS-EUROS is not small enough to take this condensation so close to the source into account, resulting in too small and too light particles and a significant underestimation of organic carbon mass in areas with significant wood burning emissions.

References

1. Asmi A et al (2011) Number size distributions and seasonality of submicron particles in Europe 2008–2009. Atmos Chem Phys 11:5505–5538
2. Denier van der Gon H et al (2010) Size-resolved Pan-European anthropogenic particle number inventory. Paper presented at IAC (oral)
3. Kuenen J et al (2011) TNO-report TNO-060-UT-2011e00588, Utrecht
4. Manders AMM, Schaap M, Querol X, Albert MFMA, Vercauteren J, Kuhlbusch TAJ, Hoogerbrugge R (2010) Sea salt concentrations across the European continent. Atmos Environ 44(20):2434–2442. doi:10.1016/j.atmosenv.2010.03.028
5. Vignati E, Wilson J, Stier P (2004) M7: An efficient size-resolved aerosol microphysics module for large-scale aerosol transport models. JGR 109:8601–8616, doi:10.1029/2003JD004485

Questions and Answers

Questioner Name: Pavel Kischka

Q: Was the effect of surf zone on SSA concentration included in the model? Did you compare modeled SSA concentrations with measured SSA concentrations?
A: No, it is not included, since the model is aimed at regional applications and the surf zone has only a small contribution on this scale. For the conventional version of LOTOS-EUROS we did a comparison [4] but not for the PN version.

Questioner Name: Jordi Vila

Q: You mentioned that small scales are very important, why do you use ECMWF data? What is your opinion on the importance of small scale processes on air quality?
A: We aim at modeling the regional scale. We know that we cannot resolve small-scale processes, although we acknowledge that these scales are very important for feedbacks or processes close to the emission source (wood burning sensitivity experiment) and thus relevant for air quality.

Chapter 22
An Advanced Scheme of Vertical Dispersion and Dry Deposition of Aerosols for Atmospheric Transport Models

Rostislav Kouznetsov and Mikhail Sofiev

Abstract A new scheme for vertical dispersion and dry deposition of atmospheric aerosols was recently developed by the authors (Kouznetsov and Sofiev, J Geophys Res 117:D01202, 1, 2012). The vertical transport scheme and deposition scheme for smooth and water surfaces are based on the exact solution of the steady-flux equation. The scheme for deposition onto rough surfaces uses a universal empirical function and two parameters describing the surface: aerodynamic roughness length and a "collection scale" that describes the surface elements. In present paper we briefly outline the scheme with some improvements of accounting for the deposition due to inertial impaction.

Keywords Chemical transport models • Aerosol • Dry deposition

22.1 Introduction

The majority of currently used atmospheric transport models have resistance-based schemes for vertical dispersion and dry deposition of aerosols. Such schemes have severe difficulties with the species with non-zero regular vertical transport. Moreover, the earlier comprehensive parameterizations of particle dry deposition either poorly agree to the experimental data [1] or use dozens of empirical parameters for fixed surface types [2], or both [3].

R. Kouznetsov (✉) • M. Sofiev
Finnish Meteorological Institute, Helsinki, Finland

A. M. Obukhov Institute of Atmospheric Physics, Moscow, Russia
e-mail: rostislav.kouznetsov@fmi.fi; mikhail.sofiev@fmi.fi

D.G. Steyn et al. (eds.), *Air Pollution Modeling and its Application XXII*,
NATO Science for Peace and Security Series C: Environmental Security,
DOI 10.1007/978-94-007-5577-2_22,

The recently-developed scheme [4], referred to as KS2011, is more or less free of the above drawbacks. It uses just two surface types (smooth and rough) and gives a clear criterion how to treat each particular surface. In KS2011 no empirical parameters are needed to evaluate the deposition rate onto smooth surfaces, whereas for rough surfaces the knowledge of their aerodynamic roughnesses and "collection scales" is required. This paper briefly describes some key features of KS2011 scheme.

22.2 The Outline of KS2011 Scheme

The vertical dispersion scheme is based on the exact solution of the transport equation (Fig. 22.1)

$$J(z) = -K(z)\frac{\partial C}{\partial z} + v(z)C, \tag{22.1}$$

(where $J(z)$ is the flux, $K(z)$ is the exchange coefficient, and $v(z)$ is regular velocity) assuming the constant flux between two levels z_i and z_j that have concentrations $C\ (z_i)$ and $C\ \left(z_j\right)$. The scheme can handle arbitrary profiles of $K(z)$ and $v(z)$. In a simple case of $v(z) = const$, the original expression for the flux between two levels reduces to the exponential form:

$$J_{ij} = \frac{C_j \exp\left(vr_{ij}\right) - C_i}{\exp\left(vr_{ij}\right) - 1} v, \tag{22.2}$$

where J_{ij} is the aerodynamic resistance between z_i and z_j.

The boundary condition at the surface is usually given in terms of the deposition velocity $V_{d0} = J_0/C(0)$. In most cases the vertical discretization scheme does not allow for direct evaluation of near-surface concentration, so the flux has to be

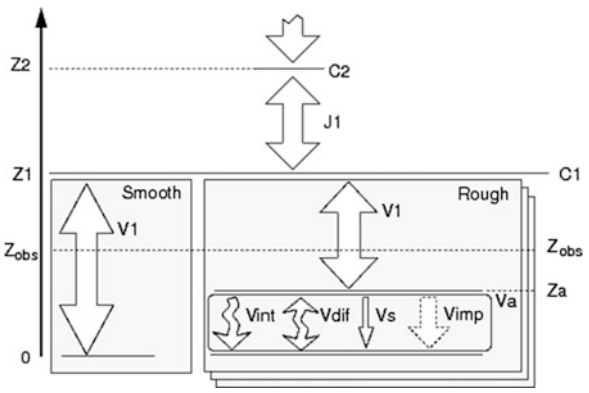

Fig. 22.1 The KS2011 scheme: $Z1$, $Z2$, etc. are the heights for concentration evaluation, steady fluxes are assumed between them. Z_0 is a roughness length for momentum [4]

evaluated using the concentration at some finite height z_1. This can be done with the assumption of constant steady-state flux below z_1. The corresponding deposition velocity $V_d\ (z_1) = J_0/C\ (z_1)$ is then evaluated by the dry deposition scheme.

The KS2011 scheme for dry deposition expresses the deposition velocity as a function of the physical properties of the species, the flow, and the surface. The scheme distinguishes between smooth and rough flow regimes and handles the transition between them. The expression for the deposition rate onto smooth surface has no tuning parameters; it results from the solution of the flux equation with universal profiles of turbulence down to the surface. It accounts for turbophoresis, gravity and (optionally) other phoretic forces. For rough surfaces V_d is evaluated stepwise: the deposition velocity within in-canopy layer is calculated and then the above-canopy layer (between the lowest model level and z_0) is accounted for in the same manner as any other atmospheric layer.

The deposition velocity within in-canopy layer is treated as a filtration process i.e. the air with given concentration and velocity flows between the canopy elements that act as collectors. No vertical structure is assumed within the in-canopy layer neither it is assumed to coincide with the canopy height. The wind speed at the canopy top U_{top} is taken as a relevant velocity scale and the concentration $C\ (z_0)$ as a concentration. U_{top} can be calculated from the friction velocity u_*, since their ratio is a function of canopy properties. For natural canopies $\mathrm{U_{top}/u^*} \approx 3$ [5].

The deposition velocity is then calculated as a sum of deposition velocities due to four main processes: Brownian diffusion (v_{dif}), interception (v_{int}), inertial impaction (v_{imp}) and gravitational settling (v_s). The Brownian motion deflects a particle from the streamlines, passing collectors so it can be captured. The interception occurs when a particle streamline happens to be closer to the collectors surface than the particle radius. The deposition by impaction occurs when a particle due to its inertia cannot follow a streamline bypassing a collector and hits it.

The deposition velocities due to the mechanisms (except for v_s), are proportional to corresponding capture efficiencies of individual canopy elements. Fitting theoretical expressions [6] for the single-element collection efficiencies due to diffusion and interception to the data of [7, 8] for grass (collector size $d_c = 5$ mm) one gets:

$$v_{dif} = U_{top} \cdot \mathrm{Re}^{-1/2}\mathrm{Sc}^{-2/3} = u_* \cdot 2\,\mathrm{Re}_*^{-1/2}\,\mathrm{Sc}^{-2/3}, \tag{22.3}$$

$$v_{\mathrm{int}} = U_{top} \cdot 80\left(\frac{d_p}{d_c}\right)^2 \mathrm{Re}^{1/2}, = u_* \cdot 80\left(\frac{d_p}{a}\right)^2 \mathrm{Re}_*^{1/2}, \tag{22.4}$$

where Sc is particle Schmidt number, $\mathrm{Re} = \mathrm{U_{top}}\ \mathrm{d}_c\ /\nu$ and $\mathrm{Re}_* = u_* a/\nu$ are Reynolds numbers, ν is the kinematic viscosity of the air, d_p is the geometrical size of a particle, and $a = d_c u_*/U_{top}$ is the collection scale, that fully describes the deposition within the canopy layer for diffusion and interception. The data for various surfaces can be described with (22.3) and (22.4) by proper choice of the collection scale [4].

The deposition due to inertial impaction is mainly controlled by Stokes number *St*, which can also be expressed in terms of u_* and a:

$$\mathrm{St} \equiv \frac{2\tau_p U_{top}}{d_c} = \frac{2\tau_p u*}{a}, \tag{22.5}$$

where τ_p is the particle relaxation time. Since the dependence of the collection efficiency due to impaction sharply increases from zero to nearly unity within an order of Stokes numbers, it is not plausible to infer v_{imp} from the deposition measurements. Instead, we derive v_{imp} from the single-element capture efficiency of impaction η_{imp} using the assumption of homogeneity of the in-canopy layer and an analogy with the deposition of momentum.

One can introduce the capture efficiency of a canopy element for momentum η_m, as the momentum deposition rate (force) per unit of momentum concentration ρU_{top} per unit speed U_{top} through the area equal to the cross-section of the element. In aerodynamics this parameter is usually expressed via drag coefficient $\eta_{imp} = C_d/2$. The deposition velocity for momentum is then simply u_*^2/U_{top}. Since the deposition velocities are proportional to corresponding capture efficiencies,

$$V_d = \frac{u_*^2}{U_{top}} \frac{\eta}{\eta_m} = \frac{u_*^2}{U_{top}} \frac{2}{C_d} \eta. \tag{22.6}$$

For inviscid flows the impaction is exclusively controlled by the Stokes number $\eta_{imp} = \eta_{imp}(\mathrm{St})$. It was shown [4] for cylinders, that the capture efficiency for impaction in viscous flow can be obtained by replacing *St* with the effective stokes number $\mathrm{St_e} = \mathrm{St} - \mathrm{Re}^{-1/2}$. The analytical approximation for $\eta_{imp}(\mathrm{St})$ can be found in [4]. In case of coniferous canopies the collectors can be considered as cylinders and corresponding drag coefficient can be taken constant $C_d = 1$. The resulting dimensionless deposition velocity due to impaction is:

$$v_{imp} = u_* \frac{2u_*}{U_{top}} \cdot \eta_{imp} \left(\mathrm{St} - \frac{u_*}{U_{top}} \mathrm{Re}_*^{-1/2} \right), \tag{22.7}$$

For other shape of roughness elements, the relevant value of C_d should be used.

The only component of the in-canopy deposition velocity, where the ratio u_*/U_{top} appears explicitly is v_{imp}, however the comparisons to experimental data [4] indicate that the impaction process is significant only at high wind speeds and within a narrow range of particle sizes, moreover in most cases $u_*/U_{top} = 3$ can be assumed. Thus, essentially the only parameter of a surface that controls the deposition is the collection scale a.

22.3 Conclusion and Outlook

The KS2011 scheme is simple enough to be used in mesoscale to global atmospheric transport models. It allows for uniform treatment of particles and gases with negligible surface resistance can be neglected. The scheme is suitable for airborne particles of nearly arbitrary size, shape, composition etc., as long as their diffusivity, geometrical size and relaxation time are provided. The transition between smooth and rough deposition regimes is allowed for the surfaces with small aerodynamic roughness.

The only surface parameter specific to the scheme is the collection scale a. Originally, a was determined for several surface types, however it still has to be parameterized for various surfaces as a function of leaf-area indexes, season, snow cover etc. The scheme performs well for the variety of wind-tunnel and outdoor experiments [4], however, like other mechanistic models, it results in severe discrepancies when compared to the data of outdoor experiments with high vegetation.

Acknowledgments This work has been supported by the EC FP7 projects ERC PBL-PMES (No.∼227915), MACC (No.∼265098), and MEGAPOLI (No.∼212520) projects, and by Academy of Finland (Projects ASTREX and IS4FIRES).

References

1. Seinfeld J, Pandis S (1998) Atmospheric chemistry and physics. Wiley, New York
2. Petroff A, Zhang L, Pryor S, Belot Y (2009) An extended dry deposition model for aerosols onto broadleaf canopies. J Aerosol Sci 40(3):218. doi:10.1016/ j.jaerosci.2008.11.006
3. Seinfeld J, Pandis S (2006) Atmospheric chemistry and physics, 2nd edn. Wiley, New York
4. Kouznetsov R, Sofiev M (2012) Methodology for evaluation of vertical dispersion and dry deposition of atmospheric aerosols. J Geophys Res 117:D01202, 1. doi:10.1029/2011JD016366
5. Raupach MR (1994) Simplified expressions for vegetation roughness length and zero-plane displacement as functions of canopy height and area index. Bound-Layer Meteorol 71:211. doi:10.1007/BF00709229
6. Parnas R, Friedlander SK (1984) Particle Deposition by Diffusion and Interception from Boundary Layer Flows. Aerosol Sci Technol 3:3. doi:10.1080/02786828408958987
7. Chamberlain AC (1967) Transport of Lycopodium Spores and Other Small Particles to Rough Surfaces. R Soc Lond Proc Ser A 296:47, doi:10.1098/rspa.1967.0005
8. Chamberlain AC, Roy QJ (1968) Transport of gases to and from surfaces with bluff and wave-like roughness elements. Meteorol Soc 94:318. doi:10.1002/qj.49709440108

Questions and Answers

Questioner Name: Kiran Alapaty

Q: The third term in resistance formulation is Rc, canopy resistance. Is your third term similar to Rc

A: No. The resistances in traditional scheme correspond to the stages of deposition: aerodynamic – quasi-laminar – surface. The latter stage is quantified by Rc

that characterizes the ability of canopy elements to absorb the tracer at finite concentration at the collector-surface. Rc is left beyond the scope of current study. It should be taken zero for particles and assigned the proper values for gases. To be used in our scheme, it should be added to $1/v_{dif}$.

The terms in the expression for the in-canopy deposition velocity correspond to concurrent processes of deposition rather than to sequential stages and, correspondingly, the velocities are summed up, but not resistances. Thus, none of the terms is similar to Rc

Chapter 23
Impact of Aerosol Activation on Modelled Regional Particulate Matter Mass and Size Distribution Due to Cloud Processing

Wanmin Gong, Sunling Gong, Junhua Zhang, Paul A. Makar, Michael D. Moran, Craig Stroud, W. Richard Leaitch, and Walter Strapp

Abstract Aerosol activation is a key process in aerosol-AQ cloud interaction. Although it is widely studied within the climate modeling community it has not been attracting significant attention within the air quality modeling community. In this study an off-line, sectional, chemically-speciated regional air quality model, AURAMS, has been used to assess the impact of aerosol activation on the modelled regional particulate matter (PM) mass concentration and size distribution. A simple activation scheme based on an empirical relationship between cloud droplet number density and aerosol number density is compared to a more physically-based activation scheme. Model simulations were compared to aircraft observations obtained during the 2004 ICARTT field campaign. Modelled aerosol light extinction and column aerosol optical depth (AOD) were computed in three different ways in the current study. Two of them based on Mie calculations and one empirical reconstructed mass extinction method. The magnitude of the modeled AOD varies significantly depending on the approach. The impact of different aerosol activation schemes on the modelled AOD in this case is generally in the range of 20–30 % for the two Mie methods. As the empirical reconstructed mass extinction method is not size dependent, it is less sensitive to aerosol activation.

Keywords Aerosol activation • Cloud processing • AURAMS-model

W. Gong (✉) • S. Gong • J. Zhang • P.A. Makar • M.D. Moran • C. Stroud
Air Quality Research Division, Environment Canada, Downsview, ON, Canada
e-mail: wanmin.gong@ec.qc.ca

W.R. Leaitch
Climate Research Division, Environment Canada, Downsview, ON, Canada

W. Strapp
Meteorological Research Division, Environment Canada, Downsview, ON, Canada

D.G. Steyn et al. (eds.), *Air Pollution Modeling and its Application XXII*,
NATO Science for Peace and Security Series C: Environmental Security,
DOI 10.1007/978-94-007-5577-2_23,

23.1 Introduction

Aerosol activation is a key process in aerosol-cloud interaction. It controls the cloud droplet number concentration, which has direct implication on cloud optical properties and precipitation formation; it can affect droplet acidity, which can in turn affect the uptake of gases and aqueous-phase reactions; it also determines where the aerosol mass addition, due to in-cloud production (e.g., of sulfate), will reside after cloud evaporation and, hence, the cloud-processed aerosol size spectrum, which will affect aerosol activation in subsequent cloud cycles, as well as other size-dependent aerosol dynamic and physical processes.

Although aerosol activation and its impact on aerosol-cloud interaction has been an active area of research within the climate modeling community, it has not been a process attracting significant attention within the air quality modeling community [5]. Here, an off-line, sectional, chemically-speciated regional air quality model, AURAMS, has been used to assess the impact of aerosol activation on the modelled regional particulate matter (PM) mass concentration and size distribution. A simple activation scheme based on an empirical relationship between cloud droplet number density and aerosol number density is compared to a more physically-based activation scheme [1]. Model simulations were compared to aircraft observations obtained during the 2004 ICARTT field campaign [4]. The impacts of aerosol activation on modelled regional PM mass and size distribution and on aerosol radiative properties are discussed.

23.2 Aerosol Activation Schemes and Simulation Setup

23.2.1 Jones Scheme [10]

This is AURAMS' default scheme for aerosol activation [6]. It assumes an empirical relationship between droplet number concentration (N_d) and aerosol number concentration (N_a):

$$N_d\left(cm^{-3}\right) = 375\left(1 - \exp\left(-2.5 \times 10^{-3} N_a\left(cm^{-3}\right)\right)\right) \tag{23.1}$$

With the AURAMS sectional representation, activated aerosol particles are determined by adding particles from bins in descending order of size until the total number of droplets, from (23.1), is reached.

23.2.2 Abdul-Razzak and Ghan Parameterization for Sectional Representation [1]

The parameterization establishes a relationship between the maximum supersaturation (S_{max}) reached by arising air parcel and an effective critical supersaturation (S_e), which in turn is determined by individual size section's critical supersaturation (S_i):

$$S_{\max} = S_e \Big/ \left[0.5(\varsigma/\eta)^{3/2} + \left(S_e^2/\eta + 3\varsigma\right)^{3/4}\right]^{1/2}, \text{ where } S_e^{2/3} = \sum_{i=1}^{nb} N_i \Big/ \sum_{i=1}^{nb} N_i / S_i^{2/3}$$

ς and η are parameters dependant on updraft velocity, growth coefficient (accounting for diffusion of heat and moisture to particles), etc., while S_i depends on size, hygroscopicity, and surface tension characteristics of the particles.

A challenge in the implementation of such parameterization is to determine the appropriate updraft velocity. Peng et al. [12] recommended the use of a updraft velocity of 0.8 times the standard deviation of the PDF of vertical velocity. Here, two approaches are tested: (1) the standard deviation of the updraft velocity (σ_w) is parameterized as a function of liquid water content (LWC) following Hoose et al. [9]:

$$\sigma_w = w_t + 2\left(\frac{m}{s}\frac{kg_{air}}{g_{water}}\right)\cdot LWC;$$

(2) σ_w from the below-cloud gust velocity measurements from the ICARTT campaign (e.g., Convair 580 flight 16 [8]) is used.

23.2.3 AURAMS Simulation Setup

Cascaded nested AURAMS simulations were carried out at 42-, 15-, and 2.5-km horizontal resolutions. The simulation setup for the 42- and 15-km runs is identical to Gong et al. [7], while the nested 2.5-km domain is set over southern Lake Michigan to eastern Lake Erie focusing on the area where Convair 580 flights 16 and 17 were conducted on August 10, 2004. Three simulations were conducted: "base case" with the Jones activation scheme, "ARG0" with the Abdul-Razzak and Ghan scheme and parameterized σ_w, and "ARG1" with the Abdul-Razzak & Ghan scheme and a prescribed observation-based updraft of 0.6 m s^{-1}.

23.3 Results and Discussion

Figure 23.1 shows the modeled cloud droplet concentrations from the 2.5-km runs at 19 Z on August 10, 2004 on the model level approximately 1,235 m above the surface from all three runs. It is immediately noticeable that the Jones scheme results

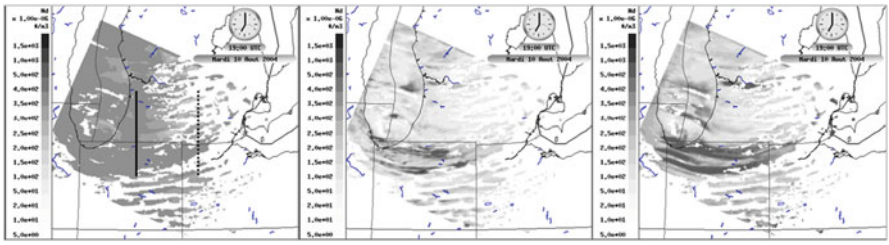

Fig. 23.1 Modelled droplet number concentration at 1,235 m (AGL) model level: base case (*left*), ARG0 (*middle*), and ARG1 (*right*). The geographical locations of Convair 580 flights are marked by the *solid* (flight 16) and *dashed* (flight 17) *lines* on the *left panel*

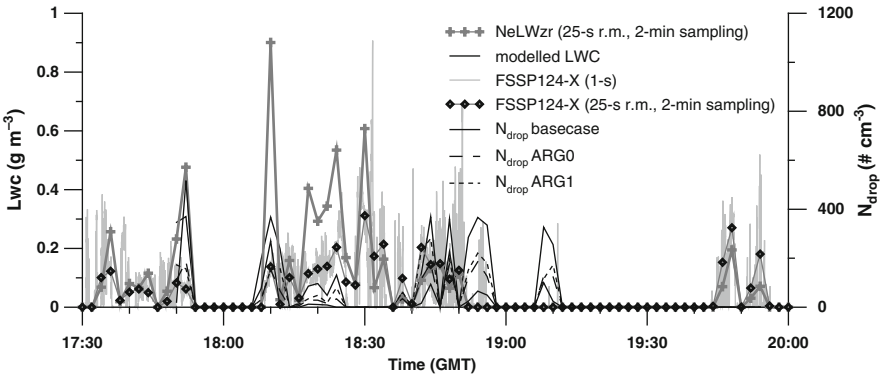

Fig. 23.2 Comparison with in-situ aircraft measurement of LWC (NeLWzr) and droplet number concentration (FSSP124-X) for Convair 580 flight 16 (August 10, 2004)

in a more uniform droplet concentration over the cloudy areas (partly due to the capping at 375 cm^{-3}). In contrast, the distribution of droplet number concentrations from the Abdul-Razzak and Ghan scheme reflects more of the aerosol sulfate distribution (see later); the differences between ARG0 and ARG1 are due to the difference in updraft only. Figure 23.2 compares the modeled LWC and droplet concentration with in-situ aircraft measurements for flight 16 (comprising primarily two level legs at different altitudes, one in-cloud and one below-cloud, along a north-south line, ca. 200 km east of Chicago, ~86 W, as indicated in Fig. 23.1). For this particular case the model predicted cloud base appears to be somewhat higher than the observed; consequently the modeled LWC is considerably lower than the observed. The 1-s droplet number concentration measurements frequently exceed the maximum imposed by the Jones scheme, but averaging the observations over a model resolution of 2.5-km results in concentrations considerably lower than the 1-s values. The droplet number concentrations predicted from the Abdul-Razzak & Ghan scheme compare better with the observations than those from the Jones scheme over the time periods when the modeled and the observed LWC values are more comparable.

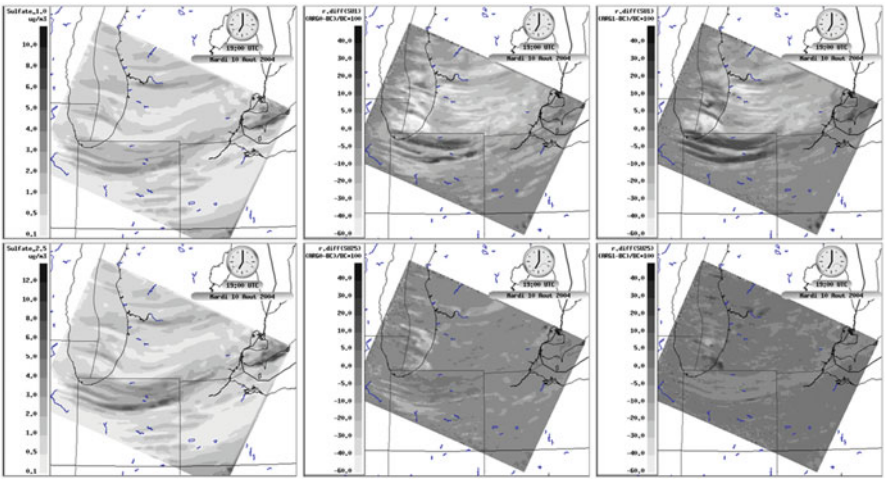

Fig. 23.3 Impact of aerosol activation on model prediction of sulfate1.0 (*top*) and sulfate2.5 (*bottom*) at 1,235 m (AGL) model level, 19 Z August 10, 2004. Modelled PM sulfate concentrations from the base case are shown in the *left panels*; the percentage differences in the modeled PM sulfate between the sensitivity runs and the base case are shown: *middle panels* – ARG0 vs. base case; *right panels* – ARG1 vs. base case

Figure 23.3 illustrates the impact of aerosol activation on the model predicted aerosol sulfate. A considerable portion of the predicted $\text{sulfate}_{2.5}$ mass is distributed below the 1 μm size range, and the impact of different aerosol activation schemes in this case is mainly the shift of the cloud-processed aerosol mass up or down the size spectrum around 1 μm (as more or less smaller particles are activated). As a consequence the impact on $\text{sulfate}_{1.0}$ is much more significant than on $\text{sulfate}_{2.5}$. This is expected to have an impact on aerosol extinction as aerosol particles of size around 0.7 μm are most effective for scattering visible radiation.

There are different approaches to how aerosol extinction can be calculated for a mixed aerosol population. Modelled aerosol light extinction and column aerosol optical depth (AOD) were computed in three different ways in the current study: (1) a Mie calculation for sectional, speciated aerosols based on [3]; (2) an empirical reconstructed mass extinction based on [11]; (3) a Mie calculation based on mapping of AURAMS sectional aerosols to a 3-mode lognormal distribution (as in CMAQ [2]). The magnitude of the modeled AOD varies significantly depending on the approach. The impact of different aerosol activation schemes on the modelled AOD in this case is generally in the range of ±20 % to ± 30 % for the two Mie methods, with the sectional based Mie calculation being the most sensitive to the aerosol activation. As the empirical reconstructed mass extinction method is not size dependent, it is less sensitive to aerosol activation.

References

1. Abdul-Razzak H, Ghan SJ (2002) A parameterization of aerosol activation. Part 3: Sectional representation. J Geophys Res 107(D3). doi:10.1029/2001JD000483
2. Binkowski FS, Roselle SJ (2003) Models-3 community multiscale air quality (CMAQ) model aerosol component 1. Model description. J Geophys Res 108(D6):4183
3. Evans BTN, Fournier GR (1990) Simple approximation to extinction efficiency valid over all size parameters. Appl Opt 29(31):4666–4670
4. Fehsenfeld FC et al (2006) International Consortium for Atmospheric Research on Transport and Transformation (ICARTT): North America to Europe – overview of the 2004 summer field study. J Geophys Res 111(D23):D23S01
5. Gong W, Stroud C, Zhang L (2011) Cloud processing of gases and aerosols in air quality modeling. Atmosphere 2(4):567–616
6. Gong W et al (2006) Cloud processing of gases and aerosols in a regional air quality model (AURAMS). Atmos Res 82(1–2):248–275
7. Gong W et al (2010) Comparative evaluation of model simulations of regional ozone and particulate matters for two distinct summers over eastern North America. In: Steyn DG, Trini Castelli S (eds) Air pollution modelling and its application XXI. Springer, Dordrecht, pp 513–518
8. Hayden KL et al (2008) Cloud processing of nitrate. J Geophys Res 113(D18):D18201
9. Hoose C et al (2010) Parameterization of in-cloud vertical velocities for cloud droplet activation in coarse-grid models: analysis of observations and cloud resolving model results. Paper presented at 13th AMS conference on atmospheric radiation, Portland, Oregon
10. Jones A, Roberts DL, Slingo J (1994) A climate model study of indirect radiative forcing by anthropogenic sulphate aerosols. Nature 370:450–453
11. Malm WC et al (1994) Spatial and seasonal trends in particle concentration and optical extinction in the United States. J Geophys Res 99:1347–1370
12. Peng Y, Lohmann U, Leaitch R (2005) Importance of vertical velocity variations in the cloud droplet nucleation process of marine stratus clouds. J Geophys Res 110(D21):D21213

Questions and Answers

Questioner Name: K. Alapaty

Q: You are looking for AOD data. This data is available from the U.S. Department of Energy's (DOE) Atmospheric Radiation Measurement (ARM) program.
A: Thank you very much for the info. We will definitely be pursuing to get hold of any suitable data for our evaluation.

Chapter 24
Dust Production by Density Currents – A Not So Well Known Source of Aerosol Particles in the Atmosphere

Stavros Solomos and George Kallos

Abstract Dust is one of the most commonly found pollutants for many areas around the globe. Recent field and satellite observations suggest the importance of convectively generated downdrafts on the mobilization processes of dust particles and on their long range transport. RAMS/ICLAMS simulations of convective storms for the area of NW Africa allowed the description of the cool pool generation and the associated dust production mechanisms. Evaporation of rain droplets as they fall through the warmer and unsaturated air is responsible for the formation of a fast propagating density current. The inner structure of this system is characterized by increased turbulence, small scale vortices and strong updrafts at the edge of the front. Mobilization of dust occurs mainly in two ways: First, due to suspension of loose soil particles as the system passes over bare soil and sandy areas and second by sweeping pre-existing dust and creating a characteristic dust wall that reaches up to 3 km height.

Keywords Aerosols • Dust production • RAMS-model

24.1 Introduction

Parameterization of dust mobilization is included in several numerical models based on soil properties and friction velocity (i.e. [3–5]). However, there is still limited number of studies on the role of more local scale meteorological features, such as density currents, for triggering dust episodes. These systems can be produced either because of deep convection in the tropics or because of orographic storm activity over the Atlas Mountains [2]. The high frequency of the phenomena

S. Solomos (✉) • G. Kallos
School of Physics, Atmospheric Modeling and Weather Forecasting Group, University of Athens, University Campus Bldg PHYS-5, 15784 Athens, Greece
e-mail: stavros@mg.uoa.gr

D.G. Steyn et al. (eds.), *Air Pollution Modeling and its Application XXII*,
NATO Science for Peace and Security Series C: Environmental Security,
DOI 10.1007/978-94-007-5577-2_24,

indicates the need for a more accurate representation of this mechanism in dust models. The main objective of this study is to describe a real case study of dust production due to convective outflow with the use of an interactive atmospheric-air quality model.

24.2 Model Study

For the current study the RAMS/ICLAMS model was used [3]. The model is an enhanced version of the Regional Atmospheric Modeling System (RAMS6.0) [1]. The experimental domain was configured with four two-way interactive nesting grids: a coarse 24 km, an intermediate of 4.8 km and two grids of 1.6 km horizontal resolution as illustrated in Fig. 24.1. During 31st of May 2006 a low-pressure system was located over Morocco (Fig. 24.1) and intense rainfall was produced over the Atlas Mountains. As the raindrops fell through a warmer and unsaturated environment, some of them evaporated before reaching the ground and the absorption of vaporization latent heat decreased the temperature of the surrounding air. The generation of a cool pool at the area resulted in the development of a fast propagating density current. The system exhibited an extended frontal line of about 300 km (see dashed lines in Fig. 24.1) and was associated with intense dust production and cloud cover.

The generation of the cool pool is indicated in Fig. 24.2a by the "dome" of the isentropes inside the precipitating area and ahead of it. The cool pool intrusion produced a region of intense updrafts ahead of the front that are indicated with black line contours in Fig. 24.2b. Vertical wind speed at the leading edge of the system often exceeded 4 m s^{-1}, while the horizontal wind component within the

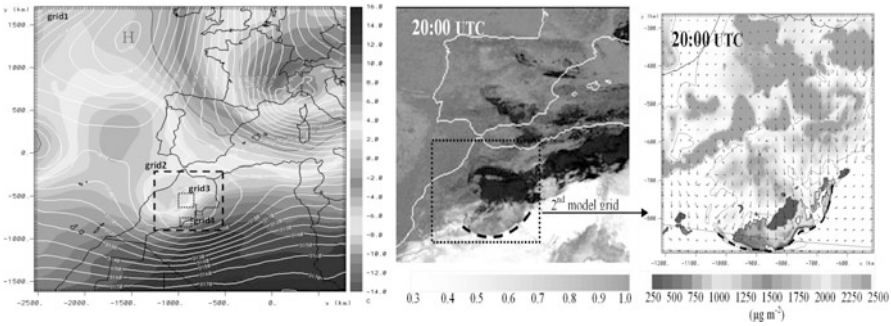

Fig. 24.1 (*left*) Geopotential height (white contour lines every 10 gpm) and temperature at 700 hPa (greycolor scale in °C) – 11:00 UTC on 31 May 2006. The dashed rectangulars indicate the locations of the nested grids. (*middle*) MSG/SEVIRI dust indicator satellite images. *Dark colors* indicate clouds and light grey indicates desert dust. (*right*) Corresponding model cloud fraction (*light grayscale*) and dust production flux (*dark greyscale* in μg m^{-2}). *Dashed lines* indicate the location of the dust front

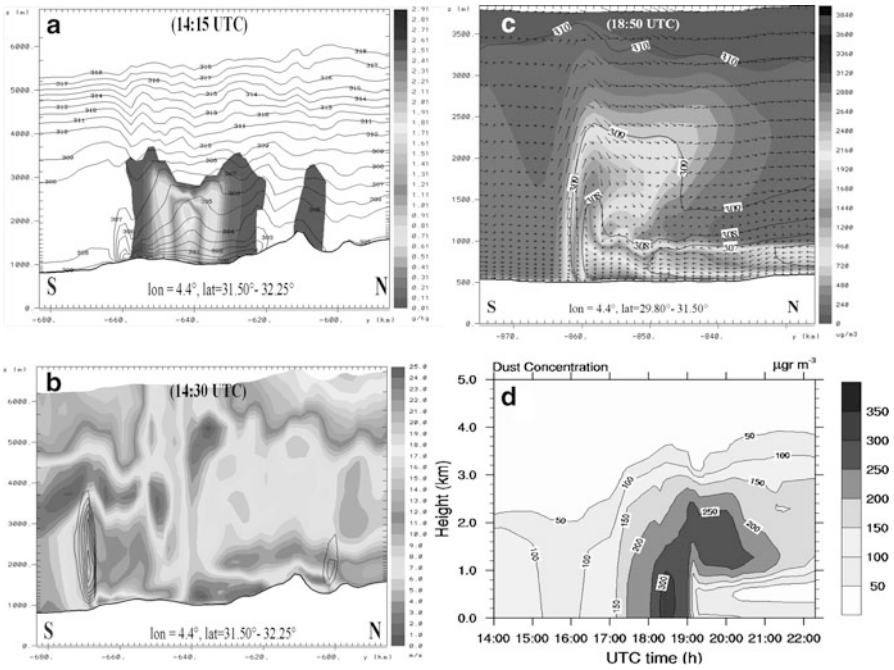

Fig. 24.2 North to south vertical cross-sections of: (**a**) Rain mixing ratio (*grayscale* in g kg^{-1}) and potential temperature (*contour lines* in K) at 14:15 UTC. (**b**) Horizontal wind speed (*grayscale* in m s^{-1}) and vertical updrafts (*black line contours* every 0.5 m s^{-1}) at 14:30 UTC. (**c**) Potential temperature (*contour lines* in K) and dust concentration (*greyscale* in μg m^{-3}) at 18:50 UTC for a reference frame relative to the propagating speed. (**d**) Time evolution of dust concentration (μg m^{-3}) over Tinfou station on 31 May 2006. Increased dust concentrations between 18:00 and 19:00 UTC are associated with the passage of the density current

propagating system ranged between 11 and 24 m s^{-1} as seen also in Fig. 24.2b. The microstructure of the density current flow and the process of dust particles uplifting are evident in the vertical cross-section (Fig. 24.2d) at 18:50 UTC when the system was fully developed.

For better understanding of the density current structure and propagation, the wind vectors in this figure are represented in the front-relative frame of reference assuming an average propagating speed of 11 m s^{-1}. This approach is useful for revealing small scale vortices within the propagating system. Due to surface friction, reversal of flow and an anticlockwise vortex is forming at the lower model layers just behind the leading edge. This flow pattern is responsible for the suspension of bigger particles (i.e. sand) and for the production of smaller dust particles through the saltation and bombardment mechanism. Increased turbulence at the edge of the system forces these particles outside of the cool pool where they enter the area of strong vertical motions ahead of the propagating system. In this way the dust particles elevate even higher than three kilometers in the troposphere and

concentrations of more than 1,000 $\mu g\ m^{-3}$ were found well above 2 km height. As the system propagates, pre-existing airborne particles are also swept along the frontal line and a "dust wall" is created.

24.3 Summary and Conclusions

The use of a high resolution limited area model that includes online dust parameterization allowed the detailed description of convective storm outdrafts. The generated density currents behaved as effective dust sources and as the flow structure and increased turbulence within these formations enhanced dust productivity. Improving the representation of these features in atmospheric models is an important step for reducing the uncertainty in global dust emissions and the related uncertainty in direct and indirect effects of dust, and aerosols in general, in the atmosphere.

References

1. Cotton WR et al (2003) RAMS 2001: current status and future directions. Meteoro Atmos Phys 82:5–29
2. Knippertz P, Deutscher C, Kandler K, Muller T, Schulz O, Schutz L (2007) Dust mobilization due to density currents in the Atlas region. Observations from the Saharan Mineral Dust Experiment 2006 field campaign. J Geophys Res 12:D21109. doi:10.1029/2007JD008774
3. Solomos S, Kallos G, Kushta J, Astitha M, Tremback C, Nenes A, Levin Z (2011) An integrated modeling study on the effects of mineral dust and sea salt particles on clouds and precipitation. Atmos Chem Phys 11:873–892. doi:10.5194/acp-11-873-2011
4. Spyrou C, Mitsakou C, Kallos G, Louka P, Vlastou G (2010) An improved limited-area model for describing the dust cycle in the atmosphere. J Geophys Res. doi:10.1029/2009JD013682
5. Zender CS, Bian H, Newman D (2003) Mineral dust entrainment and deposition (DEAD) model: description and 1990s dust climatology. J Geophys Res 108(D14):4416. doi:10.1029/2002JD002775

Questions and Answers

Questioner Name: Marina Astitha

Q: Would you consider that the dust emission parameterization is inadequate in resolving the density currents features? How important are the Habbobs in terms of generating dust mass compared to the other mechanisms?
A: The existing dust production mechanisms are adequate as a principle. The treatment of meteorology is crucial on generating density currents. Density currents are features with very strong gradients at horizontal scale of hundreds of meters to a few kilometers at the direction of propagation and tens to hundreds of kilometers

wide. Turbulence within the density current is considerable and needs appropriate treatment. Habbobs are important mechanisms for dust production because they generate sharp changes in the wind field, the flow is highly turbulent and this helps in dust mobilization. Of course habbobs are very important in near-source locations because of the high amounts of sand mobilization.

Chapter 25
Toward a New Chemical Mechanism in WRF/Chem for Direct and Indirect Aerosol Effects: A Focus on the Carbonaceous Aerosols

Paolo Tuccella, Georg A. Grell, Stuart A. Mckeen, Ravan Ahmadov, Gabriele Curci, and Guido Visconti

Abstract An updated version of Weather Research and Forecasting/Chemistry model (WRF/Chem) with a new parameterization for the secondary organic aerosol (SOA) production based on the Volatility Basis Set (VBS) is evaluated over Europe in May–June 2003. Results are compared against surface observations issued from the EC/OC 2002–2003 campaign of European Monitoring and Evaluation Program (EMEP). WRF/Chem underestimates the elemental carbon (EC) and the organic aerosol mass (OA) by −7 and −38 %, respectively. The analysis of OA: EC ratio reveals that the under prediction may be mainly explained by a misrepresentation of anthropogenic emissions of carbonaceous aerosols due to the coarse resolution of the inventory. The modeled concentration of OA constituent is nearly constant during the day. The predicted SOA/OA ratio has a value of ∼80 %. The biogenic SOA (BSOA) are 30 % of the total OA mass. Dry deposition velocity of Volatile Organic Compounds (VOC) oxidation products is a source of uncertain in the SOA budget.

Keywords WRF/Chem • SOA • VBS • Atmospheric chemistry modeling • Indirect aerosol effect • Carbonaceous aerosols

P. Tuccella (✉) • G. Curci • G. Visconti
CETEMPS – Dip. Fisica, Università degli Studi dell'Aquila, Via Vetoio, 67010 L'Aquila, Coppito, Italy
e-mail: paolo.tuccella@aquila.infn.it

G.A. Grell • S.A. Mckeen • R. Ahmadov
Cooperative Institute for Research in Environmental Sciences, University of Colorado at Boulder, Boulder, CO 80302, USA

Earth System Research Laboratory, National Oceanic and Atmospheric Administration, Boulder, CO 80302, USA

D.G. Steyn et al. (eds.), *Air Pollution Modeling and its Application XXII*,
NATO Science for Peace and Security Series C: Environmental Security,
DOI 10.1007/978-94-007-5577-2_25,

25.1 Introduction

Although the organic aerosols constitute a highly uncertain effect on global radiative forcing and represent a large fraction of sub-micron aerosol mass (20–90 %), their sources and evolution are still not well characterized [1]. As a consequence, chemical transport models (CTM) generally tend to underestimate the OA mass observed in the atmosphere, because the processes involved in the production and evolution of secondary organic aerosol are misrepresented [2]. In this paper we report on the evaluation over Europe of an updated SOA parameterization implemented in the WRF/Chem model. This work is a first step toward a new chemistry option that will be made available in WRF/Chem with microphysics fully coupled with aerosols (i.e., direct and indirect effects).

25.2 WRF/Chem Model

In this paper we use the pre-release version 3.4 of WRF/Chem. WRF/Chem is a fully coupled "online" meteorology-chemical model, a complete description is given by Grell et al. [3]. A simulation is carried out in May and June 2003 over Europe on a grid that extends from 35°N to 57°N in latitude and from 15°W to 27°E in longitude. The horizontal resolution is of 30 km with 28 vertical levels extending up to 50 hPa. The initial and boundary meteorological conditions are provided by National Center for Environmental Prediction (NCEP) analyses every 6 h. The chemical initial and boundary conditions consist of time-in variant climatological profiles. The "traditional" configuration of WRF/Chem [3] uses the Secondary Organic Aerosol Model (SORGAM) scheme to estimate the SOA formation. Several studies over USA and Europe [3–5] demonstrated that this parameterization produces very little SOA. Here we use an updated parameterization based on the volatility basis set approach, as described by Ahmadov et al. [2]. More details on model configuration are reported in Table 25.1. Dry deposition velocity of Organic Condensable Vapor

Table 25.1 WRF/Chem configuration

Physical process	WRF/Chem option
Microphysics	Morrison
Long-wave radiation	RRTM
Short-wave radiation	Goddard
Surface layer	Monin-Obukhov
Land-surface model	Noah LSM
Boundary layer scheme	Mellor-Yamada Nakanishi and Niino
Cumulus	New Grell scheme (G3)
Photolysis	Madronich
Chemistry model	New RACM-ESRL [2]
Aerosol model	MADE and VBS scheme for SOA [2]
Aerosol feedback	No

(OCV) is assumed proportional to the calculated deposition velocity of nitric acid with a factor of proportionality of 0.25. Wet deposition by large-scale precipitation is included.

The anthropogenic emissions (NOx, NMVOCs, CO, SOx, NH3 and unspeciated aerosol mass) are taken from the EMEP inventory (www.emep.int). Elemental carbon and organic carbon emissions are provided by the Laboratoired' Aerologie (www.aero.obsmip.fr). The emissions are adapted to the chemical mechanism used in this study as described by Tuccella et al. [5]. Biogenic emissions are based on the Model of Emissions of Gases and Aerosols from Nature (MEGAN).

25.3 Model Evaluation May–June 2003

WRF/Chem simulations are compared to surface measurements of EC/OC issued from the EMEP 2002–2003 campaign [6]. Observations consist in one daily sample per week. To take into account the OA mass, we multiply the observed OC by a factor of 1.6 [7]. Figure 25.1 shows the comparison between the observed and modeled mean concentrations of EC and OA at all EMEP stations. In Fig. 25.1 we also show the scatter plots of observed and simulated EC and OA with the correlation coefficient (r), mean bias error (MBE), normalized mean bias error (NMBE) and normalized mean gross error (NMGE). WRF/Chem reproduces the observations of EC and OA with a r of 0.64 and 0.70, respectively. Although the model is in agreement with the lower end of the observed distribution, it tends to underestimate the measurements. EC is simulated with a negative MBE of $-0.35\ \mu g/m^3$ (-17 %), while the modeled OA mass is low biased of $-2.44\ \mu g/m^3$ (-38 %). One possible reason of the under prediction of modeled carbonaceous aerosols could be attributed to the coarse resolution of anthropogenic emissions. Indeed the analysis of OA: EC ratio reveals that WRF/Chem underestimates the observed correlation and slope of OA: EC ratio. The modeled values are 0.60 and 2.69, respectively, against the measured 0.77 and 3.63.

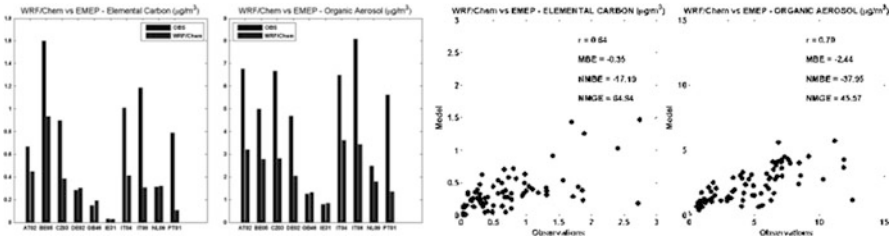

Fig. 25.1 (*left*) Inter comparison among the mean observations of EC/OA and WRF/Chem simulations at each EMEP stations in the domain. (*right*) Scatter plots of observed and simulated EC and OA. Some statistical indices (see the main text) are also shown

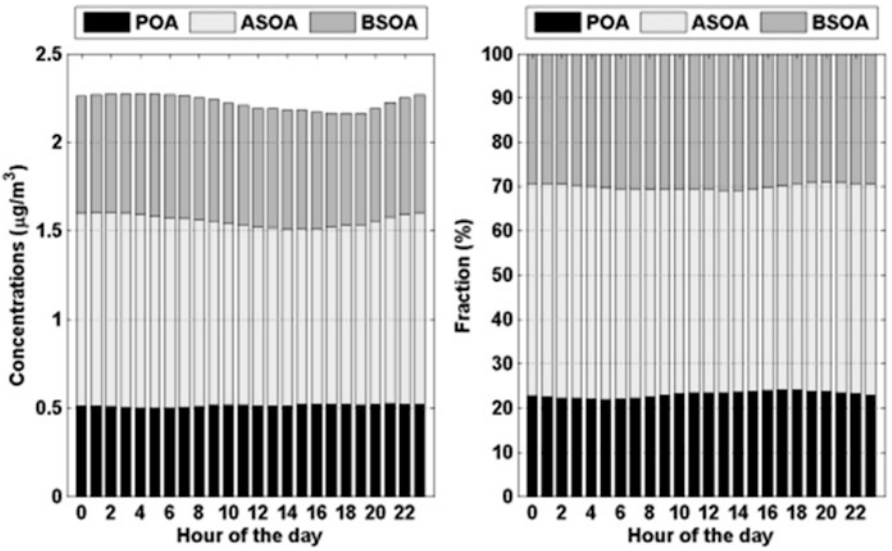

Fig. 25.2 Diurnal cycle of modeled OA composition (see the main text) averaged over all EMEP sites and over all days during May–June 2003. (*left*) Average diurnal variations in OA composition. (*right*) Mean diurnal variation in constituent fraction of OA

Another potential source of negative bias is the absence of wild fire emissions, which in spring time may contribute to 5–35 % of the European aerosol optical depth [8]. The reader should also consider that the configuration of the model used here treats the inorganic and organic aerosols only in the nuclei and accumulation mode, while the EMEP data are referred to the PM10 mass. Putaud et al. [9] reported that EC and OA over Europe contribute to 1–10 % and 5–15 % respectively to PM coarse mass. Finally, the model results should be affected by the assumption on the deposition velocity of OCV.

Figure 25.2 shows the mean diurnal cycle of modeled OA composition at EMEP station. The concentrations of primary OA (POA), anthropogenic SOA (ASOA) and biogenic SOA (BSOA) are nearly constant throughout the day. The simulated SOA/OA ratio is about 80 %, at the upper end of the 50–80 % observed over Europe [1]. Moreover, the average predicted BSOA/SOA ratio is about 30 %, but it is about 50 % at the stations in South Europe.

Future work will include the direct and in direct aerosol effects in the new chemical option used in this work and validate it over Europe.

Acknowledgments This work was founded by University of L'Aquila (Italy) and Regione Abruzzo in the frame of "Higher Education Project" (P.O.F.S.E 2007-2013), and Italian Space Agency in the frame of the PRIMES (contract I/017/11/0) projects. Paolo Tuccella is grateful to NOAA for the hospitality.

References

1. Jimenez JL et al (2009) Evolution of organic aerosol in the atmosphere. Science 326:1525. doi:10.1126/science.1180353
2. Ahmadov R et al (2012) A volatility basis set model for summer time secondary organic aerosols over the eastern U.S. in 2006. J Geophys Res 117:D6. doi:10.1029/2011JD016831
3. Grell GA et al (2005) Fully coupled "online" chemistry within the WRF model. Atmos Environ 39:6957–6975
4. Mckeen SA et al (2007) Evaluation of several PM2.5 forecast models using data collected during the ICARTT/NEAQS 2004 field study. J Geophys Res 112:D10S20. doi:10.1029/2006JD007608
5. Tuccella P et al (2012) Modeling of gas and aerosol with WRF/Chem over Europe: evaluation and sensitivity study. J Geophys Res 117:D03303. doi:10.1029/2011JD016302
6. Yttri KE et al (2007) Elemental carbon and organic carbon in PM10: a one year measurement campaign within the European Monitoring and Evaluation Program EMEP. Atmos Chem Phys 7:5711–5725. doi:10.5194/acp-7-5711-2007
7. Bessagnet B et al (2008) Regional modeling of carbonaceous aerosols over Europe – focus on secondary organic aerosols. J Atmos Chem 61:175–202. doi:10.1007/s10874-009-9129-2
8. Barnaba F et al (2011) An important finger print of wild fires on the European aerosol load. Atmos Chem Phys 11:10487–10501. doi:10.5194/acp-11-10487-2011
9. Putaud JP et al (2010) A European aerosol phenomenology-3: physical and chemical characteristics of particulate matter from 60 rural, urban, and kerbside sites across Europe. Atmos Environ 44:1308–1320. doi:10.1016/j.atmosenv.2009.12.011

Chapter 26
Impact of Aerosol Properties on Cloud and Precipitation Formation

Christelle Barbet, Laurent Deguillaume, and Nadine Chaumerliac

Abstract Clouds droplets are directly dependent on aerosols that are present in the atmosphere and on their probabilities to act as cloud condensation nuclei (CCN). So, it is necessary to study aerosols distributions native to different air masses in order to understand cloud droplets distributions. Sensitivity tests, using WRF-chem (Weather Research and Forecast), should allow an improvement in the knowledge of aerosol properties and their impacts on cloud droplets and precipitation. From this perspective, simulations for various air masses are simulated with WRF-chem using RADM2 (Stockwell et al., J. Geophys Res, 95:16343–16367, 1990) chemical mechanism associated with MADE/SORGAM aerosol module (Ackermann et al., Atmos Environ, 32(17):2981–2999, 1998) which dissociates aerosols into three modes: Aitken, accumulation and coarse modes. Furthermore, comparisons are presented between model outputs and observation data from the puy de Dôme site. This site, part of the ACTRIS network, has been equipped with many probes in order to characterize the physical, chemical and optical properties of aerosol particles, to quantify gases (O_3, CO, CO_2, NO, NO_2, ...), to measure radiation and to document typical meteorological parameters and in particular cloud parameters (cloud water content, cloud droplet concentrations and mean radius).

Keywords Aerosol Modelling • Clouds • Precipitation

C. Barbet (✉) • L. Deguillaume • N. Chaumerliac
Laboratoire de Météorologie Physique (LaMP), CNRS, Clermont Université, Université Blaise Pascal, BP 80026, 63171 Aubière, France
e-mail: c.barbet@opgc.univ-bpclermont.fr

D.G. Steyn et al. (eds.), *Air Pollution Modeling and its Application XXII*,
NATO Science for Peace and Security Series C: Environmental Security,
DOI 10.1007/978-94-007-5577-2_26, © Springer Science+Business Media Dordrecht 2014

26.1 Introduction

Since several years, a significant increase of emissions of gases and aerosols particles has been observed. Thus, efforts have been made by the scientific community to better understand the atmospheric chemistry. Therefore, one of the fundamental actors of the atmospheric chemistry is aerosol particles. These ones are classified into two categories according to their production mechanism: primary particles which are directly emitted into the atmosphere and secondary particles which are formed from gaseous precursors through gas-particle conversion. Aerosols can modify the Earth's radiative budget. In fact, they can absorb or diffuse solar and terrestrial radiations which lead to a warming or a cooling of the atmosphere (direct effect). Moreover, they can have a significant radiative impact via their interactions with clouds (indirect effect).

Modeling studies attempt to correctly represent atmospheric environment. For this, chemistry mechanisms are increasingly introduced inside transport models. Chemical species are exposed to various reaction pathways and their change between gaseous, aerosol and cloud phases are studied. Interactions between microphysical, chemical, radiative and dynamical processes are also considered. In addition, observational data are essential to make comparisons with models outputs in order to improve all the processes taken into account.

26.2 Model Description

WRF-chem model results from the coupling of the WRF (Weather Research and Forecast) with a chemistry module. This coupling between dynamics, radiation and chemistry allows for simulating gases, aerosols and cloud chemistry. A double-moment microphysical scheme module, developed by Morrison et al. [1] and predicting the number concentration of cloud water as the number concentration and the mixing ratio of rain, ice, snow and graupel, is used. The chemical mechanism, RADM2 includes 26 stable species and 16 peroxy radicals for organic species and 14 stable species, four reactive intermediates and three abundant stable species (oxygen, nitrogen and water) for inorganic species. In order to limit number of model groups, some similar organic compounds are grouped together based on the principle of reactivity weighting. Aggregation factors, computed by Middleton et al. [2], are used for VOC (Volatile Organic Compounds). RADM2 chemical mechanism is coupled with MADE. Moreover, secondary organic aerosols are simulated due to the incorporation of SORGAM into MADE [3]. Thereby, the size distribution of aerosols is represented by three modes (Aitken, accumulation and coarse mode). Each mode is represented by a log-normal distribution. The dynamical processes include condensation, coagulation, size-dependent dry deposition and sedimentation, advective and diffusive transport and aerosol-cloud interaction. Particle formation is treated by two processes: direct particle emission and secondary formation by nucleation.

26.3 Emissions Data Sets Used Within WRF-Chem Model

Three types of emissions data sets are necessary to correctly initialize chemical species in the model: anthropogenic, biogenic and biomass burning (wildfire) emissions data.

- Anthropogenic emissions come from two different data sets: TNO-MACC [4] and MACCity [5]. TNO-MACC emissions are available from 2003 to 2007 with a yearly temporal resolution and spatial resolution of 0.5° per 0.5°. Chemical species emissions used are: NMVOC, PM10 and PM2.5. MACCity provides information about a lot of gases but also about BC and OC emissions. Data are available from 1990 to 2010 with a monthly temporal resolution and spatial resolution of 0.5° per 0.5°.
- Biogenic emissions are provided by MEGAN with estimations for gas and aerosols emissions from terrestrial ecosystems into the atmosphere [6]. Its temporal resolution is around 1 km;
- Biomass burning emissions are derived from the Fire Inventory from NCAR version 1.0 (FINNv1). As described by Wiedinmeyer et al. [7], global estimates of gas and particle emissions from open burning of biomass (wildfire, agricultural fires and prescribed burning) are provided with a daily temporal resolution and a temporal resolution close to 1 km.

Emissions units are mol/km^2/h for gases and μg/km^2/h for aerosols whereas WRF-chem units are ppmv for gases and μg/kg$_{(\text{dry air})}$for aerosols.

26.4 Comparisons Between Model Outputs and Observations Data

In order to compare model outputs and observations data, measurements performed at the puy de Dôme monitoring site are used. This latter is located in central France (45°46 N 2°57E) and is equipped with probes to characterize meteorology as well as gases and aerosol particles. One of them is the Aerodyne ToF-AMS [8] which provides information about chemical composition and mass concentration of the particulate matter (Fig. 26.1).

Concerning the simulation, a domain is defined by 360 grid points in the west-east direction and 390 grid points in the south-north direction with a resolution of 10 km. The center of the domain is 52.5° latitude and 15.0° longitude. The simulation starts on the 16th and ends on the 18th September 2008. On these days, a Mediterranean air mass was observed and sampled at the puy de Dôme station as it is described in detail by Freney et al. [9].

Figure 26.1 provides a sample of comparison between AMS data and model outputs for aerosol concentrations. The model captures the variability of the concentrations induced by the diurnal cycle and topographic forcing but underestimates

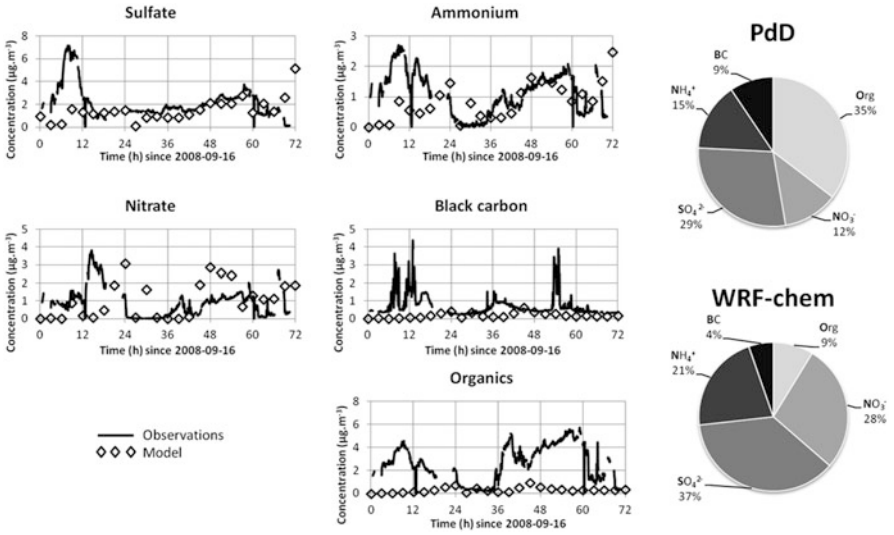

Fig. 26.1 Comparisons between WRF-CHEM outputs and observations at the puy de Dôme site for a Mediterranean air mass

their magnitude, especially in the case of particles, such as organic compounds and black carbon. Other situations from various air masses have been performed and exhibit the same behavior. Next step will be to consider cloudy situations to test the performance of the model and the impact of aerosol properties on cloud and precipitation formation.

References

1. Morrison H, Thompson G, Tatarskii V (2009) Impact of cloud microphysics on the development of trailing stratiform precipitation in a simulated squall line: comparison of one- and two-moment schemes. Mon Weather Rev 137:991–1007
2. Middleton P, Stockwell WR, Carter WPL (1990) Aggregation and analysis of volatile organic compound emissions for regional modeling. Atmos Environ 24A:1107–1113
3. Schell B, Ackermann IJ, Hass H (2011) Modeling the formation of secondary organic aerosol within a comprehensive air quality model system. J Geophys Res 106:28275–28293
4. Kuenen J, Denier Van der Gon H, Visschedijk A, Van der Brugh H (2011) High resolution European emission inventory for the years 2003–2007. TNO report, Utrecht
5. Lamarque JF, Bond T, Eyring V, Granier C, Heil A, Klimont Z, Lee D, Liousse C, Mieville A, Owen B, Schultz MG, Schindell D, Smith S, Stehfest E, VanAardenne J, Cooper O, Kainuma M, Mahowald N, McConnell J, Naik V, Riahi K, VanVuurent D (2010) Historical (1850–2000) gridded anthropogenic and biomass burning emissions of reactive gases and aerosols: methodology and application. Atmos Chem Phys 10:7017–7039
6. Guenther A, Karl T, Harley P, Wiedinmyer C, Palmer PI, Geron C (2006) Estimates of global terrestrial isoprene emissions using MEGAN (Model of Emissions of Gases and Aerosols from Nature). Atmos Chem Phys 6:3181–3210

7. Wiedinmyer C, Akagi SK, Yokelson RJ, Emmons LK, Al-Saadi JA, Orlando JJ, Soja AJ (2010) The Fire INventory from NCAR (FINN) – a high resolution global model to estimate the emissions from open burning. Geosci Model Dev Discuss 3:2439–2476
8. Canagaratna MR, Jayne JT, Jimenez JL, Allan JD, Alfarra MR, Zhang Q, Onasch TB, Drewnick F, Coe H, Middlebrook A, Delia A, Williams LR, Trimborn AM, Northway MJ, DeCarlo PF, Kolb CE, Davidovits P, Worsnop DR (2007) Chemical and microphysical characterization of ambient aerosols with the aerodyne aerosol mass spectrometer. Mass Spectrom Rev 26:185–222
9. Freney EJ, Sellegri K, Canonaco F, Boulon J, Hervo M, Weigel R, Pichon JM, Colomb A, Prévôt ASH, Laj P (2011) Seasonal variations in aerosol particle composition at the Puy-de-Dôme research station in France. Atmos Chem Phys 11:13047–13059
10. Riemer N, Vogel H, Vogel B, Schell B, Ackermann I, Kessler C, Hass H (2003) Impact of the heterogeneous hydrolysis of N2O5 on chemistry and nitrate aerosol formation in the lower troposphere under photosmog conditions. J Geophys Res 108(D4):4144
11. Zaveri RA, Easter RC, Fast JD, Peters LK (2008) Model for Simulating Aerosol Interactions and Chemistry (MOSAIC). J Geophys Res 113. doi:10.1029/2007JD008782
12. Bertram TH, Thornton JA (2009) Toward a general parameterization of N2O5 reactivity on aqueous particles: the competing effects of particle liquid water, nitrate and chloride. Atmos Chem Phys 9:8351–8363
13. Ackermann IJ, Hass H, Memmesheimer M, Ebel A, Binkowski FS, Shankar U (1998) Modal aerosol dynamics model for Europe: development and first applications. Atmos Environ 32(17):2981–2999
14. Stockwell WR, Middleton P, Chang JS, Tang X (1990) The second generation regional acid deposition model chemical mechanism for regional air quality modeling. J Geophys Res 95:16343–16367

Questions and Answers

Questioner Name: Johannes Bieser

Q: How did you create the model emissions? (temporal and vertical disaggregation, interpolation, PM speciation, biogenic emissions)
A: Anthropogenic emissions used in the model do not have a temporal evolution during the day and are produced only at surface level.
For gases such as non-methane volatile organics compounds (NMVOC), some of emitted species are lumped together into one model species. First, gaseous species are differentiated using IPCC (2007). Then, they are lumped in model species according to their aggregation factor, detailed in Middleton et al. [2].
To initialize PM, four kinds of emissions are used: PM2.5, PM10, elemental carbon (EC) and organic carbon (OC). Concerning PM2.5, they are divided between unidentified PM25, sulfate and nitrate particulate matter. The others are allocated to PM10, EC and OC respectively. For aerosol species, there are two categories: one for the Aitken mode of the aerosol distribution and one for the accumulation mode. Thus, 20 % of the emitted specie is allocated to the Aitken mode and 80 % to the Accumulation mode.
Biogenic emissions are coming from MEGAN which uses global emissions dataset with 1 km spatial resolution for the year 2003.

Questioner Name: SebnemAksoyoglusloan

Q: In both cases (WRF-Chem and WRF-CHIMERE), the meteorological model is the same, WRF. Was there any difference between two models with respect to meteorology, precipitation? If yes, where does the difference come from?
A: WRF-Chem is an online model whereas WRF-CHIMERE is an offline model. Thus, using WRF-Chem, feedbacks of aerosols and gaseous species on meteorological processes are allowed that's why we can say that precipitation and cloud formation are directly impacted and different between the two models. Also, a two-moment microphysical scheme is implemented in WRF-Chem.

Questioner Name: GolamSarwar

Q: Model predicted aerosol nitrate compare well with observed data. HNO_3 can be formed by homogeneous as well as heterogeneous conversion of N_2O_5 into HNO_3. Does the model account for heterogeneous conversion of N_2O_5 into HNO_3?
A: Even if the heterogeneous reaction of N_2O_5 plays an important role in HNO_3 formation, especially during nighttime, and consequently on aerosol nitrate [10], it is not represented in the chemical mechanism that we use (RADM2/MADE/SORGAM). However, it is possible to run WRF-Chem with MOSAIC aerosol scheme [11] which includes the N_2O_5 heterogeneous reaction scheme of Bertram and Thornton [12] based upon laboratory experiments.

Chapter 27
Numerical Study on Reduction of Ambient NOx, PM, and VOCs Concentrations by ACF (Activated Carbon Fiber) Fences: Effects of Generated Air Flow and Chemical Reactivity of the ACF Fences

Toshihiro Kitada, Yasuhiro Kurodai, Takaaki Shimohara, Takao Kanzaki, Masaaki Yoshikawa, and Takayuki Tokairin

Abstract A method to use fences of activated carbon fiber (ACF) is presented to reduce high NO_2, PM, and VOCs concentrations in urban atmosphere without excess energy use. Polluted air in road space moves with natural and car-induced winds to contact with and to flow through ACF fences, and the ACF layer removes these pollutants. That this "energy-free" equipment can reduce high NOx by 15–50 % at the roadside is numerically evaluated.

Keywords ACF fences • High NOx • Energy free removal • Natural wind

27.1 Introduction

To reduce high NO_2 concentration at the roadside with extremely heavy trafic, mainly two methods were tested in Japan for the last 15 years; one is TiO_2 coated panels which were used, for example, on Route 43 in Osaka City, Osaka Pref.

T. Kitada (✉)
Gifu National College of Technology, Motosu, Japan

Department of Environmental and Life Sciences, Toyohashi University of Technology, Toyohashi, Japan
e-mail: kitada@gifu-nct.ac.jp

Y. Kurodai • T. Tokairin
Department of Environmental and Life Sciences, Toyohashi University of Technology, Toyohashi, Japan

T. Shimohara
Fukuoka Institute of Health and Environmental Studies, Fukuoka, Japan

T. Kanzaki
Department of Mechanical Engineering, Daido University, Nagoya, Japan

M. Yoshikawa
Osaka Gas Co. Ltd., Tokyo, Japan

D.G. Steyn et al. (eds.), *Air Pollution Modeling and its Application XXII*,
NATO Science for Peace and Security Series C: Environmental Security,
DOI 10.1007/978-94-007-5577-2_27,

The panels trap NOx on their surface by oxidizing NO_2 to $NO_3^-(HNO_3)$. The other one is to use specially prepared soil layer. The method was applied, for example, on Route 43 in Nishinomiya City, Hyogo Pref. Micro-bial actibity in the soil layer scavenges NOx in the polluted air which is pumped into the soil layer after oxidation of NO to NO_2 by generated ozone. These two methods have their own demerits and did not show clear effect on reduction of high NO_2 concentration; the demerit of TiO_2 panel is its rather small contact efficiency with polluted air due to small specific active-surface area, while deficit of the soil layer method is its high running cost and requires large area for setting.

To eliminate these deficits, a method to use fences of activated carbon fiber (ACF) has been developed to reduce high NO_2, PM, and VOCs concentrations in urban atmosphere without excess energy use. Polluted air in road space moves with natural and car-induced winds to contact with and to flow through ACF fences, and the ACF layer removes NOx, PM, and VOCs from the polluted air. This idea of "energy-free" equipment for air pollution reduction is proposed and numerically evaluated.

27.2 Governing Equations

For evaluation of the ACF fence's performance in NOx concentration reduction, a set of non-thermal flow equations and advection-diffusion equation of air pollutant was applied with a standard k-ε turbulence model. ACF fence was treated as porous media [1, 2]. In this chapter some of the equations characterizing ACF fence simulation are focused. Momentum equation is written as:

$$K_{jk}U_k\frac{\partial U_i}{\partial x_j}=-\frac{1}{\rho}\frac{\partial p}{\partial x_i}+\frac{\partial}{\partial x_j}\left(\nu_t K_{jk}\left(\frac{\partial U_i}{\partial x_k}+\frac{\partial U_k}{\partial x_i}\right)\right)+B_i \quad (i,j,k=1,2,3) \tag{27.1}$$

where B_i is the resistance to the flow in the porous media (ACF fence):

$$B_i=-\gamma R_c U_i \tag{27.2}$$

Advection-diffusion equation of air pollutant is also written as:

$$\frac{\partial}{\partial x_i}\left(\rho K_{ij}U_j C-\rho\Gamma_t K_{ij}\frac{\partial C}{\partial x_j}\right)=-\gamma k_c \rho C \tag{27.3}$$

The symbol γ and K_{ij} in Eqs. 27.2 and 27.3 denote the volume porosity and the area porosity tensor, respectively. K_{ij} accounts for directivity of the flow in the porous media (ACF fence) and was assumed as a unit tensor. A similar system of equations with resistance formulation different from Eq. 27.2 and no chemical reaction was applied elsewhere [3]. R_c in Eq. 27.2 and k_c in Eq. 27.3 are two important parameters characterizing ACF fence module. Solver of these equations were CFX5 [4].

27.3 Removal Rate Coefficient, k_c and Resistance Coefficient, R_c

NOx (=NO + NO_2) removal by ACF may be influenced by several factors such as type of ACF, packing density of ACF, and coexistence of other gases [5]. For simplicity, we assumed the first order removal reaction by using laboratory experiments [5]. The rate coefficient k_c was determined for packing density of ACF at 0.066 g cm^{-3} (corresponding to $\gamma = 0.95$) as:

k_C for NOx: 1–2 s^{-1} and k_C for NO_2: 2–3 s^{-1}

In numerical experiments, we varied k_C as a parameter ranging 0–3 s^{-1}.

Coefficient R_c in the term B_i (Eq. 27.2) was estimated by laboratory experiments which determined relationship between pressure drop and flow velocity in ACF layer. Obtained R_c values for two types of ACF fence-module were as follows:

$\gamma\rho R_c \equiv \bar{R}_C \cong 3700\left(kg\ m^{-3}s^{-1}\right)$ for panel type ACF fence module, and
$\gamma\rho R_c \equiv \bar{R}_C \cong 400\left(kg\,m^{-3}s^{-1}\right)$ for slit type ACF fence module

In the panel type module ACF was packed in 10 cm thick with the density of 0.066 g cm^{-3}, while in the slit type module many thin panels of 0.6 cm thick with the same ACF packing density were placed parallel each other with a distance of 1.6 cm between adjacent thin panels [5, 6].

27.4 Calculation Domain and Simulation Conditions

Two types of calculation domain were assumed: one is for double fences set at both sides of the road as shown in Fig. 27.1, and the other one is for single fence set only at lee side of the road. Pollutant was assumed to be discharged from the

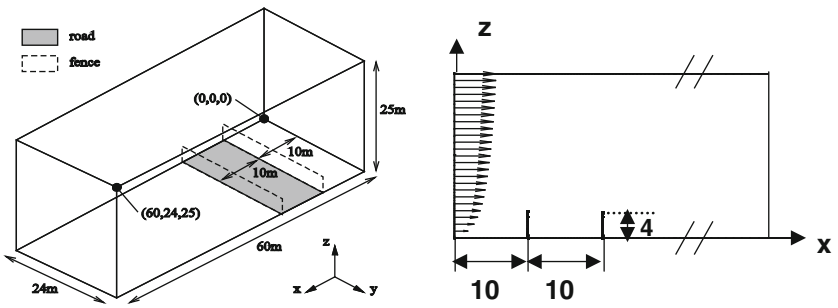

Fig. 27.1 Calculation domain for double fences case: 3D view (*left*), and x–z cross section (*right*). Wind at the upstream boundary is shown schematically on the *right panel*; velocity is 1.5 m s^{-1} at 2 m high. In the single fence case only one fence is remained at the downstream side. Road width is 10 m. Each fence is 4 m high and 10 cm thick

road surface as constant volume source. In the calculation inside of each fence of 10 cm thick was resolved with a grid size of $\Delta x = 2$ cm for main stream direction (x axis).

27.5 Results and Discussion

For double- and single-fence cases, performance of the ACF fences in NOx concentration reduction at the roadside was numerically evaluated. Two parameters characterizing ACF fence, k_c and $\bar{R}_C$ were varied based on the laboratory experiments described in the Sect. 27.3.

27.5.1 Calculated NOx Field

Figure 27.2 shows NOx fields for double-fence cases with varied parameter-values of kc and $\bar{R}_c$. Figure 27.2a, b present cases with no NOx-removal-activity of the fences $k_c = 0\ s^{-1}$, while Fig. 27.2c, d are those with $k_c = 3\ s^{-1}$. To see the effect of the other parameter $\bar{R}_c$, Fig. 27.2a, c stand for cases with smaller resistance ("slit" type fence module) $\bar{R}_C = 400\ (kg\ m^{-3}s^{-1})$, while Fig. 27.2b, c show larger resistance cases ("panel" type fence module) with $\bar{R}_C = 3700\ (kg\ m^{-3}s^{-1})$. It is shown that both types of ACF fences with NOx removal activity can largely decrease

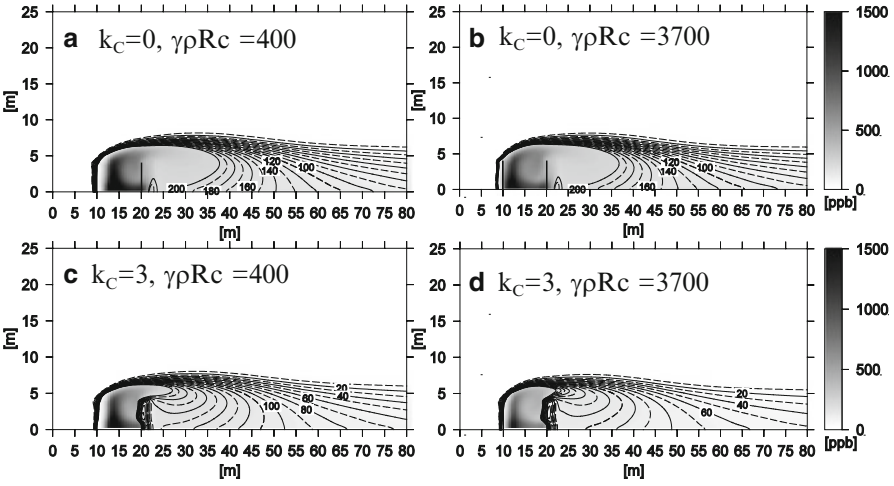

Fig. 27.2 NOx field in double-fence cases with $\bar{R}_c$ $(= \gamma\rho Rc)$ and k_C as parameters: (**a**, **b**) for no removal activity of ACF fences. (**c**, **d**) for removal activity with $k_c = 3\ s^{-1}$. Contour interval is 10 ppb

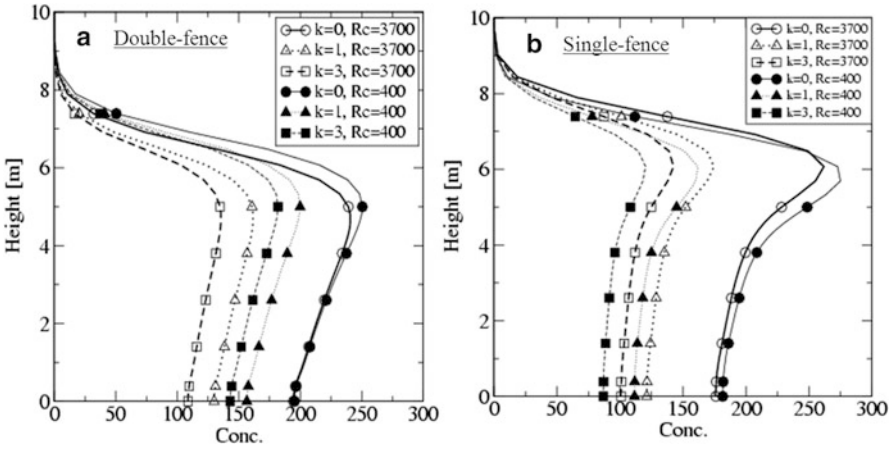

Fig. 27.3 Vertical profiles of calculated NOx (ppb) at 10 m downstream from thelee-ward fence: (**a**) double-fence, and (**b**) single-fence. Profiles are shown with parameters $\bar{R}_c$ and k_C (see text for detail)

NOx concentration at leeside of the road (Fig. 27.2c, d). Closer look at Fig. 27.2c, d further indicates that in the double-fence situation the "panel" type fence module, with larger resistance, show better performance in reduction of NOx concentration.

27.5.2 Evaluation of NOx Concentration Reduction by ACF Fence

Figure 27.3a, b shows NOx profile at 10 m downwind from the leeward side fence (namely, at x = 30 m in Fig. 27.2). Double- and single-fence cases are presented in Fig. 27.3a, b, respectively. In the single-fence situation only leeward side fence is remained from the double-fence case shown in Fig. 27.2.

Results of "double-fence" case (Fig. 27.3a) demonstrate ACF fences can reduce near-surface NOx concentration at the roadside by 15–40 % compared with the no-removal activity case ($k_c = 0$). Since the difference in NOx concentrations between cases with $k_c = 1$ and 3 is relatively small, the NOx removal by ACF fence can be rather diffusion-limited if k_c value exceeds around 1 s^{-1}. Moreover, it is suggested that fence of larger resistance, which corresponds to "panel" type module with $\bar{R}_C = 3700 \ \left(kg\ m^{-3}s^{-1}\right)$, can lead to larger decrease of NOx concentration (open symbols in Fig. 27.3a) than that of lower resistance (solid symbols in Fig. 27.3a) with "slit" type module of $\bar{R}_C = 400 \left(kg\ m^{-3}s^{-1}\right)$. This can be explained by the calculation result that the low resistance fence on upwind side allows clean air outside the fence to intrude into the road space and the clean air blocks contact of the polluted air over the road with the upwind ACF fence.

Also in single-fence situation, it is shown that the ACF fences can cut NOx concentration by 30–55 % (Fig. 27.3b). In contrast to the double-fence case, fence with small resistance ($\bar{R}_C = 400$) is better for lowering NOx concentration. In the case of single fence set on the leeside of the road, the lower resistance fence leads to higher pollutant flux into the ACF layer, and thus larger reduction of NOx can be expected.

27.6 Summary and Conclusions

Two important parameters on the ACF fence were identified: one is the resistance of ACF layer to the air flow and the other is the removal reactivity of ACF for NOx, PM, and VOCs. With these two parameters varied, performance in pollutants' removal of both double fences along the road and single fence set on the lee side of the road was investigated. Obtained results showed: (1) in the double fences case, larger resistance of the ACF layer to the air flow is rather preferable for effective reduction of ambient NOx, PM, and VOCs concentrations, because the circulating flow formed in the vertical cross section in the road space is enhanced by the larger resistance and thus contact of polluted air in the road space with the ACF fence on the upwind side is promoted, (2) in the single fence case, on the other hand, smaller resistance of the fence is better for the pollutants' removal, since higher pollutants' fluxes into the ACF layer are obtained, (3) in both cases, the phenomena are found rather diffusion-limited, indicating frequency of the contact of polluted air with the fences is important, and (4) the ACF fences can reduce ambient NOx concentrations near road by more than 30 % without excess energy use.

References

1. Nagano M, Kitada T, Shimohara T, Kanzaki T, Ichikawa Y, Yoshikawa M (2008) ACF (Activated Carbon Fiber) for reduction of ambient NO_2 concentration at the roadside. In: Advances in Wind and Structures (AWAS'08), Jeju, pp 1203–1212
2. Nagano M, Kitada T, Kanzaki T, Ichikawa Y, Shimohara T, Yoshikawa M (2009) Reduction of ambient NOx concentration at roadside by the porous fences filled with ACF: comparison of numerical model with wind tunnel experiment. Global environmental research (chikyu kankyou kenkyu ronbunshu). Jpn Soc Civ Eng 17:115–121, in Japanese with English abstract
3. Tokairin T, Kitada T (2005) Study on the effect of porous fence on air quality and traffic noise level around a double-decked road structure. Environ Monit Assess 105:121–143
4. ANSYS (2005) ANSYS CFX-Solver manuals
5. Shimohara T, Niiya S, Mitoma S, Yoshikawa M, Kitada T (2011) Air purification technology using activated carbon fiber. I. NOx purification properties and the air purification technique by forced ventilation system with ACF. J Jpn Soc Atmos Environ 46(3):187–195, in Japanese with English abstract
6. Shimohara T, Niiya S, Mitoma S, Yoshikawa M, Kitada T (2012) Air purification technology using activated carbon fiber. II. Study on de-NOx system using ACF through the natural ventilation system. J Jpn Soc Atmos Environ 47(1):58–66, in Japanese with English abstract

Questions and Answers

Questioner Name: Anthony Dore

Q: ACF was shown to capture NO_2 more efficiently than NO. With vehicle emissions changing towards a higher fraction of NO_2 in primary emissions, will the fences have a greater impact?
A: The ACF will more effectively reduce ambient NOx concentration with a higher fraction of NO_2 in vehicle emissions, since a higher fraction of NO_2 in ambient NOx concentration leads to a larger removal rate coefficient of NOx, k. However, it may also be noted that the NOx removal by the ACF fences is rather diffusion-limited if the k value is larger than about 1 s^{-1}.

Questioner Name: Peter Builtjes

Q: Does the ACF also work for PM?
A: The ACF can remove PM, and the removal is more efficient for particles coarser than sub-micron.

Chapter 28
Application of PMF for Evaluation of the Fine Particles Contribution from Vehicular Emission in Six Brazilian Cities

Maria Andrade, Beatriz Oyama, Adalgiza Fornaro, Regina Miranda, and Paulo Saldiva

Abstract The vehicular emission is the main source of fine particles in Brazilian Cities. A comprehensive study was performed from 2007 to 2009 with 24 h daily sampling of fine particles in an experimental site in six Brazilian capitals: Sao Paulo, Rio de Janeiro, Curitiba, Porto Alegre, Recife and Belo Horizonte. The polycarbonate filters collected at each site with Harvard sampling, were submitted to gravimetrical analysis for identification of PM2.5 concentration, to reflectance for Black Carbon concentration, to X-ray fluorescence analysis for elemental composition and to ion chromatography for an ion sand cations composition and concentration. The average PM2.5 concentration were 28, 19, 17, 17, 16 and 11 $\mu g/m^3$ in São Paulo, Rio de Janeiro, Belo Horizonte, Curitiba, Porto Alegre and Recife, respectively. Black Carbon accounted for approximately 30 % of the PM2.5 mass concentration in the more air pollution impacted cities: Sao Paulo, Rio de Janeiro and Belo Horizonte. The Black Carbon was used as a tracer for diesel fuel emission and biomass burning. The elemental chemical composition of the PM2.5 was used to identify source-related fractions of fine particles, by means of Receptor Models. The results were used to examine the association of these fractions with daily mortality in each of the six cities. Principal Matrix Factorization (PMF) was applied to the elemental concentration data in order to identify the sources of fine particles, specifically the participation of the vehicular emission. These results were compared to the previous analysis performed with Absolute Principal Component Analysis (APCA). The participation of the vehicular fleet to the PM2.5 mass concentration was significant, explaining in the most urbanized area even 40 % of its mass. These results show the relative importance of the vehicular emission to health injury.

Keywords Particulate matter • Vehicular emissions • Observations • Principal matrix factorization • Receptor models

M. Andrade (✉) • B. Oyama • A. Fornaro • R. Miranda • P. Saldiva
Universidade de Sao Paulo, rua do Matao 1226, Sao Paulo 05508-090, Brazil
e-mail: mftandra@model.iag.usp.br

D.G. Steyn et al. (eds.), *Air Pollution Modeling and its Application XXII*,
NATO Science for Peace and Security Series C: Environmental Security,
DOI 10.1007/978-94-007-5577-2_28,

Chapter 29
Study of Aerosol Particle Scavenging by Rain, Experiments and Modelling

Arnaud Quérel, Pascal Lemaitre, Marie Monier, Emmanuel Porcheron, and Andrea Flossmann

Abstract The understanding and the anticipation of the environmental fallout in case of severe nuclear accidents with radioactive releases is crucial for the environment. In this study we aim to improve our knowledge on the aerosol particles scavenging, in particular the washout by raindrops with a diameter larger than 1 mm.

29.1 Introduction

The Institut de Radioprotection et de Sûreté Nucléaire (IRSN) is involved in the understanding and the anticipation of the environmental fallout of a nuclear accident. In collaboration with the Meteorology Laboratory of Clermont-Ferrand (LaMP), this work is devoted to improve our knowledge on the aerosol particles scavenging, in particular the washout by raindrops with a diameter larger than 1 mm.

The analysis of ground contamination after the Chernobyl accident has indeed highlighted some differences with the results of aerosol scavenging models. The model presently used at IRSN underestimates the aerosol deposition to the ground [1, 2]. This work takes place within the IRSN efforts to improve the modelling of aerosol scavenging by rain, in order to evaluate more precisely the radioactive fallout and the ground contamination in case of a severe accident with a release of radioactivity into the troposphere.

After an emission of radioactive pollutants, radionuclides quickly react with atmospheric aerosols (adsorption and coagulation processes) to form radioactive

A. Quérel (✉) • P. Lemaitre • E. Porcheron
IRSN, BP68, 91192 Gif-sur-Yvette, France
e-mail: arnaud.querel@irsn.fr; pascal.lemaitre@irsn.fr; emmanuel.porcheron@irsn.fr

M. Monier • A. Flossmann
LaMP, Université Blaise Pascal – CNRS – OPGC, 24 avenue des Landais, Aubiere, Cedex 63177, France
e-mail: M.Monier@opgc.univ-bpclermont.fr; A.Flossmann@opgc.univ-bpclermont.fr

D.G. Steyn et al. (eds.), *Air Pollution Modeling and its Application XXII*,
NATO Science for Peace and Security Series C: Environmental Security,
DOI 10.1007/978-94-007-5577-2_29,

particles [1]. It is considered that atmospheric particles keep their physical properties (mass, density and morphology) in relation to the scavenging mechanisms.

Two aspects of aerosol particles deposition can be distinguished: the dry deposition and the wet scavenging.

However, the wet deposition "only" depends on the aerosol characteristics and the meteorological conditions, particularly on the rain characteristics. The wet scavenging itself can be divided into two mechanisms, the rainout and the washout.

This extended abstract only deals with washout; it takes place below the cloud, considering the scavenging of atmospheric aerosol particles by raindrops during their fall. It is particularly efficient in the case of a rain event during, or shortly after, an emission of radioactive aerosols, when they are still below clouds.

With the knowledge of the microscopic phenomena and an appropriate description of the rain, it should be possible to predict the mass of aerosol scavenged during a rain event.

29.2 The DESCAM Model

DESCAM [2] was developed to model aerosol and gas scavenging in the atmosphere. Today DESCAM models the cloud formation, and it is already operational to compute the aerosol washout.

Then, the DESCAM model is used to compute the evolution of the mass of aerosol particles at each altitude in the atmospheric column, during a hypothetic rain event. So, it is possible to determine easily the washout coefficient. To be executed, the DESCAM model needs a matrix of collection efficiencies. The collection efficiency is defined as the ratio between the aerosol mass collected by a single drop and the total mass of aerosol particles in the volume it has crossed [3].

In this work, the collection efficiency is presented as a function of three parameters: drop size, particle size and relative humidity. With a complete collection efficiency database, the computation of the washout coefficient is possible. In the ranges of our study of the collection efficiencies (particles between 0.1 and 10 μm and drops between 1 and 5 mm) there is a lack of collection efficiencies data.

So, the goal of this work is to obtain more reliable collection efficiencies data for these ranges of drops and particles in order to improve the DESCAM washout model.

29.3 Facility for Collection Efficiency Measurements

A free fall shaft similar to the one of Wang and Pruppacher [4] is used to measure the collection efficiency. A 10 m shaft was built in our laboratory, able to reach 98 % of the terminal velocity for a raindrop smaller than 5 mm. At the bottom of the shaft, there is an aerosol chamber filled with particles of controlled size. Drops

are collected after their path through the aerosol chamber. By this way, the mass of aerosols collected is measured.

To measure the efficiency, a fluorescein tracing method is used [5]. Fluorescein is a molecule highly detectable in liquids by its fluorescence under UV light: the lowest measurable concentration is 5.10–11 g/cm^3.

Fluorescein powder is dissolved in water, then this liquid is atomized and the droplets produced are dried, creating fluorescein aerosol particles. The droplets are created by an ultrasonic generator: a ceramic vibrates at 500 or 2,400 kHz (depending on the apparatus used), creating a fog of mono-disperse droplets. Then the resulting distribution of particles of fluorescein is almost mono-disperse. Fluorescein particles are collected by the falling drops during their path through the chamber. Finally the drops are collected after their path through the aerosol chamber and analysed with an appropriate fluorimeter. This instrument sends UV light through the collected liquid (between 100 and 250 drops), and the intensity of the fluorescent light is measured. As the fluorescence intensity is proportional to the fluorescein concentration, the fluorescein aerosol mass collected by drops is determined.

It is necessary to know the number and the size of particles in the aerosol chamber. The particle distribution measurements are done by an ELPI device (Electrical Low Pressure Impactor, Marjamäki et al. [6]) and an APS (Aerodynamic Particle Sizer TSI-3321). The APS has a better resolution (52 channels against 12), but its range of measurement is only between 0.5 and 20 μm. Thus, to measure particles smaller than 0.5 μm the ELPI is used.

The mass density of particles inside the aerosol chamber is determined by a sample on filters. Air is sampled through a HEPA filter, then the filter is withdrawn and the mass of fluorescein collected by the filter is determined. Knowing the flow and the duration of the sample, the mass density of fluorescein in the aerosol chamber is calculated.

Knowing the particle size, the number of particles in the aerosol chamber, the fluorescein mass density, the height of the aerosol chamber and the drop size, it is possible to determine the collection efficiency.

29.4 Results

At the moment, only two drops have been studied for a full range of particles: drops of 2.1 and 2.6 mm diameter.

Results are presented in Fig. 29.1. Other data are added to this figure:

- the detection limit of fluorescein,
- the two experimental points of Lai et al. [7] which are in our range of drops and particles,
- the current data in DESCAM for drops of 2.05 mm (continuous line).

Figure 29.1 shows the evolution of the collection efficiency as a function of the particle diameter between 0.3 and 4 μm for drops of 2.1 and 2.6 mm. The detection

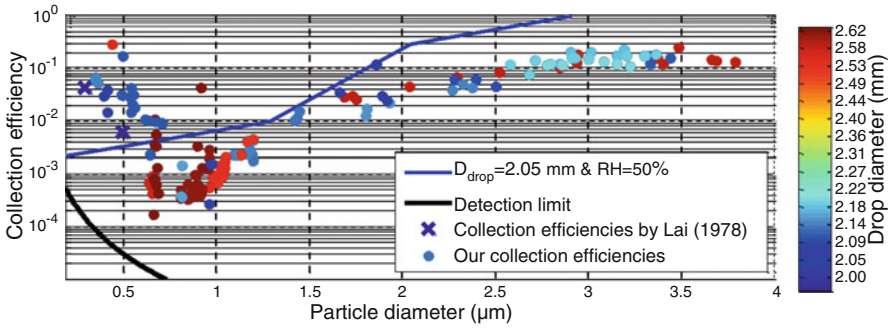

Fig. 29.1 Evolution of collection efficiencies

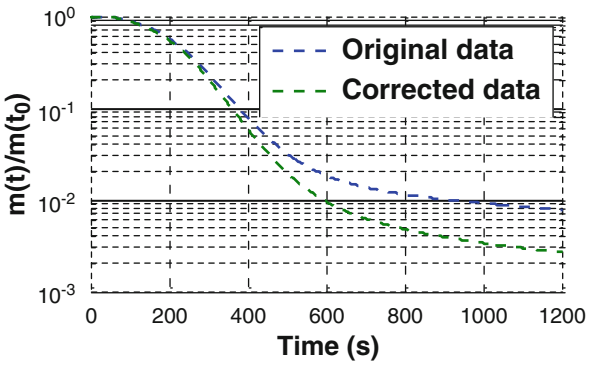

Fig. 29.2 Normalized mass of particles still in the atmosphere as a function of time

limit of the fluoresce in technique is plotted in this figure. Then we observe that the collection efficiencies are big enough to be reliably measured by this method.

Both of Lai's dots correspond to drops of 1.96 mm and particles of 0.3 and 0.5 μm. They appear well fitted with our own measurements.

The experimental points of the collection efficiency show a minimum around 0.8 μm. For particles smaller than 0.8 μm, the collection efficiency is decreasing as particle sizes increase, and is increasing for particle larger than 0.8 μm. So, the minimum of collection efficiency seems to correspond to particles of 0.8 μm for drops of 2.1 and 2.6 mm.

Present results are very different from the data used in DESCAM. Even if, for particles between 1.2 and 2 μm, DESCAM data are almost the same as our measurements, very strong differences appear for particles smaller than 1 μm and for particles larger than 2 μm.

Therefore, the extrapolation currently implemented in DESCAM must be improved by this new data. Figures 29.2 and 29.3 show the results obtained with the collection efficiencies matrix changed by these measurements and compared to the results obtained with the original matrix of collection efficiencies for a rain intensity of 10 mm/h.

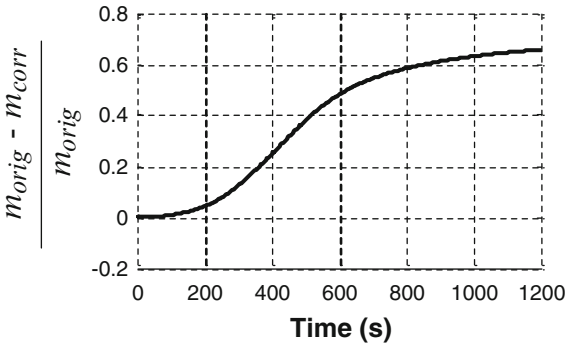

Fig. 29.3 Comparison of scavenging between the old and the new matrix of collection efficiencies

Figure 29.2 shows both evolutions of the mass of particles still in the atmosphere, with the original matrix of collection efficiencies and the corrected matrix.

The mass still in the atmosphere (and then potentially transported away) is less important with the corrected matrix. This result agrees with the very important increase of the collection efficiencies noted for particles between 0.1 and 0.8 μm. The decrease of the collection efficiencies observed for particles between 2 and 10 μm does not seem to balance the increase concerning the small particles.

To study more precisely the differences between both computations, the relative difference between the mass of particles still in the atmosphere, calculated with the original matrix (m_{orig}) and calculated with the corrected matrix (mcorr), is shown in Fig. 29.3. Both computations are done for similar rain intensity (20 mm/h).

The difference obtained with both collection efficiencies reaches 15 % after 10 min of rain. This large difference obtained with only some corrections in the matrix of collection efficiencies (only corrected for drops of 2.05 mm and for particles between 0.3 and 4 μm) confirms the great significance of the measurement of collection efficiencies for drops larger than 1 mm. Thus, we need to continue the measurements to reach an accurate model of the washout.

29.5 Conclusions

Particles between 0.1 and 10 μm and drops between 1 and 5 mm are the most important for the washout. A free fall shaft and an aerosol chamber needed to measure collection efficiencies have been designed and built to study these ranges of particles and drops.

Although we have only studied the collection efficiencies for drops of 2.1 and 2.6 mm and particles between 0.3 and 4 μm, significant changes in the results of the model of the washout by DESCAM are observed.

These first results are very encouraging to continue our investigations and to extend the measurements of collection efficiencies to other drop sizes, and finally to complete the matrix of collection efficiencies.

Now, another topic needs to be studied: the behaviour of collection efficiencies with respect to the relative humidity. Wang and Pruppacher [4] show the dependency of the collection efficiency on the humidity for drops smaller than 0.8 mm. For these drops, the collection efficiency is decreasing when an increase of humidity occurs.

Our collection efficiency measurements have been carried out for relative humidities lower than 60 %, but the relative humidity of the atmosphere increases quickly to approach 100 % during a rain event. Therefore, we have to measure the collection efficiencies with humidities closer to saturation, in order to determine (or not) the dependency of collection efficiency on humidity for drops larger than 1 mm.

A better knowledge of the scavenging of aerosol particles by rain should be a significant leap forward in the prediction of radioactive fallout and the nuclear safety.

References

1. Masson O et al (2011) Tracking of airborne radionuclides from the damaged Fukushima Dai-Ichi nuclear reactors by European networks. Environ Sci Technol 45:7670–7677
2. Flossmann AI, Pruppacher HR (1998) A theoretical study of the wet removal of atmospheric pollutants, part III: the uptake, redistribution, and deposition of (NH4)2SO4 particles by a convective cloud using a two-dimensional cloud dynamics model. J Atmos Sci 45:1857–1871
3. Pruppacher HR, Klett JD (1997) Microphysics of clouds and precipitation. Kluwer Academic, Dordrecht
4. Wang PK, Pruppacher HR (1977) An experimental determination of the efficiency with which aerosol particles are collected by water drops in subsatured air. J Atmos Sci 34:1664–1669
5. Standard (1972) Method for measuring the efficiency of filters by means of a uranine (fluorescein) aerosol [in French]. Norme NF X 44-011
6. Marjamäki M, Keskinen J, Chen D-R, Pui DYH (2000) Performance evaluation of the Electrical Low-Pressure Impactor (ELPI). J Aerosol Sci 31(2):249–261
7. Lai K, Dayan N, Kerker M (1978) Scavenging of aerosol particles by a falling water drop. J Atmos Sci 35:674–682

Part IV
Data Assimilation and Air Quality Forecasting

Chapter 30
Kalman Filter-Based Air Quality Forecast Adjustment

Koen De Ridder, Ujjwal Kumar, Dirk Lauwaet, Stijn Van Looy, and Wouter Lefebvre

Abstract We describe the implementation of a Kalman filter-based adjustment scheme for the correction of deterministic air quality forecast results. This scheme exploits the information on the mismatch between the deterministic forecast and observations of the prior period to calculate correction regression coefficients for the next forecast step. This method was applied to ground-level daily O_3 and PM_{10} concentration fields simulated by the regional-scale deterministic air quality model AURORA for the year 2007, for a domain covering Belgium, and employing observations from the AirBase data archive. From a cross-validation analysis, it was found that the correction method improved the accuracy of daily mean PM_{10} and daily maximum O_3 concentrations substantially.

Keywords Kalman filter • Air quality forecast • AURORA

30.1 Introduction

In recent years, the implementation of the Kalman filter as a relatively simple yet powerful adaptive bias adjustment scheme for the correction of air quality forecasts has grown considerably [see, e.g., 1, 2, 4]. Basically, these schemes express the corrected concentrations as a linear function of the forecast values, estimating the coefficients of this linear relation by means of the Kalman filter, and using the difference between the observed and forecasted values of the preceding period as a constraint.

K. De Ridder (✉) • D. Lauwaet • S. Van Looy • W. Lefebvre
VITO – Flemish Institute for Technological Research, Mol, Belgium
e-mail: koen.deridder@vito.be

U. Kumar
VITO – Flemish Institute for Technological Research, Mol, Belgium

Royal Netherlands Meteorological Institute, De Bilt, The Netherlands

D.G. Steyn et al. (eds.), *Air Pollution Modeling and its Application XXII*,
NATO Science for Peace and Security Series C: Environmental Security,
DOI 10.1007/978-94-007-5577-2_30,

Yet, these schemes generally focus on the correction of air quality forecasts at the level of (sets of) individual monitoring stations. In this paper, we describe the extension of a Kalman filter-based scheme *towards full domain coverage*, allowing it to generate air quality forecast corrections also in between the positions of monitoring stations. Moreover, we show results obtained with the correction scheme implemented to concentration values simulated by the regional-scale deterministic air quality model AURORA.

30.2 Method

For a given time step, the corrected concentration values are obtained from

$$\mathbf{c}^c = \mathbf{G}\,\mathbf{x}^f, \tag{30.1}$$

$\mathbf{c}^c = \left[\mathrm{c}_1^c \ldots \mathrm{c}_N^c\right]^{\mathrm{T}}$ containing the corrected concentrations at grid cell positions $i = 1, \ldots, N$. $\mathbf{G} = [\ \mathbf{I} \mid \mathbf{I}\,\mathbf{c}^f\ ]$ contains the (uncorrected) forecast concentrations at the considered time step, with $\mathbf{I}$ the $N \times N$ identity matrix, and $\mathbf{c}^f = \left[c_1^f \ldots c_N^f\right]^{\mathrm{T}}$ containing the uncorrected forecast concentration values. The vector $\mathbf{x}^f = \left[A_1^f \ldots A_N^f\ B_1^f \ldots B_N^f\right]^{\mathrm{T}}$ contains the regression coefficients of the linear relation that is used to obtain the corrected concentrations from the forecast values. Basically, row i of (30.1) contains an expression for grid cell i of the form $c_i^c = A_i^f + B_i^f\,c_i^f$, i.e., linearly relating the corrected concentration value at that position to the forecast concentration value. The aim is to estimate the regression coefficients A_i^f and B_i^f contained in $\mathbf{x}^f$ to the best possible extent, which is done here using the Kalman filter approach.

The analysis (or estimation) step of the Kalman filter applied to the regression coefficient vector is given by

$$\mathbf{x}^a = \mathbf{x}^f + \mathbf{K}\left(\mathbf{c}^o - \mathbf{H}\,\mathbf{x}^f\right), \tag{30.2}$$

$\mathbf{x}^a$ containing the updated values of the regression coefficients at the considered forecast step, and $\mathbf{c}^o$ containing the observed concentrations. The matrix $\mathbf{H}$ is similar to $\mathbf{G}$ (see above), but then sampled at the rows that correspond to grid cells containing a monitoring station. $\mathbf{K}$ is the Kalman gain, which essentially determines how the model-vs-observation mismatch (i.e., $\mathbf{c}^o - \mathbf{H}\,\mathbf{x}^f$) has to be spatially distributed over the grid cells. The Kalman gain matrix is itself a function of the model and observation error covariance matrices. A nice property of the Kalman filter framework is that it contains a prediction equation for the background error covariance matrix.

30.3 Results

The method briefly described in the previous section was applied to output fields generated by the regional-scale deterministic air quality model AURORA [see, e.g., 3, 5] for the year 2007, on a domain covering Belgium at a spatial resolution of 3 km. Even though we used results of a retrospective simulation instead of an actual forecast, the correction scheme was set up as if it were running in forecast mode, i.e., only using observed concentration values available prior to the time of the 'forecast', considering the uncorrected simulated concentration value of the next day as a 1-day model forecast, then applying the Kalman filter-based correction, and comparing the resulting corrected concentration value to the observation of that day. This exercise was done for daily mean PM_{10} and daily maximum O_3 concentrations, using observations from the AirBase data archive to do so.

In order to verify the impact of the correction scheme, we conducted a cross-validation exercise, in which the Kalman filter-based adjustment scheme was applied to AURORA output using all monitoring data except that of the station used in the validation. Figures 30.1 and 30.2 show error statistics resulting from this exercise for a number of monitoring stations within the AURORA domain. It is found that, on average, for daily mean PM_{10} the correction scheme reduced the root mean square error from 14 to 10 $\mu g\ m^{-3}$ and the bias from 8.8 to 2.9 $\mu g\ m^{-3}$, while the correlation coefficient increased from 0.65 to 0.72. For daily maximum O_3 concentrations, the root mean square error was reduced from 22.0 to 17 $\mu g\ m^{-3}$, the bias from 4.5 to 3.5 $\mu g\ m^{-3}$, and the correlation coefficient increased from 0.67 to 0.82.

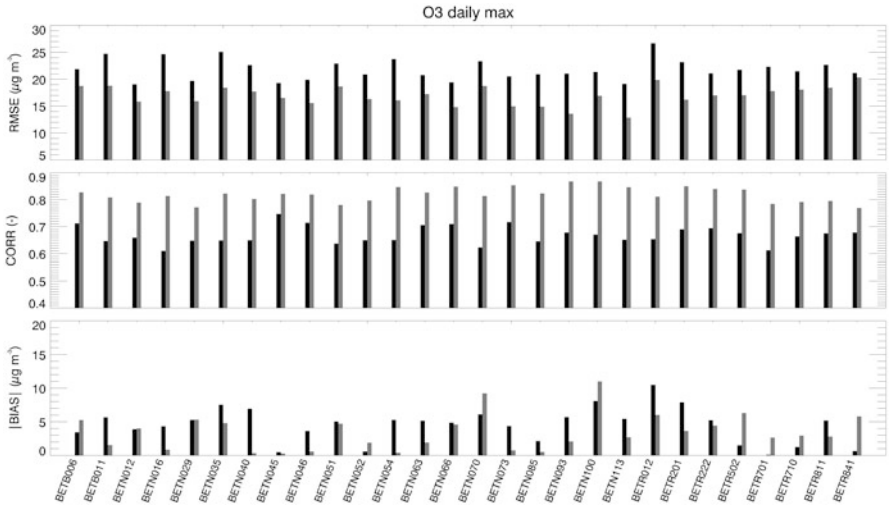

Fig. 30.1 Root mean square error, correlation coefficient, and bias, for the free (*black*) and corrected (*grey*) daily maximum O_3 concentration, at the stations shown on the abscissa

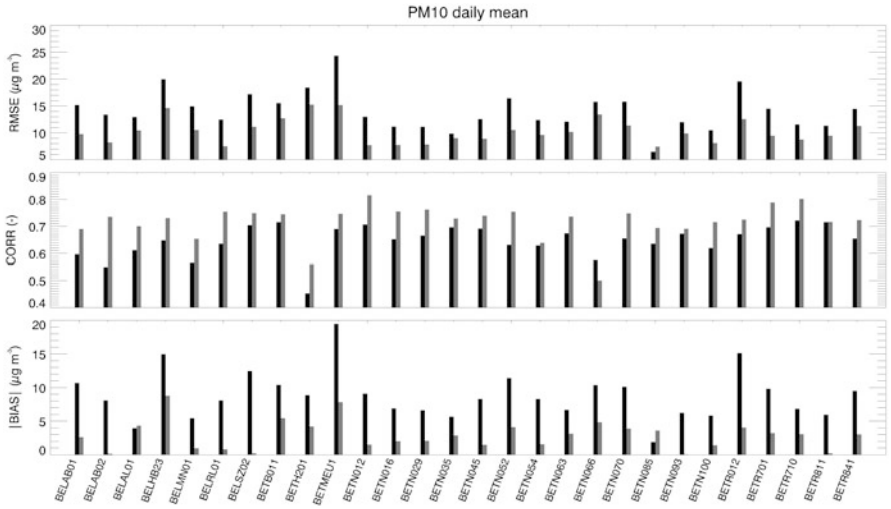

Fig. 30.2 As in Fig. 30.1, but for daily mean PM10 concentrations

30.4 Conclusions

We described a Kalman filter-based adjustment scheme for the correction of deterministic air quality forecasts, and that has the capacity to provide full spatial coverage. This method was applied to concentration fields generated by the deterministic air quality model AURORA, using AirBase observations as input for the correction scheme. Results from a cross-validation study clearly showed the ability of the scheme to improve the accuracy of the forecast concentration values.

Acknowledgments This work was carried out with support of the European Commission, within the LIFE+ project ATMOSYS and the FP7 project PASODOBLE.

References

1. Borrego C, Monteiro A, Pay MT, Ribeiro I, Miranda AI, Basart S, Baldasano JM (2011) How bias-correction can improve air quality forecasts over Portugal. Atmos Environ 45:6629–6641
2. De Ridder K, Kumar U, Lauwaet D, Blyth L, Lefebvre W (2012) Kalman filter-based air quality forecast adjustment. Atmos Environ 50:381–384
3. De Ridder K, Lefebre F, Adriaensen S, Arnold U, Beckroege W, Bronner C, Damsgaard O, Dostal I, Dufek J, Hirsch J, IntPanis L, Kotek Z, Ramadier T, Thierry A, Vermoote S, Wania A, Weber C (2008) Simulating the impact of urban 390 sprawl on air quality and population exposure in the German Ruhr area. Part I: reproducing the base state. Atmos Environ 42:7059–7069

4. Kang D, Mathur R, Rao ST (2010) Realtime bias-adjusted O_3 and $PM_{2.5}$ air quality index forecasts and their performance evaluations over the continental United States. Atmos Environ 44:2203–2212
5. Lefebvre W, Fierens F, Trimpeneers E, Janssen S, Van de Vel K, Deutsch F, Viaene P, Vankerkom J, Dumont G, Vanpoucke C, Mensink C, Peelaerts W, Vliegen J (2011) Modeling the effects of a speed limit reduction on traffic-related elemental carbon (EC) concentrations and population exposure to EC. Atmos Environ 45:197–207

Chapter 31
PASODOBLE AIRSHEDS: Regional Operational Air Quality Forecasts to Bridge the Gap Between Continental Scale and Local/Urban Scale Services

Carlijn Hendriks, Renske Timmermans, Martijn de Ruyter de Wildt, Henk Eskes, Dimitris Balis, Eleni Katragkou, Michael Sofiev, Charles Talbot, Hendrik Elbern, Martijn Schaap, and Thilo Erbertseder

Abstract Within the EU-FP7 project PASODOBLE five AIRSHED services have been developed to bridge the gap between the GMES core atmospheric service at coarse resolution and the PASODOBLE regional/local/urban downstream services at high resolution. For these Airsheds regional air quality forecasts and analysis are produced at a horizontal resolution of 5–10 km. Within this presentation we will present the PASODOBLE Airsheds focusing on the issues encountered while developing the systems.

The nesting within the European ensemble forecasts from the core atmospheric service poses a problem due to timing and lack of available information in the ensemble forecasts. Recommendations for the ensemble forecasts have been made to include more components and the timing issue will be solved by the delivery of

C. Hendriks (✉) • R. Timmermans • M. Schaap
TNO, Netherlands Organisation for Applied Scientific Research, Unit Environment, Health and Safety, P.O. Box 80015, 3508 TA Utrecht, The Netherlands
e-mail: carlijn.hendriks@tno.nl

M. de Ruyter de Wildt • H. Eskes
KNMI, Royal Meteorological Institute Netherlands, de Bilt, The Netherlands

D. Balis • E. Katragkou
AUTH – Aristotle University of Thessaloniki, Thessaloniki, Greece

M. Sofiev
FMI – Finnish Meteorological Institute, Helsinki, Finland

C. Talbot
ACRI-ST, Sophia-Antipolis, France

H. Elbern
FRIUUK, Rheinisches Institut für Umweltforschung an der Universität zu Köln, Köln, Germany

T. Erbertseder
DLR, Deutschen Zentrums für Luft- und Raumfahrt, Cologne, Germany

D.G. Steyn et al. (eds.), *Air Pollution Modeling and its Application XXII*,
NATO Science for Peace and Security Series C: Environmental Security,
DOI 10.1007/978-94-007-5577-2_31,

96 h instead of 72 h ensemble forecasts. The data assimilation of observations to improve the forecasts forms another issue due to time consuming calculations and lack of timely observations.

Keywords Forecasting • Data assimilation • Nesting

31.1 Introduction

Within the EU-project PASODOBLE user-driven information services for the regional and local air quality sector are developed by combining space based data, in-situ data and air quality models. To bridge the gap between the high-resolution local/urban PASODOBLE services and the lower resolution services on the European scale from the EU-project MACC, five operational systems have been set up that provide air quality forecasts of a.o. PM, O_3 and NO_2 at an intermediate resolution of approximately 7 km for different regions over Europe, the so-called Airsheds. The systems are developed by five different teams using different models nested within European scale MACC air quality forecasts. The Airsheds forecasts are subsequently used as boundary conditions and initialization for local/urban scale services defined within or outside PASODOBLE. One of the important advantages of PASODOBLE is that it provides a generic and harmonized infrastructure allowing easy application of new services.

31.2 Description of Airsheds

The following five airsheds have been set-up (see Fig. 31.1):

1. **Central**, **Western and Southern Europe** (∼3W–20E; 41–59N), covering BENELUX, Northrine-Westfalia, Paris, London and Marseille, Provence, Alps, Cotes d'Azur, Po Valley, Switzerland and Austria. Delivered by the Rheinisches Institut für Umweltforschung an der Universitätzu Köln (FRIUUK) with EURAD-IM model with assimilation of surface in situ measurements from Germany, France, Switzerland, and Austria as well as NO_2 retrievals from OMI.
2. **Central and Southern Europe** (4–18E; 41–51N), covering Marseille, Provence, Alps, Cotes d'Azur, Po Valley, Switzerland, Austria, Prague, Bratislava and Bavaria. Delivered by ACRI with the CHIMERE model.
3. **Northern Europe** (4–33E; 54–71N), er ingFennoscandia, the Baltic States and adjacent areas of Russia, Poland and Germany. Delivered by the Finnish Meteorological Institute (FMI) with the SILAM model.
4. **South-EastEurope** (∼13E–30E; 35N–48N), covering Greece, Bulgaria, Romania, Serbia, Croatia, Albany, Bosnia and Herzegovina and Macedonia. Delivered by the Aristotle University of Thessaloniki (AUTH) with the CAMx model.

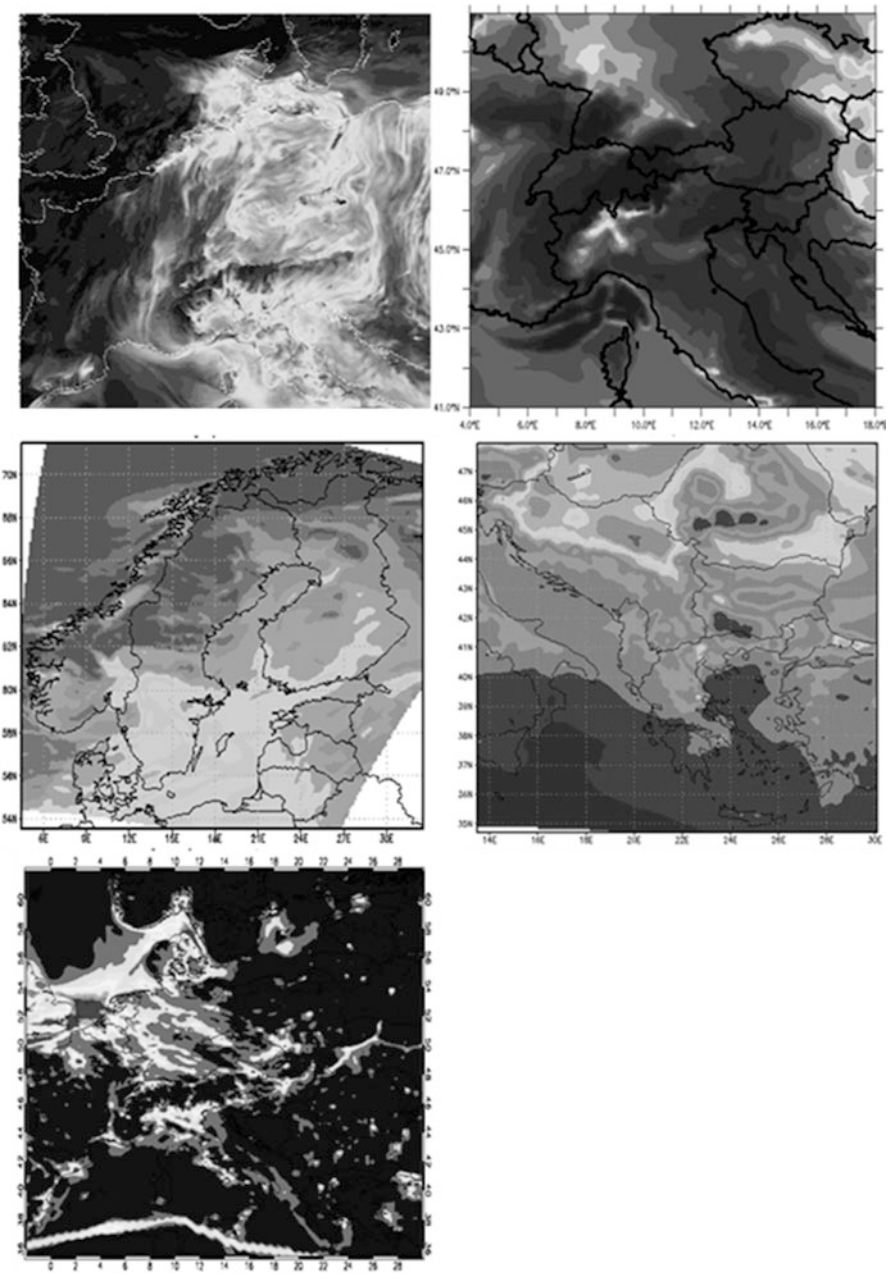

Fig. 31.1 Example forecasts from the five different airsheds. *Top left*: Centre-South and Centre-West airshed, *Top right*: Centre-South airshed, *middle left*: North airshed, *middle right*: South East airshed, *bottom*: Joint airshed

5. **Joint airshed** (2W–30E; 35–62N), covering Airsheds 1 and 2, the Southern part of Airshed 3 where the main cities are located and Airshed 4 excluding Crete. Delivered jointly by KNMI, RIVM and TNO with the LOTOS-EUROS model.

31.3 Evaluation and Issues

The evaluation of the Airsheds services will take place in a harmonized way using a tool providing e.g. target diagrams, hit rates and skill scores. As there is overlap between some Airsheds, intercomparisons between different systems/models are undertaken with the aim to improve the forecasts.

The nesting of the airsheds within the core atmospheric service (MACC) forecasts is not easy. Ideally, the MACC ensemble forecasts based on seven regional models should be used. However, both timing and the amount of information (only five layers and five species) available from the ensemble pose problems. The timing issue will be solved by the delivery of 96 h instead of 72 h ensemble forecasts.

Nesting tests have been performed to investigate the impact of missing species in the boundary conditions (see Fig. 31.2). The set of required boundary species depends on location and size of the Airshed, the model used, target species and possibly also time of year. In general however an extension of the MACC ensemble is required.

Another issue is the data assimilation of (satellite) observations within the forecast models. Most Airshed services have not (yet) been able to incorporate data

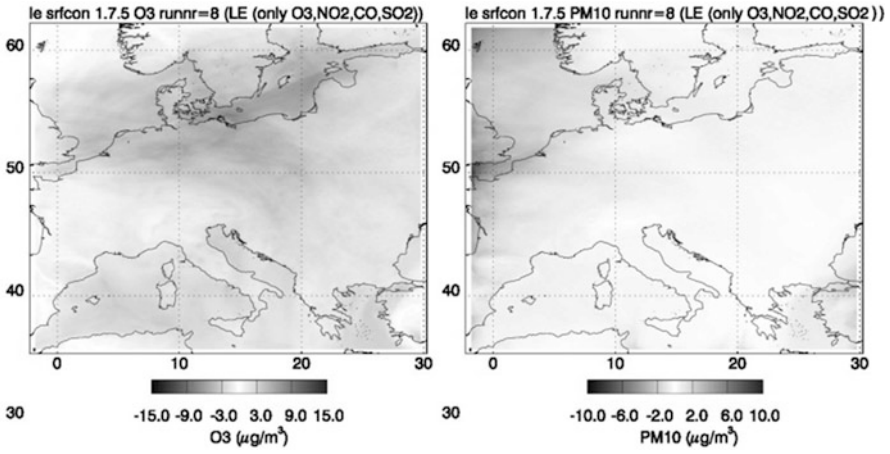

Fig. 31.2 Difference in mean surface concentration of O_3 (*left*) and PM_{10} (*right*), between the reference run with all boundary conditions and the run which only uses Lotos-Euros boundary conditions for CO, NO_2, O_3 and SO_2. The runs were performed for the period 22 June 2011–28 June 2011

assimilation in the operational system. Data assimilation is time consuming and prevents timely delivery of forecasts for further nesting of local models. Another problem is the timely availability of observations for assimilation.

Acknowledgment The work described here was carried out with support of the European Commission, within the FP7 project PASODOBLE.

Questions and Answers

Questioner Name: Stijn Janssen

Q: What is the impact of the fact that the ensemble mean is not in chemical equilibrium when it is used as boundary conditions in LOTOS-EUROS?
A: This can definitely be an issue when using boundary conditions coming from an ensemble of models. However, the issue about the lack of species and height layers present in the ensemble causes such large deviations in most cases that the chemical equilibrium issue is less important at the moment. If more species become available from the ensemble, this might become an issue, but to what extent is hard to say and would need to be investigated.

Questioner Name: Amir Hakami

Q: Have you tested whether a simplified but less expensive model would result in deteriorated forecasts?
A: No, we haven't. However, from the model intercomparison that is planned for later this year, we might get some clues about which processes are the most important and which can be modelled in less detail while retaining good-quality forecasts.

Chapter 32
Data Assimilation and Air Quality Forecasting

Henk Eskes, Renske Timmermans, Lyana Curier, Martijn de Ruyter de Wildt, Arjo Segers, Ferd Sauter, and Martijn Schaap

Abstract Lotos-Euros is a chemistry transport model developed in the Netherlands, and is used for air quality assessments and forecasts. Operational air quality forecasts for the Netherlands concerning ozone and PM10 are made available on the RIVM webpage (http://www.lml.rivm.nl/verw.html) and are used to warn the population in case of predicted exceedances of air quality standards. Lotos-Euros is also contributing to the model-ensemble based air quality forecasts for Europe (MACC project, http://macc-raq.gmes-atmosphere.eu/index.php?op=get). Currently, the system is expanded to assimilate routine surface observations from European networks as well as satellite observations such as OMI NO_2. The Ozone Monitoring Instrument (OMI) is a Dutch-Finnish instrument on the NASA EOS-Aura mission, and has a capability to detect boundary-layer NO_2 with a unique resolution of about 20 km. The assimilation in Lotos-Euros is based on the ensemble Kalman filter technique in which model parameters such as the NO_x emissions, VOC emissions, PM sources, ozone boundary conditions and/or deposition velocities are adjusted to improve the comparison with the observations. In our contribution we will discuss the experiences with the assimilation of NO_2 tropospheric columns from the OMI instrument. In particular we will focus on the model-OMI comparisons over Europe, the analysis improvements, the analysed emissions and the impact of OMI NO_2 data assimilation on other constituents such as ozone.

H. Eskes (✉) • M. de Ruyter de Wildt
KNMI, Royal Meteorological Institute Netherlands, de Bilt, The Netherlands
e-mail: henk.eskes@knmi.nl

R. Timmermans • L. Curier • A. Segers • M. Schaap
TNO, Netherlands Organisation for Applied Scientific Research, Utrecht, The Netherlands

F. Sauter
RIVM, National Institute for Public Health and the Environment, Bilthoven, The Netherlands

D.G. Steyn et al. (eds.), *Air Pollution Modeling and its Application XXII*,
NATO Science for Peace and Security Series C: Environmental Security,
DOI 10.1007/978-94-007-5577-2_32,

Keywords LOTOS-EUROS • Data assimilation • Chemistry transport modeling • OMI • NO_2

32.1 Lotos-Euros Contribution to the MACC Project

The MACC (Monitoring Atmospheric Composition and Climate, 2009–2011) and MACC II (Monitoring Atmospheric Composition and Climate – Interim Implementation, 2012–2014) projects build the current pre-operational atmospheric service of the European GMES programme. MACC (http://www.gmes-atmosphere.eu/) combines state-of-the-art atmospheric modelling with Earth observation data to provide forecasts and reanalysis information services covering European Air Quality, Global Atmospheric Composition, Climate, and UV and Solar Energy.

Seven regional air-quality analysis and forecasting systems are operated routinely for MACC (CHIMERE, EMEP, EURAD, LOTOS-EUROS, MATCH, MOCAGE and SILAM). The products provided on the MACC website are: Daily air-quality analyses for the day before from each model; Daily air-quality forecasts up to 72 h from each model; Daily ensemble air-quality analyses for the day before; Daily ensemble air-quality forecasts; Ensemble air-quality reanalyses for the years 2007, 2008 and 2009.

The LOTOS-EUROS model [6] is a 3D chemistry transport model aimed to simulate air pollution in the lower troposphere, and is currently developed by TNO, RIVM and KNMI. The RIVM is both model developer and user of the forecasts,

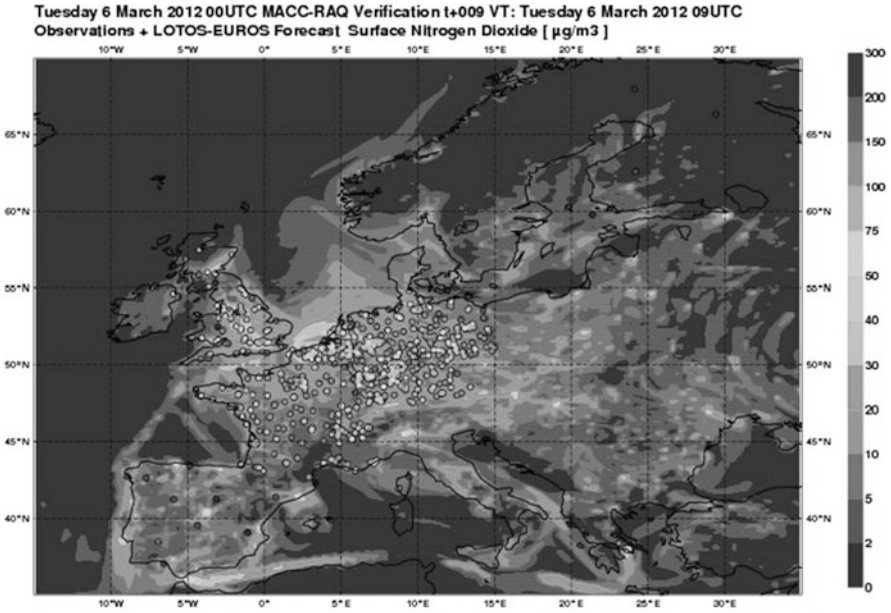

Fig. 32.1 Verification of the LOTOS-EUROS NO2 field for Tuesday 6 March 2012, 9 UTC, with the available surface observations. Plot taken from the MACC website

with a legal obligation to provide real-time air quality measurements and pollution forecasts to the Dutch public, see http://www.lml.rivm.nl/. The model has been used for the assessment of particulate air pollution in a number of studies directed to total PM10 (e.g. [4, 5]), secondary inorganic components (e.g. [1]), primary carbonaceous components and trace metals. The model has participated frequently in international model comparisons (e.g. [7, 8]) and contributes to AQMEII. In Fig. 32.1 we show an example of the verification of the LOTOS-EUROS ozone forecasts. Recently the NO_2 simulations have been compared with MaxDOAS column measurements [9].

32.2 Assimilation of OMI NO_2 Satellite Observations

The LOTOS-EUROS model is equipped with a data assimilation package based on the ensemble Kalman filter technique (e.g. [1, 3]). At this moment data assimilation is performed for ozone in the zoom region over the Netherlands in the context of

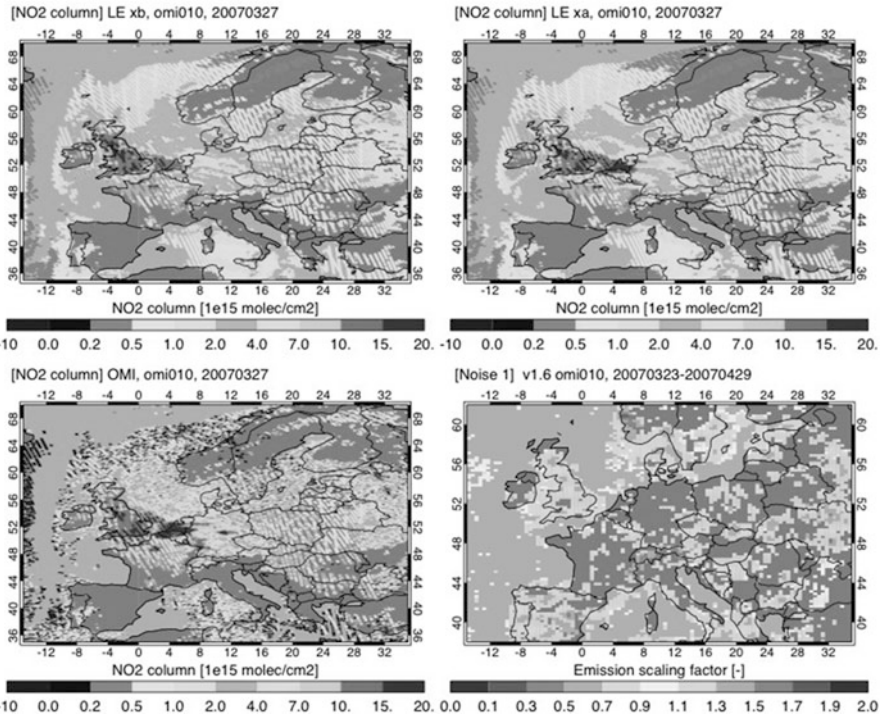

Fig. 32.2 Results for the OMI NO_2 assimilation run. *Top-left*: Free LOTOS-EUROS run for 27 March 2007. *Bottom-left*: The OMI cloud-filtered observations for 27 March 2007. *Top-left*: Analysis based on the OMI observations. *Bottom-right*: Ratio between analysed NO_x emissions and a-priori emissions for the period 23 March – 29 April 2007. Only significant emission adjustments are shown

the Dutch SmogProg project. Assimilation of surface ozone measurements, OMI NO_2 and surface PM10 has been applied Europe-wide within MACC for the 2008 and 2009 reanalyses. The combined use of other observational datasets from surface networks and satellite missions is under investigation.

Several sensitivity experiments have been performed with the assimilation of NO_2 tropospheric column data measured by the OMI instrument [2]. The OMI data had the largest impact on the NO_x emissions, which is not surprising given the direct link between NO_x emissions and NO_2 concentrations observed. Figure 32.2 shows the adjustments made to the model NO_x emissions by the Kalman filter. A consistent feature which is observed also for the other days is a relative increase in emissions over central and eastern Europe. The assimilation of OMI NO_2 data results in a slightly positive impact on ozone as compared to Dutch surface observations in these runs.

The data assimilation results for OMI NO_2 and other data sets will be discussed at the ITM-2012 meeting.

References

1. Barbu A, Segers A, Schaap M, Heemink A, Builtjes PJH (2008) A multi-component data assimilation experiment directed to sulphur dioxide and sulphate over Europe. Atmos Environ 43(9):1622–1631. doi:10.1016/j.atmosenv.2008.12.005
2. Boersma KF, Eskes HJ, Dirksen RJ, van der A RJ, Veefkind JP et al (2011) An improved tropospheric NO2 column retrieval algorithm for the Ozone Monitoring Instrument. Atmos Meas Tech Discuss 4:2329–2388. doi:10.5194/amtd-4-2329-2011
3. Curier RL, Eskes H, Timmermans R, Calabretta-Jongen S, Segers A, Schaap M, Swart D (2012) Improving ozone forecasts over Europe by synergistic use of the LOTOS-EUROS chemical transport model and in-situ measurements. Atmos Environ 60:217–226
4. de Ruyter de Wildt M, Eskes H, Manders A, Sauter F, Schaap M, Swart D, van Velthoven P (2011) Six-day PM10 air quality forecasts for the Netherlands with the chemistry transport model Lotos-Euros. Atmos Environ 45:5586–5594. doi:10.1016/j.atmosenv.2011.04.049
5. Manders AMM, Schaap M, Hoogerbrugge R (2009) Testing the capability of the chemistry transport model LOTOS-EUROS to forecast PM10 levels in the Netherlands. Atmos Environ 43(26):4050–4059. doi:10.1016/j.atmosenv.2009.05.006
6. Schaap M, Timmermans RMA, Roemer M, Boersen GAC, Builtjes PJH, Sauter FJ, Velders GJM, Beck JP (2008) The LOTOS–EUROS model: description, validation and latest developments. Int J Environ Pollut 32:270–290
7. Stern R, Builtjes P, Schaap M, Timmermans R, Vautard R, Hodzic A, Memmesheimer M, Feldmann H, Renner E, Wolke R, Kerschbaumer A (2008) A model inter-comparison study focussing on episodes with elevated PM10 concentrations. Atmos Environ 42:4567–4588. doi:10.1016/j.atmosenv.2008.01.068
8. van Loon M, Vautard R, Schaap M, Bergstrom R, Bessagnet B, Brandt J, Builtjes PJH, Christensen JH, Cuvelier C, Graff A, Jonson JE, Krol M, Langner J, Roberts P, Rouil L, Stern R, Tarrason L, Thunis P, Vignati E, White L (2007) Evaluation of long-term ozone simulations from seven regional air quality models and their ensemble. Atmos Environ 41:2083–2097. doi:10.1016/j.atmosenv.2006.10.073
9. Vlemmix T, Eskes HJ, Piters AJM, Kelder H, Levelt PF (2011) MAX-DOAS tropospheric nitrogen dioxide column measurements compared with the Lotos-Euros air quality model. Atmos Chem Phys Discuss 11:28895–28944. doi:10.5194/acpd-11-28895-2011

Chapter 33
Forecasting Sensitivities: Is Adaptive, Short-Term Air Quality Management a Viable Option?

Matthew Russell and Amir Hakami

Abstract Air quality managers have traditionally relied on deterministic and statistical approaches for forecasting concentrations. In some parts of the world, concentration forecasts are used to trigger urgent and sometimes drastic preventative measures in the hope that severe pollution episodes are alleviated or avoided altogether. These preventative measures, however, are often applied rather indiscriminately to all emission sources without accounting for specific influence of each individual source on the forecast outcome. This blanket approach fails to improve air quality in a cost-effective manner. Adjoint sensitivity analysis approach provides a unique framework for efficient forecast of the impact of individual sources on short-term air quality. We demonstrate how this method can be used for short-term emission behavior modification resulting in amelioration of pollution episodes.

Keywords Air quality management • Ozone • Attainment • AQHI • Adjoint

33.1 Introduction

Over 400 urban areas host populations in excess of one million worldwide. With these large urban areas comes harmful air pollution that is estimated to result in 4.1 million deaths annually [1]. While many governments have set in place policies to reduce hazardous air pollution, these policies generally aim to improve the air quality over the long term. This long-term strategic planning has proven to be effective in many regions of world. However, there is a great deal of day-to-day

M. Russell (✉) • A. Hakami
Department of Civil and Environmental Engineering, Carleton University, Ottawa, ON, Canada
e-mail: amir_hakami@carleton.ca

D.G. Steyn et al. (eds.), *Air Pollution Modeling and its Application XXII*,
NATO Science for Peace and Security Series C: Environmental Security,
DOI 10.1007/978-94-007-5577-2_33,

variability in pollution influences on a specific receptor. These potentially significant differences in spatial distribution of contributions imply that any long-term policy, as effective as it can be on average, would have significantly varying success rate on different days. Few jurisdictions, however, have employed policies to address short-term emergency episodes in near future, and the few that do, have typically employed heavy-handed blanket approaches. For instance, Onursal and Gautam [2] describe one such policy in Mexico City where a 2 day ban on up to 40 % of vehicles in Mexico City prohibited driving on days where air pollution exceeded certain levels. This policy proved to be so unpopular that it was almost never enacted.

Prediction of concentrations has been attempted for many years through the use of statistical or deterministic models. Concentration forecasts provide prior knowledge about pollution episodes but cannot guide short-term management efforts in an effective manner. For over a decade air quality models have been extended to include the capability to calculate sensitivities alongside concentrations. One particularly promising area has been the development of backward or adjoint sensitivity tools. Adjoint sensitivity analysis allows for calculation of contributions from individual sources to a scalar metric such as concentration at a location.

In this work, we introduce an efficient approach for Adaptive Air Quality Management (AAQM). The proposed framework is based on identification of major contributing sources to a future pollution episode by forecasting adjoint (backward) sensitivities. In so doing, air quality decision makers may adapt to the unique conditions of an oncoming adverse air quality episode and manage emission sources in near optimal way to alleviate the negative impacts.

33.2 Methodology

Adjoint sensitivity analysis requires the definition of an adjoint cost function, i.e., the scalar the sensitivity of which is being calculated. We consider ozone concentration at a specific receptor (Baltimore) and the Canadian Air Quality Health Index (AQHI) [3] in Toronto as the adjoint cost functions. Sensitivities in this work are calculated using the adjoint of the gas-phase processes in the Community Multiscale Air Quality (CMAQ) model [4]. Adjoint sensitivities are calculated using a coarse 36 km domain over the continental US for sample days with poor air quality in the summer of 2007. For the first case, the ozone concentration in Baltimore is used as the cost function. As an example of an alternative concentration-based metric, the AQHI in Toronto is taken as the cost function. We use a simplified first-order approximation of the AQHI (based on a Taylor series expansion of the original form):

$$AQHI = \frac{10}{12.8}\left(0.101\,[NO2] + 0.104\,[O3]\right)$$

We apply three emission behavior modification scenarios for major point source emitters and mobile sources affecting the adjoint cost function. As the air quality authority (e.g., a municipality) is unlikely to be able to shut down a large percentage of sectors, we assume that emission behavior modifications are 5, 10, and 15 % for point sources, and 8, 15, and 25 % for mobile sources, under the three considered scenarios, respectively. Furthermore, we consider two separate cases for daily and hourly contribution estimation from individual sources. For the daily case, emission behavior modification at the levels mentioned above is applied to sources in the top 10 % contributing cells. In the case of hourly contribution calculations, only the top 5 % grid-hour contributing sources undergo prescribed emission reductions in each scenario.

33.3 Results and Discussion

We aim to examine whether targeted emission modifications at these levels can trigger sizeable change in predicted concentrations. Figure 33.1a shows the results for the least aggressive scenario for the Baltimore case where improvement as a result of emission modification is plotted against the initial 8-h maximum concentrations for a number of days in summer of 2007. Any value above the x-axis in Fig. 33.1 indicates an improvement and the straight lines present the required improvement for reaching the current maximum 8-h standard (75 ppb) or the previously recommended lower level (65 ppb). While sizeable improvement is made, the shift is not sufficient to attain standards. Figure 33.1b depicts the results for the same exercise but for AQHI management in Toronto and under the most aggressive emission behavior modification scenario. Improvements achieved in AQHI are more significant as the emission modification in this scenario is more aggressive. Furthermore, AQHI includes NO_2 for which local controls are more effective.

The simulations shown in Fig. 33.1 are performed over a coarse grid and modest emission modification scenarios. More aggressive emission modification scenarios result in more sizeable improvements in predicted episodes. Also, higher resolution simulations would provide the opportunity to better delineate contributions and perform targeted emission modifications.

The success of an AAQM system will depend on effective recruitment of emitters for participation in the program, which may require consideration of various forms of incentives as well as public education. One particularly important challenge lies in the evaluation of the performance of the AAQM system. Since forecast sensitivities cannot be observed, a thorough evaluation of the AAQM's success is often impossible except for cases that involve long-term trend analysis. In other words, once an emission intervention is implemented, one would never know for certain how the air quality would have been without the intervention. This limitation further emphasizes the need for more thorough investigation of this approach.

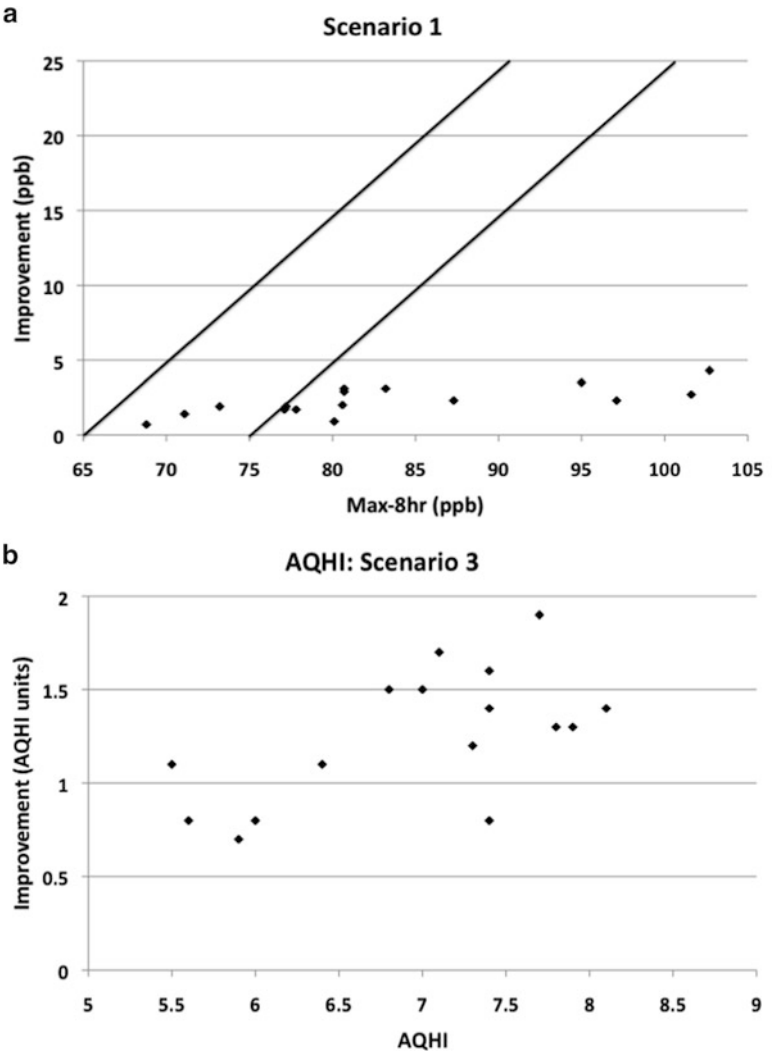

Fig. 33.1 The result of emission modification on (**a**) concentration at Baltimore and (least aggressive scenario) (**b**) AQHI in Toronto (most aggressive scenario)

References

1. Anenberg S, Horowitz L, Tong D, West J (2010) An estimate of the global burden of anthropogenic ozone and fine particulate matter on premature human mortality using atmospheric modeling. Environ Health Perspect 118(9):1189
2. Onursal B, Gautam S (1997) Vehicular air pollution: experiences from seven Latin American urban centers, vol 23. World Bank Publications, Washington D.C

3. Stieb D, Burnett R, Smith-Doiron M, Brion O, HWASHIN H, Economou V (2008) J Air Waste Manage Assoc 58(3):435–450
4. Hakami A, Henze DK, Seinfeld JH, Singh K, Sandu A, Kim S, Byun D, Li Q (2007) Environ Sci Technol 41(22):7807–7817

Questions and Answers

Questioner Name: Henk Eskes

Q: Canada has a health index which is based on O_3 and NO_2, while the US and Europe look only at O_3. This makes a significant difference as considering only O_3 could result in increased concentrations due to reduced NO_x emissions. Should Europe and the US include NO_2?
A: Inclusion of NO_2 in the Canadian health index is due to an observed association between NO_2 and health outcomes (i.e., mortality) in Canadian time series studies. Health Canada maintains that this association is not explained by other species, and therefore, that inclusion of NO_2 is not only justified but also necessary. They agree, however, that the observed association does not imply causality and that NO_2 may be a proxy for some other pollutants. This lack of causality implies that reductions in NO_x emissions may not result in reduction in the associated health outcomes. Therefore, there are good arguments for and against inclusion of NO_2 in policy-relevant air quality metrics.

Chapter 34
Sensitivity of PM Assimilation Results to Key Parameters in the Ensemble Kalman Filter

Arjo Segers, Vincent Kamphuis, and Martijn Schaap

Abstract To study and forecast atmospheric tracer concentrations at ground level, an assimilation system is available around the LOTOS-EUROS model based on the Ensemble Kalman filter technique. For applications focusing on air-quality related to aerosols, the available observation data is usually limited to ground based observations of total PM2.5 or PM10, and model uncertainty is specified for the emissions. In this study, the key parameters of the assimilation system have been varied: the assumed temporal variation in the emission uncertainty, the amplitude of the representation error, the localization length of the analysis, the averaging period of the observations, and the number of ensemble members in the filter. Although in theory these parameters are all important, the most important parameters are those related to the representation error between simulations and observations.

Keywords PM • LOTOS-EUROS model • Data-assimilations

34.1 Assimilation System

A data-assimilation system incorporates observations in model simulations. Independent of the chosen technique, the components of such a system are a simulation model with associated assumptions about the model error, observation data with associated observation errors, an observation representation operator with an assumption about the representation error, and an assimilation algorithm.

In this study, the model simulations are provided by the LOTOS-EUROS model [1]. The simulation domain is limited to an area in North-West Europe covering The Netherlands and the west part of Germany (Fig. 34.1). The model is

A. Segers (✉) • V. Kamphuis • M. Schaap
TNO, Utrecht, The Netherlands
e-mail: Arjo.Segers@tno.nl

D.G. Steyn et al. (eds.), *Air Pollution Modeling and its Application XXII*,
NATO Science for Peace and Security Series C: Environmental Security,
DOI 10.1007/978-94-007-5577-2_34,

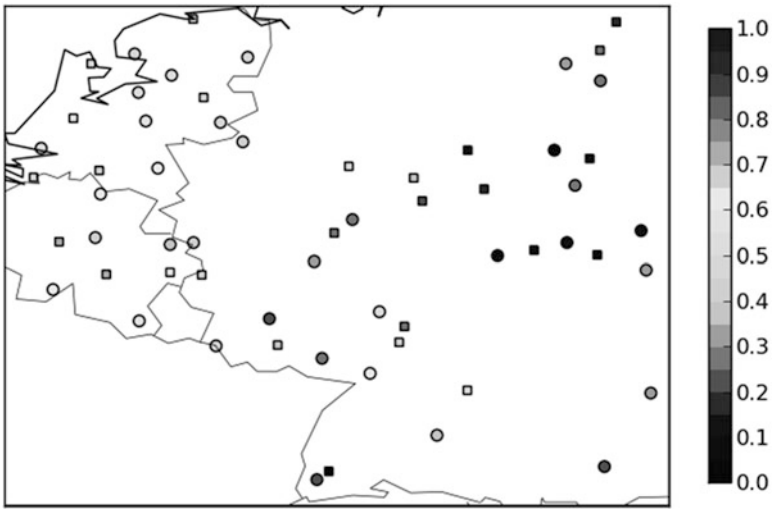

Fig. 34.1 Simulation domain and location of observations sites. *Circles* denote assimilated stations, and *squares* denote the stations used for validation only. The *colors* show the temporal correlation between observed and simulated total PM10 concentrations

configured to simulate concentrations of aerosols and trace gasses at a resolution of 25 km in this domain, during the month July 2008. The model is driven by meteorological fields from ECMWF, land cover information, and emissions from traffic, industry, and other anthropogenic sources. These emissions are considered the most uncertain input for the simulation of aerosols, and uncertainty is specified in terms of a standard deviation and a temporal correlation. A part of the observed aerosol load is of unknown origin and is therefore not represented in the model; a bias-correction factor accounts for the missing aerosol when simulating total PM concentrations.

Observations of aerosol at ground level are available from the AIRBASE database. The model is expected to provide simulations representative for rural background sites; the locations of these sites in the domain are shows in Fig. 34.1 too. The sites used here all measure the total fine (PM2.5) and coarse (PM10) aerosol load at hourly resolution. The observation operator to simulate these observation from the model state simply extracts the concentrations from the lowest grid cell in which the site is located. A representation error is assumed with a standard deviation equal to a fraction of the observed value, which also accounts for the instrumental error.

The assimilation system is based on the Ensemble Kalman Filter approach and is described in detail in Timmermans et al. [2]. In this method, an ensemble of model states is propagated in time where the spread originates from the emission uncertainty. Whenever observations are available, the ensemble is contracted in the neighborhood of the observation site, taking into account the representation uncertainty.

34.2 Sensitivity Experiments

The assimilation system contains a number of parameters that are highly uncertain but strongly determine the results. Their value is often set by trial-and-error analysis, since no other information on the best value is available. The sensitivity of the result to these parameters is evaluated by changing their value and determine the impact on the results in terms of difference between observations and analyzed ensemble mean.

The sensitivity to the emission uncertainty was examined by varying the assumed temporal correlation; the amplitude of the uncertainty has a constant high value of 40 %. A stronger temporal correlation limits the hour-to-hour variation in the emissions, but leads to a broader ensemble on long term since each member is able to build up a different emission region. For the later reason, the assimilation system is better able to follow an episode of high PM values.

A smaller representation error assigns more weight to the observations. This will contract the ensemble mean more in the direction of the observations, as long as this is in agreement with the spatial variations in the ensemble In the current application, with a rather homogeneous domain (urbanized areas) and observation sites not too close to each other, the difference between simulations and observations is quite homogeneous. Especially during an episode of high PM values a smaller representation error therefore improves the results. This suggests that the assumption of a representation error standard deviation being a constant fraction of the observed value needs a re-formulation

The observations could be assimilated hourly or at longer time steps by taking average values. If for example daily averages are assimilated, the ensemble is propagated during a longer time period and is able to build up more uncertainty. The hourly simulations are stored in the ensemble too, and are changed following the analysis of the averages. The sensitivity runs showed that preferably the averaging interval should be as small as possible. If the difference between model and simulations is rather constant then increasing the averaging interval does not improve the results. If the difference is time depended however, for example too low during the day and too low during the night, then increasing the averaging interval leads to larger difference between observations and ensemble mean.

The localization length scale determines the size of the region around an observation site when the ensemble is analyzed. This localization is necessary to let spurious correlations in the ensemble not have impact on the results. Since the uncertainty added to the emissions is part of the ensemble state too, a larger length scale changes emissions in a larger region around the sites. The impact of the localization length is not unambiguous. In regions where the difference between model and simulations is rather homogenous, a longer localization length improves the assimilation results (Fig. 34.2). In regions where differences occur due to other reasons than a simple increase or decrease of emissions, the results get worse for longer length scale. This result suggests that the localization length requires a regional value, determined by the spatial correlation in the observed differences between simulations and observations.

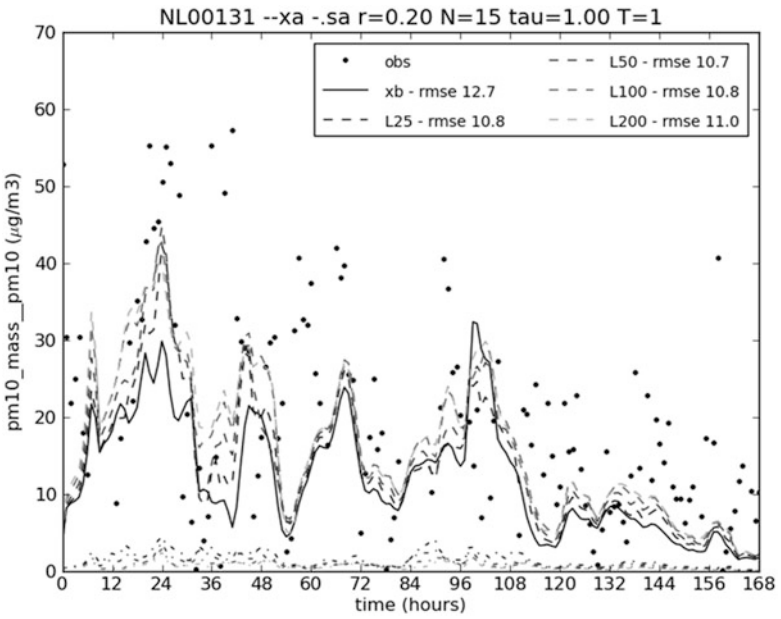

Fig. 34.2 Time series of PM10 in site Vreedepeel (The Netherlands) during the first week. The *black line* shows the model simulation, the *colored lines* the ensemble mean for assimilations with different analysis localization length scales

The final parameter tested was the ensemble size. In general, a bigger ensemble is needed if the spatial covariance's are more complicated. In the current application, with a rather homogenous uncertainty defined for the emissions, and a domain dominated by similar urbanized areas, the error structure is rather simple. A small ensemble size of about 20 member was sufficient to provide stable results. The largest impact of this parameter is seen for the ensemble spread, which quantifies the assumed accuracy of the result; the ensemble mean is quickly insensitive for the ensemble size.

34.3 Conclusions

The Ensemble Kalman Filter technique used to assimilate PM observations with simulations from the LOTOS-EUROS model is most sensitive to parameters related to the analysis of observations. Sensitivity experiments showed that the representation error, the averaging interval, and the localization length have the strongest impact on the results. In general, the averaging interval should be as small as possible. For the representation error and the localization length the results are not unambiguous and suggest that their values should not be set globally

but individually per station or region, or per episode. Analysis of the structure difference between observation and simulations should lead to proper choices for these parameters.

References

1. Schaap M, Timmermans R, Roemer M, Boersen G, Builtjes P, Sauter F, Velders G, Beck J (2008) The LOTOS–EUROS model: description, validation and latest developments. Int J Environ Pollut 32:270–290
2. Timmermanns R, Segers A, Builtjes P, Vautard R, Siddans R, Elbern H, Tjemkes S, Schaap M (2009) The added value of a proposed satellite imager for ground level particulate matter analyses and forecasts. IEEE J Sel Top Appl Earth Observ Remote Sensing 2:271–283

Questions and Answers

Questioner Name: Sebnem Aksoyoglu

Q: Are SOA included in the model? Is there any effort to implement it in LOTOS-EUROS?
A: In the current default settings of LOTOS-EUROS the formation of SOA is not enabled. However, the SOA formation is currently being revised and validated as part of the implementation of aerosol condensation, and is expected be enabled by default in the near future.

Chapter 35
A Statistical Approach to Improve Air Quality Forecasts in the PREV'AIR System

Laure Malherbe, Anthony Ung, Frédérik Meleux, and Bertrand Bessagnet

Abstract Since 2003, the national PREV'AIR system (www.prevair.org) has been delivering daily air quality forecasts of atmospheric pollutants (O_3, NO_2, PM_{10}, $PM_{2.5}$) over Europe and France. Those products are based on chemistry-transport modeling and in particular on the outputs from CHIMERE model. Analysed air quality maps of the previous day are also produced by mixing observed and simulated data through a geostatistical approach.

More recently a methodology has been developed to improve the accuracy of CHIMERE forecasts. It consists of two main stages.

In a preliminary stage, statistical short-term forecasting models are built and validated for each French and European rural or (sub)urban background monitoring site. The response variables are the O_3 daily maximum, NO_2 daily maximum and PM_{10} daily average concentrations of the current and the next 2 days. This part is based on the developments carried out and tested within CITEAIRII project (www.citeair.eu).

In the operational stage, the statistical models identified as reliable enough are applied with a daily frequency to predict concentrations at the corresponding monitoring sites. Locally forecast concentrations are then combined with CHIMERE forecast concentration fields according to the same geostatistical approach as aforementioned. This has been tested so far for O_3 and PM_{10}. Validation against independent data shows a significant improvement of the forecasts compared with raw CHIMERE outputs.

Keywords Chimere-model • Prev'air • Forecast

L. Malherbe (✉) • A. Ung • F. Meleux • B. Bessagnet
INERIS, Parch Technologique ALATA, B.P.2, 60550 Verneuil-en-Halatte, France
e-mail: laure.malherbe@ineris.fr

D.G. Steyn et al. (eds.), *Air Pollution Modeling and its Application XXII*,
NATO Science for Peace and Security Series C: Environmental Security,
DOI 10.1007/978-94-007-5577-2_35,

35.1 Introduction

The PREV'AIR system (http://www.prevair.org) was implemented in 2003 with the aim of generating and publishing daily air quality forecast maps obtained from numerical simulations on different spatial scales [1]. Analysed maps are also produced by combining simulations from the chemistry-transport model (CTM) CHIMERE with surface measurements. A geostatistical kriging based procedure is applied [2]. The resulting maps are considered as the best possible representation of the pollution situation having occurred.

Using this kriging procedure, the forecast maps can be improved as well by mixing CHIMERE predictions with forecast concentrations at individual stations. The first section deals with the local forecasts and describes how past modelling and measurement data can contribute to construct a better prediction at individual stations. The second section is at this stage a discussion on how those local forecasts can be introduced in the operational mapping.

35.2 Statistical Short-Term Forecasting at Individual Stations

The statistical methodology, which is referred to as "statistical adaptation" of the regional CTMforecast, was investigated within the framework of CITEAIRII project and presented during ITM31 [3]. It is aimed at being achievable with limited availability of environmental data. Concentrations of each pollutant at each monitoring station are written as linear function of interpolated CTM outputs, past measurements and other relevant quantitative (meteorology) or qualitative (type of day) predictors. Despite its limitations in capturing non-linear processes, the multiple linear regression technique was selected because of its efficiency, its flexibility, which makes it easy to add or remove predictors, and its low computational cost. Thorough validation studies against observation data from many cities [4] highlighted the overall robustness of the method and its ability to significantly improve raw CHIMERE forecasts on local scale.

Statistical short-term forecasting models were built for O_3 and PM_{10} for all background monitoring sites in Europe (forecasting horizons: D+0, D+1, D+2). Air Base data (http://acm.eionet.europa.eu/databases/airbase/#reporting) – completed with national measurement data – and CHIMERE data from 2010 were used as training dataset and data from 2009 as validation dataset. Usual validation scores were computed both for CHIMERE raw outputs and for the statistically adapted forecasts; for most stations they are improved by statistical adaptation (Fig. 35.1). From those results numerical bounds can be set for those scores, outside which a statistical model may be considered as less reliable and potentially unsuitable for operational use.

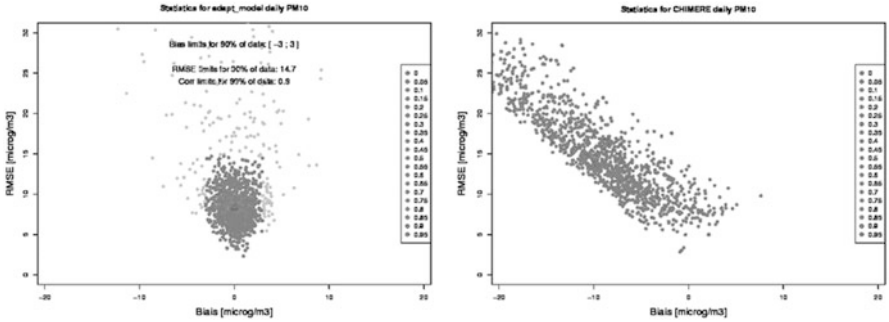

Fig. 35.1 D+0 prediction of PM_{10} daily average concentrations at monitoring sites. European domain. Validation scores for CHIMERE raw forecasts (*right*) and for the statistically adapted forecasts (*left*). X-axis: Bias; Y-axis: RMSE; *color of the points*: correlation

35.3 Operational Use of the Local Forecasts

External drift kriging is applied to combine CHIMERE model output fields with local forecasts. Three ways of selecting relevant stations for the mapping process have been so far identified:

1. In MACC2 project [5], a set of stations was selected from the Airbase database list of stations. The selection process takes account of the type of area, the type of station and the geographical coordinates.
2. In Joly and Peuch [6], a new classification of stations was proposed based on the temporal analysis of time series.
3. As a result of the previous section, numerical criteria can be defined to identify the stations for which the statistical models are more reliable.

A combination of those three approaches is being tested for operational implementation in PREV'AIR. In the meanwhile, all background stations for which data are available are taken into account (Fig. 35.2). The graph on the right represents CHIMERE raw forecast of the daily mean PM_{10} concentration for a specific day over Europe (D+0 forecast). Within the domain covered by monitoring data, the use of the local forecasts succeeds in reducing the well-known underestimation of PM_{10} concentrations by CTMs. Such map has to be compared to the D-1 analysed map, which is the best estimate obtained a posteriori using observations from all French and European background stations. Good agreement between both figures is observed. Note that in regions or countries with sparse network or no available measurement data, the forecast map is more uncertain. In extrapolation areas, kriging results should be considered with caution.

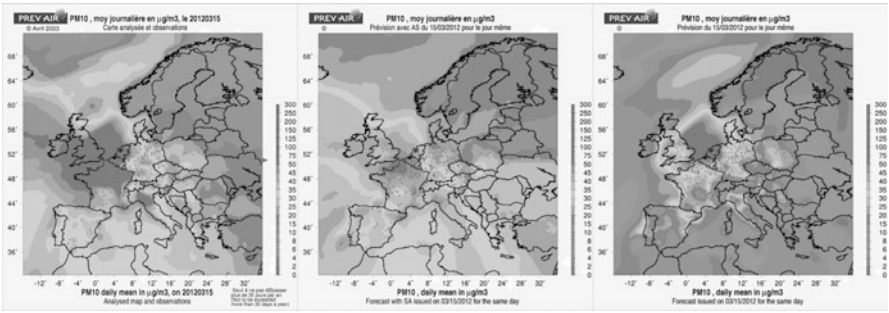

Fig. 35.2 Daily average concentrations of PM_{10} over Europe (15 March 2012). *Left*: D-1 analysed map (observations + CHIMERE simulated concentrations); *middle*: D+0 adjusted forecast map (local statistical forecasts + CHIMERE forecast field). *Right*: D+0 CHIMERE raw forecast

35.4 Conclusion and Discussion

Much effort has been devoted to improving the quality of the forecasts delivered by the national PREV'AIR system. Parallel to ongoing physical and numerical developments in the CTM, a statistical and geostatistical methodology has been worked out. It consists in combining the results from local statistical forecasting models with CHIMERE outputs on the French and European scales. Several issues are being investigated through validation tests: (1) selection of stations according to their class and location, data variability and the reliability of the statistically adapted models; (2) Evaluation of forecast performance as a function of the prediction horizon: D+0, D+1 or D+2; (3) extension to NO_2 forecast maps.

References

1. Honoré C et al (2008) Predictability of European air quality: the assessment of three years of operational forecasts and analyses by the PREV'AIR system. J Geophys Res – Atmos 113:D04301. doi:10.1029/2007JD008761
2. Malherbe L, Ung A, Colette A, Debry E (2012) Formulation and quantification of uncertainties in air quality mapping. ETC/ACM Technical Paper Sept 2011. Report available at http://acm.eionet.europa.eu/reports/ETCACM_TP_2011_9_AQmapping_uncertainties
3. Malherbe L, Songeur CH, Honoré C, Ung A, Meleux F (2010) Forecasting urban air quality over cities by statistical adaptation of deterministic chemistry transport model outputs. In: 31st NATO/SPS international technical meeting on air pollution modelling and its application, 27 Sept–01 Oct 2010, Torino, Italy
4. Honoré C, Ung A, Corbet L, Malherbe L (2011) Good practice guide on air quality forecasting. CITEAIRII publications, European Union, Interreg IVC. http://www.citeair.eu

5. Rouïl L (ed) (2011) Evaluation report of the air quality assessments in Europe for 2007, MACC report D-R-EVA_2.2, Report available at http://www.gmes-atmosphere.eu/documents/deliverables/r-eva/
6. Joly M, Peuch V-H (2012) Objective classification of air quality monitoring sites over Europe. Atmos Environ 47:111–123

Questions and Answers

Questioner Name: Ujjwal Kumar

Q: CHIMERE air quality concentrations have been used just as exogeneous variables in the statistical model to make air quality forecasts and then kriging has been applied to extend it for full domain. What if we remove "CHIMERE values" from the statistical model and then try to make forecasts with mapping? I guess, it can still give reasonable results. Has such comparison been made?

A: CHIMERE results are actually used:
– at the monitoring stations, as possible predictor in the statistical models;
– over the whole domain, as drift in the kriging.
In the statistical modelling, a set of predictors is automatically selected from a list of potential explanatory variables. It may occur that after selection CHIMERE is removed from that set. However this is usually not the case; comparison tests indicated that in general, CHIMERE significantly increased the explanatory power of the statistical models.
In the kriging, CHIMERE proved very useful as well, enabling a better estimation of the concentration spatial variability and the production of more realistic air pollution maps.

Chapter 36
Ensemble Forecasting Coupled with Data Assimilation, and Threshold Exceedance Detection on Prev'Air

Édouard Debry, Vivien Mallet, Laure Malherbe, Frédérik Meleux, Bertrand Bessagnet, and Laurence Rouïl

Abstract In this study the benefits of coupling data assimilation with ensemble forecasting are demonstrated for the production of improved air quality forecasts and detection of threshold exceedances.

Keywords Data assimilation • Ensemble forecasting • Prev'air

36.1 Introduction

Air quality models are more and more used in operational context, either in the framework of impact studies, or to forecast air pollution events. Nevertheless, they still undergo strong uncertainties [3] in their input data as well as physical parameterizations, not to mention numerical solvers. Data assimilation and ensemble forecasting have been developed for several years on the French air quality platform *Prev'Air* (http://www.prevair.org). In this talk, we aim at demonstrating the benefits of coupling data assimilation with ensemble forecasting in order to produce better forecasts and to address the detection of threshold exceedances, which is one of the crucial demand of the French ministry for environment in supporting this work.

É. Debry (✉) • L. Malherbe • F. Meleux • B. Bessagnet • L. Rouïl
National Institute for Industrial Environment and Risks (INERIS), Parc Technologique ALATA, B.P. 2, 60550 Verneuil-en-Halatte, France
e-mail: edouard.debry@ineris.fr; fabienne.carette@ineris.fr

V. Mallet
INRIA (French National Institute for Research in Computer Science and Control), Domaine de Voluceau Rocquencourt, B.P. 105, 78153 Le Chesnay Cedex, France

CEREA, École des ponts ParisTech – EDF R&D, Université Paris Est, Marne la Vallée Cedex 2, France

D.G. Steyn et al. (eds.), *Air Pollution Modeling and its Application XXII*,
NATO Science for Peace and Security Series C: Environmental Security,
DOI 10.1007/978-94-007-5577-2_36,

36.2 Coupling Data Assimilation and Ensemble Forecasting

Data assimilation and ensemble forecasting are both numerical methods designed to improve forecasts. The first one combines available observation data (e.g., ozone measurements) with the dispersion model, whereas the second combines several dispersion model predictions in order to better forecast the observations.

The coupling between data assimilation and the ensemble simulations relies on a weighted linear combination (EFA) of the ensemble members (M^m) which is designed to forecast the forthcoming analyses generated by an assimilation algorithm.

$$EF\ A_{t,x} = \sum_{m=1}^{n} \alpha_{t,x}^{m} \quad M_{t,x}^{m}$$

Before every forecast step t, the method produces new weights $\alpha_{t,x}^{m}$ (one per model, per grid cell and per pollutant) based on past ensemble simulations ($M_{t',x}$) and past analyses ($A_{t',x}$), using the Ridge Regression Discounted algorithm [4]

$$\alpha_{t,x} = \underset{a \in \mathbb{R}^n}{\arg\min}\ \lambda \|\alpha\|_2^2 + \sum_{t'=1}^{t-1} \beta_t^{-t'} \left(\alpha \cdot \mathbf{M}_{t',x} - A_{t',x}\right)^2 \tag{36.1}$$

where $\lambda > 0$ and β_t is a decreasing sequence.

We refer to this method as the Ensemble Forecast of Analyses (EFA) [2]. In the long run and in every grid cell, the ensemble forecasts approximate the analyses (i.e., the best a posteriori knowledge of the atmosphere chemical state) at least as well as the best constant (in time) linear combination of the ensemble members.

36.3 Operational Application on Prev'Air and Threshold Exceedance Detection

EFA is applied operationally on the French air quality platform *Prev'Air* which provides daily an ensemble of eight forecasts (up to 3 days ahead) for ozone, nitrogen dioxide and particles over France and Europe. The forecasts are generated by *Chimere* (IPSL, INERIS, CNRS), *Mocage* (Météo France) and *Polyphemus* (CEREA). Analyses are currently generated offline with an ordinary kriging of innovations [1].

Figures 36.1 and 36.2 show the ability of EFA respectively for ozone and PM_{10}. The *Chimere* model, its analysis and EFA are respectively labeled (a), (b) and (d). (c) is the Ensemble Forecast of Observations (EFO), which targets directly the observed data instead of the analysis and which combines the ensemble simulations with uniform weights learned from all observation stations at once.

Tables 36.1 and 36.2 respectively show the statistical performance of the ensemble for both pollutants, and the detection skill for ozone and for the regulatory threshold of 180 μ g·m^{-3}.

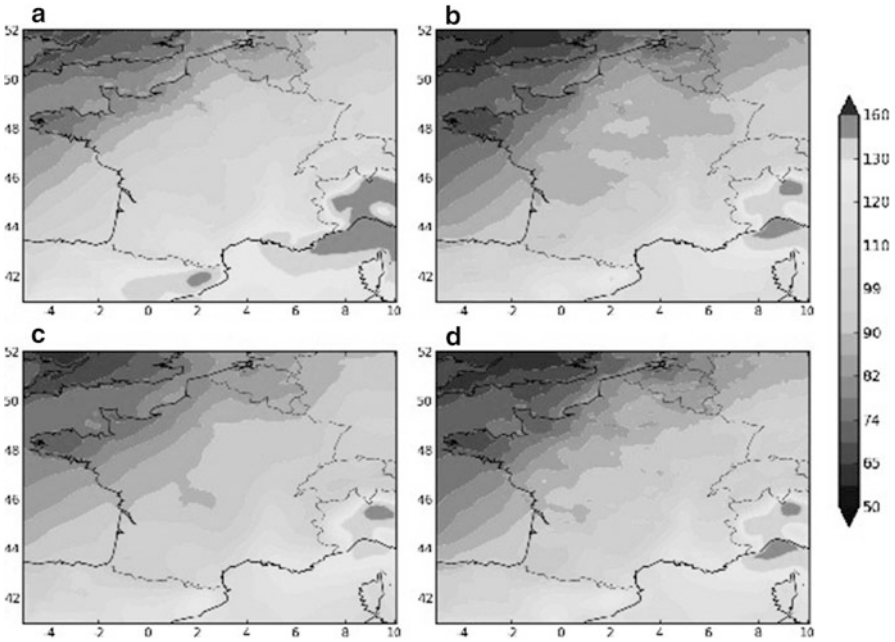

Fig. 36.1 Ozone peak map on summer 2009

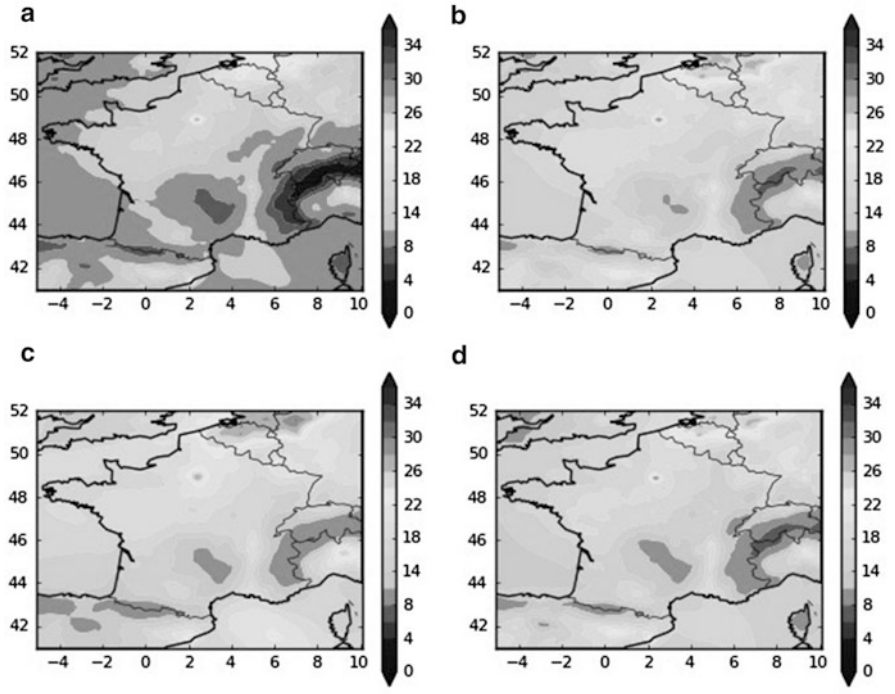

Fig. 36.2 PM_{10} daily average map on summer 2010

Table 36.1 Ozone peak and PM_{10} performance

	RMSE (μ g·m^{-3})	Correlation	Bias factor
Ozone peak			
Chimere a)	20.1	0.79	1.12
EFO c)	15.3	0.83	1.00
EFA d)	14.8	0.84	1.02
PM_{10}			
Chimere a)	10.8	0.4	0.55
EFO c)	8.4	0.51	0.82
EFA d)	8.3	0.53	0.79

Table 36.2 Ozone threshold (180 μ g·m^{-3}) exceedance detection skill

	Chimere	EFO	EFA
Hit	10	3	5
Miss	3	10	8
False alarm	10	0	1
Correct negative	100	110	109

36.4 Conclusion

The EFA improves the statistical performance for both pollutants. It also slightly improves the threshold exceedance detection. Both ensemble methods make less hits than the model itself, but produce significantly less false alarms.

The advantage of the EFA lies in its ability to compute space-dependent weights, which allows to better account for the small patterns found in the analyses. It is noteworthy that the EFA reproduces well the analyses and is therefore highly dependent on the quality of these analyses.

Further works will consist in developing an online data assimilation method based on the BLUE method and to improve the ensemble detection skills.

References

1. Honoré C et al (2004) Le système Prev'Air: cartographie et prévision de la qualité de l'air à grande échelle en Europe. Environnement Risques et Santé 3(3):156–164
2. Mallet V (2010) Ensemble forecast of analyses: coupling data assimilation and sequential aggregation. J Geophys Res 115:D24303
3. Mallet V, Sportisse B (2006) Uncertainty in a chemistry-transport model due to physical parameterizations and numerical approximations: an ensemble approach applied to ozone modeling. J Geophys Res 111:D01302
4. Mallet V, Stoltz G, Mauricette B (2009) Ozone ensemble forecast with machine learning algorithms. J Geophys Res 114:D05307. doi:10.1029/2008JD009978

Chapter 37
Recent Advances in Canada's National Operational AQ Forecasting System

Michael D. Moran, S. Ménard, R. Pavlovic, D. Anselmo, Stavros Antonopoulos, P.A. Makar, Wanmin Gong, S. Gravel, C. Stroud, J. Zhang, Q. Zheng, A. Robichaud, H. Landry, P.A. Beaulieu, S. Gilbert, J. Chen, and A. Kallaur

Abstract Environment Canada routinely issues twice-daily, 48-h public forecasts of (a) gridded surface and near-surface O_3, $PM_{2.5}$, and NO_2 concentration fields made by the GEM-MACH15 on-line chemical weather forecast model on a 15-km North American grid plus (b) point-specific forecasts for Canadian cities of the national Air Quality Health Index (AQHI) prepared by a statistical post-processing package called UMOS-AQ. The AQHI is a health-based, additive, no-threshold, hourly AQ index that ranges from 0 to 10+ and is based on a weighted sum of local O_3, $PM_{2.5}$, and NO_2 concentrations. An objective analysis scheme for surface O_3, $PM_{2.5}$, and NO_2, which will provide model-measurement data fusion and model error diagnostics, is now being tested. These recent advances as well as plans for further improvements to the AQ forecasting system are described.

Keywords AQ forecasts • Health index • AQHI • GEMS-MACH15

M.D. Moran (✉) • P.A. Makar • W. Gong • C. Stroud • J. Zhang • Q. Zheng
Air Quality Research Division, Environment Canada, Toronto, ON, Canada
e-mail: mike.moran@ec.gc.ca

S. Ménard • R. Pavlovic • D. Anselmo • H. Landry • P.A. Beaulieu • S. Gilbert • J. Chen
Air Quality Modeling Applications Section, Environment Canada, Montreal, QC, Canada

S. Antonopoulos
Weather Elements Section, Environment Canada, Montreal, QC, Canada

S. Gravel • A. Robichaud • A. Kallaur
Air Quality Research Division, Environment Canada, Montreal, QC, Canada

D.G. Steyn et al. (eds.), *Air Pollution Modeling and its Application XXII*,
NATO Science for Peace and Security Series C: Environmental Security,
DOI 10.1007/978-94-007-5577-2_37,

37.1 Elements of the Canadian National AQ Forecasting System

Environment Canada (EC) uses an information tool called the Air Quality Health Index (AQHI) to communicate the total health risk of a mixture of air pollutants, including ground-level ozone (O_3), particulate matter ($PM_{2.5}$ size fraction), and nitrogen dioxide (NO_2), to the Canadian public. This hourly index has a range from 0 to 10+ and is calculated as a weighted sum of local O_3, $PM_{2.5}$, and NO_2 surface concentrations. It was developed from a time-series analysis of air pollutant concentrations and mortality in Canadian cities by Health Canada and EC [6] in collaboration with the provinces and key health and environmental stakeholders.

The AQHI improves upon existing provincial AQ indices in several ways: (i) it considers the combined effects of a mixture of air pollutants on health (i.e., it is additive); (ii) it does not assume a minimum threshold; (iii) it provides a common national index that has the same meaning across Canada; and (iv) it is targetted, because each index value has two associated health-related messages, one for sensitive populations such as children, the elderly, and asthmatics, and one for the general population.

Hourly AQHI observations and twice-daily forecasts are made available to the public via an EC external website and various other media outlets. In order to be able to provide current AQHI values, EC receives automated near-real-time (NRT) hourly reports of local O_3, $PM_{2.5}$, and NO_2 concentrations from over 230 urban and rural AQ measurement stations located across Canada. NRT hourly O_3 and $PM_{2.5}$ concentrations are also obtained from U.S. stations from AIRNow. To provide AQHI forecasts, EC runs an operational AQ forecast model twice daily to produce 48-h forecasts of O_3, $PM_{2.5}$, and NO_2 concentrations across Canada. Recently, two post-processing packages were developed to provide forecasters with additional guidance by combining AQ model forecasts and measurements. More details about recent updates to the operational AQ forecast model, the post-processing packages, and future plans are provided in the following sections.

37.2 Status of the National Operational AQ Forecast Model

The current EC operational AQ forecast model is called GEM-MACH15 ("Global Environmental Multi-scale model – Modelling Air Quality and Chemistry with 15-km grid spacing"). GEM-MACH15 is a limited-area configuration of the GEM-MACH on-line chemical transport model, which itself is embedded in GEM, EC's multi-scale operational numerical weather prediction model [1, 4, 5]. GEM-MACH15 predicts both chemical and meteorological fields and its twice daily 48-h forecasts start at 00 and 12 UTC. Seasonal climatological vertical profiles of chemical species are currently used to provide chemical lateral boundary conditions, with the exception of O_3, which varies monthly. Hourly meteorological boundary

conditions are provided from 48-h forecasts made by the operational regional 15-km configuration of GEM (the meteorological "piloting" model) on a larger domain. Initial chemical conditions are obtained from the 12-h chemistry fields of the previous GEM-MACH15 forecast while initial meteorological conditions (based on 3DVAR) come from the regional GEM piloting run for the same forecast time.

GEM-MACH15 has undergone a number of recent upgrades since it became operational late in 2009:

Mar. 2010: New emissions files are introduced (modified spatial distribution primary $PM_{2.5}$ emissions over some Canadian provinces)
Oct. 2010: Piloting model is changed from global GEM15 to regional GEM-LAM15
Oct. 2011: New operational version of GEM-MACH15 (GEMv3.3.3, PHY4.7.2) is implemented with new U.S. emissions

The current operational version of GEM-MACH15 uses hourly emissions input files that were obtained by processing the 2006 Canadian national emissions inventory, a 2012 projected U.S. emissions inventory, and the 1999 Mexican emissions inventory. Previous versions of GEM-MACH15 had used emissions files based on the 2005 U.S. emissions inventory (v4). The 2012 inventory has decreased mobile and point-source emissions but increased marine emissions.

37.3 Status of Post-processing Packages

Two post-processing packages have been developed for use with GEM-MACH15 forecasts to provide additional guidance to EC AQ forecasters by combining AQ forecasts with AQ measurements in different ways for different purposes.

37.3.1 UMOS-AQ Package

UMOS-AQ ("Updateable Model Output Statistics – Air Quality") is a statistical post-processing package for bias correction that can compensate for systematic AQ model errors and account for unresolved subgrid-scale phenomena at selected points, namely AQ station locations. A UMOS post-processing package has been used by EC to forecast meteorological predictands such as surface temperature and probability of precipitation since 1995 [7, 8]. UMOS-AQ uses the existing EC UMOS framework and became operational in July 2010.

UMOS-AQ combines multiple sources of information: AQ forecasts; meteorological forecasts; AQ measurements; and physical variables (e.g., solar flux, sine of scaled Julian day). It consists of a large set of multi-variate linear regression (MLR) equations, where one MLR equation is generated per AQ station per pollutant per season per forecast hour per run.

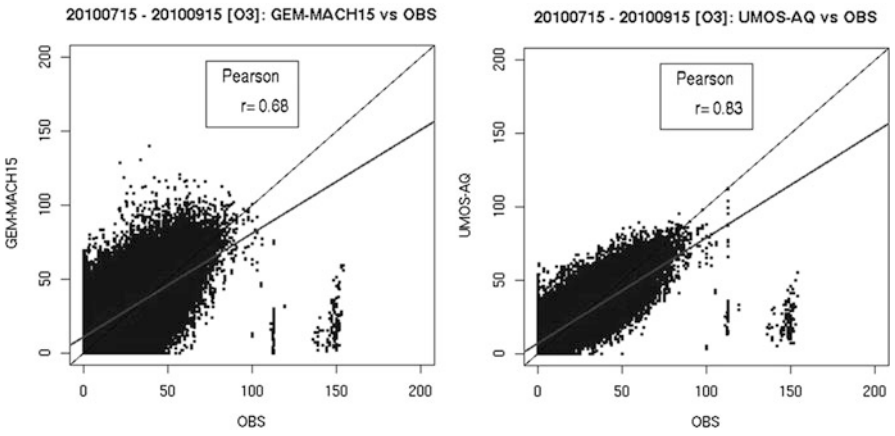

Fig. 37.1 Scatterplots of (*left*) GEM-MACH15 hourly O_3 forecasts vs. measurements at Canadian stations and (*right*) UMOS-AQ hourly O_3 forecasts vs. measurements at the same stations for the 2-month period 15 July to 15 Sept. 2010

Three predictands are currently considered by UMOS-AQ: O_3, $PM_{2.5}$, and NO_2. Possible MLR predictors include O_3, $PM_{2.5}$, and NO_2 hourly concentrations at a station for each hour of the previous day (i.e., persistence) plus 84 other chemical, meteorological, and physical predictors. Between two and five predictors are used per MLR equation on average to avoid overfitting. Two seasons – summer and winter – are considered with a transitional period of ~6 weeks. A minimum of 250 observation-model pairs per season are needed to generate robust MLR equations. The equations are regenerated with the latest model data every week. Figure 37.1 shows the impact of UMOS-AQ on GEM-MACH15 hourly O_3 forecasts for a 2-month period in summer 2010.

One limitation of UMOS-AQ is that MLR equations can only be constructed for locations where historical AQ measurements are available. This is an issue because most AQ stations are not co-located with public weather forecast stations and many do not measure all three AQHI pollutants. A solution is to blend the UMOS-AQ point forecasts with GEM-MACH15 gridded forecast fields. This is now being done by optimal interpolation (OI) using MIST (Moteur d'Interpolation STatistique), an EC statistical interpolation package that uses the OI algorithm described by Mahfouf et al. [3]. UMOS-AQ/MIST was implemented operationally by EC in Aug. 2011.

37.3.2 Objective Analysis Package

An objective analysis (OA) package for O_3, $PM_{2.5}$, and NO_2 has been developed based on an improved version of the OI technique to blend or "fuse" AQ measurements with model forecast fields in order to make maximum use of the

information contained in both. Applications include nowcasting, construction of chemical climatologies, trend analyses, and inputs for retrospective human exposure studies. The difference field between the OA and the model field (the "analysis increment") can also provide useful information about short- and longer-term model errors to both AQ forecasters and model developers.

The input measurement data used by the OA package consist of NRT surface measurements from Canadian and U.S. AQ networks, and the trial fields required for the OI scheme are GEM-MACH15 forecast fields. The package blends the hourly measurements as they become available with corresponding model forecast fields from each 48-h GEM-MACH15 run. Spatial error variances were pre-computed from historical AQ data sets and past model forecasts using a first-order auto-regressive approach. Computation of error statistics is adapted from Hollingsworth and Lönnberg [2]. The cutoff distance used is 900 km.

The OA package is currently running for O_3 and $PM_{2.5}$ in development mode, but it is expected that the package will be migrated into the operational environment later this year. Research also continues into adding NO_2 to the package.

37.4 Future Plans

Updates planned for GEM-MACH in the near term include (a) reduction of the horizontal grid spacing from 15 to 10 km while keeping the same domain size and (b) new input emissions files based on improved emissions processing methodology, including new spatial surrogate fields and temporal profiles. GEM v4, a new generation of the host meteorological model, is now available, and GEM-MACH will migrate to this version, which includes a new staggered vertical discretization and the capability of piloting a limited-area configuration at the model top. Some new process representations may be added, including the meteorological modulation of fugitive PM emissions [5], and some numerical schemes such as the operator splitting sequence and the gas-phase chemistry solver may be revised. A grid nesting capability will also be introduced for urban-scale modelling.

References

1. Anselmo D, Moran MD, Ménard S, Bouchet V, Makar P, Gong W, Kallaur A, Beaulieu P-A, Landry H, Stroud C, Huang P, Gong S, Talbot D (2010) A new Canadian air quality forecast model: GEM-MACH15. In: Proceedings of the 12th AMS conference on Atmospheric Chemistry, Jan. 17–21, Atlanta, GA. American Meteorological Society, Boston, 6 pp. See http://ams.confex.com/ams/pdfpapers/165388.pdf
2. Hollingsworth A, Lönnberg P (1986) The statistical structure of short-range forecast errors as determined from radiosonde data. Part I: the wind field. Tellus 38A:111–136
3. Mahfouf J-F, Brasnett B, Gagnon S (2007) A Canadian precipitation analysis (CaPA) project: description and preliminary results. Atmos-Ocean 45:1–17

4. Moran MD, Chen J, Ménard S, Pavlovic R, Landry H, Beaulieu P-A, Gilbert S, Makar PA, Gong W, Stroud C, Kallaur A, Robichaud A, Gong S, Anselmo D (2011) Two years of operational AQ forecasting with GEM-MACH15: a look back and a look ahead. In: Proceedings of the 10th CMAS conference, 24–26 Oct., Chapel Hill, NC, 7 pp. See http://www.cmascenter.org/conference/2011/abstracts/moran_two_years_2011.pd
5. Moran MD, Ménard S, Talbot D, Huang P, Makar PA, Gong W, Landry H, Gravel S, Gong S, Crevier L-P, Kallaur A, Sassi M (2010) Particulate-matter forecasting with GEM-MACH15, a new Canadian air-quality forecast model. In: Steyn DG, Rao ST (eds) Air pollution modelling and its application XX. Springer, Dordrecht, pp 289–292M
6. Stieb DM, Burnett RT, Smith-Doiron M, Brion O, Hyun Shin H, Economou V (2008) A new multipollutant, no-threshold air quality health index based on short-term associations observed in daily time-series analyses. J Air Waste Manage Assoc 58:435–450
7. Wilson LJ, Vallée M (2002) The Canadian Updateable Model Output Statistics (UMOS) system: design and development tests. Weather Forecast 17:206–222
8. Wilson LJ, Vallée M (2003) The Canadian Updateable Model Output Statistics (UMOS) system: validation against perfect prog. Weather Forecast 18:288–302

Questions and Answers

Questioner Name: Sarav Arunachalam

Q: You have developed an advanced air quality forecast (AQF) system. Do you have any information on how much this AQF system is used by the public for protecting public health and/or for general awareness? Documenting any information on gross usage statistics will be helpful to assess the utility and value of this system.
A: In terms of gross usage statistics, for the most recent year, 2011, there were 800,000 visits to our AQHI values on Environment Canada's public Weatheroffice website (http://www.weatheroffice.gc.ca/canada_e.html). As well, EC has been and is working with polling and market research firms to track how well the AQHI is understood by the public, how it is being used, and by whom.

Questioner Name: Sarav Arunachalam

Q: After UMOS-AQ is applied, it seems that $PM_{2.5}$ performance degrades rather than improves whereas O_3 and NO_2 seem just fine. Do you know why?
A: In comparing the scatterplots for GEM-MACH15 vs. observations and UMOS-AQ vs. observations for summer 2010, you are correct that to the eye the amount of data-point scatter appears to have increased for UMOS-AQ. However, the overall forecast skill for $PM_{2.5}$ has in fact improved: for example, the Pearson correlation coefficient r increased from 0.28 to 0.52 and the slope of the best-fit line moved closer to unity.

Chapter 38
Ensemble Perturbations for Chemical Data Assimilation

Jeremy D. Silver, Jørgen Brandt, Jesper H. Christensen, Michael Kahnert, and Lennart Robertson

Abstract The ensemble Kalman filter is a commonly used framework for chemical data assimilation. Random perturbations are required for the ensemble initial conditions and to account for model error. For a chemical transport model, such perturbations should represent appropriate scales of variation and correlations in the horizontal, vertical and chemical dimensions. We present a sampling scheme to generate normally distributed perturbations with covariances based on a climatological background covariance matrix, estimated with a spectral decomposition, assuming horizontally homogeneous and isotropic error correlations. We tested the sampling scheme with an ensemble Kalman filter coupled to the Danish Eulerian Hemispheric Model, a three-dimensional chemical transport model. Observations of CO were assimilated, leading to substantially reduced bias at surface monitoring stations.

Keywords Data assimilation • Ensemble Kalman filter • Model error

38.1 Introduction

The ensemble Kalman filter (EnKF) is a popular data assimilation technique based on Kalman filter theory [3]. The EnKF accounts for "errors of the day" in the background error covariance matrix, **B**. The EnKF relies on the assumption that ensemble spread is a good representation of model uncertainty. Appropriate ensemble spread may be achieved by perturbing the initial conditions (ICs) and

J.D. Silver (✉) • J. Brandt • J.H. Christensen
Department of Environmental Science, Aarhus University, 4000 Roskilde, Denmark
e-mail: jds@dmu.dk

M. Kahnert • L. Robertson
Swedish Meteorological and Hydrological Institute, 601 76 Norrköping, Sweden

D.G. Steyn et al. (eds.), *Air Pollution Modeling and its Application XXII*,
NATO Science for Peace and Security Series C: Environmental Security,
DOI 10.1007/978-94-007-5577-2_38,

maintained by adding random perturbations to the ensemble as part of each assimilation cycle, which corresponds to the model error (ME) term in the Kalman filter framework [3].

We present a sampling scheme for ensemble ICs and ME perturbations. The random samples are drawn from a multivariate normal distribution with a specified covariance matrix, namely the climatological **B** matrix. The **B** matrix was estimated using a spectral decomposition, and invoking assumptions of horizontally homogeneous and isotropic error correlations [1, 4, 6]. This sampling scheme ensures appropriate scales of variation and correlations in the horizontal, vertical and chemical dimensions. Results are presented for an experiment to test the sampling scheme using an EnKF coupled to the Danish Eulerian Hemispheric Model (DEHM), a three-dimensional chemical transport model. A month-long simulation was run and observations of CO were assimilated.

38.2 Sampling Scheme

Let w be a vector of independent, normally distributed random variables with zero mean and unit variance. Let **C** be a covariance matrix, thus satisfying $\mathbf{C} = \mathbf{V}\mathbf{V}^{\mathrm{T}}$ for some **V**; then $\mathbf{V}w$ will be normally distributed with zero mean and covariance matrix **C** [5, pp. 132]. The sampling scheme presented here uses this fact, in conjunction with a decomposition of the climatological **B** matrix. This spectral decomposition models covariances as horizontally homogeneous, isotropic in the horizontal plane, and non-separable in the vertical and chemical dimensions. The procedure used to estimate and decompose **B** is presented in detail by [6], and we use $\mathbf{V} := \mathbf{U}^{-1}$ from Eq. 31 of that article.

The sampling is performed by computing the product $\mathbf{V}w$. To ensure that $\mathbf{V}w$ are real, w must satisfy $w_{e,-m,-n} = w_{e,m,n}{}^{*}$ where e is the index of the eigenvector and $m = -K_x, \ldots, K_x$, $n = -K_y, \ldots, K_y$ are the indices of the Fourier coefficients [6]. Unconstrained entries of w are independent draws from a standard normal distribution.

The estimates of the background errors required for the climatological covariance matrix were derived using the NMC method. Two DEHM simulations were run for the period January to March 2006 with different meteorological data using 12 and 36 h forecasts, respectively. The difference between the concentration fields was used to estimate covariance parameters.

The power spectrum of the error statistics, derived from the decomposition [6, Eq. 49], shows that the spatial scales of error variability reflect the atmospheric lifetime of the species (Fig. 38.1), short-lived species (e.g. OH) showing far more variation at shorter spatial scales. For CO there is a slight shift towards longer length-scales at higher model layers.

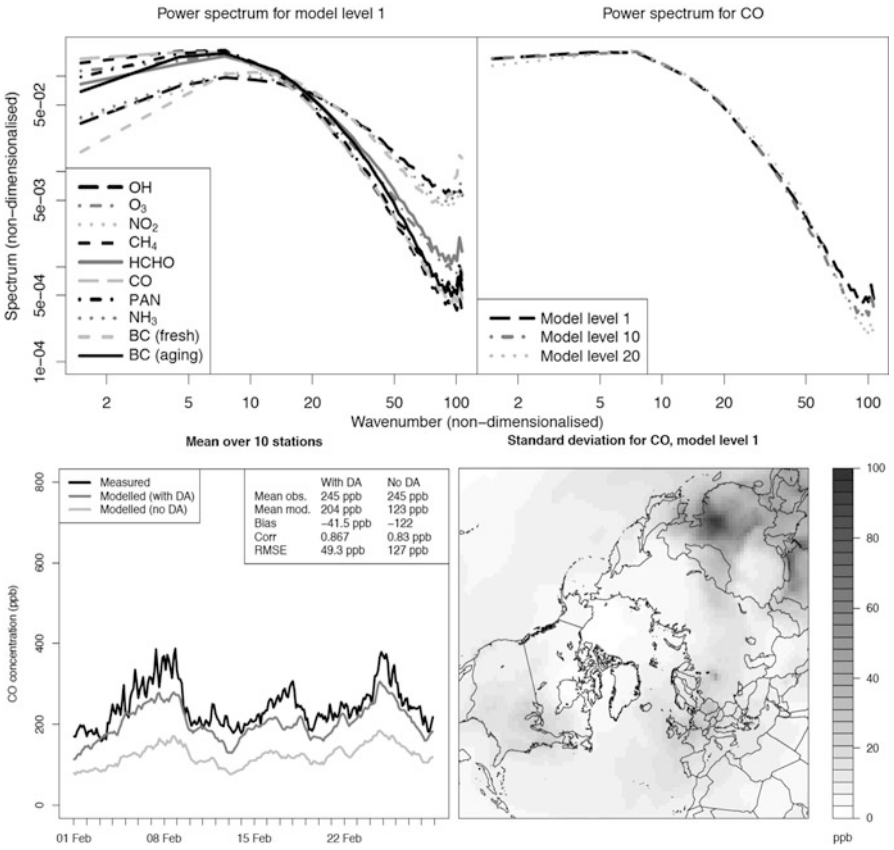

Fig. 38.1 *Top*: Power spectrum for selected species at the lowest model layer and for CO at different model layers. Levels 10 and 20 correspond to about 0.7 and 4.9 km above the surface, respectively. *Bottom left*: Time-series of mean concentrations, averaging over ten European monitoring stations. *Bottom right*: CO background error standard deviation

38.3 Experiment

An EnKF was coupled to the Danish Eulerian Hemispheric Model (DEHM) [2]. The model domain used a 96×96 horizontal grid with approximately 150×150 km resolution at 60°N, and 29 vertical layers extending up to 100 hPa; 67 species were simulated.

Two DEHM simulations were run for February 2005: one with assimilation (*test*) and one without (*reference*). Observations were assimilated every 3 h, adjusting only CO. An asynchronous EnKF was used to account for discrepancies between observation and analysis time [7]. A local analysis was performed for each grid-cell; localisation weights were based on horizontal and vertical distances between grid cells and observations. Perturbations to the ICs and ME for CO, generated

as described above, were scaled by 0.25 and 0.05 (respectively) to avoid negative concentrations and ensemble divergence.

Retrieved total column CO from the MOPITT instrument (aboard the polar-orbiting NASA satellite Terra) were assimilated. Also assimilated were in-situ CO measurements from the GAW network: 16 measurement stations within the model domain provided hourly data. For verification, we used observations of CO from the AirBase network of European AQ monitoring stations. A number of objective quality control checks were applied to select the stations, and data from only ten monitoring stations were used.

Averaging over these ten monitoring stations, the reference simulation shows a strong negative bias, which is largely corrected in the test simulation (Fig. 38.1, bottom-left). The test simulation matches the observed time-series better in terms of the amplitude of temporal variation. Climatological error variances, used to scale the perturbations, mirrored typical concentration, with largest values over central and eastern Asia (Fig. 38.1, bottom-right).

38.4 Discussion

The DEHM-EnKF system with Gaussian perturbations corrected for systematic biases in surface CO concentrations. Experiments with synthetic observations are required to assess how the EnKF increments affect the concentration field in the upper model layers or poorly observed regions. Experiments to test the potential for multi-species assimilation are also planned.

Additive perturbations can lead to negative estimates of concentration, especially for highly variable species. Log-transforming concentrations would avoid this, yet may cause the ensemble to diverge in regions with few observations. Zeroing negative estimates may create bias and degrade the analysis.

References

1. Berre L (2000) Estimation of synoptic and mesoscale forecast error covariances in a limited-area model. Mon Weather Rev 128:644–667
2. Christensen JH (1997) The Danish Eulerian hemispheric model – a three-dimensional air pollution model used for the arctic. Atmos Environ 31(24):4169–4191
3. Evensen G (2009) Data assimilation: the ensemble Kalman filter. Springer, Berlin
4. Gustafsson N, Berre L et al (2001) Three-dimensional variational data assimilation for a limited area model. Part I: general formulation and the background error constraint. Tellus A 53:425–446
5. Gut A (2009) An intermediate course in probability. Springer, Heidelberg
6. Kahnert M (2008) Variational data analysis of aerosol species in a regional CTM: background error covariance constraint and aerosol optical observation operators. Tellus 60B:753–770
7. Sakov P, Evensen G, Bertino L (2010) Asynchronous data assimilation with the EnKF. Tellus 62A:24–29

Questions and Answers

Questioner Name: Valerie Garcia

Q: How did you determine your assumptions for the error correlations (horizontal separation, vertical and chemical levels)?
A: The assumptions you refer to were a compromise between a reality and simplicity. The assumption of horizontally homogeneous and isotropic error correlations is a basic starting point for modelling error correlations, and it dramatically reduces the amount of data required to parameterise the matrices involved in the decomposition of the background error covariance matrix. The results should, however, be treated with caution; in work not presented here, we have found that that error correlations are, in general, neither horizontally homogeneous nor isotropic.
However the assumptions only applied to the ensemble perturbations (to generate initial conditions and to represent model error), and were not used explicitly in the assimilation step. The ensemble Kalman filter inherently captures flow dependent structures in error correlations, and the assumptions used in the decomposition of the climatological background covariance matrix are not invoked.

Chapter 39
Ensemble Data Assimilation for Tropospheric Ozone Analysis Within the CHIMERE Regional Chemistry Transport Model

Benjamin Gaubert, Adriana Coman, Gilles Foret, Matthias Beekmann, Maxim Eremenko, Gaelle Dufour, Denis Zyryanov, Anthony Ung, Gilles Bergametti, and Jean-Marie Flaud

Abstract The data assimilation method Ensemble Kalman Filtering has been used with the Chimere-model for tropospheric ozone over Europe and the results are presented and discussed.

Keywords Chimere model • Data assimilation • Ozone

39.1 Introduction

We present here the set-up and performance of a data assimilation system dedicated to air quality based on the Regional Chemistry Transport Model (RCTM) CHIMERE and an Ensemble Kalman Filter (EnKF). Our focus is on surface ozone concentration over the European domain. Data assimilation provides a framework to the estimation of the error budget for both observation and model. Particularly, the ensemble Kalman filter methodology [5, 6] offers a recursive flow dependant correction of both the ozone state and the associated model error covariance. Concerning the surface ozone data assimilation, the ensemble Kalman filter (EnKF) as well as the Reduced Rank Square Root filter (RRSQRT) was firstly set up within the LOTOS-EUROS model. It has been demonstrated that theses ensemble filters improve the quality of the ozone fields compare to unassimilated stations with only a small ensemble size [10, 12]. In our assimilation system, we choose to implement the deterministic Ensemble Square Root Filter (EnSRF) in order to avoid the sampling error induces by the perturbation of theobservation [7, 14]. In the

B. Gaubert (✉) • A. Coman • G. Foret • M. Beekmann • M. Eremenko • G. Dufour • D. Zyryanov • A. Ung • G. Bergametti • J.-M. Flaud
LISA, Créteil, France
e-mail: gaubert@lisa.u-pec.fr

D.G. Steyn et al. (eds.), *Air Pollution Modeling and its Application XXII*,
NATO Science for Peace and Security Series C: Environmental Security,
DOI 10.1007/978-94-007-5577-2_39,

following, we first give more details on the CHIMERE model, then we present the observation that are used. Also, the assimilation method is presented. Finally results of an assimilation exercise are presented and discussed.

39.2 The Regional Chemistry-Transport Model (RCTM) CHIMERE

CHIMERE is a state-of-the-art chemistry transport model (http://www.lmd.polytechnique.fr/chimere/). General formulation of the model is presented in Bessagnet et al. [1]. The horizontal resolution is $0.5° \times 0.5°$ for the continental domain (−15°, 35° E; 35°, 70° N) with 8 hybrid (σ, p) vertical levels from 995 to 500 hPa.

The mandatory meteorological variables are obtained from the Integrated Forecasting System (IFS) of the European Centre for Medium-Range Weather Forecasts (ECMWF). Hourly anthropogenic emission fluxes are derived from the TNO (http://www.tno.nl/) inventory [13]. The global chemistry transport model MOZART-3 [11] running at $1.875° \times 1.875°$ has been coupled to IFS [9] and provides global trace gas composition on a hourly resolution (three-hourly storage). Thus we obtain three-hourly boundary conditions that are temporally and spatially interpolated on the CHIMERE grid. The deterministic CHIMERE reference run covers June/July/August of 2009 and its output is used for the initialization of the assimilation period.

39.3 Observation Assessment

It is necessary to define an objective subset of observations in order to provide a guideline of simulation verification. In this study, we calculate the daily variability and the daily mean for the entire available background airbase stations (with altitude under 300 m above sea level) in order to get an objective classification of station type following the approach developed by Flemming et al. [8]. As urban stations are not representative of areas on the order of the model resolution, we do not use stations corresponding to urban environment. Thus, we retain three ozone stations types with an increasing daily variability from background/mountain (MOU, 96 stations) for remote site, 'RUR' for rural (240 stations), 'PUR' ('U1', 395 stations) for suburban. Despite the use of a different period and a different geographical distribution, the shape of the ozone profile is similar. Because of the variability criterion, stations located in the north Scandinavia that have in average a lowest daily mean are considered here as background stations. In general, suburban stations are situated around the pattern of polluted environment around large urbanized areas like Paris and Berlin or the Pô valley.

39.4 Data Assimilation Method (EnSRF Formulation)

Firstly introduced by Evensen [5, 6], the Ensemble Kalman Filter (EnKF) algorithm is a sequential filter where Monte-Carlo methods are used to sample the errors statistics. Here, an ensemble of 20 perturbed model state evolve forward in time by the deterministic model which determines the model forecast variances and covariances. Then, we perform a local analysis with a cutoff radius of 250 km around the analysis cell. The impact of the covariance localization is efficient dealing with air quality analysis [4]. After the analysis step, we put additive white noise perturbations to the ozone state with a fixed decorrelation length [5] of 200 km [3]. Following Boynard et al. [2], we apply the same perturbation approach applied to the main parameters driving the ozone concentrations in the CHIMERE model which are the anthropogenic emissions, boundary conditions, the land-use, the vertical diffusion coefficient and the photolysis rate. In this case, the error variance doesn't bring enough spread in the ensemble compared to the additive perturbation of the ozone field itself. As a consequence it reduces only very slightly the RMSE. Assuming no observational error correlation, the R matrix is defined by the observation error variance (diagonal terms). An observation error standard deviation of 5 ppb is used in this study which is common to previous data assimilation system [10, 15].

39.5 Description of Assimilation Experiment and Results

The CHIMERE-EnSRF has been run for ten days from the 14th of August to the 23th of August 2009 in order to obtain reliable statistics of the system. This period was characterized by a short pollution episode on 19th and 20th august, but with a large spatial extent. We define randomly an 'assimilation' and a 'validation' subset of stations (with respectively 368 and 347 stations). In this simulation, we define an arbitrary standard deviation of the additive perturbation of 25 % at night (7 p.m. to 6 a.m.) and 15 % (8 a.m. to 5 p.m.) in the day time. Result in the forecast standard deviation is very close to the prescribed noise which is slightly higher in the nighttime and lower in the day time. The amplitude is in the range of the model error distribution and is found to be sufficient relatively to the observation error by comparing the total error in the system to the resulting forecast RMSE. The RMSE of the analysis is reduced over all stations type used for validation with an average decrease of more than 2 ppb (Fig. 39.1). The temporal correlation between the analysis and the observation is enhancing for all stations type.

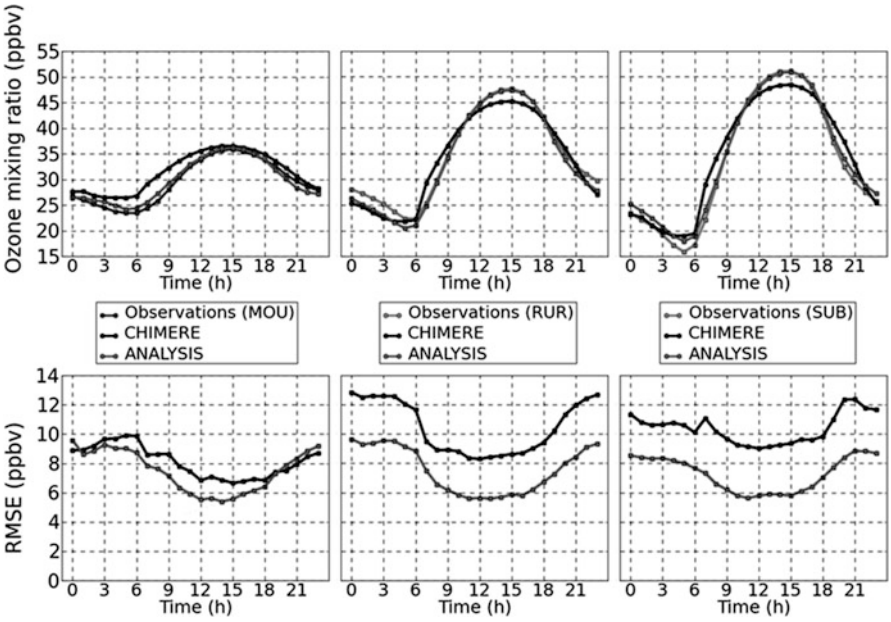

Fig. 39.1 Average ozone profile during the 10 days experiment (*top*). The assimilated profile is close to the observations whereas the observed ozone in underestimate (*overestimate*) in the daytime (*nighttime*). Average RMSE profile (*bottom*) for the reference run (*black*) and the analysis mean (*grey*). Scores are calculated over all stations used for validation for background (MOU, 17stations), rural (RUR, 101 stations) and suburban (SUB, 172 stations)

References

1. Bessagnet B, Menut L, Aymoz G, Chepfer H, Vautard R (2008) Modelling dust emissions and transport within Europe: the Ukraine March 2007 event. J Geophys Res 113:D15202. doi:10.1029/2007JD009541
2. Boynard A, Beekmann M, Foret G, Ung A, Szopa S, Schmechtig C, Coman A (2011) Assessment of regional ozone model uncertainty with a modelling ensemble using an explicit error representation. Atmos Environ 45:784–793
3. Coman A, Foret G, Beekmann M, Eremenko M, Dufour G, Gaubert B, Ung A, Schmechtig C, Flaud JM, Bergametti G (2011) Assimilation of IASI partial tropospheric columns with an ensemble Kalman filter over Europe. Atmos Chem Phys Discuss 11:26943–26997. doi:10.5194/acpd-11-26943-2011
4. Constantinescu EM, Sandu A, Chai T, Carmichael GR (2007) Ensemble-based chemical data assimilation. II: covariance localization. Q J R Meteor Soc 133:1245–1256
5. Evensen G (1994) Sequential data assimilation with a nonlinear quasi-geostrophic model using Monte Carlo methods to forecast error statistics. J Geophys Res 99:143–162
6. Evensen G (2003) The ensemble Kalman filter: theoretical formulation and practical implementation. Ocean Dyn 53:343–367
7. Evensen G (2004) Sampling strategies and square root analysis schemes for the EnKF. Ocean Dyn 54:539–560. doi:10.1007/s10236-004-0099-2

8. Flemming J, Stern R, Yamartino RJ (2005) A new air quality regime classification scheme for O3, NO2, SO2 and PM10 observation sites. Atmos Environ 39:6121–6129
9. Flemming J, Inness A, Flentje H, Huijnen V, Moinat P, Schultz MG, Stein O (2009) Coupling global chemistry transport models to ECMWF's integrated forecast system. Geosci Model Dev 2:253–265
10. Hanea GR, Velders GJM, Heemink A (2004) Data assimilation of ground-level ozone in Europe with a Kalman filter and chemistry transport model. J Geophys Res 109:D10302. doi:10.1029/2003JD004283
11. Kinnison DE, Brasseur GP, Walters S, Garcia RR, Marsh DR, Sassi F, Harvey VL, Randall CE, Emmons L, Lamarque JF, Hess P, Orlando JJ, Tie XX, Randel W, Pan LL, Gettelman A, Granier C, Diehl T, Niemeier U, Simmons AJ (2007) Sensitivity of chemical tracers to meteorological parameters in the MOZART-3 chemical transport model. J Geophys Res 112:D03303. doi:10.1029/2008JD010739
12. Van Loon M, Builtjes PJH, Segers AJ (2000) Data assimilation of ozone in the atmospheric transport chemistry model LOTOS. Environ Model Softw 15:603–609
13. Visschedijk AJH, Zandveld P, Denier van der Gon HAC (2007) A high resolution gridded European emission database for the EU integrated project GEMS, TNO, Apeldoorn, the Netherlands, TNO-report 2007-A-R0233/B
14. Whitaker JS, Hamill TM (2002) Ensemble data assimilation without perturbed observations. Mon Weather Rev 130:1913–1924
15. Wu L, Mallet V, Bocquet M, Sportisse B (2008) A comparison study of data assimilation algorithms for ozone forecasts. J Geophys Res 113:D20310. doi:10.1029/2008JD009991

Questions and Answer

Questioner Name: Dominik Brunner

Q: Model-obs difference shows diurnal cycle with a clear bias at night, probably due to the limited vertical resolution of the model. Should not you try to correct this bias rather than just increasing the uncertainty of nighttime data?
A: The absolute observation error variance of 25 ppb^2 used in this study is therefore relatively more important in the nighttime, considering the total error profile; we also decide to increase the relative model error noise. Regarding the assimilated observations, the bias is considerably reduced at the analysis step, but also in the following one hour forecast. As the bias has a spatial and temporal variability, we prefer to correct the bias in the assimilation procedure as it is based on the model error covariance matrix.

Chapter 40
Improving O3, PM25 and NO2 Surface Fields by Optimally Interpolating Updatable MOS Forecasts

Stavros Antonopoulos, Jacques Montpetit, Vincent Fortin, and Guy Roy

Abstract Updatable Model Output Statistics (UMOS) (Wilson JW, Vallée M, Weather Forecast, 17:206–222, 2001) methodology in air-quality forecasting (UMOS-AQ) has shown great ability to improve direct model output. The UMOS-AQ (Antonopoulos S, Bourgouin P, Montpetit J, Croteau G, Forecasting O_3, PM_{25} and NO_2 hourly spot concentrations using an updateable MOS methodology. In: Proceedings for the 31st NATO/SPS international technical meeting on air pollution modeling and its application, Torino, Italy, pp 309–314, 2010) system produces one equation for each station, predictand, model run, forecast hour and season. A limitation of the method however is the fact that we only obtain point forecasts. An optimal interpolation solution on the UMOS-AQ forecasts using Simple Krigging is presented in which the model's output is used as a trial field. The parametrization chosen is such that the radius of influence is approximately two grid points with most of the weight coming from the UMOS-AQ forecasts. Preliminary results showed significant improvements over the model's forecasts in regions with a high density of observation stations.

Keywords Particulate matter • Ozone • Nitrogen dioxide • Updatable MOS • UMOS • MLR • Post-processing • Krigging • Optimal interpolation

S. Antonopoulos (✉) • J. Montpetit
Weather Elements Section, Environment Canada, Dorval, Quebec, Canada
e-mail: stavros.antonopoulos@ec.gc.ca

V. Fortin
Meteorological Research Division, Environment Canada, Dorval, Quebec, Canada

G. Roy
Meteorological Service of Canada, Environment Canada, Montreal, Quebec, Canada

D.G. Steyn et al. (eds.), *Air Pollution Modeling and its Application XXII*,
NATO Science for Peace and Security Series C: Environmental Security,
DOI 10.1007/978-94-007-5577-2_40,

40.1 Introduction

UMOS-AQ provides point forecasts using Multiple Linear Regression (MLR) only on the stations that are part of the observations network. An important motivation behind the project is the non colocalization of the public forecast (Scribe) sites and the UMOS-AQ stations. In addition, the Scribe forecast sites are much more numerous than the UMOS-AQ observation stations.

An optimal interpolation of the UMOS-AQ forecasts using simple krigging in which the air quality model's (GEM-MACH15) output is used as a trial field is presented as a solution. The krigging parameters chosen are such that the radius of influence is approximately two grid points with most of the weight coming from the UMOS-AQ forecasts.

40.2 Scribe Sites vs. Air Quality Stations

The air quality stations in the database are members of the National Air Pollution Surveillance Network (NAPS) and measure all or a combination of the following pollutants: ozone (O_3), fine particulates (PM_{25}) and nitrogen dioxide (NO_2). Figures 40.1 and 40.2 below show the station and site geographical distribution where the red markers represent the AQ stations and the brown markers the Scribe stations.

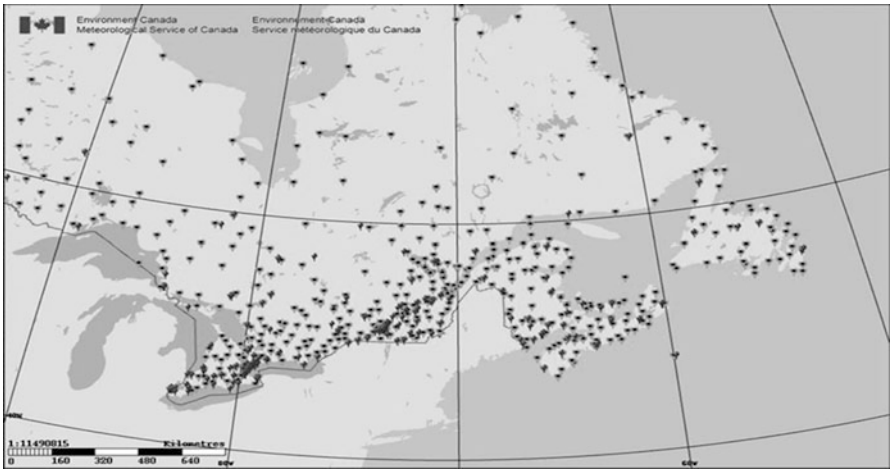

Fig. 40.1 Geographical distribution of Scribe sites and UMOS-AQ stations (East)

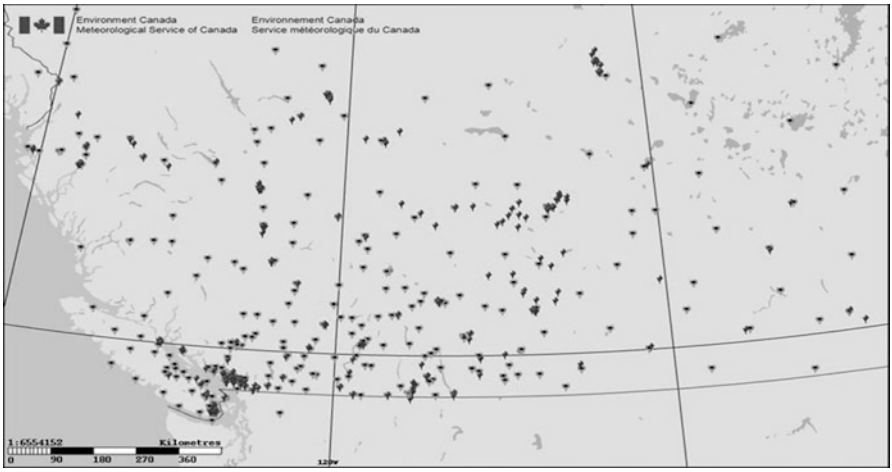

Fig. 40.2 Geographical distribution of Scribe sites and UMOS-AQ stations (West)

40.3 Method and Results

In order to produce forecasts at all Scribe sites, UMOS-AQ forecasts need to be interpolated. Traditionally, the UMOS-Scribe system uses one of two approaches to do this: the creation of virtual stations using neighbor statistics or krigging of the point forecasts. However, the virtual-stations method is intensive to maintain. Additionally, a krigging method as presently implemented on the meteorological post-processing system (UMOS) uses the average value of all the point forecasts as its background field. This approach can induce large errors for isolated Scribe points that are located far from observation stations.

Due to the disadvantages of these two methods we implemented a S*imple Krigging* method that uses the air quality model's (GEM-MACH15) forecasts as trial fields. The interpolation engine used is MIST, the same optimal interpolation engine used to prepare the Canadian Precipitation Analysis (CAPA) [3]. The interpolation parameters are quite strict with a strong localized impact so that we only affect the model's forecast in places where there is a concentration of UMOS-AQ stations. An example of the influence of the UMOS-AQ forecasts over the model's domain can be seen in Fig. 40.3.

The final field obtained is used afterwards for point-forecasts on the Scribe sites which are derived through a second interpolation. Due to this, there is a slight degradation of the quality of the forecast in the subset of UMOS-AQ/MIST *collocated* sites. Figure 40.4 shows the dispersion diagram for a typical case for ozone.

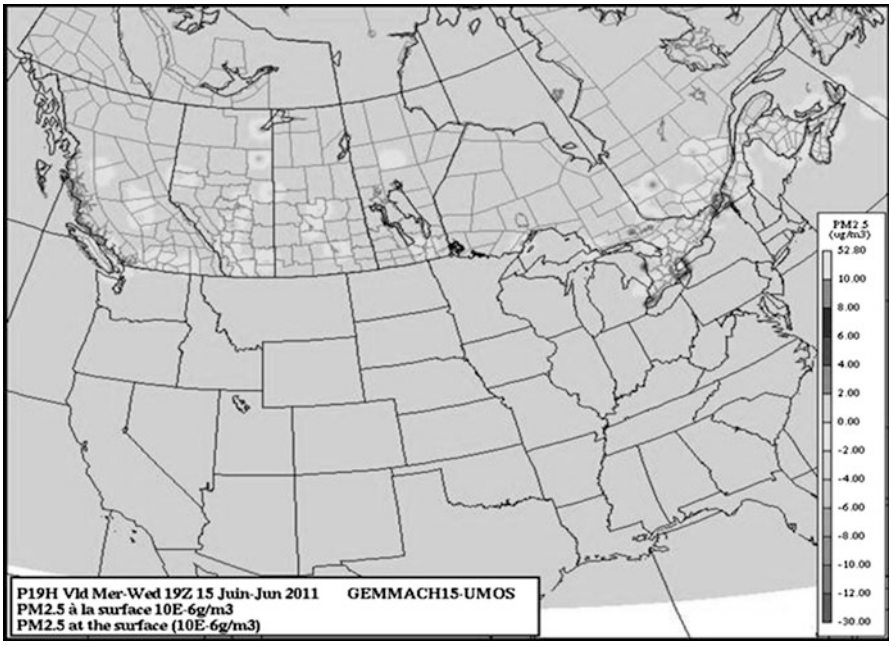

Fig. 40.3 Example of differences between the model and the interpolated field (PM25)

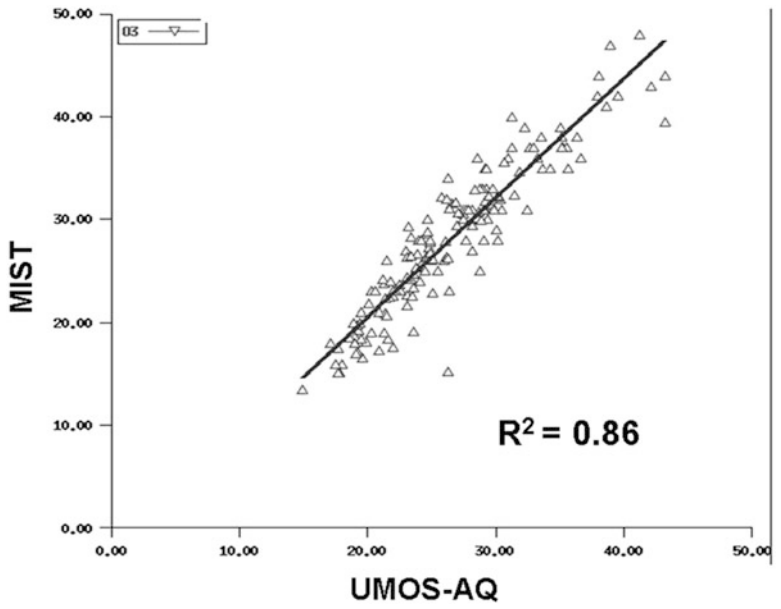

Fig. 40.4 Dispersion diagram and correlation factor between MIST interpolated forecasts and UMOS-AQ (20th June 2011)

40.4 Conclusions

The simple krigging method using MIST has significantly improved the quality of the forecasts for the vast majority of Scribe stations compared to the interpolated direct model output. In addition, the present system is much easier to maintain and update. Future improvements should concentrate on elimination of the second interpolation step through point-krigging as well as expanding the system in order to include meteorological variables.

References

1. Wilson JW, Vallée M (2001) The Canadian Updatable Model Output Statistics (UMOS) System: design and development tests. Weather Forecast 17:206–222
2. Antonopoulos S, Bourgouin P, Montpetit J, Croteau G (2010) Forecasting O_3, PM_{25} and NO_2 hourly spot concentrations using an updateable MOS methodology. In: Proceedings for the 31st NATO/SPS international technical meeting on air pollution modeling and its application, Torino, pp 309–314
3. Mahfouf J-F, Brasnett B, Gagnon S (2007) A Canadian precipitation analysis (CaPA) project: description and preliminary results. Atmos Ocean 45:1–17

Chapter 41
Synergistic Use of LOTOS-EUROS and NO2 Tropospheric Columns to Evaluate the NOX Emission Trends Over Europe

Lyana Curier, Richard Kranenburg, Renske Timmermans, Arjo Segers, Henk Eskes, and Martijn Schaap

Abstract The NOx-emission trend has been evaluated over Europe using the LOTOS-EUROS model and the NO2 tropospheric columns from OMI.

Keywords LOTOS-EUROS • Emission trends • NO2

41.1 Introduction

The quality of available information about sources (emissions) of atmospheric pollutants is a key parameter in any attempt to represent the current state or predict the future changes of the atmospheric composition. Besides natural sources and biomass burning, current estimates show that fossil fuel combustion is responsible for about 90 % of the total NOx emissions over Europe. In situ measurements in polluted areas have shown that the boundary layer contains more than two third of the tropospheric NO2. Hence, satellite remote sensing providing tropospheric NO2 columns is a suitable answer for the monitoring of pollution. Recent studies using spaceborne instruments have illustrated that the tropospheric column of nitrogen dioxide contains valuable information about its sources, transport and sinks. NO2 timeseries derived from satellites instruments have also been used to study long-term changes in anthropogenic emissions of NOx. The goal of this study is to estimate the trends in NOx emissions in Europe and subsequently identify the source sectors responsible. To this end we investigate the possibility to assess the trends in anthropogenic NOx emissions over Europe at high spatial resolution

L. Curier (✉) • R. Kranenburg • R. Timmermans • A. Segers • M. Schaap
TNO Built Environment and Geosciences, Utrecht, The Netherlands
e-mail: lyana.curier@tno.nl

H. Eskes
KNMI, Royal Netherlands Meteorological Institute, de Bilt, The Netherlands

D.G. Steyn et al. (eds.), *Air Pollution Modeling and its Application XXII*,
NATO Science for Peace and Security Series C: Environmental Security,
DOI 10.1007/978-94-007-5577-2_41,

using OMI observation and the LOTOS-EUROS chemistry transport model. The study takes place within the framework of the ENERGEO and GlobEmission projects which respectively aims to set-up monitoring system of air pollutants using earth observation data and contributes to the verification and improvement of the UNECE/EMEP emission inventory over Europe.

41.2 NOx Emission Source Apportionment

In 2005, the anthropogenic NOx emissions over Europe were dominated by combustion processes in road transport with a 40 % share, followed by power plants, industry, off-road transport and the residential sector. In the last decades the abatement strategies over Europe have principally targeted combustion processes by power generation, road transport and industries. Moreover, it is anticipated that future changes in NOx emissions will be driven by certain sectors. As the OMI satellite observes the total column at local overpass time, It is important to know the sensitivity of the OMI signal to emission changes and investigate whether OMI is suitable to observe such trends over Europe. This is especially relevant considering the short life time of NOx in the atmosphere and the large variability of the temporal (or diurnal) variation in emission strengths for the different source sectors. To this end, the LOTOS-EUROS chemical transport model was ran for 2005 over Europe using the TNO-MACC emission inventory [4] for 2005. The model includes a new source apportionment module that tracks the contribution of specified sources through each modelled process and thus through the whole simulation. This means that for all oxidised nitrogen components at every time step and each grid cell the origin is calculated. Here the emissions were categorized per source sector and hour of emission. As the life time of NOx is short, it was chosen to focus the resolution for the time of emission to the morning hours prior to OMI overpass.

Figure 41.1 presents the modelled contribution per source sector and emission hour over two industrialized area in Europe at OMI overpass time (i.e. 1.30 p.m. local time). At first glance it is observed that 50 % of the OMI signal results from NOx emissions in the 3 h prior to OMI overpass. Besides, it can be observed that over the heavily industrialized area like the BENELUX the NOx emission are mainly driven by combustion processes in the road transport whereas over the Northern Iberian Peninsula the combustion processes in road transport energy sector and non-road transport have an equal share.

41.3 Trends Analysis

The tropospheric NO2 columns retrieved from OMI measurements, DOMINO [1, 2], are used in synergy with the LOTOS-EUROS [5] chemistry transport model. LOTOS-EUROS is an operational 3D chemistry transport model which simulates

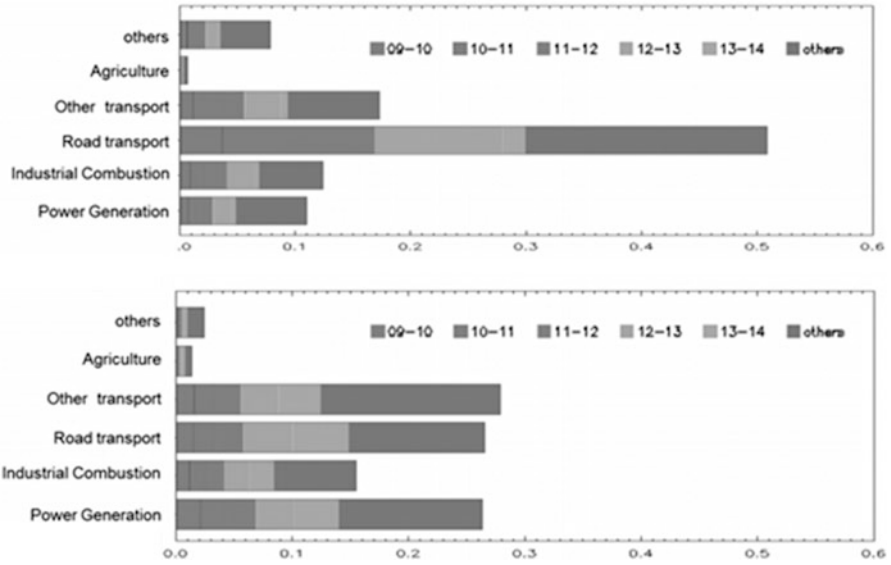

Fig. 41.1 Barchart of the contribution of various source sectors for different emission time to the total NOx emission

the air pollution in the lower troposphere over Europe. The OMI tropospheric NO¬2 column product has been validated in several studies [1, 2] and recently a comparison of OMI NO2 tropospheric columns with an ensemble of global and European regional air quality models was performed [3]. This last study concluded that the vertical column of the regional air quality models ensemble median shows a spatial distribution which agrees well with the tropospheric OMI NO2 tropospheric columns. The discrepancies observed between the tropospheric OMI NO2 tropospheric column and its modelled counterparts should occur mainly in the higher part of the atmosphere due to a lack of sources such as lightning and incorrect estimates of the lifetime of NO2 at higher altitude. In this study, a multi-year simulation is performed for 2005–2010 by LOTOS-EUROS using a constant a priory NOx emission database [4], to model the NO2 tropospheric columns at the overpass location and time of OMI. As we are using a fixed NOx emission database the inter-annual and seasonal variability present in these columns will solely represent the changes in the meteorology, transport and chemistry. In a second step the NO2 tropospheric columns from both OMI and LOTOS-EUROS were meshed into a 0.25×0.5 grid and for each pixel the time series of the monthly mean NO2 tropospheric columns are fitted using a model with a linear trend and a seasonal component which accounts for the annual cycle of NO2 [8]. This model has been validated for mean NO2 tropospheric columns using GOME and SCIAMACHY data at a global scale and over China [6, 7]. Figure 41.2 shows an example of a measured time series and the fitted function. The monthly averaged NO2 tropospheric column is plotted as a function of the month number starting in

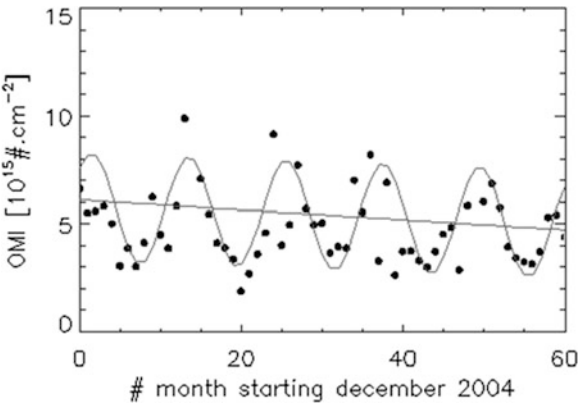

Fig. 41.2 Example of a timeseries for one grid cell near Paris (France). The Y axis shows the monthly mean NO2 tropospheric column, and the X axis shows the month index starting January 2005. The *dots* represent the measurement while the *straight* and *sinusoidal lines* represent respectively the linear decrease and seasonal component of the fitting result

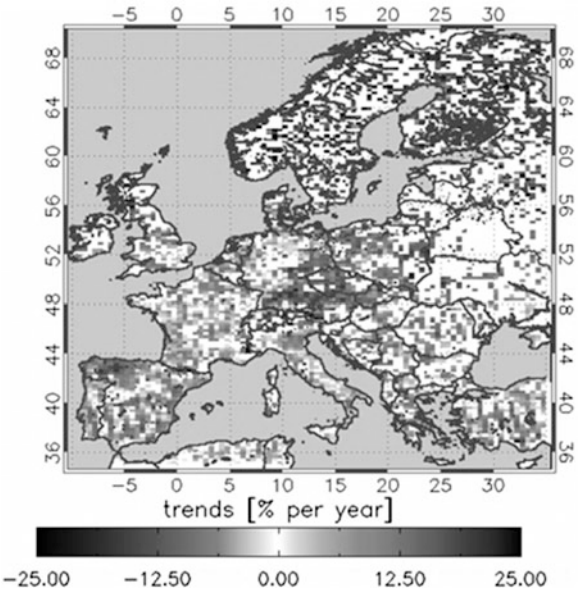

Fig. 41.3 Linear trends per year for tropospheric NO2 for 2005–2009 derived from OMI observations over Europe

January 2005. The fitting model is applied to each grid cell over Europe, which allow for a spatial distribution of each of the fitting parameters. Figure 41.3 presents the annual linear trends per year for tropospheric NO2 for 2005–2010 derived from OMI observations over Europe due to change in the NOx emission. A clear negative trend is observed over Europe. Significant negatives trends, ranging between −8 and −4 % are found over the dominant anthropogenic source regions of Western Europe such as Western Germany, Benelux, Po-Valley. The largest decreases coincide with well-known industrialized areas such as the Benelux, the Po-Valley in Italy and the Ruhr area in Germany. This can be explained by the fact that over Europe the decrease of NOx emissions is mainly due to a better control of road transport and

Table 41.1 Comparison table for the average trends (% per year) derived for three heavily industrialized area over Europe

	Area		
Study	Benelux	Po Valley	Northern Spain
Konovalov et al. [4]	−3.7	−2.7	−1.3
Zhou et al. [9]	−6.	−6.	−20 to −10
This study	−4.1	−6.1	−7.5 with hotspot −20

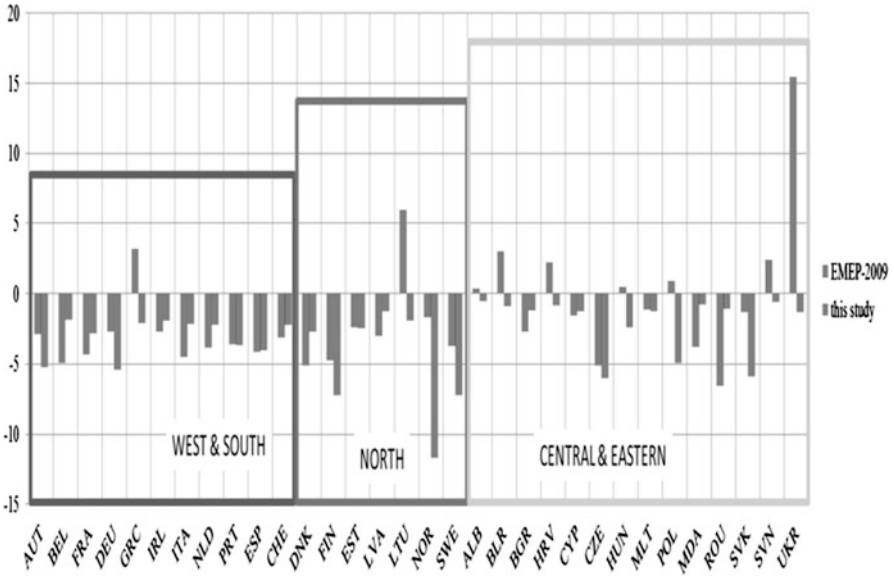

Fig. 41.4 Barchart of the yearly trends derived per country within the framework of this study (*left bars*) and the trends derived from officially reported data by countries (*right bars*)

power plants. A comparison of our results with recent trend studies using satellite is presented Table 41.1 for the BENELUX, Po Valley and Northern Spain. In general, a good agreement is observed. However, discrepancy occurs between the study carried out by Konovalov et al. [4] and the other two studies for Northern Spain. In fact, the strongest decreases occurred over Northern Spain (−20 to −10 %) and we believe it to be strongly related to emission abatement strategies targeting power plants implemented since beginning of 2008.

The trends derived for each country from this study are presented in Fig. 41.4 and compared to official reported data by countries. In general, the reported and retrieved trends are of similar amplitudes and providing confidence in the trends deduced in this study. However, a dichotomy between European countries appears and the reported and estimated NOx emissions tends compare better over Western Europe than over Central and Eastern Europe. This dichotomy may illustrate the differences between countries in re-updating their emission inventories but may also

reflect that the dominant NOx source in Western Europe is road transport with a well-documented and, here confirmed, decrease in emissions due to implementing new technologies, whereas trends in other source sectors in eastern Europe are less known. The difference in sensitivity of the OMI instrument to source sectors may also play a role here and is under investigation. Besides, the large differences observed for Finland, Norway and Sweden are believed to be due to surface reflectance contamination and are under further investigations.

41.4 Conclusion and Outlook

A trend was derived from synergistic use of LE and OMI NO2. The results were in agreement with recent studies and reported emission inventories per country from EMEP. Significant negative changes were found in highly industrialized areas over Western Europe i.e. ∼5–6 %/year. Strong decrease in were observed over a regions with many power plants in Northern Spain (up to 20 %) and over the Po-Valley (∼11 %). The method described here is a promising methodology to complement and evaluate trends in bottom up emission reportings. A strong point is the fact that the methodology using satellite date is in principle consistent throughout the entire domain. Besides, satellite data are available in near real time. Remote sensing observations can therefore provide a top-down constraint which allows for a near real time estimate of the emissions.

Acknowledgement The work described in this paper is supported by ENERGEO, a Collaborative Project (2009–2012) funded by the European Union under the 7th Framework Programme and TNO internal funding.

References

1. Boersma KF, Jacob DJ, Bucsela EJ, Perring AE, Dirksen R, van der A RJ, Yantosca RM, Park RJ, Wenig MO, Bertram TH, Cohen RC (2006) Validation of OMI tropospheric NO2 observations during INTEX-B and application to constrain Nox emissions over the eastern United States and Mexico. Atmos Environ 42(19):4480–4497. doi:10.1026/j.atmosenv.2008.02.004, 2008. 4304, 4309
2. Boersma KF, Jacob DJ, Trainic M, Rudich Y, DeSmedt I, Dirksen R, Eskes HJ (2009) Validation of urban NO2 concentrations and their diurnal and seasonal variations observed from space (SCIAMACHY and OMI sensors) using in situ measurements in Israeli cities. Atmos Chem Phys 9:3867–3879
3. Huijnen V, Eskes HJ, Amstrup B, Bergstrom R, Boersma KF et al (2010) Comparison of OMI NO2 tropospheric columns with an ensemble of global and European regional air quality models. Atmos Chem Phys 10:3273–3296
4. Konovalov IB, Beekmann M, Burrows JP, Richter A (2008) Satellite measurement based estimates of decadal changes in European nitrogen oxides emissions. Atmos Chem Phys 5(8):2623–2641

5. Kuenen J, van der Gon D , Visschedijk AH, van de Brugh H, van Gijlswijk R (2011) MACC European emission inventory for the years 2003–2007. Technical Report. report TNO-060-UT-2011-00588. TNO, Utrecht, the Netherlands
6. Schaap M, Renske MA, Timmermans MR, Boersen GAC, Builtjes PJH, Sauter FJ, Velders GJM, Beck JP (2007) The LOTOS–EUROS model: description, validation and latest developments. Int J Environ Pollut (IJEP) 32(2)
7. van der A RJ, Peters DHMU, Eskes H, Boersma KF, Van Roozendael M, De Smedt I, Kelder HM (2006) Detection of the trend and seasonal variation in tropospheric NO2 over China. J Geophys Res 111:D12317. doi:10.1029/2005JD006594
8. van der A RJ et al (2008) Trends, seasonal variability and dominant NOx source derived from a ten year record of NO2 measured from space. J Geophys Res 113:D04302. doi:10.1029/2007JD009021
9. Zhou Y, Brunner D, Hueglin C, Henne S, Staehelin J (2012) Changes in OMI tropospheric NO2 columns over Europe from 2004 to 2009 and the influence of meteorological variability. Atmos Environ 46:482–495. doi:10.1016/j.atmosenv.2011.09.024

Questions and Answers

Questioner Name: W. Lefebvre

Q: How does the changing NO2/NOx ratio affect your results?.
A: The downward trend observed in NOx emissions partly resulted in the development of new technologies that influence the ratio. Changes in NO2/NOX ratios during the period of interest may result in additional uncertainty in NOX emissions.

Questioner Name: J. Silver

Q: The comparison between OMI and LOTOS-EUROS showed a seasonal bias. Is this mainly due to the model or the observations?
A: Many studies shown this bias between chemistry transport model and observation. The discrepancies observed between the tropospheric OMI NO2 tropospheric column and its modelled counterparts should occur mainly in the higher part of the atmosphere due to a lack of sources such as lightning and incorrect estimates of the lifetime of NO2 at higher altitude. On the other hand, comparison studies between OMI and ground based observations have also shown that OMI was biased high.

Chapter 42
On the Data Assimilation for Operational Forecasting and Re-analysis of Allergenic Pollen Dispersion

Mikhail Sofiev, Marje Prank, and Julius Vira

Abstract Operational forecasting of allergenic pollen faces several challenges, which are not common in the air chemical composition forecasting. One of them is practical inapplicability of the standard data assimilation (DA) methods, which originates from basic features of the problem. The pollen observations are manual and become available with a delay of about a week. The bulk of the information has daily resolution, whereas the diurnal variability of the concentrations exceeds one order of magnitude. Finally, the season duration at each particular place is rarely more than 1–2 weeks, which makes the 1–2 days old information outdated. Adaptation of the DA methods for pollen forecasting has to target the emission source parameters, which would have a longer lasting effect. Some of these parameters also have long correlation distance, which increases the value of sparse observational network.

Keywords Data assimilation • Forecasting • Pollen

42.1 Current Status of SILAM Pollen Forecasting System

The pollen emission module of SILAM v.5 includes four species: birch, grass, olive, and ragweed. All sources cover the whole Europe and evaluated against the data of European Aeroallergen Network for last 5–10 years. The basic approach to the heat-controlled phenological processes is described in Sofiev et al. [1]. The model evaluation for birch is given in Siljamo et al. [2].

M. Sofiev (✉) • M. Prank • J. Vira
Department of Physics, Finnish Meteorological Institute, Helsinki, Finland
e-mail: mikhail.sofiev@fmi.fi

D.G. Steyn et al. (eds.), *Air Pollution Modeling and its Application XXII*,
NATO Science for Peace and Security Series C: Environmental Security,
DOI 10.1007/978-94-007-5577-2_42,

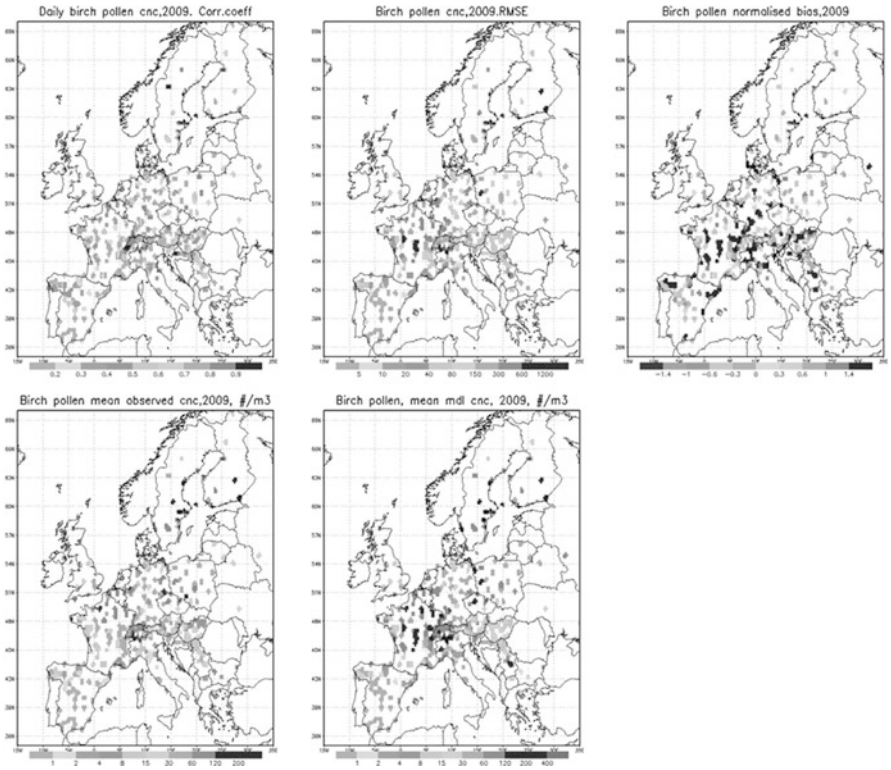

Fig. 42.1 SILAM performance indicators, 2009. (correlation coefficient, RMSE [pollen/m^3], fractional bias, mean observed, March–July, [pollen/m^3], mean predicted, March–July [pollen/m^3])

42.2 MACC Re-analysis for Birch, 2008–2009

The MACC regional air quality assessment reports describe with yearly frequency the state and evolution of background concentrations of air pollutants in European countries. The assessments involve DA procedures to obtain the best representation of pollution patterns. Re-analysis from 2008 forward include birch pollen.

For 2008 and 2009 re-analysis, the DA procedure included a simple iterative adjustment of the seasonal total emitted from a particular region, in relation to the model-measurement (dis)agreement. Fractional bias of seasonally-averaged concentrations was used as the cost function (Fig. 42.1).

42.3 Features of the 2009 Birch Pollen Season

Important characteristics for sensitive people are the total number of hours with the pollen concentrations exceeding 50 grain/m^3 and the total pollen load over the season for a specific location (Fig. 42.2). The bulk of the heavily loaded areas is in

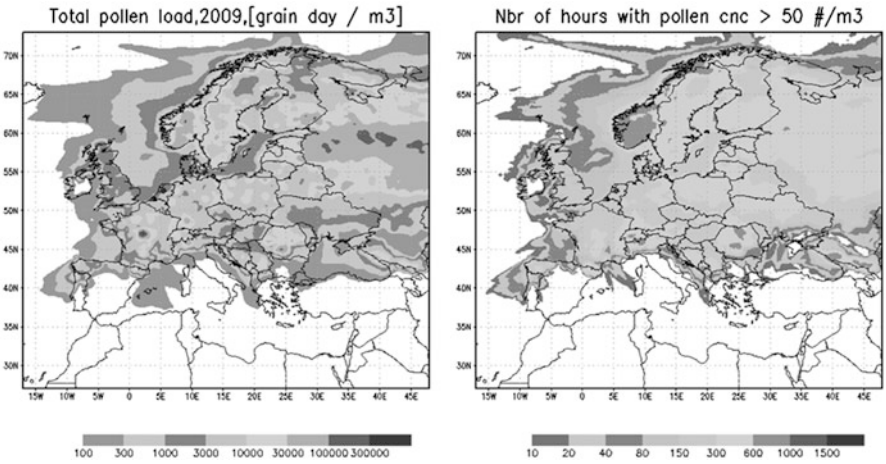

Fig. 42.2 Characteristics of birch pollen season in 2009: total pollen load, [pollen day/m^3]; number of hours with concentration exceeding 50 grains/m^3

the north-eastern part of Europe. However, the allergy-triggering threshold in these areas is presumed to be higher. The total pollen load also indicates the potential sensitization of presently non-sensitive individuals – a high pollen load during long period of time can provoke individual's sensitization.

42.4 Correction to the Seasonal Pollen Total Using Observations

The number of iterations in the procedure was kept to minimum (up to 3) since: (i) already the first iteration has shown to eliminate the bulk of the model-measurement disagreement, (ii) starting from the second iteration, the system was adjusting the high-frequency uncertainties in the observational data and birch map, (iii) each iteration required recalculation of the whole season, which, despite fast model, made the analysis quite costly.

Specific problem in the analysis was that uncertainties in the birch habitation density map can reach orders of magnitude in regions with sparse birch population (e.g. Southern Europe). Over these territories, the system was inflating the correction up to unphysical levels, thus making the third and further iterations unfeasible (Fig. 42.3). The final results were using the first-iteration correction.

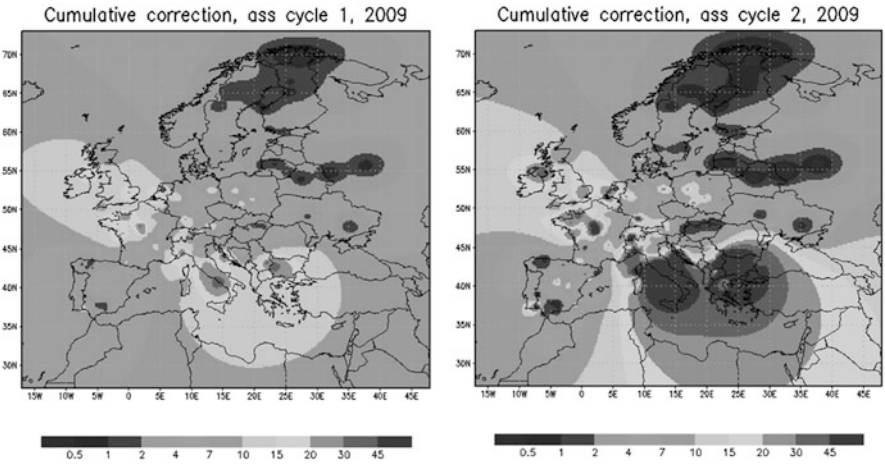

Fig. 42.3 Season-total correction of the first and second iterations

42.5 Summary

Current status of pollen monitoring and modelling makes application of standard data assimilation procedures unfeasible for both short forecasting and re-analysis. However, experience of SILAM re-analysis for 2008 and 2009 shows that very significant improvement can be obtained with quite simple bulk corrections of the total pollen emission parameter in the model. Such correction not only brings about unbiased estimates of pollen load but also improves temporal correlation with the daily observations, owing to more accurate patterns of pollen distribution.

Acknowledgements The work has been done within the scope of FP7-MACC and FP7-HIALINE projects. Networking was supported by the COST Action ES0603 EUPOL.

References

1. Sofiev M, Siljamo P, Ranta H, Linkosalo T, Jaeger S, Rasmussen A, Rantio-lehtimaki A, Severova E, Kukkonen J (2012) A numerical model of birch pollen emission and dispersion in the atmosphere. Description of the emission module. Int J Biometeorol. doi:10.1007/s00484-012-0532-z
2. Siljamo P et al (2012) A numerical model of birch pollen emission and dispersion in the atmosphere. Model evaluation and sensitivity analysis. Int J Biometeorol. doi:10.1007/s00484-012-0539-5, [online] Available from: http://www.ncbi.nlm.nih.gov/pubmed/22434484 (Accessed 14 May 2012)

Chapter 43
Improved Meteorological Data for Air Quality Forecasting Models: Assessment

Sergio Borghi, Maurizio Favaron, and Giuseppe Frustaci

Abstract In this study we assess the impact of improved meteorological data over the Milan area for the forecasting of air quality.

Keywords Meteorological variability • Forecasts • Urban air quality

43.1 Introduction

One of the most important operational aspects addressed by dispersion models is the short-term forecast of air quality expressed as the spatial distribution of key pollutants concentration. These products are used as a basis to take decisions (e.g. on traffic stop or other measures), in addition to advice to the public.

For this application to be viable, a detailed knowledge of emissions and transport/diffusion processes is paramount. Of these phenomena, transport and diffusion are consequences of the state and dynamical evolution of the atmosphere, that is, of large-scale circulation, local circulation and turbulent diffusion, which must be modelled for Europe at the level of accuracy and in the modalities prescribed by Directive 2008/50/EC.

In practical terms, this means that the meteorological information normally available is to be supplemented by quality measurements able to detect local effects.

The availability of an urban resolving observational network is a prerequisite for urban model initialization and verification. The "Climate Network®" presented and described in this paper, has several stations of high quality standards over the Milan urban and sub- urban area, allowing a good characterization of the local variability of the main meteorological variables.

S. Borghi (✉) • M. Favaron • G. Frustaci
Osservatorio Meteo di Milano Duomo, Italy
e-mail: sergio.borghi@meteoduomo.it

D.G. Steyn et al. (eds.), *Air Pollution Modeling and its Application XXII*,
NATO Science for Peace and Security Series C: Environmental Security,
DOI 10.1007/978-94-007-5577-2_43,

43.2 The "Climate Network®"

This work is based on data of the start operational phase of a new meteorological network, aimed at measuring surface atmospheric conditions in the urban environment for several different applications, especially energy management, air quality, and climate.

The so named "Climate Network®" (in the following briefly CN), still in an expanding phase, has been already presented at the last IEEE-EEMS Workshop [2], and has been proposed to contribute to MeteoMet project (in the framework of EMRP-EURAMET) at the kick off Meeting held in Turin, 12–13th October 2011. CN's main characteristics are:

- Use of homogeneous core instruments, data logger and station software,
- Redundant measurement of temperature at all nodes,
- Power supply independent of power mains allowing for easy relocation,
- Adoption of a standardized calibration procedure for critical measurements (e.g. temperature),
- Adoption of strict quality assurance practice:
  - Level-1 (station level) and level-2 (network level) human-operated validation, based on automatic level-0 plausibility checks,
  - Systematic check and calibration of non-critical measurements,
- Systematic use of oversampling at station level (2 s acquisition period),
- Station-level averaging on 10 min basis, allowing use of data also for alarm generation,
- Final averaging performed at central database level.

Collection and configuration management of metadata is to be stressed, as functional to the climatological nature of CN. In a meteorological network focus is typically on short-term measurements, their accuracy, and time and space coverage, with only minor concerns for data remaining comparable in the long term. In a climatological network, on the other side, focus goes on the need that measurements can be used over network lifetime spans in the order of many decades and some centuries, independently of which instruments are currently in use, and in full knowledge of local conditions possibly affecting measurements. Planned to cover a large number of towns all over Italy (80 stations), CN has already a good coverage over the most important urban agglomeration in the Po Valley, the great Milan area.

In the present preliminary work only CN's data from the inner area are used and discussed. Table 43.1 summarizes the main characteristics of this strictly urban network.

Table 43.1 Coordinates of the six CN stations in the Milan urban area

Name	Site	Lon. [°]	Lat. [°]	H above msl [m]
Milano Centro	Univ. Statale	9,194933	45,459733	140
Milano I-N	Sempione	9,171008	45,477275	155
Milano E-E	Politecnico	9,229608	45,480094	149
Milano E-N	Broglio	9,163792	45,502517	152
Milano E-S	Noto	9,200516	45,431210	134
Milano E-W	San Siro	9,125299	45,478850	189

43.3 Data Base and Data Quality

Each CN station is composed by a unified set of core instruments, plus site-specific additions. The core set consists of:

- A Vaisala WXT-520 compact weather station (2D ultrasonic anemometer, capacitive thermometer, capacitive hygrometer, barometer, and an acoustic precipitation sensor),
- A thermistor-based thermometer,
- A Campbell CR-800 data logger,
- A site-aware data acquisition and 10-min averaging program. Additional instruments consist of a third thermometer, a rain bucket, a global radiometer.

Site-aware data acquisition and 10-min averaging program includes logic to compute derived quantities (e.g. 1 min pressure gradients, dominant wind direction, wind direction histogram, wind gust detection), and automatic plausibility checking. The program is subject to strict configuration control, under direct control of network management personnel, following network and knowledge evolution.

Collected data are then fed to a DBMS; data ingestion process completes plausibility checking. Resulting data, structured as a relational table exactly matching data acquisition format, are averaged on user-significant time basis (30 and 60 min) and dispatched to specialized tables. Those are then available in both text and graphic form for level-1 and level-2 validation, routinely performed by qualified operators through a continuously updated standard procedure. Validation ensures data are labelled as “useable” in CN applications, including modelling.

43.4 Calibration Procedures

Based on the quality of instrumentation, a detailed quality control procedure has been designed and implemented [3]. In synthesis, the data quality is assessed through redundant sensors, calibration of every single station using a climatic

chamber controlled by an automated computer program, instrument comparison field test, traceable first and second line standards (for temperature: Reference Platinum Resistance Thermometer and 3 PT 100 ohm Class A calibrated with dedicated digital multimeter), 3rd degree polynomial regression on a sequence of measuring points (for temperature: 20 °C, −20 °C, +50 °C, +30 °C accounting for sensor hysteresis), field testing of calibration, and automatic control to detect anomalies.

43.5 Verification and Validation

In addition to the calibration procedure outlined above data validation has also been planned using high resolution Limited Area Models (LAM), considering the peculiar environment of the installed CN stations (generally on roofs of urban buildings) and in order to test the feasibility of data assimilation to improve short term numerical modeling in the complex urban terrain. In this preliminary work, only Milan has been considered because of the number of stations already installed and the economical importance of this urban area, located well in the middle of the polluted Po Valley region. For convenience and as a first investigation tool, analysis data from a RAMS model implementation over Italy is used. The model is initialized with a GFS operational forecast and runs in three levels nested mode. After still ongoing testing period, comparison of model analysis values at the grid points and interpolation at the station sites shall provide a verification of observational network efficiency and valuable hints for assimilation of fine scale measurements into LAMs. Anyway, the first network data set obtained after installation in 2011 has already been used for 1–2 days forecast verification of several operational limited area models with different resolutions and characteristics (Table 43.2). In a longer than a monthly verification time span, the correlation has been evaluated, for example, between mean daily temperatures: measured (arithmetic mean of the six CN stations), and – forecast as a mean of the $+27 \div 48$ h model predicted 3-hourly values interpolated for the coordinates of Milan downtown, generally with simple methods. Results are summarized in Table 43.2, where correlations coefficients

Table 43.2 Model T scores over Milan between Jan. and Feb. 2012

LAM	Initializ.	Resol. [km]	R	E [°C]	B [°C]
RAMS	*GFS*	*16,0*	*0,768*	*7,7*	*+2,8*
Moloch	GFS	2,3	0,916	3,0	−2,5
EDM WRF	GFS	1,6	0,860	5,4	−1,5
NMM	GFS	12,0	0,922	3,3	−1,6
WRF ARW ECM	IFS	3,0	0,860	6,1	−1,5
WRF NMM	GFS	4,0	0,859	4,8	−1,3
ETA Model	GFS	5,0	0,862	4,7	−2,2
COSMO LM-ME	IFS	7,0	0,877	3,1	−1,8
EMM WRF	GFS	1,1	0,878	1,4	−2,7

R, Stand. Error (E) and Bias (B) for nine the different LAMs are reproduced. "Ensemble" predicted daily mean temperature (arithmetic mean of the eight model forecasts, excluding RAMS) correlate to the mean CN measured temperatures with a correlation coefficient $R = 0{,}92$, mean error $E = 1{,}3\ ^{\circ}C$ and a negative bias $B = -1{,}4\ ^{\circ}C$, last value being an expected effect of the urban heat island [1].

Note, as reference, that last year ECMWF (28 km horizontal resolution) B scores for surface temperature over Italy in the same season were in the range of $0{,}5 \div -1{,}5\ ^{\circ}C$ (forecast $+24 \div 48$ h, verification station: WMO 16080 M. Linate, in the SE outskirts, about 9 km from Milan downtown).

43.6 Case Studies

The temporal evolution of the daily mean temperature as observed and predicted covers some very different meteorological situations, as the extended exceptional cold spell in February (which affected most of Europe). Therefore, specific case studies shall be necessary to investigate residuals in terms of model characteristics and of the meteorological situation at the synoptic as well as the mesosynoptic scale.

43.7 Conclusions and Further Work

In this preliminary work a first assessment of a new meteorological network in urban area has been performed, showing the importance of high quality data for the characterization of high resolution meteorological fields, to be used as primary input in atmospheric as well as in air quality. Further validation and verification studies shall be necessary for other meteorological variables of relevant interest in air quality forecasting. Assimilation experiments of the CN high quality data into high resolution models will be eventually performed to set up an integrated observational and forecasting tool.

Acknowledgements Cristina Lavecchia and SavinoCurci (Climate Consulting s.r.l.) provided data, metadata and technical information about CN stations and procedures.

References

1. Borghi S, Corbetta G, De Biase L (2000) A heat island model for large urban areas and its application to Milan. Il Nuovo Ci- mento C 23(5):547–566
2. Borghi S, Favaron M, Frustaci G (2011) Surface meteorological monitoring network at mesoscale β, γ and microscale α: quality, reliability and representativeness requirements. In: EESMS 2011 Proceedings, Milan
3. Curci S, Virlan M, Lavecchia C (2011) Traceability and reliability on meteorological measures. In: EESMS 2011 Proceedings, Milan

Chapter 44
Ingestion of Intermittent Wild Fire Sources Inside and Outside the Forecasting Domain

Pius Lee, Hyuncheol Kim, and Henk Eskes

Abstract In this study we address the real-time emission capturing of intra- and exo-domain wild fires in the US National Air Quality Forecasting Capability (NAQFC).

Keywords Intermittent sources • Wild fire • Dynamic boundary condition

44.1 Introduction

The US National Air Quality Forecasting Capability (NAQFC) is aiming at providing quantitative forecast for particulate matters (PM) smaller than 2.5 μm diameter in a few years. The highly variable spatial and temporal distribution of PM together with its numerous combination of chemical composition, mixing states, coatings of organics, and characteristics of origination pose challenges to predict its mass, speciation, and distribution over space and time. An equally considerable challenge is the potential strengthening of the US EPA ozone standards. This will make background concentration of ozone a more relevant topic. Furthermore, there is evidence that long range transport is causing the background concentrations to increase in recent decades. Capturing real-time concentrations of the various constituents in the inflowing air-mass to the Conterminous US (CONUS) domain

P. Lee (✉)
Air Resource Lab., NOAA, 1315 East West Highway, Room 3316,
Silver Spring, MD 20910, USA
e-mail: pius.lee@noaa.gov

H. Kim
Earth Resources Technology, Incorp., Annapolis, MD, USA

H. Eskes (✉)
Royal Netherlands Meteorological Institute, De Bilt, The Netherlands

D.G. Steyn et al. (eds.), *Air Pollution Modeling and its Application XXII*,
NATO Science for Peace and Security Series C: Environmental Security,
DOI 10.1007/978-94-007-5577-2_44,

is important. It was reported that PM emitted during large fires can stay in the atmosphere for multiple days. Therefore PM25 forecasting should include the best real-time emission information on intra- and- extra-domain wild fires. By the same token the wild fire information helps ozone forecasting. In this study we address the real-time emission capturing of intra- and exo-domain wild fires. Wild fires is a major originator and precursor emitter of PM and ozone. A large North America parent domain is setup to facilitate the generation of dynamic boundary condition for a nested CONUS domain. A Blue-skies framework-based Hazard Mapping System (HMS) is used to ingest near real-time wild fire information within the parent as well as the CONUS domains. Result of this nested run will be compared to that without nesting to delineate its impact. Both ground-based and airborne measurement will be used to quantify the fidelity of the forecast for July 2011, where there were numerous fires in North America both within and without the CONUS.

44.2 Methodology and July 2011 Case

To incorporate real-time wild fire sources into an Air Quality (AQ) forecasting modeling prototype for NAQFC, a β-version of it [6] is used to facilitate the study. NAQFC is an off-line system consists of the National Centers for Environmental Prediction (NCEP) Non-hydrostatic Meso-scale Model with Arakawa B-grid staggering (NMMB) coupled with the US Environmental Protection Agency (EPA) Community Multi-scale Air Quality (CMAQ) Model [5]. The former provides meteorological data feed to the latter, a chemical transport model accounting for projected emission, transformation, transport, and removal of atmospheric chemical constituents owing to physical and chemical processes. To validate the methods used in this β version, the July 2011 period is chosen for sensitive studies. The (DISCOVER-AQ) campaign with space, air-borne and ground based coordinated measurements was conducted in the period over the Baltimore and Washington area [2]. Selected data from the campaign is utilized to quantify the attributions of the wild-fire emissions.

44.2.1 Operational NAQFC

In concert with accurate description of the meteorology and processes stated by the governing equation of NMMB [4] and CMAQ [1], NAQFC uses the following procedures to project emission: (1) Point sources: The US EPA 2005 National Emission Inventory (NEI) is used as the base data for Electric Generation Unit (EGU) and non-EGU point emission rates and initial thermal characteristics. The EGU emission rates for NOx and SO2 were calculated by multiplying the measured 2009 point source fluxes from Continuous Emission Monitoring (CEM) with the ratio of US Department of Energy Annual Energy Outlook (AEO) for 2011 and 2009. Across the Northern and Southern borders, the province-level 2000 Canadian,

Fig. 44.1 North American Model driven HYSPLIT domain and the NAQFC CONUS domains are depicted as the outer and inner domain, respectively. The *shading* represents the fire-counts reported by MODIS during the month of April 2009

and the 1999 Mexican national inventories were used, respectively; (2) Area and off-road vehicular sources: The same national inventories as used in by point source were used. The data were processed through the Sparse Matrix (SMOKE) system to obtain spatial and temporal specifications. Climatology wild fire, agricultural prescribed burns have been removed; (3) Biogenic sources: An online version of (BEIS) version 3.10 was employed to generate biogenic reactive (VOC) modulated by meteorological parameters such as 2 m temperature and moisture; and (4) Mobile sources: The aforementioned national inventories were again the base data. The (OTAQ) 2005 on-road emission inventory is used to generate on-road mobile emissions over the U.S. The data were processed through (MOBILE) version 6 system to obtain spatial and temporal specifications.

44.2.2 β-Version of NAQFC

Ingestion of near real-time wild fire emissions was carried out in two steps: (A) Fires within the so-called NAQFC Conterminous US (CONUS) domain (see Fig. 44.1) – dubbed as intra-domain fire emission, was derived through a real-time

wild fire detection/quantification product by (NESDIS). It is based on HMS which integrates satellite-retrieval fire-counts and the Blue Skies framework of quantifying variable burn-rates utilizing vegetation fuel-type, loading and moisture inventories. This information was fed into a fire-specific modified SMOKE system to obtain plume-rise and speciation information as additional 3-dimensional pollutant injections. Modifications included speciation mapping based on mass-scaling using CO [3] and plume rise treatments as additional point sources of buoyant plumes. And (B), for fires outside the CONUS but within the NMMB-North American Model (NAM) (HYSPLIT) domain (see Fig. 44.1) – dubbed the exo-domain fire emissions to the NAQFC CONUS domain, was used to perform a simultaneous wild-fire specific HYSPLIT model run to Step (A). HYSPLIT – a Lagrangian dispersion model, predicts the dispersion of CO as a trace gas. Identical speciation mapping and plume rise treatments used in step (A) was used. However, the fire hotspots identified as intra-domain emission sources are removed from the fire-specific HYSPLIT run so as not to double-count those fires already accounted for by the SMOKE system in step (A). Hourly concentration of CO forecasted in the NAM domain by HYSPLIT along the lateral boundaries of the NAQFC CONUS domain is extracted, species-mapped and merged with other chemical constituents of the otherwise static Boundary Condition (BC) to be fed into the β-NAQFC forecast as dynamic BC's.

44.3 Results and Verification

Two runs were performed for this study: (Base) Base-case with no wild fire as described in Sect. 44.2.1, (Fire) with both intra- and exo-domain wild fire emissions as described in Sect. 44.2.2; namely: (1) base-run with no wild fire, (2) with intra domain fire, and (3) with both intra- and exo-domain wild fires. Figure 44.2a and b show the time series of model predicted and observed concentrations for O_3 and Pm25 for these cases averaged over the available monitoring AIRNow sites in Northeastern US: 263 O_3 monitors and 134 PM25 monitors. In general both sensitivity runs showed high bias for O_3 for both day time and night time.

This study concentrates on the Baltimore and Washington (BW) area to take advantage the many collocated ground and air-borne data obtained by the DISCOVER-AQ campaign. During the campaign month of July 2011, the HMS system detected fires near the BW areas on July 2, 5, 10, 20, and 27. All these days there were flight measurement and (AIRNow) data. The study further selected the 20th data as the prime set for model sensitivity study as it has the longest hours of flight data. Figure 44.2 shows the fight path of the July 20 flight. Figure 44.3a, b show the NOAA P3 flight along-track measurement of O_3 and CO, respectively.

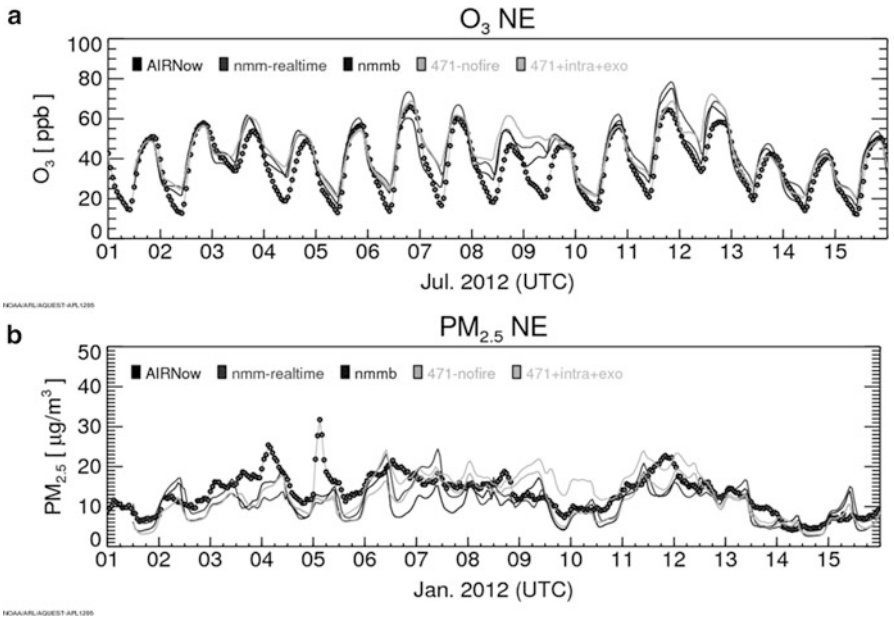

Fig. 44.2 Time series of model bias for daily hourly averaged surface concentration for (**a**) O_3 and (**b**) PM25, respectively. It is averaged over the Northeastern US as depicted as the "NE region" in the *upper-left inset* US map, verified with collocated AIRNow measurements: 263 O_3 monitors and 134 PM25 monitors between July 1 and 15, 2011

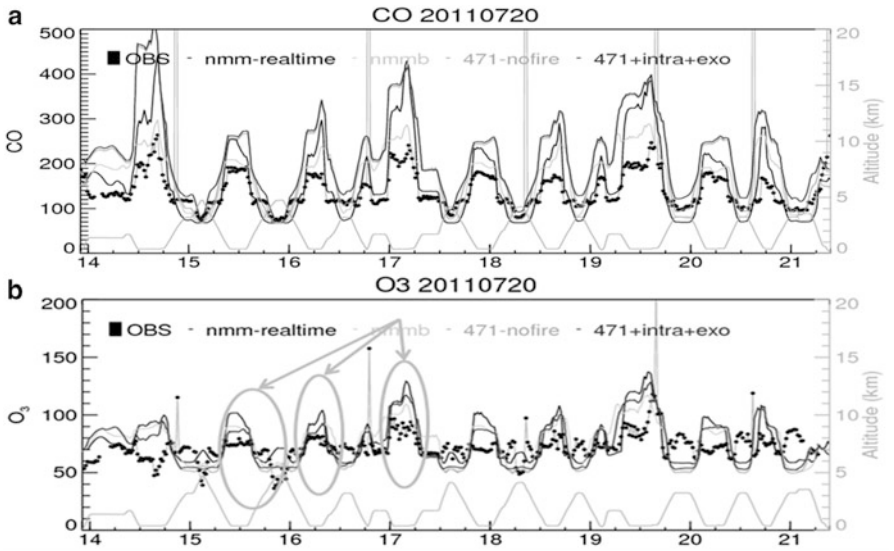

Fig. 44.3 NOAA P3 flight along-track measurement in ppb for (**a**) O_3 and (**b**) CO

44.4 Summary

Real time intra- and exo-domain wild fire emissions are included in a β version of the US National Air Quality Forecasting Capability (NAQFC). Three sensitivity runs were performed with this β version: (1) base-run with no wild fire, (2) with intra domain fire, and (3) with both intra- and exo-domain wild fires. The period of July 2011 was chosen since an intensive measurement campaign was carried out in the Baltimore and Washington area that month. Selected land, aircraft and satellite-based measurement have been employed to verify run results of the sensitivity runs. There was slight exacerbation of over bias for O_3 for cases (2) and (3), but considerable reduction of under-bias of PM25 for the two cases especially for case (3). There were sizable uncertainties involved in the mass flux quantification of the pertinent emission species. These results are preliminary.

Disclaimer Although the research presented here has been reviewed by NOAA and approved for publication, it does not necessarily reflect its policies or views.

References

1. Byun D, Schere K (2006) Review of the governing equations, computational algorithms, and other components of the models3 Community Multiscale Air Quality (CMAQ) modeling system. Appl Mech Rev 59(2). doi:10.1115/1.2128636
2. Crawford and Pickering (2012) The DISCOVER-AQ campaign website http://discover-aq.larc.nasa.gov/
3. Janhäll S, Andreae MO, Pöschl U (2012) Biomass burning aerosol emissions from vegetation fires: particle number and mass emission factors and size distribution. Atmos Chem Phys 10:1427–1439
4. Janjic ZI (2001) Nonsingular implementation of the Mellor-Yamada level 2.5 scheme in the NCEP meso-model, NCEP Office Note 437. Available at http://www.emc.ncep.noaa.gov/officenotes/FullTOC.html
5. Lee P, Ngan F (2011) Coupling of important physical processes in the planetary boundary layer between meteorological and chemistry models for regional to continental scale air quality forecasting: an overview. Atmosphere 2(3):464–483, http://www.mdpi.com/2073-4433/2/3/464/
6. McQueen J and co-authors (2011) Recent improvements towards improving the NOAA National Air Quality Forecasting Modeling Capability. Preprint: 3rd international workshop on Air Quality Forecasting and Research. Washington, DC. http://www.arl.noaa.gov/IWAQFR_presentations.php. Nov 29–Dec 1, 2011

Part V
Regional and Intercontinental Modelling

Chapter 45
The EMEP MSC-W Modelling Programme: Its Relationship to Policy Support, Current Challenges and Future Perspectives

David Simpson

Abstract The EMEP MSC-W group have as their main aim the support of air pollution policy in Europe, primarily under the Convention on Long-range Transboundary Air Pollution, but also for the European Commission. Traditionally, the EMEP MSC-W model has covered all of Europe with a grid-size of about 50 km, and extending vertically from ground level to the tropopause (100 hPa). The model has undergone substantial development in recent years, and is now applied on scales ranging from local (ca. 5 km grid size) to global. The main scientific challenges include those associated with e.g. formation of organic aerosols, but all activities are limited by uncertain inputs, particularly emissions (e.g. BVOC), and too few measurements of key compounds. In a longer-term perspective EMEP needs to develop links covering a range of scales and issues, including the interaction with Earth-system models.

Keywords EMEP • LRTAP • Modelling

45.1 The EMEP Programme

The UNECE European Monitoring and Evaluation Programme for Transboundary Long-Range Transported Air Pollutants (EMEP) started in 1977, a successful initiative between almost all European countries to pool efforts in tackling the major environmental problem of the day, acid deposition. That international action was required to tackle this problem was established through an earlier OECD study, in

D. Simpson (✉)
EMEP MSC-W, Norwegian Meteorological Institute, Oslo, Norway

Department of Earth & Space Sciences, Chalmers University of Technology, Gothenburg, Sweden
e-mail: david.simpson@met.no

D.G. Steyn et al. (eds.), *Air Pollution Modeling and its Application XXII*,
NATO Science for Peace and Security Series C: Environmental Security,
DOI 10.1007/978-94-007-5577-2_45,

which a Lagrangian model developed in Norway was used to track the transport and deposition of sulphur compounds across Europe [4]. When the Convention on Long-range Transboundary Air Pollution (CLRTAP, www.unece.org/env/lrtap) was established in 1979, EMEP became an integrated part of the Convention. The main objective of the EMEP programme within CLRTAP is to regularly provide governments and subsidiary bodies under the Convention with qualified scientific information to support the development and further evaluation of the international protocols on emission reductions negotiated within the Convention. Indeed, EMEP has since played an important part in the development of emission reduction scenarios, for both the Convention (now comprising 51 Parties, including U.S.A. and Canada) and increasingly for the European Commission.

The Meteorological Synthesizing Centre – West (MSC-W), based in Oslo, and the Eastern Centre, MSC-E, based in Moscow, are the two modelling centres established by EMEP. A third Centre, EMEP Chemical Coordinating Centre (CCC) takes care of the EMEP measurement network, and provide the main source of data against which the EMEP models are evaluated [30]. In 1999 the Executive Body of the Convention decided to include integrated assessment into the core activities of EMEP and to establish a Center for Integrated Assessment Modelling (CIAM) building on past modelling work, in particular the RAINS (now GAINS) model. The EMEP Centre on Emission Inventories and Projections (CEIP) has the task to collect emissions and projections of acidifying air pollutants, heavy metals, particulate matter and photochemical oxidants. More information and links to the activities of these Centres can be found at http://www.emep.int.

45.2 EMEP MSC-W Models

Originally both MSC-E and MSC-W conducted modelling studies of sulphur compounds, providing two independent estimates and thus a degree of cross-checking on the models results. As the models have become more complex and resource demanding over the decades (in terms of number of pollutants, computer and man-time), the Centres now focus on different pollutants. MSC-E works largely with heavy metals and persistent organic pollutants, MSC-W works largely with acidifying compounds, ozone, and particulate matter (PM).

Eliassen et al. [6] and Eliassen and Saltbones [5] presented the first long-range transport model within the EMEP framework. The model was Lagrangian, developed for modelling sulphur compounds, and covered the whole of Europe using a 150 km grid. This model was further developed for nitrogen compounds [11, 12], and ozone [21, 22]. Eulerian models were subsequently developed for acidification [1], and photo-oxidants [13, 14]. In Simpson et al. [23] the first 'unified' MSC-W EMEP model was presented, in which one Eulerian model code was developed for both acidification and photo-oxidant activities. Applications of this unified model have been presented in, for example, Fagerli et al. [7]; Jonson

et al. [15]; Simpson et al. [24, 25]. Research versions of the model have been developed for studies including aerosol dynamics [31], secondary organic aerosol [2, 26], and local to global scale photo-oxidant studies [15–17, 33].

In 2008 the EMEP model was released as public domain code. The next update is targeted for Autumn 2012. Documentation of the latter code can be found in Simpson et al. [27]. The model code itself can be obtained through www.emep.int.

45.3 Current Challenges

The biggest challenges for reliable modelling today probably lie in the estimation of particulate matter, especially for the fine fraction ($PM_{2.5}$). This fraction is thought to that most relevant for health issues, and as such is a key driver for air quality policy. $PM_{2.5}$ consists of a large number of compounds however, including the traditional inorganic pollutants (sulphate, nitrate, ammonium), some fraction of sea-salt and dust emissions, and a host of organic aerosol (OA) compounds, both primary and secondary (formed through chemical processes). Although we have a great deal of information on some of the inorganic compounds, there are still surprisingly many areas where knowledge is inadequate, for example in the deposition rates applied to nitrogen compounds [8], the size-distribution of nitrate (across fine and coarse modes), or whether we can reproduce the equilibrium partitioning associated the ammonium formation [19].

The biggest problems are probably associated with two OA sources: residential biomass burning in wintertime, and biogenic secondary organic aerosol (BSOA) in summertime. Measurements clearly indicate the predominance of these sources (e.g. [9]), but emissions are very uncertain, and formation mechanisms for SOA still not clear (e.g. [10]). In the EMEP MSC-W model, several schemes for secondary organic aerosol (SOA) formation have been tested. The standard model uses a so-called volatility basis set (VBS) approach [3, 20]. Results from various VBS setups are presented in Bergström et al. [2], and can be summarised:

1. Summertime levels are quite well captured by some versions of the VBS scheme. Those VBS schemes which include aging processes (reactions of OH with semivolatile compounds) seem to do a better job of reproducing summertime OA levels than schemes without such a mechanism.
2. It is hard however to know if the biogenic volatile organic compound (BVOC) emissions which are the major summertime precursor to SOA are correct there are significant uncertainties in European BVOC estimates (e.g. [18]).
3. There are problems matching wintertime OA levels, with the model in general underestimating. Some of these problems may stem from dispersion issues (in stable boundary layers), but there are signs that there are also problems with the emission inventories. Several other studies confirm the importance of residential wood combustion in wintertime, and also point to problems and inconsistencies with the emissions.

45.4 Future Challenges

Global change, involving both climate and emission changes (e.g. the significant growth in Asian emissions), needs to be accounted for in the policy process, and hence in models. The traditionally separate fields of air quality research and global climate modelling are increasingly integrated, not least through the recognition of the potential role of the so-called short-lived climate forcers (black carbon, CH_4, O_3), pollutants whose reduction would benefit both air quality and the climate [32].

The pollutants traditionally dealt with by EMEP are in any case significant for climate issues in many respects. Changes in ozone affect plant functioning, leading to changes in biomass, carbon-sequestration, and with feedbacks to climate and hydrology [28]. Reactive nitrogen (Nr, as opposed to non-reactive compounds N_2 or N_2O), can be a nutrient which can aid plant growth in some areas (and which is of course applied liberally as fertilizer across the world), but which also causes many environmental problems, not least acidification and eutrophication, increases in tropospheric ozone, and health issues through PM formation. The recently completed European Nitrogen Assessment (ENA, [29]) was a major effort to capture the complexity of the Nitrogen cycle for the European continent, mapping emissions, transformation, sources and sinks to both land and waters. The ENA report discusses many of the complex interactions of Nr in the environment, as well as future possibilities and policy option.

A growing recognition of the complexity of these interactions is driving a need for better treatments of the biosphere in both air pollution and climate models. Models inevitably become more complex (the trend to Earth-system models), which in principal should give more realism, but it becomes harder for individual scientists (or even groups of scientists) to understand all aspects of the models. As models grow, the main challenge may be to ensure that they get the right answer for the right reasons. For such efforts to be successful, careful consideration and evaluation will be needed of the whole model chain, which includes emissions, vegetation characteristics (and dynamics) and other inputs, chemistry and transport issues, process descriptions, scaling-issues, and the quality and representativeness of measurements which are used to evaluate and or guide the model development.

References

1. Berge E, Jakobsen HA (1998) A regional scale multi-layer model for the calculation of longterm transport and deposition of air pollution in Europe. Tellus 50:205–223
2. Bergström R, Denier van der Gon H, Prevot A, Yttri K, Simpson D (2012) Modelling of organic aerosols over Europe (2002–2007) using a volatility basis set (VBS) framework with application of different assumptions regarding the formation of secondary organic aerosol. Atmos Chem Phys Discuss 12:5425–5485
3. Donahue N, Robinson A, Stanier C, Pandis S (2006) Coupled partitioning, dilution, and chemical aging of semivolatile organics. Environ Sci Technol 40:2635–2643, http://pubs3.acs.org/acs/journals/doilookup?in_doi=10.1021/es052297c

4. Eliassen A (1978) The OECD study of long-range transport of air pollutants: long-range transport modelling. Atmos Environ 12:479–487
5. Eliassen A, Saltbones J (1983) Modelling of long-range transport of sulphur over Europe: a two year model run and some experiments. Atmos Environ 17:1457–1473
6. Eliassen A, Hov Ø, Isaksen I, Saltbones J, Stordal F (1982) A Lagrangian long-range transport model with atmospheric boundary layer chemistry. J Appl Met 21:1645–1661
7. Fagerli H, Legrand M, Preunkert S, Vestreng V, Simpson D, Cerquira M (2007) Modeling historical long-term trends of sulfate, ammonium and elemental carbon over Europe: a comparison with ice core records in the Alps. J Geophys Res 112:D23S13
8. Flechard CR, Nemitz E, Smith RI, Fowler D, Vermeulen AT, Bleeker A, Erisman JW, Simpson D, Zhang L, Tang YS, Sutton MA (2011) Dry deposition of reactive nitrogen to European ecosystems: a comparison of inferential models across the NitroEurope network. Atmos Chem Phys 11:2703–2728, http://www.atmos-chem-phys. net/11/2703/2011/
9. Gelencser A, May B, Simpson D, Sánchez-Ochoa A, Kasper-Giebl A, Puxbaum H, Caseiro A, Pio C, Legrand M (2007) Source apportionment of PM2.5 organic aerosol over Europe: primary/secondary, natural/anthropogenic, fossil/biogenic origin. J Geophys Res 112:D23S04
10. Hallquist M, Wenger JC, Baltensperger U, Rudich Y, Simpson D, Claeys M, Dommen J, Donahue NM, George C, Goldstein AH, Hamilton JF, Herrmann H, Hoffmann T, Iinuma Y, Jang M, Jenkin ME, Jimenez JL, Kiendler-Scharr A, Maenhaut W, McFiggans G, Mentel TF, Monod A, Prevot ASH, Seinfeld JH, Surratt JD, Szmigielski R, Wildt J (2009) The formation, properties and impact of secondary organic aerosol: current and emerging issues. Atmos Chem Phys 9:5155–5236
11. Hov Ø, Eliassen A, Simpson D (1988) Calculation of the distribution of NOx compounds in Europe. In: Isaksen I (ed) Troposheric ozone. Regional and global scale interactions. D. Reidel, Dordrecht, pp 239–262
12. Iversen T (1990) Calculations of long-range transported sulphur and nitrogen over Europe. Sci Total Environ 96:87–99
13. Jonson J, Bartnicki J, Olendrzynski K, Jakobsen H, Berge E (1998) EMEP Eulerian model for atmospheric transport and deposition of nitrogen species over Europe. Environ Poll 102:289–298
14. Jonson J, Sundet J, Tarrasón L (2001) Model calculations of present and future levels of ozone and ozone precursors with a global and a regional model. Atmos Environ 35:525–537
15. Jonson J, Simpson D, Fagerli H, Solberg S (2006) Can we explain the trends in European ozone levels? Atmos Chem Phys 6:51–66, Ref-ID: 1680-7324/acp/2006-6-51
16. Jonson J, Stohl A, Fiore A, Hess P, Szopa S, Wild O, Zeng G, Dentener F, Lupu A, Schultz M, Duncan B, Sudo K, Wind P, Schulz M, Marmer E, Cuvelier C, Keating T, Zuber A, Valdebenito A, Dorokhov V, De Backer H, Davies J, Chen G, Johnson B, Tarasick D, Stubi R, Newchurch M, von der Gathen P, Steinbrecht W, Claude H (2010) A multi-model analysis of vertical ozone profiles. Atmos Chem Phys 10:5759–5783
17. Jonson JE, Travnikov O, Gauss M, Gusev A, Iyin I, Valiyaveetil S, Valdebenito A, Wind P, Sokovykh V, Shatalov V, Lin C-J, Dastoor A, MacLeod M, Hollander A (2010) Development of the EMEP global modelling framework: progress report, EMEP/MSCW technical report 1/2010. The Norwegian Meteorological Institute, Oslo
18. Rinne J, Back J, Hakola H (2009) Biogenic volatile organic compound emissions from the Eurasian taiga: current knowledge and future directions. Boreal Environ Res 14:807–826
19. Schaap M, Otjes RP, Weijers EP (2011) Illustrating the benefit of using hourly monitoring data on secondary inorganic aerosol and its precursors for model evaluation. Atmos Chem Phys 11:11 041–11 053, http://www.atmos-chem-phys.net/11/11041/2011/
20. Shrivastava MK, Lane TE, Donahue NM, Pandis SN, Robinson AL (2008) Effects of gas particle partitioning and aging of primary emissions on urban and regional organic aerosol concentrations. J Geophys Res 113
21. Simpson D (1993) Photochemical model calculations over Europe for two extended summer periods: 1985 and 1989. Model results and comparisons with observations. Atmos Environ 27A:921–943

22. Simpson D (1995) Biogenic emissions in Europe 2: implications for ozone control strategies. J Geophys Res 100:22 891–22 906
23. Simpson D, Fagerli H, Jonson J, Tsyro S, Wind P, Tuovinen J-P (2003) The EMEP unified Eulerian model. Model description, EMEP MSC-W report 1/2003. The Norwegian Meteorological Institute, Oslo
24. Simpson D, Butterbach-Bahl K, Fagerli H, Kesik M, Skiba U, Tang S (2006) Deposition and emissions of reactive nitrogen over european forests: a modelling study. Atmos Environ 40:5712–5726
25. Simpson D, Emberson L, Ashmore M, Tuovinen J (2007) A comparison of two different approaches for mapping potential ozone damage to vegetation. A model study. Environ Poll 146:715–725
26. Simpson D, Yttri K, Klimont Z, Kupiainen K, Caseiro A, Gelencsér A, Pio C, Legrand M (2007) Modeling carbonaceous aerosol over Europe. Analysis of the CARBOSOL and EMEP EC/OC campaigns. J Geophys Res 112:D23S14
27. Simpson D, Benedictow A, Berge H, Bergstrom, Emberson LD, Fagerli H, Hayman GD, Gauss M, Jonson JE, Jenkin ME, Nyíri, Richter AC, Semeena VS, Tsyro S, Tuovinen J-P, Valdebenito Á, Wind P (2012) The EMEP MSC-W chemical transport model – Part 1: model description. Atmos Chem Phys Discuss 12:3781–3874
28. Sitch S, Cox PM, Collins WJ, Huntingford C (2007) Indirect radiative forcing of climate change through ozone effects on the land-carbon sink. Nature 448:791–795
29. Sutton M, Howard C, Erisman J, Billen G, Bleeker A, Grennfelt P, van Grinsven H, Grizetti B (2011) The European nitrogen assessment. Sources, effects and policy perspectives. Cambridge University Press, Cambridge, http://www.nine-esf.org/ENA-Book
30. Tørseth K, Aas W, Breivik K, Fjæraa AM, Fiebig M, Hjellbrekke AG, Lund Myhre C, Solberg S, Yttri KE (2012) Introduction to the European Monitoring and Evaluation Programme (EMEP) and observed atmospheric composition change during 1972–2009. Atmos Chem Phys 12:5447–5481, http://www.atmos-chem-phys.net/12/5447/2012/
31. Tsyro S (2008) Regional model for formation, dynamics, and long-range transport of atmospheric aerosol: study of atmospheric aerosol properties in Europe. Russ Met Hydrol 33:300–309
32. UNEP (2011) Intergrated assessment of black carbon and tropospheric ozone. Summary for decision makers, tech. rep. UNEP/WMO
33. Vieno M, Dore AJ, Stevenson DS, Doherty R, Heal MR, Reis S, Hallsworth S, Tarrason L, Wind P, Fowler D, Simpson D, Sutton MA (2010) Modelling surface ozone during the 2003 heat-wave in the UK. Atmos Chem Phys 10:7963–7978

Questions and Answers

Questioner Name: Sergey Napelenok

Q: Any emission estimates of b-caryophellene?
A: We do not include this in the EMEP modelling as the emissions of this compound, and indeed all sesquiterpenes are so uncertain, both in magnitude and timing. In fact, all BVOC emissions are problematic – this is one of the major issues I tried to stress.

Questioner Name: S.T. Rai

Q: Very nice presentation, thank you David. If I were to give you $10 M and 10 years time, what model developments would you make to address our human health and

ecosystem problems in a cooperative manner. For example, there is a concern that AQ models need to be connected to human exposure models, watershed models, etc. Would you build a "one-environment" model to address the needs of policy makers. **A**: Sorry to say this in a room full of modellers, but I would use most of the money on measurements, or better use of them. I think the main limitation for model development at the moment is lack of observations on some fundamental issues, e.g. NOy partitioning, or near-source data to improve emission estimates. As to models, there is a clear trend towards harmonised and more complex models, but these easily become too complex to understand. These are needed, but have to be well founded at the process level (comparison with observations) – this will be a real challenge.

Chapter 46
Modelling Clean Air

Peter Builtjes and Richard Kranenburg

Abstract An attempt has been made by a combination of theory, observations, and especially modeling to determine the concentrations of trace gases and aerosols in the troposphere, without the influence of human beings.

Keywords Chemical transport modeling • Biogenic and anthropogenic emissions • Clean air

46.1 Introduction

Determination of the natural background is important to understand the chemical composition of the atmosphere and for application studies in order to know the contribution of biogenic and natural emissions to current concentration levels. The study of the composition of "clean air" consists of four aspects: observations, like in ice-cores, theoretical considerations concerning the development of the chemical composition of the atmosphere of the earth, smog-chamber studies-if at all possible-, and chemical transport modeling.

The definition of clean air deserves some attention. Often, clean air is defined as the chemical composition of the atmosphere before the industrial revolution, so before 1850, the IPCC takes 1750 as the base year. However, it is clear that

P. Builtjes (✉)
TNO, PO Box 80015, Utrecht 3508 TA, The Netherlands

Free Univ. Berlin, Berlin, Germany
e-mail: peter.builtjes@tno.nl

R. Kranenburg
TNO, PO Box 80015, Utrecht 3508 TA, The Netherlands

D.G. Steyn et al. (eds.), *Air Pollution Modeling and its Application XXII*,
NATO Science for Peace and Security Series C: Environmental Security,
DOI 10.1007/978-94-007-5577-2_46,

"clean air" did not exist in medieval cities, or even in caves, were the level of EC will have been rather high. A possibility might be to define the start of the new area, the anthropogene, when people got control over fire, which is about 400,000 years ago.

46.2 Observations

For a number of species the natural concentrations of the trace gases can be interfered from observations in ice-cores. The natural concentration of CO2 is about 270 ppm, for CH4 about 700 ppb. Based on a concentration of CO2 of 270 ppm, the natural Ph of rainwater would be 5.5. Concerning tropospheric O3 an estimate has been made by Volz and Kley [4] based on observations during 1840–1870 at Mont Souris, Paris, resulting in an annual averaged value of about 15 ppb.

46.3 Theoretical Considerations

An analysis has been made concerning aerosols/PM by Andreae [1]. Based on estimates concerning seasalt, windblown dust and aerosol-formation theory, values were derived of about 100 particles/cm^3, which is about 5 ugr/m^3. The remarkable aspect is that the spatial gradients would be rather small, also between land and sea.

46.4 Modelling

Over the years a number of modelling studies, both on the regional and the global scale, have been performed to assess the natural background. Using as emission input to the CTM's the estimated biogenic and natural emissions, concentrations have been calculated which might reflect the clean air concentrations.

Global modeling with the ECHAM-model, [2, 3] resulted in natural concentrations of summertime tropospheric O3-concentrations in the northern hemisphere of about 15 ppb, which is remarkable similar to the Mont Souris data. From their paper it can estimated that the natural CO-level would be about 40 ppb.

Model calculations have been made with the chemical transport model LOTOS-EUROS over Europe to estimate the natural background for O3 and for aerosols/PM. To calculate natural O3-levels next to natural NMVOC, also natural NO-emissions from the soil have to be taken into account using the approach of Yienger and Levy [5]. In the base run, calculations for the year 2006 over Europe have been made. In the second run the natural NO-emissions have been added. In Fig. 46.1, one can see that in general the annual averaged O3 concentrations of 40 ppb, increases by 0.5 ppb over sea, and decreases by 0.5 ppb over land. For the natural run the anthropogenic NMVOC and NO/NO2-emissions have been put to zero. The

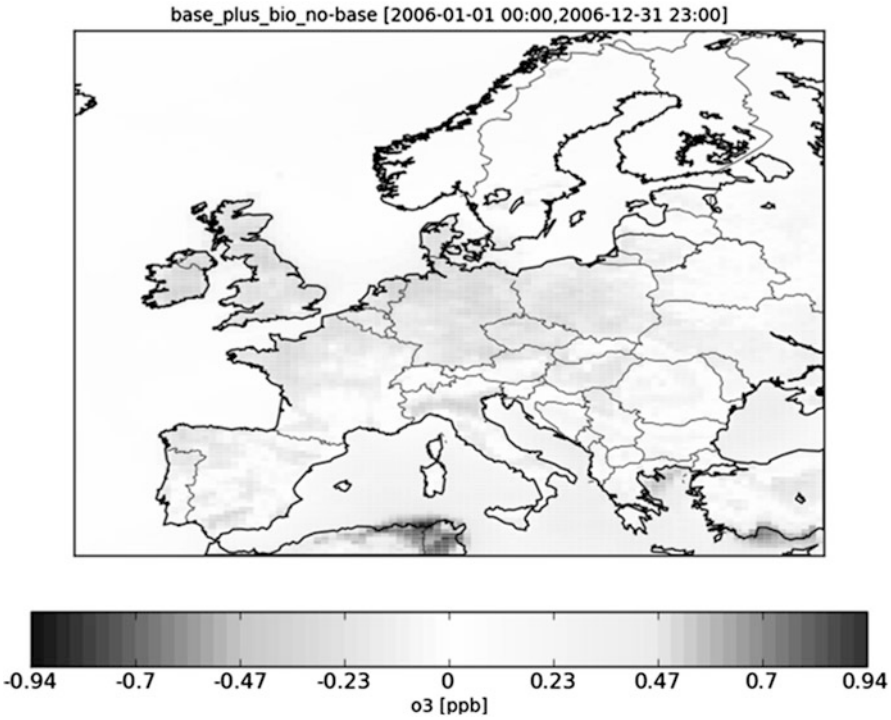

Fig. 46.1 Difference in annual ozone concentrations between run with natural NO emissions and a run without natural NO emissions

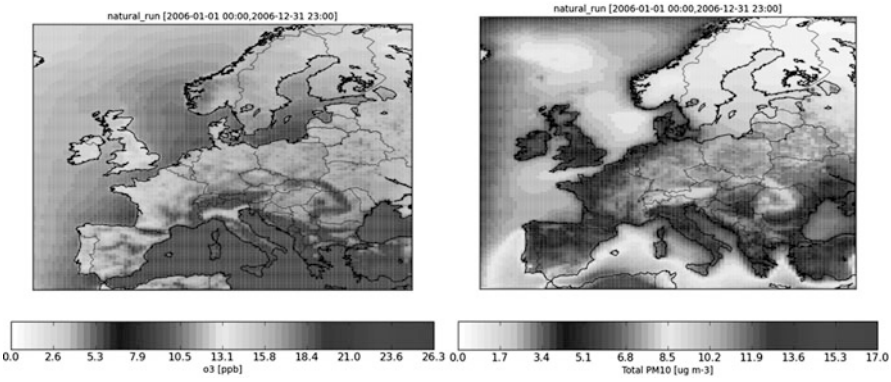

Fig. 46.2 Annual average ozone concentration (*left*) and annual average PM concentration (*right*) from natural sources

anthropogenic emissions of SO2, PPM, NH3 and CO have been multiplied by 5 %, to create natural emissions. The boundary conditions in the base run have been taken from the MOZART-model. Because no MOZART-run with natural emissions was available, the results of Roelofs [2] have been used. The left panel of Fig. 46.2 shows

the calculated yearly averaged natural O3 levels which are about 15 ppb in central Europe. In July, values up to 20 ppb are reached. These values are in nice agreement with the Mont Souris data.

The right panel of Fig. 46.2 shows the – very preliminary-annual averaged results of natural PM10 concentrations. Values of about 7–10 ugr/m^3 are found over the sea due to sea-salt, and about 3–5 ugr/m^3 over land. These results are promising, and at least not in contradiction with the results of Andreae. It should be noted that these results are preliminary, and that for example BSOA has not yet be included, which might increase the land-based PM10 concentrations by 2–3 ugr/m^3.

46.5 Conclusions

An attempt has been made to derive natural O3-and PM-concentrations from model calculations using estimates of natural emissions. For tropospheric annual averaged O3, concentrations are found of 15 ppb. Annual averaged PM10-concentrations are about 7–10 ugr/m^3 over the sea and about 3–5 ugr/m^3 over land. These values are not in contradictions with theoretical considerations.

References

1. Andreae M (2007) Aerosol before pollution. Science 315(5808):50–51
2. Roelofs G-J, Lelieveld J, van Dorland R (1997) A three-dimensional chemistry/general circulation model simulation of anthropogenically derived ozone in the troposphere and its radiative forcing. J Geophys Res 102(D19):23389–23401
3. Roelofs G-J, Lelieveld J, Feichter J (1998) Model simulations of the changing distribution of ozone and its radiative forcing of climate: past, present and future. Max. plamck-Inst. of Meteorology, Hamburg, Germany, Rep. no 283
4. Volz A, Kley D (1988) Evaluation of the Montsouris series of ozone measurements in the nineteenth century. Nature 332:240–242
5. Yienger J, Levy H (1995) Empirical model of global soil-biogenic NOx-emissions. J Geophys Res 100:11447–11464

Questions and Answers

Questioner name: Sergey Napelenok

Q. How do you classify “wild fires” in your analysis
A. I in fact did not take them into account. Focusing on Europe, most forest fires might be caused by humans

Questioner name: Mark Janssen.

Q. You should be able to include forest fire return frequency and create a good statistical model for forest fires. Fire return frequency is a well understood science in the forestry field
A. Thanks for this information. In case these forest fires are natural fires, it would be useful to take them into account. However, in that case I should also consider the forest coverage in previous times, Europe might well have been nearly completely covered by forest

Questioner name: Stefano Galmarini.

Q. How it looks if you consider "clean air" as that produced in stationary state of interaction between life and the atmosphere. To what extent can we say that prior to the anthropogene the atmosphere reached already not "equilibrium" and onto which the anthropogenic perturbation occurred?. Why not running a super long simulation without man and see what happens?
A. I need to think about this in more detail. The chemical lifetimes of species will play a role there, like the 6,000 years for O2.

Questioner name: Douw G. Steyn.

Q. Have you tried to put your interesting ideas into the context provided by the "big history" movement
A. No, I didn't, but will certainly have a look into this.

Chapter 47
An Online Coupled Two Way Interactive Modelling Study of Air Pollution Over Europe and Mediterranean

Jonilda Kushta, Stavros Solomos, Marina Astitha, Christina Mitsakou, and George Kallos

Abstract During the last decade, the efforts in the field of atmospheric modeling have been directed towards a joint 'online' approach of the meteorological and chemical processes in order to treat, in an integrated way, their complex and interactive links. This approach allows for the use of all meteorological fields as input in the chemical submodel, at each model time step, as well as takes into consideration the concentration of the pollutants on the meteorological processes (radiation and cloud microphysics). In this work, the air pollution over East Mediterranean is assessed with the use of the fully coupled, two-way interactive modeling system ICLAMS. Simulations have been performed for several test cases enhancing on the feedback mechanisms that occur. The summer case (July 2005) is used as base evaluation case due the increased insolation and high photolytic activity. The ozone model results are compared with measurements from stations from the European Monitoring and Evaluation Programme (EMEP). The correlation coefficient over all model domain reaches 0.7 with a root mean square error 22.78 $\mu g/m^3$ and mean bias 0.74 $\mu g/m^3$. The spring case (April 2004) highlights on the impact of mineral dust and sea salt on the photolysis rates that in turn determine the concentration of ozone in the area. The presence of dust over Finokalia station (Crete, Greece) leads to a decrease in the photolysis rates of NO2 and O3. Another winter case has also been discussed regarding the role of anthropogenic aerosols on clouds and precipitation.

Keywords Online modeling • ICLAMS-model • Ozone

J. Kushta • S. Solomos • C. Mitsakou • G. Kallos
School of Physics, University of Athens, Athens, Greece

M. Astitha (✉)
School of Physics, University of Athens, Athens, Greece

The Cyprus Institute, Energy, Environment and Water Research Centre, Nicosia, Cyprus
e-mail: m.astitha@cyi.ac.cy

D.G. Steyn et al. (eds.), *Air Pollution Modeling and its Application XXII*,
NATO Science for Peace and Security Series C: Environmental Security,
DOI 10.1007/978-94-007-5577-2_47,

47.1 Introduction

The assessment of weather processes and atmospheric chemistry in a combined way is a necessity in chemical weather modeling. Traditional chemical transport modeling systems use an offline approach that has several drawbacks. Chemical weather forecasting is based on online integrated modeling systems since this approach gives the possibility to consider the links between air pollution and meteorological processes. These links consist of several feedback mechanisms of direct, semi-direct and non-direct type on radiation, clouds and precipitation. The thermally induced circulation is responsible for the distribution of the gases and aerosols, and therefore any changes, from the direct effects, in the temperature and wind field, will lead to changes in their concentrations. Additionally the indirect effect plays a crucial role in the pollutants levels through removal processes.

Another important link between chemistry and meteorology refers to the strong dependency of the photolysis rates on the actinic fluxes that in an integrated model can be achieved through the online calculation of them, therefore giving the possibility to reflect any changes on the actinic fluxes due to the changes on the cloud cover. The present work focuses on the feedbacks between air pollution and meteorology over East Mediterranean in an attempt to define certain conditions when the impact of these links is magnified. The integrated fully coupled model ICLAMS is used for this study. A detailed description of the development related to the natural aerosols and several meteorological schemes is given in [1]. The chemical component of the model constitutes of the gas (SAPRC99) and aqueous chemistry module (RADM) and the gas-particle interaction module (ISORROPIA). The photochemical scheme uses basic formulations and it is directly coupled with the radiation scheme.

47.2 Results and Discussion

47.2.1 Model Evaluation: Test Case 1–31 July 2005

The performance of the integrated model for a summer test case, characterized by enhanced radiation and low cloud cover (increased photolytic activity), is discussed for four sub-regions: West Europe (WE 12 stations), Central Europe (CE 38 stations), Iberian Peninsula (IP 10 stations) and East Europe (EE 7 stations) to reflect different characteristics and measurements availability. The comparison of the modelled and observed ozone concentrations reveals a satisfactory performance overall domain with single station correlations above 0.6, apart from several distinct areas of lower correlation (lower than 0.4) along Austrian Alps, and coastal areas due to coarse resolution. Low correlations are also noted over Greece and Cyprus but the RMSE in these cases is low (less than 20 $\mu g/m^3$) indicating the lack of diurnal ozone cycle in these areas that are mostly affected by long range transport.

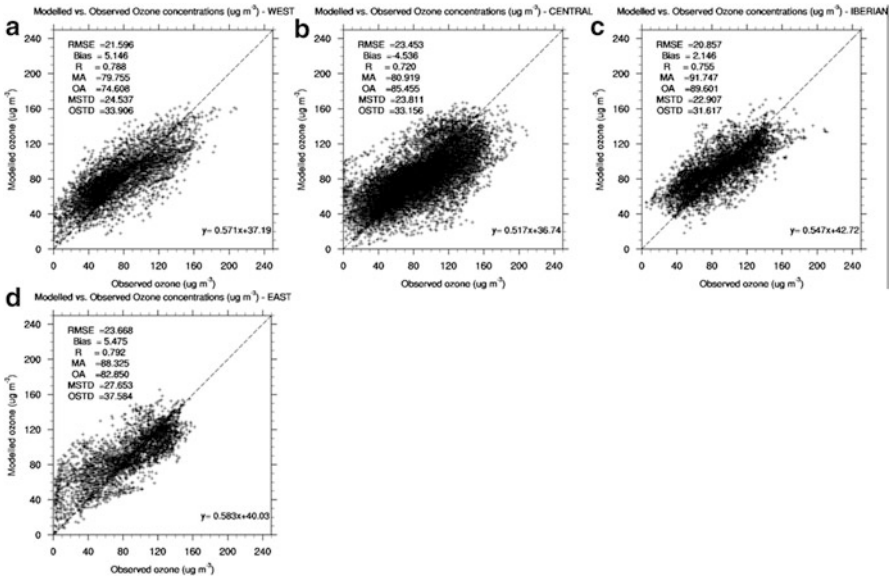

Fig. 47.1 Statistical parameters in $\mu g/m^3$ (RMSE, Bias, correlation, model and observed average, model and observed standard deviation) for each of the sub-regions included in the model domain (**a**) WE, (**b**) CE, (**c**) IP and (**d**) EE resulting from the comparison of modeled with observed hourly mean ozone concentrations

Overall domain, the absolute mean biases are also low. Several discrete statistical parameters are summarized in Fig. 47.1 for each sub-region. In all sub-regions the R coefficient is above 0.7 and absolute mean biases less than 6 $\mu g/m^3$. RMSE varies from 20.86 to 23.69 $\mu g/m^3$. The standard deviations of the model and observed averages differ by approx. 10 $\mu g/m^3$ indicating a lower diurnal span of modeled hourly ozone concentrations. The spatial resolution of the model (24 km) is adequate for a satisfactory description of the chemical and meteorological mechanisms that take place but may be low for areas with complex terrain and high altitudes therefore nesting configuration must be applied for local air quality studies.

47.2.2 Impact of Aerosols on Photolysis Rates: 10–20 April 2004

Mineral dust and sea salt are aerosols of natural origin that are often found in significant concentrations over East Mediterranean. One such event is that of 17 April 2004. The comparison of model results with (WD) and without dust impact

(ND) on radiation (and subsequently on actinic fluxes) revealed that, over Finokalia station (Crete, Grece), the greater differences are noticed close to the

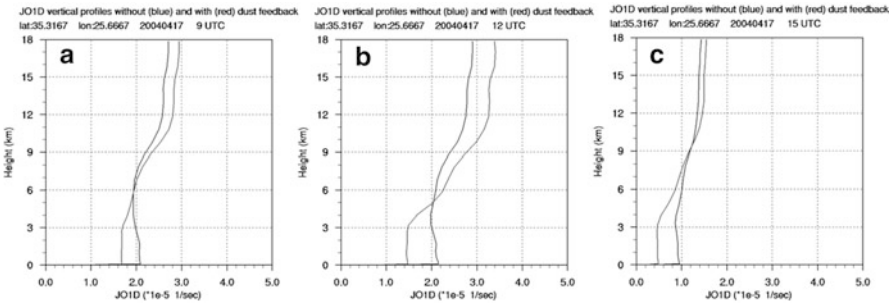

Fig. 47.2 Vertical profile of JO1D (s^{-1}) over Finokalia station (latitude = 35° 19′ N longitude = 25° 40′ E, altitude 250 m above sea level) with (*light gray*) and without (*dark grey*) dust effect on solar radiation on (**a**) 09:00, (**b**) 12:00 and (**c**) 15:00 UTC

surface during noon reaching up to 0.7×10^{-5} s^{-1} for JO1D and 1.5×10^{-3} s^{-1} for JNO2 (Fig. 47.2). The correlation coefficient R^2 from the comparison of the modeled and observed photolysis rates increased with the inclusion of the impact of dust on the heating rates. Also the spread of values was minimized and the linear correlation was closer to 1:1 reflecting the correction of the overestimation of the photolysis rates that was caused by larger amounts of actinic fluxes in the ND run.

47.2.3 Impact of Aerosols on Clouds and Precipitation: 26–30 January 2003

Solomos et al. [1] studied the case of 26–30 January 2003 when a low pressure system and a dust storm coexisted over East Mediterranean, showing that prognostic natural aerosol treatment gave better results than simulations with prescribed aerosol properties. In this study anthropogenic aerosols are explicitly represented and their impact on precipitation is discussed. In order to assess the respective effect of sulphate aerosols on precipitation two runs were performed with a solely difference the inclusion of the sulphates activation as CCN (Run with dust and salt – RD; Run with dust, salt and sulphate aerosols – RS). Over East Mediterranean there are two spots of increased sulphate activity that may result in considerable levels of sulphate aerosols over the coastline of Israel: Cairo mega city and west coast of Israel (power plants). The RS cloud system exhibits lower cloud top, enhancement of ice formation and suppression of cloud development over sea (Fig. 47.3a, b). Over the entire domain the 24 h accumulated precipitation remains the same in both cases but the spatiotemporal features of hourly precipitation differ (Fig. 47.3c). The maximum values of the hourly precipitation in the RD case are noticed more inland that in the RS case.

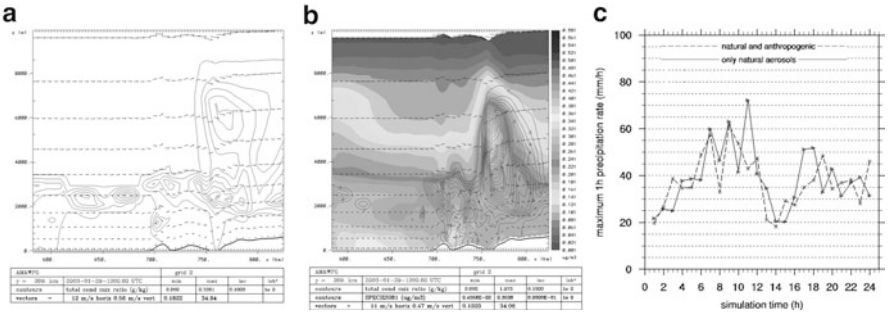

Fig. 47.3 Sulfate aerosols concentration (*grey fillings*) and total condensates (*contours*) at the west-east cross section located over Haifa (heavy rain) on January 29th, 2003 at 12:00UTC from (**a**) the simulation without the sulphate aerosols and (**b**) the simulation with the sulphate aerosols and (**c**) the diurnal variation of hourly precipitation maxima with and without sulphate aerosols

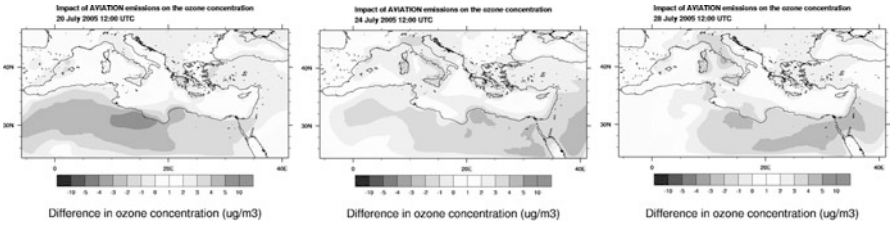

Fig. 47.4 Difference in the mean hour surface ozone concentration due to the utilization of the aviation emissions in the emission inventory for the 20, 24 and 28th of July 2005, at 12:00 UTC. The difference is expressed as C with aviation emissions minus C without aviation emissions

47.2.4 Impact of Aviation Emissions on Ozone Levels Over Europe and GMR

The inclusion of aviation emissions in the emission inventory leads to an increase in the ozone levels over Europe and GMR. The higher differences are noticed over Mediterranean due to the prevailing westerly flow over continental Europe and the etesian winds over the Aegean Sea that transfers the pollutants from East Europe over Eastern Mediterranean and Northeast Africa (Fig. 47.4).

47.3 Conclusions

The online approach for chemical weather modelling systems gives the opportunity to capture features that cannot be accurately described by the conventional meteorological and air quality models. Apart from configuration advantages, the integrated

model can assess links and feedbacks between atmospheric processes. The order of magnitude of these interactions is a necessary quantification for local applications to climatological studies.

Reference

1. Solomos S et al (2011) An integrated modelling study on the effects of mineral dust and sea salt particles on clouds and precipitation. Atmos Chem Phys 11:873–892

Questions and Answers

Questioner Name: S. Arunachalam:

Q: The AQ impacts of O3 (∼10–20 ppb) due to aviation emissions seem too high. Can you report these as a recent of total anthropogenic O3 over your domain? A similar analysis of NOx emissions budgets (aircraft as a percent of total anthropogenic NOx) will be helpful.
A: What was shown is O3 difference in the lower troposphere (runs with minus without aviation emissions of all type). The numbers mentioned in the presentation as too high are spotted at specific locations and are instant values, not averaged as in the paper. As an average, aviation emissions contribute to a relatively small percentage but for specific locations and seasons it can become more important (e.g. near or downwind from a major airport). This analysis is not finished yet and therefore is hard to quantify at this stage.

Chapter 48
A Retrospective Analysis of Ozone Formation in the Lower Fraser Valley, Canada

Douw G. Steyn, Bruce Ainslie, Christian Reuten, and Peter Jackson

Abstract We conducted a study of ozone formation in the Lower Fraser Valley (LFV), using WRF-SMOKE-CMAQ models, observations and emission inventories in order to understand relationships between the reduction in both amount and location of precursor emissions and spatio-temporal changes in episodic ambient ozone concentrations over the last 20 years. A dynamical model evaluation shows that the modeling framework is able to capture the changes in both magnitude and spatio-temporal structure of ozone concentrations over the 20-year period. We model ozone formation for four episodes, which both capture the observed changes in ozone reduction and the different meteorological regimes that occur during LFV ozone episodes. The SMOKE emission inventories are adjusted to account for temporal changes in amount, and location of emissions, based on population shifts. Model runs allow us to isolate the effects of emission changes from meteorological changes. Results show that the western LFV has been, and remains VOC-sensitive; the central LFV has changed from VOC-limited to NOx-limited; and the eastern LFV has been, and remains NOx-limited. Analysis shows that the ozone production efficiency as a function of NO has increased noticeably in the eastern LFV. This has likely offset some of the benefits resulting from local NOx emission reductions.

Keywords Ozone • Decadal changes • Model evaluation • Process analysis

D.G. Steyn (✉) • B. Ainslie
Earth, Ocean and Atmospheric Science, The University of British Columbia, Vancouver, BC, Canada
e-mail: dsteyn@eos.ubc.ca

C. Reuten
RWDI Calgary, Calgary, AB, Canada

P. Jackson
Environmental Science & Engineering Program, University of Northern BC, Prince George, BC, Canada

D.G. Steyn et al. (eds.), *Air Pollution Modeling and its Application XXII*,
NATO Science for Peace and Security Series C: Environmental Security,
DOI 10.1007/978-94-007-5577-2_48,

48.1 Introduction

Regional tropospheric ozone in the LFV are subject to interaction of local emissions of ozone precursors; the local background concentration of ozone and its precursors; and meteorological [1, 5]. Local air quality management strategies [3, 4] implemented over the past 20 years have reduced total emissions of ozone precursors in the valley, while the spatial distribution of population (and hence ozone precursors) has shifted markedly. There has been a marked eastward shift in the ozone plume over the same period The objective of this research is to use the WRF-SMOKE-CMAQ modeling system to explore emissions ambient relations in the LFV and to elucidate whether spatial shifts in the ozone "plume" arise from changes in amount, reactivity or spatial location (or all three) of emissions.

48.2 Methods

The SMOKE-generated emissions inventory was adjusted to account for changes in both amount of emissions and the location of emission sources, with separate emission inventories for: light and heavy duty vehicles (through the MOBILE 6.2 and MOBILE 6.2C), off-road vehicles, railroads, aircraft, marine, other mobile sources, biogenic emissions, point sources, and area sources. Total annual emission rates of NOx, VOCs, CO, SO2, PM10, PM25, and NH3 within the LFV for each of the source categories, were taken from the Metro Vancouver forecast and backcast emission inventories [4]. Biogenic emissions were modelled the MEGAN modelling framework. The spatial distribution of emissions was achieved using 38 different spatial surrogates, gridded to 36, 12 and 4-km domains. The 4-km surrogates were dynamically adjusted, by changes in local population density.

The Weather Research and Forecasting model (WRF V 3.1) employing three two-way nested domains with grid cell resolutions of 36, 12 and 4 km at 48 vertical eta-levels was used to produce high-resolution meteorological fields. Each 96 h WRF run was initialized at 1800Z using North American Regional Re-analysis fields at a 32-km resolution. Nudging was used in outer domains to the analysis fields outside of the boundary layer.

The EPA Models-3 CMAQ modelling system version 4.7.1 was used for the photochemical modelling. Allowing for a 12-h spin up-period in the 96-h runs provided in excess of three full days of modelling for each episode. Background ozone, CO, and NOx were obtained from RETRO monthly average output fields created from the ECHAM5-MOZ coupled GCM/chemical and aerosol model. The carbon bond version 5 (CB05) gas phase chemical mechanism with chlorine using the AE-5 aerosol module was used.

48.3 Model Evaluation

Detailed evaluation was applied to meteorological and chemical fields over four episodes, spanning the analysis period: July 1985, July 1995, August 2001 & June 2006. Particular attention was paid to the ability of the modeling system to respond to spatio-temporal ozone field changes over the analysis period. The episodes modeled included all four meso-meteorological types associated with ozone episodes in the LFV [1]. WRF performance was evaluated against a wide range of meteorological data from fixed stations, tethered balloon, lidar and aircraft data. CMAQ performance was evaluated against routine and special study data, chemical canister and balloon borne measurements of a wide range of modeled chemicals.

Based on this model evaluation, we conclude that the WRF-SMOKE-CMAQ modelling system produces ozone fields over the 20-year study period that are responsive to the estimated changes in local precursor emissions and are in generally good agreement with observations from the monitoring network. Some episodes show better comparisons with observations than others. This is in part due to weaknesses in the meteorological modelling. The model shows a changing bias over time, which might be related to uncertainties in the emissions backcasting.

Using model evaluation approaches outlined in Galmarini et al. [2] and especially the idea that a model is validated if it is judged to be "fit for purpose", we conclude that, while the model output does not exactly match all details of observed meteorological and chemical fields it is responsive to the changes in emissions between 1985 and 2005. Furthermore, the magnitude of the response is comparable to observed changes in the ozone plume. We therefore conclude that the modelling system is indeed fit for the intended purpose and that we can proceed to investigate the causes underlying observed spatio-temporal shifts in ozone fields in the LFV.

48.4 Mechanistic Analysis of Ozone Changes

Using the four evaluated episodes, which are representative of the four meso-scale meteorological regimes found during summertime ozone episodes [1], we re-ran each episode with emissions drawn from the 1985 and 2005 inventory years. We also performed a series of four sensitivity runs in order to identify NOx- and VOC-sensitive regions, using 15 % overall increases and decreases in NOx and VOC, and the ratio $[O_3]/[NOy] = 7$ as an indicator of the spatial location of the VOC/NOx ridgeline to track how emission changes have altered the spatial location of the ridgeline in the LFV.

Sensitivity runs, the 1985- and 2005-emission runs along with observations, emission inventory data and previous studies were used to identify causes of spatio-temporal shifts in ozone air quality. A further set of simulations was performed to examine the influence of the changes in land-use patterns and population density versus the absolute change in precursor emission rates on modeled ozone levels.

Composite analysis of ridgeline positions from the full set of individual runs shows that over the 20-year span of this study, the ridgeline has shifted westward by about 40 km in the core of the LFV whose full length is 100 km. In addition, the ridgeline has shifted and downslope along mountain slopes defining the valley.

48.5 Conclusions

The western LFV has been and remains VOC-sensitive. Large VOC emission reductions, stemming from light duty vehicles and petroleum refining emission controls, have been effective in reducing ozone concentrations in the western LFV. Some benefits of the VOC emissions reductions have been offset by the simultaneous NOx emission reductions that have occurred in and around the Vancouver urbanized area. Nonetheless, these precursor emissions reductions have led to decreasing 1- and 8-h episodic ozone concentrations.

The mid-valley region has gone from being VOC-limited to NOx-limited over the 20-year period; however, given the variability due to meteorology, it is probably better to characterize it as showing mixed sensitivity. VOC reductions (largely from VOC emission reductions in light duty vehicle; petroleum refining emissions not being greatly influential here) along with NOx emission reductions, appear to have offset one another in this part of the LFV. Ozone production efficiency as a function of NO has increased noticeably in this part of the valley. This efficiency increase has likely offset some of the benefits resulting from NOx emission reductions. The change in ozone sensitivity and the increased ozone production efficiency have changed the shape of the diurnal ozone profile to one that is less peaked around the daily maximum. As a result of this broadening, for a fixed peak ozone level, 8-h averaged concentrations calculated around the peak concentration have increased. An eastward shift in population from 1985 to 2005 have likely had a greater affect at mid-valley than in the western part of the valley. The net effect of these changes is consistent with the modest decline in peak 1-h ozone concentrations with the weakly declines in 8-h averaged concentrations.

Acknowledgments Metro Vancouver provided the air-quality data. Funding for the research was derived from NSERC grants to Douw G. Steyn and Peter Jackson and from the British Columbia Clean Air Research Fund supported by the Fraser Basin Council, Fraser Valley Regional District, and Metro Vancouver.

References

1. Ainslie B, Steyn DG (2007) Spatiotemporal trends in episodic ozone pollution in the lower Fraser Valley, British Columbia, in relation to mesoscale atmospheric circulation patterns and emissions. J Appl Meteor Climatol 46:1631–1644
2. Galmarini S, Steyn DG, Schere KL, Moran MD (2010) Tech. Rep. 2010JRC56481, Office for Official Publications of the European Communities
3. Greater Vancouver Regional District (1994, 2004) GVRD Air quality management plan. Tech rep, GVRD Policy and Planning Department, Burnaby, BC

4. Greater Vancouver Regional District (2007, 2005) Lower Fraser Valley air emissions inventory & forecast and backcast. Tech rep, GVRD Policy and Planning Department, Burnaby, BC
5. Steyn DG, Bottenheim JW, Thomson RB (1997) Atmos Environ 31:2025–2035

Questions and Answers

Questioner Name: Talat Odman

Q: What did you learn from the cluster analysis in terms of model improvement?
A: The cluster analysis made the modeling strategy possible, but really did not help improve the models we employed.

Questioner Name: Stefano Galmarini

Q: Did you account for land use changes, especially in terms of vegetation and the impact of biogenic emission changes?
A: We adjusted the emissions spatial allocation factors dynamically through the 20-year period based on changes in population per grid square. This changed the proportion of vegetated surface in each grid square, and therefore the biogenic emission. We did not change the vegetation type with time.

Questioner Name: Marina Astitha

Q: What about the transport of pollutants into the valley from remote sources? Could that affect the shift of ozone regimes?
A: We performed extensive back trajectory analyses to show that the LFV really is an isolated region. Emissions from Seattle (the nearest source region of any note) simply do not get to the LFV during ozone episodes.

Questioner Name: Golam Sarwar

Q: What caused the ozone production efficiency to increase from 1985 to 2005?
A: As in other regions where this has been noted, it is driven by the NOx/VOC ratio and to a certain extent by the VOC composition.

Questioner Name: Jeff Weil

Q: (1) Was the main source of NOx & VOC light duty vehicles? If so, how was the factor of 2 reduction achieved?
A: Yes, LDV has always been the main emissions source in the LFV. The reduction has been achieved by a sequence of AQ management plans over the past 20 years. Mostly the reduction has been thanks to an aggressive emissions monitoring program linked to vehicle insurance and registration. Of course this has been facilitated by improvements in engine efficiency and emissions controls.
Q: (2) Is valley meteorology, particularly slope and valley flows important in ozone formation?
A: Allow me to defer answering this until the next paper (by Annie Seagram), which demonstrates the crucial importance of such flows.

Chapter 49
Modelled Recirculation of Pollutants During Ozone Episodes in the Lower Fraser Valley, B. C.

Annie Seagram, Douw G. Steyn, and Bruce Ainslie

Abstract Recirculation of pollutants is often invoked as a cause of degraded air quality episodes. In this modelling study, we investigated recirculation in order to explore its behaviour in the Lower Fraser Valley (LFV), British Columbia. HYSPLIT was used to produce trajectories from WRF output for seven severe episodes, covering the four main circulation regimes conducive to ozone episodes. Both internal and external recirculations within our domain of interest were observable, but they do not have the same frequency for all regimes.

Keywords Recirculation • Ozone episode • Lower Fraser Valley • HYSPLIT

49.1 Introduction

49.1.1 Background

In the LFV, ozone episodes occur under a narrow set of synoptic conditions with weak forcing [3], which drive the photochemical conversion of precursor species into ozone, and are also characteristic of the mesoscale land-sea breeze circulation (e.g. [5]). These circulations can also interact with mountain-valley slope flows, and tributary valleys (e.g. [2]). Given that the LFV has relatively small total emissions [1], the severity of ozone episodes is often attributed to the strong recirculation of pollutants coincident with the mesoscale circulations aforementioned.

A. Seagram (✉) • D.G. Steyn • B. Ainslie
Department of Earth and Ocean Sciences, University of British Columbia, Vancouver, BC, Canada
e-mail: aseagram@eos.ubc.ca

D.G. Steyn et al. (eds.), *Air Pollution Modeling and its Application XXII*, NATO Science for Peace and Security Series C: Environmental Security,
DOI 10.1007/978-94-007-5577-2_49,

In this modelling study, we seek to define and provide evidence of recirculation during seven 3-day, summertime ozone episodes. These episodes were previously examined and described at length by Steyn et al. [6], and form the basis of the current study. The episodes are representative of the four regional mesoscale circulation regimes for ozone episodes, described by Ainslie and Steyn [1].

49.1.2 Defining Recirculation

We find that the term "recirculation" lacks a precise definition in the context of air pollution episodes. Here, we define the following: a trajectory is said to have *externally recirculated* at the point where it exhibits a minimum distance from its origin, if and only if: (a) the trajectory *left and returned* to a domain deemed chemically active for the region of interest, and (b) the point is within the mixed layer. If the trajectory fails to leave the domain but does re-approach its origin (given that (b) is true), we say it has *internally recirculated*.

49.2 Methods

49.2.1 Modelling

WRF (v3.1) meteorological fields were run for the seven episodes, using three, two-way nested domains (36, 12, 4 km resolution) at 48 sigma levels, for 96 h using NARR fields. The output was then evaluated against observed meteorological data (see [6]). The WRF fields served as input for HYSPLIT4. We selected the release point for trajectories to coincide with the point of maximum NO_x and VOC (precursors) emissions, modelled by SMOKE [6]. Trajectories were released at 10 m agl every hour, for the duration of the episodes (72 h, totaling 72 trajectories).

49.2.2 Trajectory Analysis

Based on our definition, we chose a chemically active domain to encompass the triangular-shaped LFV (see Fig. 49.1). The vertical limit allowance of recirculations was set to 800 m to represent the mixed layer height. Segments of trajectories that met these criteria were then identified, and labeled according to the circulation regime that prevailed on the day they occurred.

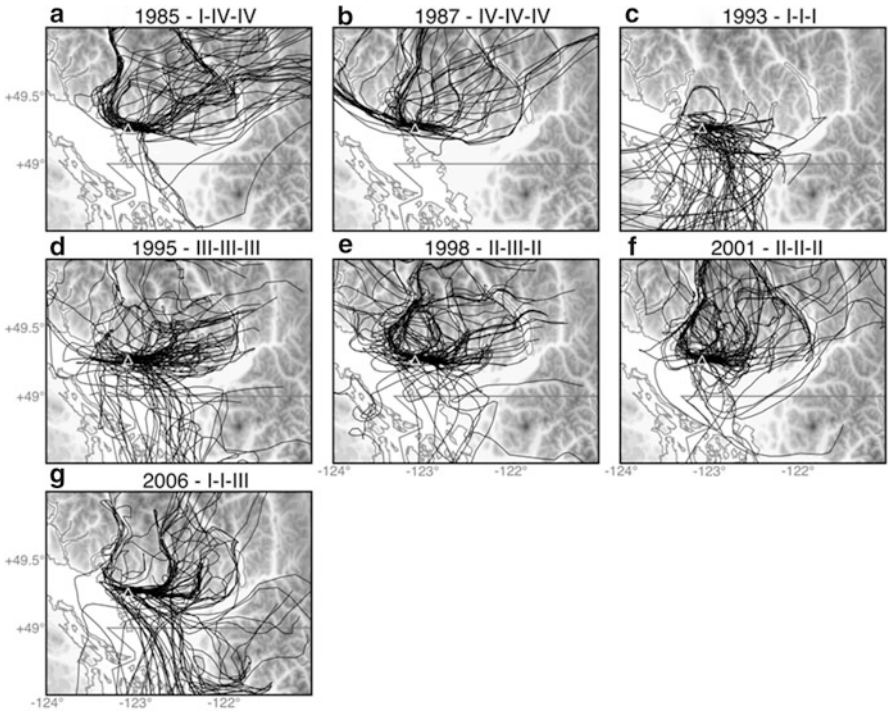

Fig. 49.1 All trajectories (*black*) for the seven ozone episodes, released from the origin (*triangle*). The domain of interest is outlined by a *dashed grey line*. The circulation regime for the three episode days are labeled above each plot

49.3 Results and Discussion

Similarities in the spatial distribution of trajectories are noted between the 1985 (Fig. 49.1a) and 1987 (b) episodes, with very few southward, and many northwestward trajectories. Both of these episodes are Type IV, which substantiates that trajectories are geometrically similar within circulation regimes. In contrast, 1993 (c) bears little resemblance to 2006 (g) (both Type III), which may be a result of the uncharacteristic, unstable conditions during the 1993 episode [4].

We note that almost all identified external recirculations exit the domain on the western and northern boundaries, and most internal recirculations occur toward the east (Fig. 49.2). Only a single external recirculation was identified for the Type IV regime. In general, external recirculations were found to either:(1) begin after midnight or in the morning hours, and last 6–30 h, or (2) begin in the early evening or before midnight, and last <12 h. In effect, this means that particles

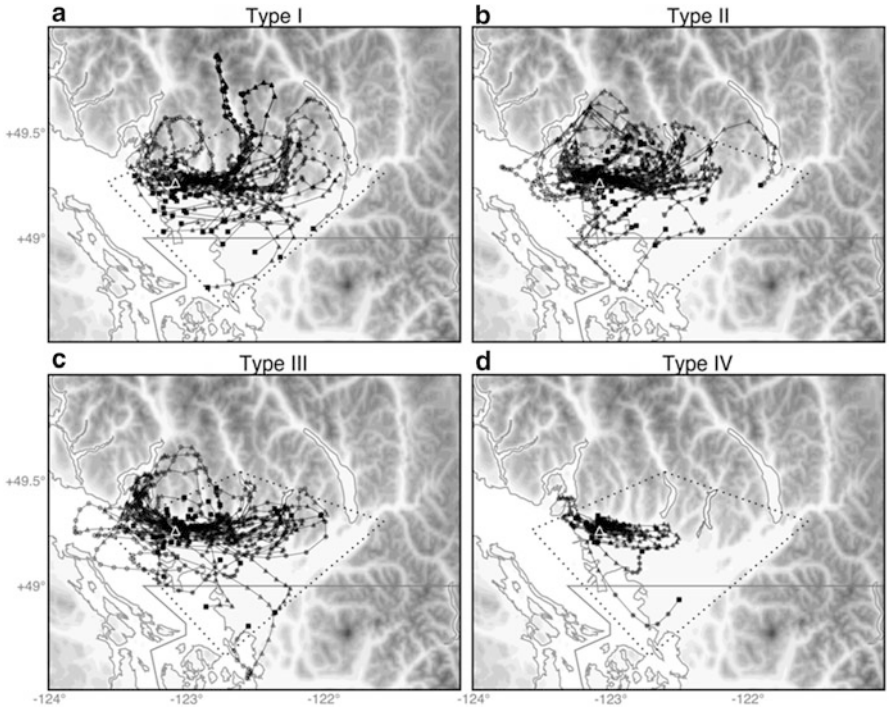

Fig. 49.2 External (*gray*) and internal (*black*) recirculation segments by circulation regime. Daytime and nighttime hours are represented by *circles* and *squares*, respectively

released on 1 day are "carried over" to the next. There is also strong evidence that particles released from the origin can recirculate through several tributary valleys (e.g. Fig. 49.2a).

49.4 Conclusion

There is good evidence to suggest that recirculation does play a role in the distribution of pollutants in the LFV during ozone episodes, and that it contributes to day-to-day "carryover" of pollutants. Recirculating trajectories under the same circulation regime tend to have similar spatial distributions. The frequency of recirculation depends on circulation regime, with a low frequency in regime IV.

Acknowledgments Funding for the research was derived from the NSERC USRA grant to Annie Seagram, and from NSERC grants to Douw G. Steyn and Peter Jackson and from the British Columbia Clean Air Research Fund supported by the Fraser Basin Council, Fraser Valley Regional District, and Metro Vancouver.

References

1. Ainslie B, Steyn DG (2007) Spatiotemporal trends in episodic ozone pollution in the Lower Fraser Valley, British Columbia, in relation to mesoscale atmospheric circulation patterns and emissions. J Appl Meteorol Climatol 46:1631–1644
2. Banta RM, Shepson PB, Bottenheim JW, Anlauf KG, Wiebe HA, Gallant A, Biesenthal T, Olivier LD, Zhu C-J, McKendry IG, Steyn DG (1997) Nocturnal cleansing flows in a tributary valley. Atmos Environ 31(14):2147–2162
3. McKendry IG (1994) Synoptic circulation and summertime ground-level ozone concentrations at Vancouver, British Columbia. J Appl Meteorol 33:627–641
4. McKendry IG, Steyn DG, Banta RM, Strapp W, Anlauff K, Pottier J (1998) Daytime photochemical transport over a tributary valley lake in southwestern British Columbia. J Appl Meteorol 37:393–404
5. Steyn DG, Faulkner DA (1986) The climatology of sea-breezes in the Lower Fraser Valley, B. C. Climatol Bull 20(3):21–39
6. Steyn DG, Ainlie B, Rueten C, Jackson PL (2011) Retrospective analysis of ozone formation in the Lower Fraser Valley, B. C. The University of British Columbia, Department of Earth and OceanSciences. Available from: http://hdl.handle.net/2429/36587

Questions and Answers

Questioner Name: Jeff Weil

Q: How sensitive was the recirculating trajectory (extent and time) to source/origin; e.g. being on valley floor or on sidewalls, was initial behavior affected by slope flows and being within a slope boundary layer?
A: We performed a very rough sensitivity test of the origin's location, and noted that placing it further north significantly increased the number of north-south recirculations, which were generally linked to mountain-valley wind reversals. However, the initial position must be constraint to some degree, as we would like to investigate the release of precursor pollutants, which primarily originate near the downtown center of Vancouver and not within the valleys.

Questioner Name: Mark Janssen

Q: Would your results look any different if you only picked a trajectory that resulted in high ozone?
A: We did not investigate this since we wanted to focus on forward trajectories as a means of detecting recirculation. It would be very interesting to do as you suggested, and determine the impact to which recirculating trajectories affect ozone values observed at various stations. We would predict that trajectories that directly result in "high ozone" at a station would also show recirculation, as our results show a lot of this behaviour during most episodes.

Chapter 50
An Assessment of the Emission and Dispersion of Volcanic Ash and Sulphur Dioxide in the Recent Eruptions in Iceland

Julius Vira, Marje Prank, Janne Hakkarainen, and Mikhail Sofiev

Abstract The chapter presents an assessment of the continental scale atmospheric dispersion of volcanic ash and sulphur dioxide from the recent eruptions of the Eyjafjallajökull (2010) and Grimsvötn (2011) volcanoes. The study is based on a combination of modelling, remote-sensing, and in-situ observations: while the release height is obtained from in-situ observations, the emitted mass flux of SO2 and particulate matter is calibrated using the satellite-based instruments. The analysed features include the split of the Grimsvötn plume to high-altitude SO2 and middle-troposphere ash clouds and the temporal variation of the Eyjafjallajökull emission composition.

Keywords Volcanic ash • Dispersion • SO2

50.1 Introduction

The airspace restrictions following the recent volcanic eruptions in Iceland established a strong need for quantitative predictions of volcanic ash dispersion. However, the uncertainties in especially the source term limit the accuracy of such predictions. The model computations are therefore frequently complemented with observations from remote-sensing instruments, soundings and measurement aircraft.

This study aims to assess the atmospheric dispersion of volcanic ash and sulphur dioxide (SO2) following the eruptions of Eyjafjallajökull (2010) and Grimsvötn (2011). The Eyjafjallajökull eruption began on 14 April and lasted

J. Vira (✉) • M. Prank • J. Hakkarainen • M. Sofiev
Finnish Meteorological Institute, Helsinki, Finland
e-mail: julius.vira@fmi.fi

D.G. Steyn et al. (eds.), *Air Pollution Modeling and its Application XXII*,
NATO Science for Peace and Security Series C: Environmental Security,
DOI 10.1007/978-94-007-5577-2_50,

about 40 days with alternating periods of lower and higher activity. The Grimsvötn eruption, in contrast, mainly consisted of the explosive outbreak starting 22 May, 2011.

50.2 Materials and Methods

In this study, the modelled dispersion was compared with satellite-based measurements to infer the emission flux, while the predictions were evaluated using ground-based measurements.

50.2.1 Observations

The primary observational sources of information were the MODIS aerosol optical depth (AOD) product and the OMI column product for aerosols and SO2, respectively. The AOD observations were supplemented by the OMI Absorbing Aerosol Index (AAI).

The satellite observations were used for adjusting the emission flux, whereas the plume height for Eyjafjallajökull was taken as the 6-h averaged values from the dataset of radar observations provided in Arason et al. [1]. For Grimsvötn, the evolution of plume height was taken from the status reports distributed by the Icelandic Meteorological Office.

Evaluating the simulation results, especially regarding the adjusted emission rates requires a separate set of quantitative observations. In case of Eyjafjallajökull, the plume was observed by several sun-photometers in the Aeronet network. However, the continental location of these sites necessities additional considerations to determine the background level of AOD. For Grimsvötn, sun-photometer observations were not readily available due to the plume trajectory, however, the plume was detected by several air quality monitoring networks, including the those in Finland [2], UK and Norway.

50.2.2 The Dispersion Model and Source Terms

The dispersion of the volcanic aerosol and SO2 release was simulated using the SILAM dispersion model [7] at 0.25° horizontal resolution and ECMWF operational meteorological fields. The volcanic ash was represented by a passive aerosol with a mean diameter of 3.0 μm. For the simulations of SO2, the sulphate formation was parameterised according to Sofiev [6].

The emission of SO2 was estimated by using the OMI SO2 columns and adjusting the daily emission rate to reproduce the observed plumes. This resulted

in ∼2.0 Tg of total SO2 emission. In contrast to ash, which was mainly emitted during start of the eruption and after mid-May, the SO2 emission flux was strongest during early May.

The aerosol source term for Eyjafjallajökull was based on the empirical relation between plume height and volume flux given by Mastin et al. [3]. For the Grimsvötn eruption, the formula resulted in strongly overestimated total columns, and the emission fluxes for both ash and SO2 were adjusted by comparing the modelled and observed optical thickness. This resulted in ∼0.6 Tg releases of both SO2 and transportable ash.

50.3 Results and Discussion

For the Eyjafjallajökull eruption, the dispersion patterns of SO2 and ash were rather similar. The initially emitted plume reached Europe by 16 April. The emission fluxes for SO2 and ash had broadly similar evolution throughout the eruption, however, the maxima of SO2 and ash emission flux did not coincide. This corroborates with the aircraft measurements published by Schumann et al. [5].

The SO2 and aerosol plumes (Fig. 50.1) from the Grimsvötn eruption had notably distinct dispersion patterns. The SO2 was mainly observed over the Arctic sea eventually extending towards Greenland and Siberia. The dispersion modelling shows the area to correspond to emission in upper troposphere.

The observations show no evidence of significant aerosol loads north of Iceland, which is confirmed also by more qualitative products like the OMI AAI. This suggests that the long-range transportableash was injected mainly into the middle or lower troposphere. In this work, the ash release was limited below 5 km, resulting in the patterns shown in Fig. 50.1

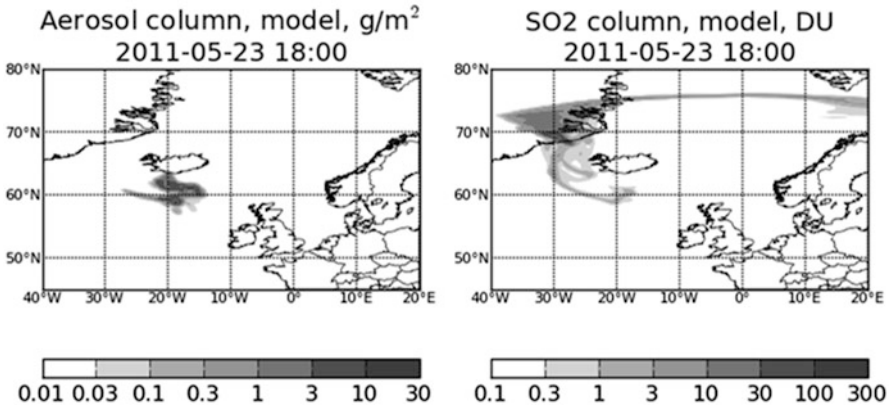

Fig. 50.1 The modelled ash (g/m^3) and SO2 (Dobson units) total column densities during the Grimsvötn eruption approximately 23 h after the start of eruption

The altitude-driven separation between ash and SO2 emissions has been observed previously for instance by Prata and Kerkmann [4], however, it was in sharp contrast to the situation with Eyjafjallajökull, where the dispersion of both SO2 and ash could be satisfyingly simulated using the reported plume heights.

50.4 Conclusion

The study shows that remote-sensed information can be used to refine and even reconstruct volcanic ash and SO2 emissions. In the Grimsvötn eruption, the SO2 and ash emission were transported almost entirely separately due to different injection altitude. This made it impossible to rely only on the plume height as a proxy for emission flux. In the Eyjafjallajökull eruption, the altitude-dependent split was not observed, however, the time development of the emission fluxes of ash and SO2 were only moderately correlated.

References

1. Arason P, Petersen GN, Bjornsson H (2011) Observations of the altitude of the volcanic plume during the eruption of Eyjafjallajökull, April–May 2010. Earth Syst Sci Data Discuss 4:1–25
2. Kerminen V-M, Niemi JV, Timonen H, Aurela M, Frey A, Carbone S, Saarikoski S, Teinilä K, Hakkarainen J, Tamminen J, Vira J, Prank M, Sofiev M, Hillamo R (2011) Characterization of a volcanic ash episode in Southern Finland caused by the Grimsvötn eruption in Iceland in May 2011. Atmos Chem Phys 11:12227–12239
3. Mastin LG, Guffanti M, Servranckx R, Webley P, Barsotti S, Dean K, Durant A, Ewert JW, Neri A, Rose WI (2009) A multidisciplinary effort to assign realistic source parameters to models of volcanic ash-cloud transport and dispersion during eruptions. J Volcanol Geotherm Res 186: 10–21
4. Prata AJ, Kerkmann J (2007) Simultaneous retrieval of volcanic ash and SO2 using MSG-SEVIRI measurements. Geophys Res Lett 34:1–6
5. Schumann U, Weinzierl B, Reitebuch O, Schlager H, Minikin A, Forster C, Baumann R, Sailer T, Graf K, Mannstein H, Voigt C, Rahm S, Simmet R, Scheibe M, Lichtenstern M, Stock P, Rüba H, Schäuble D, Tafferner A, Rautenhaus M, Gerz T, Ziereis H, Krautstrunk M, Mallaun C, Gayet J-F, Lieke K, Kandler K, Ebert M, Weinbruch S, Stohl A, Gasteiger J, Groß S, Freudenthaler V, Wiegner M, Ansmann A, Tesche M, Olafsson H, Sturm K (2011) Airborne observations of the Eyjafjalla volcano ash cloud over Europe during air space closure in April and May 2010. Atmos Chem Phys 11:2245–2279
6. Sofiev M (2000) A model for the evaluation of long-term airborne pollution transport at regional and continental scales. Atmos Environ 34:2481–2493
7. Sofiev M, Siljamo P, Valkama I, Ilvonen M, Kukkonen J (2006) A dispersion modelling system SILAM and its evaluation against ETEX data. Atmos Environ 40:674–685

Questions and Answers

Questioner name: Jeff Weil

Q: Concerning the lower ash cloud height than SO2 cloud height, do you consider the particle inertial effects with particles being "thrown out" of the cloud due to the buoyant cloud/plume internal circulation + higher inertia of particles? This effect is in addition to the standard gravitational settling of particles (particles don't/can't follow gas/fluid streamlines due to their inertia).
A: Internal dynamics of the buoyant plume were not included in the simulations. While such effects are likely to be important in explaining the observed behaviour, the stress of this study was rather on inferring their consequences using a dispersion model and satellite data.

Chapter 51
Representing the Effects of Long-Range Transport and Lateral Boundary Conditions in Regional Air Pollution Models

Rohit Mathur, Shawn Roselle, Jeffrey Young, and Daiwen Kang

Abstract The Community Multiscale Air Quality (CMAQ) modeling system was applied to a domain covering the northern hemisphere; meteorological information was derived from the Weather Research and Forecasting (WRF) model run on identical grid and projection configuration, while the emission inputs were derived from global inventories. The ability of the model to represent long-range transport of pollutants is analyzed through comparisons with aircraft measurements from the 2006 INTEX-B field campaign, ozonesonde profiles, and remotely sensed observations of aerosol optical depth. Time varying lateral boundary conditions from these hemispheric scale calculations were used to drive regional-scale air quality simulations over a finer resolution domain covering the continental United States. Comparison of model predictions with surface O_3 and $PM_{2.5}$ measurements indicate comparable or better performance relative to other approaches (e.g., other global models, static profiles). The successful expansion of CMAQ to the hemispheric scales now provides a conceptual framework to examine interactions between atmospheric processes occurring at various spatial and temporal scales in a consistent manner.

Keywords CMAQ-model • WRF • Ozone • PM 2.5

R. Mathur (✉) • S. Roselle • J. Young
United States Environmental Protection Agency, Research Triangle Park, NC, USA
e-mail: mathur.rohit@epa.gov

D. Kang
Computer Science Corporation, Research Triangle Park, NC, USA

D.G. Steyn et al. (eds.), *Air Pollution Modeling and its Application XXII*,
NATO Science for Peace and Security Series C: Environmental Security,
DOI 10.1007/978-94-007-5577-2_51,

51.1 Introduction

Both observational and modeling studies have demonstrated that pollutants near the Earth's surface can be convectively lofted to higher altitudes where strong winds can efficiently transport them from one continent to another, thereby impacting air quality on intercontinental to global scales. Changes in emission patterns over different regions of the world are likely to exacerbate the impacts of long-range pollutant transport on background pollutant levels in other regions, which may then impact the attainment of local air quality standards. Thus, strategies for reduction of pollution levels of the surface air over a region are complicated not only by the interplay of local emissions sources and several complex physical, chemical, dynamical processes in the atmosphere, but also hemispheric background levels of pollutants. Consistent modeling frameworks that can represent the interactions between various physical and chemical atmospheric processes at the disparate space and time scales are thus needed.

51.2 Model Setup

The Community Multiscale Air Quality (CMAQ) modeling system [1] was applied over a domain encompassing the northern hemisphere. The horizontal domain, set on a polar stereographic projection was discretized using grid cells with a 108 km resolution (see Fig. 51.1), while the vertical extent ranging from the surface to 50 mb was discretized with 44 layers of variable thickness with a 20 m deep lowest layer. 3-D meteorological fields were derived from the Weather Research and Forecasting (WRF) modeling system operating on the exact same projection and grid configuration as CMAQ. Observations from NCAR's global upper air observation data set combined with the GFS 1-degree analysis provided the reanalysis fields every 6 h for grid nudging in the WRF simulations. CMAQ v4.7.1 was configured with CB05 chemical mechanism and the AER05 aerosol module. In addition, O_3 mixing ratios in the top most model layer ($\sim$50mb) were modulated based on scaling to the spatially and temporally varying potential vorticity fields to represent possible effects associated with stratosphere-troposphere exchange [2]. Emissions of NO_x, SO_2, CO, volatile organic compounds, and particulate matter from anthropogenic and biomass burning sources were derived from the ARCTAS global emission inventory (http://www.cgrer.uiowa.edu/arctas/emission.html). Monthly varying biogenic emissions of isoprene and terpene were based on the Precursors of Ozone and their Effects on the Troposphere (POET) inventory.

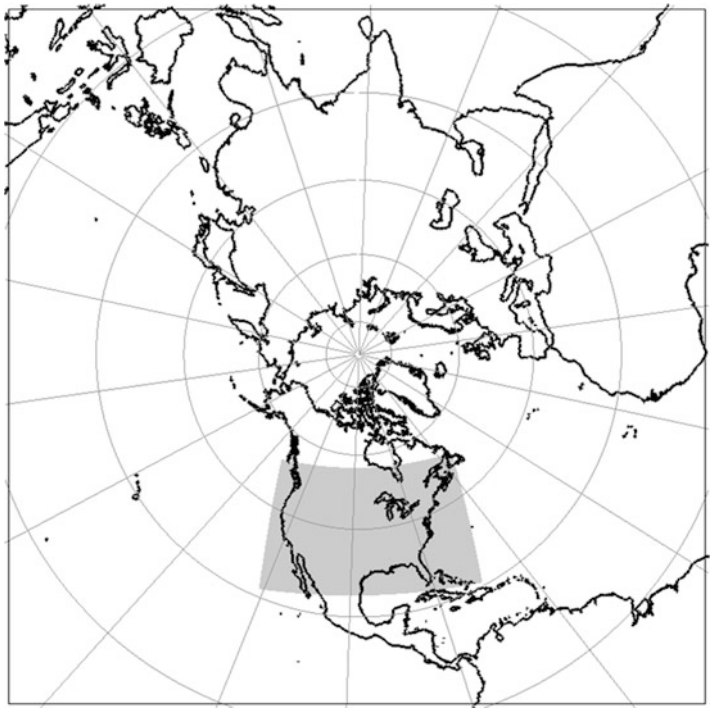

Fig. 51.1 The northern hemisphere modeling domain discretized using a 108 km resolution grid. The *shaded region* shows the extent of the Continental U.S. nested domain discretized using a 12 km resolution horizontal grid

51.3 Results and Discussion

Model simulations were conducted for the entire 2006 calendar year with a 20 days spin-up. Previous comparisons of 3-dimensional model estimates of O_3 against ozonesonde profiles and aircraft measurements over the Pacific demonstrated the feasibility of extending CMAQ to the hemispheric scale [3]. To further investigate the ability of the model to capture the variability in daily maximum 8-h O_3 levels at the surface, Fig. 51.2 compares distributions of modeled and observed (at CASTNET sites) max-8 h. O_3 for the spring season when transport across the Pacific and from the stratosphere influence O_3 mixing ratios in the surface air over the U.S.; these comparisons suggest that the model is able to capture the dynamic range of the observations.

The ability of the hemispheric model to provide spatially and temporally varying and consistent lateral boundary conditions (LBCs) to limited area finer resolution calculations was examined through nesting a 12 km grid over the Continental

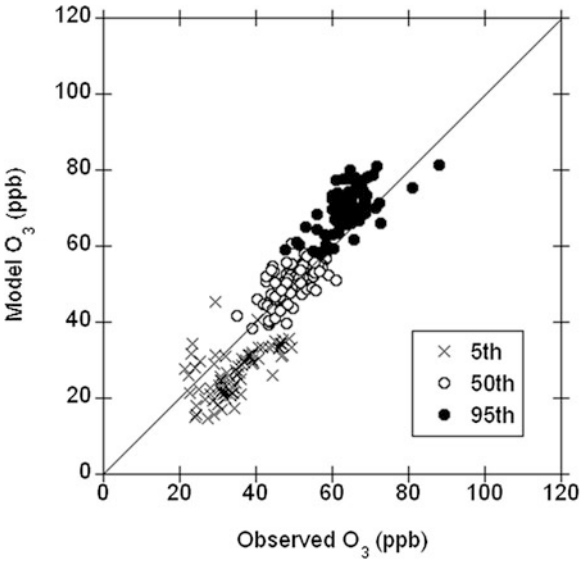

Fig. 51.2 Comparisons of modeled and observed (CASTNET) daily maximum 8-h. O_3 mixing ratio distributions during Spring (March–May, 2006). At each observation location the time-series of modeled and observed daily maximum −8-h. O_3 is examined and percentiles of the distributions are computed

U.S. within the hemispheric domain. During the late July – early August period, particulate matter levels over large portions of the southeastern U.S. were influenced by long-range transport over the Atlantic of dust from the Sahara, as evidenced by the increase in measured $PM_{2.5}$ concentrations at monitors in Florida (Fig. 51.3a). Also shown in Fig. 51.3, are comparisons of simulated $PM_{2.5}$ levels in the regional calculations driven with LBCs derived from the hemispheric model with those in which the LBCs were based on GEOS-Chem. As illustrated, the regional calculations with LBCs derived from hemispheric-CMAQ show comparable or better performance (reduced bias, Fig. 51.3b) relative to other approaches, further illustrating that the extension of CMAQ to hemispheric scales provides a conceptual framework to examine interactions between processes occurring at various spatial and temporal scales in a consistent manner.

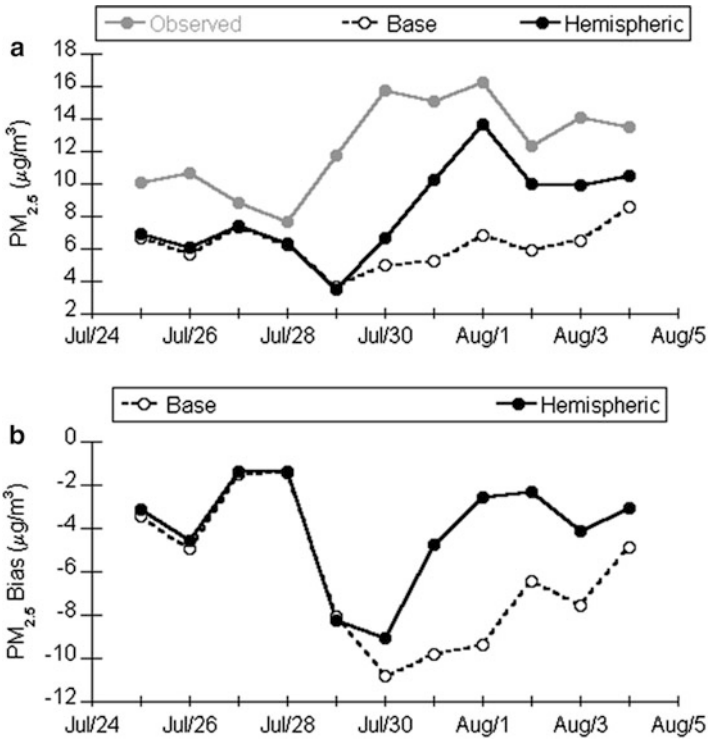

Fig. 51.3 Comparison of regional average (across 31 sites in Florida) (**a**) modeled and measured daily average $PM_{2.5}$ concentrations, and (**b**) corresponding model bias. The Base calculation used LBCs derived from GEOS-Chem, while the Hemispheric calculation used LBCs derived from CMAQ calculations over the northern hemisphere

Disclaimer Although this paper has been reviewed by EPA and approved for publication, it does not necessarily reflect EPA's policies or views.

References

1. Byun DW, Schere KL (2006) Review of the governing equations, computational algorithms, and other components of the Models-3 Community Multiscale Air Quality (CMAQ) modeling system. Appl Mech Rev 59:51–77
2. Mathur R, Lin H-M, McKeen S, Kang D, Wong D (2008) Three-dimensional model studies of exchange processes in the troposphere: use of potential vorticity to specify aloft O_3 in regional models. In: 2008 CMAS conference, Chapel Hill, North Carolina. Available at: http://www.cmascenter.org/conference/2008/slides/mathur_three-dimension_model_cmas08.ppt
3. Mathur R, Gilliam R, Bullock OR, Roselle S, Pleim J, Wong D, Binkowski F, Streets D (2012) Extending the applicability of the community multiscale air quality model to hemispheric scales: motivation, challenges, and progress. In: Steyn DG, Trini S (eds) Air pollution modeling and its applications, XXI. Springer, Dordrecht, pp 175–179

Questions and Answers

Questioner Name: M. Astitha

Q: Given the very good correlation of the modeled vs. observed O_3 at the flight tracks using 108 km horizontal resolution, did you test different setups of the vertical layers to get the optimal one?
A: We conducted tests with two different vertical layer configurations: a 35-layer and a 44-layer configuration. Both configurations have comparable resolution within the nominal daytime boundary layer ($\sim$3 km); the latter configuration better resolves the atmosphere between 3 and 20 km, especially near the tropopause. The comparisons shown were based on the 35-layer configuration results. The 44-layer simulated distributions within the lowest 10 km (examined in these comparisons) are similar. However, as expected much larger differences between the two configurations are seen in the upper troposphere.

Questioner Name: M. Astitha

Q: About the dust transport towards the U.S., you mentioned $PM_{2.5}$ measurements were used. Maybe PM_{10} would be most likely associated to dust particles?
A: Yes, wind-blown dust emissions influence both ambient $PM_{2.5}$ and PM_{10} levels and our simulation results also show that. In future analyses we will also examine the influence of this transport event on coarse PM levels in the region.

Chapter 52
Modeling the European Nitrogen Budget: Effects of Including the Bi-directional Surface-Atmosphere Exchange of Ammonia

Roy J. Wichink Kruit, M. Schaap, F.J. Sauter, M.C. van Zanten, and W.A.J. van Pul

Abstract Modelling has been performed of the European nitrogen budget, and the effects of including the bi-directional surface-atmosphere exchange of ammonia have been investigated.

Keywords Ammonia • Surface-atmosphere exchange

52.1 Introduction

Eutrophication due to nitrogen deposition is an important aspect in the conservation of ecosystems and biodiversity. For ecosystems close to populated areas with intensive animal housing, the dry deposition of ammonia is the most important form of nitrogen deposition. It is difficult, expensive and time consuming to measure the atmospheric input of ammonia on ecosystems. Therefore, atmospheric transport models (ATMs) are generally used to calculate the nitrogen deposition on ecosystems. An example of such an ATM is the LOTOS-EUROS model of the Dutch research consortium TNO-RIVM-PBL-KNMI [1]. The LOTOS-EUROS model is an Eulerian model in which atmospheric processes are modelled on a high time resolution, which makes the model useful for studying dynamic exchange processes at the earth's surface. In the description for the surface-atmosphere

R.J.W. Kruit (✉) • M. Schaap
Department of Climate, Air and Sustainability, TNO, P.O. Box 80015,
3508 TA Utrecht, The Netherlands
e-mail: roy.wichinkkruit@tno.nl

F.J. Sauter • M.C. van Zanten • W.A.J. van Pul
RIVM, P.O. Box 1, 3720 BA Bilthoven, The Netherlands

D.G. Steyn et al. (eds.), *Air Pollution Modeling and its Application XXII*,
NATO Science for Peace and Security Series C: Environmental Security,
DOI 10.1007/978-94-007-5577-2_52,

exchange of ammonia, a surface concentration or compensation point has long time been neglected, although many studies have shown that these concentrations are important for the exchange of ammonia with the surface. This is especially the case in ATMs, in which generalizations of parameterizations derived for inferential models need to be made. In this study, a new surface-atmosphere exchange model for ammonia proposed by Wichink Kruit et al. [3] is implemented in the LOTOS-EUROS model, called DEPAC3.11 hereafter [2]. This model includes compensation points for ammonia in vegetation (both stomata and external leaf surface), soils and water surfaces. In this way, the surface is not only able to adsorb ammonia but can also emit it under certain atmospheric conditions. The new model is compared with the earlier version of deposition model DEPAC, DEPACold hereafter, which is still widely used throughout Europe to model the atmospheric deposition of ammonia. We will show the effects of including bi-directional surface-atmosphere exchange of ammonia on the concentrations as well as on the NH_x deposition. To validate the ammonia mass balance calculations, ammonia concentration measurements are used.

52.2 Concentration Distribution

Figure 52.1 shows the yearly average NH_3 concentration as calculated by the LOTOS-EUROS model using DEPAC3.11 (upper right panel) and DEPACold (upper left panel) and the absolute (lower left) and relative (lower right) differences between them for the year 2007. The ammonia distribution largely follows the emission density distribution as the atmospheric lifetime of ammonia is rather short. Not surprisingly, the highest concentrations are modeled in the Po-Valley, Brittany, the Netherlands and north western Germany with NH_3 concentrations in the range of 4–10 μgm^{-3}. Concentrations between 1 and 4 μgm^{-3} occur over large regions in central Europe, whereas low concentrations of <1 μgm^{-3} are modeled across remote continental and marine regions. Including the compensation point approach causes the modeled ammonia concentrations to increase almost everywhere.

The largest absolute increase in ammonia concentrations is observed in agricultural areas, where the increase generally amounts 1–2 μgm^{-3}, while in the Po Valley an increase of more than 4 μgm^{-3} is found. In a relative sense, concentrations increase by about 30 % in the source regions, whereas at some distance the increase is about 10 %. Hence, the transport distance of ammonia is increased. The introduction of the compensation point for water leads to the largest relative concentration increases of a factor 2–3. This is because the concentrations over sea were very small with the DEPACold scheme.

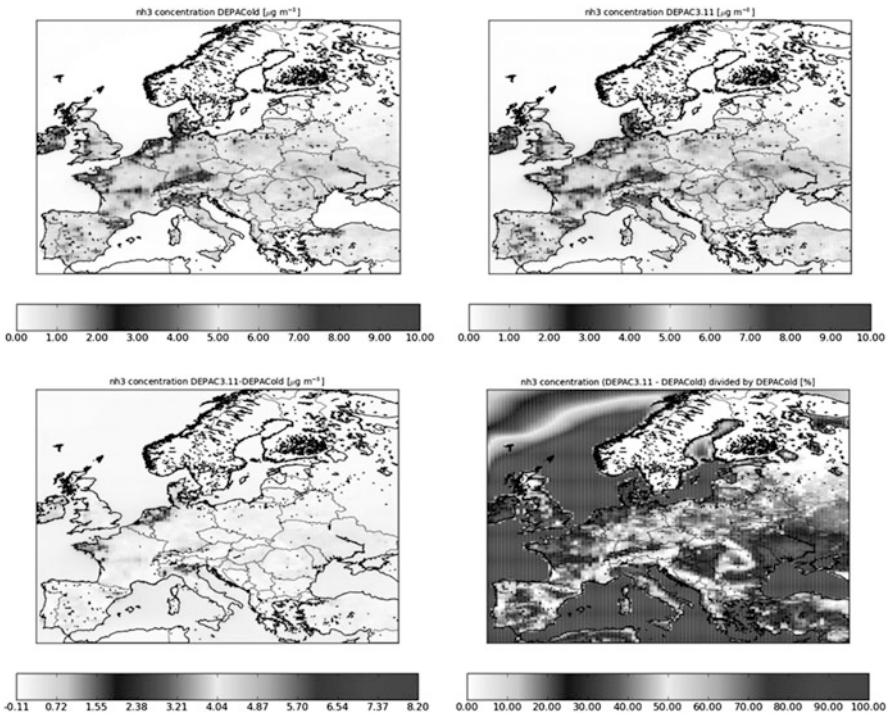

Fig. 52.1 The yearly average NH_3 concentrations as calculated by the LOTOS-EUROS model with the old DEPAC (*upper left*) and DEPAC3.11 module (*upper right*) for the year 2007. The *lower left figure* shows the absolute difference and the *lower right figure* shows the relative difference between the two model calculations [4]

52.3 Surface-Atmosphere Exchange

Figure 52.2 shows absolute differences in yearly dry NH_x, wet NH_x and total NH_x deposition (upper left, upper right and lower left respectively) and the relative difference (%) in total NH_x deposition (lower right) between DEPAC3.11 and DEPACold as calculated with the LOTOS-EUROS model for the year 2007.

The figure shows that the total NH_x deposition is mainly determined by the dry NH_x deposition, while reduced dry NH_x deposition is partly compensated by increased wet NH_x deposition due to the higher ambient air concentrations. The largest reductions in the total NH_x deposition (>200 mol NH_x ha^{-1} reduction) are calculated in agricultural source areas, while the largest increases (up to about 100 mol NH_x ha^{-1}) are found in remote nature areas. The lower right figure shows that the introduction of the compensation point for water leads to a relatively large reduction in the NH_x deposition over sea. This figure also shows that more remote

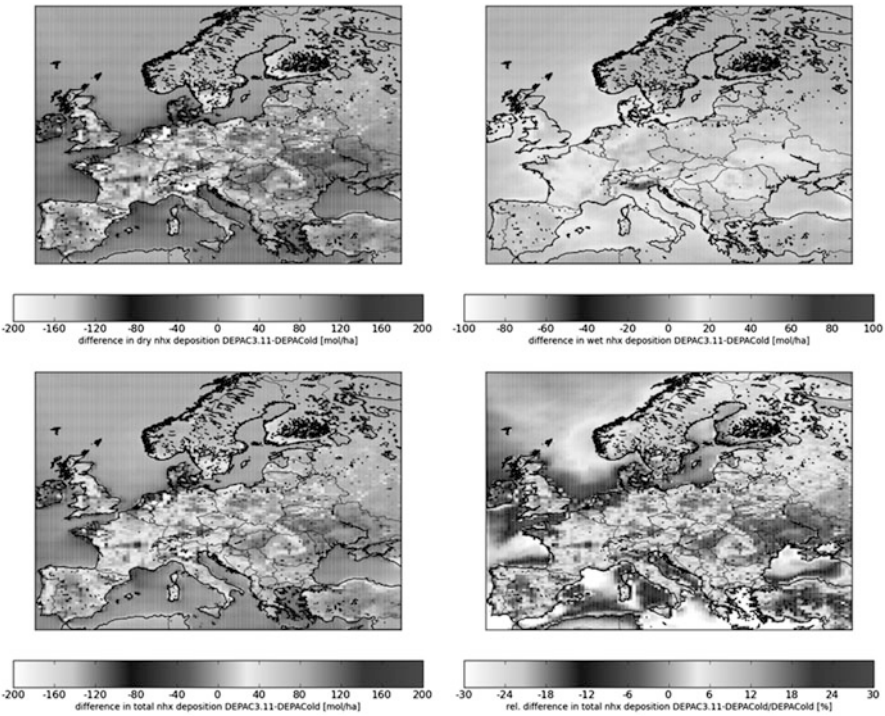

Fig. 52.2 Absolute differences (mol/ha) in yearly average dry NH_x, wet NH_x and total NH_x deposition (*upper left*, *upper right* and *lower left* respectively) and relative difference (%) in total NH_x deposition (*lower right*) between DEPAC3.11 and DEPACold as calculated by the LOTOS-EUROS model for the year 2007 [4]

areas in Scandinavia receive about 20 % more NH_x. This is because the lifetime of NH_3 increases due to reduced deposition elsewhere and due to the conversion of NH_3 into NH_4^+ aerosol, which can travel over much larger distances than NH_3.

52.4 Validation with Measurements

Figure 52.3 shows a comparison of the model runs with DEPACold and DEPAC3.11 with the available total ammonia concentration measurements (ammonia and particulate ammonium) at 33 EMEP stations in 2007. It is shown that the model generally underestimates the concentrations at the 33 EMEP stations. An increasing underestimation is present with increasing measured ammonia levels. The three points with the highest observed total ammonia concentrations are Jerczew (PL), Payerne (CH) and Els Thorms (ES), of which the latter two are located at elevation heights larger than 400 m with some agricultural activity in their surroundings. Although the ammonia levels that are calculated by the model run with DEPAC3.11

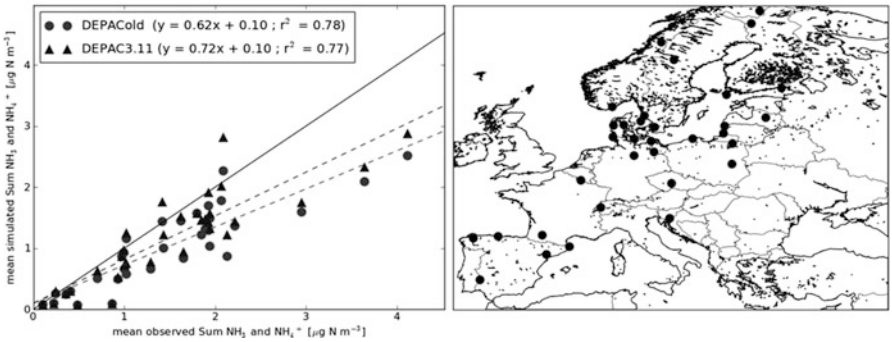

Fig. 52.3 Comparison of the modeled total ammonia concentrations (sum of ammonia and particulate ammonium modeled with 'DEPACold' (*red*) and 'DEPAC3.11' (*blue*)) with the EMEP measurement stations (n = 33) in Europe in 2007 [4] (Color figure online)

are better, the scatter between the measurements and the model calculations remains the same. The EMEP network contains a range of station types with locations in remote areas as well as in areas with intense agricultural. Hence, the limited number of sites can not cover the range of conditions present in Europe. A validation with other datasets is planned.

References

1. Schaap M, Timmermans RMA, Roemer M, Boersen GAC, Builtjes PJH, Sauter FJ, Velders GJM, Beck JP (2008) The LOTOS–EUROS model: description, validation and latest developments. Int J Environ Pollut 32(2):270–290
2. Van Zanten MC, Sauter FJ, Wichink Kruit RJ, Van Jaarsveld JA, Van Pul WAJ (2010) Description of the DEPAC module: dry deposition modelling with DEPAC_GCN2010. RIVM report 680180001/2010, Bilthoven, p 76
3. Wichink Kruit RJ, Van Pul WAJ, Sauter FJ, Van den Broek M, Nemitz E, Sutton MA, Krol M, Holtslag AAM (2010) Modeling the surface-atmosphere exchange of ammonia. Atmos Environ 44:945–957
4. Wichink Kruit RJ, Schaap M, Sauter FJ, Van Zanten MC, Van Pul WAJ (2012) Modelling the distribution of ammonia across Europe including bi-directional surface-atmosphere exchange. Biogeosci Discuss 9:4877–4918

Questions and Answers

Questioner Name: M. Sofiev

Q: Did you use the EMEP wet deposition monitoring data? This network may be the major evaluation data source for your study.

A: That's true. We will include this data source in a further model inter-comparison study within the ÉCLAIRE project.

Questioner Name: T. Dore

Q: Comparison of modeled ammonia concentrations with measurements at nature reserves in the UK also shows an over-estimate in modeled concentrations. Could reducing your model grid resolution successfully resolve source (agricultural) regions from sink (nature reserve) regions?
A: Many studies have shown that the model resolution is extremely important in areas where local sources are present and therefore we expect that increasing the model resolution will definitely improve the correspondence with the measurements. Especially in the Netherlands, the size of the nature areas is generally much smaller than the size of the grid cells. Therefore, a grid cell in the model will generally include some emissions of NH_3 from agricultural sources, which are spread over the whole grid cell, thus overestimating the amount of NH_3 in the nature areas. By increasing the model resolution, this problem might be reduced.

Chapter 53
Multiscale Air Quality with the NMMB/BSC Chemical Transport Model

Oriol Jorba, Carlos Pérez, Karsten Haustein, Zavisa Janjic, José MaríaBaldasano, Donald Dabdub, Alba Badia, and Michele Spada

Abstract The NMMB/BSC Chemical Transport Model (NMMB/BSC-CTM) is a new air quality modeling system under development at the Earth Sciences Department of BSC in collaboration with several research institutions. It is an on-line model based on the NCEP new global/regional Nonhydrostatic Multiscale Model on the B grid (NMMB). NMMB is an evolution of the WRF-NMMe model extending from meso to global scales. Its unified nonhydrostatic dynamical core allows regional and global simulations and forecasts. NMMB/BSC-CTM incorporates an aerosol module that simulates the global life cycle of mineral dust, sea salt, black carbon and organic carbon, and sulfate. Additionally, a gas-phase chemistry module has been implemented.

Keywords NMMB/BSC-model • Global modeling • Regional modeling • Aerosols

O. Jorba (✉) • K. Haustein • A. Badia • M. Spada
Earth Sciences Department, Barcelona Supercomputing Center (BSC), Barcelona, Spain
e-mail: oriol.jorba@bsc.es

C. Pérez
Earth Institute at Columbia University, NASA, GISS, New York, USA

Z. Janjic
NOAA/NWS/National Centers for Environmental Prediction, Camp Springs, MD, USA

D. Dabdub
Department of Mechanical and Aerospace Engineering, University of California, Irvine, USA

J. MaríaBaldasano
Earth Sciences Department, Barcelona Supercomputing Center (BSC), Barcelona, Spain

Environmental Modeling Laboratory, Technical University of Catalonia, Barcelona, Spain

D.G. Steyn et al. (eds.), *Air Pollution Modeling and its Application XXII*,
NATO Science for Peace and Security Series C: Environmental Security,
DOI 10.1007/978-94-007-5577-2_53,

53.1 Introduction

A new integrated meteorology-air quality model is under development at the Earth Sciences Department of the Barcelona Supercomputing Center (BSC). The model, the NMMB/BSC Chemical Transport Model (NMMB/BSC-CTM), is an online chemical weather prediction system for short-term applications from global to sub-synoptic scales. The system incorporates a tropospheric gas-phase photochemical module and an aerosol module accounting for the relevant global aerosols. Meteorology, gas-phase and aerosol processes are on-line coupled in order to incorporate feedback interactions among modules. In this contribution, the state of development of NMMB/BSC-CTM model and results at both global and regional scale are presented.

53.2 Model Development

Developments are focused on the coupling of aerosol and gas-phase processes within the meteorological driver NMMB.

53.2.1 Meteorological Driver

The Nonhydrostatic Multiscale Model on the B grid (NMMB; [4]) is the new unified atmospheric model developed at the National Centers for Environmental Prediction (NCEP) for a broad range of spatial and temporal scales. It evolves from the regional WRF-NMMe model. The regional NMMB is the regional North American Mesoscale (NAM) model in operations at NCEP. Isotropic horizontal finite volume differencing is employed so a variety of basic and derived dynamical and quadratic quantities are conserved (e.g., energy, enstrophy). The global model is constructed in the latitude-longitude grid with polar filtering and regional applications use the rotate longitude-latitude system. Advection of passive tracers is Eulerian, positive definite and monotone. The reader is referred to Janjic et al. [4] for a further description of the model.

53.2.2 Aerosol Module

An aerosol module for the relevant global aerosols (e.g., mineral dust, sea salt, black carbon, organic carbon and sulfate) is on-line coupled within the NMMB/BSC-CTM. From all the aerosols, the mineral dust scheme is inherited from the NMMB/BSC-Dust model [5]. The sea salt, black carbon, organic carbon and sulfates are currently under development.

The Dust module includes eight dust size bins, within each transport bin, dust is assumed to have time-invariant, subbin lognormal distribution. The dust emission scheme takes into account the effects of saltation and sandblasting, soil moisture and viscous diffusion close to the ground. Dust shortwave and long wave radiative feedbacks on meteorology are fully taken into account through the coupling of dust aerosols with the RRTM SW/LW radiation scheme of NMMB [5].

The sea-salt aerosol is implemented through eight bins in the dry radius interval (0.1–15 μm) to describe mass concentrations and optical depth. A sub-bin lognormal approach is assumed to calculate the optical properties of the particles. An open-ocean emission scheme is implemented, accounting for bubble-bursting and spume production. The water uptake is taken into account by using prescribed growth factors for different relative humidity values. The parameterizations of the aerosol processes affected by the water-uptake (i.e., sedimentation, dry deposition, wet deposition, etc.) have been extended to wet particles from those implemented in the dust module of NMMB/BSC-CTM [6].

53.2.3 Gas-Phase Chemistry Module

The gas-phase module simulates the tropospheric chemistry of ozone and is coupled with a simplified linear scheme of the stratospheric chemistry of ozone. Thus, a fully consistent balance in O3 concentrations is achieved within the troposphere on global configurations. The modular structure of the system allows configuring the model with feedbacks among the different processes implemented (e.g., radiation-aerosols-gases, photolysis-gases-aerosols). Chemical species are advected and mixed at the corresponding time steps of NMMB tracers using the same numerical scheme as the meteorological driver. The Carbon Bond 2005 (CB05) chemical mechanism has been implemented. The photolysis scheme is based on the Fast-J scheme, coupled with physics of each model layer (e.g., aerosols, clouds, absorbers as ozone). The dry deposition scheme follows the deposition velocity analogy for gases. The Wesley scheme is implemented to compute the canopy resistance in the dry-deposition process. The cloud-chemistry processes are included in the system considering both sub-grid and grid-scale processes following Foley et al. [2]. A linear ozone photochemistry parameterization for use in upper troposphere and stratosphere, Cariolle v2.9, is implemented within NMMB/BSC-CTM.

An emission process allows the coupling of a vast variety of emission inventory sources (e.g., POET, RETRO, EDGAR, MACC, EMEP, HERMES) with the model. Natural emissions are computed on-line. Currently, only biogenic emissions are implemented through the coupling of the MEGAN model within NMMB/BSC-CTM.

53.3 Results

The mineral dust module has been extensively evaluated at global and regional scales on an annual basis [3, 5]. In this section a preliminary evaluation of the gas-phase chemistry of NMMB/BSC-CTM, configured at both global and regional scale, is briefly presented. The global simulation is configured at $1° \times 1.4°$ and 64 vertical levels up to 0 hPa and the regional domain covers Europe at 12 km × 12 km and 24 vertical levels up to 100 hPa. Both configurations use the same physics and chemistry. Chemical boundary conditions for the regional run are obtained from the global simulation. POET emissions are used in the global run and EMEP emissions for the regional configuration.

Table 53.1 and Fig. 53.1 present a brief summary of the statistics computed for August 2004 with both global and regional runs. Background stations from EMEP network are used. For the global results, only stations below 1,000 m are used. Results show how the coupling of the model from global to regional scales have a positive impact on the results, as expected. The correlation of the ozone concentrations is 0.51 on average for August. However, several stations present a correlation over 0.6–0.7. The MNGE and MNBE for both configurations fall within the recommended values of EPA. The variability on the model and observations is highly improved at high resolution. In this sense, the daily ozone cycle is qualitative and quantitatively well captured in most of the stations. Downscaled model results

Table 53.1 Ozone evaluation against EMEP European stations for global and regional runs on August 2004

Run	Corr.	MB ($\mu g/m^3$)	RMSE ($\mu g/m^3$)	MNBE (%)	MNGE (%)	MFB (%)	MFE (%)
Global	0.33	−12.9	41.4	−11.5	30.9	−21.3	36.7
Regional	0.51	0.7	23.1	2.1	17.2	−0.3	17.1

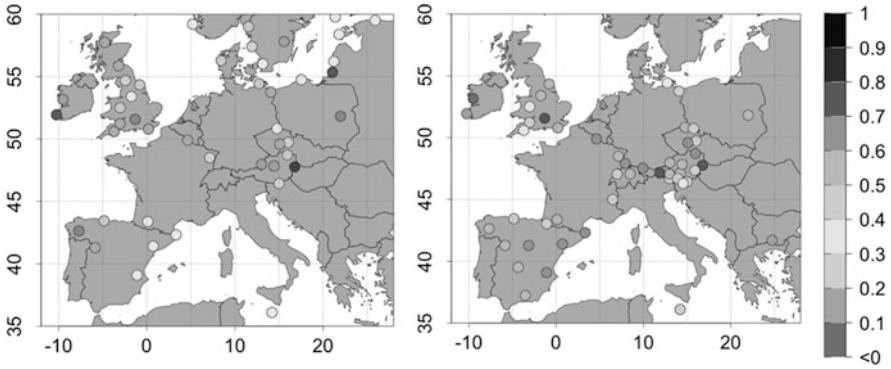

Fig. 53.1 Correlation r over Europe for the global (*left panel*) and regional (*right panel*) runs for August 2004

over Spain and Central Europe present a very good agreement with observations. This preliminary evaluation provides general overview of the capabilities of the on-line multi scale modeling system developed.

53.4 Conclusions

The NMMB/BSC-CTM model is a powerful tool for air quality tropospheric studies from global to sub-synoptic scales. The NMMB/BSC-CTM is expected to start providing pre-operational dust forecasts both at global and regional scale within the Sand and Dust Storm-Warning Assessment System (http://sds-was.aemet.es/).

Acknowledgments This work is funded by grants CGL2008-02818-CLI and CGL2010-19652 of the Spanish Ministry of Economy and Competitiveness. All the numerical simulations were performed with the Mare Nostrum supercomputer hosted by the BSC.

References

1. Chin M, Ginoux P, Kinne S, Torres O, Holben BN, Duncan BN, Martin RV, Logan JA, Higurashi A, Nakajima T (2002) Tropospheric aerosol optical thickness from the GOCART model and comparisons with satellite and Sun photometer measurements. J Atmos Sci 59:461–483
2. Foley K et al (2010) Incremental testing of the community multiscale air quality (cmaq) modeling system version 4.7. Geosci Model Dev 3:205–226
3. Haustein K et al (2011) Atmospheric dust modeling from meso to global scales with the online NMMB/BSC-dust model – part 2: experimental campaigns in Northern Africa. Atmos Chem Phys Discuss 11:30273–30331
4. Janjic Z et al (2011) A class of conservative fourth-order advection schemes and impact of enhanced formal accuracy on extended-range forecasts. Mon Weather Rev 13(5):1556–1568
5. Pérez C et al (2011) Atmospheric dust modeling from meso to global scales with the online NMMB/BSC-dust model: part 1: model description, annual simulations and evaluation. Atmos Chem Phys 11:13001–13027
6. Spada M et al (2012) Implementation of a sea-salt module within the NMMB/BSC Chemical Transport Model: global simulations and comparisons with observations. In 2012 EGU General Assembly, Vienna, Austria, 22–27 April 2012
7. Zender CS, Bian H, Newman D (2003) Mineral Dust Entrainment And Deposition (DEAD) model: description and 1990s dust climatology. J Geophys Res 108(D14):4416. doi:10.1029/2002JD002775

Questions and Answers

Questioner Name: Pavel Kishcha

Q: Could you elaborate on hygroscopic properties of SSA included in your model?
A: The SSA in the model is assumed as pure hydrophilic, and the hygroscopic factors are calculated following Zender et al. [7]. All the aerosol processes

(dry deposition, wet deposition, sedimentation, convective mixing) have been extended from the dust module [5], while the aerosol water-uptake has been introduced as a specific process for SSA. The water uptake is parameterized following Chin et al. [1].

Q: With respect to dust, did you compare DREAM and NMMB/BSC-Dust model results? What is better?

A: The new NMMB/BSC-Dust model performs better in emission regions. A more physically based emission scheme has been implemented in the model (see [5]), and the results of the system have improved compared with BSC-DREAM8b. Indeed, a positive impact on the dust transport is identified. The Northern Africa-Middle East-Europe Regional Center of the WMO Sand and Dust Storm Warning Advisory and Assessment System is providing compared dust forecast of different models. Quantitative evaluation is performed there for several dust models, among them several versions of the DREAM model and NMMB/BSC-Dust.

Chapter 54
Sea-Salt Aerosol Forecasts Over the Mediterranean Sea Evaluated by Daily Measurements in Lampedusa from 2006 to 2010

Pavel Kishcha, Boris Starobinets, Roberto Udisti, Silvia Becagli, Alcide di Sarra, Slobodan Nickovic, and Pinhas Alpert

Abstract Detailed knowledge of sea-salt aerosol (SSA) space-time variations is essential for a deeper understanding of the process of SSA loading in the atmospheric boundary layer. In order to reproduce variability of SSA concentrations over the Mediterranean Sea, the regional DREAM-Salt model has been running daily at Tel-Aviv University since February 2006 (http://wind.tau.ac.il/salt-ina/salt.html). The model performance in producing accurate SSA forecasts over the Mediterranean Sea was evaluated using a 5-year record (2006–2010) of daily SSA mass concentration measurements at the island of Lampedusa. Model-vs.-measurement comparisons showed a distinct dependence of model performance on wind direction. On average, for wind direction from 30° to 300°, the model performance was quite acceptable. It was characterized by a relatively high correlation of over 0.65 and a rather small mean bias. For north winds (0°–30°, and 300°–360°), some discrepancy between modeled and measured SSA concentrations was observed. This was characterized by the model underestimation of SSA measurements and a rather low correlation between model data and measurements. Probably, for north winds, SSA production in the surf zone, located in the vicinity of the monitoring site, contributed to observed SSA concentrations.

P. Kishcha (✉) • B. Starobinets • P. Alpert
Department of Geophysical, Atmospheric, and Planetary Sciences, Tel-Aviv University, Tel-Aviv, Israel
e-mail: pavel@cyclone.tau.ac.il

R. Udisti • S. Becagli
Department of Chemistry, University of Florence, Florence, Italy

A. di Sarra
National Agency for New Technologies, Energy, and Economic Sustainable Development, Rome, Italy

S. Nickovic
World Meteorological Organization, Geneva, Switzerland

D.G. Steyn et al. (eds.), *Air Pollution Modeling and its Application XXII*,
NATO Science for Peace and Security Series C: Environmental Security,
DOI 10.1007/978-94-007-5577-2_54,

Keywords Marine aerosol • Sea-salt aerosol forecast • Aerosol modeling

54.1 Introduction

Marine aerosol is mechanically produced by breaking waves during whitecap formation [6]. As soon as SSA is introduced by wind into the boundary layer, SSA can contribute to the intensity of Mediterranean storms by changes in the energy balance, as it does in intensifying tropical hurricanes [2]. In order to reproduce variability of SSA concentrations over the Mediterranean Sea, the regional DREAM-Salt model has been running daily at Tel-Aviv University since February 2006. In our previous studies, the model performance over the open sea was indirectly verified by comparing modeled SSA concentrations with wave height measurements collected by the ODAS Italia one buoy and the Llobregat buoy in the Western Mediterranean [5]. In addition, modeled concentrations were compared directly with SSA measurements taken at the island of Lampedusa in the Central Mediterranean [4]. In the current study, the DREAM-Salt model performance in simulating the main temporal features of SSA distribution was evaluated against a long-term record of daily SSA measurements taken at the Mediterranean island of Lampedusa over the 5-year period 2006–2010.

54.2 Sea-Salt Aerosol Model and Measurements

The DREAM-Salt prediction system has been producing daily forecasts of 3-D distribution of sea-salt aerosol concentrations over the Mediterranean model domain 20°W–45°E, 15°N–50°N [4, 7]. The model incorporates parameterizations of all major phases of the atmospheric sea-salt aerosol cycle such as: diffusion, advection, gravitational settling, and wet removal of sea-salt aerosols. DREAM-Salt has 0.3° horizontal resolution, and 24 vertical levels. And eight particle size bins ranging from 1 to 8 μm. Forecasts are made once every day, starting from the 12:00 UTC objective analyses and providing forecasts up to 72 h ahead. The NCEP/Eta regional atmospheric model drives the aerosol. The sea-salt emission scheme defines the lower boundary condition using the source function of Erickson et al. [3]. In our model setup, we used $N = 8$ particle size bins (1.0–1.5, 1.5–2.5, 2.5–3.5, 3.5–4.5, 4.5–5.5, 5.5–6.5, 6.5–7.5, and 7.5–8.5 μm). The mass going into each of the eight particle size bins is in percentages 0.5, 1.5, 6.0, 11.0, 16.0, 19.0, 21.0, and 25.0 of the total source, respectively. Note that the dependence of SSA productions and size distributions on relative humidity was not included in the model.

In order to evaluate the model performance over the Mediterranean Sea, numerical simulations of sea-salt aerosol (SSA) were compared with sea-salt ground-based measurements taken at the tiny Mediterranean island of Lampedusa, Italy, during the

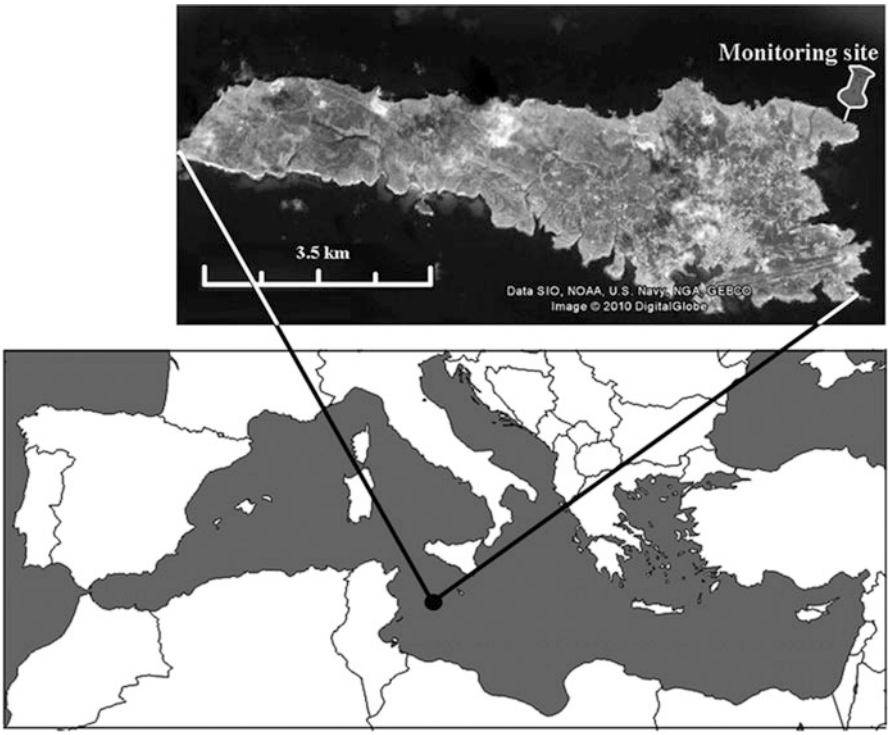

Fig. 54.1 A map of the Mediterranean Sea with a map of the island of Lampedusa with the monitoring site (*the grey place mark*)

5-year period 2006–2010. Lampedusa, which measures several kilometers across, is located far from any land areas and is characterized by clean air without industrial pollution. The monitoring site is located at approximately 10 m from the north-east coastline of Lampedusa, at 50 m elevation (Fig. 54.1). SSA measurements were based on chemical analysis of PM10 measurements on a daily basis. SSA concentration was calculated as the sum of the weight of $ssNa^{+}$ (i.e. sea salt Na^{+}), Cl^{-}, $ssCa^{2+}$, and $ssMg^{2+}$ [1].

54.3 Results and Discussion

Shown in Figs. 54.2a and c, polar diagrams of measured SSA mass concentration and wind speed reveal their maximum under north winds. This can be explained by the location of the monitoring site near the northern coast. Strong north winds create a surf zone, within which sea-waves, approaching the coastline, start breaking. SSA production in the surf zone, located in the vicinity of the monitoring site, can

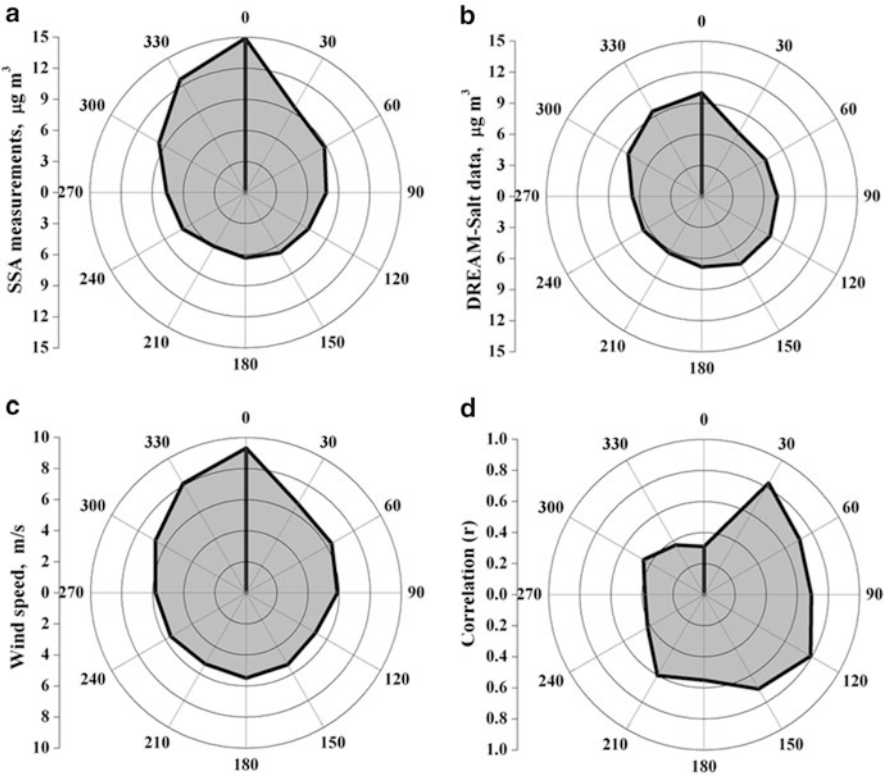

Fig. 54.2 Polar diagrams of 5-year (2006–2010) mean values of (**a**) measured SSA mass concentration, (**b**) DREAM-Salt modeled SSA concentration, and (**c**) measured wind speed, as a function of wind direction. (**d**) is the polar diagram of correlation between daily measured and modeled SSA concentrations over the 5-year period under consideration as a function of wind direction. All diagrams are *centered* at the monitoring site in Lampedusa

contribute to observed SSA concentrations. Our regional model could not take into account the effects of surf zones; this results in some model underestimation of measured SSA concentrations under north winds (Figs. 54.2a, b).

Moreover, model-vs.-measurement comparisons on a daily basis at Lampedusa over the 5-year period under consideration showed that the correlation between model data and measurements depended on wind direction (Fig. 54.2d). On average, for wind direction from 30° to 300°, the model performance was characterized by a relatively high correlation of over 0.65. For north winds (0°–30°, and 300°–360°), a rather low correlation between model data and measurements was observed. This was because of the aforementioned additional source of SSA aerosol production in the surf-zone, which was not included in the model.

The island of Lampedusa was chosen for the model evaluation because it was considered to have open sea measurement conditions. However, based on our

analysis of long-term SSA measurements during the period 2006–2010, it was found that this was not the case. Despite the relatively small size of Lampedusa of approximately several kilometers across, measurement conditions there are not exactly as those in the open sea, because SSA concentrations depend on wind direction.

References

1. Becagli S, Ghedini C, Peeters S et al (2011) MBAS and LAS in the Mediterranean coastal aerosols: sources and transport processes. Atmos Environ 45:6788–6801
2. Emanuel K (2003) A similarity hypothesis for air-sea exchange at extreme wind speeds. J Atmos Sci 60:1420–1428
3. Erickson DJ, Merril JT, Duce RA (1986) Seasonal estimates of global atmospheric sea-salt distribution. J Geophys Res 91:1067–1072
4. Kishcha P, Nickovic S, Starobinets B, di Sarra A, Udisti R, Becagli S, Sferlazzo D, Bommarito C, Alpert P (2011) Sea-salt aerosol forecasts compared with daily measurements at the island of Lampedusa (Central Mediterranean). Atmos Res. doi:10.1016/j.atmosres.2010.12.021
5. Kishcha P, Starobinets B, Bozzano R, Pensieri S, Canepa E, Nickovic S, di Sarra A, Udisti R, Becagli S, Alpert P (2012) Sea-salt aerosol forecasts compared with wave height and sea-salt measurements in the open sea. In: Air pollution modeling and its applications XXI, Chapter 51, pp 299–303. Springer, Dordrecht. doi: 10.1007/978-94-007-1359-8_51
6. Lewis ER, Schwartz SE (2004) Sea salt aerosol production: mechanisms, methods, measurements, and models—a critical review. Geophysics monograph series, vol 152. AGU, Washington, DC, 412 p
7. Nickovic S, Janjic Z I, Kishcha P, Alpert P (2007). Model for simulation of the sea salt aerosol atmospheric cycle. Research Activities in Atmospheric Ocean Modelling. WMO, CAS/JSC WGNE, Geneva, Sect. 20, pp 19–20

Questions and Answers

Questioner Name: Douw G. Steyn

Q: You mentioned the possibility of a sea-breeze at Lampedusa having an effect not captured in your model. I think Lampedusa is too small an island to generate a true sea-breeze. So do the data show existence of a sea-breeze?
A: Yes. In general, there are two requirements for sea-breeze formation. First, the natural wind flow due to high- and low-pressure systems must be weak, and the middle of an anticyclone is, therefore, an ideal region for this to occur. Second, the land must be significantly warmer than the sea by approximately 5 °C or more. These two requirements are fulfilled in Lampedusa in the summer months, when sea-breezes take place. Note that sea-breeze winds are relatively weak over such a small island as Lampedusa, and can not produce high sea-salt aerosol concentrations. However, these sea-breeze winds are capable of carrying sea-salt aerosol particles produced by breaking waves near the coastline to the monitoring site. Due to its coarse resolution, our model can not take sea-breeze processes into consideration.

Chapter 55
An Enhanced Sub-grid Scale Approach to Characterize Air Quality Impacts of Aircraft Emissions

Saravanan Arunachalam, Matthew Woody, Jeffrey Rissman, Francis Binkowski, Hsi-Wu Wong, Shantanu Jathar, and Allan Robinson

Abstract We present an overview of results from an enhanced sub-grid scale approach to characterize air quality impacts of aircraft emissions at the Hartsfield-Jackson Atlanta International airport (in the U.S.) for June and July 2002 using an adaptation of CMAQ called the Advanced Modeling System for Transport, Emissions, Reactions, and Deposition of Atmospheric Matter (AMSTERDAM). Aircraft emissions during the landing and takeoff cycle (LTO) and below 3,000 m were represented as plume-in-grid (PInG) emissions using AMSTERDAM's PInG treatment. Initial results from CMAQ-AMSTERDAM focusing on impacts from aircraft emissions to inorganic $PM_{2.5}$ and total $PM_{2.5}$ indicated aircraft increased average total $PM_{2.5}$ concentrations by up to 235 ng m^{-3} near the airport and by 1–7 ng m^{-3} throughout the Atlanta metro area. However, aircraft reduced concentrations by 0.5–1 ng m^{-3} downwind of the airport, attributable to reductions in sulfate aerosol. The subgrid-scale concentrations were an order of magnitude higher than the grid-based concentrations due to aircraft. In an earlier study when aircraft emissions were modeled by CMAQ as traditional point sources within

S. Arunachalam (✉) • M. Woody • J. Rissman • F. Binkowski
Institute for the Environment, University of North Carolina at Chapel Hill,
137 E. Franklin St., #645, Chapel Hill, NC 27599-6116, USA
e-mail: sarav@email.unc.edu

H.-W. Wong
Aerodyne Research, Inc, Center for Aerothermodynamics, Billerica, MA 01821, USA

S. Jathar
Department of Engineering and Public Policy, Carnegie Mellon University, Pittsburgh,
PA 15213, USA

A. Robinson
Department of Engineering and Public Policy, Carnegie Mellon University, Pittsburgh,
PA 15213, USA

Department of Mechanical Engineering, Carnegie Mellon University, Scaife Hall 420,
Pittsburgh, PA 15213, USA

D.G. Steyn et al. (eds.), *Air Pollution Modeling and its Application XXII*,
NATO Science for Peace and Security Series C: Environmental Security,
DOI 10.1007/978-94-007-5577-2_55,

the ATL airport grid cell, we showed that modeled secondary organic aerosol (SOA) concentrations increased by 2 % due to primary organic aerosol (POA) emissions from aircraft, which provided additional surface area for SOA to partition onto. We now present results from additional modeling work performed to a) enhance organic treatment in a 1-D aerosol microphysics model used to provide engine-specific emissions parameters for CMAQ, and b) examine aircraft's impacts on secondary organic aerosol concentrations using the volatility basis set (VBS) within CMAQ-AMSTERDAM to represent the formation and aging of organic aerosols. Parameterization for the VBS components was determined using current and ongoing field study measurements, chamber studies, and box models specific to aircraft SOA formation, which showed that non-traditional precursors of SOA (NTSOA) were a much higher contributor to aircraft-specific SOA than previously understood.

Keywords CMAQ • AMSTERDAM • PInG • Aviation Emissions • $PM_{2.5}$

55.1 Introduction

Given the projected future growth of aircraft usage and emissions, it is critical to understand the effects of aircraft emissions on air quality. However, traditional modeling techniques simplify the representation of aircraft emissions, using a 1-dimensional source treatment. Adding additional uncertainty, the First Order Approximation 3 (FOA3) [1], the typical method used to estimate $PM_{2.5}$ emissions from aircraft, has known limitations, particularly in regards to POA. Here we present an investigation of the simulated impacts of aviation emissions when treated at the sub-grid scale as PInG emission sources, focusing on impacts to $PM_{2.5}$ and provide future considerations to enhance predictions of organic contributions.

55.2 Modeling Approach

CMAQ-AMSTERDAM [2] was used to estimate the effects of aircraft emissions on air quality at and around the Hartsfield-Jackson Atlanta International Airport (ATL). Modeling simulations were performed for June and July 2002 at a 4-km horizontal grid resolution with 19 vertical layers. Meteorological inputs were based on 2002 conditions and generated using MM5. Non-aviation emissions were estimated using the EPA's 2002 NEI and excluded the NEI reported emissions from commercial aircraft.

Aircraft emissions were estimated for Landing and Takeoff (LTO) cycle activity of commercial aircraft below 3,000 ft based on 2002 historical flight activity (CSSI, 2007). For each commercial aircraft engine, mode specific (taxiing, takeoff, approach and landing) LTO emission factors for total organic gases (TOG), NO_x,

CO, and SO_2 were taken from the ICAO database [3]. TOG was speciated using the recommend FAA and EPA aircraft speciation profile [4]. PM emission factors of elemental carbon, POA, and sulfate aerosol were estimated using the FOA3 methodology [1]. Computed emission factors were applied to annual activity data to produce an annual inventory. This annual inventory was allocated in time and space using 51 PInG emitter sources (8 takeoff, 20 climbout, 20 approach, and 3 taxi) which were mapped onto 4 runways at ATL (2 designated for landing, 2 for takeoff) to represent typical takeoff and landing trajectories.

Three additional model scenarios were performed over a 2-day period (June 6 and 7, 2002) to analyze sensitivities to varying the number of PInG emitter sources used to represent aircraft. In these three scenarios, total emissions were identical to the initial PInG scenario but the number of PInG emitter locations was increased from 51 to 102 (2×), 153 (3×), and 202 (∼4× and currently the maximum allowable within CMAQ-AMSTERDAM).

55.3 Results

CMAQ-AMSTERDAM results indicated that, on a 2 month average basis, aircraft emissions increased $PM_{2.5}$ concentrations by 235 ng m^{-3}at the ATL airport when PInG was used, compared to 217 ng m^{-3} without PInG. The PInG treatment also predicted higher contributions from aircraft emissions to $PM_{2.5}$ downwind of ATL compared to the non-PInG treatment. Differences in impacts between PInG and non-PInG greater than 2 ng typically occurred within 50-km of the airport but extended as far as 75-km downwind. In general, the higher predicted $PM_{2.5}$ contributions were attributable to inorganic $PM_{2.5}$ species.

Examining hourly results for June 6, 2002, grid based contributions with PInG exhibited a higher average but lower range of values at the airport compared to without PInG (Fig. 55.1). However, the maximum subgrid scale concentrations in the puffs were an order of magnitude higher than the grid averages. Furthermore, puffs tended to have higher concentrations downwind than near the airport source, and their concentrations were higher aloft than in the surface layer (Fig. 55.1).

Increasing emitters by 2× and 3× increased contributions to $PM_{2.5}$ compared to the original PInG simulation. These increased contributions were similar to differences when using PInG vs. non-PInGand suggest that doubling or tripling the number of emitters enhances the impacts of using a PInG treatment for aircraft. Conversely, increasing emitters by approximately 4xloweredcontributions from aircraft emissions compared to the original PInG simulation. This is possibly attributable to an increase in the number of plumes, which are diluted and more readily merge into the grid, reducing PInG effects. It should be noted that with each increase in the number of emitter locations used (1× to 2×, 2× to 3×, etc.), model run time increased by approximately 15 %.

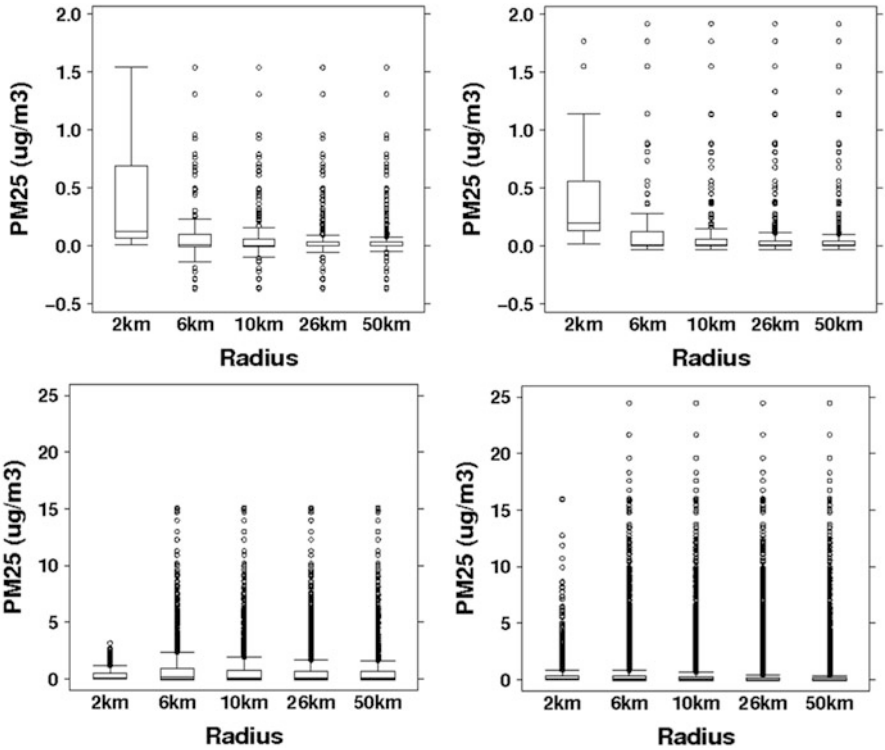

Fig. 55.1 Hourly grid based contributions from aircraft without PInG (*top left*) and with PInG (*top right*) and sub-grid scale contributions at the surface [below 36 m] (*bottom left*) and aloft [above 36 m] (*bottom right*) on July 6, 2002

55.4 Discussion

This work provides a framework to model aircraft emissions as PInG sources using CMAQ-AMSTERDAM at ATL. Ongoing efforts include coupling the existing CMAQ-AMSTERDAM framework with the one-dimensional Aerosol Dynamics Simulation Code (ADSC) [5] model and the VBS approach [6] to modeling aerosols. ADSC provides near field predictions of engine specific organic aerosol emissions for CMAQ-AMSTERDAM. The VBS portion predicts SOA formation and partitioning with aircraft specific parameterizations based on current and ongoing field study measurements [7], chamber studies, and box models [8]. Initial testing of the contributions of aircraft emissions to SOA using VBS in CMAQ is underway. Preliminary results using this VBS parameterization have indicated that the use of VBS increases SOA production from aircraft emissions, particularly downwind of the airport while also improving model performance for both OC and $PM_{2.5}$ at two monitoring locations near the airport.

Acknowledgements This work was funded by PARTNER under a grant to UNC. Opinions, findings, conclusions and recommendations expressed in this material are those of the author(s) and do not necessarily reflect the views of PARTNER sponsoring organizations. PARTNER is funded by FAA, NASA, Transport Canada, DOD &EPA.

References

1. Wayson RL, Fleming GG, Iovinelli R (2009) Methodology to estimate particulate matter emissions from commercial aircraft engines. J Air Waste Manage Assoc 59:91–100
2. Karamchandani P et al (2010) Development and application of a parallelized version of the advanced modeling system for transport, emissions, reactions and deposition of atmospheric matter (AMSTERDAM): 1. Model performance evaluation and impacts of plume-in-grid treatment. Atmos Pollut Res 1(4):260–270
3. ICAO (2010) International Civil Aviation Organization Aircraft Engine Emissions Databank. Available at: http://www.caa.co.uk/default.aspx?catid=702
4. USEPA (2009) Recommended best practice for quantifying speciated organic gas emissions from aircraft equipped with turbofan, turbojet, and turboprop engines. EPA-420-R-09-901
5. Wong H-W, Yelvington PE, Timko MT, Onasch TB, Miake-Lye RC (2008) Microphysical modeling of ground-level aircraft-emitted aerosol formation: roles of sulfur-containing species. J Propuls Power 24(3):590–602
6. Donahue NM, Robinson AL, Pandis SN (2006) Coupled partitioning, dilution, and chemical aging of semivolatile organics. Environ Sci Technol 40:2635–2643
7. Miracolo MA, Hennigan CJ, Ranjan M, Nguyen NT, Gordon TD, Lipsky EM, Presto AA, Donahue NM, Robinson AL (2011) Secondary aerosol formation from photochemical aging of aircraft exhaust in a smog chamber. Atmos Chem Phys 11:4135–4147
8. Jathar SH, Miracolo MA, Presto AA, Adams PJ, Robinson AL (2012) Modeling the formation and properties of traditional and non-traditional secondary organic aerosol: problem formulation and application to aircraft exhaust. Atmos Chem Phys Discuss 12:9945–9983. doi:10.5194/acpd-12-9945-2012

Questions and Answers

Questioner Name: Stefano Galmarini

Q: Would your new approach/improvements be more visible if you considered an airport less busy than the Atlanta one? Preferential pathways may lead to differences that grid method would smear down.

A: Yes, we agree that the grid-based approach would dilute some of these impacts due to preferential pathway changes. However, that limitation is precisely the reason we need an enhanced subgrid-scale treatment of aircraft sources to characterize their air quality impacts in the near field. We believe that our new approach for modeling aircraft emissions will likely show improvements in characterizing air quality even for less busy airports, specifically where commercial aircraft activity that have bigger engines dominate, but unlikely for small airports where most of the activity is dominated by regional jets.

Questioner Name: Jeff Weil

Q1. How far downstream (in space) do you go before the puff concentrations blend into the background, and do not stand out?
A: Based upon this modeling application, up to 99 % of all the aircraft-related puffs are chemically active at a distance of 60 km from the airport, with a few puffs active even at a distance of 145 km, before they are "handed over" to the host grid in CMAQ, based upon physical or chemical criterion for puff maturity.
Q2. Do you see the 3D puff of PInG contribution when you compare with observations?
A: We don't have direct comparison of 3D puffs from aircraft with observations. However, since 21 % of all aircraft-related puffs from the Atlanta airport have at least 0.1 $\mu g/m^3$ $PM_{2.5}$ concentrations (mean of 0.14 $\mu g/m^3$and max of 42.1 $\mu g/m^3$from all puffs during the 2-month simulation), these concentrations are definitely measurable.
Q3. If the 3D puffs do matter, should you consider a TC0 case where you explicitly model individual aircraft plumes as "line-thermal" or 2D puffs because they would better retain their buoyancy?
A: We haven't considered that. But we will investigate this in ongoing work, which is focused on improving treatment of aircraft sources in 3-D models, and understanding subgrid-scale variability due to these sources.

Questioner Name: Biliaiev N

Q: From the physical point of view, there must be the interaction between puffs. I don't see this in these results. Does your model take into account this interaction?
A: Yes, CMAQ-AMSTERDAM supports both intra-plume and inter-plume interactions by treating both splitting and merging of puffs from aircraft to account for wind shear effects, and varying chemistry across the plume.

Chapter 56
Sensitivity of Fine PM Levels in Europe to Emissions Changes

A.G. Megaritis, C. Fountoukis, and S.N. Pandis

Abstract A three-dimensional chemical transport model (CTM), PMCAMx-2008, was applied to Europe to study the influence of emissions changes on fine PM levels. Various emissions scenarios were studied, covering summer and winter periods to quantify also the seasonal variation. Reduction of NH_3 emissions seems to be the most effective control strategy for reducing $PM_{2.5}$ over Europe, in both seasons, mainly due to reduction of NH_4NO_3. A reduction of SO_2 emissions has a significant effect on $PM_{2.5}$ levels over the Balkans during summer, due to decrease of sulfate, while the reduction of anthropogenic OA emissions has a strong effect on total OA mainly in areas close to emissions sources. The NO_x emissions control strategy seems to be problematic in both seasons. Our analysis in European Megacities, based on a scenario zeroing all anthropogenic emissions, showed that the contribution of local emissions on total $PM_{2.5}$, depends on the chemical component, with local sources being especially important mainly for black carbon (BC).

A.G. Megaritis (✉)
Department of Chemical Engineering, University of Patras, Patras, Greece

Institute of Chemical Engineering Sciences, Foundation for Research & Technology-Hellas (FORTH), 26504 Patras, Greece
e-mail: athmegaritis@chemeng.upatras.gr

C. Fountoukis
Institute of Chemical Engineering Sciences, Foundation for Research & Technology-Hellas (FORTH), 26504 Patras, Greece

S.N. Pandis
Department of Chemical Engineering, University of Patras, Patras, Greece

Institute of Chemical Engineering Sciences, Foundation for Research & Technology-Hellas (FORTH), 26504 Patras, Greece

Department of Chemical Engineering, Carnegie Mellon University, Pittsburgh, PA 15213, USA

D.G. Steyn et al. (eds.), *Air Pollution Modeling and its Application XXII*,
NATO Science for Peace and Security Series C: Environmental Security,
DOI 10.1007/978-94-007-5577-2_56,

Keywords PM2.5 • Emission changes • PM-CAMx model

56.1 Introduction

Air pollution is one of the challenging environmental problems in Europe since particulate matter (PM), ozone and other pollutants often exceed the air quality limits, having adverse effects on human health, climate change and visibility [3].

In order to improve air quality in Europe we need to quantify how gaseous and particulate pollutants respond to emissions changes of their precursors and in which extend major urban area emissions impact local and regional air quality. For this purpose we applied a three-dimensional chemical transport model (PMCAMx-2008) [2] which can accurately and efficiently describe the physical and chemical transformations of gas and aerosol species. PMCAMx-2008 includes state-of-the-art organic and inorganic aerosol modules which make it well suited to quantify the response of the system to emission controls.

56.2 Model Description

PMCAMx-2008 [2] simulates the processes of horizontal and vertical advection, horizontal and vertical dispersion, wet and dry deposition, and gas-phase chemistry. The model includes a state-of-the-art organic aerosol module which is based on the volatility basis set framework [1]. PMCAMx-2008simulates the partitioning of primary emissions assuming primary organic aerosol to be semivolatile. Nine surrogate POA species with effective saturation concentrations at 298 K ranging from 10^{-2} to 10^{6} $\mu g\ m^{-3}$ are used. The model treats all organic species (primary and secondary) as chemically reactive. Chemical aging through gas-phase oxidation of OA vapors is also simulated.

The model was applied over Europe covering a $5{,}400 \times 5{,}832\ km^2$ region with 36×36 km grid resolution and 14 vertical layers. The necessary meteorological inputs were taken using the meteorological model WRF (Weather Research and Forecasting) [4]. In addition updated anthropogenic [5] and biogenic gridded hourly emission fields were developed for gases and primary particulate matter.

56.3 Methods

To study the response of fine particulate matter ($PM_{2.5}$) to emissions changes, we performed a sensitivity analysis reducing the emissions of the major gaseous precursors (SO_2, NH_3, NO_x, anthropogenic VOCs) by 50 %. A 50 % reduction of anthropogenic primary OA emissions (POA) was also studied. In addition, a

special focus was given to European Megacities (Paris, London, Rhine-Ruhr, and Po Valley), exploring their contribution in their air quality as well as the impact that they have on the surrounding regions. For this purpose, we applied hypothetical "annihilation" scenarios, zeroing all the anthropogenic emissions of Megacities. Different simulation periods were used representing summer and winter to quantify also the seasonal variation.

56.4 Results and discussion

The reduction of NH_3 emissions by 50 % seems to be the most effective control strategy in reducing $PM_{2.5}$, in both periods (Fig. 56.1), mainly due to a significant decrease of ammonium nitrate. During summer, NH_3 emissions reduction resulted in a decrease of ammonium nitrate by 22 % in the entire model domain. The highest reduction is predicted in UK and Southwest Europe where ammonium nitrate is reduced by 35 and 31 %, while the corresponding decrease of total $PM_{2.5}$ in these areas was 15 and 10 % respectively. Similarly in winter, ammonium nitrate is decreased by 22 %.

The 50 % reduction of SO_2 emissions, during the summer, leads to a significant decrease of sulfate in the entire domain (23 % on average). The SO_2 control strategy is more effective over the Balkans where sulfate is reduced by 30 %, while the respective decrease of total $PM_{2.5}$ was 10 %. Additionally in winter, sulfate is also reduced (15 % on average) although its decrease is lower because its formation was limited by H_2O_2 availability.

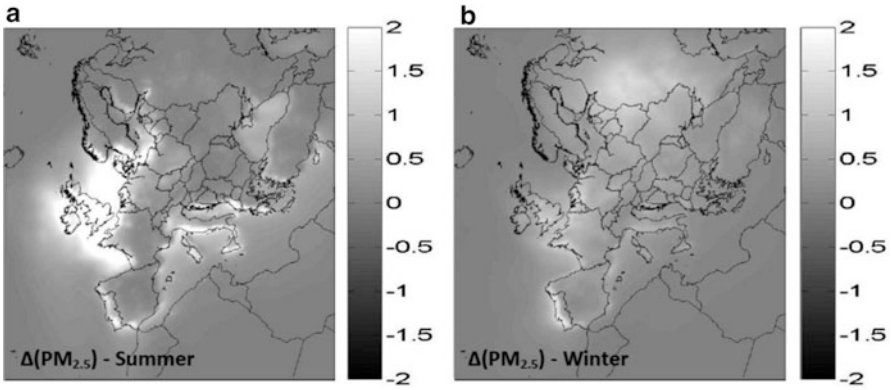

Fig. 56.1 Predicted reduction ($\mu g\ m^{-3}$) in ground-level concentrations of total $PM_{2.5}$ after a 50 % reduction of NH_3 emissions during (**a**) summer 2008 and (**b**) winter 2009. A negative value corresponds to an increase

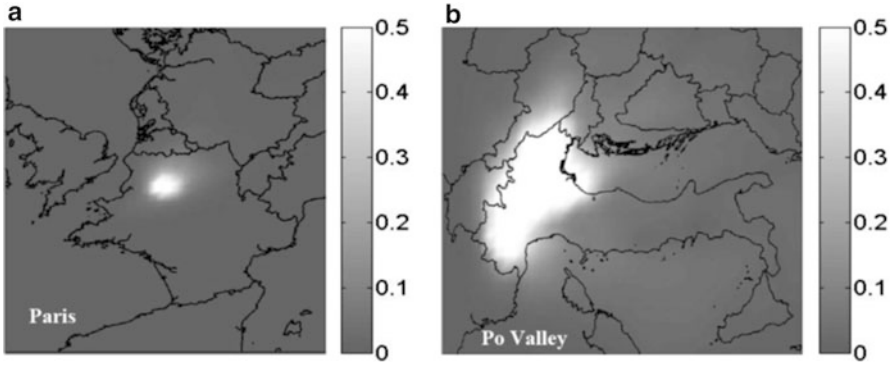

Fig. 56.2 Fractional change of BC in (**a**) Paris and (**b**) Po Valley after an emissions "annihilation" scenario during winter 2010. A negative value corresponds to a decrease

The 50 % reduction of anthropogenic VOCs and POA produced a decrease of total OA concentration in both periods with the POA control strategy being more effective in areas close to emissions sources. By reducing VOCs emissions, total OA is predicted to decrease in the whole domain, by 8 % during summer and 4 % in winter, while the respective average decrease of total OA after the 50 % reduction of POA emissions was 15 % during winter and 8 % in the summer.

The NO_x emissions control strategy seems to be problematic in both periods. During the summer, the 50 % reduction of NO_x emissions leads to an increase of ozone levels, mainly in the major urban areas such as London, Paris and Madrid (up to 40 %), and also over Western Europe (4 % on average). Additionally, in the winter, the reduction of NO_x emissions results in an increase of sulfate and total OA by 8 and 12 % respectively.

The results from the Megacities "annihilation" scenarios showed that the impact of local emissions on total $PM_{2.5}$ levels is quite variable depending on location, time and chemical component. In Po Valley, total $PM_{2.5}$ was found to be largely local in both periods (over 50 % in summer and more than 60 % during winter), while in Paris and Rhine-Ruhr the contribution of local sources is also significant mainly during winter. On the contrary, London emissions have a smaller effect on local $PM_{2.5}$ and long range transport of pollutants often dominates.

In addition, local emissions are especially important for black carbon (BC) levels in all the European Megacities. In both periods more than 40 % of BC is found to originate from local sources, while in Paris and Po Valley the contribution of local emissions to BC levels during summer, exceeds 60 and 80 % respectively (Fig. 56.2). At the same time, Megacities do not influence only their air quality, but their impacts extend to the surrounding regions several hundred kilometres away from the source.

56.5 Conclusions

The analysis we performed to quantify how total $PM_{2.5}$ levels respond to emissions changes of their precursors, using PMCAMx-2008 showed that reduction of NH_3 emissions could be an effective control strategy for reducing $PM_{2.5}$ in Europe, in both periods. The reduction of SO_2 emissions has a significant effect on $PM_{2.5}$ levels over the Balkans during summertime, while reduction of anthropogenic VOCs and POA emissions will reduce total OA, especially in areas close to emissions sources. On the other hand reduction of NO_x emissions does not seem to be effective for reducing $PM_{2.5}$ levels.

Our findings from the "annihilation" scenario of Megacities anthropogenic emissions, suggest that the influence of local sources on the concentration of total $PM_{2.5}$ varies by space, time and the chemical component. Local sources are more significant for primary aerosol species like BC, while they do not only impact their air quality but their impacts extend to the surrounding regions.

This work was funded by the European Commission 7th Framework Programme projects MEGAPOLI and PEGASOS.

References

1. Donahue NM et al (2006) Coupled partitioning, dilution, and chemical aging of semivolatile organics. Environ Sci Technol 40:2635–2643
2. Fountoukis C et al (2011) Evaluation of a three-dimensional chemical transport model (PMCAMx) in the European domain during the EUCAARI May 2008 campaign. Atmos Chem Phys 11:10331–10347
3. Seinfeld JH, Pandis SN (2006) Atmospheric chemistry and physics: from air pollution to climate change, 2nd edn. Wiley, Hoboken
4. Skamarock WC et al (2005) A description of the advanced research WRF version 2. NCAR technical note. NCAR/TN–468+STR. NCAR, Boulder, Colorado. Available from: http://www.mmm.ucar.edu/wrf/users/docs/arw_v2.pdf
5. Visschedijk AJH et al (2007) TNO Report 2007 A-R0233/B: a high resolution gridded European emission database for the EU integrated project GEM., Netherlands, Organization for Applied Scientific Research

Questions and Answers

Questioner Name: Nicholas Savage

Q: You concluded that NO_x emission control alone was a bad idea in Europe. In winter, the O_3 concentration increased widely but does this matter if O_3 is well below O_3 concentration limits anyway?

A: One of the objectives of this study was to examine how effective emissions reductions of the major precursors could be for reducing fine particulate matter levels and subsequently for improving European air quality. Indeed, during wintertime the

predicted increase of O_3 levels was below O_3 concentration limits but the 50 % reduction of NO_x emissions alone lead also to a significant increase of sulfate and OA levels in most areas of the domain. Taking also account that during summer, O_3 is predicted to increase up to 40 % in the major European cities (e.g. Paris, London, Madrid) and also in Western Europe, we concluded that a reduction of NO_x emissions on its own seems to be a bad idea for improving air quality in Europe.

Questioner Name: Volker Matthias

Q: What is the impact of reduced ammonia emissions on the NO_2 concentrations? It was this in the expected concentration enhancement?
A: The main focus on this study was on fine particulate matter and their corresponding response to emissions changes in Europe. Thus, we gave little attention to the predicted concentration changes on gaseous species like NO_2. Nevertheless, from results we predicted small increases on NO_2 levels after the reduction of NH_3 emissions but without any further analysis.

Chapter 57
ATMOSYS: A Policy Support System for Atmospheric Pollution Hot Spots

Clemens Mensink, L. Blyth, K. De Ridder, W. Lefebvre, N. Veldeman, and P. Viaene

Abstract The LIFE + Environmental Policy & Governance project ATMOSYS has the objective to implement an advanced and comprehensive air quality modeling system as a web-based service used by policy makers. The ATMOSYS system is based on advanced technology, including prognostic 3-D atmospheric computer models, data assimilation techniques, CFD modeling, and on results from recent and on-going national and European research projects. Its comprehensive character resides in the multiple scales and scale interactions covered by the system and in a coherent approach for forecasts, assessments, and scenario studies alike.

Keywords CFD modeling • Data assimilation • Policy support • Scale interactions • ATMOSYS

57.1 Introduction

ATMOSYS is a LIFE + Environmental Policy & Governance project co-financed by the European Commission. The project began on the 1st September 2010 and will be completed at the end of 2013. The overall objective of the project is to set up, evaluate and demonstrate an advanced and comprehensive air quality modeling system and associated web-based service, containing novel elements specifically designed for air pollution policy support in hot spot regions. The system will be implemented for the European hot spot region of Flanders by VITO together with the Flemish Environmental Agency (VMM).

Several regions in the EU have difficulty in attaining the limits for specific air pollutants, such as NO_2, and $PM_{2.5}$. The 2008/50/EC directive on ambient air quality and cleaner air for Europestipulates that measures should be taken to reduce

C. Mensink (✉) • L. Blyth • K. De Ridder • W. Lefebvre • N. Veldeman • P. Viaene
Flemish Institute for Technological Research (VITO), Boeretang 200, 2400 Mol, Belgium
e-mail: clemens.mensink@vito.be

D.G. Steyn et al. (eds.), *Air Pollution Modeling and its Application XXII*,
NATO Science for Peace and Security Series C: Environmental Security,
DOI 10.1007/978-94-007-5577-2_57,

emissions and states that modeling techniques can be applied to obtain geo-spatial insights in the air quality problem and provide possible solutions.

Recently the cost of air pollution to the Flemish region of Northern Belgium has been estimated at several hundred million euros per year [2], among other things by increased absence at work caused by respiratory disease. The European Commission [1] has estimated that in hot spot areas, owing to the effect of anthropogenic fine particulate matter ($PM_{2.5}$) alone, there is an associated loss in life expectancy of up to 13–36 months per individual, as compared to values of 2–9 months elsewhere in Europe.

57.2 Methodology

The ATMOSYS air quality policy support system to be implemented includes: (i) an operational daily forecasting system (up to 3 days ahead), (ii) a re-analysis service (i.e., retrospective simulations) and (iii) a scenario tool. The system contains urban/regional (AURORA) and local (ENVI-Met) components.

The AURORA regional/urban scale model will yield output for relevant gases (e.g. NO_2, benzene, O_3) and particles ($PM_{2.5}$ and its constituent elements, such as elemental carbon, ammonium and sulphates), although the focus will be on pollutants with a local character. The model will contain a module to calculate concentrations near line sources (highways) at a resolution of up to a few tens of metres. The AURORA model is described in the Model Documentation System of the European Topic Centre on Air and Climate Change (EIONET).

The ENVI-Met micro scale model is a 3-D atmospheric CFD (computational fluid dynamics) model which was developed at the Universities of Bochum and Mainz and extended by VITO with an air quality module capable of calculating PM_{10}, $PM_{2.5}$, EC, NO_2, NO and O_3 transport, chemical reactions, and deposition. Research is currently in progress aiming to implement the full UFP size distribution and its relevant dynamics. Further details on ENVI-Met are available at http://www.envi-met.com.

The use of 3-D atmospheric computer models for air quality policy support is not a straightforward task because of the advanced and complex nature of the models and because of the computation intensive character of the models. Performing annual simulations is therefore a great challenge, however essential in order to be compliant with the European Air Quality Directives. The targeted accuracy for the air quality forecasting will be of the order of 10 % for the most common gases, and 20–30 % for the particles. Occupying a central position, the web-based platform collects results from many other individual system modules, in particular the air quality forecasts and re-analysis simulations, provided by the AURORA and ENVI-Met models. The web-based interface also ingests information regarding the validation strategy and metrics. Finally, the model evaluation is done by accessing results contained in the web-based platform, and combining those with measurements from the experimental campaigns as well as from the routine monitoring station network.

57.3 Results and Discussion

Despite the fact that the project is only halfway at the moment, several project elements have already been realized. The AURORA regional/urban scale model has been implemented in the system and coupled to a Gaussian module to calculate concentrations near line sources (highways) at a resolution of up to a few tens of meters.

Results for Flanders are shown in Fig. 57.1, revealing hot spot areas near the city of Antwerp, the capital Brussels and the area of Ghent. The ENVI-Met micro-scale model yields output for most of the primary emitted gases and has been extended with a limited chemistry module for gases subject to short-range chemistry (e.g. NO-NO_2-O_3). Figure 57.2 shows NO_2 concentrations for a street canyon in an urban area. The ENVI-Met model has also been extended with a module for ultrafine particles (UFP). A fast method to calculate annual statistics from the ENVI-Met results is in development.

With respect to the system design and architectural framework, the discussions on user requirements resulted in the use of the DELTA benchmarking tool, developed by the EC JRC within FAIRMODE, as a common functionality for model validation within ATMOSYS. Users can use ATMOSYS as an initial explorative validation tool and assess their model performance prior to entering the official JRC Benchmarking service web application.

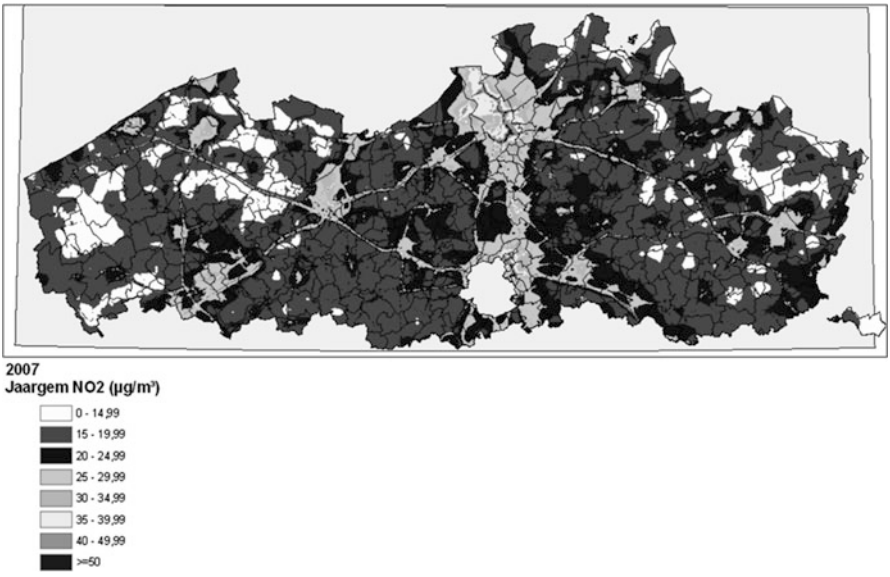

Fig. 57.1 Annual average NO_2 concentrations modeled with AURORA, showing the air quality hot spot regions of Antwerp, Brussels and Ghent

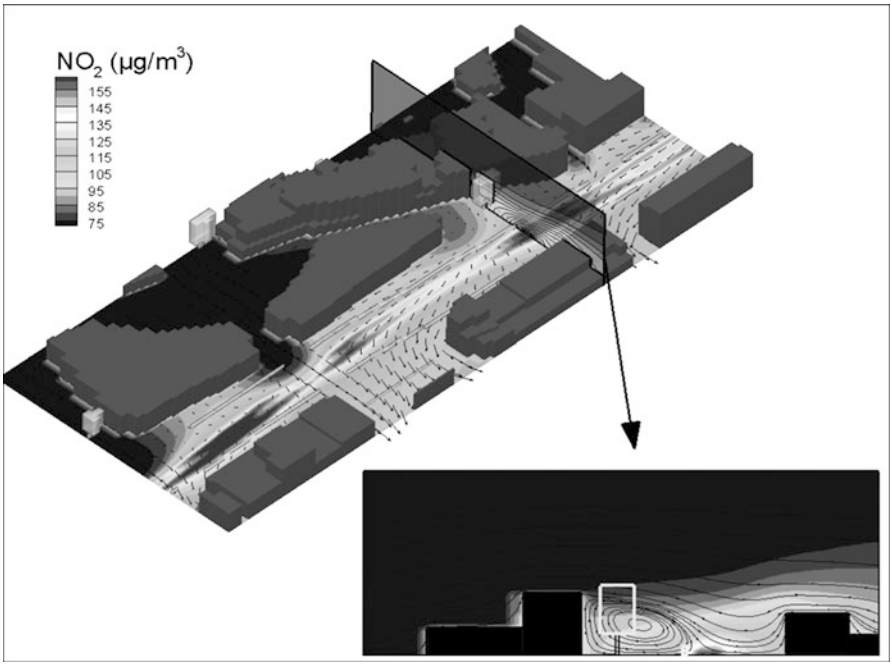

Fig. 57.2 Instantaneous NO_2 concentrations modeled in an urban street canyon using the ENVI-Met model

Automatic validation of the AURORA model is obtained by first specifying the representativeness of the in-situ air measurement locations. Additional urban measurement campaigns (PM_{10} monitors, chemical analysis thereof and passive samplers of NO_2) are organized to further assess the validation for urban background, urban location close to a major regional road and a street canyon. Another intensive measurement campaign is planned for all of 2012 where Black Carbon, PM_{10}, $PM_{2.5}$ and NO_2 will be sampled at locations close to motorways.

57.4 Conclusions

The ATMOSYS policy support system combines prognostic 3-D atmospheric computer models, data assimilation techniques and CFD modeling, in order to provide a coherent and validated approach for forecasts, assessments, and scenario studies at multiple scales and scale interactions.

Acknowledgments This research has been supported by the LIFE + programme of the European Commission.

References

1. Amann M et al (2005) Target setting approaches for cost-effective reductions of population exposure to fine particulate matter in Europe. CAFE Report #4. February 2005
2. Bossuyt M et al (2007) Environmental report flanders (Milieurapport Vlaanderen MIRA: achtergronddocument: milieu, mens & gezondheid), VMM, 2007

Questions and Answers

Questioner Name: Sarav Arunachalam

Q: At the local scales, you are only considering NO2-O3 chemistry, and not PM (aerosols). Was that an intentional omission, or do you plan to incorporate that later?
A: This is a correct observation. For the moment the aerosol chemistry is only included in the AURORA model to account for PM formation at the urban and regional scales. At the local scale the ENVI-Met model simulates the fate of PM_{10}, $PM_{2.5}$ and EC as tracers. However, the ENVI-Met chemistry model has been extended with a detailed aerosol (UFP) model at the local scale. At the moment it is extensively tested validated.

Questioner Name: Kiran Alapaty

Q: Have action 11 such that evaluation results are available to action 1 audience and policy makers in a digestible language / format / wordings.
A: Thank you for this suggestion. Since many of the policy makers are on board as project partners, constant feedback is given throughout the project. This also includes more formal evaluation sessions for a broader audience of policy makers. It is indeed a very important aspect of the project as you have pointed out.
Q: For CFD gas phase chemistry GCM's have several simplified packages.
A: This might indeed be useful. However, the relevant time scales might be very different for chemistry at the local scale. Therefore one should be careful in just copying chemistry modules from other models. We look for fast chemistry modules that represent the (fast) local chemistry correctly. Besides we think that a thorough validation and careful testing is needed before implementing the system in a policy context.

Chapter 58
Atmospheric Dispersion of Radioactive Material from the Fukushima Daiichi NuclearPower Plant

Pontus von Schoenberg, Jonas Boson, Håkan Grahn, Torbjörn Nylén, Henrik Ramebäck, and Lennart Thaning

Abstract Model calculations have been performed of the emissions of radioactive material from the Fukushima Daiichi nuclear power plant over the northern hemisphere.

Keywords Radioactive material • Fukushima power plant • Hemispherical transport

58.1 Introduction

One of the consequences of the devastating earthquake and the subsequent tsunami close to the Japanese east coast on Friday 11 March 2011 was large cooling problems of the nuclear reactors in Fukushima Daiichi. It resulted in a series of releases of radioactive material into the atmosphere. These releases mainly affected Japan in the vicinity of Fukushima but were also monitored around the northern hemisphere. At FOI a global/regional stochastic particle model has been used to simulate transport and deposition of particulate ^{137}Cs and the model results have been compared with measurements at different locations on the northern hemisphere. In the past, the model has been used primarily for dispersion of particles or gases on the European scale. The motive for this study was to investigate the dispersion model behaviour over the whole northern hemisphere and on timescales up to a few weeks. It is important to understand the accurateness of the model and in which way the model result can be used in the emergency preparedness system.

P. von Schoenberg (✉) • J. Boson • H. Grahn • T. Nylén • H. Ramebäck • L. Thaning
FOI, Swedish Defence Research Institute, SE-901 82 Stockholm, Sweden
e-mail: pontus.von.schoenberg@foi.se

D.G. Steyn et al. (eds.), *Air Pollution Modeling and its Application XXII*,
NATO Science for Peace and Security Series C: Environmental Security,
DOI 10.1007/978-94-007-5577-2_58,

58.2 Method

The stochastic particle model Pello, an acronym for ***P**article model in an **E**ta **L**atitude **LO**ngitude* coordinate system, is a random displacement model, with dry and wet deposition (using large scale precipitation only). It's developed at FOI, the Swedish Defence Research Agency [1]. For the calculations with dispersion from the Fukushima accident the model had to be adjusted for dispersion on the entire northern hemisphere. Periodic boundary conditions for transport of the particles were included for the east-western boundary and a coordinate transformation was made, in order to avoid singularity in the model, in the North Pole area.

The weather fields driving the model come from ECMWF, *European Centre for Medium Range Weather Forecasts*. A time resolution of 6 h was used for the weather fields. Calculations were made with two different geographical domains, the northern hemisphere (1.0° resolution) and a locally over Japan (0.1° resolution). In the first tests dispersion of particulate ^{137}Cs was evaluated using an estimate of the source term [2]. It was assumed that the radioactivity was evenly distributed over the surface of the particle already present in the surroundings. Typical particle distributions for urban, rural and maritime air were used in several model calculations. Each distribution is described as a sum of three different log-normal distributions as defined by Guide to Global Aerosol Models [3].

58.3 Result

For the high resolution geographical domain over Japan the modelled deposition have been compared with deposition measurements of ^{137}Cs from MEXT, *Ministry of Education*, *Culture*, *Sports*, *Science* & *Technology in Japan*. The model represents the levels and the location of deposition reasonably well. However, most of the deposition in Japan comes from a rainy period (15–16 March 2011) when the cloud went inland, and since the movement of this is not captured by the 6 h resolution in the weather data, the model shows discrete locations with deposited material. This could be smoothed out by using better time resolution in weather data, which on the other hand would require more computational resources.

There are six air filter stations in Sweden. In Fig. 58.1 a comparison between model data and measurement results for these sites are visualized for the time period when the cloud reaches Sweden, about 11 days after the first release. The timing of the cloud arriving to Sweden is very well described, as well as the order of magnitudes of the concentration of ^{137}Cs. Even tendencies are in good agreement between model and measurements.

Comparisons have also been done between the model and air filter measurements in Taiwan Chih-An [4]. There was good agreement between the stations at low altitudes.

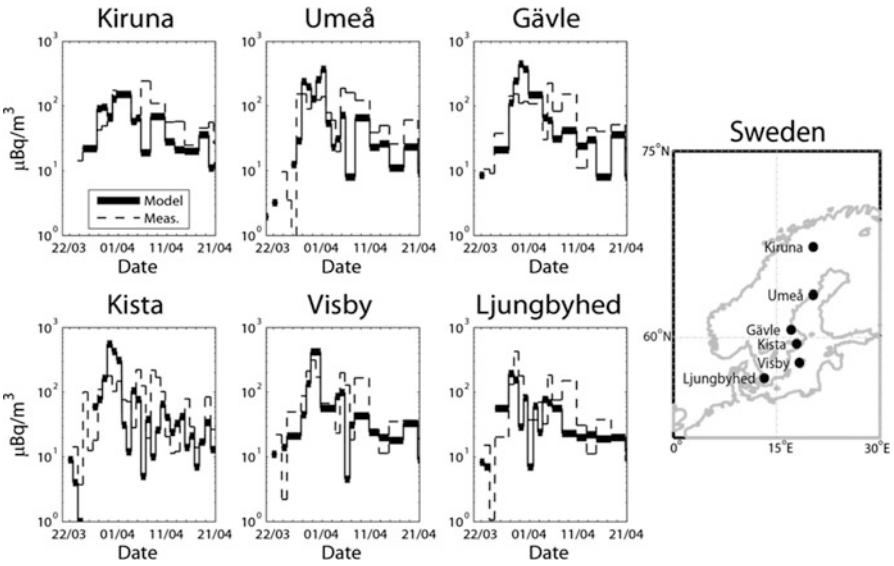

Fig. 58.1 Comparison between model data (*solid line*) and air filter measurements (*dashed line*) for the Swedish air filter stations. Averaging periods for the model is the same as the measurement periods for the stations (*left*). Station locations in Sweden (*right*)

However, at a site located in the mountains at about 3,000 m height above sea level the model showed between one and two orders of magnitude higher concentrations than the measurements. One aspect of this discrepancy is that our model does not resolve the high mountains in the orography data. Another is the modelling of the boundary layer details in this complex, high terrain. Further work has to be done on how to use the model in these extreme cases.

If we compare the different particle distributions of urban, rural and maritime air there is little difference between them for long distances, see Fig. 58.2. There are greater uncertainties in the model than those that come from the different particle distributions for the long scale modelling, as long as a reasonable distribution is used. The wet deposition is noted to be crucial for these scales i.e. without precipitation the concentration levels in Sweden became 100 times larger due to lack of wash out.

58.4 Conclusions

The Pello model is a very useful tool for many purposes in an emergency preparedness situation. The time of arrival is an important decision aid for determining whether to e.g. evacuate people or put cattle inside. The time of arrival shows

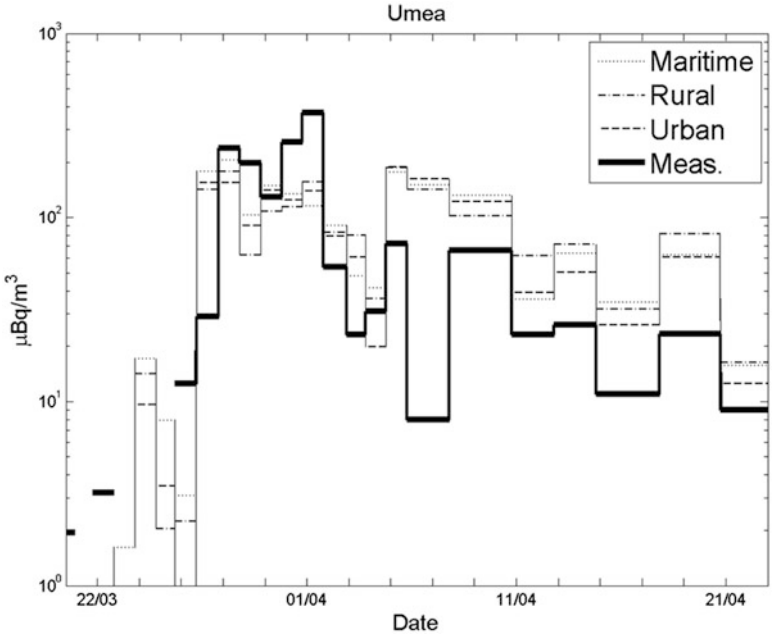

Fig. 58.2 Example of result of model data with different particle distributions for maritime, rural and urban air compared with measurements in Umeå, one of the measurement sites in Sweden, see Fig. 58.1

good agreement between model data and measurement results. Furthermore, the air concentration from the model involves greater uncertainties especially in the early stages of an accident since the source term might be poorly known.

References

1. Lindqvist J (1999) En stokastisk partikelmodell I ett ickemetriskt koordinatsystem. FOI-R—99-01086-862-SE. ISSN 1107-9154
2. Personal contact with, Dr Mashimoto Chino (2011) JAEA, Japan Atomic Energy Agency
3. Guide to Global Aerosol Models (GAM) (1999) American Institute of Aeronautics and Astronautics, AIAA G-065-1999
4. Huh C-A, Hsu S-C, Lin C-Y (2012) Fukushima-derived fission nuclides monitored around Taiwan: free tropospheric versus boundary layer transport. Earth Planet Sci Lett 319–320:9–14

Questions and Answers

Questioner Name: Jeff Weil

Q: For the Taiwan monitor in elevated terrain is the disagreement between the model + measurement due to inaccuracy in specifying the diffusivities for your RDM or in getting the flow field right for this monitor which is in complex terrain?
A: The resolution used in this comparison is 1° in both latitude and longitude. For that reason the model misses the complexity of the terrain which one reason for the disagreement. Another reason is the modeling of the boundary layer details in this complex terrain and on these altitudes. Further investigations have to be made to understand how to interpret the model under these conditions and tests with higher resolution is a first step in this work.

Chapter 59
Ensemble Modelling of Surface-Level Ozone in Europe and North America for AQMEII

Efisio Solazzo, Stefano Galmarini, Roberto Bianconi, and S. Trivikrama Rao

Abstract Eleven state-of-the-science regional air quality (AQ) models, exercised by 20 independent groups in Europe and North America, have been assembled for the Air Quality Model Evaluation International Initiative (AQMEII). The modelled ground-level ozone mixing ratios are collectively examined from the ensemble perspective and evaluated against observations from both continents. We aim at creating optimized ensembles in order to capture the data variability while keeping the error low. It is shown that the most commonly used ensemble approach, namely the average over all available members, can be outperformed by subsets of members optimally selected in terms of bias, error, and correlation, independent of the skill of the individual members. A clustering methodology is applied to discriminate among members and to build a skilful ensemble based on model association and data clustering.

Keywords AQMEII • Clustering • Multi-model ensemble • Ozone

59.1 Introduction

In this study, we analysed the ozone mixing ratios provided by simulations from 11 state-of-the-science regional AQ models run by 18 independent groups from North America (NA) and Europe (EU). Model predictions have been made available,

E. Solazzo (✉) • S. Galmarini
Joint Research Centre, European Commission, Ispra, Italy
e-mail: efisio.solazzo@jrc.ec.europa.eu

R. Bianconi
Enviroware srl, Concorezzo, Milano, Italy

S.T. Rao
Atmospheric Modeling and Analysis Division, U.S. Environmental Protection Agency, Research Triangle Park, NC, USA

D.G. Steyn et al. (eds.), *Air Pollution Modeling and its Application XXII*,
NATO Science for Peace and Security Series C: Environmental Security,
DOI 10.1007/978-94-007-5577-2_59,

along with observational data, to the ENSEMBLE system [1]. The ability of the ensemble mean and median to reduce the error and bias of single model (SM) outputs is examined, and co regarding the size of the ensemble and its quality are made. The level of repetition provided by each individual model to the ensemble is quantified by applying clustering analysis to examine whether the improvement in error using the mean or median of the model ensemble is due to the increased ensemble size, or if information carried by each model contributes to the multi-model (MM) superiority.

59.2 Participating Models and Settings

The meteorological and the AQ models participating in AQMEII are:

- WRF – CMAQ;
- WRF/MM5 – CAMx;
- MM5 – CHIMERE;
- COSMO – MUSCAT;
- MM5 – DEHM;
- MM5 –POLYPHEMUS;
- LOTOS – EUROS;
- ECMWF – SILAM;
- GEM – AURAMS;
- PARLAM-SP – EMEP;
- WRF – WRF/Chem.

Some AQ models were run over the two continents driven by different meteorology (as for example, CAMx). Full details, settings and references can be found in Solazzo et al. [2]. In total there are eleven AQ models that were run over EU and seven AQ models over NA. The models' outputs were compared against observational data at over 1,000 receptor locations over the two continents.

59.3 Multi-model Analysis: Selected vs. Unselected Model Ensembles

We consider the distribution of some metrics (e.g. root-mean square error (RMSE) and Pearson correlation coefficient (PCC)) of the mean of all possible combinations of available ensemble members n. An example of such a distribution, for any possible k-member combination ($k < n$) of the statistical analysis, is presented in Fig. 59.1 for a European sub-region. The continuous lines on each plot represent the mean and median of the distribution of any k-model combinations. Analysis of mean RMSE for EU sub-regions, for which a large set of members is available,

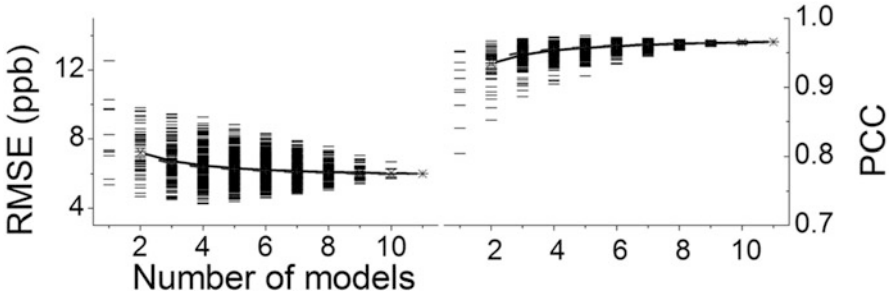

Fig. 59.1 RMSE and PCC of the ensemble mean of any possible combination of members for EU. *Continuous lines* denote the mean and the median of the distributions

shows that a plateau is reached for $k > 5$. This indicates that there is no advantage, on average, to combine more than six members as the benefit in minimizing the mean RMSE is negligible. Furthermore, a minimum of RMSE, among all combinations, systematically emerges for ensembles with a number of members $k < n$. Similarly, a maximum of PCC is achieved by combinations of a subset of members. This result has been found for a number of regions in Europe and North America. This suggests that the ensemble of a few members systematically outperforms the ensemble of all members. Also, adding new members to such an optimal ensemble (thus moving towards a higher value of k) deteriorates the quality of the ensemble since the minimum RMSE increases and the maximum PCC decreases.

The next step in the analysis was to rank the ensemble members by their individual RMSE and track the RMSE positioning within the optimal ensemble combinations (full details and results are given in [2]). The RMSE ranking shows that the optimal ensemble is in some cases achieved by the MM ensemble containing low-ranking members, suggesting that all members should be considered in building a skilful ensemble. Therefore, an ensemble of top-ranking models can be worse than an ensemble of top-ranking and low-ranking models: that is, outliers may need to be included in the ensemble to obtain the best performance. Moreover, further analysis comparing the variability of MM combinations of selected members vs. full member ensembles shows that reducing the number of members does not degrade the ensemble variability, but instead actually compares better to the spread of the observations.

59.4 Reduction of Data Complexity: A Clustering Approach

To discern which members should be included in the ensemble, a method for clustering highly associated models and then discarding redundant information was developed using the PCC as the determining metric. The most representative models of each cluster, chosen based on a distance metric, are then used to

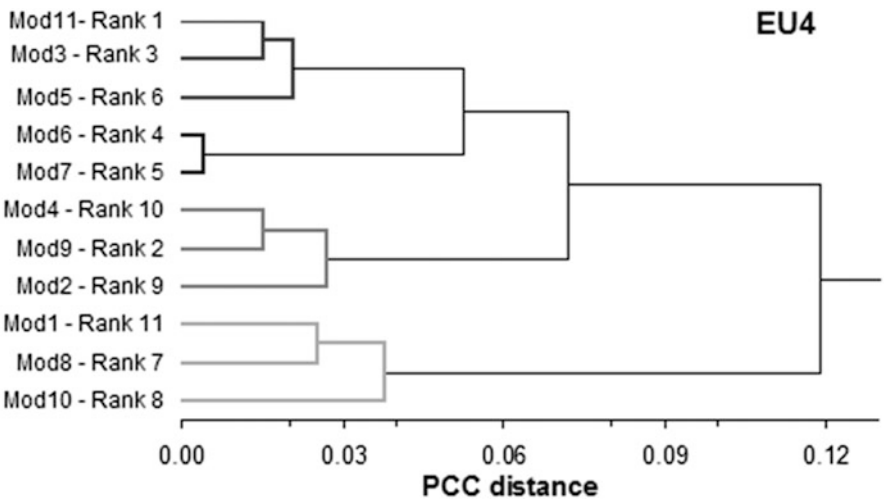

Fig. 59.2 Model clustering as function of mutual PCC distance

generate a reduced or selected-member ensemble. In this way, the information that each member provides to the ensemble is "unique" to the greatest possible degree. The clustering has been applied to eight sub-regions of Europe and North-America, with individual models ranked by the RMSE for that particular sub-region. An example is given in Fig. 59.2, where highly associated members (low PCC distance) belong to the same cluster. Thus, an ensemble of independent members is generated by selecting one member from each cluster. We note two aspects: (*a*) a cluster's representatives are not necessarily those with higher RMSE ranking, and (*b*) the number of independent clusters matches the number of models needed to generate the MM ensembles with minimum RMSE of Fig. 59.1, for all the analysed sub-regions in both continents. The two methods are in fact independent, as the clustering analysis makes no use of observational data (only model-to-model PCC is used in the cluster analysis).

59.5 Conclusions

This study collectively analysed the performance of 11 regional AQ models and their ensembles in the context of the AQMEII inter-comparison exercise. While MM ensembles demonstrate improved performance over the individual model realizations, the most skilful ensemble is not necessarily generated by including all available model results, but instead by selecting models that result in a minimization of ensemble error. In addition, an ensemble of top-ranking model results can be worse than an ensemble of top-ranking and low-ranking model results. Until now, the prevailing assumption has been that as long as a large set of results was treated

statistically in one ensemble, the ensemble would perform better than any individual ensemble member. Furthermore, it was assumed that the better the model results the better would be the ensemble. However, the analysis presented here suggests that this is not necessarily the case, as outliers also needed to be included in the ensemble to enhance performance. Furthermore, the skill score does not necessarily improve by increasing the number of models in the ensemble. By contrast, the level of inter-dependence of model results may lead to a deterioration of the results and to an overall worsening of performance. We apply a method for reducing data complexity through a clustering technique, which has the advantage of simplifying information provided by AQ model outputs by clustering the data into groups based on a selected metric, where there is no prior knowledge of grouping. Results show that by selecting the appropriate cluster distance and association criteria, one can generate an ensemble of selected members whose error is significantly lower than that of the full-member ensemble mean.

Acknowledgments The AQMEII community is kindly acknowledged for providing the modeling data. Although this paper has been reviewed by EPA and approved for publication, it does not necessarily reflect EPA's policies or views.

References

1. Galmarini S et al (2012) ENSEMBLE and AMET: two systems and approaches to a harmonised, simplified and efficient assistance to air quality model developments and evaluation. Atmos Environ 53:51–59. doi:10.1016/j.atmosenv.2011.08.076
2. Solazzo E et al (2012) Model evaluation and ensemble modelling and for surface-level ozone in Europe and North America. Atmos Environ 53:60–74. doi:10.1016/j.atmsenv.2012.01.003

Question and Answers

Questioner Name: David Simpson

Q: The analysis was based only on ozone. Models might be good for ozone but not for other pollutants. Is this a problem?
A: The analysis presented has been based on ozone for four different sub-regions of Europe and North-America. We found that, even for ozone only, the best combination of models is region-dependant. We expect that when other compounds are examined, models other than those for ozone will agree the best with the observations. However, it is important to point out that aim of the study is not to find out the best models, but to show that a subset of independent models (where the dependency is measured by means of the correlation) can outperform the ensemble mean of all available models. We expect the independence of models (and group clustering) not to depend on the specie, but for all species to find a common

clustering of independent models (although the representative model of each cluster may be pollutant-dependant) (see also reply to next question). Ongoing work is devoted to clarify these aspects for a range of pollutants.

Questioner name: Michail Sofiev

Q: In the framework of the MACC project the multimodel evaluation showed that models performing best for ozone were those with the poorest performance for NO2. It is interesting whether the clustering made for ozone will be the same for other pollutants.
A: We do not expect to find the same model to be representative of clusters generated for different pollutants. The clustering analysis produces groups of models that can be considered "independent" in the sense that they are uncorrelated, but it does not provide any information about the "best model". That said, it is expected that models that are independent for one specie (e.g. ozone) are also independent for other species (e.g. NO2), although the most representative models from each independent cluster might not be the same. This is because the variance (spread) and error (accuracy) are highly specie-dependant, whilst independency should be not.

Questioner name: Volker Matthias

Q: Are the modeling systems within a given cluster sharing common features?
A: Indeed, clustering of models reflects the sharing of important commonalities, such as air quality system, meteorological driver, emissions and boundary conditions.

Chapter 60
A Case Study on the Impact of Aerosol-Radiation Feedback on Meteorology and Regional Pollutant Distributions

R. Forkel, J. Werhahn, S.A. McKeen, S.E. Peckham, G.A. Grell, and P. Suppan

Abstract The impact of aerosol-radiation feedback on meteorology and subsequent changes in pollutant distributions over Europe and the North Atlantic were investigated with WRF/Chem. The case studies for two summer months show that the direct effect of aerosol particles on solar radiation is dominated by semi-direct effects that are developing after a few days. Strong deviations from the baseline case, which does not include any feedback, were found for the global radiation over the North Atlantic and Northern Europe when the indirect aerosol radiative effect is considered.

Keywords WRF/CHEM • Aerosol- radiation feedback

60.1 Introduction

Fully coupled "online" meteorology-chemistry models provide the possibility to account for feedback mechanisms between simulated aerosol concentrations and meteorological variables, which cannot be accounted for in traditional off-line coupled air quality models. Here, simulations with the fully coupled meteorology-chemistry model WRF/Chem [2] – one just including the direct aerosol-radiative effect and two cases considering the direct as well as the indirect effect – are compared against a baseline case without any feedback effects.

R. Forkel (✉) • J. Werhahn • P. Suppan
Institute for Meteorology and Climate Research (IMK-IFU), Karlsruhe Institute of Technology (KIT), Kreuzeckbahnstr. 19, 82467 Garmisch-Partenkirchen, Germany
e-mail: renate.forkel@kit.edu

S.A. McKeen • S.E. Peckham • G.A. Grell
Earth System Research Laboratory, National Oceanic and Atmospheric Administration (NOAA), Boulder, CO 80305-3337, USA

D.G. Steyn et al. (eds.), *Air Pollution Modeling and its Application XXII*,
NATO Science for Peace and Security Series C: Environmental Security,
DOI 10.1007/978-94-007-5577-2_60,

Table 60.1 Labels of the simulated cases

Case	Description
BASE	Baseline case; without any aerosol feedback effects
RFB	Direct aerosol-radiative effect only (also including semi-direct effect)
RFBC	Direct aerosol-radiative effect plus indirect aerosol effect (also including semi-direct effect and second indirect effect) for zero PM10 boundary values
RFBC2	As RFBC but with higher PM10 boundary values

60.2 Method

WRF/CChem simulations are carried out for an episode from May 30 2006 to July 31 2006. Equal to the WRF/Chem contribution to the AQMEII (Air Quality Model Evaluation International Initiative; [3]) model inter-comparison, which initiated this investigation, the 3-modal MADE/SORGAM aerosol module was applied [1]. The simulation domain with a horizontal grid size of 22.5 km covers Europe and the North Atlantic. In order to observe the free development of feedback effects no nudging was applied for the considered 2-month episode for this study.

Four cases are compared, a baseline case without any feedback (BASE), a case just including the direct aerosol effect on radiation (RFB), and two cases including the direct as well as the indirect aerosol effect (RFBC and RFBC2). The RGBC and the RFBC2 case differ in so far as zero PM10 boundary values were applied for the RFBC case and high lateral PM10 concentrations for the RFBC2 case (Table 60.1).

60.3 Results and Discussion

Over Central Europe the mean reduction of global radiation due to aerosol extinction alone was mostly 3–7 Wm^{-2} for clear sky conditions. However, the subsequent changes in temperature and boundary layer height result in changed cloud cover. Already after a few days these semi-direct effect dominates the reduction of solar radiation due to the direct aerosol extinction. The semi-direct effect on solar radiation increases with time. Changes in cloud cover due to semi-direct effects resulted in monthly mean changes of ± 50 Wm^{-2}.

The inclusion of the indirect aerosol effect resulted in an up to 70 % lower cloud water content for the RFBC case than for the BASE case and almost 100 % higher mean solar radiation over the North Atlantic and Northern Europe [1]. The simulated low cloud droplet concentrations, which are significantly smaller than the 250 droplets cm^{-3} that are assumed for the baseline case, are a result of the low aerosol concentrations in this area. The higher boundary values for PM concentrations in the

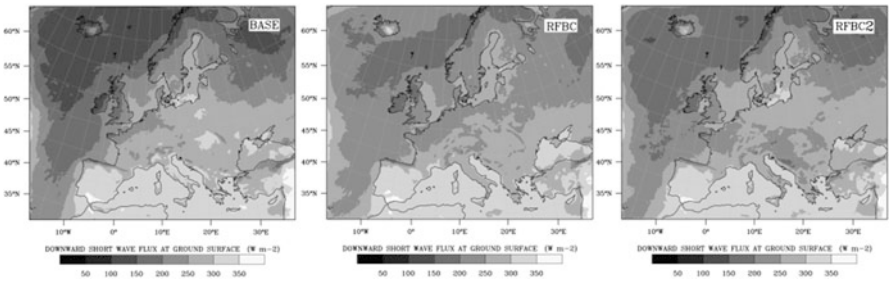

Fig. 60.1 July 2006 mean solar radiation in W m^{-2} for the BASE case (*left*), the RFB case (*middle*), and the RFB2 case (*right*)

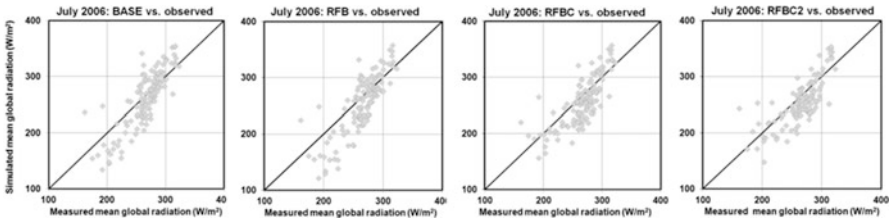

Fig. 60.2 Simulated versus observed (http://wrdc.mgo.rssi.ru) mean incoming solar radiation over Europe for the four considered cases

RFBC2 case result in a higher cloud water content and a less pronounced increase of solar radiation over the North Atlantic (Fig. 60.1). In contrast to the temporal development of the semi-direct effect the changes in solar radiation due to the indirect effect occur immediately after cloud formation.

Except for pollution hotspots, cloud droplet numbers are mostly lower over continental Europe when the indirect aerosol effect is included. Better agreement between observed and simulated global radiation over Europe was found for cloudy conditions when the indirect effect was taken into account (Fig. 60.2).

Mean ozone mixing ratios over Europe in July were modified by up to 4 ppbv or 10 % over continental Europe (figure not shown). These changes are mostly related to changes in cloud cover [1]. For PM_{10} the inclusion of the direct effect resulted for the considered episode in a mean decrease by 20–50 %. By additionally taking indirect aerosol effect into account an increase of the monthly PM_{10} concentration by 1–3 $\mu g\ m^{-3}$ was found for July 2006 over large parts of continental Europe (Fig. 60.3), which can mostly be related to a decreased atmospheric boundary layer height and changes in precipitation patterns. Different from the analysis of short episodes, the changes in meteorological variables and pollutant fields cannot always be related with the underlying aerosol concentrations any more due to the development of the semi-direct effect and the second indirect effect.

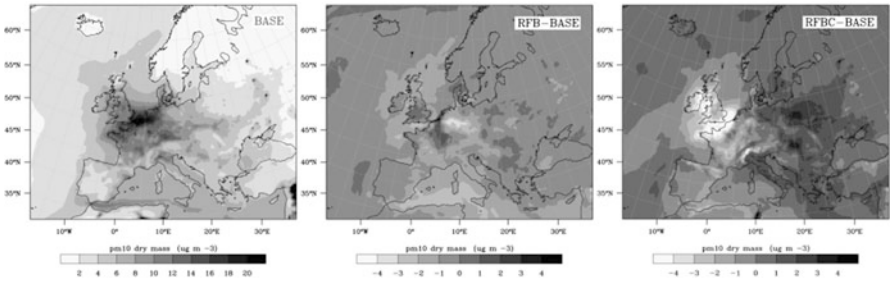

Fig. 60.3 July 2006 mean PM_{10} in $\mu g\ m^{-3}$ for the BASE case (*left*), for the difference between RFB and BASE case, and for the difference between RFBC and BASE case (*right*)

60.4 Concluding Remarks

WRF/Chem simulations were performed to study the impact of aerosol direct and indirect radiative effects on meteorology and pollutant distributions. As the results shown here refer to one particular summer episode details of the spatial patterns of changes in meteorological parameters and pollutants over continental Europe due to aerosol effects will depend on the considered meteorological situation.

However, some more general conclusions are still possible. The continuous simulations for two summer months show that the comparatively small direct effect of aerosol particles on solar radiation is dominated by the effect of changed cloud cover due to semi-direct effects that are developing after a few days. The inclusion of the indirect aerosol effect results in smaller cloud droplet numbers and cloud water and higher global radiation in particular over the North Atlantic and unpolluted regions in Northern Europe. In contrast to the immediate impact of the indirect and also of the direct aerosol effect on solar radiation the semi-direct effect and the second indirect effect develop with time.

Continuous nudging of the meteorological variables during runtime, which is a common practice for hindcasts with offline air quality models, is not an option if feedback effects are studied with online coupled models since semi-direct effects are suppressed when continuous nudging is applied. However, also without nudging the simulated development of semi-direct effects will depend on the length of the episode and whether the simulation is done with one continuous run or whether it is split into a sequence of shorter episodes where the meteorological variables are re-initalized in order to attach the regional simulation closer to the reanalysis. In this case, it is still necessary to find the right balance between the frequency of re-initializing the meteorology and allowing for the development of the semi-direct and the second indirect effects.

Acknowledgments The present study was partly financed by the German Federal Ministry of Education and Research (BMBF). Also we like to acknowledge the AQMEII initiative for initiating this modelling exercise.

References

1. Forkel R, Werhahn J, McKeen S, Peckham S, Grell G, Suppan P (2012) Effect of aerosol-radiation feedback on regional air quality – a case study with WRF/Chem. Atmos Environ 53:202–211. doi:10.1016/j.atmosenv.2011.10.009
2. Grell G, Freitas SR, Stuefer M, Fast J (2011) Inclusion of biomass burning in WRF-Chem: impact of wildfires on weather forecasts. Atmos Chem Phys 11:5289–5303. doi:10.5194/acp-11-5289-2011
3. Solazzo E et al (2012) Operational model evaluation for particulate matter in Europe and North America in the context of the AQMEII project. Atmos Environ 53:75–92. doi:10.1016/j.atmosenv.2012.02.045

Questions and Answers

Questioner Name: Nicholas Savage

Q: Would data assimilation be a way to balance between needing a realistic simulation and allowing indirect and direct effects develop and will you do it?
A: Data assimilation a good thing for generating good initial conditions. This is also the case when I do a hindcast in the same way as a forecast is made, i.e. the hindcast episode is composed of a sequence of single runs in 'forecast' mode. This allows for the development of aerosol indirect and semi-direct effects. However, I hope that it is sufficient for our AQMEII simulation that we start each of the 'forecast' cycles with initial conditions which are derived from a meteorological reanalysis and will not need anything extra.

Nevertheless, the question remains, whether this procedure should be applied e.g. daily or with some other frequency. This frequency will certainly determine how strong the meteorology of the regional simulation is attached to the reanalysis (or observational data) and to which extent semi-direct effects can develop and to which amount they are suppressed.

Chapter 61
Impact of Fire Emissions on Air Quality in the Euro-Mediterranean Region

S. Turquety, P. Messina, S. Stromatas, A. Anav, L. Menut, B. Bessagnet, J.-C. Péré, P. Drobinski, P.F. Coheur, Y. Rhoni, C. Clerbaux, and D. Tanré

Abstract We present a regional emission inventory constructed based on satellite observations of fire activity (MODIS) and the ORCHIDEE vegetation model, and its application to air quality forecasting. After a brief description of the variability of fire activity in the Euro-Mediterranean region during the past 8 years, a full evaluation of the emissions is performed for the case study of the summer of 2007, during the large Greek fires event. Therefore, regional simulations undertaken with the CHIMERE chemistry-transport model (CTM) are compared to surface and satellite observations of trace gases and aerosols.

Keywords Chimere model • Fire emissions • MODIS

S. Turquety (✉) • L. Menut
LMD-IPSL, Université Pierre et Marie Curie – Paris 6, Paris, France
e-mail: solene.turquety@lmd.polytechnique.fr

P. Messina • S. Stromatas • P. Drobinski
LMD-IPSL, CNRS, Ecole Polytechnique, Palaiseau, France

A. Anav
LMD-IPSL, CNRS, Ecole Polytechnique, Palaiseau, France

Present Affiliation: University of Exeter, Exeter, UK

B. Bessagnet • J.-C. Péré
INERIS, Verneuil-en-Halatte, France

P.F. Coheur • Y. Rhoni
Université Libre de Bruxelles, Brussels, Belgium

C. Clerbaux
Université Libre de Bruxelles, Brussels, Belgium

LATMOS, IPSL, CNRS, INSU, UPMC, Paris, France

D. Tanré
LOA, CNRS, Université de Lille 1, Villeneuve d'Ascq, France

D.G. Steyn et al. (eds.), *Air Pollution Modeling and its Application XXII*,
NATO Science for Peace and Security Series C: Environmental Security,
DOI 10.1007/978-94-007-5577-2_61,

61.1 Introduction

Fires are recognized to have a major impact on atmospheric chemistry at local to regional scales through the emission of large amounts of trace gases and aerosols. In Europe, regulations and public information have helped reducing the number of fires in the past decades, but thousands of hectares of forest are burned every summer, and agricultural fires remain large in Eastern Europe. The additional emissions thus need to be accounted for in air quality analysis and forecasts.

Here we present a high resolution regional emission inventory developed for the Euro-Mediterranean region. The calculated emissions are integrated into the CHIMERE regional CTM for evaluation of the resulting fire plumes against atmospheric observations. We present results for the case study of the Greek fires in August 2007 [3, 11].

61.2 Quantifying Emissions for Air Quality Purposes

Following the classical approach described by Seiler and Crutzen [10], emissions E_i (g) for a given species i is calculated using:

$$E_i = \sum_f A_f BD_f CC_f EF_{i,f} \tag{61.1}$$

where A is the area burned (m^2) in a given fuel type f, BD is the biomass density (kg dry matter m^{-2}), CC is the combustion completeness factor and EF is the emission factor (g species/kg dry matter). Areas burned are derived from a combination of the MODIS area burnt product (MCD45, [9]) and active fire product (MOD14, [4]), at a 1 km resolution. The biomass density is estimated based on regional simulations from the ORCHIDEE vegetation dynamics and carbon cycle [6], combustion completeness is attributed following Hoelzemann et al. [5], and emission factors are from the Akagi et al. [1] review. Comparisons to other inventories [12, 13] show good general agreement in the temporality but the intensity of the emissions can differ by more than a factor of two. The main differences maybe attributed to the fire detection products used, but uncertainties in other parameters (e.g. CC) can also explain this large range of values.

The analysis of the MODIS fire data from 2005 to 2010 (Fig. 61.1) shows that fires are mainly burning in Southern and Eastern Europe, and Russia. In Eastern Europe and Russia, burning occurs from about March to October, with largest areas during the summer (but largest number of active fires in spring), and is mostly detected in croplands. In other regions, fires have a clear peak during the summer, with more than half of the burning in forested areas in the Iberic Peninsula, and a large fraction of fires in shrubland in the Mediterranean countries.

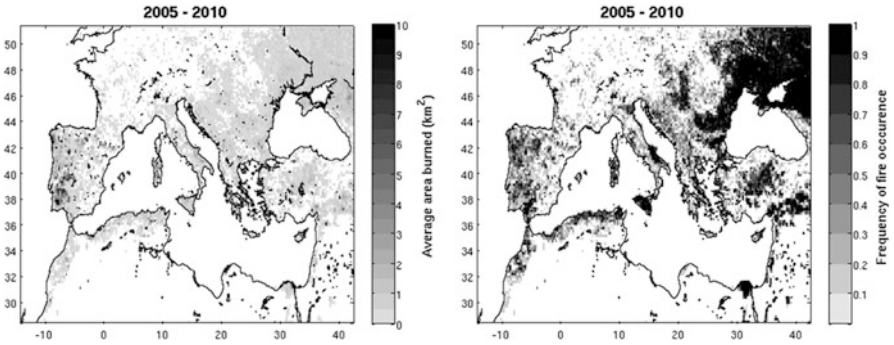

Fig. 61.1 Average area burnt according to MODIS within a 20 km × 20 km grid and corresponding frequency (number of years when a fires was detected within a grid cell) during the period 2005–2010

61.3 Evaluation on a Case Study: Greek Fires in August 2007

The impact of fire emissions is evaluated using the CHIMERE CTM [2] forced by simulations from the WRF meteorological model. It includes anthropogenic emissions from the EMEP inventory, biogenic emissions from the MEGAN model, and dust emissions parameterization [7]. In the results presented here, CHIMERE was run with a horizontal resolution of 20 km and 18 levels from the surface up to 200 hPa. Fire emissions are considered mixed in the boundary layer (but no lower than 1 km).

The temporal variability of the emissions during the Greek fires event, and the transport pathways have been evaluated through comparisons to the IASI/METOP retrievals of carbon monoxide (CO) [11] used as a tracer of long-range transport. Figure 61.2 shows the total CO columns for both model and observations, averaged on a box directly above the emission region (21°E–23°E, .36.5°N–38°N). Comparisons to aerosol optical depth (AOD) from the POLDER/PARASOL instrument above the same region show similar results. Emissions seem underestimated, particularly the fine mode fraction for aerosols, but the temporal variability and transport pathways are well reproduced. The vertical structure of the plume has been evaluated based on comparisons to the CALIOP/CALIPSO lidar attenuated backscattered profiles, showing good agreement with a transport at ∼2–3 km for this event.

Observations of more reactive species (nitrogene dioxide from OMI, ammonia and ethylene from IASI, AirBase surface observations) have also been analyzed, highlighting the importance of accounting for the impact of dense aerosol plumes on photolysis rates. This is currently being implemented in the CHIMERE model following Péré et al. [8].

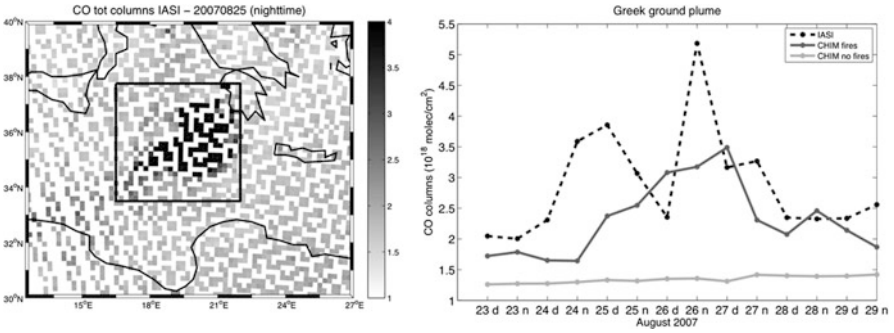

Fig. 61.2 *Left*: CO total columns (10^{18}molec/cm^2) observed by IASI during the Greek fire event; *Right*: Average CO observed within the fresh plume, closest to the Peloponnese, (*red line*) and CHIMERE simulated total CO in the same region with fire emissions included (*black*) and without including fires (*light blue*) (Color figure online)

61.4 Summary

The high resolution regional fire emissions inventory developed at LMD shows good performance for the modeling of fire plume transport, considering the large uncertainties on each parameter involved in the calculation. A near-real time version of the algorithm has been developed. Emissions are updated daily, and will be included in an experimental forecasting system (daily maps available at www.lmd.polytechnique.fr/cosy).

Acknowledgments This work is done in the framework of the APIFLAME project (www.lmd.polytechnique.fr/apiflame), supported by the PRIMEQUAL program (contract number 0962c0068). Work on satellite observations is supported by CNES. S. Stromatas is supported by a fellowship from CNES and ADEME.

References

1. Akagi SK, Yokelson RJ, Wiedinmyer C, Alvarado MJ, Reid JS, Karl T, Crounse JD, Wennberg PO (2011) Emission factors for open and domestic biomass burning for use in atmospheric models. Atmos Chem Phys 11:4039–4072
2. Bessagnet B, Menut L, Curci G, Hodzic A, Guillaume B, Liousse C, Moukhtar S, Pun B, Seigneur C, Schulz M (2009) Regional modeling of carbonaceous aerosols over Europe – focus on secondary organic aerosols. J Atmos Chem 61:175–202
3. Coheur P-F, Clarisse L, Turquety S, Hurtmans D, Clerbaux C (2009) IASI measurements of reactive trace species in biomass burning plumes. Atmos Chem Phys 9:5655–5667
4. Giglio L, Csiszar I, Justice CO (2006) Global distribution and seasonality of active fires as observed with the terra and aqua MODIS sensors. J Geophys Res 111:G02016. doi:10.1029/2005JG000142
5. Hoelzemann JJ, Schultz MG, Brasseur GP, Granier C, Simon M (2004) Global Wildland Fire Emission Model (GWEM): evaluating the use of global area burnt satellite data. J Geophys Res 109:D14S04. doi:10.1029/2003JD003666

6. Maignan F, Bréon F-M, Chevallier F, Viovy N, Ciais P, Garrec G, Trules J, Mancip M (2011) Evaluation of a dynamical global végétation model using time series of satellite végétation indices. Geosci Model Dev Discuss 4:907–941
7. Menut L, Chiapello I, Moulin C (2009) Previsibility of mineral dust concentrations: the CHIMERE-DUST forecast during the first AMMA experiment dry season. J Geophys Res 114:D07202. doi:10.1029/2008JD010523
8. Péré JC, Mallet M, Pont V, Bessagnet B (2011) Impact of aerosol direct radiative forcing on the radiative budget, surface heat fluxes, and atmospheric dynamics during the heat wave of summer 2003 over western Europe: a modeling study. J Geophys Res 116:D23119. doi:10.1029/2011JD016240
9. Roy DP, Jin Y, Lewis PE, Justice CO (2005) Prototyping a global algorithm for systematic fire affected area mapping using MODIS time series data. Remote Sens Environ 97:137–162
10. Seiler W, Crutzen PJ (1980) Estimates of gross and net fluxes of carbon between the biosphere and the atmosphere from biomass burning. Clim Change 2(3):207–247. doi:10.1007/BF00137988
11. Turquety S, Hurtmans D, Hadji-Lazaro J, Coheur P-F, Clerbaux C, Josset D, Tsamalis C (2009) Tracking the emission and transport of pollution from wildfires using the IASI CO retrievals: analysis of the summer 2007 Greek fires. Atmos Chem Phys 9:4897–4913
12. van der Werf GR, Randerson JT, Giglio L, Collatz GJ, Mu M, Kasibhatla PS, Morton DC, DeFries RS, Jin Y, van Leeuwen TT (2010) Global fire emissions and the contribution of deforestation, savanna, forest, agricultural, and peat fires (1997–2009). Atmos Chem Phys 10:11707–11735. doi:10.5194/acp-10-11707-2010
13. Wiedinmyer C, Akagi SK, Yokelson RJ, Emmons LK, Al-Saadi JA, Orlando JJ, Soja AJ (2011) The Fire INventory from NCAR (FINN): a high resolution global model to estimate the emissions from open burning. Geosci Model Dev 4:625–641. doi:10.5194/gmd-4-625-2011

Questions and Answers

Questioner name: Jordi Vilà (Wageningen University, The Netherlands)

Q:
1. Do you take into account the influence of fire on the meteorology (transport, radiation, microphysics)
2. How important is it?

A:We are currently using an offline chemistry-transport model (CHIMERE), and the impact of fires on meteorology is therefore not accounted for, although several studies have shown that it is important (using WRF-Chem case studies for instance, Grell et al. Have shown a strong short term impact on cloud formation, storm developments, etc.).

Regarding the radiative impact, we are currently implementing an online calculation of the photolysis rates to account for the impact of these dense plumes on photochemistry. Several studies have shown that the attenuation of radiation by the plume lowers ozone formation.

Ongoing work also involves the integration of a pyroconvection code to inject emissions at a correct altitude depending on the fire energy and atmospheric stability. This is critical for long-range transport since emissions injected in the free troposphere are expected to travel farther away.

Chapter 62
Influence of Physical Parameterization Changes in the ALARO High Resolution NWP Model for Belgium on the CTM CHIMERE

A.W. Delcloo, R. Hamdi, A. Deckmyn, P. Termonia, H. De Backer, and H. Van Langenhove

Abstract At the Royal Meteorological Institute of Belgium the chemical transport model (CTM) CHIMERE runs at a spatial resolution of 7 km. The CTM is first run on a coarse resolution of 50 km covering Western Europe. As a NWP input, the meteorological fields of ECMWF are consulted. The emission database is provided by EMEP. This model run is used as input for the boundary conditions for the coupled high resolution (7 km) chemical transport model run.

This one-way nested coupling with the high resolution limited area NWP model ALARO (spatial resolution of 7 km) improved already significantly the modelling of ozone concentrations by improving the physical parameterization, i.e. cloud cover, surface temperature, surface sensible heat flux, surface latent heat flux and relative humidity fields.

The model domain of ALARO covers Belgium and the Netherlands (680×680 km^2). The emission database used as input for this high-resolution model is the TNO/GEMS emission database (Visschedijk AJH, Zandveld PYJ, Denier van der Gon HACA, High resolution gridded European database for the EU integrate project GEMS, TNO-report 2007-A-R0233/B, 2007).

We will present the influence from the improved physical parameterizations of the NWP model on air quality model forecast performance for two different time periods. Also the influence on the implementation of a new surface scheme (SURFEX including The Town Energy Balance (TEB) scheme) in the NWP limited area model will be shown.

Keywords Chimere-model • Ozone • Town-Energy-Balance

A.W. Delcloo (✉) • R. Hamdi • A. Deckmyn • P. Termonia • H. De Backer
Royal Meteorological Institute of Belgium, Brussels, Belgium
e-mail: andy.delcloo@meteo.be

H. Van Langenhove
Research group EnVOC, Department of Sustainable Organic Chemistry and Technology, Faculty of Bioscience Engineering, Ghent University, Brussels, Belgium

D.G. Steyn et al. (eds.), *Air Pollution Modeling and its Application XXII*,
NATO Science for Peace and Security Series C: Environmental Security,
DOI 10.1007/978-94-007-5577-2_62,

62.1 Introduction

The chemical transport model CHIMERE [4] has been coupled to the IFS/ECMWF at a coarse resolution of 50 km. The CHIMERE model is able to catch most of the day-to-day variability when verified against observations for Belgium at this coarse resolution.

Running CHIMERE on a coarse resolution of 50 km, using a large domain (Europe) helps us understand the contribution of synoptic weather phenomena to pollution events. However, to study the ability of a CTM to capture the day-to-day variability on a local scale, it is necessary to feed the model with high-resolution meteorological data from a NWP-model. The NWP-models we use for our analysis run four times a day in an operational context at our institute; the ALADIN model and its updated version ALARO receive their boundary conditions from ALADIN France, run by Météo France.

Also the performance of the use of the Town Energy Balance (TEB, [3]) single-layer module within the ALARO and ALADIN 7 km resolution NWP model within an operational configuration will be tested, with the SURFEX module online and offline. SURFEX is a new externalized (i.e., it can run independently from the ALADIN model) land surface scheme that has recently been implemented at the RMI for off-line applications [2]. SURFEX contains four modules, describing the exchanges of water, momentum, and energy on four tiles of surface: sea, lake, vegetation, and urban area. The vegetation tile is considered as a composition of various sub-homogenous entities called patches (forest, meadows, fields . . .).

62.2 Results and Discussion

To validate our results, observation data is used from IRCELINE. Four different versions of our NWP-model are verified: ALADIN and ALARO applying the SURFEX scheme, further referred as ALD-SFX and ALR-SFX. When the option TEB is activated, the simulations are referred as ALD-SFX-TEB and ALR-SFX-TEB. These runs will be compared with the output of the simulations, ran with ALADIN and ALARO [1].

We will use the following method to integrate the cloud cover from the NWP model in the CTM: we will use 3 h mean cloud cover values, representative for the three consecutive hours as shown to be the best approach in [1].

The improved physical parameterization scheme of ALARO should lead to an improved precipitation-, temperature- and cloud field. A qualitative and quantitative evaluation is made between the one-way nested couplings of CHIMERE with the four different LAM's. Table 62.1 gives an overview of some general statistics on the modeling of maximum ozone concentrations for 1 month during the summer (July 2008) for some specific observation stations and different scenarios. Figure 62.1 shows a time series of modelled- against observed maximum ozone concentrations for the station of Destelbergen, applying the ALARO-SFX-TEB scenario.

Table 62.1 Correlation, rmse ($\mu g/m^3$) and bias ($\mu g/m^3$) for the time period 01/07/2008–31/07/2008 are shown for some stations for the scenarios ALD-SFX, ALD-SFX-TEB, ALR-SFX, ALR-SFX-TEB for the analysis (D-1)

		Dessel	Houtem	Moer-kerke	Destel-bergen	Hasselt	Ukkel
ALD-SFX	Corr	0.93	0.87	0.90	0.92	0.87	0.83
	Rmse	19.1	15.1	16.8	14.1	15.6	31.5
	Bias	9.7	3.2	7.7	3.8	6.1	−20.4
ALD-SFX-TEB	Corr	0.93	0.89	0.90	0.92	0.89	0.84
	Rmse	19.6	14.4	16.8	14.4	15.3	29.2
	Bias	10.8	2.9	8.1	5.4	7.0	−16.1
ALR-SFX	Corr	0.90	0.88	0.85	0.90	0.88	0.80
	Rmse	19.3	14.9	18.6	14.6	13.8	34.0
	Bias	7.8	2.9	7.8	1.6	2.4	−22.7
ALR-SFX-TEB	Corr	0.90	0.88	0.85	0.91	0.88	0.80
	Rmse	20.6	14.8	18.5	14.5	14.0	31.3
	Bias	9.3	3.1	8.1	4.1	4.4	−18.3

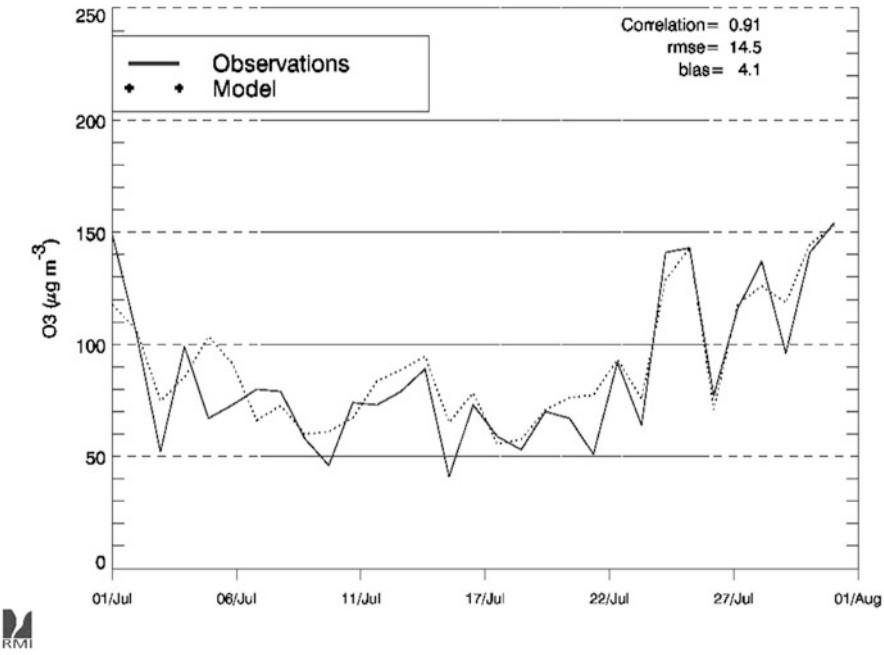

Fig. 62.1 Time series of observed- and modelled maximum ozone concentrations for the time period 01/07/2008–31/07/2008 for the station of Destelbergen (D-1)

Table 62.1 shows that the updated versions, using TEB reduces the bias in the sub-urban stations considerably and improves the modeling of the day-to-day variability of the maximum ozone concentrations. In general, ALARO with SURFEX shows less bias.

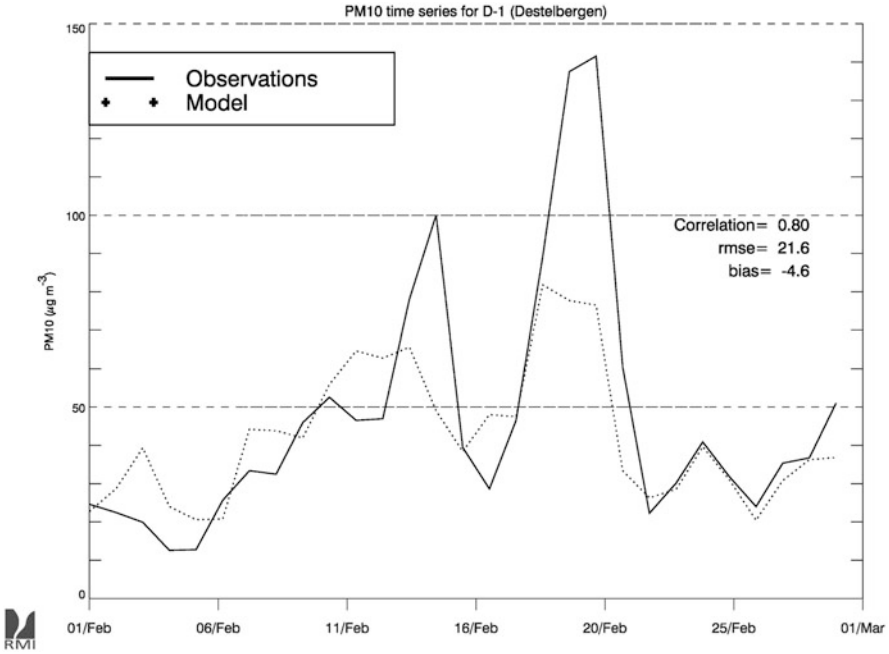

Fig. 62.2 Time series of observed- and modelled PM10 concentrations for the time period 01/02/2008–29/02/2008 for the station of Destelbergen (D-1)

PM10 concentrations have been modelled during 1 month in the winter period (February 2008). Figure 62.2 shows an example of the time series for the station of Destelbergen.

In the previous version without SURFEX and TEB, correlations between modelled- and observed PM10 concentrations vary between 0.5 and 0.8. The statistics for PM10 shows a major improvement (reduction) in the representation of the day-to-day variability and the bias when implementing both schemes, especially for the sub-urban stations (6–8 $\mu g/m^3$).

62.3 Conclusions

When the CTM was coupled to the updated ALADIN/ALARO NWP-models, using the SURFEX and the TEB scheme, statistics significantly improved for both modelling maximum ozone- and PM10 concentrations, especially for the sub-urban stations.

It will be useful to perform a full year simulation in order to examine if there are seasonal dependencies detectable in the CTM output.

Acknowledgments The authors would like to thank IRCELINE for providing the ozone and PM10 data.

References

1. Delcloo AW, Deckmyn A, Hamdi R, Van Langenhove H, Foret G, De Backer H (2012) Coupling of the CTM CHIMERE to the high resolution LAM ALADIN for Belgium, air pollution modeling and its application XXI, NATO science tor peace and security series C: environmental security volume 4 part 2, pp 315–319. doi: 10.1007/978-94-007-1359-8_54
2. Hamdi R (2009) The offline version of SURFEX coupled to the operational ALADIN forecast over Belgium: a tool to improve winter screen temperature. Publication Scientifique Interne, RMI, Brussels
3. Masson V, Grimmond CSB, Oke TR (2002) Evaluation of the Town Energy Balance (TEB) scheme with direct measurements from dry districts in two cities. J Appl Meteorol 41:1011–1026
4. Vautard R, Beekmann M, Roux J, Gombert D (2001) Validation of a deterministic forecasting system for the ozone concentrations over the Paris area. Atmos Environ 35:2449–2461
5. Visschedijk AJH, Zandveld PYJ, Denier van der Gon HACA (2007) High resolution gridded European database for the EU integrate project GEMS, TNO-report 2007-A-R0233/B

Chapter 63
Model Evaluation for Surface Concentration of Particulate Matter in Europe and North America in the Context of AQMEII

Efisio Solazzo, Stefano Galmarini, Roberto Bianconi, and S. Trivikrama Rao

Abstract Ten state-of-the-science regional air quality (AQ) modeling systems have been applied to continental-scale domains in North America and Europe for full-year simulations of 2006 for the Air Quality Model Evaluation International Initiative (AQMEII), whose main goals are model inter-comparison and model evaluation. Model simulations are inter-compared and evaluated with a large set of observations for ground-level particulate matter (PM_{10} and $PM_{2.5}$) and its chemical components. Analyses of PM_{10} time series show a large model underestimation throughout the year. Moreover, a large variability among models in predictions of emissions, deposition, and concentration of PM and its precursors has been found.

Keywords AQMEII • Model intercomparison • Model evaluation • Particulate matter

63.1 Introduction

The main objective of the Air Quality Model Evaluation International Initiative (AQMEII) is to assess the state-of-the-science in current regional-scale AQ models in order to improve their ability to accurately characterize the spatial and temporal features embedded in air quality observations. Within AQMEII, a cooperative

E. Solazzo (✉) • S. Galmarini
Joint Research Centre, European Commission, Ispra, Italy
e-mail: efisio.solazzo@jrc.ec.europa.eu

R. Bianconi
Enviroware srl, Concorezzo, Milano, Italy

S.T. Rao
Atmospheric Modeling and Analysis Division, U.S. Environmental Protection Agency, Research Triangle Park, NC, USA

D.G. Steyn et al. (eds.), *Air Pollution Modeling and its Application XXII*,
NATO Science for Peace and Security Series C: Environmental Security,
DOI 10.1007/978-94-007-5577-2_63,

exercise was launched for modelling groups to use their AQ models retrospectively to simulate the entire year 2006 for the continents of Europe (EU) and North America (NA), with the goal of evaluating the ability of regional AQ models in reproducing atmospheric pollutant concentrations. In this paper, we focus on the evaluation of PM in EU and NA using simulated results from ten different state-of-the-science regional AQ models run by 15 independent groups from both continents. In addition to the model results, observational PM data from over 2,000 monitoring stations have also been gathered and made available on the ENSEMBLE system [1]. The scale of the regional model evaluation and inter-comparison presented in this study is unprecedented given the number of models evaluated, the length of the simulation period, the spatial extent of the model domains, and the amount of observational data collected over the two continents.

63.2 Participating Models

Outputs from the regional AQ models participating in the AQMEII exercise are compared to observations over the full year of 2006. Modelling groups have provided gridded surface concentrations of PM_{10} and $PM_{2.5}$ for two continental areas: Europe and North America (US and Canada). The meteorological drivers and AQ models providing PM concentrations are

- MM5/WRF – CHIMERE;
- MM5 – POLYPHEMUS;
- WRF – CAMx;
- COSMO – MUSCAT;
- ECMWF – SILAM;
- MM5 – DEHM;
- WRF – CMAQ;
- ECMWF – LOTOS-EUROS;
- GEM – AURAMS;
- WRF – WRF/Chem.

Some AQ models were run over the two continents driven by different meteorology (as for example, CHIMERE). Full details, settings and references can be found in Solazzo et al. [2]. The models' outputs were compared against observational data at over 2,000 receptor locations over the two continents.

63.3 PM_{10} Evaluation and Model Cross-Comparison

Time series of monthly and daily continental-scale mean PM_{10} surface concentrations are presented in Fig. 63.1 for EU and NA.

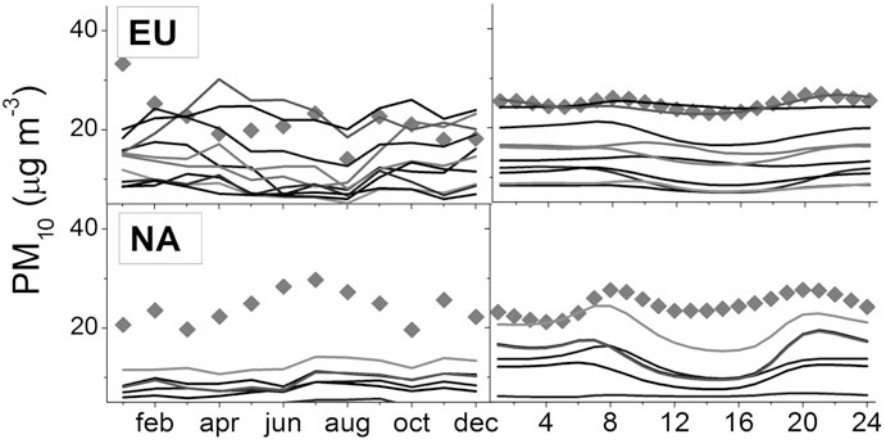

Fig. 63.1 Monthly time series (*right column*) and daily cycle (local time, *left column*) for PM_{10} over Europe (*first row*) and North America (*second row*) continental domains for 2006 (*solid gray diamonds*: observations; *colored lines*: model predictions)

A persistent underestimation of PM_{10} by all models is common to both continents. The satisfactory agreement between two models for EU (green and black lines, most noticeable for the daily cycle) is achieved at the expense of the fine fraction. In fact, as discussed later, these models show a tendency to overestimate $PM_{2.5}$. Reasons for the severe model underestimation are attributable to (*a*) missing sources in the emission inventories (such as natural dust), (*b*) unmodelled PM components, (*c*) negative bias in the PM gaseous precursors (such as SO_2 and NO_x), and (*d*) bias introduced by the meteorological drivers (such as wind speed). See Solazzo et al. [2] for explanations of possible sources of model bias for PM_{10}.

Levels of the root mean square error (RMSE), Pearson correlation coefficient (PCC), arithmetic mean, and spread (Std Dev) for each model simulation (entire continent, full year) are provided in Table 63.1 (only the non-urban receptors providing daily observations have been included here). PCC values for the simulations vary greatly and are generally higher for EU than NA, ranging for EU from a minimum of 0.2 to a maximum of 0.7, and for NA from 0.15 to 0.4. The variability seen in the observations for NA is underestimated by all models by a factor of two on average, indicating that these models were unable to simulate the same range of variability as the measurements.

While the standard deviation for the EU observed data (7.3 $\mu g\ m^{-3}$) is larger than that of NA (5.4 $\mu g\ m^{-3}$), the majority of the models underestimate the observed variability, with the exception of Mod5, which agrees well with the observed variability. Such large differences among models depend strongly on PM composition and on the chemical components of PM_{10} included in each model's chemistry module.

Table 63.1 Statistical analysis for PM_{10} EU and NA – whole continents

		RMSE	PCC	Mean	Std Dev
EU	Mod1	7.3	0.4	22.9	5.4
PM_{10} daily averaged hourly data	Mod2	14.2	0.5	8.9	2.8
	Mod3	11.2	0.5	12. 5	5.3
	Mod4	15.2	0.7	7.5	2.2
	Mod5	10.8	0.4	14.4	7.7
	Mod6	9.8	0.2	22.3	6.6
	Mod7	9.8	0.7	13.2	4.6
	Mod8	14.5	0.7	8.0	3.2
	Mod9	13.9	0.4	9.3	3.9
	Mod10	7.7	0.5	17.7	5.3
	Obs			21.5	7.3
NA	Mod12	20.9	0.3	10.5	2.0
PM_{10} daily averaged hourly data	Mod13	25.6	0.3	5.7	1.6
	Mod14	17.2	0.2	14.5	3.0
	Mod15	17.5	0.2	14.2	3.2
	Mod16	19.9	0.4	11.5	2.2
	Mod17	5.3	0.15	20.1	2.9
	Obs			30.7	5.4

RMSE root mean square error, *PCC* Pearson correlation coefficient, *Std Dev* standard deviation

63.4 $PM_{2.5}$ Evaluation and Model Cross-Comparison

Time series of monthly continental mean $PM_{2.5}$ surface concentrations are presented in Fig. 63.2 for EU and NA. Compared to PM_{10} concentrations model bias is much lower for both continents, demonstrating an enhanced capability of the AQ models to simulate $PM_{2.5}$. For EU, the models underestimate the monthly mean continental $PM_{2.5}$ surface concentrations, with several exceptions. In particular, the models that overestimate PM_{10} concentrations also overestimate $PM_{2.5}$ concentrations. The majority of the NA models also tend to underestimate $PM_{2.5}$ concentrations.

Model-to-measurement correlation is slightly higher for the NA sub-regions (total $PM_{2.5}$, not shown), with PCC for the majority of models between 0.5 and 0.75 for NA and between 0.4 and 0.7 for EU, indicating that the daily variability of $PM_{2.5}$ is better reproduced for NA, possibly due to differences in the PM emission datasets [2].

Analysis of $PM_{2.5}$ components (not shown here, but reported in [2]) showed more homogenous model performance for the speciated compounds than for total $PM_{2.5}$ mass. This result might suggest that, while AQ models are reliable for simulation of inorganic aerosol, there are still gaps in the representation of some processes other than inorganic aerosol chemistry that strongly influence the $PM_{2.5}$ concentrations.

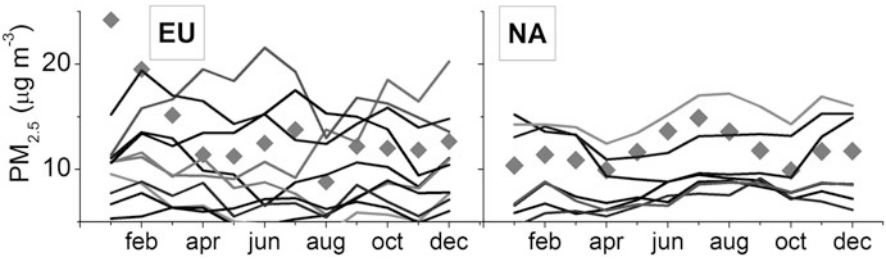

Fig. 63.2 Monthly time series for $PM_{2.5}$ over Europe (*left*) and North America (*right*) continental domains for 2006 (*solid gray diamonds*: observations; *colored lines*: model predictions)

63.5 Conclusions

We have analysed predictions of PM_{10} and $PM_{2.5}$ by ten AQ models run by 15 groups in Europe and North America, quantifying bias and model performance with the aid of a number of statistical metrics. We conclude that a large variability exists among models (and even among different simulations performed using the same model), especially for PM_{10}, with model concentrations varying by up to a factor of seven between the different model simulations. All models severely underestimate PM_{10} concentrations over the entire year, often with mean fractional errors exceeding 0.75 for both continents.

Model performance for $PM_{2.5}$ was much better than that for PM_{10}, with PCC values often exceeding 0.7 (higher on average for NA than EU). Work still remains to be undertaken to eliminate large uncertainty in the simulation of secondary organic aerosols and unspeciated $PM_{2.5}$.

Acknowledgments The AQMEII community is kindly acknowledged for providing the modeling data. Although this paper has been reviewed by EPA and approved for publication, it does not necessarily reflect EPA's policies or views.

References

1. Galmarini S et al (2012) ENSEMBLE and AMET: two systems and approaches to a harmonised, simplified and efficient assistance to air quality model developments and evaluation. Atmos Environ 53:51–59. doi:10.1016/j.atmosenv.2011.08.076
2. Solazzo E et al (2012) Operational model evaluation for particulate matter in Europe and North America in the context of AQMEII. Atmos Environ 53:75–92

Chapter 64
Multi-scale Atmospheric Composition Modelling for Bulgaria

Georgi Gadzhev, Kostadin Ganev, Maria Prodanova, Dimiter Syrakov, Emanouil Atanasov, and Nikolai Miloshev

Abstract The present work aims to studying the local to regional atmospheric pollution transport and transformation processes over Bulgaria and to tracking and characterizing the main pathways and processes that lead to atmospheric composition formation in the region. The US EPA Models-3 system is chosen as a modelling tool. As the NCEP Global Analysis Data with 1° resolution is used as meteorological background, the MM5 and CMAQ nesting capabilities are applied for downscaling the simulations to a 9 km resolution over Balkans and 3 km over Bulgaria. The TNO emission inventory is used as emission input. Special pre-processing procedures are created for introducing temporal profiles and speciation of the emissions. The study is based on a large number of numerical simulations carried out to four emission scenarios – with all the emissions and with excluded biogenic emissions, emissions from energetics and road transport. Some results from the numerical simulations concerning the main features of the atmospheric composition in Bulgaria and the contribution of the different emission categories are demonstrated in the paper.

Keywords MM5-CMAQ • NO_2 • O_3 • SO_2

G. Gadzhev (✉) • K. Ganev • N. Miloshev
National Institute of Geophysics, Geodesy and Geography, Bulgarian Academy of Sciences, Acad. G. Bonchev Str., Bl.3, Sofia 1113, Bulgaria
e-mail: ggadjev@geophys.bas.bg

M. Prodanova • D. Syrakov
National Institute of Meteorology and Hydrology, Bulgarian Academy of Sciences, 66 Tzarigradsko shaussee Blvd, Sofia 1784, Bulgaria

E. Atanasov
Institute of Information and Communication Technologies, Bulgarian Academy of Sciences, Acad. G. Bonchev Str., Bl.2, Sofia 1113, Bulgaria

D.G. Steyn et al. (eds.), *Air Pollution Modeling and its Application XXII*,
NATO Science for Peace and Security Series C: Environmental Security,
DOI 10.1007/978-94-007-5577-2_64,

64.1 Introduction

Air Quality (AQ) is a key element for the well-being and quality of life of European citizens. Bulgaria also faces AQ problems. It should be noted that, while in Western Europe the photo-oxidant and PM air pollution are at present the major environmental problem, in Bulgaria the classic acidifying pollutants (SO_2, NOx,), the heavy metals (Hg, Cd, Pb) and the persistent organic pollutants are still a serious problem and so the study of their environmental impact is absolutely necessary. The reduction of the emissions of these compounds is a major task in the environmental policy of the country.

The air pollution transport is subject to a different scale phenomena, each characterized by specific atmospheric dynamic mechanisms, chemical transformations, typical time scales etc. The air pollution pattern is formed as a result of interaction of different processes, so knowing the contribution of each for different meteorological conditions and given emission spatial configuration and temporal behavior is by all means important. That is why the one of the overall study goals is to make some evaluations of the contribution of different processes to the local to regional pollution over the Balkans and/or Bulgaria.

The main scientific challenge of local to regional atmospheric composition pattern modelling probably is the accounting for the strong dependence of concentrations on fluctuations of local and regional meteorological conditions, the complex interaction of transport scales (different life times of the pollutants make it even more complex), uncertainties and responses to emission forcing and boundary conditions, both introducing information noise.

64.2 Methodology and Input Data

The simulations are based on the US EPA Model-3 system [1–4]. The MM5/CMAQ simulations were performed day by day for 8 years – from 2000 to 2007. Thus a quite extensive data base was created, which could be used for different studies and considerations of the main features and origins of the atmospheric composition in Bulgaria.

The large scale (background) meteorological data used by the study is the NCEP Global Analysis Data with $1^\circ \times 1^\circ$ resolution. At the moment the created database contains all the necessary information since year 2000.

The TNO high resolution emission inventory [6] is exploited. The TNO emissions are distributed over ten SNAPs classifying pollution sources according the processes leading to harmful material release to the atmosphere. The inventory contains eight pollutants: CH_4, CO, NH_3, NMVOC (VOC), NOx, SOx, PM10 and PM2.5. The biogenic emissions, which depend on the vegetation type and the meteorological conditions, are calculated by the SMOKE model. The temporal allocation is made on the base of daily, weekly and monthly profiles, provided in [5].

Four emission scenarios will be considered in the present paper: Simulations with all the emissions, simulations with biogenic emissions and the emissions of SNAP categories 1 (energetics) and 7 (road transport) for Bulgaria reduced by a factor of 0.8.

64.3 Results, Comments and Discussion

The most simple atmospheric composition evaluations are, of course, the surface concentrations. By averaging over the 8-year simulated fields ensemble the mean annual and seasonal surface concentrations can be obtained and treated as respective "typical" daily concentration patterns. That can be seen in the plots (Fig. 64.1) and it is not surprising: the big cities, the road network and the big power plants are clearly outlined in the surface concentrations.

The averaged over the ensemble 2D concentration fields can be themselves averaged over the territory of Bulgaria and thus some easier to comprehend the plots of the "typical" diurnal course of the concentrations for the year and the four seasons to be obtained (Fig. 64.2) for Ozone [ppb] and SO_2 [ppb]. What can be seen in the

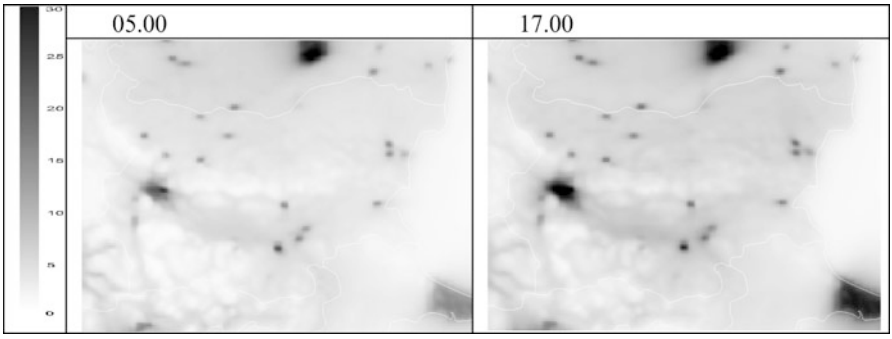

Fig. 64.1 Surface concentrations of NO_2 [ppb] annually averaged in 05.00 and 17.00 GMT

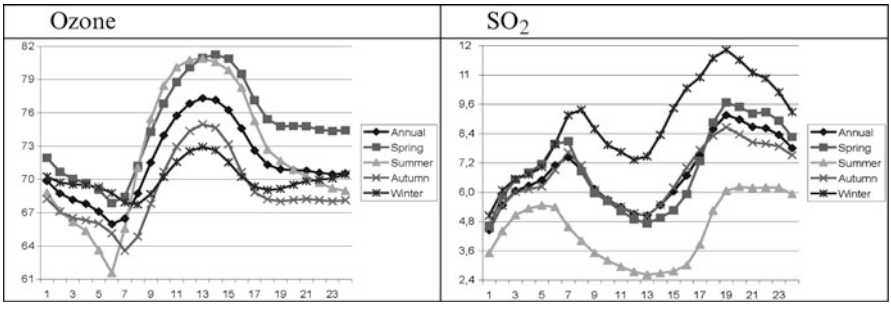

Fig. 64.2 Plots of O_3 and SO_2, averaged annually, spring, summer, autumn and winter

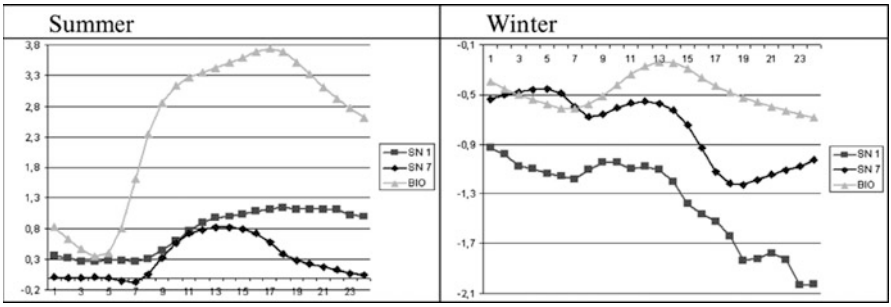

Fig. 64.3 Plots of the contributions [%] of the emissions from SNAP categories 1 (SN1) and 7 (SN7) and of the biogenic emissions (BIO) to the concentrations of O_3 [ppb]

plots does not defy the common sense and does not oppose the schematic concepts about how the air pollution near earth surface is formed. SO_2 has its minimums during daytime and its concentrations are higher during the winter than those in the summer. The ozone concentrations, as they should, have their maximum during daytime and are higher in the warmer part of the year.

In order to demonstrate the emission contribution behavior in a more simple and easy to comprehend way, the respective fields can be averaged over some domain (in this case the territory of Bulgaria), which makes it possible to jointly follow and compare the diurnal behavior of the respective contributions for different species (Fig. 64.3).

The contributions of different emission categories to different species surface concentrations have different diurnal course and different importance. The biogenic emissions have near to zero and negative contributions for O3 during the winter. Smaller and more significant differences than those of summer could be seen, this is quite natural, of course, having in mind that in the warm period of the year the biogenic emissions are higher. That is an important result which means, in particular, that the ozone in Bulgaria during the winter is mostly due to transport from other countries.

The contribution of the emission from SNAP categories 1 and 7, which are the major sources of the other ozone precursor – nitrogen oxides, is also small. This once again is an indirect indicator that the surface ozone in Bulgaria is to a small extend due to domestic sources, but is mostly imported.

64.4 Conclusions

The performed numerical experiments produced a huge volume of information which have to be carefully analyzed and generalized so that some final conclusions could be made.

The demonstrations, presented in the present paper are just a first glance on the atmospheric composition status in Bulgaria, so very few decisive conclusions can be made at this stage of the study.

The obtained ensemble of numerical simulation results is extensive enough to allow statistical treatment – calculating not only the mean concentrations and different SNAP categories contribution mean fields but also standard deviations, skewness, etc. with their dominant temporal modes (seasonal and/or diurnal variations). Some advanced and sophisticated methods for statistical treatment of the results should also be appropriately applied in order to: study the atmospheric pollution transport and transformation processes from urban to local to regional (Balkan and country) scales. Track and characterize the main pathways and processes that lead to atmospheric composition formation in different scales, and provide high quality scientifically robust assessments of the atmospheric composition and its origin – the air pollution fields response to emission changes (model sensitivity to emission input) is obviously a task of great practical importance, obviously connected with formulating short-term (current) pollution mitigating decisions and long-term pollution abatement strategies.

Acknowledgments The present work is supported by the Bulgarian National Science Fund (grants № Д 002-161/16.12.2008 and ДЦВП-02/1/29.12.2009), and by the 7FP projects PASODOBLE, Grant № 241557 and EGI-InSPIRE Grant № 261323.

References

1. Byun D, Ching J (1999) Science algorithms of the EPA models-3 Community Multiscale Air Quality (CMAQ) modeling system EPA report 600/R-99/030 Washington, DC http://www.epa.gov/asmdnerl/models3/doc/science/science.html
2. CEP (2003) Sparse Matrix Operator Kernel Emission (SMOKE) modeling system. University of Carolina, Carolina environmental programs, Research Triangle Park, NC
3. Dudhia J (1993) A non-hydrostatic version of the Penn State/NCAR Mesoscale model: validation tests and simulation of an Atlantic cyclone and cold front. Mon Weather Rev 121:1493–1513
4. Grell G, Dudhia J, Stauffer DR (1994) A description of the fifth generation Penn state/NCAR Mesoscale Model (MM5) NCAR technical note NCAR TN-398-STR pp. 138
5. Schaap M, Timmermans RMA, Roemer M, Boersen GAC, Builtjes PJH, Sauter FJ, Velders GJM, Beck JP (2008) The LOTOS–EUROS model: description, validation and latest developments. Int J Environ Pollut 32(No.2):270–290
6. Visschedijk AJH, Zandveld PYJ, Denier van der Gon HAC (2007) A high resolution gridded European emission database for the EU Integrate Project GEMS, TNO-report 2007-A-R0233/B, Apeldoorn, The Netherlands

Chapter 65
Source Apportionment in the LOTOS-EUROS Air Quality Model

Richard Kranenburg, Martijn Schaap, Elja Huibregtse, Carlijn Hendriks, and Arjo Segers

Abstract Source apportionment/labeling has been inserted in the LOTOS-EUROS model, and tests have been performed to show the impact of different source areas and categories.

Keywords LOTOS-EUROS model • Source apportionment

65.1 Introduction

One of the main targets in air quality modeling is to know the origin of air pollution. Ideally, information about the contribution of individual emission sources is known at a certain location, for example locations within a large urban or industrialized area. The different sources can be for example road traffic versus industry, emissions from abroad versus emissions from inside the country of interest and many others. This information of the origin of air pollution can be used for policy measures to create an effective reduction of air pollution.

65.2 Theory

Until now the individual contributions of sources to pollutant concentrations are mostly calculated by so-called scenario runs. In such a scenario run, the emissions of only one (or a few) sources are turned off in the model. The difference between the original run and the scenario run is used to determine the impact of the emission source.

R. Kranenburg (✉) • M. Schaap • E. Huibregtse • C. Hendriks • A. Segers
TNO, Climate Air and Sustainability, PO Box 80015, 3508 TA Utrecht, The Netherlands
e-mail: richard.kranenburg@tno.nl

D.G. Steyn et al. (eds.), *Air Pollution Modeling and its Application XXII*,
NATO Science for Peace and Security Series C: Environmental Security,
DOI 10.1007/978-94-007-5577-2_65,

This means that for each emission source of interest, the model must be run separately. This implies a lot of computer time and possible inconsistency between several runs. Another issue in the approach of scenario runs is that for chemical active tracers, the chemical regime is influenced. This implies that the difference between the basis run and the scenario run is not equal to only the contribution of the emission source(s), which is (are) switched off.

For example, the formation of ammonium-nitrate is an equilibrium reaction of ammonia (NH_3) and nitric acid (HNO_3). NH_3 is mainly emitted by agricultural sources while HNO_3 mainly originates from NO_x emissions. If the agricultural sources are reduced in a scenario run, there will be a decrease of the ammonium-nitrate concentrations. This implies that the origins of ammonium nitrate are mainly agricultural emissions. If the most important NO_x emission sources (burning processes) are reduced, there will also be a decrease of the ammonium-nitrate concentration. This implies that the burning processes are the main source of ammonium-nitrate.

65.3 Labeling Method

Within the chemistry transport model LOTOS-EUROS [1], a labeling method is developed to make a better source apportionment study. In this labeling method, the emissions of several sources of interest can be labeled. During all the model processes, the labels are tracked, such that the resulting concentrations can be coupled with the originating emissions. For the linear processes in the model, this approach is results in exactly the same as the scenario method. For the non-linear processes, the labeling method is more accurate to make a coupling of concentrations with originating emissions.

The problem with the influenced chemical regime is solved in the labeling module. In the labeling module the total amount of emissions is not changed, while the scenario method changes emissions. Because the total emissions are not changed, and the contribution of each label is treated separately, the chemical regime is not influenced.

On the other hand some, some assumptions must be made in the labeling routine for the chemistry. In the developed method, only the species containing a C, N or S atom are labeled [2]. Look for example to the reaction $NO_3 + NO_2 \rightarrow N_2O_5$. In this reaction the amount of produced N_2O_5 is assumed to be half of the label distribution of NO_3 and half of NO_2. This is a logical assumption, but the back reaction in this equilibrium $N_2O_5 \rightarrow NO_3 + NO_2$, leads to the assumption that both NO_3 and NO_2 get the labels from the reacted amount of N_2O_5. This is possible contrary with reality. But overall it holds that both NO_3 radical and NO_2 mainly originate from NO_x emissions, thus the sources are the same.

The problem with the source contribution of ammonium nitrate is not solved explicitly, but within the model it is now possible to allocate the ammonium part of the aerosol to the NH_3 emissions and the nitrate part to the NO_x emissions per source.

Overall, it can be said that the method with labeling has a more accurate view on the origin of air pollution, while the scenario method fits better to view different emission scenarios.

65.4 Results

If this algorithm is used to track ten different emission sources, the run time for the model increases with only a factor three, so the total computer time is reduced by 70 % with respect to the scenario runs. This is because some calculations have to be to done only ones for all different labels. Another advantage is that the results for the contributions of each specific emission source are based on the same model run, which means that all the results are consistent.

The labeling method is used in several projects. For example, an application of the labeling method is used for the EU FP7 project ENERGEO. The emissions are labeled by the combustion of the originating fuel. The labels are put on emission from combustion of Coal fuels, liquid fuels, gas fuels etc. In Fig. 65.1, the contributions over Europe from the combustion of solid fuels (upper) and heavy liquid fuels (lower) to the total concentration of sulphate aerosol in Europe is given. The solid fuels mainly contribute in Eastern Europe and the north of Spain, while the heavy fuels mainly contributes on the international shipping lanes.

Another application of this method is used in the BOP campaign; in this campaign a study of the origin of modeled PM concentrations in the Netherlands is done. The total contribution of Dutch sources is about 30 %, while the sources abroad contribute about 50 %. The rest of the concentrations are from natural sources, or from outside the boundary of the model domain (Fig. 65.2). In these

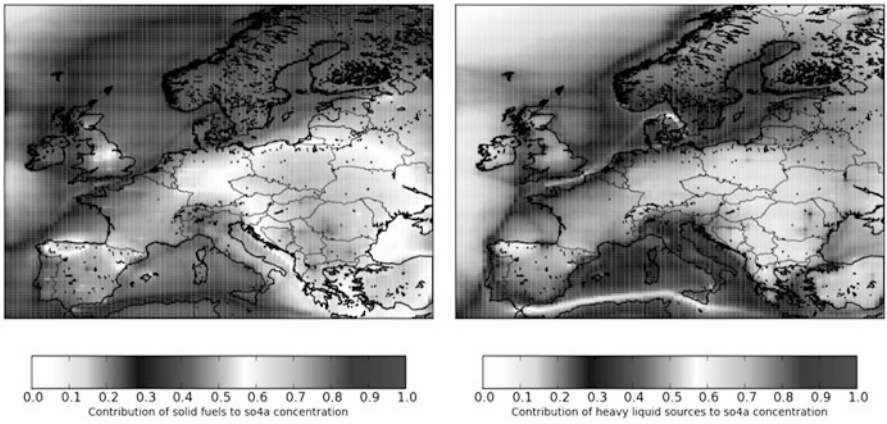

Fig. 65.1 Relative contribution of solid (*upper*) and heavy liquid (*lower*) fuels to the total concentration of sulphate aerosol in Europe

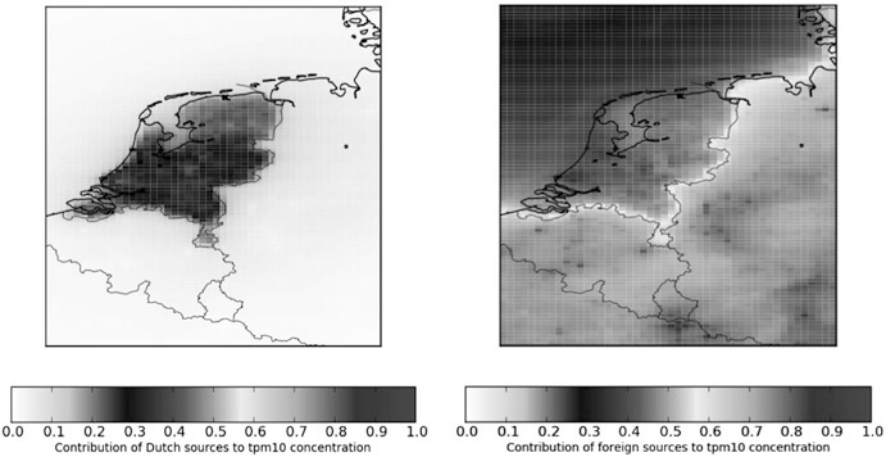

Fig. 65.2 Relative contribution of Dutch emissions (*left*), and abroad emissions (*right*) to the total modeled PM concentration in the Netherlands

figures it is clear that there is a significant gradient on the Dutch borders, this is mainly the result of tracers which are not transported very far, thus have a high local contribution.

References

1. Schaap M, Timmermans RMA, Roemer M, Boersen GAC, Builtjes PJH, Sauter FJ et al (2008) The LOTOS-EUROS model: description, validation and latest developments. Int J Environ Pollut 32(2):270–290
2. Wagstrom KM, Pandis SN, Yarwood G, Wilson GM, Morris RE (2008) Development and application of a computationally efficient particulate matter apportionment algorithm in a three dimensional chemical transport model. Atmos Environ 42:5650–5659

Chapter 66
Numerical Simulation of the Atmosphere Pollution After Accident at the "Tolliaty – Odessa" Ammonia Pipe

M.M. Biliaiev, L.V. Amelina, and M.M. Kharytonov

Abstract The results of numerical simulation of environment pollution after accident at the ammonia pipe are presented in this paper. The problem was solved for two different scenarios. Firstly only the ammonia ejection into the atmosphere was considered. 3D equation of pollutant dispersion (k – gradient model) and model of potential flow were used to simulate the process of air pollution. At the second step the problems of river Dnepr pollution and evaporation of ammonia from the water surface were considered. The developed numerical models and the code were used to calculate the scale of the air and water pollution. The code was used to calculate the toxic gas penetration into the dwellings of the settlements which are situated near the ammonia pipe. It allowed obtaining the information about the possibility of safety people evacuation.

Keywords Environment • Pollution • Numeric modeling • Ammonia pipe • Evacuation

66.1 Introduction

Transportation of liquid ammonia from Tolliaty City (the city where the ammonia is produced, Russia) to Odessa sea port (Ukraine) is carried out in ammonia pipe which is known as "*Tolliaty – Odessa*" pipe. This ammonia pipe was built in the former USSR according to the USA project. This pipe crosses 14 rivers on its 2,424 km route and only one river it crosses over the water surface. This is the river Dnepr which is the main water supply source of Ukraine.

M.M. Biliaiev (✉) • L.V. Amelina • M.M. Kharytonov
Railway Transport University, Dnipropetrovsk, Ukraine
e-mail: envteam@ukr.net

D.G. Steyn et al. (eds.), *Air Pollution Modeling and its Application XXII*,
NATO Science for Peace and Security Series C: Environmental Security,
DOI 10.1007/978-94-007-5577-2_66,

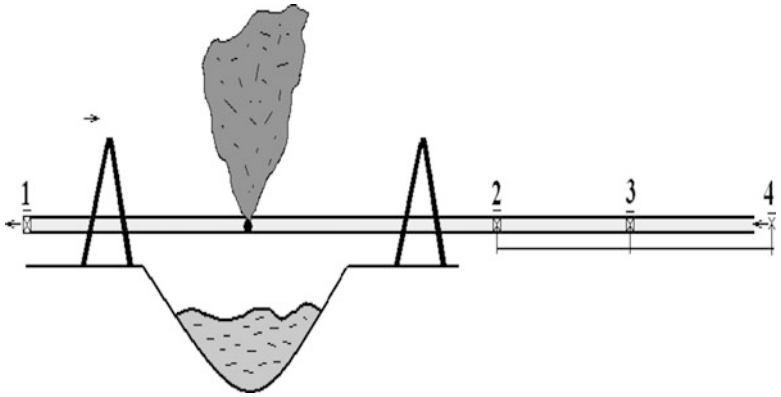

Fig. 66.1 Sketch of NH_3 emission from the opening at the ammonia pipe

The prediction of the possible air pollution level after accidents at this pipe was carried out in the seventies years of the past century on the basis of empirical models and later this prediction was carried out using the analytical models. Today the Ministry of Emergency of Ukraine needs more detailed and realistic information about the scale of environment pollution and risk assessment in the case of the different accidents or terror acts at this pipe.

In this paper two problems of the atmosphere pollution after accident at the ammonia pipe are considered.

1. *The first problem* is the scenario when the emission of NH_3 takes part at the ammonia pipe above the water surface (Fig. 66.1).

In this case to simulate the process of NH_3 dispersion in the atmosphere the equation of pollutant transport is used

$$\frac{\partial C}{\partial t}+\frac{\partial uC}{\partial x}+\frac{\partial vC}{\partial y}+\frac{\partial wC}{\partial z}+\sigma C = \frac{\partial}{\partial x}\left(\mu_x \frac{\partial C}{\partial x}\right)+\frac{\partial}{\partial y}\left(\mu_y \frac{\partial C}{\partial y}\right)+\frac{\partial}{\partial z}\left(\mu_z \frac{\partial C}{\partial z}\right) + \sum Q_i(t)\delta(x-x_i)\,\delta(y-y_i)\,\delta(z-z_i)\cdot$$

where u, v, w – are the wind velocity components; C – is the concentration of NH_3; σ – is the parameter taking into account the process of NH_3 washout;

μ_x, μ_y, μ_z are the turbulent diffusion coefficients; x_i, y_i, z_i are the coordinates of the point source of NH_3 emission; $Q_i(t)$ – is the intensity of NH_3 emission; $\delta(x-x_i)\delta(y-y_i)\delta(z-z_i)$ – is Dirac's delta-function.

In the numerical model developed the following models to approximate the velocity component u and coefficients of diffusion are used:

$$u = u_1\left(\frac{z}{z_1}\right)^n, \quad \mu_z = k_1\left(\frac{z}{z_1}\right)^m, \quad \mu_y = \kappa_0 u,\ \mu_y = \mu_x$$

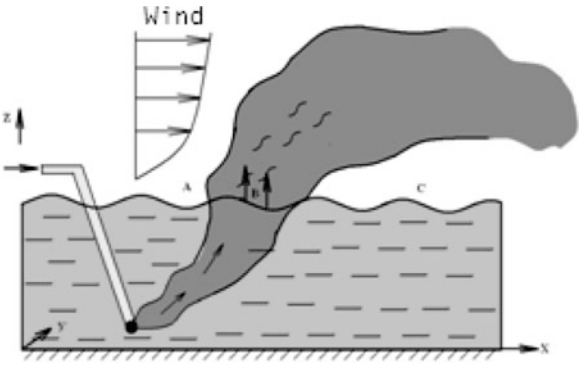

Fig. 66.2 Sketch of NH_3 emission from the ammonia pipe to the river

where u_1 is the wind speed at the height $z_1 = 10$ m; $n = 0.15$; k_0 is the empirical parameter; $k_1 = 0.2$; $m \approx 1$.

In the case of the accident the NH_3 propagation will take place in the region with the complex terrain. To simulate the wind flow in the case of the complex terrain and among buildings of the settlement which is situated near the ammonia pipe the 3D model of potential flow is used

$$\frac{\partial^2 P}{\partial x^2} + \frac{\partial^2 P}{\partial y^2} + \frac{\partial^2 P}{\partial z^2} = 0,$$

where is the potential of velocity.

The wind velocity components are calculated as follows:

$$u = \frac{\partial P}{\partial x}, \quad v = \frac{\partial P}{\partial y}, \quad w = \frac{\partial P}{\partial z}.$$

The process of the atmosphere pollution modeling in the case of the accident at the ammonia pipe consists of two steps. At the first step the wind velocity components are determined on the basis of the potential flow model and after that the NH_3 dispersion is studied using pollutant transport model.

2. *The second problem* is the scenario when the ammonia pipe has fallen into the river. In this case NH_3 discharges from the pipe contaminating the river and rising in the water to the water surface. This results in NH_3 plume formation over the river free surface (Fig. 66.2). This plume causes the atmosphere pollution.

In this scenario it is necessary to solve two problems. The first problem is the problem of the river pollution. To simulate the flow in the river Dnepr in this case the 2D Navier-Stokes equations which are written in the variables "vortex – flow function" are used:

$$\frac{\partial \omega}{\partial t} + \frac{\partial u\omega}{\partial x} + \frac{\partial v\omega}{\partial y} = \frac{1}{\mathrm{Re}}\left(\frac{\partial^2 \omega}{\partial x^2} + \frac{\partial^2 \omega}{\partial y^2}\right)$$

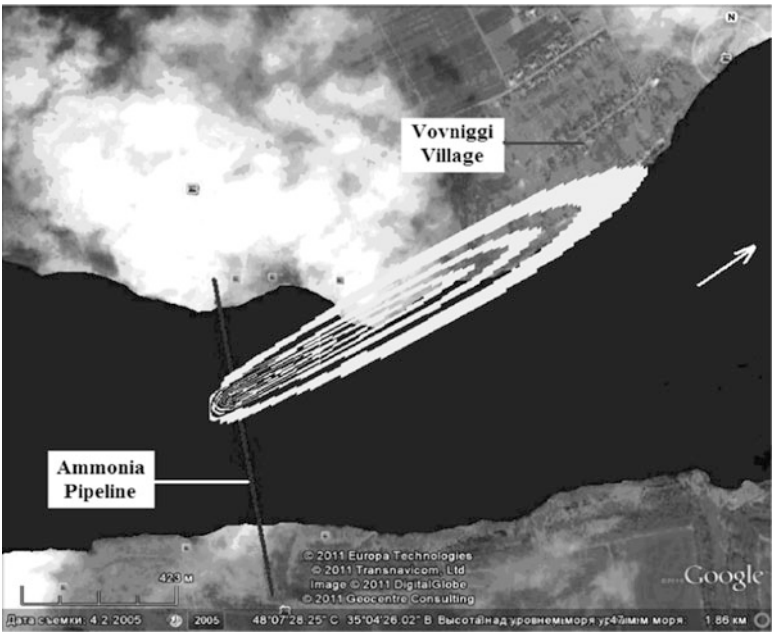

Fig. 66.3 Air pollution area after accident with NH_3 emission (t = 30s)

$$\frac{\partial^2 \psi}{\partial x^2} + \frac{\partial^2 \psi}{\partial y^2} = -\omega$$

where $\omega = \frac{\partial v}{\partial x} - \frac{\partial u}{\partial y}$ is the vortex; ψ is the flow function; Re is Reynolds number; $u = \frac{\partial \psi}{\partial y}; v = -\frac{\partial \psi}{\partial x}$ are the components of the velocity vector.

To simulate the NH_3 dispersion in the river the equation of pollutant transport is used.

For the '*pilot*' numerical simulation of the water flow the model of potential flow is also used.

The intensity of NH_3 emission from the pipe is calculated on the basis of the hydraulics formulae. The dimension of the NH_3 bubbles in the water and the speed of their rising in the water is calculated using empirical models.

The air pollution under the influence of the plume which is formed over the river surface is modeled on the basis of the equation of pollutant transport.

Numerical solution of the equations of the models is carried out using implicit difference schemes of splitting [1, 2]. On the basis of the numerical model the code '*Ammonia Release*' was developed.

Air pollution area after accident with NH_3 emission (t = 30 s) is shown in Fig. 66.3. The plume is forming over the water surface.

66.2 Conclusion

The developed code was used to simulate the intensity of the atmosphere pollution after the possible accidents at the ammonia pipe. This information allowed evaluating the risk of people hitting in their buildings and on the routes of evacuation.

References

1. Belayev NN, Kazakevitch MI, Khrutch V (1999) Computer simulation of the pollutant dispersion among buildings. // Wind Engineering into 21st century. In: Proceedings of the tenth international conference on wind engineering. A. A. Balkema/Rotterdam/Brookfield, Copenhagen/Denmark, pp 1217–1220
2. Belayev NN, Khrutch VK (2000) An engineering approach to simulate the 3-d wind flows over buildings. In: Proceedings of the fourth international colloquium on bluff body aerodynamics & applications. Ruhr-Universitat, Bochum, Germany. Volume of Abstracts, 11–14 Sept 2000, pp 471–475

Chapter 67
An outlook of System for Integrated modeLling of Atmospheric coMposition SILAM v.5

Mikhail Sofiev, Julius Vira, Marje Prank, Joana Soares, and Rostislav Kouznetsov

Abstract Chemical composition of the troposphere is controlled by several major emission sources, such as anthropogenic releases, biogenic gaseous and particulate emission, wild-land fires, wind-driven dust and sea salt emissions, lightning, and transport from the upper atmosphere. These sources contribute to a comparatively limited list of inorganic species and a vast variety of organic substances, which are transported and mixed in the troposphere but also take part in chemical and physical transformations. Due to inter-relation of the transformation processes and synergetic effects of the pollutants impacting human health and ecosystems, modern chemical transport models include a wide range of species, as well as their interactions. This paper presents a new generation of dispersion model SILAM, an open-code system developed at FMI in collaboration with VTT Energy (Finland), Main Geophysical Observatory (Russia), University of Tartu (Estonia), Medical University of Wien (Austria), Danish Meteorological Institute (Denmark).

Keyword Model evaluation

67.1 Components of SILAM v.5

SILAM v.5 includes six transformation modules (Fig. 67.1): CB4-based gas-phase scheme of NOx, VOCs and O3, basic acidification scheme for SIA formation from SOx, NOx, NHx and some VOCs [5], linearized scheme for sulphur oxides, generalized inert tracer with self-degradation, radioactive decay [7], and allergenic pollen [4, 6].

M. Sofiev (✉) • J. Vira • M. Prank • J. Soares • R. Kouznetsov
Finnish Meteorological Institute, Helsinki, Finland
e-mail: mikhail.sofiev@fmi.fi

D.G. Steyn et al. (eds.), *Air Pollution Modeling and its Application XXII*,
NATO Science for Peace and Security Series C: Environmental Security,
DOI 10.1007/978-94-007-5577-2_67,

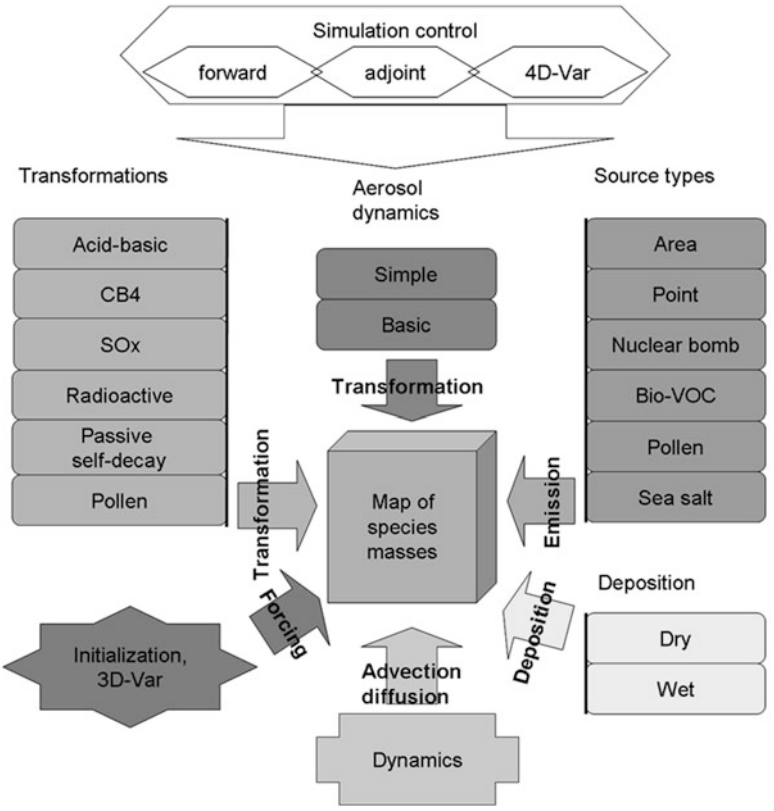

Fig. 67.1 Main modules of SILAM v.5

Two original schemes for aerosols processes – equilibrium-based and with basic aerosol dynamics – are connected with the sectional representations of particle size spectrum, chemical transformation routines, and dry and wet deposition modules [2].

The source terms include point and area emission source types for anthropogenic emission, nuclear bomb explosion, as well as the sub-models for BVOC, pollen, sea salt, with the sub-model for desert dust being developed.

The embedded data assimilation modules include 3D- and 4D-VAR [10], which allow the system initialization from the observations, dynamic adjustment of concentrations, and identification or adjustment of source characteristics. The adjoints to the transport and some chemical modules can also be used for analysis of the observational results.

67.2 Evaluation of SILAM v.5

SILAM evaluation is comprised of several-levels: algorithm testing, evaluation of past-time computations, in-depth analysis of specific episodes, and near-real-time evaluation of the previous-days model forecasts (Fig. 67.2).

In general, SILAM performance is at the level of other state-of-the-art atmospheric composition and air quality models [1, 3]. For some species, such as sea salt, its performance is better than standard, owing to more detailed representation of important processes [8, 9]. However, simplified representation of gas-phase chemical transformations (basic CB4 scheme) brings certain under-estimation of ozone concentrations. Finally, the SILAM, as all other models, under-estimates aerosol concentrations, especially the course fraction. The latter problem is being addressed via the new development of the wind-blown dust source term.

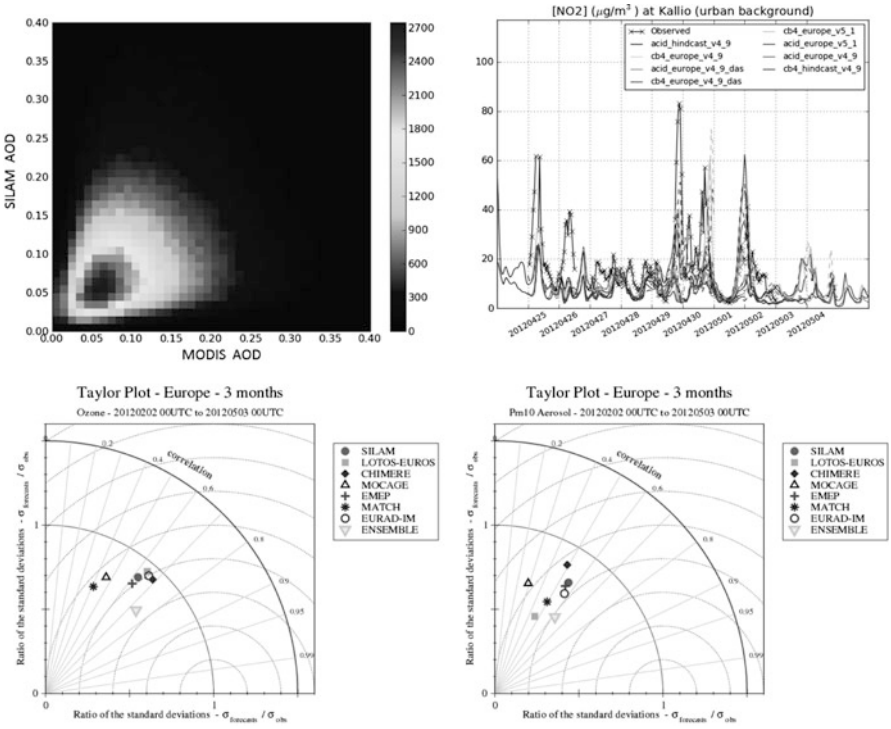

Fig. 67.2 Evaluation examples:
- sea salt (Southern Pacific, AOD scatter plot, colours depict the number of points in bin)
- NO2 (Helsinki, time series May 2012)
- O3 Taylor diagram for Central Europe, Feb–May 2012
- PM10 Taylor diagram for Central Europe, Feb–May 2012

67.3 Applications of SILAM at Various Scales

The model flexibility and a wide range of covered processes and species allowed its applications at practically any scale starting from the whole globe down to mesoscale computations with resolution ∼1 km. Operational forecasts and regular re-analyses are performed for European continent, Fennoscandia and Baltic, and the region of Gulf of Finland. Global applications, as well as other regional simulations address scientific aspects and performed offline.

References

1. Huijnen V et al (2010) Comparison of OMI NO2 tropospheric columns with an ensemble of global and European regional air quality models. Atmos Chem Phys 10(7):3273–3296
2. Kouznetsov R, Sofiev M (2012) A methodology for evaluation of vertical dispersion and dry deposition of atmospheric aerosols. J Geophys Res 117(D01202). doi:10.1029/2011JD016366
3. Kukkonen J et al (2012) A review of operational, regional-scale, chemical weather forecasting models in Europe. Atmos Chem Phys 12(1):1–87. doi:10.5194/acp-12-1-2012, [online] Available from: http://www.atmos-chem-phys.net/12/1/2012/. Accessed 3 Jan 2012
4. Siljamo P et al (2012) A numerical model of birch pollen emission and dispersion in the atmosphere. Model evaluation and sensitivity analysis. Int J Biometeorol. doi:10.1007/s00484-012-0539-5. [online] Available from: http://www.ncbi.nlm.nih.gov/pubmed/22434484 Accessed 14 May 2012
5. Sofiev M (2000) A model for the evaluation of long-term airborne pollution transport at regional and continental scales. Atmos Environ 34(15):2481–2493
6. Sofiev M, Siljamo P, Ranta H, Linkosalo T, Jaeger S, Rasmussen A, Rantio-Lehtimaki A, Severova E, Kukkonen J (2012) A numerical model of birch pollen emission and dispersion in the atmosphere. Description of the emission module. Int J Biometeorol. doi:10.1007/s00484-012-0532-z. [online] Available from: http://www.ncbi.nlm.nih.gov/pubmed/22410824 Accessed 14 May 2012
7. Sofiev M, Siljamo P, Valkama I, Ilvonen M, Kukkonen J (2006) A dispersion modelling system SILAM and its evaluation against ETEX data. Atmos Environ 40(4):674–685. doi:10.1016/j.atmosenv.2005.09.069
8. Sofiev M, Soares J, Prank M, de Leeuw G, Kukkonen J (2011) A regional-to-global model of emission and transport of sea salt particles in the atmosphere. J Geophys Res 116(D21). doi:10.1029/2010JD014713. [online] Available from: http://www.agu.org/pubs/crossref/2011/2010JD014713.shtml. Accessed 25 July 2012
9. Tsyro S, Aas W, Soares J, Sofiev M, Berge H, Spindler G (2011) Modelling of sea salt concentrations over Europe: key uncertainties and comparison with observations. Atmos Chem Phys 11(20):10367–10388. doi:10.5194/acp-11-10367-2011, [online] Available from: http://www.atmos-chem-phys.net/11/10367/2011/. Accessed 12 July 2012
10. Vira J, Sofiev M (2011) On variational data assimilation for estimating the model initial conditions and emission fluxes for short-term forecasting of SOx concentrations. Atmos Environ 46:318–328. doi:10.1016/j.atmosenv.2011.09.066, [online] Available from: http://linkinghub.elsevier.com/retrieve/pii/S1352231011010296. Accessed 5 Dec 2011

Chapter 68
Evaluating the Influence of Regional Gridded Emissions Distribution on Air Quality Simulation

Angel Rodríguez, Maria Dios, Santiago Saavedra, Jose A. Souto, Juan J. Casares, David Cartelle, Jose M. Vellón, C. Borrego, A.I. Miranda, J. Ferreira, A. Monteiro, N. Gallego, A. Sáez, and Maria L. Macho

Abstract The aim of this work is the assessment of changes in modelled regional air quality, by the comparison of the EMEP inventory vs. the application of a regional inventory based in a mixed top-down and bottom-up methodology over the NW of the Iberian Peninsula. Air quality simulations were carried out with the CHIMERE model for an ozone episode in 2008. Comparison against measurements using the Delta Tool show better scores for the regional inventory daily maxima 8 and 1 h ozone simulation results.

Keywords Emission inventories • Bottom-up and top-down • Ozone simulations • Performance evaluation

68.1 Introduction

The compilation of emission information is a critical stage in air quality modeling. The uncertainties related to emissions inventories are unavoidable, as all the emissions sources cannot be monitored individually. These uncertainties are partly

A. Rodríguez (✉) • M. Dios • S. Saavedra • J.A. Souto • J.J. Casares
Department of Chemical Engineering, University of Santiago de Compostela, 15782 Santiago de Compostela, Spain
e-mail: angel.rodriguez@usc.es; ja.souto@usc.es

D. Cartelle • J.M. Vellón
Troposfera SC, Ferrol, Spain

C. Borrego • A.I. Miranda • J. Ferreira • A. Monteiro
CESAM & Department of Environment and Planning, University of Aveiro, 3810-193 Aveiro, Portugal

N. Gallego • A. Sáez • M.L. Macho
Laboratorio de Medio Ambiente de Galicia, Consellería de Medio Ambiente, Territorio e Infraestructuras, Xunta de Galicia, Santiago de Compostela, Spain

D.G. Steyn et al. (eds.), *Air Pollution Modeling and its Application XXII*, NATO Science for Peace and Security Series C: Environmental Security,
DOI 10.1007/978-94-007-5577-2_68,

responsible for the lack of accuracy in results obtained by air quality modeling. Thus, a continuous development is needed to improve those results.

Typically bottom-up approaches are a very time-consuming task, due to the large amount of information handled. On the other side, the accurate distribution of emissions required in regional applications is not always well represented by using a top-down approach. The EMEP grid emission inventory with a spatial resolution of 50 km × 50 km is taken as reference in many European research applications.

However, the inner variability within each cell of this grid is not considered, affecting the final result of air quality simulations [3, 8].

68.2 Methodology

The CHIMERE model [5] was applied to a domain covering the NW of Iberian Peninsula (from 10.0°W to 6.0°W, and 41.0°N to 44.8°N), comprising Galicia and part of northern Portugal, with an horizontal resolution of 3×3 km^2. Meteorological fields were provided by WRF simulations [9]. 1–15 August 2007 period including ozone peaks was considered.

A mixed top-down and bottom-up methodology was designed and applied to estimate year 2008 emissions. For point sources, a bottom-up validated inventory provided by the Galician regional government was used [4]; major road traffic sources (>50,000 inhabitants cities and highways) were also obtained by bottom-up approach; other emissions were estimated following a top-down approach based in the EMEP inventory [2] with disaggregation criteria dependent on the source type [1, 6]. For the Portuguese region, the available inventory by municipality [7] was segregated to the same high grid resolution using a GIS to process data.

Ozone results were compared to measurements using the Delta Tool developed in the scope of FAIRMODE [10].

68.3 Results and Concluding Remarks

Figure 68.1 shows as an example the spatial distribution of annual nitrogen oxides (NOx) emissions from road traffic as estimated by the mixed approach and as directly coming from the EMEP inventory.

From the comparison of simulation results vs. measurements using the Delta Tool ozone daily maximum 8 h mean values are always within the criteria for all Delta Tool scores (Table 68.1), with the exception of the target for ozone estimated with the EMEP inventory.

The scale ranges from bad to good performances levels, with colored circles: black for worse than criteria, dark grey for between criteria and goal, and light grey for better than goal.

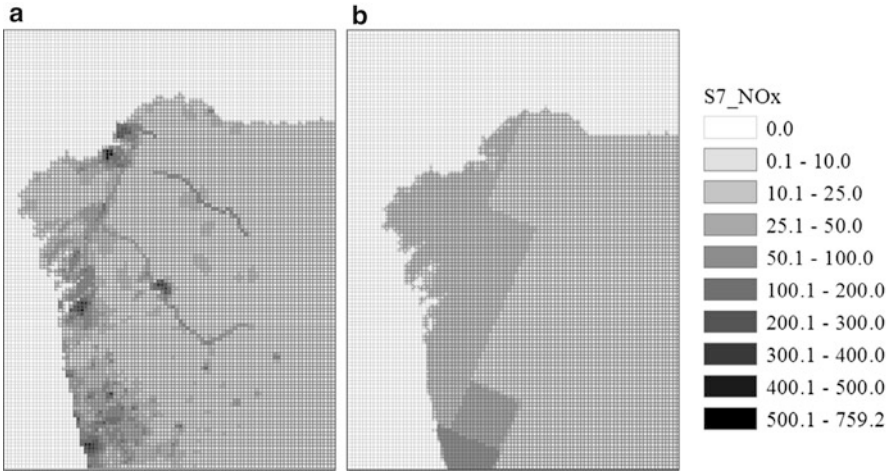

Fig. 68.1 Comparison between NOx emissions (t) from the road traffic sector estimated based on: (**a**) combined bottom-up and top-down inventory; and (**b**) EMEP inventory

Table 68.1 Scores diagrams (DeltaTool) for the simulations of the daily max 8 h mean ozone for (a) combined bottom-up and top-down inventory, and (b) EMEP inventory

No of stations: 26 valid/56 selected			
INDIC	(Crit – Goal)	(a) 90 % percentile	(b) 90 % percentile
MFB	(0.30 − 0.15)	0.22	0.27
FAC2	(0.50 − 0.60)	1.00	1.00
MFE	(0.45 − 0.30)	0.22	0.27
IOA	(0.65 − 0.78)	0.74	0.72
R	(0.65 − 0.78)	0.73	0.74
TARGET	(1.0 − 0.80)	0.97	1.08
RDE	(0.50 − 0.42)	0.22	0.22
RPE	(0.50 − 0.42)	0.23	0.28

Regarding the EMEP emissions simulations, only TARGET score is not accomplished, which is mainly due to a higher overestimation of the O_3 concentrations, according to the BIAS/σ plotted in Fig. 68.2.

In general ozone simulations were better using the mixed top-down/ bottom-up methodology to estimate emissions. This methodology is based on EMEP and other public information sources, which are easily updated and spatially distributed and analysed using geographical parameters.

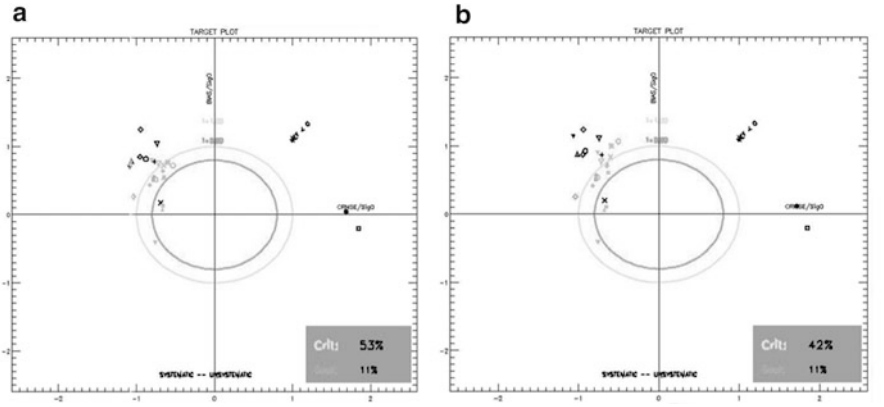

Fig. 68.2 Target plots for the CHIMERE simulation of the hourly maximum O_3 from DeltaTool for (**a**) combined bottom-up and top-down inventory and (**b**) EMEP inventory

Acknowledgements The Galician regional government "Xunta de Galicia" is acknowledged for the support of project "XIMERE/FUXIMERE" (10MDS009E), PhD grants of M. Dios and A. Rodríguez ('María Barbeito" Programme), and the research stay abroad grant of M. Dios (09.02.561B.444.0) at the University of Aveiro. Thanks are extended to the Portuguese 'Ministério da Ciência, da Tecnologia e do Ensino Superior' for the post-doc grants of A. Monteiro (SFRH/BPD/63796/2009) and J. Ferreira (SFRH/BPD/40620/2007). Support of As Pontes Power Plant is also acknowledged.

References

1. Butler TM et al (2008) The representation of emissions from megacities in global emission inventories. Atmos Environ 42(4):703–719
2. CEIP EMEP Centre on Emission Inventories and Projections (2008) Officially reported emission data, year 2008. http://www.ceip.at/. Last accessed July 2011
3. Denby B, Cassiani M, Smet P, Leeuw F, Horálek J (2011) Sub-grid variability and its impact on European wide air quality exposure assessment. Atmos Environ 45(25):4220–4229
4. Dios M et al (2012) Evaluation of the E-PRTR emissions inventory: the Galician case. In: 20th international conference on modelling, monitoring and management of air pollution, A Coruña, Spain, 16–18 May 2012 (accepted for oral presentation)
5. INERIS, Institut National de l'Environnement Industriel et des Risques (2008) Documentation of the chemistry-transport model CHIMERE [version chimere2008c]. Institut Pierre-Simon Laplace, LISA & CNRS
6. Karvosenoja N (2008) Emission scenario model for regional air pollution. Monographs of the boreal environment research. Monograph No. 32, Finnish Environment Institut, Finland
7. Monteiro A, Borrego C, Miranda AI, Gois V, Torres P, Perez A T (2007). Can air quality modeling improve emission inventories? In: Proceedings of the 6th international conference on urban air quality, Limassol, Cyprus, 26–30 March, pp 13–14
8. Pulles T, Heslinga D (2010) The art of emission inventorying TNO. TNO, Utrecht

9. Saavedra S et al (2012) Validation of WRF model during O_3 episodes in an Atlantic coastal region. In: 32nd NATO/SPS international technical meeting on air pollution modelling and its application, Utrecht, The Netherlands, 7–11 May 2012
10. Thunis P, Georgieva E, Pederzoli A (2011) The DELTA tool and benchmarking report template. Concepts and user guide, version 2. Joint Research Centre, Ispra. Available at: http://aqm.jrc.it/DELTA/data/DELTA_SG4_V2.pdf

Chapter 69
Modelling the Emission, Air Concentration and Deposition of Heavy Metals in Poland

Małgorzata Werner, Maciej Kryza, Anthony J. Dore, and Stephen Hallsworth

Abstract The aim of this paper was to calculate emission, air concentration and deposition of cadmium (Cd), and lead (Pb) for Poland with the Fine Resolution Atmospheric Multi-pollutant Exchange model (FRAME). Calculations of anthropogenic sources of heavy metals (HM) were based onPM_{10} emissionsand coefficients of activity and emission, dependent on SNAP sector and type of fuel. Natural emissions were estimated using PM_{10} wind blown dust from the Nat Air project and HM concentration in topsoil, taken from the Geochemical Atlas of Europe. Emission maps were used in the FRAME model, and annual average concentration and total deposition of individual HM were calculated at a 5 km × 5 km spatial resolution. It was found that the regions with the highest values of HM concentration and deposition were Upper Silesia (industrial region), as also legally protected areas of National Parks.

Keywords Heavy metals • Air concentration • Deposition • Cd • Pb

69.1 Introduction

Heavy metals (HM) are one of the most important pollutants emitted to the atmosphere due to their toxic effects on the environment and human health [5]. HM particles in the air are especially dangerous for human health, whereas their deposition to a soil surface can adversely affect growth of vegetation.

M. Werner (✉) • M. Kryza
Department of Climatology and Atmosphere Protection, University of Wroclaw, Wroclaw, Poland
e-mail: malgorzata.werner@uni.wroc.pl

A.J. Dore • S. Hallsworth
Centre for Ecology and Hydrology, Edinburgh, Scotland, UK

D.G. Steyn et al. (eds.), *Air Pollution Modeling and its Application XXII*,
NATO Science for Peace and Security Series C: Environmental Security,
DOI 10.1007/978-94-007-5577-2_69,

HM are released into the atmosphere both from anthropogenic and natural sources. The main source of HM emissions in Poland are combustion processes. The contribution of combustion in manufacturing industry (SNAP03) in total anthropogenic emission dominates for Pb (52 %). In the case of Cd the prevailing sources are non industrial combustion plants (SNAP02). In total, SNAP02 and SNAP03 contribute to 70–80 % of particular HM emission [2]. Wind blow emission also has a significant contribution to the total HM emission in European countries (re-suspension, [7]). Re-suspended particles may have both natural and anthropogenic origin (historical particles). It is not possible to distinguish between these two components. Poland, as well as Italy, Bulgaria and the Ukraine, belongs to the group of European countries with the highest HM emission, concentration and deposition [7]. According to the authors' knowledge, using atmospheric transport modelling tools for calculating HM concentration or deposition in Poland is limited.

The aim of this work is to calculate a HM (Cd, Pb) emissions inventory and spatial distribution and use this data to estimate air concentration and deposition of HM for Poland in year 2007, with the FRAME model.

69.2 Data and Methods

69.2.1 FRAME Model Description

The atmospheric transport model, FRAME provides information on the annual mean deposition and concentrations of atmospheric pollutants. A detailed description of the FRAME model is provided by e.g. Fournier et al. [6], Dore et al. [4]. Originally FRAME was developed to simulate nitrogen and sulphur deposition and primary particulate matter concentrations. Recently FRAME has been further developed to include base cation and heavy metal modelling, with the aim to develop a complex tool supporting environmental policy in the United Kingdom and Poland. FRAME is a Lagrangian model with a grid resolution of 5 km $\times$ 5 km and grid dimension of 160 $\times$ 160 cells for Poland [9]. Aerosol concentrations at the boundary of the model domain are calculated with the FRAME-Europe model. FRAME-Europe is a similar model to FRAME, but runs for the entire Europe on the EMEP grid at 50 $\times$ 50 km resolution. The FRAME model was run with emission inventory prepared according to the methodology described below and meteorological data for the year 2007.

69.2.2 Calculation of the Emission Data

The only spatial data of HM (As, Cd, Pb) emission for Poland is from the E-PRTR database (http://prtr.ec.europa.eu/). The database contains information about emissions from the largest point sources (about 20 industrial plants for each species), which contributes less than 10 % for individual species of their total

Table 69.1 Summary of the model performance statistics (MB in g ha^{-1} $year^{-1}$, the rest statistics are dimensionless)

HM	R	MB	MNB	NMAE
Cd	0.72	−1.00	−0.24	0.43
Pb	0.53	2.00	0.80	0.67

national emission, reported in Dębski [2]. An anthropogenic emissions inventory of Cd and Pb was prepared using PM_{10} point and area emissions for the year 2007, together with activity and emission factors dependent on SNAP sector and fuel type, reported by the Institute of Environmental Protection

The calculation was made according to the equation:

$$E_{HM} = \frac{E_{PPM} * W_{HM}}{W_{PPM}}$$

E_{HM}, E_{PPM} – HM or PM_{10} emission (kg)
W_{HM}, W_{PPM} – HM or PM_{10} emission factor (kg TJ^{-1})

The area emission sums to the official national emissions reported by Dębski et al. [2]. The missing mass of point sources emission (20 % for Pb) was distributed as an area emission. Anthropogenic emissions for Europe were taken from the EU-Project ESPREME (Integrated Assessment of Heavy Metal Release in Europe).

To calculate natural emission of HM from soil erosion, the estimation of PM_{10} wind blown dust emission from the Nat Air project [8] and concentration of HM in topsoil were used. Nat Air data is provided for all Europe with a 10 km × 10 km spatial resolution for years 1997, 2000, 2001 and 2003. An average value from available years was taken for calculations of HM emissions. Detailed data on HM concentration in topsoil was taken from the Geochemical Atlas of Europe (www.gsf.fi/publ/foregsatlas). To get continuous information about topsoil, point data was interpolated in the resolution of 10 km × 10 km. An increased emissions factor was used for the urban area and along roads, after Abbott [1].

69.2.3 Evaluation of the Model Results

FRAME modelled wet deposition results were evaluated by comparison with available measurements gained at 25 stations of the Polish Chief Inspectorate of Environment Protection. To summarize the model performance, the following statistics were used [10]: Pearson Correlation Coefficient (R), Mean Bias (MB), Mean Normalised Bias (MNB) and Normalised Mean Absolute Error (NMAE). The MB indicates that FRAME underestimates wet deposition of Cd and overestimates Pb (Table 69.1). A higher total error (NMAE) is found for wet deposition of Pb. Reasonable values are obtained for R coefficient.

69.3 Results

The modelled average air concentrations of Cd and Pb for Poland in 2007 were 0.20 and 3.00 ng m^{-3}, respectively. The highest values were observed relatively close to the emission sources (Fig. 69.1). The maxima concern the Upper Silesia region (S Poland, industrial region) and the center of the country, especially in urban complexes (e.g., Warszawa, Łódź, Poznań, Kraków, Wrocław), where the concentration reaches 3.50 and 25.00 ng m^{-3}, respectively for Cd and Pb.

The average values of wet deposition are 1.0 g $ha^{-1}year^{-1}$ for Cd and 14.0 g $ha^{-1}year^{-1}$, for Pb. The highest values of wet deposition are also, as for concentration, calculated for the Upper Silesia region (Fig. 69.1) but increased deposition does not appear so evidently in the city centers. The increased values concern the mountainous areas (SudetyMts, SW Poland and KarpatyMts., S and SE Poland),

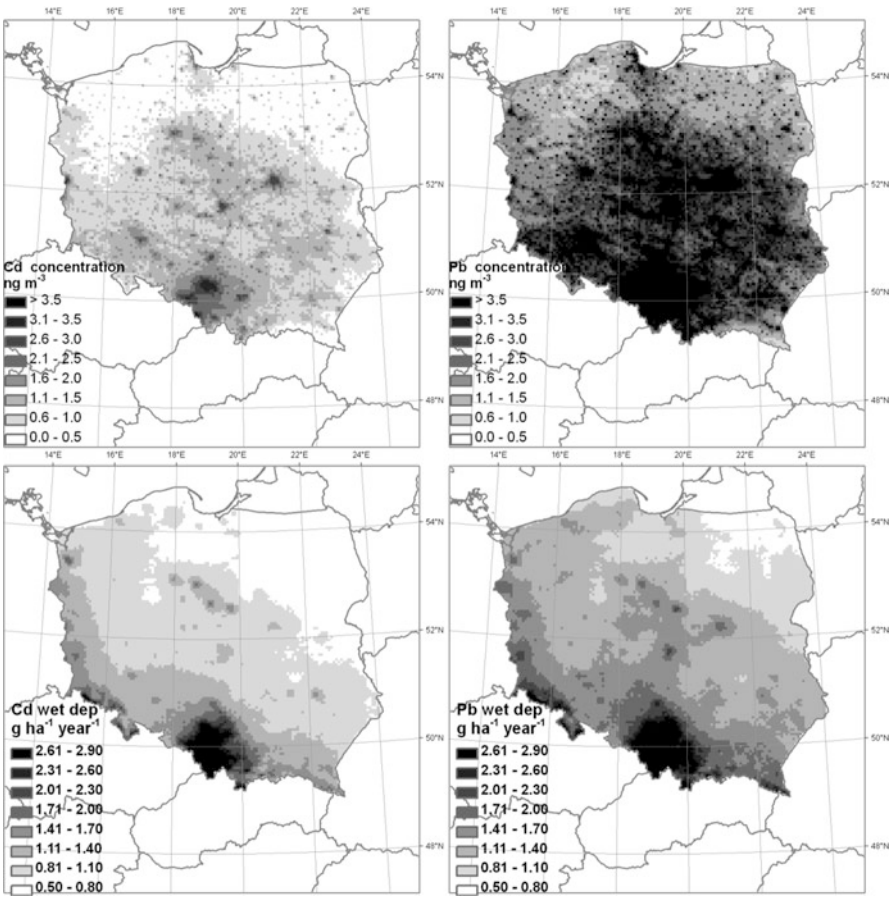

Fig. 69.1 Air concentration (*top*) and wet deposition (*bottom*) of Cd and Pb in year 2007

where values reach 11.0 and 107.0 g $ha^{-1}year^{-1}$, for Cd and Pb. These areas are the location of several National Parks with protected mountainous ecosystems. The substantial enhancement in wet deposition with altitude can be partially explained with the seeder-feeder mechanism, causing an increased total rainfall amount and ion content (e.g. [3]).

69.4 Summary

The main aim of the paper was to assess the spatial distribution of HM (Cd, Pb) emission, concentration and deposition in Poland for the year 2007. HM emission maps were calculated using spatial distribution of PM_{10} emissions and information about HM content in particulate matter. The emission estimates were used in the FRAME model to obtain the spatial distribution of HM concentration and deposition. The model results for wet deposition were found to be in good agreement with measurements. The region with high values of HM concentration and deposition is the Upper Silesia, which is the most industrialized area in Poland. High wet deposition values were also observed in the legally protected areas of National Parks.

Acknowledgments This work was supported by the Polish Ministry of Science and Higher Education grants N N306 044540.

References

1. Abbott J (2008) Resuspended heavy metal emissions. Report to the Department for the environment, food and rural affairs. AEA Energy & Environment, Didcot, Wielka Brytania
2. Dębski B, Olendrzyński K, Cieślińska J, Kargulewicz I, Skośkiewicz J, Olecka A, Kania K (2009) Inwentaryzacja emisji do powietrza SO2, NO2, CO, NH3, pyłów, metali ciężkich NMLZO i TZO w Polsce za rok 2005. Instytyt Ochrony Środowiska, Krajowe Centrum Inwentaryzacji Emisji, Warszawa
3. Dore AJ, Choularton TW, Fowler D (1992) An improved wet deposition map of the United Kingdom incorporating the seeder–feeder effect over mountainous terrain. Atmos Environ 26A:1375–1381
4. Dore AJ, Vieno JM, Fournier N, Weston K, Sutton MA (2006) Development of a new wind-rose for the British Isles using radiosonde data, and application to an atmospheric transport model. Q J R Meteorol Soc 132:2769–2784
5. Fang G, Chang C, Wu Y, Fu PY (1999) Characterization of chemical species in PM10 and PM2.5 aerosols in suburban and rural sites of central Taiwan. Atmos Environ 234:203–212
6. Fournier N, Dore A, Vieno M, Weston K, Dragosits U, Sutton M (2004) Modelling the deposition of atmospheric oxidized nitrogen and sulphur to the UK using a multi-layer long-range transport model. Atmos Environ 38:683–694, Elsevier
7. Ilyin I, Travnikov O, Aas W (2006) Heavy metals: transboundary pollution of the environment. EMEP Status Report 2006. Meteorological Synthesizing Centre – East, Chemical Coordinating Centre, 79pp

8. Korcz M, Fudala J, Klis C (2009) Estimation of wind blown dust emissions in Europe and its vicinity. Atmos Environ 43:1410–1420, Elsevier
9. Kryza M, Matejko M, Błaś M, Dore A, Sobik M (2010) The effect of emission from coal combustion in non-industrial sources on deposition of sulphur and nitrogen oxides in Poland. J Air Waste Manag Assoc 60:856–866
10. Yu S, Eder B, Dennis R, Chu S-H, Schwartz S (2006) New unbiased symmetric metrics for evaluation of air quality models. Atmos Sci Lett 7:26–34

Chapter 70
Impact of NOX Ship Emissions on the Baltic Sea Area: Present Status and Future Prospects

Joana Soares, Mikhail Sofiev, and Jukka-Pekka Jalkanen

Abstract The study is dedicated to perform a quantitative assessment of the present status and future prospects of the Baltic Sea (BS) area for two possible emission control measures. The consideration is given to environmental impact, mainly happening via total oxidised nitrogen (TON) deposition.

Keywords Ship emissions • Scenarios • Baltic Sea

70.1 Introduction

The excessive inputs of nitrogen nutrients remain one of the key threats to the BS ecosystems causing eutrophication and resulting in negative impacts on biodiversity, including alteration of the natural food-web structure, changed the species composition and disturbed the population dynamics [1].

70.2 Methodology

70.2.1 Emission Scenarios

The assessment considered: (i) the baseline case representing the ship traffic and in-land emission of 2007, (ii) the estimated ship traffic emission following the so-called Tier-II, and (iii) the Tier III scenario [3]. In all scenarios the in- land emission rates were taken constant at the present level from EMEP (www.emep.int) emissions

J. Soares (✉) • M. Sofiev • J.-P. Jalkanen
Finnish Meteorological Institute, FI-00101 Helsinki, Finland
e-mail: joana.soares@fmi.fi

D.G. Steyn et al. (eds.), *Air Pollution Modeling and its Application XXII*,
NATO Science for Peace and Security Series C: Environmental Security,
DOI 10.1007/978-94-007-5577-2_70,

inventories. The EMEP ship emissions were scaled according to Tier II and III requirements allowing for 2 % annual growth in ship emissions and, by the year 2045, the ship traffic is assumed to double while the emission per traffic-unit would decrease by 20 % in Tier-II and by 80 % by Tier-III.

Since, the EMEP ship emission inventory did not include the emissions from harbours, the emission database based on the methodology of Jalkanen et al. [4] was considered. This new case will provide the indication of the emission uncertainty for the cases (i)–(iii) and its impact on the results of the assessment. It also enabled a quantitative estimation of the impact of emission reduction measures in major harbours. To estimate the missing contribution of the harbour ship emissions, 1 month (January 2007) was recomputed with this ship emission inventory.

70.2.2 Modelling Tool: SILAM v.4.9

The dispersion modelling tool used in this study is the System for Integrated Modelling of Atmospheric coMposition, SILAM [5]. The chemical transformation scheme considers both gas-phase and heterogeneous SOx-NOx- NHx transformations. For aerosols, the mechanisms of dry deposition varies from primarily turbulent diffusion driven removal of fine aerosols to primarily gravitational settling of coarse particles. The wet deposition distinguishes between sub- and in-cloud scavenging and between rain and snow. Meteorological information and land cover maps were taken from the ECMWF (www.ecmwdf.int) meteorological model.

The dispersion results were obtained from the model runs for the whole year of 2007, repeated for each emission scenario. The year was selected almost arbitrarily, with the only requirement to be free from extreme meteorological events. The results describe the spatial distribution of the NOX, among other pollutants, in terms of surface concentrations and wet and dry deposition.

70.2.3 Ecosystems Impact Evaluation: Eutrophication

Protection levels against adverse effects of eutrophication and acidification (critical levels) for European countries which are set by the Coordination Centre for Effects – Environmental Impact Assessment (CCE-EIA) have been preferential to evaluate the maximum deposition allowed to avoid eutrophication or induce any type of nutrient imbalance [6]. By definition, critical loads are steady–state quantities thus; using critical loads is the most straightforward assessment strategy to evaluate the ecosystem impact when enforcing the different emission scenarios. The difference between emission scenarios depositions will be compared the exceedances of the harmless thresholds based on the critical load maps of the CCE-EIA. The exceedances of critical loads are the differences between present loads of nitrogen and the 1st and 5th percentile for the critical load nitrogen, and are expressed as average accumulated exceedances per grid cell.

70.3 Results and Discussion

70.3.1 Impact of TIER Scenarios in Eutrophication

Comparing the results obtained by SILAM model for the year 2007 with the critical loads map (Fig. 70.1), the load of nutrient nitrogen in the present situation is complying, in general, only in the northern-most part of the domain. The critical levels are exceeded in Central Finland and Sweden and the exceedance grows towards the south reaching a factor of a few times for Denmark, Poland, Germany and Baltic States. The absolute level of exceedances varies from a few tens of equivalents per hectare per year (eq ha^{-1} a^{-1}) up to several hundreds.

Comparing the exceedances with the difference between the Tier II and Tier III scenarios (Fig. 70.2), one can notice that in the countries with the major exceedances, such as Denmark, the impact will be negligible due to the bulk of the eutrophying nitrogen originated from terrestrial sources and Northern Sea ship traffic. However, the situation is different for several other regions: coastal areas of the Baltic States, Finland, Sweden and Poland. There, with the exceedances being between 100 and 300 eq ha^{-1} a^{-1}, the difference between Tier II and III can reach up to 60 eq ha^{-1} a^{-1} (84 mg m^{-2}), i.e., 20–30 % of the exceedances themselves. The second positive effect of Tier III scenario in comparison with Tier II is that the area where the critical loads are exceeded will reduce, mainly, in central parts of Finland and Sweden.

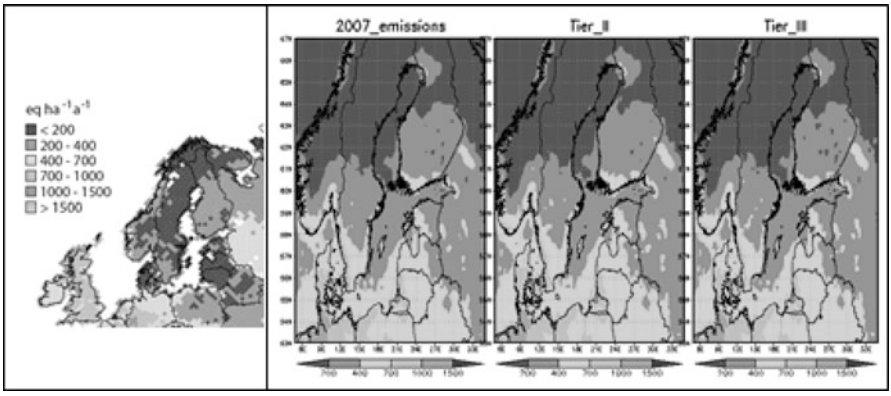

Fig. 70.1 *Left panel*: European map of critical loads for eutrophication which protects 95 % of natural areas in a 50* 50 km^2 EMEP grid [2]. *Right panel*: annual nutrient nitrogen deposition for emission scenarios: EMEP 2007 (*left panel*), Tier II (*middle*) and Tier III (*right*). Unit: eqN ha^{-1} a^{-1}

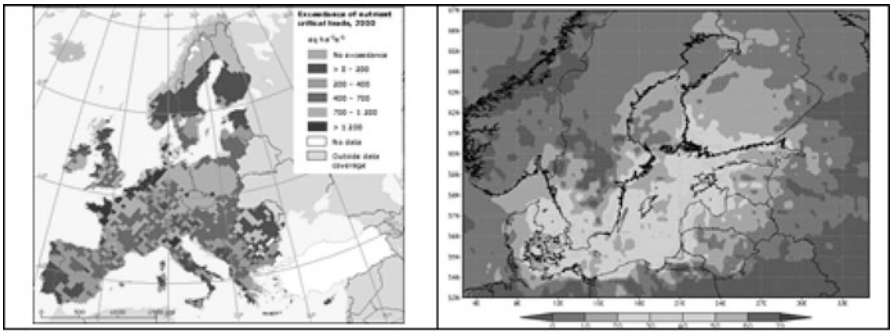

Fig. 70.2 *Left panel*: European map of exceedances of critical loads for eutrophication due to the deposition of nutrient nitrogen in 2000, in a 50×50 km^2 EMEP grid [2]. *Right panel*: difference between nutrient nitrogen deposition for emission scenarios Tier II and Tier III. Unit: eqN ha^{-1} a^{-1}

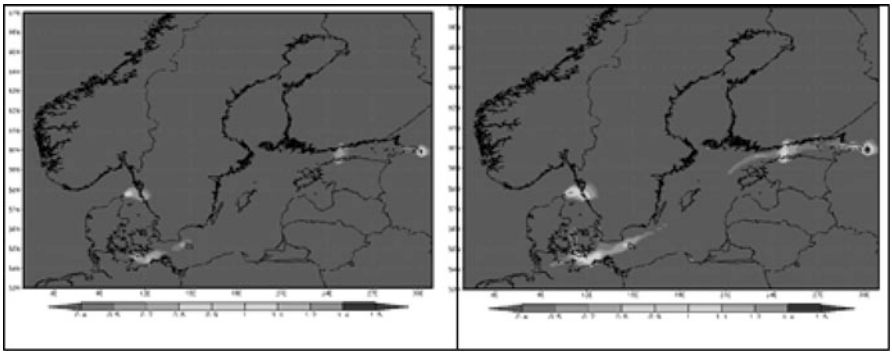

Fig. 70.3 *Left panel*: estimates of the contribution of the in-harbour emission to NOx concentrations in 2007. *Right panel*: Tier III emission scenario gain over Tier II. Unit μgN m^{-3}

70.3.2 Baltic Sea Harbours

As shown by Jalkanen et al. [4], the harbour emissions can be substantial and can add-up to the air quality burden in the major cities. By utilising EMEP ship emission inventory results in under-estimation of 1 μgN m^{-3} of the NOx concentrations, if averaged over 20 km (the resolution of the current simulations) (Fig. 70.3, left panel). Consequently, the application of Tier III scenario, in comparison with Tier II, would reduce approximately 1.4–1.5 μgN m^{-3} of the ship-induced "background" NOx in several major cities around the BS (Fig. 70.3 right panel).

70.4 Conclusions

The scenario simulations showed reduction by tens of % over the coastal regions for Tier-III whereas Tier-II leads to its increase in comparison with present levels. Comparison with critical load maps showed exceedances up to 100–300 eq ha^{-1} a^{-1} in 2045 with the difference between Tier-II and Tier-III reaching up to 60 eq ha^{-1} a^{-1}. Two ship emissions were considered: the EMEP top-down (50 km × 50 km, annual) and the AIS-based bottom-up (1 km × 1 km, hourly) inventories. Accounting for the harbour emission, absent from the EMEP inventory, leads to a bulk increase of NOx concentrations by about 1 μgNm^{-3} areas around harbours.

References

1. HELCOM (2010) Ecosystem health of the Baltic Sea – HELCOM initial holistic assessment. Baltic Sea Environ Proc 122. Available at: www.helcom.fi/publications
2. Hettelingh J-P, Posch M, Slootweg J (eds) (2008) Critical load, dynamic modelling and impact assessment in Europe: CCE Status Report 2008. Report No. 500090003, ISBN No. 978-90-6960-211-0, Coordination Centre for Effects, Bilthoven, The Netherlands
3. IMO, International Maritime Organisation (2007) Revision of MARPOL Annex VI and the NOx technical code, BLG 12/INF.10
4. Jalkanen J-P, Brink A, Kalli J, Pettersson H, Kukkonen J, Stipa T (2009) A modelling system for the exhaust emissions of marine traffic and its application in the Baltic Sea area. Atmos Chem Phys 9:9209–9223
5. Sofiev M, Siljamo P, Valkama I, Ilvonen M, Kukkonen J (2006) A dispersion modeling system SILAM and its evaluation against ETEX data. Atmos Environ 40:674–685
6. Sverdrup H, De Vries W, Henriksen A (1990) Mapping critical loads: a guidance to the criteria, calcuations, data collection and mapping of critical loads. Miljørapport (Environmental report) 1990:14. NORD: 1990:98. Nordic Council of Ministers, Copenhagen, 124 pp

Chapter 71
AQMEII and MOZAIC: Evaluating Regional Scale Model Ability to Capture the Vertical Distribution of Pollutants

Efisio Solazzo, Stefano Galmarini, Roberto Bianconi, C. Hogrefe, and S. Trivikrama Rao

Abstract As part of the AQMEII project, vertical profiles of a number of variables simulated by several state-of-the-science regional-scale air quality (AQ) models are evaluated against measurements collected by instrumented aircraft over Europe (EU) and North America (NA) continental-scale domains for the full year of 2006. Tropospheric profiles of ozone, carbon monoxide, wind speed, temperature and relative humidity simulated by the AQ models at 12 selected airport locations in NA and 3 in EU are considered here for model evaluation. Moreover, in this study, several model outputs are inter-compared to examine the models' ability to reproduce the observed variability for ozone.

Keywords Model evaluation • Vertical profiles

71.1 Introduction

Within the framework of the Air Quality Model Evaluation International Initiative (AQMEII), it was possible to access the MOZAIC (Measurements of OZone, water vapour, carbon monoxide and nitrogen oxides by in-service AIrbus aircraft) dataset for 2006, which provided more than 2,000 vertical profiles of aircraft measurements. Profiles of a number of chemical species and meteorological variables (ozone, CO,

E. Solazzo (✉) • S. Galmarini
Joint Research Centre, European Commission, Ispra, Italy
e-mail: efisio.solazzo@jrc.ec.europa.eu

R. Bianconi
Enviroware srl, Concorezzo, Milano, Italy

C. Hogrefe • S.T. Rao
Atmospheric Modeling and Analysis Division, U.S. Environmental Protection Agency, Research Triangle Park, NC, USA

D.G. Steyn et al. (eds.), *Air Pollution Modeling and its Application XXII*,
NATO Science for Peace and Security Series C: Environmental Security,
DOI 10.1007/978-94-007-5577-2_71,

temperature, relative humidity, wind speed and direction) were measured by aircraft during landings and take-offs to and from 12 selected airports in North America (Portland, Dallas, Vancouver, Philadelphia, Charlotte, Boston, Chicago, Montreal, New York, Atlanta, Toronto, Washington) and 3 in Europe (Frankfurt, Munich, and Vienna). Over ten regional-scale chemical transport models, applied by 13 institutions in EU and NA, delivered model data corresponding to the grids covering the domain of the flights at 13 identified altitudes (from ground to 8,500 m). Model outputs and MOZAIC data have been uploaded to the web-shared platform ENSEMBLE system [4]. For all the airports included in this study, data gathered during take-offs and landings mostly occurred between the early morning and the early afternoon (local times), and ∼25 % more frequently in summer than in winter. The availability of observations varied greatly, depending on the species and airport. For example, there are over 1,000 flights at Frankfurt, but only 120 at Philadelphia.

71.2 Participating Models and Settings

In total, five modelling groups for NA and eight for EU delivered data to compare against the MOZAIC profiles. The AQ models employed in the model evaluation are:

- AURAMS [6];
- CAMx (http://www.camx.com);
- CMAQ [3];
- DEHM [2];
- SILAM [7];
- CHIMERE [1];
- EUROS [5];
- WRF/Chem (http://www.acd.ucar.edu/wrf-chem/).

All model results have been presented and evaluated independently in individual studies. However, the inter-comparison of modeled and observed vertical data at several airports in two continents along with the large number of regional AQ models used in this study are unique developments that can help in understanding the models' performance. Some of the models participating in the analysis share one or more aspects in common (meteorological driver, emissions, chemical boundary conditions), although in general, each model adopted its own settings, including horizontal and vertical resolutions. Full detail on the models' settings are provide in Solazzo et al. [8, 9].

71.3 General Statistics

Analyses of bias, error, and correlation have been carried out for each of the investigated variables. The variables have been spatially averaged (at each altitude) over the MOZAIC domains for which the larger number of hourly data (flights) are available (i.e. Portland, Philadelphia, Dallas, Atlanta, and Frankfurt). A large number of plots have been generated, some of which are presented in Fig. 71.1, where modeled ozone, CO and wind speed are examined for Portland (US west coast), Philadelphia (US east coast), and Frankfurt (central EU). Overall, results indicate that performance for temperature (not shown) is satisfactory for all models and in all domains for, at least, the first 5,000 m above ground (Pearson correlation coefficient (PCC) in excess of 0.90), while for all the other variables errors are not negligible, particularly within the boundary layer. CO and, to a lesser extent ozone, had the largest error, mainly in central EU and on the west coast of NA.

Analysis of the error by season (not shown) has revealed that, among the investigated fields, modelled ozone is the most sensitive to seasonal variations, as expected, with the largest bias in the winter (all airports), probably due to biases in the boundary conditions used for the AQ models.

The performance of AQ models in replicating the variability seen in the observed fields has also been evaluated by means of the coefficient of variation, expressed as the ratio of the standard deviation to the mean value of the distribution. An example

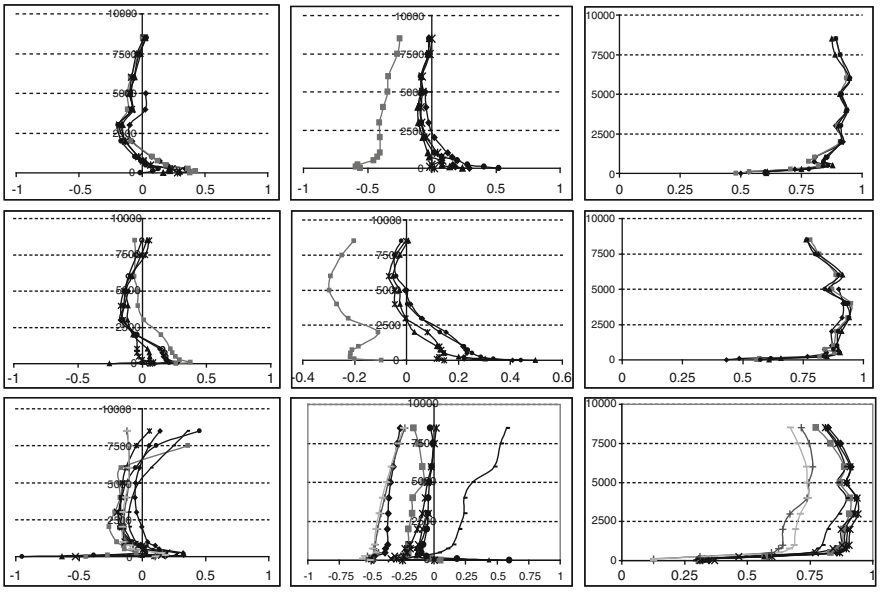

Fig. 71.1 Mean fractional bias for ozone (*left column*), CO (*middle column*), and PCC for wind speed (*right column*) for Portland (*top row*), Philadelphia (*middle row*), and Frankfurt (*lower row*)

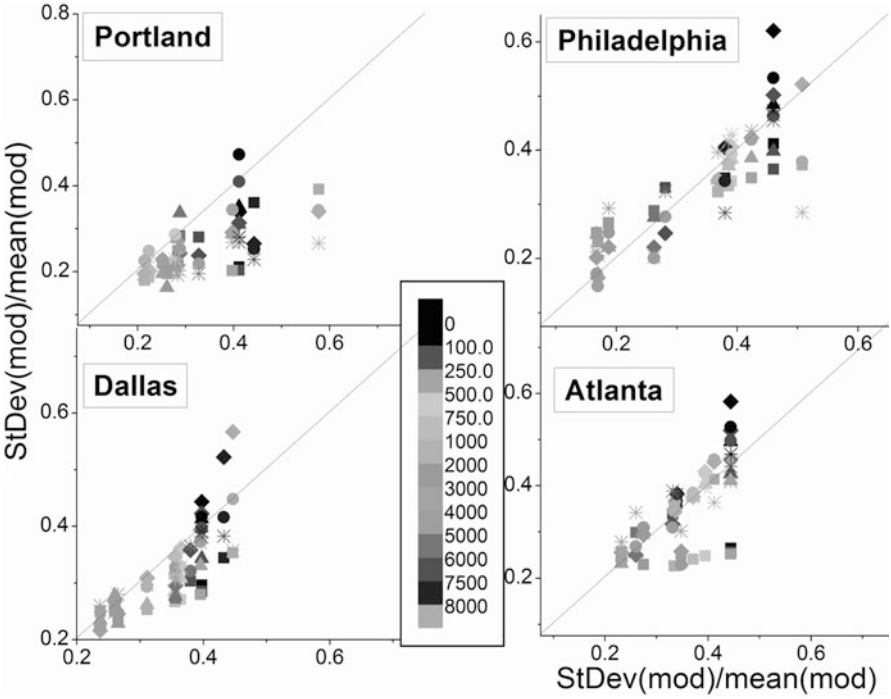

Fig. 71.2 Observed vs. modelled coefficient of variation for ozone in NA. Models by symbols, and altitude by color

of such an analysis is given in Fig. 71.2, where the coefficients of variation for ozone are shown for four airports in NA (averaged over the full year of 2006). This analysis is helpful in determining the spread of modeled ozone and its variation with height. From Fig. 71.2, we can infer that the largest variability is typically observed for $z \leq 500$ m and $z = 8{,}500$ m, with models underestimating the spread of ozone particularly for Portland and Dallas. Models exhibit considerable scatter, with some models being able to replicate the observed variability quite satisfactorily (although not at all heights for all airports), while others have some systematic deficiencies (for example the square symbols in Fig. 71.2), under-predicting the observed spread, possibly due to bias in the emissions or in the boundary conditions. Further work is on-going to investigate this behavior.

71.4 Conclusions

This study, conducted as part of the AQMEII exercise, presents AQ model inter-comparison results for a number of vertical fields relevant to air quality (ozone, CO, wind speed), calculated for several airport locations in Europe and North America

for the year of 2006. Furthermore, AQ model outputs have been evaluated against observational data collected by instrumented aircraft within MOZAIC. Results reveal the models' difficulty in simulating CO and ozone within the boundary layer, while errors aloft are small but still significant. In contrast, temperature and wind speed are satisfactorily simulated by the models. Analysis of the variability has indicated that, at least for ozone, the spread in the first 500 m is, on average, underestimated, while it is adequately reproduced between 1,000 and 4,000 m. Current analyses are focusing on assessing the influence of the lateral boundary conditions for ozone and other species on the seasonal performance of AQ models for both continents.

Acknowledgments The AQMEII community is kindly acknowledged for providing the modeling data. Although this paper has been reviewed by EPA and approved for publication, it does not necessarily reflect EPA's policies or views.

References

1. Bessagnet B et al (2004) Aerosol modeling with CHIMERE: preliminary evaluation at the continental scale. Atmos Environ 38:2803–2817
2. Brandt J et al (2007) THOR – an operational and integrated model system for air pollution forecasting and management from regional to local scale. In: Proceedings of the 2nd ACCENT Symposium, Urbino, Italy, 23–27 July 2007
3. Byun DW, Schere KL (2006) Review of the governing equations, computational algorithms, and other components of the models-3 Community Multiscale Air Quality (CMAQ) modeling system. Appl Mech Rev 55:51–77
4. Galmarini S et al (2012) ENSEMBLE and AMET: two systems and approaches to a harmonised, simplified and efficient assistance to air quality model developments and evaluation. Atmos Environ. doi:10.1016/j.atmosenv.2011.08.076
5. Schaap M et al (2008) The LOTOS-EUROS model: description, validation and latest developments. Int J Environ Pollut 32:270–290
6. Smyth SC et al (2009) A comparative performance evaluation of the AURAMS and CMAQ air quality modelling systems. Atmos Environ 43:1059–1070
7. Sofiev M et al (2006) A dispersion modeling system SILAM and its evaluation against ETEX data. Atmos Environ 40:674–685
8. Solazzo E et al (2012) Operational model evaluation for particulate matter in Europe and North America in the context of AQMEII. Atmos Environ 53:75–92
9. Solazzo E et al (2012) Model evaluation and ensemble modelling and for surface-level ozone in Europe and north America. Atmos Environ 53:60–74

Chapter 72
CTM: Numerical Recipes and Their Implementations

Eugene Genikhovich, Mikhail Sofiev, Irene Gracheva, Julius Vira, Marje Prank, and Alexandra Ryzhakova

Abstract Numerical implementation of CTM should satisfy a set of contradictory requirements related to the quality of the model predictions, minimization of the volume of computations, applicability of the model to different meteorological situations etc. In this paper we present several numerical recipes that were proven to be efficient in constructing CTMs and dispersion models developed at the Voeikov Main Geophysical Observatory (St. Petersburg, Russia) and Finnish Meteorological Institute (Helsinki, Finland). Assuming splitting, we discuss approximations of the physical processes separately but they can be used jointly as well.

Keywords Numerical recipes • CTM

72.1 Introduction

We present here the numerical "recipes" for solution of the system of differential equations like (72.1) (with summation over i and u_i usually satisfying the continuity equation):

$$\frac{\partial c}{\partial t} + u_i \frac{\partial c}{\partial x_i} = \frac{\partial}{\partial x_i} K_i \frac{\partial c}{\partial x_i} + S \tag{72.1}$$

E. Genikhovich • I. Gracheva • A. Ryzhakova
Voeikov Main Geophysical Observatory, Saint Petersburg, Russia

M. Sofiev (✉) • J. Vira • M. Prank
Finnish Meteorological Institute, Helsinki, Finland
e-mail: mikhail.sofiev@fmi.fi

D.G. Steyn et al. (eds.), *Air Pollution Modeling and its Application XXII*,
NATO Science for Peace and Security Series C: Environmental Security,
DOI 10.1007/978-94-007-5577-2_72,

Description of the following processes simulated in the framework of splitting is considered:

- numerical approximation of the vertical turbulent transport using the "MSB approach" originally introduced by Marchuk, Samarski, and Berlyand [1, 3, 4]. The resulting numerical schemes in a sense are analogous to the shock-capturing method in the gas dynamics;
- advection of pollutants. An advanced version of the scheme of M. Galperin is combined with pre-processing module ensuring the continuity equation. The scheme extension handling possible violation of the continuity is also discussed.
- combined description of the vertical diffusion, transport, and sedimentation in a single transport term suitable also for dry deposition computations;
- simplified NOx – ozone scheme and its implementation in non-stationary and stationary problems. The scheme is based on mathematical analysis of the ozone production cycle and captures its main features with a fraction of the usual computational costs for such schemes. In the local-to-urban scale it allows for the first integral of the corresponding differential equation.

72.2 MSB Scheme

The equation $\frac{\partial c}{\partial t} = \frac{\partial}{\partial z} K \frac{\partial c}{\partial z}$ is approximated with the finite differences scheme $\frac{\partial c_i^h}{\partial t} = \frac{K_{i+1/2}\left(c_{i+1}^h - c_i^h\right) - K_{i-1/2}\left(c_i^h - c_{i-1}^h\right)}{h^2} + O\left(h^n\right)$. In the MSN scheme $K_{i+1/2} = \frac{z_{i+1} - z_i}{\int_{z_i}^{z_{i+1}} dz/K}$ and $n \to \infty$ if $t \to \infty$ ("exact solution").

72.3 Advection Scheme

The scheme [2], also presented in details by [5], is one of the highly accurate developments with zero numerical diffusion and acceptable computational demands. An example of the rotational test of a cube with one revolution (Fig. 72.1) demonstrates its capabilities; here, the sequential plume positions are shown with one full revolution computed. A variation of this scheme can be derived to further reduce its sensitivity to violation of the continuity equation.

To reduce the related errors, one can substitute a component of the wind speed generated by the met driver, with the reconstructed one based on integration of the continuity equation using two other components. Another option is to modify the main equation $\frac{\partial c}{\partial t} + u_i \frac{\partial c}{\partial x_i} = S$ in the following way: $\frac{\partial c}{\partial t} + u_i \frac{\partial c}{\partial x_i} = ac \frac{\partial u_i}{\partial x_i} + S$ with the first term in the right-hand side of this equation equal to zero because of the continuity equation. The resulting equation could be approximated using splitting and the adjustment parameter "a" could be selected here between 0 and 1. With

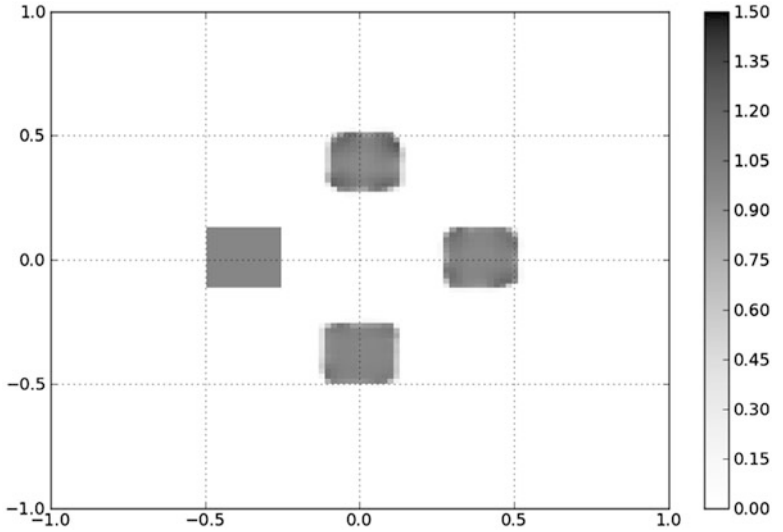

Fig. 72.1 Rotational test for Galperin's advection scheme

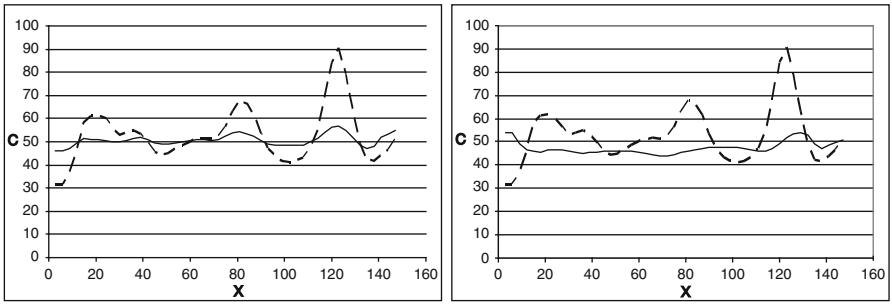

Fig. 72.2 Generalized advection scheme (*solid line*) with a = 0.8 (*left panel*) and a = 1 (*right panel*) vs. Galperin's (*dotted line*) scheme

a = 0.5 such a scheme was introduced by Marchuck in 2D case. Some results of numerical experiments are shown on the following picture (Fig. 72.2).

72.4 Combined Description of the Vertical Diffusion, Transport and Sedimentation

The governing equation $\frac{\partial c}{\partial t} + \left(w - w_g\right)\frac{\partial c}{\partial z} = \frac{\partial}{\partial z}K\frac{\partial c}{\partial z}$ can be transformed into an equivalent form $f\frac{\partial c}{\partial z} = \frac{\partial}{\partial z}Kf\frac{\partial c}{\partial z}$ where $f = \exp\left\{-\int \left(w - w_g\right)dz/K\right\}$. It could be discretized applying the MSB scheme and additionally used when approximating the dry-deposition boundary condition.

72.5 Simplified NOx-Ozone Scheme

A chemical mechanism written as

$$\frac{d\,[NO_2]}{dt} = k_1\,[NO]\,[O_3] + k_4\,[NO]\,[RO_2] - J\,[NO_2] - k_5\,[NO_2]\,[OH] \qquad (72.2)$$

is simplified to the following one:

$$\begin{aligned}
\frac{d\,[NO]}{dt} &= J\,[NO_2] - k_1\,[NO]\,[O_3] - k'_4[NO] \\
\frac{d\,[NO_2]}{dt} &= -J\,[NO_2] + k_1\,[NO]\,[O_3] + k'_4\,[NO] \\
\frac{d\,[O3]}{dt} &= J\,[NO_2] - k_1\,[NO]\,[O_3]
\end{aligned} \qquad (72.3)$$

If the temporal and spatial scales of the process are large enough, the coefficients there are functions of t and x_i, and the problem should be solved numerically. In the local-to-urban scales, however, they could be considered as constants. In this case, the system is autonomous and allows for the first integral. The last one could be expressed via the pre-tabulated auxiliary solution y(x) of the following nonlinear ordinary differential equation:

$$\frac{dy}{dx} + \frac{1}{y} = m\left(1 + \frac{1}{x^2}\right) \qquad (72.4)$$

Its solution y(x) depends also on the constant m and on the boundary condition $y(x_0) = y_0$, i.e., on three parameters.

References

1. Berlyand ME (1982) Moderne problemen der atmospharischen diffusion und der Verschmutzung der Atmosphare. Academie-Verlag, Berlin, 435 s
2. Galperin M (2000) The approaches to correct computation of airborne pollution advection. In: Problems of ecological monitoring and ecosystem modelling, Gidrometeoizdat, pp 54–68
3. Marchuk GI (1977) Methods of computational mathematics. Nauka, Moscow, 456 p
4. Samarski AA (1971) Introduction in the theory of finite-difference schemes. Nauka, Moscow, 552 p
5. Sofiev M, Galperin M, Genikhovich E (2008) Construction and evaluation of Eulerian dynamic core for the air quality and emergency modeling system SILAM. NATO science for piece and security series C: environmental security. In: Borrego C, Miranda AI (eds) Air pollution modelling and its application, XIX. Springer, Dordrecht, pp 699–701

Chapter 73
Fine Resolution Modeling of Climate Change Impact on Future Air Quality Over BULGARIA

Dimiter Syrakov, Kostadin Ganev, Maria Prodanova, Nikolai Miloshev, and Kiril Slavov

Abstract A meteorological database of high resolution (∼10 km) climate modeling results for three time slices – 1960–2000 (Control Run, CR), 2020–2050 (Near Future, NF) and 2070–2100 (Far Future, FF), produced by ALADIN-Climate model following the IPCC scenario A1B, future concentrations of many air pollutants are estimated. The dispersion calculations are made basically by US EPA Models-3 system (MM5, CMAQ, SMOKE). The mean concentrations of four main polluters (ozone ADM, SO2, NO2 and PM10) for the last 10 years of each time slice are calculated. The changes in pollution levels are presented and commented.

Keywords Climate change • Climate scenario's • Air pollutants

73.1 Introduction

Many scientific projects and publications are aimed to assessment of the possible climate changes and on its impact on various areas of human activity and environment. The EC FP6 project CECILIA (http://www.cecilia-eu.org/) is only one of them. CECILIA's Work Packages 1 and 2 are connected with long-term meteorological simulations aiming creation of respective databases of high resolution (10 km) meteorological fields capable to retrieve climate estimates. WP7 aims at long-term simulations of chemistry air quality models driven by Regional Climate Models (RCMs) for present climate and for future projections with fine

D. Syrakov (✉) • M. Prodanova • K. Slavov
National Institute of Meteorology and Hydrology, Bulgarian Academy of Sciences,
66 Tzarigradsko shaussee Blvd, Sofia 1784, Bulgaria
e-mail: dimiter.syrakov@meteo.bg

K. Ganev • N. Miloshev
Geophysical Institute, Bulgarian Academy of Sciences, Acad. G. Bonchev Str.,
Bl.3, Sofia 1113, Bulgaria

D.G. Steyn et al. (eds.), *Air Pollution Modeling and its Application XXII*,
NATO Science for Peace and Security Series C: Environmental Security,
DOI 10.1007/978-94-007-5577-2_73,

resolution of 10 km for some target regions of Central and Eastern Europe (including Bulgaria). The chemical boundary conditions for these regions are prepared by calculations covering the whole of Europe with coarser grid resolution of 50 km.

73.2 Meteorological Modeling and Meteorological Data Base

The meteorological data base for this study is created off-line by the ALADIN Regional Climatic Model. It is a modification of the current operative weather forecast system in the National Institute of Meteorology and Hydrology (NIMH) of Bulgaria. Its creation is a result of a project between France and Bulgaria [6–8]. ALADIN-Climate is a regional version of ARPEGE–Climate [1]. ARPEGE and ALADIN use the same executable (same dynamical core, same physical parameterizations).

The simulations spans three scenario time slices: 1961–2000 (Control Run, **CR**), 2021–2050 (Near Future, **NF**) and 2071–2100 (Far Future, **FF**). They are driven at the lateral boundaries by meteorological fields from a corresponding global simulation with the ARPEGE model under forcing from the SRES-A1B IPCC greenhouse gas IPCC scenario [3]. Only the CR-period is driven with ERA40 [11] data set as boundary conditions.

The ALADIN output is a binary file with 6-h time resolution transformed to standard GRIB-forma. The created by ALADIN-Climate meteorological data base consists of such 6-h GRIB files containing the main meteorological parameters in 31 standard p-levels going up to 50 hPa.

The CR simulations are used for validation by comparing the respective model climate with present climate estimates. Compared are daily precipitation and temperature taken from 56 stations in Bulgaria. Generally, the simulations show colder and wetter behavior of the model in comparison with the measured climate. The temperature error shows colder model simulations of about 2 °C. The errors of other GCMs over the same time slice show temperature cooling of about 4 °C, so the decrease of the resolution to 10 km definitely increase the quality of simulations.

The verification shows that the errors are relatively permanent in the period, i.e. they can be considered as systematical. The difference between the simulated future period and the present one gives the tendencies in the future, i.e. the climate change dimensions for the domain used. This difference eliminates in big extent the systematical error of ALADIN. The two future periods (NF and FF) are simulated.

The temperature shows positive tendency of increasing of 2 °C in NF and 3.7 °C in FF. There could not be mentioned significant differences of the temperature distribution in the integration domain. The precipitations tendencies show steady signal for decreasing of 15–20 % comparing with the reference run in the South-East part of the domain and North Greece. The decreasing of precipitation is approximately the same in both simulations for NF and FF.

73.3 Air Pollution Modeling and Air Quality Database

For assessing the climate change impact on air quality, a modeling System was elaborated based on the open source US EPA Models-3 air quality modeling tool, consisting of:

- CMAQ (http://www.cmaq-model.org/), **C**ommunity **M**ulti-scale **A**ir **Q**uality model, being the chemical-transport model of the System;
- MM5 (http://box.mmm.ucar.edu/mm5/), The 5th generation PSU/NCAR **M**eso-Meteorological **M**odel, used as meteorological pre-processor to CMAQ; and
- SMOKE (http://www.smoke-model.org/), **S**parse **M**atrix **O**perator **K**ernel **E**missions modeling system, being the emission pre-processor to CMAQ.

A number of interfaces (Linux scripts and FORTRAN codes) are created as to link those models with different types input information in a chain capable to perform long term calculations. The calculations are performed for a region containing mainly Bulgaria with 10×10 km resolution nested in the ALADIN domain. Here, a very short description of the System will be presented. One can find more detailed description in [9, 10].

ALADIN data drives MM5. Its output feeds MCIP (Meteorology-Chemistry Interface Processor of CMAQ) that produces formatted meteorological input to both CMAQ and SMOKE. The CAMx database [4, 5] is based in the Aristotle University of Thessalonica, Greece, and contains air pollution calculations for Europe on a 50-km grid. It is used for off-line interpolations to the CMAQ boundary points, results uploaded to a dedicated server in Sofia. This data is used by the System for on-line elaboration of CMAQ boundary conditions for the current day.

CMAQ demands its emission input in specific format reflecting the time evolution of all pollutants accounted for by the chemical mechanism used. The main groups of emission sources are Area Sources (AS), Large Point Sources (LPS) and Biogenic Sources (BgS). The emission scenario in CECILIA is fixed – only EMEP 50 km emission database (http://webdab.emep.int/) for 2000 is applied. In fact, its disaggregation to higher resolution ($\sim 15 \times 15$ km) made by [12] is exploited.

AS- and LPS-inventories feed the interface programs AEmis and PEmis which produce respective emission files. The gridded land-use information for the domain is introduced in SMOKE which calculates the biogenic emissions exploiting the ambient meteorological data provided by MCIP. Finally, SMOKE merges these files as to produce common emission input for CMAQ.

The System performance is verified for Ozone for 2000. Hourly measured data in two points [2] are compared with simulated ones. The results are quite good [9, 10].

The Air Quality data base comprises three 10-year time slices: 1991–2000 (CR), 2041–2050 (NF) and 2091–2100 (FF). GRID technology is used for the calculations.

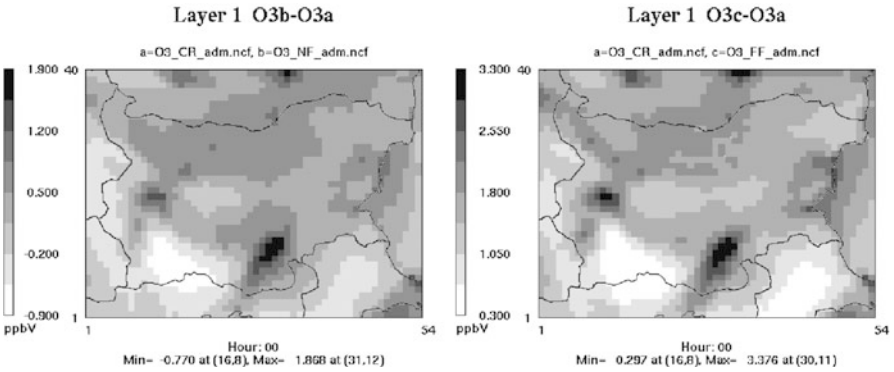

Fig. 73.1 Differences in the 10-year ADM fields for "NF-CR" (*left*) and "FF-NF" (*right*)

73.4 Comparison of Various Air Pollution Climate Values

Here, results only for ozone Averaged Daily Maxima (ADM) are given. For other pollutants see [9]. In the Figure, the ADM differences are displayed. It is seen that the differences "FF-CR" are higher than "NF-CR", being in correspondence with temperature tendencies. The maximal values are over 3 ppb that is about 5–10 % of ADM maximums. There is a definite separation between positive and negative difference values in both cases – they are positive in the plain parts of the domain and negative in the mountain areas. The maximal positive differences are concentrated around the main pollution sources (Fig. 73.1).

73.5 Conclusion

In the present work some estimates of the dimensions of the climate changes for the region of Bulgaria are presented. They are calculated by the ALADIN-Climate model following IPCC scenario A1B. This Scenario is considered as the most realistic one.

Considering the changes in ozone ADM levels, it can be concluded that the changes are quite small (5–10 % of maximal values). The maximal positive changes are located around the main pollution sources in the region. In the main part of the country and in higher extent in the mountain areas the changes are at decreasing pollution levels.

Acknowledgements This study is made under the financial support of EC, – FP7 Project CECILIA.

References

1. Déqué M, Piedelievre J-P (1995) High-resolution climate simulation over Europe. Clim Dyn 11:321–339
2. Donev E, Zeller K, Avramov A (2002) Preliminary background ozone concentrations in the mountain and coastal areas of Bulgaria. Environ Pollut 17:281–286
3. IPCC (2000) IPCC special report: emissions scenarios, ISBN: 92-9169-113-5. http://www.grida.no/publications/other/ipcc_tar/?src=/climate/ipcc_tar/wg3/081.htm
4. Katragkou E, Zanis P, Tegoulias I, Melas D, Krueger BC, Huszar P, Halenka T (2008) Tropospheric ozone over Europe: an air quality model evaluation for the period 1990–2001. In: Proceedings of IX EMTE national-international conference of meteorology-climatology and atmospheric physics, 28–31 May 2008, Thessaloniki, Greece, p 649
5. Krueger BC, Katragkou E, Tegoulias I, Zanis P, Melas D, Coppola E, Rauscher SA, Huszar P, Halenka T (2008) Regional decadal photochemical model calculations for Europe concerning ozone levels in a changing climate. Időjαrαs – Q J Hung Meteorol Serv 112(3–4):285–300
6. Somot S, Spiridonov V, Marquet P, Deque M (2004) Climate version of the LAM ALADIN. In: Workshop on regional climate modeling, MAGMA EC Project No EVG3-CT-2002-80006, Prague
7. Spiridonov V, Braun Al, Deque M, Somot S (2004) High resolution climate adaptation of ERA40 data over the Bulgarian domain. In: Workshop on regional climate modeling, MAGMA EC Project No EVG3-CT-2002-80006, Prague
8. Spiridonov V, Déqué M, Somot S (2005) ALADIN-CLIMATE: from the origins to present date. ALADIN Newsletter, 29
9. Spiridonov V, Syrakov D, Ganev K, Prodanova M, Bogachev A, Miloshev N, Jordanov G, Slavov K (2010) Model estimates of regional climate changes and its impact on the air quality over Bulgaria. In: 19th international symposium ECOLOGY & SAFETY, 7–11 June 2010, Sunny Beach, Bulgaria (on a CD, volume 4, Part 1, http://www.science-journals.eu), ISSN: 1313-2563
10. Syrakov D, Ganev K, Spiridonov V, Prodanova M, Bogatchev A, Miloshev N, Jordanov G (2009) Assessment of climate change impact on air pollution levels in Bulgaria. In: 7th international conference on air quality science and application Istanbul, 24–27 March 2009 (on a CD)
11. Uppala SM, Kållberg PW, Simmons AJ, Andrae U, da Costa Bechtold V, Fiorino M, Gibson JK, Haseler J, Hernandez A, Kelly GA, Li X, Onogi K, Saarinen S, Sokka N, Allan RP, Andersson E, Arpe K, Balmaseda MA, Beljaars ACM, van de Berg L, Bidlot J, Bormann N, Caires S, Chevallier F, Dethof A, Dragosavac M, Fisher M, Fuentes M, Hagemann S, Hólm E, Hoskins BJ, Isaksen L, Janssen PAEM, Jenne R, McNally AP, Mahfouf J-F, Morcrette J-J, Rayner NA, Saunders RW, Simon P, Sterl A, Trenberth KE, Untch A, Vasiljevic D, Viterbo P, Woollen J (2005) The ERA-40 re-analysis. Q J R Meteorol Soc 131:2961–3012. doi:10.1256/qj.04.176
12. Visschedijk AJH, Zandveld PYJ, Denier van der Gon HAC (2007) A high resolution gridded European Emission Database for the EU Integrate Project GEMS, TNO-report 2007-A-R0233/B, Apeldoorn

Chapter 74
Ensemble Modeling of Air Pollution Due to April 2010 Island Volcano Eruption

Dimiter Syrakov, Maria Prodanova, Stefano Galmarini, Efisio Solazzo, Roberto Bianconi, Roberto Bellasio, Andrew Jones, Robert Buckley, Slavomir Potemski, and Maud Maret

Abstract The eruption of Island volcano in April 2010 caused enormously big troubles for air transport over Europe for a long period of time. The losses and inconveniences for air companies, common business and usual passengers are difficult to be estimated but in any case are rather considerable. The insights from this extraordinary event are that serious efforts must be put in studding not only the volcanic events but in creating tools for reliable forecast of volcano products (mainly ash) distribution in case of eruption. There are few centers devoted to observation and forecast of such events. Some meteorological services lately created respective systems. The ENSEMBLE consortium leaded by European JRC in Ispra, Italy, which is aimed at elaborating ensemble forecast on the base of individual forecasts of almost all European Early Warning Systems (EWS) in case of nuclear accident decided to launch a series of exercises devoted to simulation of the first week air

D. Syrakov (✉) • M. Prodanova
National Institute of Meteorology and Hydrology, Bulgarian Academy of Sciences,
66 Tzarigradsko Chausee, Sofia 1784, Bulgaria
e-mail: dimiter.syrakov@meteo.bg

S. Galmarini • E. Solazzo
European Commission – DG Joint Research Centre, Institute for Environment
and Sustainability, 21027 Ispra, VA, Italy

R. Bianconi • R. Bellasio
Enviroware srl C. Dir Colleoni, Pzo Andromeda, 1 20041 Agrate Brianza, Italy

A. Jones
Met Office, FitzRoy Road, Exeter EX1 3PB, UK

R. Buckley
Savannah River National Laboratory, Savannah River Site, Aiken, SC 29808, USA

S. Potemski
Institute of Atomic Energy, 05-400 Otwock-Swierk, Poland

M. Maret
Meteo France, Dir. Prod., Serv./Environ, 42 av. Coriolis, 31057 Toulouse, France

D.G. Steyn et al. (eds.), *Air Pollution Modeling and its Application XXII*,
NATO Science for Peace and Security Series C: Environmental Security,
DOI 10.1007/978-94-007-5577-2_74,

pollution dilution caused by Island volcano eruption. Bulgarian ERS (BERS) was upgraded as to be able to take part in these exercises and its results and comparisons with other model results are the object of this work.

Keywords Ensemble modelling • Volcanic eruption

74.1 Introduction

The severe atmospheric events like powerful volcano eruption do not cause serious problems for air quality at ground surface except for the neighboring territories. But sometimes they can cause serious economic problems. The disruption in ground transport caused by snow, floods etc. paled into insignificance compared with the havoc caused by the ash cloud spewed out by Eyjafjallajokull volcano in Iceland. The event started on 14 April 2010. It lasted with different intensity more than a month. The eruption has been characterized by two main phases of intense ash emissions spanning April 14–21 and May 1–10.

Volcanic eruptions are often referred to as violent explosions which spew huge rocks and hot lava. Some times volcanic eruptions can create very large clouds of ash that can be quite dangerous. When ash particles pass through the extremely hot jet engines, they melt into glass which coats any exposed areas. This can cause the engines to malfunction, including total engine failure. A detail description of these effects can be found in [12].

Due to the damaging effect of ash particles to aircraft engines, during the Eyjafjallajokull eruption a lot of airports all over Europe have been closed sporadically for different periods of time. Even at open airport conditions many flights have been cancelled or delayed according to the volcanic ash distribution. The cancelled flights are estimated to more than 100,000. Millions of passengers were stranded not only because of the dust clouds, but due to the ultra-strict safety rules which banned flying if there was even a slightest trace of volcanic ash. The European Union's executive body estimates the losses from the first 2 weeks of the disaster to 1.5–2.5 billion euros.

It is obvious that such extremely harmful events, in spite very rare, do not get away from the monitoring and forecast practice of meteorological services and other devoted institutions. All around the world, nine Volcanic Ash Advisory Centers (VAACs) are set, responsible for advising international aviation of the location and movement of clouds of volcanic ash. The Icelandic volcano was handled by the VAAC in London, England. Advisory charts have been issued several times per day during the entire event. Quite good description of London VAAC activity connected with Eyjafjallajokull eruption is presented in [11]. Apart VAAC activities many other institutions had intensive activity, including modeling.

The modeling activity performed in real or near-real time during the event suffers from different uncertainties. In [11], special attention is paid on it. The main feature

of the modeling activities is that only individual forecasts are issued. That is why the ENSEMBLE consortium (described in the next paragraph) decided to launch series of modeling exercises in attempt to obtain more realistic simulations of this event.

74.2 ENSEMBLE Project and Volcano Exercise

Ensemble modeling, originally developed for weather prediction, is lately being extended to atmospheric dispersion applications [1, 2]. Following this ideology the EU 5FP project ENSEMBLE was launched as a natural continuation and further development of ETEX project [3] and of the follow-up RTMOD project [1]. After its completing, the European Commission, recognizing the importance of the project achievements, converted its consortium to a permanent structure lead by JRC in Ispra, Italy. From that time many other institutions join the Consortium (see the ENCSEMBLE web-site [10]). Now a day ENSEMBLE is a web-based decision support system that produces a comprehensive forecast based on the multi-model ensemble dispersion concept. The tool provides also a number of various statistics and plots that allows users to perform on-line ensemble analysis.

ENSEMBLE Consortium launched a volcano exercise for the first week of the event (14–21 April 2010). The vertical structure was enlarged up 12,000 m. Four cases are foreseen; here results of Case 3 (^{137}Cs-like aerosol) only are presented. Source term is produced after Mastin [6–8]. Eleven modeling systems from ten countries took part in this Case.

74.3 BERS' Simulation Results

Bulgarian Emergency Response System (BERS) in case of nuclear accident works operationally since 2001. Its creation and development was highly stimulated by the ETEX experiment. NIMH took part in all activities of with a puff-type dispersion model. Lately, the new 3D model EMAP was tested; performing better than the puff model and now it is the core of BERS. Description of the system and of EMAP is given in [4, 5]. The EMAP model is verified many times in the frame of various projects as ETEX, RTMOD, ENSEMBLE and others.

For ENSEMBLE applications EMAP is realized in a domain of 250×210 points with 20 km resolution covering the whole Europe on stereographic map projection. The vertical levels are 6 (up to 3,000 m). The participation of BERS in ENSEMBLE volcano exercise laid essential upgrades of EMAP and the whole system. First, the number of EMAP levels was increased and set as required by the exercise's technical documents. As far as the operational met-data transferred from German Met Office (DWD) is quite limited, the high level data was downloaded from the free NCEP data base [9].

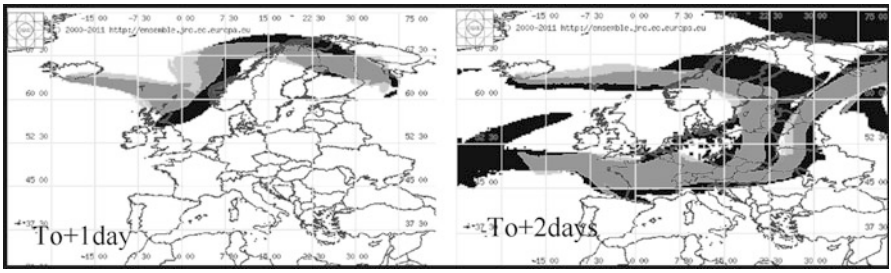

Fig. 74.1 Forecasted time evolution of EMAP simulation versus ensemble one: Case 3, concentration at height 6,000 m, threshold 1 μg/m^3; *light gray plume* – EMAP simulation, *black one* – ENSEMBLE simulation, *dark gray one* – overlap

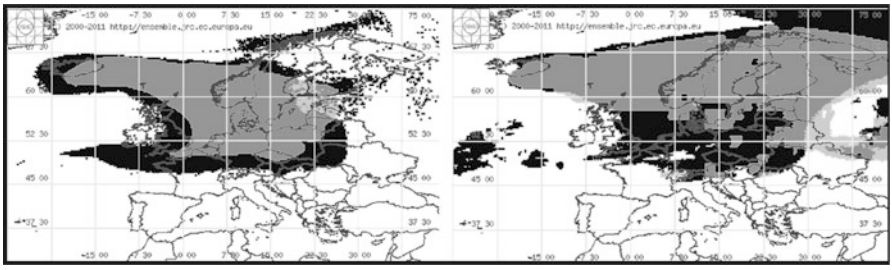

Fig. 74.2 Forecasted time evolution of EMAP simulation versus ensemble one: Case 3, accumulated dry (*left*) and wet (*right*) deposition, threshold 1,000 μg/m^3; *light gray plume* – EMAP simulation, *black one* – ENSEMBLE simulation, *dark gray one* – overlap

BERS took part in all ENSEMBLE volcano exercise cases; results encrypted and uploaded to the ENSEMBLE web server. From all statistical parameters supported by ENSEMBLE system only "overlap in space" is used and respective images presented, here. It is done because of its quite illustrative character. This is the percentage of overlapping area to the common area of both comparable plumes. Here, only part of BERS results versus ensemble ones are presented. All images are produced by ENSEMBLE system. Many simulations were made by BERS in attempt to tune the EMAP model.

The next two figures demonstrate the EMAP simulation abilities in comparison with an ensemble composed by the other ten models. In Fig. 74.1, the concentration spots of both simulations are shown for two particular moments. The percentage of overlap, as usual, decreases in time. Despite, EMAP plume coincides with ensemble one in big extent.

In Fig. 74.2, the accumulated deposition fields (dry and wet) are presented for 3 days after **To**. The percentage of overlapping here is much higher than in case of concentration fields that is quite natural taking into account the accumulation character of these fields.

74.4 Conclusion

The Bulgarian Emergency Response System took part in the volcano exercise launched by ENSEMBLE consortium. The possibilities of the ENSEMBLE web-based system were used for tuning the BERS models. Despite all four cases of the exercise were calculated, BERS reliability was demonstrated only on Case 3. The main conclusion is that despite many unfavorable circumstances as different source of meteorological information for low and high layers, met-data set low time resolution, simplest numerical schemes etc., EMAP produces quite satisfactory results. All main features of volcanic ash distribution are caught by the model. The comparison of the levels of agreement of all models that took part in the exercise versus the ensemble of the remaining ten models shows that EMAP results are in the middle of the ranking. This entire means that NIMH with its BERS is a useful member of ENSEMBLE consortium.

Acknowledgments This work is based on the results obtained within the ENSEMBLE Consortium which is acknowledged.

References

1. Galmarini S, Bianconi R, Bellasio R, Graziani G (2001) Forecasting the consequences of accidental releases of radionuclides in the atmosphere from ensemble dispersion modelling. J Environ Radioact 57:203–219
2. Galmarini S et al (2004) Ensemble dispersion forecasting - Part I: concept, approach and indicators. Atmos Environ 38(28):4607–4617
3. Girardi F, Graziani G, van Velzen D, Galmarini S, Mosca S, Bianconi R, Bellasio R, Klug W, Fraser G (1998) ETEX – The European tracer experiment. EUR 18143 EN, 1-108. Office for Official Publications of the European Communities, Luxembourg
4. Syrakov D, Prodanova M, Slavov K (2003) Description and performance of Bulgarian Emergency Response System in case of nuclear accident (BERS). Int J Environ Pollut 20:1–6
5. Syrakov D, Veleva B, Prodanova M, Popova T, Kolarova M (2009) The Bulgarian Emergency Response System for dose assessment in the early stage of accidental releases to the atmosphere. J Environ Radioact 100:151–156
6. Syrakov D, Prodanova M, Galmarini S, Solazzo E, Bianconi R, Bellasio R, Jones A, Buckley R, Potemski S, Maret M (2011) Model simulation of air pollution due to April 2010 Iceland Volcano Eruption. J Int Sci Publ Ecol Saf 5:127–142, Part 1 (http://www.science-journals.eu), ISSN: 1313-2563
7. Thomson D (2010) The Met Office Volcanic Ash Advisory Centre (VAAC) response to the Eruption. In: Annual science conference national centre for earth observation, University of Leicester, UK. 29 September 2010. http://www.nceo.ac.uk/documents/18.%20Dave%20Thomson.pdf
8. UCL (2010) Volcanic hazard from Iceland: analysis and implications of the Eyjafjallajökull eruption. Report of the Institute for Risk and Disaster Reduction, University College London. https://www.ucl.ac.uk/rdr/publications/icelandreport
9. http://rda.ucar.edu/datasets/ds083.2/
10. http://ensemble2.jrc.ec.europa.eu/

11. Thomson D (2010) The Met Office Volcanic Ash Advisory Centre (VAAC) response to the Eruption. In: Annual science conference national centre for earth observation, University of Leicester, UK. 29 September 2010. http://www.nceo.ac.uk/documents/18.%20Dave%20Thomson.pdf
12. UCL (2010) Volcanic hazard from Iceland: analysis and implications of the Eyjafjallajökull eruption. Report of the Institute for Risk and Disaster Reduction, University College London. https://www.ucl.ac.uk/rdr/publications/icelandreport

Chapter 75
Evaluations of WRF-CMAQ/CAMx Performance in East Asia Focusing on the Seoul Metropolitan Area

Youn-Seo Koo, Dae-Ryun Choi, and Jin-Sik Cho

Abstract Comparative study of two chemical transport models of CMAQ and CAMx with WRF (Weather Research and Forecasting) model under the identical conditions of meteorological field as well as emission inventory was carried out to evaluate their performances to predict atmospheric aerosols in East Asia focusing on the Seoul Metropolitan Area. Predicted concentrations of PM10, PMC (particulate matter with less than 10 μm and larger than 2.5 μm), PM2.5, sulfate, nitrate, organic carbon, elemental carbon and soil component were compared with those measured in Korea especially with intensive measurements in the SMA. CMAQ and CAMx generally depicted the variation of temporal trend and spatial distribution of the aerosols components but the PM10 and PMC were intrinsically underestimated by both models due to inherent uncertainty and lack of information for emission data of fugitive soil dusts. CAMx has a tendency to predict higher PM species concentrations than those of CMAQ. According to soccer plots of fractional bias vs. fractional gross error in annual PM chemical species, both CMAQ and CAMx, however, are acceptable in the range of between good performance and average performance. It is inferred from this study that the main reasons to induce differences between CMAQ and CAMx in predicting PM species are due to dry deposition mechanism and nesting method.

Keywords Aerosols • Model evaluation

Y.-S. Koo (✉) • D.-R. Choi • J.-S. Cho
Department of Environmental Engineering, Anyang University, Anyang, Gyeonggi-do, South Korea
e-mail: koo@anyang.ac.kr

D.G. Steyn et al. (eds.), *Air Pollution Modeling and its Application XXII*,
NATO Science for Peace and Security Series C: Environmental Security,
DOI 10.1007/978-94-007-5577-2_75,

75.1 Introduction

The East Asia region is world's most populous area with a rapid growing economy resulting in the large air pollutant emissions. The urban and industrial development of China in this region is especially prominent and it causes heavy and complex air pollution problems in Korea. The air quality in the SMA (Seoul Metropolitan Area) had deteriorated due to the emission in the SMA itself as well as growing influence from China [4].

The Korean Ministry of Environment put into operation of a comprehensive program, so-called 'Blue Sky 21' project, to improve air quality in the SMA. To assess the air quality improvement according to various control policies, a chemical transport modeling reflecting the long-range transport from China is necessary. The U.S. EPA's Models-3/CMAQ and CAMx (Comprehensive Air-quality Model with extension) have been used in assessing future air quality and regional contribution according to various emission reduction plans in the SMA.

Comparative study of two chemical transport models of CMAQ and CAMx with WRF (Weather Research and Forecasting) model under the identical conditions of meteorological field as well as emission inventory was carried out to evaluate their performances to predict atmospheric aerosols in East Asia focusing on the SMA. Predicted concentrations of PM10, PMC (particulate matter with less than 10 μm and larger than 2.5 μm), PM2.5, sulfate, nitrate, organic carbon, elemental carbon and soil component were compared with those measured in Korea especially with intensive measurements in the SMA.

75.2 Modeling System

Emission inventory and meteorological modeling used for the CMAQ and CAMx performance test with key characteristics of both models were briefly described below. The anthropogenic emissions from the Intercontinental Chemical Transport Experiment Phase B (INTEX-B) inventory for 2006 [7] was used for Asia region except South Korea. The CAPSS (Clean Air Policy Support System) emission inventory for 2007 from Korean Ministry of Environment was used with updates of fugitive dust and bio-mass emissions in South Korea.

The WRF model with version 3.1 is used as the meteorological model [1, 5]. The number of vertical layers of WRF was 46 and the WRF with three domains of 27 km for East Asia, 9 km for Korean peninsula, and 3 km for the SMA. The National Centers for Environmental Prediction (NCEP) Final Analyses (FNL) data of 1° resolution have been used to provide the initial and boundary conditions for WRF model.

Table 75.1 A summary of CMAQ and CAMx model configurations

Model option	CMAQ	CMAx
Model version	Version 4.6	Version 5.2.1
Horizontal resolution	27/9/3Km	27/9/3Km
Grid nesting	One-way	Two-way
Vertical layers	NZ = 12	NZ = 12
Horizontal advection	PPM	PPM
Vertical advection	PPM	Implicit
Horizontal diffusion	K-theory	K-theory
Vertical diffusion	Eddy diffusion	Eddy diffusion
Gas-phase chemistry	CB4	CB4
Gas-phase chem. solver	EBI	EBI
Aerosol chemistry	AE4/ISORROPIA	M4/ISORROPIA
Dry deposition	Pleim-Xiu	Wesely
Emissions	2006 INTEX-B & 2007 CAPSS	2006 INTEX-B & 2007 CAPSS

Grid FDDA (Four dimensional data assimilation) nudging was applied to temperature, wind and moisture parameters for the domains of 27 and 9 km, respectively.

CMAQ and CAMx are three-dimensional Eulerian multi-scale chemical transport models and open source modeling systems [2]. They have been updated by reflecting state-of-art of science findings in the academic society. Although they have many similarities in model conceptions, numerical methods and operational usage, there are several key differences reflecting the technical preference and development history of each model. The summary of CMAQ and CAMx model configurations used in this study is listed in Table 75.1. Key differences between CMAQ and CAMx are nesting method, dry deposition method, PM size distribution, SOA formulation and probing tools [6]. The CMAQ is one-way nesting and the CAMx is multiple two way nesting. The CMAQ normally uses three lognormal modes of Aitken, accumulation and coarse modes while CAMx uses a two-size section module with fine and coarse modes. The more details of modeling system can be found in Koo et al. [3].

The ability of the CMAQ and CAMx models to reproduce observed ground level concentrations of gas-phase species and major aerosol species observed in Korea was tested. The intense measurement campaign led by Seoul Metropolitan Government was carried out to understand the effect of trans-boundary and local effect on the air quality in Seoul and clarify further action to improve the air quality in Seoul. During the campaign period of 2008–2010, the chemical speciated species of sulfate, nitrate, ammonium, OC, EC, total mass of PM2.5 and PM10 were observed in SMA. The air quality monitoring stations are shown in Fig. 75.1.

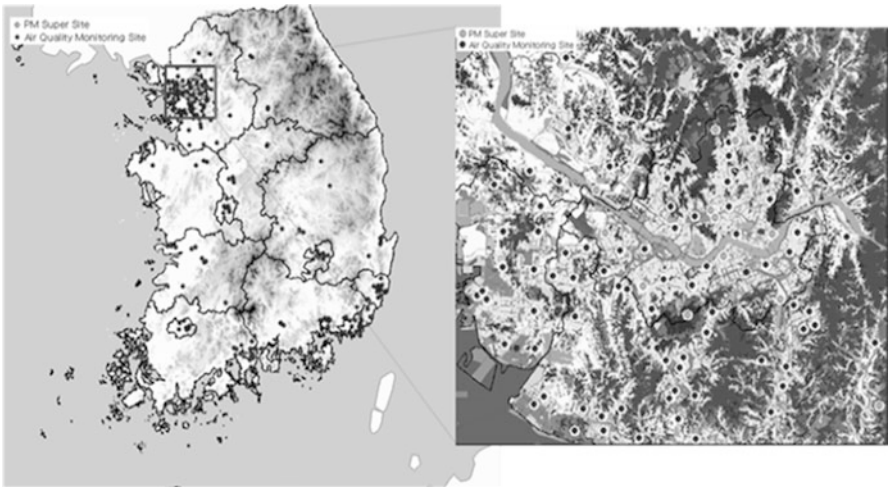

Fig. 75.1 The locations of ambient air quality monitoring stations in Korea with highlight of PM supersite to measure chemically speciated aerosols in the SMA

75.3 Results and Discussion

In order to test the performance of WRF-CMAQ and CAMx modeling systems, the model predictions were compared with meteorological and air quality data observed in SMA.

The observed meteorological variables such as temperature, wind speed, wind direction and relative humidity were compared with the WRF predictions at Seoul meteorological monitoring station. WRF surface temperatures had warm bias and the relative humidity simulated by WRF showed generally lower value than the measured one especially in high humidity period. Wind speeds in WRF has shown slight over-prediction with normalized mean bias of 13.8 %. The artifact in the calculated meteorological field is expected to have an impact on the formation of secondary aerosols. Generally, the meteorological field predicted by WRF was quite acceptable.

Predicted concentrations of PM10, PMC, PM2.5, sulfate, nitrate, organic carbon, elemental carbon and soil component were compared with those measured at ambient air quality monitoring sites in Korea as well as PM supersite for measurements of chemical speciated aerosol species in the SMA.

Daily PM10, PMC, and PM2.5 concentrations calculated from CMAQ and CAMx for 2009 were compared with the data measured at Guui PM supersite in Fig. 75.2 and the resulting statistics of CMAQ and CAMx performance for each

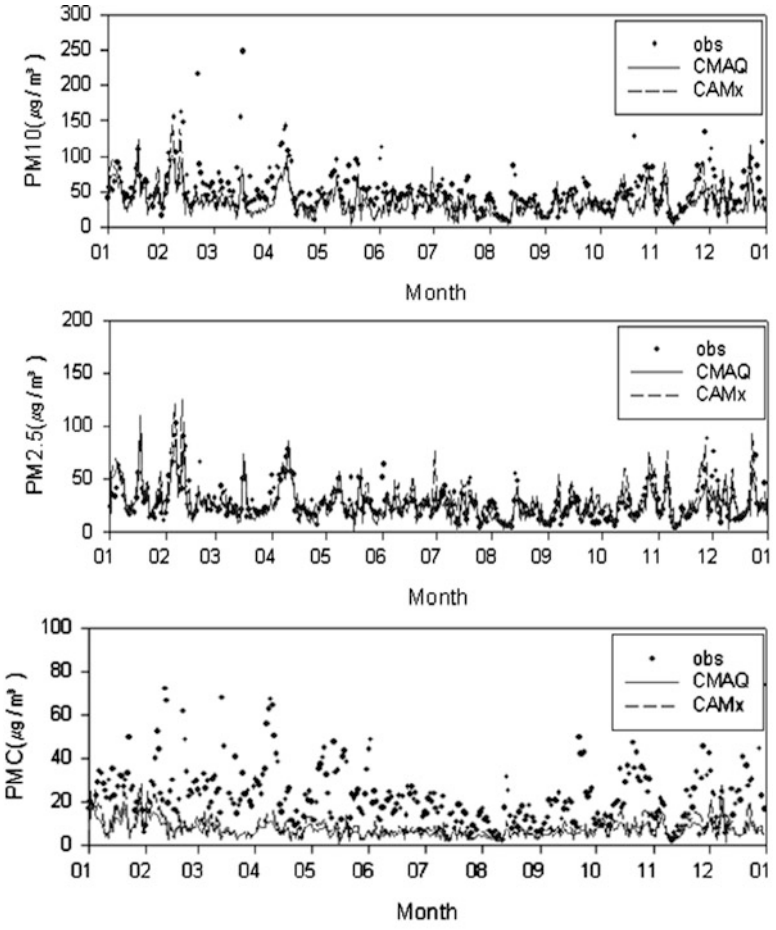

Fig. 75.2 Comparison of daily PM10, PMC and PM2.5 concentrations measured at Guui PM supersite with predicted ones by CMAQ and CAMx for 2009

aerosol species for 2009 are summarized in Fig. 75.3. The soccer plots of fractional bias vs. fractional gross error in annual PM chemical species calculated by CMAQ and CAMx at Guui supersite for 2009 is in Fig. 75.4.

Across the full year of 2009, CMAQ and CAMx in general depicted the variation of temporal trend and spatial distribution of the aerosols components but the PM10 and PMC were intrinsically underestimated by both models due to inherent uncertainty and lack of information for emission data of fugitive soil dusts [3].

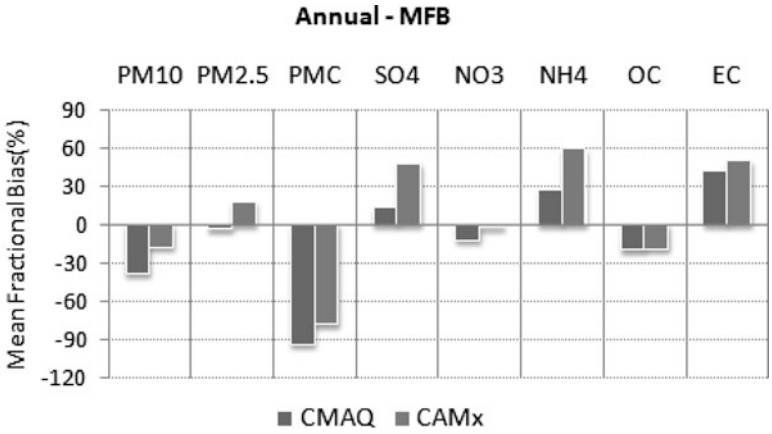

Fig. 75.3 Annual performance statistics of PM chemical species predicted by CMAQ and CAMx at Guui PM supersite for 2009

CAMx has predicted higher PM species concentrations than those of CMAQ: mean fractional biases of CAMx for PM10 and PM2.5 are −19 and 5 while those of CMAQ are −30 and −3, respectively. According to soccer plots in Fig. 75.4, the performance of CMAQ and CAMx is acceptable in the range of between good performance (2nd dotted box) and average performance (3rd dotted box).

75.4 Conclusions

CMAQ and CAMx generally depicted the variation of temporal trend and spatial distribution of the aerosols components but the PM10 and PMC were intrinsically underestimated by both models due to inherent uncertainty and lack of information for emission data of fugitive soil dusts. CAMx has a tendency to predict higher PM species concentrations than those of CMAQ. According to soccer plots of fractional bias vs. fractional gross error in annual PM chemical species, both CMAQ and CAMx, however, are acceptable in the range of between good performance and average performance. It is inferred from this study that the main reasons to induce differences between CMAQ and CAMx in predicting PM species are due to dry deposition mechanism and nesting method.

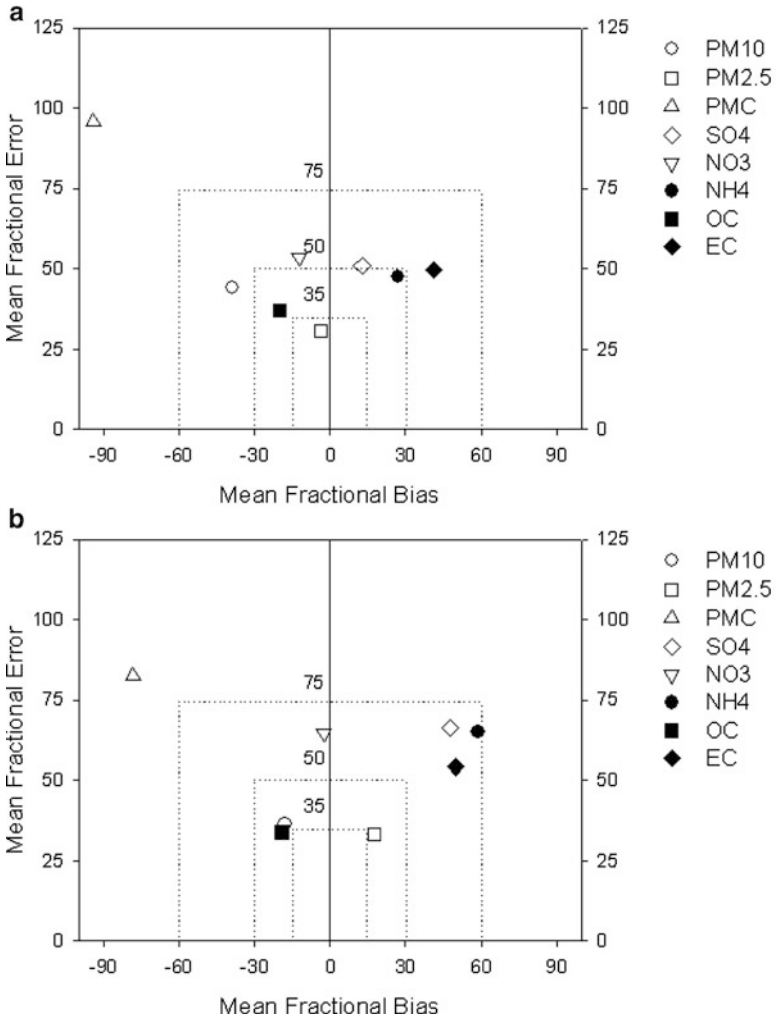

Fig. 75.4 Soccer plots of fractional bias vs. fractional gross error in annual PM chemical species calculated by CMAQ and CAMx at Guui PM supersite for 2009

Acknowledgements This subject is supported by Korea Ministry of Environment as "The Eco-technopia 21 project".

References

1. Borge R, Alexandrov V, del Vas JJ, Lumbreras J, Rodríguez ME (2008) A comprehensive sensitivity analysis of the WRF model for air quality applications over the Iberian Peninsula. Atmos Environ 42:8560–8574
2. Byun F, Ching JKS (1999) Science algorithm of the EPA Model-3 Community Multiscale Air Quality (CMAQ) modeling system. United States Environmental Protection Agency Rep. EPA-600/R-90/030, 727 pp
3. Koo YS, Kim ST, Cho JS, Jang YK (2012) Performance evaluation of the updated air quality forecasting system for Seoul predicting PM10. Atmos Environ 58:56–69. doi:10.1016/j.atmosenv.2012.02.004
4. Koo YS, Kim ST, Yun HY, Han JS, Lee JY, Kim KH, Jeon EC (2008) The simulation of aerosol transport over East Asia region. Atmos Res 90:264–271. doi:10.1016/j.atmosres.2008.03.014
5. Skamarock WC, Klemp JB (2008) A time-split non-hydrostatic atmospheric model for weather research and forecasting applications. J Comput Phys 227:3465–3485. doi:10.1016/j.jcp.2007.01.037.1
6. Tesche TW, Morris R, Tonnesen G, McNally D, Boylan J, Brewer P (2006) CMAQ/CAMx annual 2002 performance evaluation over the eastern US
7. Zhang Q, Streets DG, Carmichael GR, He K, Huo H, Kannari A, Klimont Z, Park I, Reddy S, Fu JS, Chen D, Duan L, Lei Y, Wang L, Yao Z (2009) Asian emissions in 2006 for the NASA INTEX-B mission. Atmos Chem Phys 9(1):4081–4139

Chapter 76
Modelling of Air Quality in Europe in the Framework of the Revision of the Gothenburg Protocol

Sebnem Aksoyoglu, Johannes Keller, and Andre S.H. Prévôt

Abstract In this study, we investigate the effects of revised Gothenburg target emissions on ozone and particulate matter in Europe with a focus on Switzerland by means of the 3-dimensional air quality model CAMx and the meteorological model WRF. We use the GAINS emissions for the CORINAIR SNAP sectors and the European countries to prepare gridded emission scenarios. In this paper, we discuss the project goals and preliminary model results for various emission scenarios with respect to the reference case.

Keywords CAMX • WRF • Ozone • PM

76.1 Introduction

In an earlier study we calculated the effects of numerous regulations enforced in Europe since 1985 and predicted the effects of Gothenburg targets for 2010 on air quality [2]. In 2007, the Convention on Long-Range Transboundary Air Pollution initiated the revision of its Gothenburg multi-pollutant/multi-effect protocol. In the revised protocol, PM2.5, PM10 and greenhouse gases were included. Various emission control scenarios for cost-effective improvements of air quality in Europe in 2020, were prepared by the EMEP Centre for Integrated Assessment Modeling (CIAM) and IIASA using the GAINS (Greenhouse gas – Air pollution Interactions and Synergies) model. We study the effects of those emissions scenarios on ozone and particulate matter in Europe with a focus on Switzerland by means of a regional air quality model. In this paper, we discuss the preliminary model results of various emission scenarios for 2020 with respect to the reference year 2005.

S. Aksoyoglu (✉) • J. Keller • A.S.H. Prévôt
Paul Scherrer Institute, Laboratory of Atmospheric Chemistry, 5232 Villigen PSI, Switzerland
e-mail: sebnem.aksoyoglu@psi.ch

D.G. Steyn et al. (eds.), *Air Pollution Modeling and its Application XXII*,
NATO Science for Peace and Security Series C: Environmental Security,
DOI 10.1007/978-94-007-5577-2_76,

76.2 Method

We perform the simulations using the air quality model CAMx (Comprehensive Air Quality Model with extensions) (http://www.camx.com) and the meteorological model WRF (Weather Research and Forecasting Model) (http://wrf-model.org/index.php). In CAMx, we use CB05 gas-phase mechanism and the SOAP aerosol model to calculate gaseous and particulate species concentrations (see [1] for details). The cloud chemistry is also included. Our coarse model domain covers whole Europe with a horizontal resolution of $0.250° \times 0.125°$. A second, nested domain with three times higher resolution covers Switzerland. European emissions for anthropogenic sources for 2006 are provided by TNO (http://www.gmes-atmosphere.eu/). Biogenic emissions are calculated using the meteorological fields from WRF model. The gridded emissions for scenarios are prepared using the GAINS emissions for various snap sectors and countries (http://gains.iiasa.ac.at/index.php/policyapplications/gothenburg-protocol-revision). The selected scenarios studied in this project are given in Table 76.1. The model validation is performed for 2006 using data from measurement campaigns and networks. The reference year is 2005 for comparison with revised Gothenburg scenarios. The relative changes in emissions with respect to the reference year (2005) are determined from the GAINS database and are transformed to TNO gridded emission data. Additionally, we run the model with emissions of 1990 as a retrospective study. Simulations for the reference year 2005 and for 2020 with various emission scenarios are carried out using the constant meteorology. The changes in the air quality between 2020 and the reference case are analyzed.

76.3 Results

Calculations of emissions and other input data were completed and simulations started. Each scenario is simulated for whole year. Only some preliminary results could be shown since simulations have not yet been completed. These results refer to 1 week in June. As an example, changes in PM2.5 concentrations in scenarios 2020 BL and 2020 MTFR relative to 2005 BL are shown in Figs. 76.1

Table 76.1 Selected scenarios studied in this project

Scenario	Year	Description
1	2006	Model validation
2	2005	CIAM4/2011 Baseline (BL), reference
3	2020	CIAM4/2011 Baseline (BL)
4	2020	CIAM4/2011 MTFR (max. technically feasible reduction)
5	2020	CIAM4/2011 Mid
6	2020	Revised Gothenburg Protocol
7	1990	Retrospective study

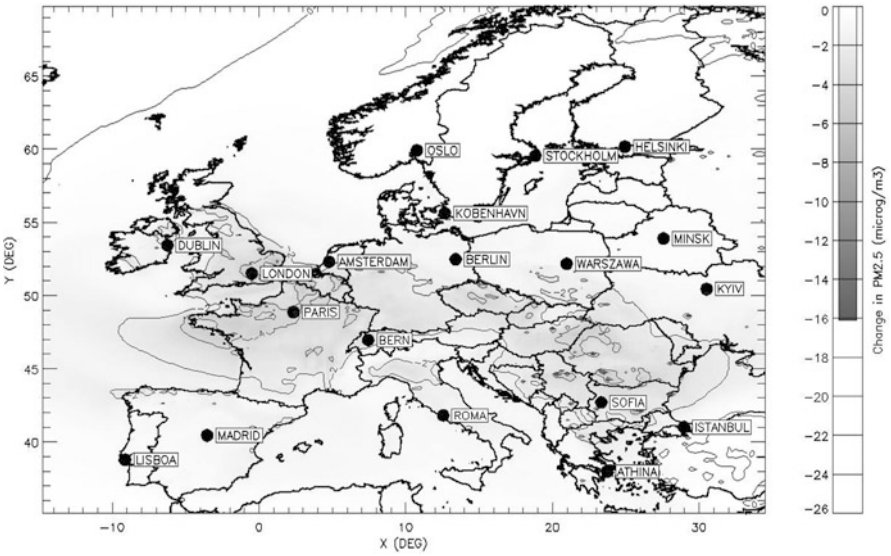

Fig. 76.1 Decrease in PM2.5 concentration in 2020 BL relative to 2005

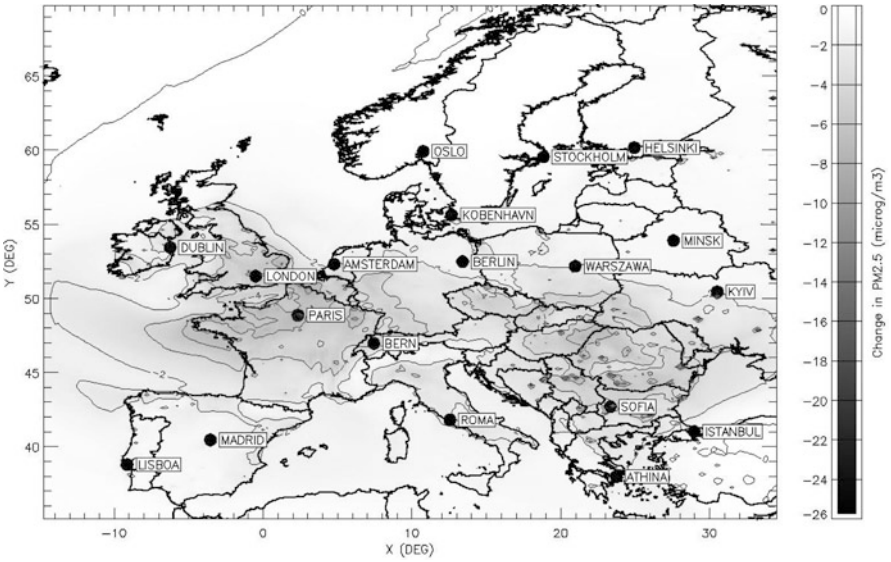

Fig. 76.2 Decrease in PM2.5 concentration in 2020 MTFR relative to 2005

and 76.2, respectively. These preliminary results suggest that the largest decrease in PM2.5 concentrations in Europe would be achieved with the MTFR scenario. On the other hand, results of the BL and MID (not shown) scenarios are quite similar. The first preliminary results of the retrospective simulations indicate a

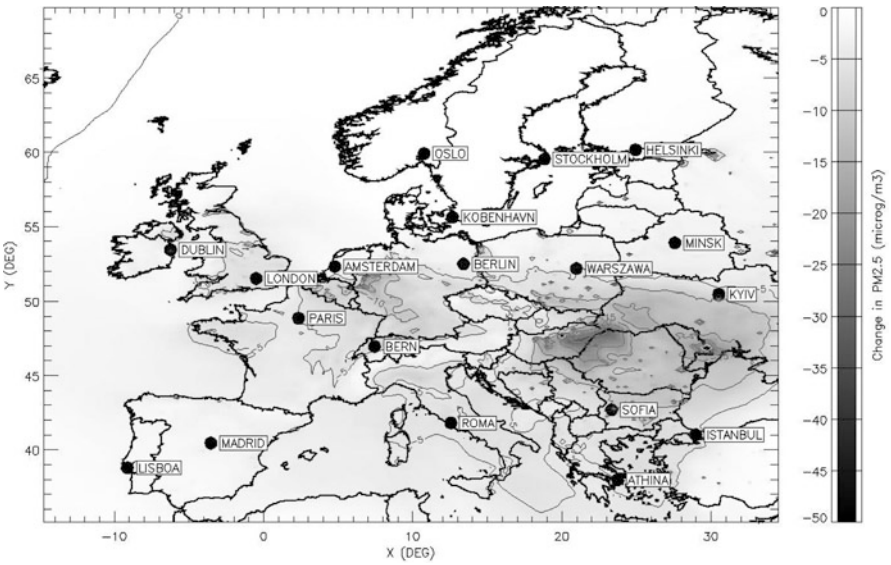

Fig. 76.3 Decrease in PM2.5 concentration between 1990 and 2005

large decrease in PM2.5 concentrations in Europe since 1990, especially in Eastern Europe (Fig. 76.3). The final discussion and conclusions will be carried out when whole year simulations for each emission scenario are completed.

Acknowledgements We thank Meteotest, INFRAS and TNO for providing various data. We extend our thanks to the European Centre for Medium-Range Weather Forecasts (ECMWF) for allowing the use of its Mozart data and the boundary conditions for WRF. Web access of IIASA for GAINS data is gratefully acknowledged. This study was financially supported by the Swiss Federal Office of Environment (FOEN).

References

1. Aksoyoglu S, Keller J, Barmpadimos I, Oderbolz D, Lanz VA, Prévôt ASH, Baltensperger U (2011) Aerosol modelling in Europe with a focus on Switzerland during summer and winter episodes. Atmos Chem Phys 11(14):7355–7373. doi:10.5194/acp-5111-7355-2011
2. Andreani-Aksoyoglu S, Keller J, Ordonez C, Tinguely M, Schultz M, Prevot ASH (2008) Influence of various emission scenarios on ozone in Europe. Ecol Model 217:1209–1218. doi:10.1016/j.ecolmodel.2008.1006.1022

Part VI
Model Assessment and Verification

Chapter 77
Air Quality Model Evaluation International Initiative (AQMEII): A Two-Continent Effort for the Evaluation of Regional Air Quality Models

S.T. Rao, Rohit Mathur, Christian Hogrefe, Efisio Solazzo, Stefano Galmarini, and Douw G. Steyn

Abstract With the endorsement and support from the U.S. Environmental Protection Agency, European Commission, and Environment Canada, a project entitled Air Quality Model Evaluation International Initiative (AQMEII) was launched in 2009 by bringing together scientists from Europe and North America (Rao ST, Galmarini S, Puckett K, Bull Am Meteorol Soc 92:23–30, 2011). Several regional-scale numerical photochemical models were applied over the North American and European domains with 2006 emissions inventory. Several papers resulting from this international collaborative effort were accepted for publication in the AQMEII special issue of *Atmospheric Environment*. Also, a large 4-D database, assembled by EU Joint Research Centre for the AQMEII project, is now available to all scientists interested in developing innovative model evaluation techniques (Galmarini S, Rao ST, Atmos Environ 45(14):2464, 2011). Having successfully completed the first phase of AQMEII, Phase 2 of AQMEII was launched at the 2011 AQMEII workshop in Chapel Hill, NC, USA to focus on the interactions of air quality and climate change. In Phase 2, coupled meteorology-atmospheric chemistry models will be exercised over the two continents with a common emissions database to assess how well the current generation of coupled regional-scale air quality models can simulate the spatio-temporal variability in the optical and radiative characteristics of atmospheric aerosols and associated feedbacks among aerosols, radiations, clouds, and precipitation. The results from AQMEII Phase 2 would be useful to policy makers for developing effective policies to deal with air pollution and climate change.

S.T. Rao (✉) • R. Mathur • C. Hogrefe
Atmospheric Modeling and Analysis Division, U.S. Environmental Protection Agency, 1200 Pennsylvania Ave NW, Washington, DC 20460, USA
e-mail: strao@ncsu.edu

E. Solazzo • S. Galmarini
Institute for Environment and Sustainability, European Union Joint Research Centre, Ispra, Italy

D.G. Steyn
Department of Earth and Ocean Sciences, University of British Columbia, Vancouver, Canada

D.G. Steyn et al. (eds.), *Air Pollution Modeling and its Application XXII*,
NATO Science for Peace and Security Series C: Environmental Security,
DOI 10.1007/978-94-007-5577-2_77,

Keywords Model evaluation • AQMEII

77.1 Introduction

Regional air quality modelling has undergone considerable development during the last three decades worldwide because of the increased concern regarding the impact of air pollution on human health and ecosystems. Both in North America and Europe, a few tens of models have been developed by different research groups. As compared to other geophysical sciences like climate, the regional character of air quality issues have not led to the development of international collaborative research efforts with participation of scientists from both continents for systematically assessing models' performance. Nonetheless, regional air quality models are now being widely used for designing emission control policies and forecasting air quality. Recognizing the need for collaboration and coordination of research among scientists in North America and Europe, a workshop was held in Stresa, Italy in April 2009 and the project "Air Quality Model Evaluation International Initiative (AQMEII)" was launched [6].

77.2 Approach

The need for a common basis for evaluating regional-scale air quality models was identified based on Dennis et al. [2]. The North American model domain covered the United States and southern part of Canada while the European domain covered all countries in the European Union (Fig. 77.1). For the 2006 annual simulation, 18 regional models from 13 countries were exercised (Table 77.1). Several articles by the AQMEII research team will be published in the special issue of *Atmospheric Environment* [3] in early 2012. Further analyses on the AQMEII dataset are being carried out by the research team and, hence, additional papers on techniques for evaluating regional-scale air quality models can be expected to appear in the literature.

AQMEII provided a set of time-varying gridded emissions (referred to as "standard" emissions) for each continent, focusing on the evaluation of the air quality and meteorological models. Full details are given in Galmarini et al. [5]. Standardised modelling outputs over a full year (2006) from each modeling group have been shared on the web-distributed ENSEMBLE system [3], which allows for statistical and ensemble analyses to be performed by each group. The observational data for several fields, based on several surface monitoring networks over both continents, have been loaded into the ENSEMBLE system. Model evaluations have been performed by pairing the model output with the observation at the same time and location.

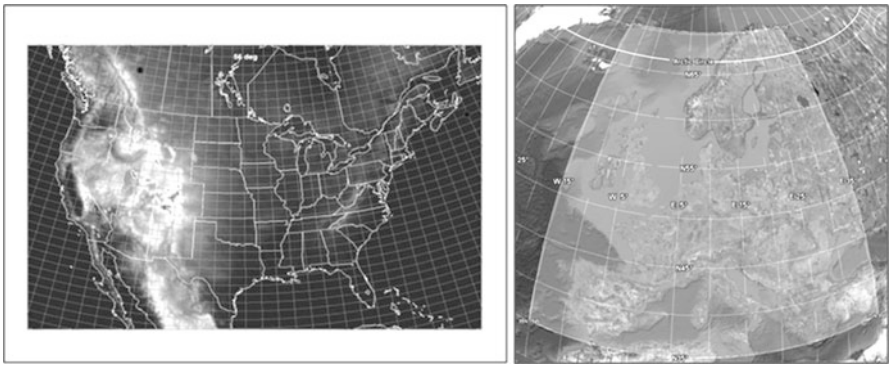

Fig. 77.1 AQMEII modelling domains for North America and Europe

77.3 Results and Discussion

Collective examination of model performance and model inter-comparison during the first phase of AQMEII have involved a number of variables and types of analyses, as detailed in Solazzo et al. [7, 8] and Vautard et al. [10]. There was considerable variability among model predictions because of the use of different configurations or post-processing of the same model. There were systematic positive model biases, particularly for Europe, in the surface and boundary layer wind speed; overestimation is particularly marked in stable wintertime or nighttime conditions. The day-to-day variability in the low-level wind speed is also systematically overestimated for Europe. Furthermore, models had a tendency to underestimate the occurrence of non-precipitation conditions and extreme precipitation events, but overestimate the occurrence of light to moderate precipitation conditions, leading to an overestimation of wet removal of particles and water-soluble gases.

The systematic biases in the meteorological inputs should induce significant and systematic concentration biases, in particular for the primary pollutants. This was in fact one of the conclusions of the AQMEII multi-model analysis of air quality model skill in simulating particulate matter (PM) (see [7]). In particular, model wind speed bias was found to be correlated with negative PM biases, especially for Europe. Overestimated rainfall frequency was also found to be consistent with underestimated PM concentrations. The operational model evaluation carried out by Solazzo et al. [7] on the air quality model outputs of PM10 and PM2.5 revealed a large variability among models (and even among different versions/users of the same model), especially for modeled PM10 concentration. Concerning the model skill in estimating the major components of PM2.5 (SO4, NH4, NO3, Elemental Carbon), a more homogenous performance was found for the selected compounds than for total PM2.5 mass. This result might suggest that, while air quality models are reliable to simulate inorganic aerosol, there is still a lack of good representation

Table 77.1 Configuration of the meteorology (Met) air quality (AQ) models in the AQMEII project (From Solazzo et al. [8])

Domain	Meteorological model	Air quality model	Horizontal resolution (km)	Number of vertical layers	Emissions	Chemical boundary conditions
EU	MM5	DEHM	50	29	Global emission databases, EMEP	Satellite measurements
EU	MM5	Polyphemus	24	9	Standard[a]	Standard
EU	PARLAM-PS	EMEP	50	20	EMEP model	From ECMWF and forecasts
EU	WRF	CMAQ	18	34	Standard[a]	Standard
EU	WRF	WRF/Chem	22.5	36	Standard[a]	Standard
EU	WRF	WRF/Chem	22.5	36	Standard[a]	Standard
EU	ECMWF	SILAM	24	9	Standard anthropogenic; In-house biogenic	Standard
EU	MM5	Chimere	25	9	MEGAN, Standard	Standard
EU	LOTOS	EUROS	25	4	Standard[a]	Standard
EU	COSMO	Muscat	24	40	Standard[a]	Standard
NA*	GEM	AURAMS	45	28	Standard+	Climatology
NA*	WRF	Chimere	36	9	Standard	LMDZ-INCA
NA*	MM5	CAMx	24	15	Standard	LMDZ-INCA
NA*	WRF	CMAQ	12	34	Standard	Standard
NA*	WRF	CAMx	12	26	Standard	Standard
NA*	WRF	Chimere	36	9	Standard	Standard
NA*	MM5	DEHM	50	29	Global emission databases, EMEP	Satellite measurements

[a]Standard anthropogenic emission and biogenic emission derived from meteorology (temperature and solar radiation) and land use distribution implemented in the meteorological driver

*Standard inventory for North America includes biogenic emissions

+Standard anthropogenic inventory but independent emissions processing, exclusion of wildfires, and different version of BEIS (v3.09) used

of the processes strongly influencing PM2.5 concentration other than inorganic aerosol chemistry. Finally, analysis of two high PM2.5 concentration episodes in Europe and North America revealed that while there is a considerable scatter of model results about the observations with significant biases, models seem to be able to capture the episode peaks and the sharp oscillations around them, especially for North America. Further analysis of model outputs is being carried out by the AQMEII team to examine if models behave differently for different weather conditions.

The focus of the investigation of surface ozone by Solazzo et al. [8] was on the ensemble analysis of the surface ozone mixing ratios, rather than on inter-comparing statistical metrics for each individual model. The main findings of the investigations, involving 11 different air quality models, was that while multi-model ensembles demonstrate improved performance over the individual model realizations, the most skillful ensemble is not necessarily generated by including all available model results, but instead by selecting models that result in a minimization in ensemble error. In addition, an ensemble of top-ranking model results can be worse than an ensemble of top-ranking and low-ranking model results. Furthermore, it was found that the skill score does not necessarily improve by increasing the number of models in the ensemble. In contrast, the level of dependence of model results may lead to a deterioration of the results and to an overall worsening of performance.

77.4 Future Directions

In the Phase 1 activity, model evaluations were performed on uncoupled regional air quality models and the database is available to the larger scientific community for developing and applying innovative methods for model evaluation [4]. Additional analyses on these models are being carried out by various groups. In light of the experience gained, the AQMEII community identified the need for moving forward with the next phase of AQMEII to continue international collaboration on modelling research and its applications, focusing this time on the evaluation of regional-scale coupled (i.e., integrated meteorology-atmospheric chemistry) models' capability to simulate the interactions of air quality and climate change. The Phase 2 activities will be aimed at addressing the following questions [1].

- Can the current versions of the coupled models developed in North America and Europe accurately simulate aerosol-radiation feedback processes?
- How important is scale interaction in air quality and climate change studies?
- Are air quality-climate change interactions simulated by the global model comparable to the regional models?
- Can global models learn from regional-scale models and vice versa?

A workshop for the Phase 2 activity of AQMEII will be held in Utrecht, Netherlands during May 2012 in conjunction with NATO/SPS's International Technical Meeting on Air Pollution Modelling and Its Application. At this workshop,

the pertinent databases from both sides of the Atlantic Ocean will be shared for conducting model inter-comparison studies by modelling groups. It is envisioned that annual simulations for 2006 and 2010 will be performed using several coupled or on-line regional-scale models.

While AQMEII is underway, there has been an intense effort by the HTAP community to better understand the intercontinental transport of air pollution [9]. The HTAP community addresses the following question:

- What is the observational evidence for the intercontinental transport of O_3, PM, Hg, and POPs in the northern hemisphere?
- What are the main processes that drive these intercontinental flows and determine their magnitudes?
- What are the source-receptor relations for transboundary air pollution?

After completing the first phase of this modeling activity, the HTAP community embarked on a continuing collaborative effort to further study the intercontinental transport of air pollution under both current and future emission scenarios. Given the common interests of the HTAP and AQMEII communities, it has become clear that these two groups need to work together to improve our understanding of the interplay between air quality and climate change. To this end, it is envisioned that both hemispheric and regional models will be applied to 2006 and 2010 – a period where there were large reductions in emissions stemming from economic downturn and regulations – to inter-compare whether the observed dynamic signal in air quality is replicated by the current air quality modelling systems. This type of dynamic evaluation of models' response to the reductions in emissions would help build confidence in the use of these modelling systems for policy analysis.

Acknowledgments The authors are grateful for the support of the U.S. Environmental Protection Agency, European Union Joint Research Center, and Environment Canada to the AQMEII. Several researchers from the private sector and academia from the United States, Europe, and Canada have contributed to the AQMEII and HTAP projects.

Disclaimer Although this paper has been reviewed and approved for publication by the U.S. Environmental Protection Agency, it does not reflect the views and policies of the Agency.

References

1. Alapaty K et al (2012) New directions: understanding interactions of air quality and climate change at regional scales. Atmos Environ. doi:10.1016/j.atmosenv.2011.12.016
2. Dennis R et al (2010) A framework for evaluating regional-scale numerical photochemical modeling systems. Environ Fluid Mech 10:471–489. doi:10.1007/s10652-009-9163-2
3. Galmarini S, Rao ST, Steyn DG (2012) Preface: Special issue of Atmospheric Environment for AQMEII. ATMOSPHERIC ENVIRONMENT. Elsevier Science Ltd, New York, NY, 53(June):1–3
4. Galmarini S, Rao ST (2011) The AQMEII two-continent regional air quality model evaluation study. Atmos Environ 45(14):2464

5. Galmarini S, Bianconi R, Appel W, Solazzo E et al (2012) ENSEMBLE and AMET: two systems and approaches to a harmonised, simplified and efficient assistance to air quality model developments and evaluation. Atmos Environ. doi:10.1016/j.atmosenv.2011.08.076
6. Rao ST, Galmarini S, Puckett K (2011) Air quality model evaluation international initiative (AQMEII). Bull Am Meteorol Soc 92:23–30. doi:10.1175/2010BAMS3069.1
7. Solazzo E, Bianconi R, Pirovano G, Volker M, Vautard R et al. (2012) Operational model evaluation for particulate matter in Europe and North America in the context of AQMEII. Atmos Environ 53:75–92. doi:10.1016/j.atmosenv.2012.02.045
8. Solazzo E, Bianconi R, Vautard R et al (2012) Model evaluation and ensemble modelling for surface-level ozone in Europe and North America in the context of AQMEII. Atmos Environ. doi:10.1016/j.atmosenv.2012.01.003
9. UNECE (2010) Hemispheric transport of air pollution, Part D: answers to policy-relevant science questions. United Nations Publication, Geneva, ISBN 978-92-1-117047-4
10. Vautard R, Moran M, Solazzo E, Gilliam R, Volker M, Bianconi R et al (2012) Evaluation of the meteorological forcing used for the Air Quality Model Evaluation International Initiative (AQMEII) air quality simulations. Atmos Environ 53:1–224. doi:10.1016/j.atmosenv.2011.10.065

Questions and Answers

Questioner Name: D.G. Steyn

Q: I believe that we must engage competent statisticians to work with us on probabilistic model evaluation. This will help us employ sophisticated, robust, statistically mature methods to evaluate AQ models.
A: Agreed. We published a short note in *Atmospheric Environment*, announcing the availability of the AQMEII database to the scientific community for developing innovative model evaluation methodologies. Unfortunately, since AQMEII doesn't have extramural research funds to support the development of model evaluation techniques, we were not able to engage statisticians. Now that an unprecedented database has been made available to the scientific community, I hope scientists from different disciplines and institutions can team-up and prepare research proposals to potential funding agencies to analyze the AQMEII data and help advance model evaluation.

Questioner Name: P. Builtjes

Q: Finding good statistical measures for model evaluation in Phase 1 is already a problem, but what about model evaluation for on-line models?
A: Yes, as you noted model evaluation is not a simple task. The results in Phase 1 demonstrated that the statistical metrics that have been developed for dispersion models for non-reactive pollutants in the early 1980's are not very useful to evaluate regional-scale photochemical simulation models. Given that the on-line models explicitly treat the various interactions occurring between chemistry and meteorology, it is important that we select the right variables for model evaluation. The AQMEII community is now paying particular attention to the right variables and right statistical metrics appropriate for judging the performance of on-line models.

Questioner Name: J. Weil

Q: The existing AQMEII effort can be considered a physical, meteorological, chemical model evaluation. Why not extend this AQMEII effort to include health effects to see how well the model predictions correlate with health effects whether it be hospital visits, epidemiology, or other health impact measures?
A: As you saw, we are having difficulties in discerning the relative performances of different air quality models using statistical metrics such as correlation. I should note that the models that the atmospheric sciences community uses try to understand and explain the cause and effect relationships, namely, the pollutant concentration is a function of the source emission strength, meteorology, and removal processes. In contrast, the models that the health sciences community uses try to find associations between air pollution and health outcomes. Although there have been some accountability studies that tried to assess whether reduced pollutant concentrations have resulted in reduced hospital admissions, it is difficult if not impossible, to evaluate health effects modeling because of a myriad of confounding factors. However, it may be useful to consider issues relating to the evaluation of impacts on human health and ecosystems in future phases of AQMEII.

Chapter 78
Diagnostic Evaluation of Carbon Sources in CMAQ

Sergey L. Napelenok, Prakash V. Bhave, Heather Simon, George A. Pouliot, Michael Lewandowski, and Rebecca Sheesley

Abstract Traditional monitoring networks measure only total elemental carbon (EC) and organic carbon (OC) routinely. Diagnosing model biases with such limited information is difficult. Measurements of organic tracer compounds have recently become available and allow for more detailed diagnostic evaluation of CMAQ modeling results, which allow for more explicit representation of secondary organic aerosols. An enhanced version of the model makes it possible to track contributions from various sources of primary organic aerosols and elemental carbon, providing more in-depth evaluation of model biases. An ambient $PM_{2.5}$ measurement campaign conducted in four Midwestern U.S. cities in March 2004 February 2005 allows for direct comparison of modeled and measured organic carbon concentrations by primary and secondary source category.

Keywords CMAQ • Air quality modeling • Diagnostic model evaluation • Elemental carbon • Organic carbon • Organic tracer

78.1 Introduction

Routine monitoring networks measure only total elemental carbon (TEC) and total organic carbon (TOC). These measurements are useful to ascertain how an air quality model performs in predicting these quantities and have been used for this purpose in the past [1, 2]. However, it is difficult to diagnose model biases with such limited data. Instead, specialized measurement campaigns are necessary.

S.L. Napelenok (✉) • P.V. Bhave • H. Simon • G.A. Pouliot • M. Lewandowski
United States Environmental Protection Agency, Washington, DC 20460, USA
e-mail: napelenok.sergey@epa.gov

R. Sheesley
Baylor University, Waco, TX 76706, USA

D.G. Steyn et al. (eds.), *Air Pollution Modeling and its Application XXII*,
NATO Science for Peace and Security Series C: Environmental Security,
DOI 10.1007/978-94-007-5577-2_78,

One such specialized measurement campaign was conducted in the midwestern United States between March 2004 and February 2005. During this time, data was collected at four sites in the region: Bondville, IL; Northbrook, IL; Cincinnati, OH; and Detroit, MI. At each site, over 80 particle-phase organic compounds, including alkanes, hopanes, steranes, organic acids were measured on filters sampled every 6th day. The filter extracts were composited on a monthly basis and analyzed by chemical derivatization and gas chromatography. The composites were also analyzed by EPA scientists for highly polar compounds, which are known tracers of secondary organic aerosol (SOA) production [3].

In this study, the tracer measurements were compared to modeling results obtained from a simulation over the entire episode using a version of the CMAQ model outfitted with the ability to track 16 individual sources of primary EC and OC. This version of the model also included the recent enhancement to the SOA module allowing for a complete comparison with the measured tracer compounds.

78.2 Method

At first a traditional evaluation of total carbon (TC) was performed for the four sites listed above. While model performance varied in time, five scenarios of interest emerged.

1. Small (-0.3 ug/m^3) bias was recorded in the spring months in Detroit.
2. Large (-1.0 ug/m^3) bias was recorded in the spring months in the three other cities.
3. Large (-1.7 ug/m^3) bias was recorded in the summer months at all four sites.
4. Large (-1.4 ug/m^3) bias was recorded in the winter months at Northbrook.
5. Small (-0.2 ug/m^3) bias was recorded in the winter months in the three other cities.

To explain the sources of these biases, the CMAQ model was modified to keep track of 16 different categories of EC and OC including on road diesel exhaust, coal combustion, nonroad diesel exhaust, oil combustion, on road gasoline exhaust, natural gas combustion, nonroad gasoline exhaust, food cooking, aircraft exhaust, paved road dust, anthropogenic biomass combustion, crustal material, wildfires, misc. industrial processes, waste combustion, and other. The resulting source specific EC and OC modeled concentrations were paired with laboratory determined source profiles to transform TC concentrations to predictions of the measured organic tracers according to the following:

$$[Tracer]_i = \sum_j Profile_{i,j}[C]_j, \tag{78.1}$$

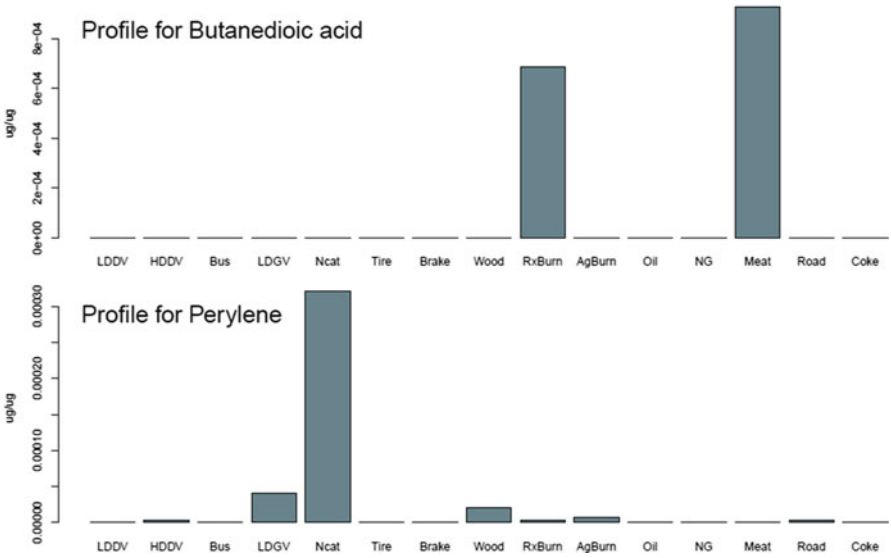

Fig. 78.1 Source profiles for two organic tracers. Butanedioic acid (*above*) originates mainly from prescribed burning and meat cooking, while Peryle (*below*) ne originates mainly from mobile sources

where $[Tracer]_i$ is the concentration of a measured organic tracer i, $[C]_j$ is the TC concentration from source j, and $Profile_{i,j}$ is the laboratory measured profile of tracer i from source j. An example of source profiles for butanedioic acid and Perylene appears in Fig. 78.1.

78.3 Results and Discussion

Several categories of emissions were analyzed to discern possible sources of biases in the emissions of EC and OC. Among these, it was found the model performed relatively well at simulating TC emissions from mobile sources at all sites, which were characterized by measurements of hopanes and steranes. Sources of biomass combustion, characterized by measurements of levoglucosan, were found to explain the negative summer-time bias at all of the sites. Production of secondary organic aerosol characterized by model predictions of isoprenes, monoterpenes, sesquiterpenes, and aromatics was also a source of large bias throughout the year. The good TC model performance during the spring in Detroit was found to be caused by compensating errors, where overestimation in emissions from burning natural gas were found to offset TC sources from other categories. The five cases of interest

Table 78.1 Biases in Emission categories for 5 selected regions/seasons

All quantities in $\mu gC/m^3$	Spring (Mar, Apr, May)		Summer (Jun, Jul, Aug)		Winter (Nov, Dec, Jan, Feb)
	Detroit	Non-Detroit	All cities	Northbrook	Non-Northbrook
TC bias	−0.3	−1.0	−1.7	−1.4	−0.2
Mobile	0.1	0.2	0.1	0.1	0.0
Natural gas	−0.2	−0.0	−0.0	−0.0	−0.1
Biomass	−0.1	0.1	0.4	0.3	0.1
α-pinene SOA	0.2	0.1	0.3	0.0	0.1
Aromatic SOA	0.2	0.1	0.2	0.0	0.0
Isoprene SOA	0.1	0.2	0.7	−0.0	0.0
β-caryophyllene SOA	0.3	0.1	0.1	0.2	0.2

identified above were found to be influenced by biases in the emissions categories according to Table 78.1, which can be used to guide further model development efforts in order to improve prediction of TC concentrations.

Disclaimer The United States Environmental Protection Agency through its Office of Research and Development funded and managed the research described here. It has been subjected to Agency's administrative review and approved for publication.

References

1. Carlton AG, Bhave PV, Napelenok SL, Edney EO, Sarwar G, Pinder RW, Pouliot GA, Houyoux M (2010) Model representation of secondary organic aerosol in CMAQv4.7. Environ Sci Technol 44(22):8553–8560
2. Foley KM, Roselle SJ, Appel KW, Bhave PV, Pleim JE, Otte TL, Mathur R, Sarwar G, Young JO, Gilliam RC, Nolte CG, Kelly JT, Gilliland AB, Bash JO (2010) Incremental testing of the Community Multiscale Air Quality (CMAQ) modeling system version 4.7. Geosci Model Dev 3(1):205–226
3. Lewandowski M et al (2008) Primary and secondary contributions to ambient PM in the Midwestern United States. Environ Sci Technol 42:3003–3309

Questions and Answers

Questioner Name: D. Simpson

Q: In European source-apportionment efforts, we have used typically 14C, levoglucosan, etc. to test models. We have also used similar SOA tracers as was shown here, but found large differences. More work is needed on these issues.
A: This type of comparison is limited mostly by measurement data availability. I agree that more work is needed on these issues, and to accomplish that, stronger

collaborations are needed between modelers and the measurement community. Also, it would be interesting to apply our techniques to the European data.

Questioner Name: C. Fountoukis

Q: Would using high time resolution measurements give more inside information about model bias?
A: It is unlikely that higher time resolution would give any additional information for a comparison such as this, because the organic tracers are measured in extremely small quantities already and require longer composite sampling.

Questioner Name: S. Aksoyoglu

Q: Comment about missing b-caryophyllene in winter: it seems that some terpenes are released when trees are cut and burned in winter. This might be one of the missing sources.
A: We are currently pursuing a related effort focused specifically on biomass combustion emissions. We appreciate this comment and will definitely investigate further.

Chapter 79
Evaluation of a Year-Long Ozone Hindcast for 2006 as Part of a DEFRA Model Intercomparison

Robert Thorpe, Nicholas Savage, Lucy Davis, and Paul Agnew

Abstract A variant of the operational forecast configuration of the Met Office's newly developed Eulerian Air Quality Forecast Model was used to generate an air quality hindcast for 2006 as part of a DEFRA model intercomparison. Verification of predicted ozone concentrations was carried out by comparing against hourly observations from 15 rural and urban background sites spread over the UK. Models were primarily assessed statistically using standard metrics including bias, mean error, correlation, and fraction of predictions within a factor of 2 of observations for (a) all observations, and (b) periods of elevated ozone (>100 $\mu g/m^3$). We will present results showing that the Met Office model is competitive with other models for hourly ozone, but is best in class at modelling episodes of elevated ozone. The results indicate that the availability of high quality met data and interactive treatment of chemistry and meteorology are both important in modelling ozone episodes.

Keywords Intercomparison • Model assessment • Ozone • 2006 • Statistical evaluation • Air quality

79.1 Introduction

The Met Office Eulerian Air Quality forecast model has been statistically validated against observational records of ozone at 15 sites spread across the UK for 2006 as part of a model intercomparison for DEFRA. Here we present some results from this study and briefly discuss the implications.

R. Thorpe • N. Savage (✉) • L. Davis • P. Agnew
UK Met Office, 1 FitzRoy Road, Exeter X1 3PB, UK
e-mail: nicholas.savage@metoffice.gov.uk

D.G. Steyn et al. (eds.), *Air Pollution Modeling and its Application XXII*,
NATO Science for Peace and Security Series C: Environmental Security,
DOI 10.1007/978-94-007-5577-2_79,

79.2 Model Description

The hindcast is performed with AQUM (Air Quality in the Unified Model), a limited area configuration of the Met Office Unified model UM with $182 \times 146 \times 38$ grid boxes at a horizontal resolution of 12 km and centred on the UK. The domain is shown in Fig. 79.1a. Initial meteorology is from Met Office global forecast, incorporating 4D-VAR analysis. Lateral boundary data is from Met Office global model (met) and GEMS (chemistry). The model uses the Regional Air Quality (RAQ) chemistry scheme [4] with: 40 tracers, 23 photolysis reactions and ~115 gas-phase reactions. Aerosols are modeled using the CLASSIC scheme [1], which includes explicit treatment of sulphate, black carbon, organic carbon, biomass burning, nitrate aerosols and allows two way coupling with aerosol direct and indirect effects AQUM is an online model – the chemistry and meteorology can interact with each other at each model timestep.

79.3 Defra Intercomparison

AQUM was compared with other models as part of the recent Defra Intercomparison [2] involving a year-long hindcast of near surface ozone concentrations for 2006. Each model's predictions were compared with hourly data for 15 sites spread across

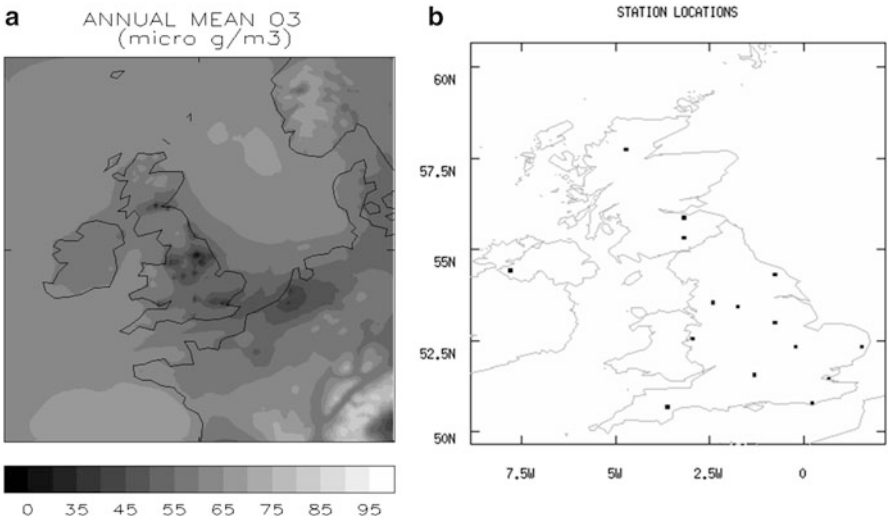

Fig. 79.1 (**a**) Modelled annual mean ozone for 2006, showing extent of model domain with UK in the centre. Areas of high orography are associated with higher mean annual ozone, lower concentrations result from interactions with NOx associated with large urban or industrial areas. (**b**) Map showing the locations of the 15 sites used in the analysis

the UK (Fig. 79.1b). Statistical assessment of the results was carried out using standard metrics such as FAC2 (the fraction of predictions within a factor of 2 of observations, bias, error and correlation.

79.4 Results

Table 79.1 shows the results of statistical evaluation of ozone predictions against all the hourly observations at the 15 observing sites. AQUM performs less well than NAME, the Met Office's Lagrangian dispersion model [3], but is competitive with other models in the intercomparison.

If we restrict our analysis to times when observed ozone is greater than 100 μg/m3 (ozone episode conditions), which are the times of greatest interest to policymakers due to the possible health impacts [5], a different picture emerges, which can be seen from Table 79.2.

The error terms generally increase during times of elevated ozone, and this increase is more than proportional to the increase in ozone itself, such that FAC2 declines. But the deterioration in performance for AQUM is significantly less than for other models, such that it is now the best performing model on some measures, and comparable to NAME on the others. Both NAME and AQUM perform significantly better than the average of the other models in ozone episode conditions.

During July 2006 there were several ozone episodes, interspersed with conditions when levels were much lower. Figure 79.2 shows modeled versus observed ozone during July at Aston Hill, a rural site in the midlands.

Table 79.1 Statistical evaluation of the ozone hindcast for 2006, for AQUM, NAME, and the average across all other models

Model	FAC2	MB	MGE	NMB	NMGE	RMSE	R
AQUM	0.78	−4.96	18.76	−0.08	0.33	24.23	0.64
NAME	0.87	2.05	16.87	0.04	0.29	22.12	0.62
Av of others	0.80	5.05	19.90	0.09	0.35	25.94	0.52

MB mean bias, *MGE* mean gross error, *NMB* normalized mean bias, *NMGE* normalized mean gross error, *RMSE* root mean square error, *R* temporal correlation

Table 79.2 Statistical evaluation of the ozone hindcast for observations >100 μg/m^3 in 2006, for AQUM, NAME, and the average across all other models

Model	FAC2	MB	MGE	NMB	NMGE	RMSE	R
AQUM	0.73	96.20	148.07	0.29	0.45	176.29	0.71
NAME	0.73	−81.93	139.53	−0.25	0.42	198.19	0.49
Av of others	0.50	−67.61	209.47	−0.17	0.64	256.27	0.25

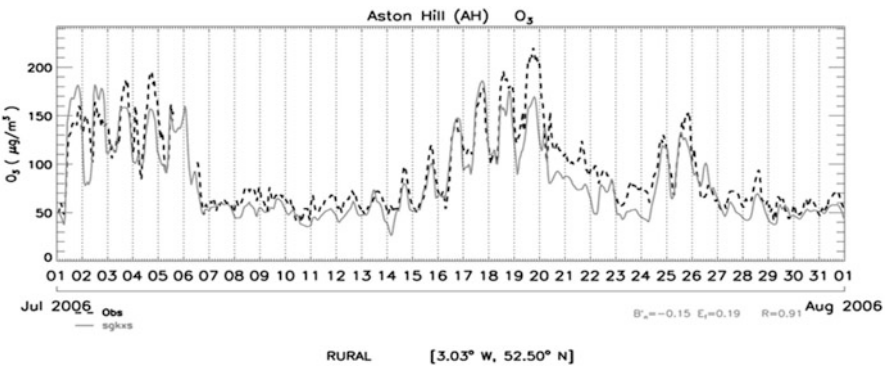

Fig. 79.2 Modeled versus observed ozone at Aston Hill. *Black* observations, *grey* model

There are three discrete ozone episodes at this site, and the model does a good job of representing them, both in magnitude and duration, whilst it also captures the periods of lower ozone between the episodes.

79.5 Summary

We have run AQUM for a full year hindcast of 2006. We find that performance is competitive with other models: mid-range for hourly ozone; best in class for modelling elevated ozone. The fact that NAME also performs well illustrates the importance of high-quality met data. The relative improvement in AQUM's performance during ozone episode conditions may reflect the online nature of the model and the feedbacks between chemistry and meteorology. These results give confidence in the Met Office's operational air quality forecast as the model set up is very similar.

References

1. Bellouin N, Rae J, Jones A, Johnson C, Haywood J, Boucher O (2011) Aerosol forcing in the Climate Model Intercomparison Project (CMIP5) simulations by HadGEM2-ES and the role of ammonium nitrate. J Geophys Res Atmos 116. doi:10.1029/2011J0016074
2. Carslaw D (2011) Defra regional and transboundary model evaluation analysis – phase I, 15 Apr 2011. http://uk-air.defa.gov.uk/library/reports?report_id=653
3. Jones AR, Thomson DJ, Hort M, Devenish B (2007) The U.K. Met Office's next-generation atmospheric dispersion model, NAME III. In: Borrego C, Norman A-L (eds) Air pollution modeling and its application XVII. Proceedings of the 27th NATO/CCMS international technical meeting on air pollution modelling and its application, Springer, Dordrecht, pp 580–589
4. O'Connor F (2009) Tropospheric configurations of UKCA. Met Office Report
5. Stedman JR, Kent AJ (2008) An analysis of the spatial patterns of human health related surface ozone metrics across the UK in 1995, 2003, and 2005. Atmos Environ 42:1702–1716

Questions and Answers

Questioner Name: Dominik Brunner

Q: Lateral boundary conditions are important and will be important for AQMEII. How well is ECMWF MACC and GEMS evaluated itself?
A: Both the GEMS and MACC reanalysis have been evaluated. For more details of the evaluation of the MACC reanalysis see ECMWF Technical Memorandum 671.
A: Inness et al. 2012. They conclude that Surface CO from the MACC reanalysis agrees well with NOAA/GMD observations, NO_2 fields from the reanalysis show the right seasonality over polluted urban areas of the NH and over tropical biomass burning areas, but underestimate wintertime NO_2 maxima over anthropogenic regions and tropospheric HCHO is quite well simulated in the MACC reanalysis even though no satellite data are assimilated.

Chapter 80
Investigating the Influence of Model Coupling by Comparing CAMx and WRF/Chem Over Italy

Alessandra Balzarini, Guido Pirovano, Giuseppe M. Riva, and Anna Toppetti

Abstract In order to assess the effects of model coupling on air quality simulations, the on-line meteorology and chemistry model WRF/Chem has been compared to the well known chemistry and transport model CAMx. Models have been applied over the Italian domain with a grid resolution of 15 km for both a winter and summer episode of 2005. The comparison of winter PM10 and summer O3 shows an overall agreement between the two models results, although some systematic differences have been highlighted. PM10 is usually higher in WRF/Chem than CAMx, especially in the Po Valley area for both winter and summer times. Models have been also evaluated against some measurement stations. Winter PM10 values are underestimated by the two models, while summer O3 data are generally overestimated.

Keywords WRF-Chem • CAMx • Model intercomparison

80.1 Introduction

Modern air quality models, such as CAMx, do not allow the estimation of the coupled interactions between climate change and air quality and, hence, their effects on policies. Otherwise, in the fully coupled Weather Research and Forecasting/Chemistry model (WRF/Chem) the chemistry transformations are embedded into the meteorological model WRF, so that such interactions can be investigated with a full modular approach. In this contribution we present the preliminary results over Italy of two different modelling systems, WRF/Chem and CAMx, for both a winter and summer period of 2005.

A. Balzarini (✉) • G. Pirovano • G.M. Riva • A. Toppetti
RSE S.p.A, via Rubattino 54, 20134 Milano, Italy
e-mail: alessandra.balzarini@rse-web.it

D.G. Steyn et al. (eds.), *Air Pollution Modeling and its Application XXII*,
NATO Science for Peace and Security Series C: Environmental Security,
DOI 10.1007/978-94-007-5577-2_80,

80.2 Modelling Systems

Air quality simulations have been performed by means of two chemical and transport models. The first one, WRF/Chem (version 3.3.1; [4]), is a coupled on-line meteorology and chemistry model with CBM-Z gas phase chemistry [11] and MOSAIC algorithm for aerosol simulation [10]. The second one, CAMx (version 5.4; [2]), is a fairly popular tri-dimensional model with Carbon Bond 2005 gas phase chemistry [9] and ISORROPIA aerosol module [7]. Models shared the same computational domain, emission inventories and boundary conditions. Anthropogenic emissions were computed by the SMOKE model (version 2.6; [8]) using the Italian official inventory [6] and the EMEP database (http://www.emep.int/). Off-line natural emissions were accounted for too [3, 5]. CAMx model has been driven by an off-line WRF meteorological simulation. WRF and WRF/Chem were initialized by the same ECMWF analysis fields (http://www.ecmwf.int), but adopted different physics parameterisations (e.g., PBL height, microphysics, ...). Finally, initial and boundary conditions were derived from a CHIMERE model run at European scale [1]. WRF/Chem and CAMx have been applied and compared over Italy for two episodes of 2005: winter (January and February 2005) and summer (June and July 2005). The computational domain extends over a $1{,}290 \times 1{,}470$ km^2 area with horizontal resolution of 15 km.

80.3 Results and Discussion

Figures 80.1 and 80.2 show the PM10 winter mean concentration and the O_3 summer mean values for both models results. In *winter* PM10 concentrations of WRF/Chem are higher than CAMx in the Po Valley area and in the city of Milan because of a bigger amount of secondary inorganic aerosols and coarse particulate (not shown). On the contrary, CAMx is higher over the rest of Italy and, more markedly, in the Mediterranean sea. In the leftover part of the domain the two models are quite similar.

During the *summer*, WRF/Chem concentrations of O_3 are usually lower than CAMx for the whole Italian domain. The discrepancies between the two model applications are mainly related to the different approach used to calculate the vertical mixing, one of the controlling factors of pollutant concentrations at the ground level.

Finally, models have been evaluated against ground-based chemical observations. For instance, we reported winter PM10 and summer O_3 time series of daily values in the city of Milan (Fig. 80.3). WRF/Chem and CAMx reproduce quite well the measured trend of daily values. In winter both models underestimate the winter PM10 daily mean, however WRF/Chem generally performs better than CAMx. In summer, O_3 concentrations are overestimated by the two models, but WRF/Chem is closer to the observed trend than CAMx.

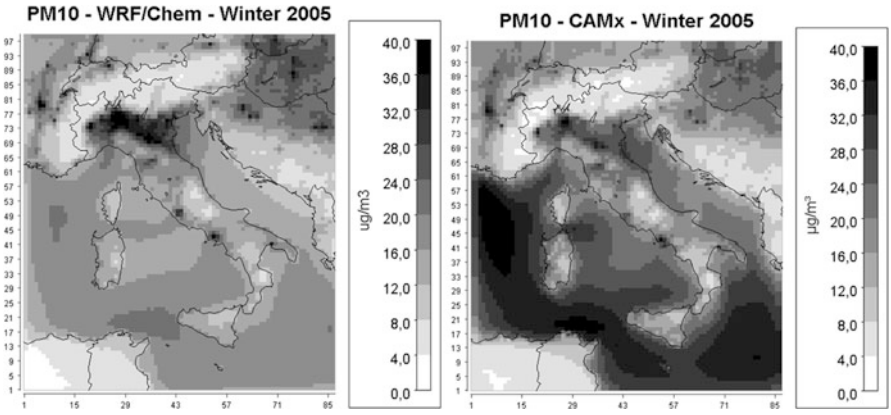

Fig. 80.1 Winter mean concentration of PM10 for WRF/Chem (*left*) and CAMx (*right*)

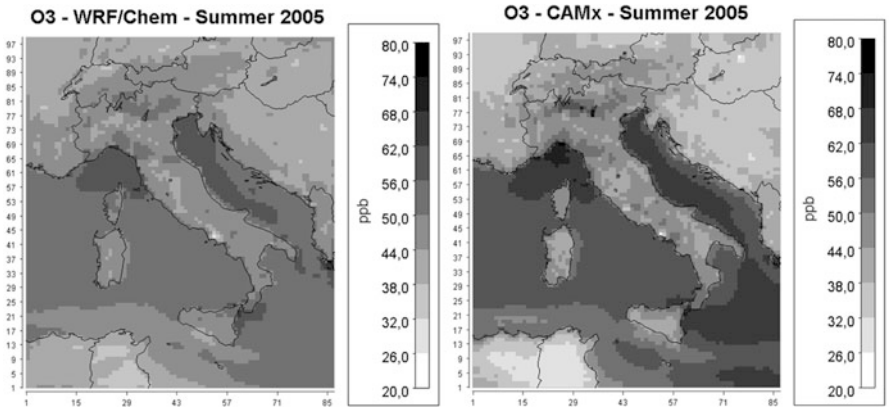

Fig. 80.2 Summer mean concentration of O_3 for WRF/Chem (*left*) and CAMx (*right*)

80.4 Conclusions

WRF/Chem and CAMx have been applied over the Italian domain with a grid step of 15 km for both a winter and summer episode of 2005. Models shared the same emission inventories and boundary conditions, while different chemical mechanisms and meteorological parameterisations have been selected. Comparisons showed an overall agreement of the two models for both winter PM10 and summer O_3. although some systematic differences have been highlighted. In winter WRF/Chem is usually higher than CAMx, especially in the Po Valley area, while in summer models revealed an opposite behaviour. Models performances were evaluated against some ground–based measurements. In the city of Milan, models showed an underestimation of winter PM10 values and an overestimation of summer O_3 concentrations, but WRF/Chem always performs better than CAMx.

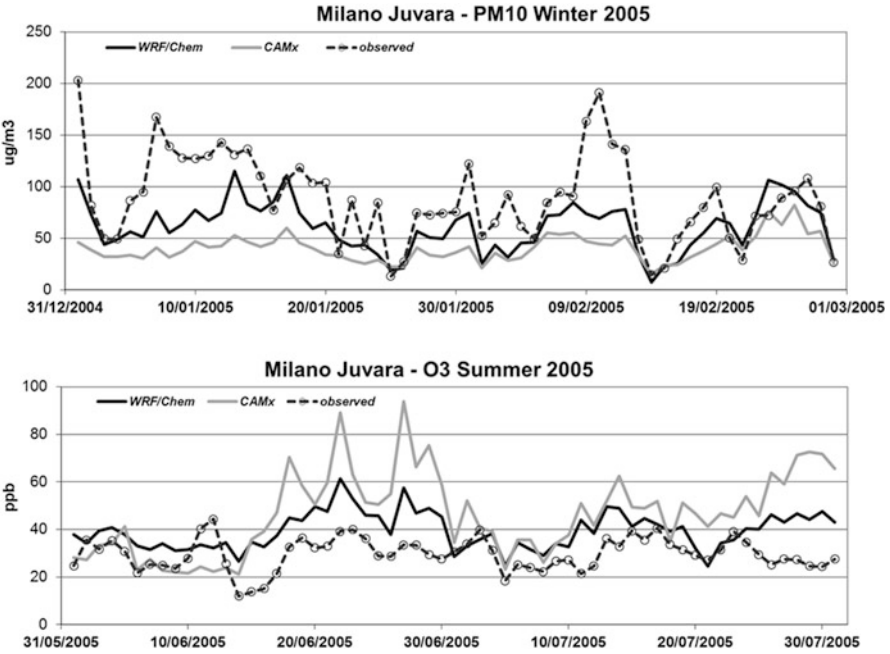

Fig. 80.3 Time series of winter PM10 (*top*) and summer O_3 (*bottom*) daily mean concentrations in the city of Milan

Acknowledgments This work has been financed by the Research Fund for the Italian Electrical System under the Contract Agreement between RSE (formerly known as ERSE) and the Ministry of Economic Development – General Directorate for Nuclear Energy, Renewable Energy and Efficiency stipulated on July 29, 2009 in compliance with the Decree of March 19, 2009.

References

1. Bessagnet B, Hodzic A, Vautard R, Beekmann M, Cheinet S, Honore C, Liousse C, Rouil L (2004) Aerosol modeling with CHIMERE-preliminary evaluation at the continental scale. Atmos Environ 38:2803–2817
2. ENVIRON (2011) CAMx (comprehensive air quality model with extensions) user's guide version 5.4. Environ Int Corp. http://www.camx.com/. Accessed 27 Feb 2012
3. Gong SL, Barrie LA, Lazare M (2002) Canadian aerosol module (CAM): a size-segregated simulation of atmospheric aerosol processes for climate and air quality models 2. Global sea-salt aerosol and its budgets. J Geophys Res 107:4779. doi:10.1029/2001JD002004
4. Grell GA, Peckham SE, Schmitz R, McKeen SA, Frost G, Skamarock WC, Eder B (2005) Fully coupled "online" chemistry within the WRF model. Atmos Environ 2:6–8. doi:10.1016/j.atmosenv.2005.04.027
5. Guenther A, Karl T, Harley P, Wiedinmyer C, Palmer P, Geron C (2006) Estimates of global terrestrial isoprene emissions using MEGAN (Model of Emissions of Gases and Aerosols from Nature). Atmos Chem Phys 6:3181–3210

6. ISPRA (2009) La disaggregazione a livello provinciale dell'inventario nazionale delle emissioni. Report number 92/2009
7. Nenes A, Pandis SN, Pilinis C (1998) ISORROPIA: a new thermodynamic equilibrium model for multiphase multicomponent inorganic aerosols. Aquat Geochem 4:123–152
8. UNC (2007) SMOKE v2.6 user's manual. Center for Environmental Modeling for Policy Developer. http://www.smoke-model.org/index.cfm. Accessed 27 Feb 2012
9. Yarwood G, Rao S, Yocke M, Whitten GZ (2005) Updates to the carbon bond chemical mechanism: CB05. Environ Int Corp. http://www.camx.com/. Accessed 27 Feb 2012
10. Zaveri R, Easter RC, Fast JD, Peters LK (2008) Model for simulating aerosol interactions and chemistry (MOSAIC). J Geophys Res 104:30387–30415. doi:10.1029/2007JD008782
11. Zaveri RA, Peters LK (1999) A new lumped structure photochemical mechanism for large-scale applications. J Geophys Res 104(D23):30,387–30,415

Questions and Answers

Questioner Name: Amela Jericevic

Q: You have concluded that vertical mixing (Kz) in CAMx is less efficient that in WRF/Chem model. However from your vertical ozone profile it is obvious that there is a strong ozone decrease in CAMx while in WRF/Chem concentrations are constant with height, which implies that vertical mixing is stronger in CAMx. Have you actually compared the Kz values from both models?
A: The Kz values from the two models haven't been compared, but we made some preliminary tests using a different algorithm to perform Kz in WRF-CAMx. This test shows that changing the vertical mixing calculation, the ozone concentrations of CAMx model are more mixed inside the PBL, making ground level concentrations in better agreement with the WRF/Chem ones.

Questioner Name: Christos Fountoukis

Q: Why the vertical mixing is so different?
A: The vertical mixing between WRF-CAMx and WRF/Chem is different because of the different calculation of Kz. In WRF-CAMx the Kz values are computed off-line with a specific pre-processor (WRFCAMx) using the O'Brien (1970) approach, while in WRF/Chem the Kz is calculated on-line, inside the coupled model.

Questioner Name: Sebnem Aksoyoglu

Q: I'm surprised that you overestimate O_3 in summer. Is O_3 overestimated everywhere? Did you compare model results at other sites?
A: We compared model results with measurement data of different Italian stations and we show a quite systematic tendency of overestimating the O_3 observed concentrations during summer months for both WRF/Chem and WRF-CAMx.

Chapter 81
Simulation of Atmospheric Oxidation Capacity in Houston, Texas

Golam Sarwar, Shuang Chen, Barron Henderson, Kathleen Fahey, Robert Gilliam, George Pouliot, Beata Czader, and Bernhard Rappenglueck

Abstract Air quality model simulations are performed and evaluated for Houston using the Community Multiscale Air Quality (CMAQ) model. The simulations use two different emissions estimates: the EPA 2005 National Emissions Inventory (NEI) and the Texas Commission on Environmental Quality (TCEQ) Emissions Inventory. A comparison of predictions with observed data from the 2006 TexAQS-II Radical and Aerosol Measurement Project (TRAMP) suggest that while the predicted oxides of nitrogen are greater than observations, predicted volatile organics (e.g., ethane, acetone) are substantially lower than the observations. Predicted hydroxyl radical predictions are in good agreement with the observations. Hydroperoxy radical predictions, however, are substantially lower than the observations.

Keywords CMAQ-model • Model evaluation • Aerosols

81.1 Introduction

Hydroxyl radical (OH) reacts with numerous chemical species present in the atmosphere, thereby determining the atmospheric oxidation capacity. Atmospheric OH, however, is not routinely measured. Hydroxyl radical, hydroperoxy radical (HO_2), and a suite of other chemical species were measured during the 2006

G. Sarwar (✉) • B. Henderson • K. Fahey • R. Gilliam • G. Pouliot
Atmospheric Modeling and Analysis Division, U.S. Environmental Protection Agency, Durham, NC, USA
e-mail: sarwar.golam@epa.gov

S. Chen
Department of Meteorology, Penn State University, University Park, PA, USA

B. Czader • B. Rappenglueck
Institute for Climate and Atmospheric Science, University of Houston, Houston, TX, USA

D.G. Steyn et al. (eds.), *Air Pollution Modeling and its Application XXII*,
NATO Science for Peace and Security Series C: Environmental Security,
DOI 10.1007/978-94-007-5577-2_81,

TexAQS-II Radical and Aerosol Measurement Project (TRAMP) [10, 11] and represent an opportunity for model evaluation. Chen et al. [6] used a constrained zero-dimensional box model and compared the predictions to observed OH and HO_2 levels from the TRAMP. In the constrained box-model, measured precursors are used to predict OH and HO_2 concentrations while in three-dimensional models emissions and meteorological fields drive the model predictions. Here, we compare OH and HO_2 predictions of a three-dimensional air quality model to observed data from the TRAMP.

81.2 Method

The study uses the CMAQ modeling system (version 5.0) [3, 7] to simulate air quality. Evaluations for the CMAQ modeling system have previously been conducted by comparing model predictions to measured ambient pollutants [1, 7, 12]. The CMAQ model has displayed considerable skill in simulating ozone and other chemical species in the atmosphere. The modeling domain covers most of Texas and Louisiana with 4-km grid spacings. It contains 35 vertical layers with the surface layer thickness of approximately 20-m. Model simulations are performed for August 30–September 4, 2006. This simulation period covers an ozone episode in Houston during which measured ozone reached over 160 ppb. Initial and boundary conditions are obtained from a larger modeling domain using 12-km horizontal grid-spacings covering the continental US. Meteorological fields are obtained from the Weather Research and Forecasting (version 3.2) model. Two different emissions inventories are used: the EPA 2005 National Emissions Inventory (NEI) and the Texas Commission on Environmental Quality (TCEQ) Emissions Inventory (EI). The Biogenic Emissions Inventory System (version 3.14) is used to prepare biogenic emissions for the study [13]. The Statewide Air Pollution Research Center (SAPRC-99) chemical mechanism [5] is used.

81.3 Results and Discussion

Predicted oxides of nitrogen (NO_x) are compared to the observed data in Fig. 81.1. Model predictions with the 2005 NEI are much greater than the observed data while predictions with the TCEQ EI agree better with the observed data. Thus, the modeling results using the TCEQ EI are presented.

Predicted ethane levels are compared to observed values in Fig. 81.2. Predicted ethane levels are substantially lower than observed data, with predicted mean value 11 times lower than mean observed data. While not shown here, predicted mean acetone level is ten times lower than observed data. Predicted levels of some other VOCs are lower than the observed values by factor of 2 or less. Thus, the model

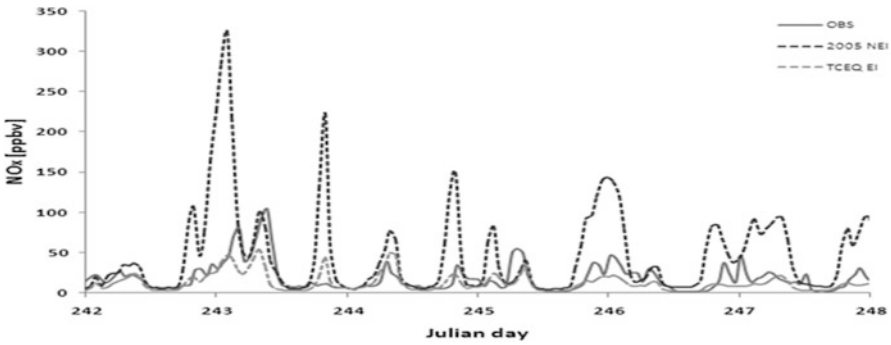

Fig. 81.1 A comparison of CMAQ predicted NO_x with TRAMP data

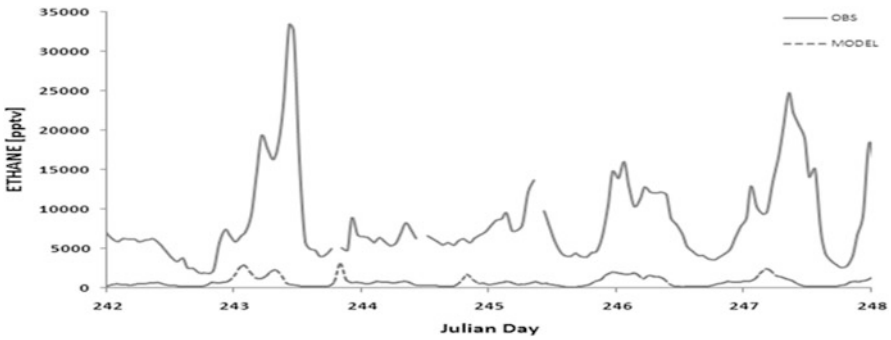

Fig. 81.2 A comparison of CMAQ predicted ethane with TRAMP data

emissions are enhanced by multiplying emissions estimates in the TCEQ EI with appropriate factors and the CMAQ model was re-run with the enhanced emissions. Kim et al. [9], Brioude et al. [2], and Byun et al. [4] also report that model with 2005 NEI predicts greater NO_x and lower VOCs than observed values.

Predicted OH levels are compared to observed values in Fig. 81.3. Predicted OH closely levels follow the diurnal trend of the observed data. Predicted daytime values are in good agreement with observed data although predicted peak values are somewhat lower. Predicted daily peak values reach to within 20 % of the observed data on all days except on September 2 (Julian day 245). Predicted nighttime OH values are lower than the observed data.

Predicted HO_2 levels are compared to the observed values in Fig. 81.4. Predicted HO_2 generally follow the diurnal trend of the observed data. While the model captures the observed day-to-day variability in OH levels reasonably well, predicted daytime peak HO_2 levels are lower than the observed data by factor of up to 4. Predicted nighttime values are also lower than the observed data. Fuchs et al. [8] suggested that several organic peroxy radicals can interfere with the measurements

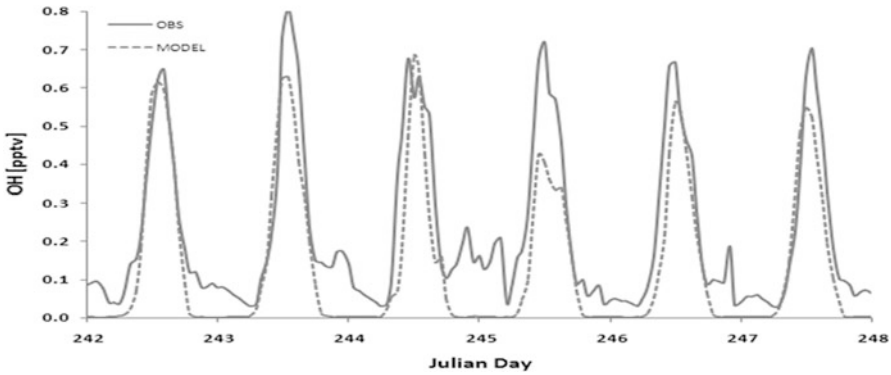

Fig. 81.3 A comparison of CMAQ predicted OH with TRAMP data

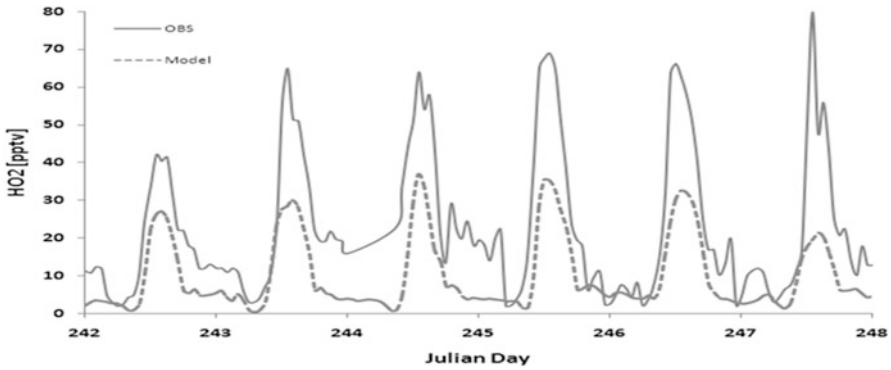

Fig. 81.4 A comparison of CMAQ predicted HO_2 with TRAMP data

of HO_2; thus true HO_2 values are lower than the observed values. Unfortunately, peroxy radicals were not measured in Houston. However, we estimate the true HO_2 values are within 20 % of the observed data.

81.4 Summary

The 2005 NEI contains more NO_x emissions than those in the TCEQ EI. Model predicted NO_x levels with 2005 NEI are much greater than the observed data. Predicted ethane levels with the TCEQ EI are substantially lower than the observed data. Predicted OH levels compare well with the observed data from TRAMP. However predicted daytime peak HO_2 levels are substantially lower than the observed data.

Disclaimer Although this paper has been reviewed by EPA and approved for publication, it does not necessarily reflect EPA's policies or views.

References

1. Appel KW, Gilliland AB, Sarwar G, Gilliam RC (2007) Evaluation of the Community Multiscale Air Quality (CMAQ) model version 4.5: sensitivities impacting model performance part I-ozone. Atmos Environ 41:9603–9615
2. Brioude J et al (2011) Top-down estimate of anthropogenic emission inventories and their interannual variability in Houston using a mesoscale inverse modeling technique. J Geogr Res 116:D20305. doi:10.1029/2011JD016215
3. Byun D, Schere KL (2006) Review of the governing equations, computational algorithms, and other components of the models-3 community multiscale air quality modeling system. App Mech Rev 59:51–77
4. Byun D, Lee D-G, Ngan F, Kim S, Kim H-C, Li X, Czader B, Rappenglueck B, Lefer B, Estes M, Olaguer E (2012) Retrospective air quality simulations of the 2006 TexAQS II TRAMP episode. Atmos Environ (in preparation)
5. Carter WPL (2000) Implementation of the SAPRC-99 chemical mechanism into the Models-3 Framework, report to the United States Environmental Protection Agency. Available at http://www.cert.ucr.edu/~carter/absts. htm#s99mod3
6. Chen S et al (2010) A comparison of chemical mechanisms based on TRAMP-2006 field data. Atmos Environ 44:4116–4125
7. Foley KM et al (2010) Incremental testing of the Community Multiscale Air Quality (CMAQ) modeling system version 4.7. Geosci Model Dev 3:205–226
8. Fuchs H, Bohn B, Hofzumahaus A, Holland F, Lu KD, Nehr S, Rohrer F, Wahner A (2011) Detection of HO_2 by laserinduced fluorescence: calibration and interferences from RO_2 radicals. Atmos Meas Tech 4:1209–1225
9. Kim SW et al (2011) Evaluations of NO_x and highly reactive VOC emission inventories in Texas and their implications for ozone plume simulations during the Texas air quality study 2006. Atmos Chem Phys 11:11361–11386
10. Lefer L, Rappenglueck R (2010) The TexAQS-II radical and aerosol measurement project. Atmos Environ 44:3997–4004
11. Mao J, Ren X, Chen S, Brune WH, Chen Z, Martinez M, Harder H, Lefer B, Rappenglück B, Flynn J (2010) Atmospheric oxidation capacity in the summer of Houston 2006: comparison with summer measurements in other metropolitan studies. Atmos Environ 44:4107–4115. doi:10.1016/j.atmosenv.2009.01.013
12. Ngan F, Byun D, Kim H, Lee D, Rappenglueck B, Pour-Biazar A (2012) Performance assessment of retrospective meteorological inputs for use in Air Quality Modeling during TexAQS 2006. Atmos Environ. doi:10.1016/j.atmosenv.2012.01.035
13. Schwede D, Pouliot G, Pierce T (2005) Changes to the biogenic emissions inventory system version 3 (BEIS3). In: 4th annual CMAS Models-3 users' conference, September 26–28, 2005, UNC-Chapel Hill, NC

Questions and Answers on NATO-ITM Paper No. 6.04

Questioner Name: Sarav Arunachalam

Q: Previous studies suggested Houston emissions have large episodic releases which are not captured in emissions inventory. Does the new emissions inventory account for these episodic releases?

A: Indeed previous studies suggested Houston emissions have large episodic releases. The new inventory attempted to capture these episodic releases. However, incorporation of these episodic releases in the inventory is a huge challenge. While significant improvement has been made in improving the emissions inventory, the model with the new inventory suggests that it still lacks VOCs although to a much lower extent than suggested by previous studies.

Chapter 82
Simulating Organic Aerosol Over Europe: Concentration, Chemical Composition and Sources

Christos Fountoukis, A.G. Megaritis, Hugo. D. van der Gon, P.E. Charalampidis, Christodoulos Pilinis, and Spyros N. Pandis

Abstract PMCAMx-2008, a detailed three-dimensional chemical transport model, was applied for the first time in Europe to simulate fine organic aerosol concentrations during the months of May 2008, February 2009, July 2009 and January 2010. The model includes a state-of-the-art organic aerosol module which is based on the volatility basis set framework treating both primary and secondary organic components as semivolatile and photochemically reactive. The model predicts that fresh primary OA (POA) is a small contributor to organic PM concentrations in Europe during the summer and spring, and that oxygenated species (oxidized primary and biogenic secondary) dominate the ambient OA. During the winter model results suggest a significant underestimation of OA emissions from wood burning. Use of very high resolution emissions inventory does not result in a significant improvement of the predictions of the model over the Megacity of Paris.

C. Fountoukis (✉)
Institute of Chemical Engineering & High Temperature Chemical Processes, Foundation for Research & Technology-Hellas (FORTH), 26504 Patras, Greece
e-mail: cfountoukis@iceht.forth.gr

A.G. Megaritis
Department of Chemical Engineering, University of Patras, Patras, Greece

H.D. van der Gon
TNO Built Environment and Geosciences, Utrecht, The Netherlands

P.E. Charalampidis • C. Pilinis
Department of Environment, University of the Aegean, 81100 Mytilene, Greece

S.N. Pandis
Institute of Chemical Engineering & High Temperature Chemical Processes, Foundation for Research & Technology-Hellas (FORTH), 26504 Patras, Greece

Department of Chemical Engineering, University of Patras, Patras, Greece

Department of Chemical Engineering, Carnegie Mellon University, Pittsburgh, PA 15213, USA

D.G. Steyn et al. (eds.), *Air Pollution Modeling and its Application XXII*,
NATO Science for Peace and Security Series C: Environmental Security,
DOI 10.1007/978-94-007-5577-2_82,

Keywords Organic aerosol • Model evaluation

82.1 Introduction

Organic aerosol, although a significant component of submicron particles throughout the world, is poorly simulated by predictive models. Current Chemical transport models (CTMs) consistently underpredict OA mass concentrations at the surface during summertime conditions. CTMs have traditionally treated POA as non-volatile and non-reactive and SOA as semi-volatile products of VOCs' oxidation. However, several recent studies (e.g. [2]) have shown that POA is semi-volatile while SOA can be seriously under predicted by models that use traditional SOA precursors and do not take into account further oxidation of these compounds.

In this study we applied PMCAMx-2008 [1], a regional 3-D CTM, to the European domain, in order to simulate the OA formation during the months of May 2008, February 2009, July 2009 and January 2010. PMCAMx-2008 includes the recently developed volatility basis set framework to describe OA absorptive partitioning by organizing the total OA mass into surrogates along an axis of volatility. Nine surrogate POA species are used, with effective saturation concentrations at 298 K ranging from 10^{-2} to 10^{6} $\mu g\ m^{-3}$. POA is simulated in the model in two types, "fresh" (not oxidized) POA and oxidized POA (OPOA). The SOA volatility basis-set approach used in the current version of the model includes four SOA species for each VOC with four volatility bins (1, 10, 100, 1,000 $\mu g\ m^{-3}$). Laboratory results from recent smog-chamber experiments have been used to update the SOA module in PMCAMx in order to include anthropogenic aerosol yields. The model treats all organic species (primary and secondary) as chemically reactive. Chemical aging through gas-phase oxidation of OA vapors is modeled using a gas-phase reaction with OH. Each reaction step is assumed to decrease the volatility of the vapor material by a factor of 10.

During the photochemically active period of May 2008, we evaluated the performance of the model against AMS ground measurements taken from various sites in Europe as well as airborne data. During the winter period of 2009 the model results are used to gain more insight into the sources and production of organic aerosol over Europe. Finally, during the July 2009 and January 2010 periods, we study the impact of horizontal grid resolution on predicted fine PM levels in the Megacity of Paris.

82.2 Results and Discussion

During the late spring period (May 2008), the model reproduces more than 87 % of the hourly data and more than 94 % of the daily averaged data within a factor of 2, for PM_1 OA. PMCAMx-2008 performs well in reproducing the high degree of oxidation as well as the average diurnal profile of the organic concentrations

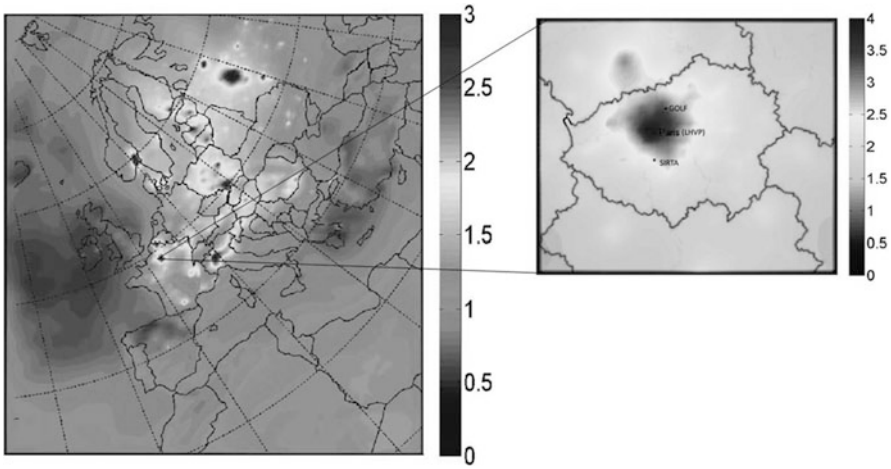

Fig. 82.1 Ground-level concentration predictions of PM_1 organic aerosol averaged over the winter period (January 10–February 10, 2010) in Europe (36×36 km grid resolution) and in Paris (4×4 km grid resolution) (in $\mu g\ m^{-3}$). Different scales are used

observed in the Eastern Mediterranean region. The model performance against the high time resolution airborne measurements of OA at multiple altitudes and locations is quite similar to its performance against the ground level hourly measurements. The model predicts that the Mediterranean region is the only area in Europe where PM_1 sulfate concentrations are much higher than the PM_1 OA during late spring, while organic matter is predicted to be the dominant PM_1 species over a large part of continental Europe. The model predicts low levels of fresh POA and that OA is dominated by oxidized primary OA (including IVOC oxidation products) (55–60 %) and biogenic SOA (30–35 %).

During February 2009, PMCAMx-2008 predicts a higher contribution of fresh POA to total PM_1 OA (approximately 12 %) compared to the May period, on average over the entire domain. Oxidized POA is predicted to be the dominant OA component during this wintertime period with an average contribution of 46 % to the total predicted PM_1 OA. Contrary to the May period, a more distinct diurnal variation is predicted in most major urban areas following the diurnal variation of combustion emissions rates. When compared to AMS measurements from various sites all over Europe, the model performs reasonably well at most sites, however the results suggest missing wood-burning emissions in the inventories used, mostly in Scandinavia, east Germany, etc.

The model was also used in a two-way nesting configuration to study the impact of different grid resolutions on organic aerosol predictions over the greater Paris area during a summer and winter. In an effort to stress more the differences between the two model grid configurations we combined high resolution emissions (1×1 km) with AMS measurement data and applied a high model grid resolution (4-km) over this Megacity in Europe (Fig. 82.1).

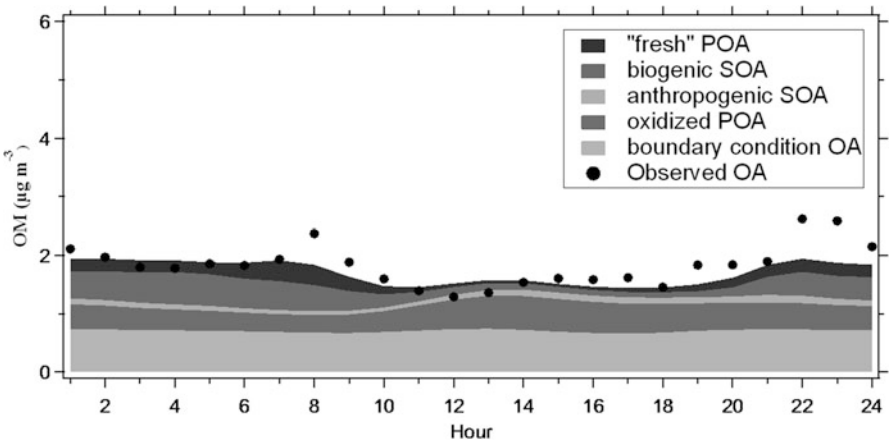

Fig. 82.2 Average diurnal profile of PM_1 organic aerosol and its components (in $\mu g\ m^{-3}$) in Paris (SIRTA station) during July 2009

The model reproduces reasonably well the average observed diurnal profile of OA, while the contribution of local sources to OA in Paris is small to moderate during both periods (Fig. 82.2). Differences between the two grid simulation results in the Paris area are, on average, small for all species during the summer period. During the winter period there are significant differences in model predictions of mainly primary organics and black carbon. The major differences are seen for the maximum (morning peak) values in the two most polluted sites (LHVP and GOLF). The 4-km grid simulation captures the average diurnal concentration of fine organic aerosol better than the coarse grid.

82.3 Conclusions

Much of the traditionally thought as particulate primary OA emissions are actually evaporating to produce low-volatility organic vapors which are the source (through photochemical aging) of a substantial amount of oxygenated OA that is distributed not only in urban and suburban areas but rural regions as well. PMCAMx-2008 tends to predict relatively flat diurnal profiles for PM_1 OA in many areas, both rural and urban during the late spring and summer. The model reproduces the relatively low OA concentrations in the free troposphere over Europe, suggesting that at least for this period there were no major missing OA sources aloft.

During the winter, both the model results and the measurements point towards missing wood-burning emissions in the inventories used, mostly in Scandinavia. The improvement in model predictions with the use of fine grid is modest during the summer and somewhat more significant during winter in the Megacity of Paris.

The use of very high resolution emissions does not lead to a significant improvement in the predictions of the fine grid simulation. These results suggest that the major reasons for the discrepancies between the model predictions and observations in both seasons are not due to the grid size used, but to other problems (e.g., emissions, process description, and meteorology).

This work was funded by the European Community's 6th (EU project EUCAARI) and 7th Framework Programme (EU projects MEGAPOLI and PEGASOS).

References

1. Fountoukis C et al (2011) Evaluation of a three-dimensional chemical transport model (PMCAMx) in the European domain during the EUCAARI May 2008 campaign. Atmos Chem Phys 11:10331–10347
2. Robinson AL, Donahue NM, Shrivastava MK, Weitkamp EA, Sage AM, Grieshop AP, Lane TE, Pierce JR, Pandis SN (2007) Rethinking organic aerosol: semivolatile emissions and photochemical aging. Science 315:1259–1262

Chapter 83
Meteorology, Emissions, and Grid Resolution: Effects on Discrete and Probabilistic Model Performance

Christian Hogrefe, Prakash Doraiswamy, Brian Colle, Kenneth Demerjian, Winston Hao, Michael Erickson, Matthew Souders, and Jia-Yeong Ku

Abstract In this study, we analyze the impacts of perturbations in meteorology and emissions and variations in grid resolution on air quality forecast simulations. The meteorological perturbations considered in this study introduce a typical variability of ~1 °C, 250–500 m, 1 m/s, and 15–30° for temperature, PBL height, wind speed, and wind direction, respectively. The effects of grid resolution are typically smaller and more localized. Results of the air quality simulations show that the perturbations in meteorology tend to have a larger impact on pollutant concentrations than emission perturbations and grid resolution effects. Operational model evaluation results show that the meteorological and grid resolution ensembles impact a wider range of model performance metrics than emission perturbations. Probabilistic model performance was found to vary with exceedance thresholds. The results of this study suggest that meteorological perturbations introduced through ensemble weather forecasts are the most important factor in constructing a model-based O_3 and $PM_{2.5}$ ensemble forecasting system.

C. Hogrefe (✉)
U.S. Environmental Protection Agency, Research Triangle Park, Durham, NC, USA

Atmospheric Sciences Research Center, University at Albany, Albany, NY, USA

New York State Department of Environmental Conservation, Albany, NY, USA
e-mail: hogrefe.christian@epa.gov

P. Doraiswamy
Atmospheric Sciences Research Center, University at Albany, Albany, NY, USA

RTI International, Research Triangle Park, Durham, NC, USA

B. Colle • M. Erickson • M. Souders
School of Marine and Atmospheric Sciences, Stony Brook University, Stony Brook, NY, USA

K. Demerjian
Atmospheric Sciences Research Center, University at Albany, Albany, NY, USA

W. Hao • J.-Y. Ku
New York State Department of Environmental Conservation, Albany, NY, USA

D.G. Steyn et al. (eds.), *Air Pollution Modeling and its Application XXII*,
NATO Science for Peace and Security Series C: Environmental Security,
DOI 10.1007/978-94-007-5577-2_83,

Keywords Ensemble modeling • Model evaluation • Direct decoupled method

83.1 Introduction

The development of ensemble forecast systems is a promising avenue for improving air quality forecast guidance and to develop probabilistic forecast products. The goal of this study is to quantify and compare the impacts of perturbations in meteorology, emissions, and grid resolution on predictions of O_3, NO_2, CO, Elemental Carbon (EC), and total $PM_{2.5}$ over the Northeastern U.S. and to evaluate these ensembles with operational and probabilistic metrics.

83.2 Database and Methods

All simulations analyzed in this study were performed for August 1–31, 2010 and January 1–February 15, 2011 over the Northeastern U.S. Air quality fields for the meteorological perturbation ensemble were generated by using 12 different MM5 and WRF weather forecasts from the Stony Brook University ensemble system to drive CMAQ4.7.1 on two nested horizontal domains with a grid spacing of 36 and 12 km, respectively. The 12 weather forecast ensemble members differ in their choice of initial and boundary conditions as well as different convective parameterization, boundary layer, and microphysical schemes. Members of the grid resolution perturbation ensemble were generated by performing WRF-Urban Canopy Model (UCM)/CMAQ4.7.1 simulations for nested 36, 12, and 4 km domains and considering the nine 4 km cells within each 12 km cell as perturbations from the 12 km base case. To create the emission perturbation ensemble, we used the Direct Decoupled Method (DDM) [1] implemented in CMAQ. CMAQ-DDM simulations were performed with one MM5 member of the meteorological perturbation ensemble. Following the general approach described in Napelenok et al. [2] and Pinder et al. [3], the CMAQ-DDM sensitivity fields were used to develop reduced-form models for O_3, NO_2, EC, and $PM_{2.5}$. For calculating pollutant variations caused by emission uncertainties, we used perturbations in NO_x, VOC, and $PM_{2.5}$ emissions sampled from a uniform distribution representing an uncertainty range of $+/-50$ %. These MM5/CMAQ-DDM simulations were performed on two nested horizontal domains with a grid spacing of 36 and 12 km, respectively. All analyses were performed for the smallest domain common to all simulations, i.e. the 4 km domain used for the WRF-UCM/CMAQ 4.7.1 simulations. The focus of this analysis was on daily maximum 8-h O_3 and CO, daily maximum 1-h NO_2, and 24-h average EC and total $PM_{2.5}$. Observations for model evaluation were obtained from the U.S. EPA's Air Quality System (AQS).

83.3 Results and Discussion

To quantify the variability of key meteorological variables (2 m temperature, PBL heights, 10 m wind speed and 10 m wind direction) introduced by the meteorological and grid resolution ensembles, we computed the standard deviation of these variables across all ensemble members at 2 pm EST for each day for each grid cell in the analysis domain and then averaged these resulting daily maps for both the summer and winter simulation periods. These seasonally averaged maps of ensemble standard deviations reveal that the meteorological perturbations considered in this study introduce a typical variability of $\sim$1 °C, 250–500 m, 1 m/s, and 15–30° for temperature, PBL height, wind speed, and wind direction, respectively. The effects of grid resolution on meteorological variables are typically smaller and more localized, with the largest effects near land/sea interfaces and in complex terrain.

As stated in the previous section, in addition to meteorological perturbation and grid resolution effects, we also considered the effects of emission perturbations for the analysis of variability in O_3, CO, NO_2, EC, and $PM_{2.5}$ concentrations simulated by CMAQ. The analysis was performed in the same way as described above for the meteorological variables except that the ensemble standard deviation was divided by the ensemble mean to compute the coefficient of variation (CV), which can then be compared between different pollutants. In general, results showed that the impact of meteorological perturbations, grid resolution and emission perturbations on CMAQ air quality simulations varies by time, location, and species. CV for NO_2, EC, and $PM_{2.5}$ are generally larger than CV for CO and O_3. For O_3 and $PM_{2.5}$, the meteorological ensemble caused larger variability than the emission and grid resolution ensembles. For NO_2 and EC, the variability caused by the emission and meteorological ensembles are comparable. Grid resolution effects are largest in urban and coastal grid cells but generally cause less variability than the meteorological and emission ensembles.

Operational evaluation results for O_3, CO, NO_2, and total $PM_{2.5}$ showed that emission perturbations can have a pronounced impact on model bias, especially in urban areas for species with a large primary component (NO_2, wintertime $PM_{2.5}$); this is consistent with the previous finding that the CV for the emission ensemble is largest in urban areas. However, with the exception of NO_2, meteorological perturbations still were found to have a larger effect on model bias than grid resolution effects even at urban locations, again consistent with the CV discussed above.

When considering model performance in a Taylor diagram representation that simultaneously depicts correlation coefficient, ratio of modeled to observed standard deviation, and centered root mean square error (RMSE), the results show that the members of the meteorological and grid resolution ensembles span a wider range of "model performance space" (i.e. they have an impact on all three model performance metrics depicted in the Taylor diagram) while the main effect of

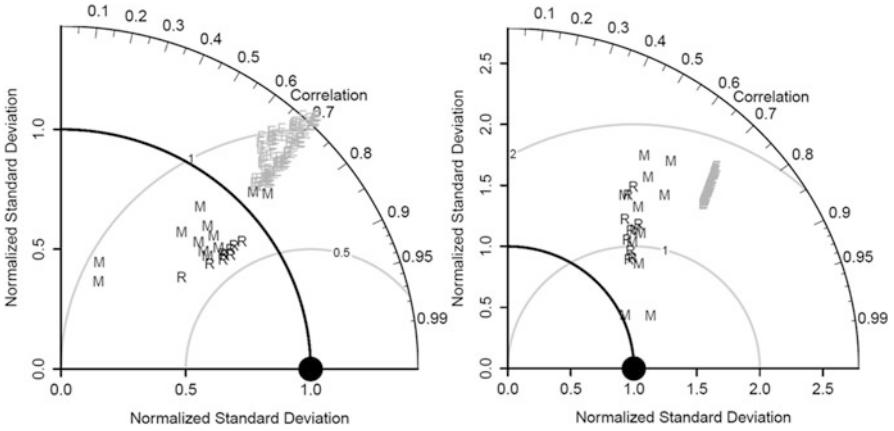

Fig. 83.1 Taylor diagram for daily maximum O3 (*left*) and 24-h average PM2.5 (*right*) at a monitor in Queens, NY during August 2010. "M" (*medium grey*), "R" (*dark grey*), and "E" (*light grey*) denote the meteorological, grid resolution, and emission perturbation ensemble members, respectively

emission perturbations is on the ratio of modeled-to-observed standard deviations with little impact on correlations and centered RMSE. Two examples of this analysis are shown in Fig. 83.1.

Probabilistic model performance for O_3 and $PM_{2.5}$ was assessed through Talagrand diagrams and reliability diagrams. Results showed that all ensemble predictions were underdispersed. This was especially true for the grid resolution and emission perturbation ensembles, consistent with the finding above that these two ensembles introduced less variability than the meteorological ensemble. Probabilistic model performance, as measured by Brier Skill Scores (BSS) with respect to climatology, was found to vary with exceedance thresholds. For O_3, ensembles showed improvement with respect to climatology for exceedance thresholds up to about 70 ppb while this threshold was about 15 $\mu g/m^3$ for $PM_{2.5}$. Overall, the results of this study suggest that, at least for the region and ensemble configurations considered here, meteorological perturbations introduced through ensemble weather forecasts are the most important factor in constructing a model-based O_3 and $PM_{2.5}$ ensemble forecasting system.

Acknowledgments and Disclaimer Although this work has been reviewed and approved for publication by the U.S. Environmental Protection Agency, it does not reflect the views and policies of the agency. The model simulations analyzed in this presentation were performed by the New York State Department of Environmental Conservation (NYSDEC) with partial support from the New York State Energy Research and Development Authority (NYSERDA) under agreement #10599. The views expressed here do not necessarily reflect the views or policies of NYSDEC or NYSERDA.

References

1. Hakami A, Odman MT, Russell AG (2003) High-order, direct sensitivity analysis of multidimensional air quality models. Environ Sci Technol 37(11):2442–2452
2. Napelenok SL, Cohan DS, Odman MT, Tonse S (2008) Extension and evaluation of sensitivity analysis capabilities in a photochemical model. Environ Model Software 23:994–999
3. Pinder RW, Gilliam RC, Appel KW, Napelenok SL, Foley KM, Gilliland AB (2009) Efficient probabilistic estimates of surface ozone concentration using an ensemble of model configurations and direct sensitivity calculations. Environ Sci Technol 43(7):2388–2393

Chapter 84
Improvement of Ensemble Technique Using Spectral Analysis and Decomposition of Air Pollution Data

Oxana Tchepel, Isabel Ribeiro, Alexandra Monteiro, Anabela Carvalho, Elisa Sá, Joana Ferreira, Ana Isabel Miranda, and Carlos Borrego

Abstract The current study proposes a novel approach for the multi-model ensemble to be applied in air pollution forecasting. The methodology is based on decomposition of air pollution time series on different components (short-term, daily fluctuations, synoptic scale, etc.) and calibration of the ensemble for each of these components independently taking into account the performance of individual predictors. Therefore, the same model may have a different contribution for the ensemble at high and low frequency fluctuations. The Kolmogorov-Zurbenko (KZ) low-pass filter is used for the time series decomposition. The Fourier analysis is implemented to determine the contribution of different frequencies to the data variance allowing better understanding of the model performance and to define the ensemble weights. The methodology was tested using a group of four different air quality models that were applied over mainland Portugal for the 2006 year, and for main pollutants like O_3 and PM10. The approach implemented in this work was compared with one of the most used ensemble technique showing clear advantages.

Keywords Ensemble techniques • Forecasting

84.1 Introduction

Ensemble modelling, originally developed for weather prediction, is being extended to air quality modelling applications demonstrating the advantage of deterministic ensemble compared with simulations provided by individual models (e.g. [6]). Nevertheless, they are still facing several problems. Furthermore, the mean and

O. Tchepel (✉) • I. Ribeiro • A. Monteiro • A. Carvalho • E. Sá • J. Ferreira • A.I. Miranda • C. Borrego
CESAM & Department of Environment and Planning, University of Aveiro, 3810-193 Aveiro, Portugal
e-mail: oxana@ua.pt

D.G. Steyn et al. (eds.), *Air Pollution Modeling and its Application XXII*, NATO Science for Peace and Security Series C: Environmental Security, DOI 10.1007/978-94-007-5577-2_84,

median ensembles as well as more advanced and complex ensemble techniques using multiple linear regression, Kalman filtering or Bayesian Model Averaging BMA approach have already been applied to improve the ensemble by specifying weights for members of the ensemble of models [2]. These techniques can be time-resolving (weights are not function of time and only vary in space) or time function.

The purpose of this work is to develop a new ensemble approach, based on decomposition of air pollution time series on different components and on the calibration of the ensemble for each of these components independently taking into account the performance of the individual predictors. This novel approach is compared with one of the most used mean ensemble technique.

84.2 Methodology

Spectral analysis is used to characterise time series in the frequency domain [1, 4, 5]. Based on the Fourier series, this method allows to determine the contribution of different frequencies to the data variance and hence to analyse the contribution of various underling processes to the concentration fluctuations. The application of the Kolmogorov-Zurbenko (KZ) filter allows decomposing the original time series on different components [3]. In this work the KZ filter was designed taking into account information provided by the spectral analysis. Thus, separation frequencies are defined in order to separate between the baseline and short-term fluctuations ($KZ_{3,5}$), daily ($KZ_{5,5}$) and synoptic ($KZ_{31.5}$) components (Fig. 84.1).

The spectral analysis and decomposition was applied for both observed and modelled O_3 hourly time series data, for five background monitoring sites (spatially distributed over mainland Portugal). The ensemble methodology was tested using four different air quality models: CAMx, CHIMERE; EURAD-IM and TAPM [2]. All models are regional-scale models designed for short-term and long-term simulations of oxidants and aerosol formation, besides different degrees of complexity. Descriptions can be consulted on the online Model Documentation System (http://pandora.meng.auth.gr/mds/mds.php).

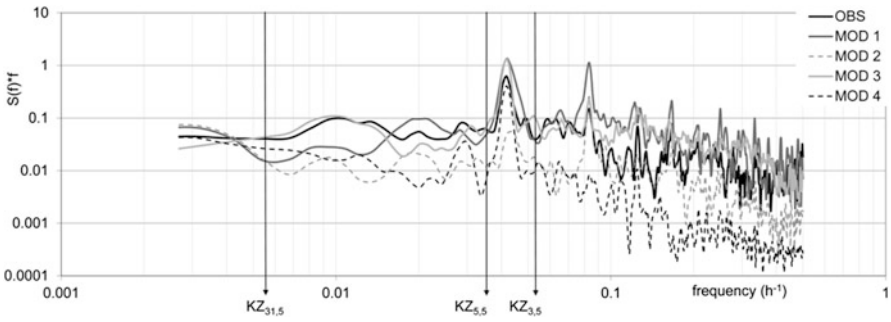

Fig. 84.1 Spectrum for O_3 data measured and modelled at REB station and separation frequencies used for KZ filter

The analysis of results was performed for O_3 and PM10 (only O_3 is presented here). Similar results and conclusions were obtained for both pollutants.

84.3 Results and Discussion

Decomposed data obtained from the air quality models were analysed and compared with observations separately for each component (short-term, daily, synoptic and baseline) allowing a better understanding of the model performance and the definition of the ensemble weights.

Figure 84.2 presents the comparison between the model ensemble and observations for higher frequencies at one of the monitoring sites (REB). The correspondence between both terms is very satisfactory, which means that the model ensemble is able to reproduce the intra-diurnal, diurnal and synoptic fluctuations (in this case the period of fluctuations is less than 6 days) of the O_3 concentrations. These results are consistent over all the monitoring sites analysed.

However, when comparing to the baseline obtained from the observations a significant bias (systematic error) in the models baselines is notorious as presented in an example for REB station in Fig. 84.3. Similar results were found for others monitoring sites, showing that the low frequencies are deficiently simulated, with high deviations exhibited by all the models analysed. Therefore, the performance of final ensemble is affected by the systematic errors presented in the baseline.

In order to investigate how the ensemble approach can benefit from the decomposition methodology, a statistical analysis of the obtained results was performed and they were compared with results from alternative mean ensemble technique. The new ensemble for O_3improves the correlation between observations and modelling from 0.66 to 0.72, in comparison with the alternative ensemble approach, and reduces the root mean square error (RMSE) from 26.2 to 23.7 $\mu g \cdot m^{-3}$ as an average over all the analysed monitoring sites.

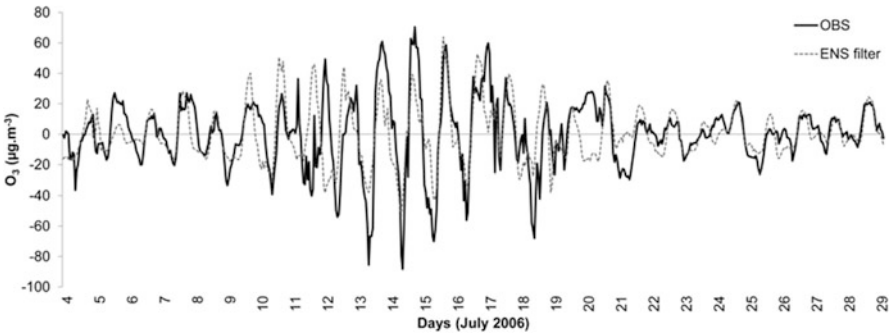

Fig. 84.2 Comparison of the models ensemble with observations considering a composite of intra-diurnal, diurnal and synoptic components at REB station

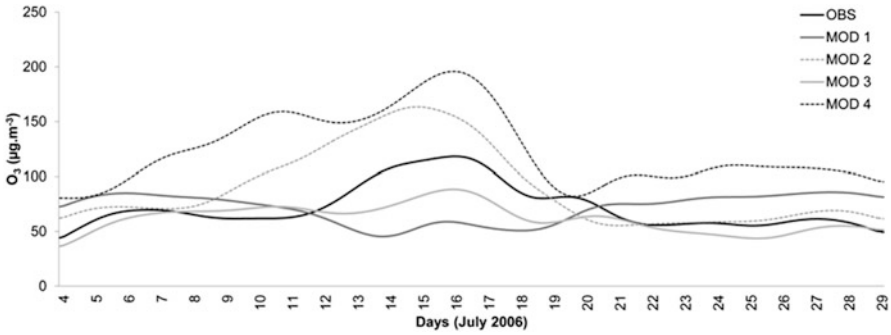

Fig. 84.3 Comparison of the baseline for each individual model and observations, for REB station

84.4 Conclusions

The ensemble methodology proposed in this work is based on spectral analysis and decomposition of time series on different components and calibration of the ensemble for each of these components. This approach allows a better understanding of the models performance: the high frequencies fluctuations are well reproduced by the majority of the models while high biases are detected for the low frequencies (baseline term). In terms of the calibration of the ensemble, this novel approach shows to be successful when compared with a traditional mean ensemble technique in terms of improving correlation and reducing RMSE. The low frequencies (baseline) should be the focus of future research work in order to improve the models performance.

Acknowledgments The authors acknowledge the Portuguese Environmental Protection Agency for the observational dataset support. The work was partly developed under the research projects POCI/AMB/66707/2006 and PTDC/CTE-ATM/103253/2008. Thanks are extended to the Portuguese Science Foundation (FCT) for the grants: SFRH/BPD/66874/2009, SFRH/BD/60370/2009, SFRH BPD/40620/2007 and SFRH/BD/60474/2009.

References

1. Eskridge R, Ku JY, Rao ST, Porter PS, Zurbenko IG (1997) Separating different time scales of motion in time series of meteorological variables. Bull Am Meteorol Soc 78(7):1473–1483
2. Monteiro A, Ribeiro I, Tchepel O, Carvalho A, Sá, Ferreira J, Galmarini S, Miranda AI Borrego C (2011) Bias correction and ensemble techniques to improve air quality assessment: focus on O_3 and PM over Portugal. In Proceedings of the 14th international conference on Harmonisation within Atmospheric Dispersion Modelling for Regulatory Purposes, Kos, Greece, 2–6 October 2011, 22–26
3. Rao ST, Zurbenko IG, Neagu R, Porter PS, Ku JY, Henry RF (1997) Space and time scales in ambient ozone data. Bull Am Meteorol Soc 78(10):2153–2166

4. Sebald L, Treffeisen R, Reimer E, Hies T (2000) Spectral analysis of air pollutants. Part 2: ozone time series. Atmos Environ 34:3503–3509
5. Tchepel O, Costa AM, Martins H, Ferreira J, Monteiro A, Miranda AI, Borrego C (2010) Determination of background concentrations for air quality models using spectral analysis of monitoring data. Atmos Environ 44(1):106–114
6. Vautard R, Schaap PM, Bergström R et al (2009) Skill and uncertainty of a regional air quality model ensemble. Atmos Environ 43(31):4822–4832

Questions and Answers

Questioner Name: Nicholas Savage

Q: For use as a forecasting tool you need to use past data to get forecast. Have you tried doing this and how much memory do you think these weights have?
A: Application of this technique to the operational forecast will be implemented as a next step. Taking into account that the methodology presented in this work is based on harmonic functions we expect a good "memory" of the weights for all the components (e.g. daily, synoptic, baseline) with possible exception for the highest frequencies.

Questioner Name: Efisio Solazzo

Q: Have you done any sensitivity test on the threshold value of driving forces? How does the ensemble change?
A: We tested different window size to separate the baseline component and the results confirm a robustness of the applied methodology.

Questioner Name: Rostislav Kouznetsov

Q: Separate weighting of harmonics might result in negative predicted concentrations. How such situations should be treated?
A: In theory it is possible to obtain negative values because of the negative signal in the filter residuals. However, the baseline of time series is always positive and it is very important for the final ensemble. In practice, the negative value means that the ensemble is not properly calibrated and the model weights should be analyzed more carefully.

Questioner Name: Jeremy Silver

Q: Were there gaps in the time-series of observations? If so, how did deal with this?
A: The completeness of the time series was one of the criteria to select the monitoring stations for the current analysis. Moreover, one of the advantages of KZ filter is its good performance in the presence of gaps in the time series.

Chapter 85
Evaluation and Inter-comparison of Acid Deposition Models for the UK

Anthony J. Dore, D. Carslaw, C. Chemel, R.G. Derwent, B.E.A. Fisher, S.J. Griffiths, S. Lawrence, S.E. Metcalfe, A. Redington, David Simpson, R. Sokhi, P. Sutton, M. Vieno, and J.D. Whyatt

Abstract An evaluation has been made of a range of simple and complex atmospheric transport models, applied to estimate sulphur and nitrogen deposition in the UK in order to provide information to policy makers to support decisions on future model use. The models were evaluated by comparison with annually averaged measurements from the national monitoring networks. A number of statistical metrics were output to assess model performance and the models were compared graphically by plotting cross-country transects of concentrations in air.

Keywords Nitrogen • Sulphur • Inter-comparison • Acid deposition • Atmospheric transport model

A.J. Dore (✉) • M. Vieno
Centre for Ecology and Hydrology, Edinburgh, Scotland, UK
e-mail: todo@ceh.ac.uk

D. Carslaw
Kings College, University of London, London, UK

C. Chemel • R. Sokhi
Centre for Atmospheric & Instrumentation Research, University of Hertfordshire, Hertfordshire, UK

R.G. Derwent
Rdscientific, Berkshire, UK

B.E.A. Fisher
Risk and Forecasting Science, Environment Agency, Bristol, UK

S.J. Griffiths
E.ON New Build and Technology, Rotterdam, UK

D.G. Steyn et al. (eds.), *Air Pollution Modeling and its Application XXII*,
NATO Science for Peace and Security Series C: Environmental Security,
DOI 10.1007/978-94-007-5577-2_85,

85.1 Description of Models

The models involvedin this study included two simple Lagrangian models (employing annually averaged meteorology) and three complex models driven by dynamic meteorology and using photo-chemical reaction schemes. A summary of the models is given in Table 85.1. The evaluation was generated with the Open air software using the R statistical language. A report blending text and graphical output was automatically generated. This approach has the advantage that the results are easily reproducible by a third party and updates to submitted model data can rapidly be incorporated by re-running the software.

Table 85.1 Summary of models participating in the inter-comparison including model grid resolution

Model name and grid	Type	References
CMAQ-JEP (5 km)	Complex Eulerian	Chemel et al. [1]
CMAQ-UH (5 km)	Complex Eulerian	Chemel et al. [1]
EMEP unified (50 km)	Complex Eulerian	Simpson et al. [5]
EMEP4UK (5 km)	Complex Eulerian	Vieno et al. [6]
FRAME (5 km)	Simple Lagrangian	Matejko et al. [2]
HARM (10 km)	Simple Lagrangian	Page et al. [3]
NAME (5 km)	Complex Lagrangian	Redington et al. [4]

Two independent applications of the CMAQ and EMEP models (the latter at different grid resolutions) are included

S. Lawrence
Department for the Environment, Food and Rural Affairs, London, UK

S.E. Metcalfe
School of Geography, University of Nottingham, Nottingham, UK

A. Redington
Met Office, London, UK

D. Simpson
Norwegian Meteorological Institute, Oslo, Norway

Chalmers University of Technology, Gothenburg, Sweden

P. Sutton
RWE npower, Swindon, UK

J.D. Whyatt
Lancaster Environment Centre, University of Lancaster, Lancaster, UK

85.2 Results

The models were evaluated by comparison with annually averaged measurements of gas concentrations (SO_2, NO_2, NH_3, HNO_3) and aerosol concentrations (sulphate, nitrate and ammonium) in air as well as ion concentrations in precipitation. Plots of the correlation of the modelled concentrations of ammonium in precipitation with measurements are illustrated in Fig. 85.1 and performance statistics are listed in Table 85.2.

The criteria for a model to be considered 'fit for purpose' were set as: FAC2 > 0.5 and $-0.2 < \text{NMB} < 0.2$. The first of these criteria was generally satisfied by the

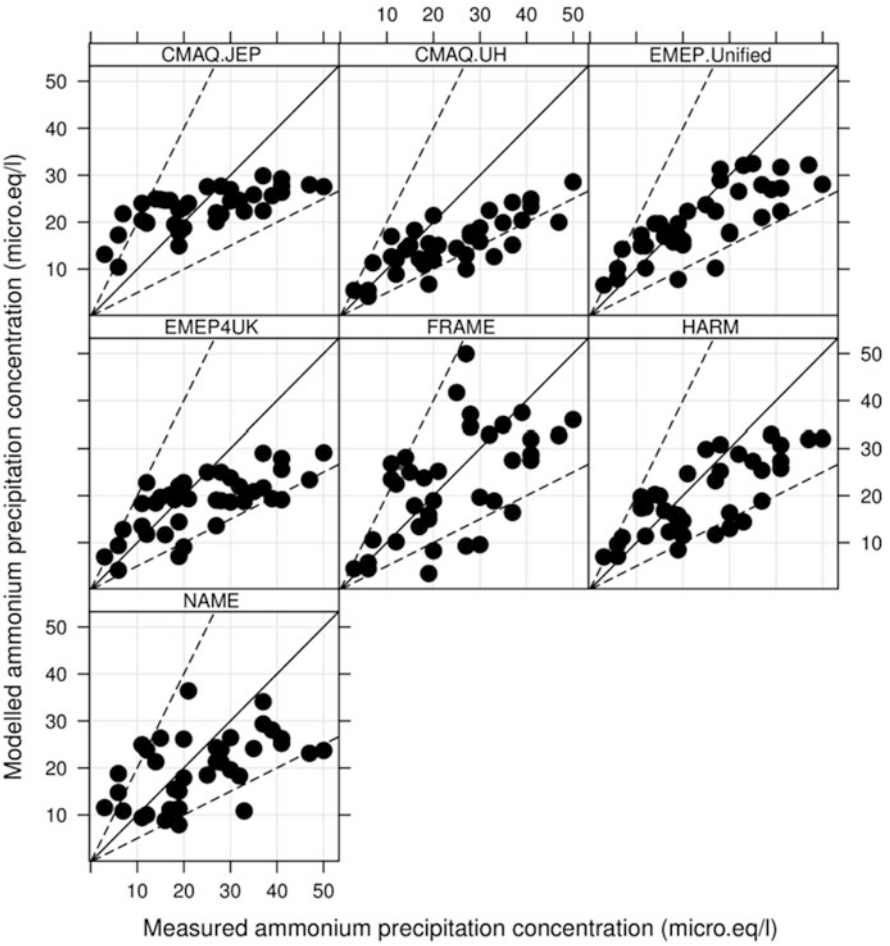

Fig. 85.1 Correlation of the annual average modeled concentrations of ammonium in precipitation with measurements from the national precipitation chemistry monitoring network

Table 85.2 Model performance statistics for comparison with measurements of ammonium in precipitation

Group	FAC2	NMB	NMGE	RMSE	r
CMAQ.JEP	0.89	−0.05	0.34	9.72	0.70
CMAQ.UH	0.84	−0.36	0.40	12.00	0.79
EMEP4UK	0.84	−0.23	0.35	10.62	0.70
EMEP.Unified	0.89	−0.17	0.28	8.78	0.79
FRAME	0.78	−0.07	0.38	11.17	0.57
HARM	0.86	−0.19	0.32	9.43	0.75
NAME	0.78	−0.16	0.39	11.17	0.52

FAC2 fraction of points greater than 0.5× and less than 2× the measured value, *NMB* normalised mean bias, *NMGE* normalised mean gross error, *RMSE* root mean square error, r correlation coefficient

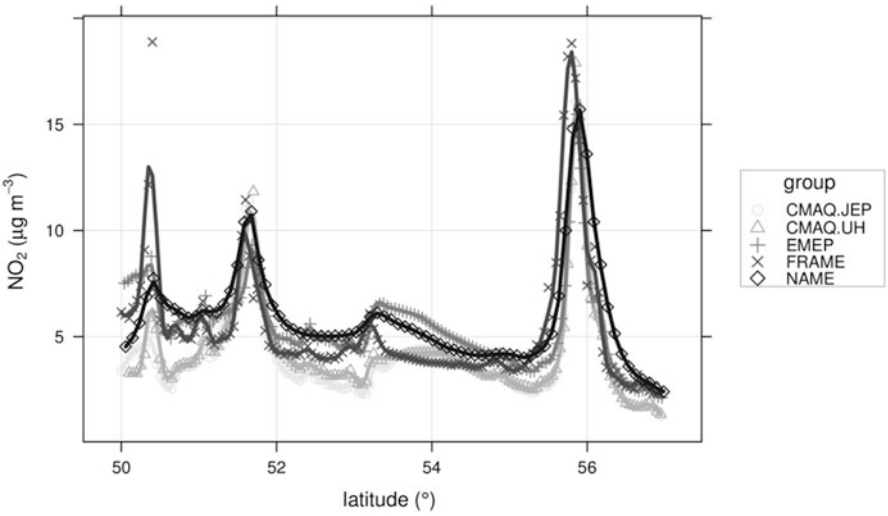

Fig. 85.2 Transect of NO_2 concentrations along −4.05 longitude

models, but the second condition was not satisfied for all variables by the models (as illustrated in Table 85.1, for ammonium concentration in precipitation). The overall results showed that whilst simple models were able to obtain good correlation with measured gas concentrations, the more advanced chemical schemes and detailed dynamics in complex models resulted in improved correlation with measured concentrations in precipitation and with aerosol concentrations. Plots of modeled air concentrations of NO_2 across a transect (Fig. 85.2) were found to be a useful way of comparing the models spatially. Significant differences between models were found for SO_2 concentrations (not illustrated here) but much smaller differences for NO_2. This may be due to the different treatments of elevated and surface emissions by the models. A full report of the deposition model evaluation analysis (PHASE 1 of the model inter-comparison exercise) is available at: http://uk-air.defra.gov.uk/library/reports?report_id=65. PHASE 2 of this exercise will focus on comparison of

modeled deposition (national budget calculation and transect plots) and application of modeled data to calculate the exceedance of critical loads for acid deposition and nitrogen deposition.

Acknowledgement This work was supported by the Department for the Environment, Food and Rural Affairs.

References

1. Chemel C, Sokhi RS, Yu Y, Hayman GD, Vincent KJ, Dore AJ, Prain HD, Fisher BEA (2010) Evaluation of a CMAQ simulation at high resolution over the UK for the calendar year 2003. Atmos Environ 44:2927–2939
2. Matejko M, Dore AJ, Hall J, Dore CJ, Błaś M, Kryza M, Smith R, Fowler D (2009) The influence of long term trends in pollutant emissions on deposition of sulphur and nitrogen and exceedance of critical loads in the United Kingdom. Environ Sci Policy 12:882–896
3. Page TP, Whyatt JD, Metcalfe SE, Derwent RG, Curtis C (2008) Assessment of uncertainties in a long range atmospheric transport model: methodology, application and implications in a UK context. Environ Pollut 156:997–1006
4. Redington AL, Derwent RG, Witham CS, Manning AJ (2009) Sensitivity of modelled UK sulphate and nitrate aerosol to cloud, pH and ammonia emissions. Atmos Environ 43:3227–3234
5. Simpson D, Benedictow A, Berge H, Bergstrom, Emberson LD, Fagerli H, Hayman GD, Gauss M, Jonson JE, Jenkin ME, Nyíri A, Richter C, Semeena VS, Tsyro S, Tuovinen J-P, Valdebenito A, Wind P (2012) The EMEP MSC-W chemical transport model – part 1: model description. Atmos Chem Phys Discuss 12:3781–3874
6. Vieno M, Dore AJ, Stevenson DS, Doherty R, Heal MR, Reis S, Hallsworth S, Tarrason L, Wind P, Fowler D, Simpson D, Sutton MA (2010) Modelling surface ozone during the 2003 heat-wave in the UK. Atmos Chem Phys 10:7963–7978

Questions and Answers

Questioner Name: Jeff Weil

Q: Don't you need uncertainty estimates in addition to mean concentration to assess whether or not finer grid resolution is giving meaningful results? Can you resolve the difference in mean correlation between two neighbouring grids outside the uncertainty limits?
A: For the example presented (exceedance of the critical level for ammonia over nature reserves) we are confident that the higher resolution (1 km) simulation is an improvement over the coarser (5 km) grid. The reason for this is that the source (agricultural) areas are better spatially resolved from the sink (nature reserve) areas. i.e. cattle are not permitted to graze in Special Areas of Conservation in a more effective manner using 1 km resolution NH_3 emissions.

In a generic sense, uncertainty in chemical transport models may be higher with increased grid resolution depending on success in resolving the driving process (emissions, chemistry, meteorology or land use).

Questioner Name: Jordi Vila

Q: Can you comment on the difference between the resolution of measurements (very much influenced by local micro-meteorological effects) and the model resolution (∼5 km)?
A: The models (with ∼5 km grid resolution) are not able to capture in detail local meteorological effects on air concentrations and these may be significant. Only rural sites were used in the inter-comparison (located >2.5 km from a major road for NO_2 measurements). The models generally gave good correlation with NO_2 measurements but correlation was less good for NH_3 (where emissions are mixed into the rural landscape).

Questioner Name: Peter Builtjes

Q: What would be your guess of the uncertainty of total N deposition over the UK?
A: Taking into account uncertainties in emissions (magnitude and mapping), modelled nitrogen concentrations (in air and precipitation), deposition velocities and annual precipitation, uncertainty in total modelled nitrogen deposition at a grid point could be $\sim +/-50$ %.

Chapter 86
Clustering for Model Validation/Improvements

Christopher Fung, Anson Cheung, K.M. Wai, Peterson Wong, and Eric Cheung

Abstract Photochemical model evaluation has been performed by clustering all relevant parameters.

Keywords Clustering • Model validation

86.1 Background

Photochemical model evaluation usually involves comparing output of each component module against measurements when they are available. Mostly, this comparison is limited to meteorological and air quality while emissions are held as an unverifiable. Yet even such limited comparison can be mired in the overwhelming number of parameters that have to be considered to answer the question: Has performance improved or has the targeted improvement in some parameters (e.g. horizontal wind speed) brought about deterioration to others (e.g. temperature or vertical wind). Fung et al. [1] made use of clustering of all relevant parameters in each module (assuming non-changing emission patterns) to gain insights into the overall performance of a photochemical modeling system.

86.2 Basic Procedures

This work focuses on the meteorological part of *Fung's scheme* for evaluation and practical improvements. Confining the analyses to a small area (Hong Kong (HK) of no more than 50×50 km with 33 ground level meteorological stations) relative

C. Fung (✉) • A. Cheung • K.M. Wai • P. Wong • E. Cheung
Environmental Protection Department, Wan Chai, Hong Kong
e-mail: cfung@epd.gov.hk

D.G. Steyn et al. (eds.), *Air Pollution Modeling and its Application XXII*,
NATO Science for Peace and Security Series C: Environmental Security,
DOI 10.1007/978-94-007-5577-2_86,

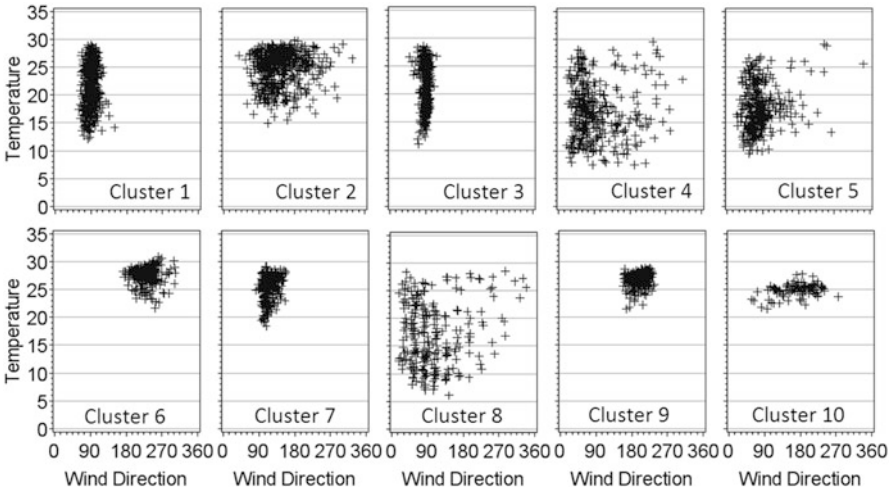

Fig. 86.1 Characteristics of reference set of ten clusters (2000–2009): temp. vs. wind direction

to the controlling synoptic features (high/low pressure systems ... etc.) to meet the criterion of homogeneity, we explore the most appropriate ways to average data and impute missing observations and show that non-wind parameters are best averaged over all station measurements after standardization and imputing missing wind data is best done through replacement by the 'closest' station according to a hierarchy table constructed from statistical comparison (R^2 for wind speed and smallest angle difference for wind direction) among all the stations. The resulting hourly data of 11 stations, after judiciously dropping unsuitable ones, are then averaged over each day for meteorological clustering.

Ten years (2000–2009) of meteorological data are used for clustering by the SAS software. Previous explorations determined that the *k*-means method gives the best results and is used. The best number of clusters is determined to be 10, based on trends of normalized sum of square distances in conjunction with judgment of the physical reasonableness of each set of clusters (e.g. emergence of a distinct cluster with low cloud cover, number of days in the smallest cluster ... etc.). This set of ten observed clusters, used as the reference here, gives interpenetration of the different weather types over seasons which agrees with experience (e.g. a summer-like day occurring in late autumn ... etc.). Figure 86.1 (a sample of this cluster characteristics) shows good time and wind direction differentiation between clusters.

86.3 Models Performance Evaluation

To determine the overall performance of model outputs, nine model simulations with different input data source, land-use classification, physics options, run segment lengths ... etc. are made for a full year (2010) over four nested domains with

horizontal grid spacing going from 40.5 km in steps of three down to 1.5 km for the innermost domain which covers HK and its vicinity with 61×55 grid cells. Forced clustering using the cluster definitions of the reference 10 years of observation was made to both modeled output and observations for 2010. The Cramer's V statistics (abbreviated as V which varies between 0 and 1 with 1 indicating perfect binning) is used to determine the extent each simulation has been able to reproduce the observed cluster distribution. By plotting various statistical measures (e.g. R^2, biases, RMSE ... etc.) against the V of the simulations, no obvious trend is discerned. Table 86.1 shows that the range of V is small, between 0.526 and 0.599 with the poorest model only correctly binning 178 days and the best model 216 days out of the 365 days, i.e. less than 60 %. Noise has prevented teasing out any trend from this collection of simulations that are performing statistically similarly.

86.4 Construction of an Improved Meteorological Driver

Given the purpose of meteorological simulations in a photochemical modeling system is only to drive the chemical transport model (CTM), improvement to this meteorological driver can be made by stitching together best performing output segments from the various simulations. The preceding observation clustering results provide a quantitative template to choose the best segments – individual day – for constructing the '*super-set*'. The following rules are used:

1. Days without any model binning correctly:
   - Use results from the best performing model based on maximum number of days matched for that category, i.e. the champion, and
   - In case of multiple champions, break deadlock using highest V
2. Days with one model binning correctly: model output used
3. Days with more than one model binning correctly:
   - Pick out only the models that get the category right;
   - Use results from the champion among the modeling binning correctly, and
   - In case of multiple champions, break deadlock using highest V.

The resulting *super-set* was able to bin 312 of the 365 days correctly (85+ %), in-creasing V to 0.831. Using the above criteria, the worst performing simulation (8, second worst V and least number of days correctly binned – the two do not necessarily go in tandem) has contributed 17 unique days (i.e., days which no other models bin correctly) to the *super-set*. Table 86.1 shows that other models can only contribute at most three unique days to the *super-set*). Since simulation 8 is produced from 12-h segments (taken from 72-h runs started every 12 h for air quality forecast) rather than monthly segments and uses a regional (ORSM) rather than hemispheric data set (FNL or ECMWF for simulations 1–7), its unique niche despite relatively inferior overall performance is indispensable for meteorological driver improvement in a photochemical modeling system.

Table 86.1 Binning statistics of the models

Observation		Simulation case[a]										
Clus.	Freq.	1	2	3	4	5	6	7	8	9	No Match	*Super-set*
1	79	32/2	34/2	35/6	37/0	38/50	24/0	29/0	31/4	37/15	12	67
2	26	11/20	7/0	6/1	8/2	6/0	7/1	6/0	8/2	3/0	9	17
3	39	21/0	16/0	26/32	19/0	20/0	25/4	22/0	17/3	24/0	6	33
4	33	16/3	17/29	4/0	14/0	16/0	5/0	10/0	7/1	6/0	12	21
5	26	24/24	22/1	16/0	20/0	20/0	7/0	7/0	13/1	16/0	0	26
6	36	18/0	21/31	15/0	20/2	18/0	18/0	19/0	17/2	12/1	10	26
7	54	27/1	22/0	35/0	32/0	33/2	38/6	35/0	33/5	39/40	1	53
8	25	24/0	22/0	25/25	24/0	23/0	24/0	24/0	25/0	24/0	0	25
9	38	38/38	38/0	38/0	36/0	36/0	34/0	33/0	26/0	36/0	0	38
10	9	0/0	2/0	0/0	6/9	4/0	4/0	3/0	1/0	0/0	3	6
Total	365	211/88	201/63	200/64	216/13	214/52	186/11	188/0	178/18	197/56	53	312
Cramer's *V*		0.591	0.574	0.544	0.599	0.583	0.537	0.526	0.529	0.529		0.831
No match[b]		56	54	56	54	54	53	53	70	56	53	
Unique contr.[c]		3	1	3	1	1	0	0	17	3		

[a]Under each case: number of days correctly binned/number of days used to construct *super-set*
[b]Number of days no simulation bins correctly after removing the case in question
[c]Increase in number of no-match days after removing the case in question

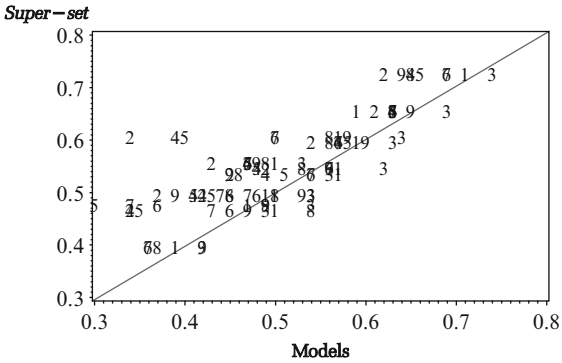

Fig. 86.2 R2 of hourly wind speed of the super-set vs. individual sets (numbers in plot) for all meteorological stations for year 2010. Points above the 1:1 line indicate higher R2 for the super-set

But does the *super-set* translate to overall better model performance? Here, we will only answer the question based on meteorological observation and leave the quantification of consequential CTM outputs improvement to future work. To avoid being buried under an unmanageable number of indicators – the motive that prompted this work, we distill the statistics for comparison. One way is to plot the statistical performance indicators of the individual models against that of this *super-set*. Results show that with some of these plots, an improvement (or any trend) is not obvious, but for correlation statistics (e.g., R^2 versus the magnitude statistics like bias) for some parameters (e.g., wind speed and cloud cover), the improvements are undeniable (Fig. 86.2). Given the unmistakable improvements in correlative statistics and no obvious deterioration in others, it can be concluded that the *super-set* does perform better in an overall sense based on observations.

86.5 Conclusions

Clustering can be a powerful guide to constructing an improved meteorological driver set for CTM from an ensemble of outputs. Diversity in individual simulations, regardless of overall performance, can contribute greatly to the resulting set.

Reference

1. Fung C, Yau P, Lam C, Yu P, Yu L (2010) Clustering analysis of air quality model performance. In: Steyn DG, Rao, ST (eds) Air pollution modeling and its application, vol XX, Springer, Dordrecht, pp 355–360

Questions and Answers

Questioner Name: Nicholas Savage

Q: Won't using a *super-set* introduce unphysical jumps in the CTM?
A: Using the *super-set* meteorological information as a driver to the CTM does not violate any of the conservation equations – momentum, mass (both of air and pollutants), energy – in the air quality simulation modeling system. The transition between one day and the next may not be as smooth as using meteorological information generated from a continuous model simulation of meteorology. Nevertheless, even in these continuous meteorological simulations, nudging and re-initialization are still used. Re-initialization of the meteorological simulations, being an extreme form of nudging, also introduces 'unphysical jumps' in the CTM. Using the *super-set* in our case can thus be seen as a cross-model-cross-simulation form of re-initialization and the 'unphysical jumps' is of the same order of magnitude. Weighing the down side of the unphysical jumps and the potential performance improvements, we decided in favor of using the *super-set*.

Questioner Name: Dominik Brunner

Q: If main goal was to get a simulation as close to observed meteorology as possible, why did you not use data assimilation?
A: There are different forms of data assimilation one can employ. We explored observation nudging and found it unsatisfactory because of the introduction of the unphysical and artificial nudging term which distorts the flow in an unnatural way. Analysis nudging – guiding the system in time by another model's output through a set of nudging coefficient – has been used, but the results of any single simulation still leave a lot to be desired. The present approach takes meteorological model results using analysis nudging and builds on their strengths. The resulting meteorological driving set has shown much improved model performance over the area of interest because undistorted – hence smoother and more natural – segments are joined together to form the final set.

Chapter 87
Development and Evaluation of an Air Quality Model for Predicting the Impacts of Prescribed Burns

M. Talat Odman, Aika Yano, Fernando Garcia-Menendez, Yongtao Hu, Scott L. Goodrick, Yongqiang Liu, and Gary L. Achtemeier

Abstract A modeling system has been developed to predict accurately the downwind air quality impacts of prescribed burns. The system has been evaluated in applications to monitored burns and a long-range smoke event detected by the regional $PM_{2.5}$ monitoring network in Southeastern USA. Uncertainties in the estimation of emissions have been identified and sensitivities of predicted $PM_{2.5}$ levels to smoke injection height versus PBL height, and wind speed and direction have been quantified. More accurate wind predictions, currently provided by WRF, would significantly improve the performance of the modeling system.

Keywords Burns • PM 2.5 • WRF

87.1 Introduction

Prescribed burning (PB) is an economical way of maintaining the forest ecosystem and reducing wildfire risk. However, pollutants emitted from the burns may contribute to air quality problems in downwind urban areas. An example of this happened in Atlanta, Georgia on 28 February 2007 when two burns ignited in the morning 80 km upwind led to 150 $\mu g\ m^3$ $PM_{2.5}$ concentrations citywide in the evening. To continue PB operations without violating ambient air quality standards,

M. Talat Odman (✉) • A. Yano • F. Garcia-Menendez • Y. Hu
School of Civil and Environmental Engineering, Georgia Institute of Technology, Atlanta, GA 30332-0512, USA
e-mail: odman@gatech.edu

S.L. Goodrick • Y. Liu • G.L. Achtemeier
Forestry Sciences Laboratory, USDA Forest Service, Athens, GA 30602-2044, USA

D.G. Steyn et al. (eds.), *Air Pollution Modeling and its Application XXII*,
NATO Science for Peace and Security Series C: Environmental Security,
DOI 10.1007/978-94-007-5577-2_87,

it is extremely important to be able to accurately predict the impacts of the burns. The objective of this research was to develop such a prediction system that can be used by land managers for conducting PB under favorable air quality conditions.

87.2 Modeling System

The prediction system consists of models for estimation of emissions, and prediction of meteorology, dispersions of smoke plumes, their long-range transport and chemical interactions with the background atmosphere. Emissions estimation starts with the estimation of fuel loads, in mass per unit area of the burn plot, for the fuel types (e.g., duff, litter, green and woody fuels) defined in the Fuel Characteristic Classification System (FCCS). For this, the pictures that look most like the burn plot are chosen from a photo-series and the loads associated with these pictures in a catalogue are weighted to obtain a best estimate. The next step is to estimate the fuel consumption using CONSUME. This model calculates the amount of fuel consumption under different fire conditions. One of the most important determinants of consumption is fuel moisture. Finally, total emissions are estimated using emission factors (EFs) defined as mass of pollutant emitted per unit mass of fuel consumed. The EFs used here are based on field measurements [8]. For the type of fuels concerned here, the difference between the $PM_{2.5}$ EF used here and the EF derived from burns simulated in a laboratory [4] is less than 10 %.

The temporal distribution of burn emissions are estimated by Rabbit Rules, a free-agent cellular automata model [1]. Given a description of the fuel distribution/density over the burn plot, which can be obtained from satellite imagery, along with an ignition pattern, this model simulates fire progression over the burn plot. Ignition is performed typically by helicopter or all-terrain vehicles, starting from the downwind edge of the plot to keep the fire under control and following lateral stripes towards the upwind edge. Rabbit Rules computes the intensities of fire induced drafts converging towards the flames and the resulting pressure fields. Around low pressure zones, smoke organizes into updraft cores the number of which is important for plume rise calculations in the dispersion model, as fewer cores would result in higher plumes. Rabbit Rules also computes the diameter of the cores and their updraft velocities.

The meteorological variables needed to model the dispersion and transport of the smoke plume (ambient pressure, temperature, humidity and wind fields) are calculated using the Weather Research and Forecasting (WRF) model [6]. The dispersion of the smoke in the near-field is modeled by Daysmoke, empirical model specifically designed for prescribed burn plumes [2]. Given the number of updraft cores, core diameters, updraft velocities, plume and ambient temperatures, wind fields, and emission rates, Daysmoke tracks the particles up to a predetermined distance from the burn plot, assuming the smoke is an inert substance. Long-range transport and chemistry are modeled by AG-CMAQ, an adaptive grid regional air quality model that can dynamically refine the grid around the plume [5]. In this

prediction system, Daysmoke has been coupled with AG-CMAQ as a subgrid-scale plume model through a process called *handover*. With this process, the plume is transferred from Daysmoke to AG-CMAQ at an optimal downwind distance with minimum loss of accuracy in smoke concentrations.

87.3 Model Evaluation

A comprehensive field study was conducted at a military base on Florida's Gulf of Mexico coast to collect data for evaluating the modeling system. As part of this study, the fuels were measured both before and after the burn [7]. Emissions of CO_2 and $PM_{2.5}$ were measured with a platform mounted on a tethered aerostat [3]. Winds were measured with a Doppler sodar, airborne (mounted on the aerostat) and ground-based sonic anemometers, and piball soundings. Plume height was measured with a lidar ceilometer. Ground-level $PM_{2.5}$ was also measured, both with fixed and mobile platforms.

Comparison to measurements reveled that although both fuel loads and consumptions were overestimated, by 20 and 10 % respectively, total emissions were underestimated by 15 %. Low wind speeds (WS) and varying wind directions (WD), particularly during transition from land to sea breeze, were difficult to predict with WRF. For sustained and steady wind periods, typical WS errors were 10–30 % and WD errors were 10–20° at altitudes most relevant to plume transport. Predicted plume heights were in agreement with the ceilometers measurements during initial flaming stages of the burns but modeled plumes collapsed faster. The agreement of predicted ground-level concentrations with observations varied; typically there was better agreement near the burn plot and the differences grew with downwind distance (Fig. 87.1).

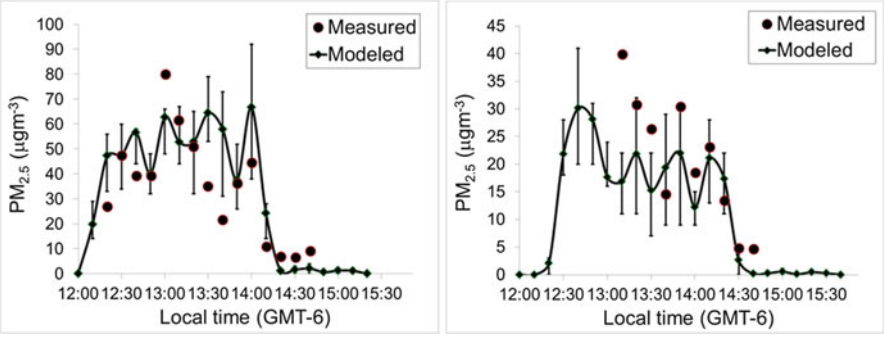

Fig. 87.1 Measured and modeled ground-level $PM_{2.5}$ concentrations (in $\mu g\ m^{-3}$) at 4 (*left*) and 9 km (*right*) downwind during the 8 February 2011 burn at Eglin AFB. WRF wind directions were corrected by 12° in accordance with tethered-aerostat lofted sonic anemometer measurements

Long-range impacts of PB were evaluated by simulating the Atlanta smoke event. Predicted peak $PM_{2.5}$ concentrations were about 70 $\mu g\ m^{-3}$ lower than the observations. The reasons for this under prediction were investigated through a sensitivity analysis. The model predictions can be raised to the level of observations by increasing the emissions by a factor of 4–6. However, based on the evaluation of emission estimates with field measurements, such a level of increase is not acceptable. On the other hand, vertical redistribution of emissions may be justified since the plume height is subject to uncertainties. The sensitivities of $PM_{2.5}$ concentrations to $PM_{2.5}$ emissions injected into different CMAQ layers at different times were calculated. The sensitivity of peak $PM_{2.5}$ concentrations in Atlanta to emissions injected into the PBL was 0.5 $\mu g\ m^{-3}\ ton^{-1}$ at 20:00 GMT, the most sensitive time for emissions. Modeled $PM_{2.5}$ peaks would increase if the emissions penetrating into the free troposphere were redistributed into the PBL. However, the maximum increase that can be achieved in this manner is estimated to be less than 5 $\mu g\ m^{-3}$. Allocating a greater fraction of emissions to 20:00 GMT would increase the peak also but its effect would be small for a realistic increment.

WS and WD are the two other parameters that were analyzed for their contribution to $PM_{2.5}$ concentrations. The Atlanta smoke event was dominated by strong and steady southeasterly winds and WD was predicted more accurately than what is typically achievable by meteorological models. However, sensitivity to WD is very large as $\pm 10°$ rotation of the wind field would make the plume totally miss Atlanta. Reducing WD, in this case making it more easterly, by 5° resulted in 15 $\mu g\ m^{-3}$ increase in peak $PM_{2.5}$ concentrations but advanced the time of the peak by 1 h. WS proved to be the most important parameter for prediction of peak concentrations. Reducing WS by 30 % increased the modeled $PM_{2.5}$ peaks in Atlanta by 50 $\mu g\ m^{-3}$. Also, it delayed the time of the peak by 1 h. Therefore, combined with $-5°$ adjustment of WD, 30 % reduction of WS would make modeled peaks match the magnitude and timing of observed peaks. But, do such adjustments of WS and WD have any basis? When compared to the most proximate sounding at Peachtree City, midway between the burn locations and Atlanta, WRF-predicted WD and WS are respectively 7–12° more southerly and about 30 % larger than the observations at the most relevant altitudes; hence, the adjustments are justified.

87.4 Conclusions

The modeling system developed incorporate new elements for emission, dispersion and transport processes that are critical for accurate prediction of the air quality impacts of PB plumes. These elements were evaluated using field data and their sources of uncertainty were identified. Uncertainties in emission strength and plume injection height are significant but their contributions to the under prediction of long-range $PM_{2.5}$ concentrations are relatively small. Uncertainties in WS and WD remain to be the limiting factors. With more accurate wind predictions, the system can be a viable tool for dynamic management of PB operations.

Acknowledgments This research was supported by the Strategic Environmental Research and Development Program, with substantial cost sharing from the US Forest Service. Supports by the Joint Fire Science Program and US Environmental Protection Agency are also acknowledged.

References

1. Achtemeier GL (2012) Field validation of a free-agent cellular automata model of fire spread with fire-atmosphere coupling. Int J Wildland Fire 22:148–156. doi:10.1071/WF11055
2. Achtemeier GL et al (2011) Modeling smoke plume-rise and dispersion from southern united states prescribed burns with daysmoke. Atmosphere 2(3):358–388
3. Aurell J, Gullett B, Pressley C, Tabor D, Gribble R (2011) Aerostat-lofted instrument and sampling method forr determination of emissions from open area sourrces. Chemosphere 85:806–811
4. Burling IR et al (2010) Laboratory measurements of trace gas emissions from biomass burning of fuel types from the southeastern and southwestern United States. Atmos Chem Phys 10(22):11115–11130
5. Garcia-Menendez F, Yano A, Hu Y, Odman MT (2010) An adaptive grid version of CMAQ for improving the resolution of plumes. Atmos Pollut Res 1(4):239–249
6. Michalakes J et al (2005) The weather research and forecast model: software architecture and performance. In: Zwieflhofer W, Mozdzynski G (eds) Proceedings of the 11th ECMWF workshop on the use of High Performance Computing in Meteorology. Reading, UK, World Scientific, pp 156–168
7. Ottmar RD, Vihnanek RE (2009) Fuel loading and fuel consumption for the RxCADRE fires. In: 4th international Fire Ecology Management Congress. Association for Fire Ecology, Savannah
8. Urbanski SP, Hao WM, Baker S (2009) Chemical composition of wildland fire emissions. In: Bytnerowicz A, Arbaugh M, Riebau A, Andersen C (eds) Developments in environmental science. Elsevier, Amsterdam, pp 79–107

Questions and Answers

Questioner Name: Amir Hakami

Q: How significant is the effect of the fire on transport winds?
A: Currently, we are not applying any fire effects to the transport winds but it is conceivable that strong fires would affect the wind fields around them.

Questioner Name: Peter Builtjes

Q: Fuel moisture is important, you mentioned. How do they determine this fuel moisture?
A: Fuel moisture is observed by personnel who make the go/no-go decision for the burn. Typically, observed fuel moistures are reported as wet, moist or dry.

Chapter 88
Assessing Sensitivity Regimes of Secondary Inorganic Aerosol Formation in Europe with the CALIOPE-EU Modelling System

María Teresa Pay, Pedro Jiménez-Guerrero, and José María Baldasano

Abstract Sulphur dioxide (SO_2) and nitrogen oxides (NO_x) form two of the largest contributors to PM2.5 in Europe: ammonium sulphate, $(NH_4)_2SO_4$, and ammonium nitrate, NH_4NO_3. Understanding the formation regimes for these components is important for the achievement of the reduction objectives established in the European legislation for PM2.5. The present work uses the CALIOPE air quality forecasting system to investigate the formation of secondary inorganic aerosols (SIAs) and their gaseous precursors over Europe. Results points out that the continental regions in Europe tend to be HNO_3^- limited for nitrate formation. Regulatory strategies in such regions should focus on reductions in NO_x rather than NH_3 to control NH_4NO_3.

Keywords Caliope-modelling system • Secondary inorganic aerosol

M.T. Pay
Earth Sciences Department, Barcelona Supercomputing Center – Centro Nacional de Supercomputación (BSC-CNS), Barcelona, Spain

P. Jiménez-Guerrero (✉)
Physics of the Earth, University of Murcia, Murcia, Spain
e-mail: pedro.jimenezguerrero@um.es

J.M. Baldasano
Earth Sciences Department, Barcelona Supercomputing Center – Centro Nacional de Supercomputación (BSC-CNS), Barcelona, Spain

Environmental Modelling Laboratory, Technical University of Catalonia, Barcelona, Spain

D.G. Steyn et al. (eds.), *Air Pollution Modeling and its Application XXII*,
NATO Science for Peace and Security Series C: Environmental Security,
DOI 10.1007/978-94-007-5577-2_88,

88.1 Introduction

The European directive 2008/50/EC has established regulations regarding PM10 concentration and recently for PM2.5 in order to protect human health. Policies must focus not only on the reduction of primary PM emissions, but also on the reduction of precursor emissions of secondary PM. Within the National Emission Ceiling (NEC) directive and the multi-pollutant and multi-effect Gothenburg protocol, NECs for SO_2, NO_x, NH_3 and NMVOC have been agreed upon to reduce acidification and eutrophication effects and to reduce human exposure to ozone. Due to the complex relationship between SIAs, the control of PM concentrations is still nowadays a difficult challenge; in this sense Chemical Transport Models (CTMs) are useful tools for PM assessment. The main purpose of this work is to characterize SIA formation regimes and understand the sensitivity of SIAs vs. their gaseous counterpart over Europe by means of the CALIOPE system [1, 2].

88.2 Model Formulation and Application

CALIOPE [2] is a complex air quality forecasting system that integrates a meteorological model (WRF-ARWv3.6.1), an emission model (HEMES-EMEP), a chemistry transport model (CTM) (CMAQv4.5) and a mineral dust dynamic model (BSC-DREAM8b). CALIOPE provides 48-h air quality forecasts with high spatial resolution in Europe (12 km × 12 km) and Spain (4 km × 4 km) (www.bsc.es/caliope/). Several evaluation studies [1] and near-real time evaluation support the confidence on the system. CALIOPE simulations over the European domain in 2004 are named hereafter as CALIOPE-EU.

Modelled SIA and gaseous counterpart are evaluated at rural background environments against ground-based measurements from the EMEP network (www.emep.int) for the year 2004. As a result, 31 stations were selected to evaluate SO_2, 53 for SO_4^{2-}, 8 for HNO_3, 31 for NO_3^-, 7 for NH_3, and 15 for NH_4^+, for respectively.

To characterize SIA formation regimes and understand their sensitivity to their gaseous precursors, we introduce three indicators. S-ratio [3] (Fig. 88.1, Eq. 88.1) stands for the ability of the model to form sulphate aerosols where concentrations are expressed as $\mu g\ m^{-3}$. A ratio close to unity indicates that only a small fraction of the emitted SO_2 has been converted to the SO_4^{2-}. Free ammonia (F-NH_x) (Fig. 88.1, Eq. 88.2) quantifies the amount of ammonia available, after neutralizing SO_4^{2-}, for NH_4NO_3 formation. This indicator is based on the fact that $(NH_4)_2SO_4$ is the favoured form for SO_4^{2-}. F-NH_x is defined on a molar basis. The gas-aerosol equilibrium in the $SO_4^{2-}/NO_3^-/NH_4^+$ system is analysed using the G-ratio [4] (Fig. 88.1, Eq. 88.3) which indicates whether fine-particle NO_3^- formation is limited by the availability of HNO_3 or NH_3. All the terms in the G-ratio equation are expressed in molar basis ($\mu mol\ m^{-3}$). G-ratio > 1 indicates that nitric acid

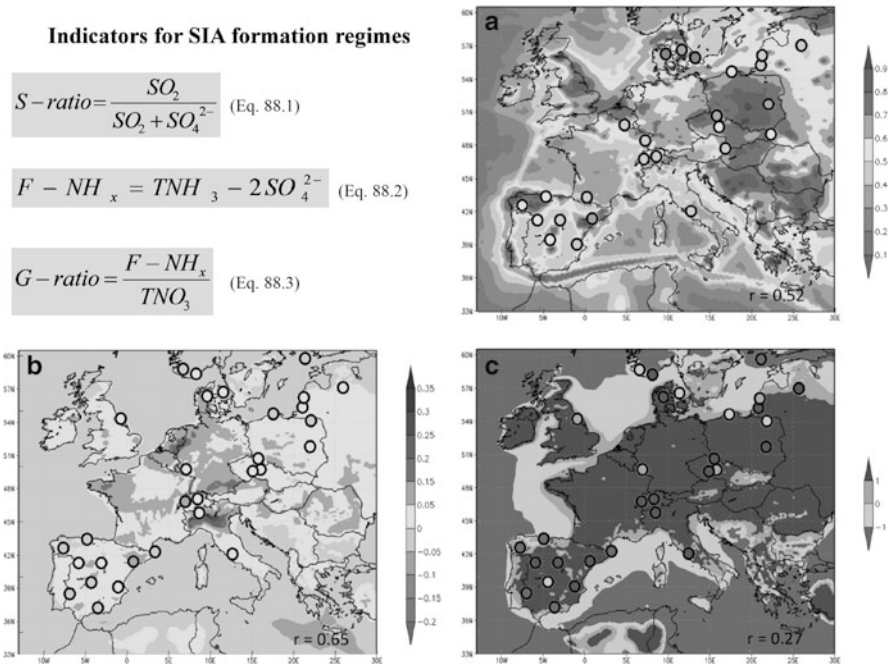

Fig. 88.1 Annual spatial distribution of the indicators: S-ratio (**a**), Free ammonia (**b**), in molar basin, and G-ratio (**c**) calculated within the CALIOPE-EU system over Europe in 2004. *Dots* represent the estimated indicators based on EMEP measurements

is limiting, while G-ratio < 0 indicates the ammonia is severely limiting. G-ratio between 0 and 1 indicates ammonia is available for reaction with nitric acid, but ammonia is the limiting species.

88.3 Results and Discussions

Although not shown here, CALIOPE-EU is able to reproduce SIA concentrations across Europe with coefficients ranging from 0.76 to 0.80. Although the total amount of SIAs is on average underestimated by 18–50 % in most regions of Europe, the temporal variability and hence the transport patterns of these species are captured rather well, as indicated by the correlation coefficients, which range between 0.49 and 0.62. Based on fractional biases and errors, the CALIOPE-EU's performance for HNO_3 and NH_3 gaseous precursors is not as accurate as for NO_3^- and NH_4^+ aerosols. The temporal treatment of ammonia emission is a probable source of uncertainty in the model representation of SIA.

Figure 88.1 presents the annual distribution of indicators for SIA formation regimes over Europe in 2004 modelled with CALIOPE-EU and measured at EMEP

stations. The highest S-ratio (Fig. 88.1a) (S-ratio > 0.5) is found over eastern Europe and western Iberian Peninsula, which indicates that fresh sulphur dominates these regions (oxidation processes are limiting). In this case, CALIOPE-EU overestimates these ratios, which is consistent with the model overestimation of the highest SO_2 concentrations, especially in eastern Europe. S-ratios between 0.4 and 0.5 are found over the Mediterranean Basin, central, north-western, and northern Europe where sulphur is dominated by SO_4^{2-} generated during the long-range transport. Under this regime, CALIOPE-EU tends to overestimate S-ratio, mainly dominated by the SO_4^{2-} underestimations, which depicts deficiencies in the SO_4^{2-} parameterizations.

Observed F-NH_x is between −0.05 and 0.13 μmol m^{-3} (Fig. 88.1b). Calculated spatial correlation is relatively high (r = 0.65). However, CALIOPE-EU presents a tendency to overestimate F-NH_x. Under this condition, NH_4NO_3 could be enhanced in the model. Nevertheless, the partition of the nitrogen species between the gas and aerosol is very sensitive to ambient conditions (temperature and relatively humidity) on the area. Modelled F-NH_x decreases from the coastal areas to the ocean. The lowest free ammonia (F-NH_x < 0 μmol m^{-3}) is mainly confined to coastal stations where neutralization by sea salt take place. The highest F-NH_x (F-NH_x >0.04 μmol m^{-3}) is found in central (south Germany and Po valley) and north-western Europe (Benelux and eastern France) where the highest and extended NH_3 emissions (>1,400 Mg $year^{-1}$) together with meteorological conditions (low temperature and high relatively humidity) favoured the partition of NO_3^- to aerosol phase.

The spatial distribution of G-ratio (Fig. 88.1c) indicates that, based on annual average concentration, over continental Europe the NH_4NO_3 formation is limited by the formation of HNO_3 (G-ratio > 1). Such findings indicate that NH_4NO_3 concentration in these areas could increase dramatically given an increase in HNO_3 concentration, or indirectly given an increase of NO_x emissions.

88.4 Conclusions

The model evaluation in terms of SIA indicators suggests that the CALIOPE-EU system is appropriate for regulatory modelling applications. S-ratios indicates that fresh sulphur dominate eastern Europe, western Iberian Peninsula, and the major shipping routes, where oxidants are limiting the formation of SO_4^{2-}. On the other hand, central Europe and the Mediterranean Basin are regions affected by the secondary SO_4^{2-} transported from the aforementioned emissions. NO_3^- formation is mostly limited by the availability of HNO_3 over continental regions in Europe. Based on the analysis of the three studied indicators, the SIA formation in Europe tends to be limited by SO_2 and HNO_3 due to the relatively high NH_3 emissions, mainly from agriculture, namely in north-western Europe. Regulatory strategies in this part of Europe could be focused on the reduction of NO_x and SO_2 rather than in NH_3 to control NH_4NO_3 and $(NH_4)_2SO_4$, respectively. The reduction of secondary PM needs international agreements, as it is a long-range transport problem.

References

1. Pay MT, Piot M, Jorba O, Basart S, Gassó S, Jiménez-Guerrero P, Gonçalves M, Dabdub D, Baldasano JM (2010) A full year evaluation of the CALIOPE-EU air quality system in Europe for 2004: a model study. Atmos Environ 44:3322–3342
2. Baldasano JM, Pay MT, Jorba O, Gassó S, Jiménez-Guerrero P (2011) An annual assessment of air quality with the CALIOPE modeling system over Spain. Sci Total Environ 409:2163–2178
3. Hass H, van Loon M, Kessler et al (2003) Aerosol modeling: results and intercomparison from European regional scale modeling system. Technical report. EUROTRAC 2 Report, EUREKA Environmental Project, GLOREAM
4. Ansari AS, Pandis S (1998) Response of inorganic PM to precursor concentrations. Environ Sci Technol 32:2706–2714

Questions and Answers

Questioner Name: Dominik Brunner

Q: You suggest that NO_x emission reduction is best measure to reduce $NH_4^+NO_3^-$. In several countries NO_x emissions have been reduced without significant effects on $NH_4^+NO_3^-$. How does this fit to your conclusions?
A: The reduction of NO_x from emissions is produced primarily in an urban environment and its effects are converged by the urban plume, which determines its spatial effects what does not happen in the same way with the plumes from power plants. Another significant factor is the high degree of resilience of the gas-to-aerosol formation, which requires high rates of reduction to cause significant effects. Finally, the oxidation conditions and the competition between different chemical species affect the response as well.

We are facing a chemical system that does not have a linear behaviour.

Chapter 89
Effect of the Turbulence Parameterizations on the Simulation of Pollutant Dispersion with the RMS Modelling System

Silvia Trini Castelli, Simona Falabino, G. Tinarelli, and Domenico Anfossi

Abstract The effect of using in dispersion modeling different parameterizations for the wind velocity fluctuations standard deviations is investigated for low-wind conditions.

Keywords Turbulence parameterizations • Surface layer • Low wind

89.1 The Wind Velocity Standard Deviations in Low-Wind Conditions

The turbulent variables are key parameters in determining the dispersion of pollutant in the atmosphere. Recently, we analyzed the wind-velocity fluctuation standard deviations as functions of the atmospheric stability with a particular attention to low-wind conditions. Three different datasets of wind velocity observations from sonic anemometers were considered: UTP dataset (Italy) collected at 5, 9 and 25 m heights, GRAZ dataset (Austria) at 10 m and TISBY dataset (Sweden) at 6.8 m. UTP and GRAZ sites are characterized by heterogeneous conditions (suburban areas), while the TISBY site is located on a flat terrain. In all threesites a remarkable

S.T. Castelli (✉) • D. Anfossi
Institute of Atmospheric Sciences and Climate, CNR-ISAC, Turin, Italy
e-mail: s.trinicastelli@isac.cnr.it

S. Falabino
Institute of Atmospheric Sciences and Climate, CNR-ISAC, Turin, Italy

Department of Physics, University of Turin, Turin, Italy

G. Tinarelli
Arianet S.r.l, Milan, Italy

D.G. Steyn et al. (eds.), *Air Pollution Modeling and its Application XXII*,
NATO Science for Peace and Security Series C: Environmental Security,
DOI 10.1007/978-94-007-5577-2_89,

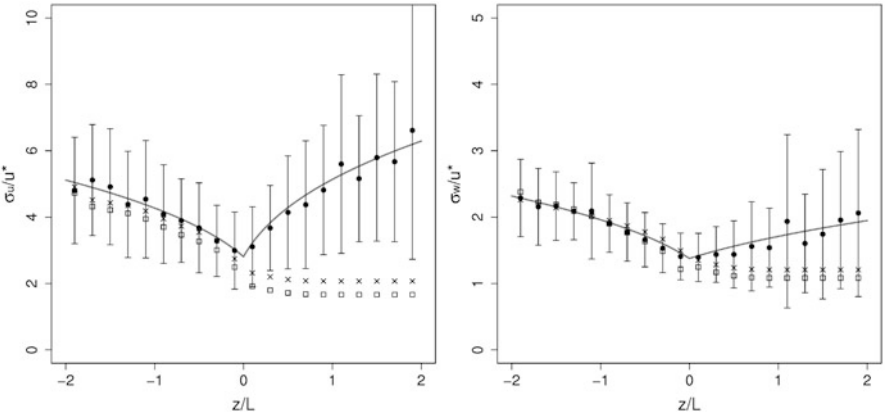

Fig. 89.1 Observed normalized standard deviations at UTP site at the height of 5 m (*dots* and *bars*), best-fit curve of Eq. (89.1) (*line*), H82 predictions (*squares*) and D00 predictions (*crosses*)

percentage of low-wind episodes, here defined as $U < 1.5\ ms^{-1}$ where U is the wind speed, were observed: 92 % of the cases in the set UTP-5 m set, 86 % for UTP-9 m, 87 % for GRAZ and 25 % for TISBY sets.

We drew an analytical function, based on a best fit of the observations and inspired by the formulation used in Moraes et al. [3], to calculate standard deviations σ_i (being u_* the friction velocity, z the height and L the Obukhov length):

$$\frac{\sigma_i}{u_*} = A_i\left[1 + B_i\left(\frac{z}{L}\right)\right]^{C_i} \tag{89.1}$$

where A_i, B_i and C_i are empirical coefficients, with $i = u,v,w$. A_i coefficients were estimated as the average of the normalized standard deviations in neutral cases ($z/L = 0$). We assigned a literature value to C_i and evaluated B_i from the non-linear best fit, separately for stable and unstable cases.

Figure 89.1 shows the predicted UTP along-wind and vertical normalized standard deviations at 5 m height (solid line) versus the stability parameter z/L, in the range $-2 \leq z/L \leq 2$, compared to the observations (dots). The values were averaged in different z/L classes (width equal to 0.2), the bars correspond to their standard deviations in each set and are representative of the variability in the single class.

The analogous plots for GRAZ and TISBY (not shown) present a similar modulation versus z/L but of course the values of the empirical coefficients are slightly different from UTP case. We verified that the main differences are ascribed to the wind velocity range of the measurements and to the different distributions of the friction velocity values.

The curves obtained through Eq. (89.1) and the empirical coefficients, which therefore account for the specificity of the low-wind regime, where then compared

(Fig. 89.1) to the predictions obtained using two literature turbulence parameterizations, Hanna [1982 – H82] [2] and Degrazia et al. [2000 – D00] [1], widely used in advanced dispersion models. We notice that the parameterizations show a good agreement with the observations in the unstable case but they fail in capturing the distribution of the observed data in stable conditions, where the similarity analytical function, fitted to data, is superior. In UTP case the stable conditions are mostly related to low-wind regime (in 96 % of the cases), for which the 'classical' parameterizations are not designed. We may infer that the low wind in stable stratification plays a major role in affecting their performances. Moreover, these formulations were established for flat terrain and not for complex geometries.

89.2 Effect of the Different Parameterizations on the Dispersion

It may be expected that the differences in the performances highlighted in Fig. 89.1 lead to different dispersion scenarios. To investigate this aspect, the analytical function of Eq. (89.1) was implemented in the (micro-) MIRS meteorological processor interfacing RAMS atmospheric model and (micro-)Spray Lagrangian dispersion model in the system (micro-)RMS.

For the new formulation given by Eq. (89.1) with UTP empirical coefficients (hereafter turbUTP), the Lagrangian time scales were evaluated from the equation:

$$T_{Li} = \frac{2\sigma_i^2}{C_{0i}\,\varepsilon}. \tag{89.2}$$

with $i = u,v,w$. C_{0i} is the Kolmogorov constant (here set $C_{0u} = 3.2$; $C_{0v} = 4.3$; $C_{0w} = 4.3$) and ε is the turbulent kinetic energy dissipation rate. This last was estimated using the surface layer similarity function proposed by Wyngaard and Coté [4].

In MIRS, H82 and D00 parameterizations are already available.

Here we present the results of a numerical experiment for a simplified case study.

We selected the observed wind speed and direction profiles at the three UTP anemometers, with the surface-layer parameters, for 2 h, respectively for unstable and stable conditions: see the example in Table 89.1 for reference.

Table 89.1 Measured mean wind and surface layer parameters at UTP site at the height of 5 m for the selected unstable and stable profiles

	Date	Local time	U (ms^{-1})	dir (°)	u_* (ms^{-1})	θ_* (K)	L (m)	PBL h (m)
Unstable	2007/04/25	14:00	0.75	12.91	0.18	−0.37	−6.54	1,080
Stable	2007/04/25	20:00	0.59	38.93	0.13	0.10	13.72	54

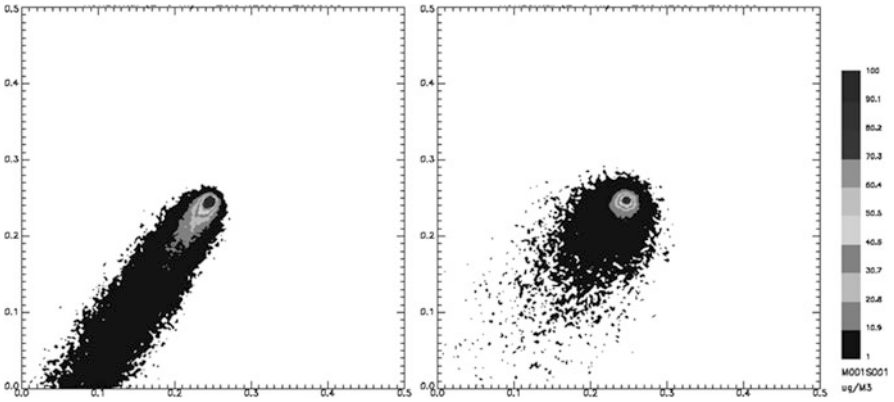

Fig. 89.2 Stable case. MicroSpray concentration field using H82 (*left*) and turbUTP (*right*)

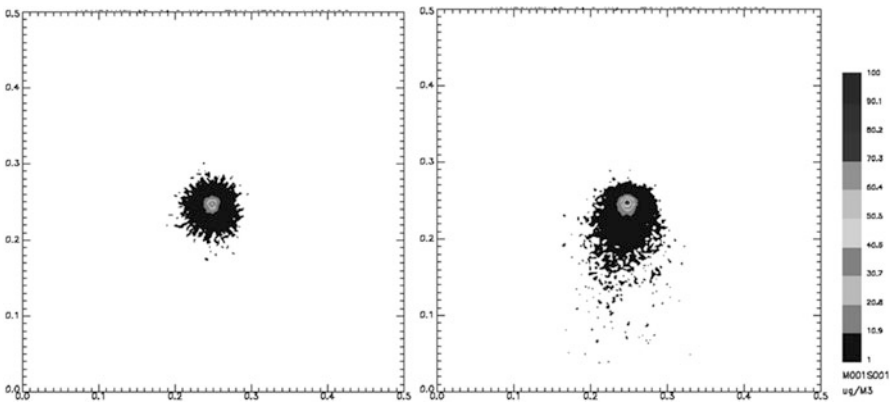

Fig. 89.3 Unstable case. MicroSpray concentration field using D00 (*left*) and turbUTP (*right*)

With the SWIFT mass-consistent model we produced two correspondent 3D-gridded homogeneous meteorological fields. These were used in input to MIRS to calculate the Lagrangian turbulent variables and then MicroSpray model was run, considering an emission at 2 m height. Two sets, unstable and stable, of three dispersion simulations, using turbUTP, H82 and D00 schemes, were obtained.

The use of the turbUTP formulation produces in fact significant differences in the stable case (example in Fig. 89.2) with respect to the classical parameterizations. The meandering, producing larger horizontal variances, prevails and leads to an enhanced spreading around the source, as expected in low-wind conditions. For both classical parameterizations instead the transport along wind dominates. For the unstable case (example in Fig. 89.3) the turbulence is more intense for the classical parameterizations and the diffusion is more efficient both in the horizontal and the vertical, even if the differences with respect to turbUTP are less pronounced.

In conclusion, the approach used in turbUTP formulation can be a valid alternative to the classical turbulence parameterizations in case of low-wind conditions. Since this type of formulations are originated from surface-layer similarities laws, next development will be to extend them to the full boundary layer.

References

1. Degrazia G, Anfossi D, Carvalho J, Mangia C, Tirabassi T, Campos Velho H (2000) Turbulence parameterisation for PBL dispersion models in all stability conditions. Atmos Environ 34:3575–3583
2. Hanna SR (1982) Applications in air pollution modelling. In: Nieuwstadt F, Van Dop H (eds) Atmospheric turbulence and air pollution modelling. Reidel, Dordrecht, pp 275–310
3. Moraes OLL, Acevedo OC, Degrazia GA, Anfossi D, Da Silva R, Anabor V (2005) Surface layer turbulence parameters over a complex terrain. Atmos Environ 39:3103–3112
4. Wyngaard JC, Coté OR (1971) The budgets of turbulent kinetic energy and temperature variance in the atmospheric surface layer. J Atmos Sci 28:190–201

Questions and Answers

Questioner Name: Jeff Weil

Q: (1) For the unstable case, have you looked at the number of independent eddies that pass your wind sensor over the averaging time? Since the large eddy scale $\sim z_i$ and the wind speed is U, the number of eddies that pass the sensor in the averaging time T_{av} is $n \cong T_{av}U/z_i$ (e.g. see Briggs 1993 JAM). The lower the number, the greater is the uncertainty in the $\sigma_{u,v,w}$ as your data seem to suggest.
(2) For the stable case, have you looked at the surface temperature in homogeneity as a source of horizontal wind fluctuations? For example, a velocity scale due to temperature fluctuations σ_θ could be given by $v_\theta = (gL_s\sigma_\theta/\theta)^{1/2}$, where Ls is the relevant length scale (TBD).
A: We appreciate the questions and related suggestions and we will take care of them in future research activity. However, our experience in low wind turbulence tells us that in such conditions there is not a clear distinction between unstable and stable conditions and that the mixing height z_i is not a proper scaling parameter. A thorough analysis of this specific dataset confirmed that low-wind conditions are critical for the definition of the atmospheric stability, since the boundaries between stable and unstable stratification are less defined than for windy cases.

Questioner Name: Bertrand Carissimo

Q: If the measurement tower was close to the building you would not use the homogeneous terrain formula as you did. What do you think is the limit for using this formula?

A: Surely we can expect that in complex geometry the formula should be corrected to account for the presence of buildings and obstacles, for instance through morphometric parameters. We are investigating this aspect trying to estimate the possible limits of it. Up to now, a thorough analysis of the data showed that in our case the low-wind regime dominates in determining the flow dynamics and the stratification conditions with respect to the urban morphology. We found a good agreement between the observed and the predicted standard deviations. Moreover, the obstacles closest to the mast are at a distance of 70 m and about 4 m high. In the simulation presented here we are looking at the microscale effect on the dispersion using the observed data as input. It will be different when considering larger scales, for which the effects of the surrounding buildings can play a major role.

Chapter 90
Information-Theoretic Approaches for Models Selection in Multi-model Ensemble Atmospheric Dispersion Predictions

Angelo Riccio, Angelo Ciaramella, Stefano Galmarini, Efisio Solazzo, and Slawomir Potempski

Abstract In this work we explore the effectiveness of theoretical information approaches, based on uncorrelation and Mutual Information, for the reduction of data complexity in multi-model ensemble systems. A distance matrix, measuring the inter-dependence between data, is derived, with the scope of clustering correlated/dependent models together and selecting a few representative models from each cluster. We test the efficacy of these distance measures to detect dependence structures and select "representative models". We apply this analysis in the context of atmospheric dispersion modeling, by using the ETEX-1 dataset and the data made available by the more recent AQMEII (Air Quality Model Evaluation International Initiative) efforts. We show how the selection of a small subset of models data, according to uncorrelation or mutual information distance criteria, usually suffices to achieve a statistical performance comparable to, or even better than, that achieved from the whole ensemble dataset, thus providing a simpler description of ensemble results without sacrificing accuracy

Keywords Multi-model ensemble • ETEX-1

A. Riccio (✉) • A. Ciaramella
Department of Applied Science, University of Naples "Parthenope",
Centro Direzionale, Isola C4, 80147 Naples, Italy
e-mail: angelo.riccio@uniparthenope.it

S. Galmarini • E. Solazzo
Institute for Environment and Sustainability, European Commission,
Joint Research Centre TP 441, 21020 Ispra, Varese, Italy

S. Potempski
National Centre for Nuclear Research, Otwock-Swierk, Poland

D.G. Steyn et al. (eds.), *Air Pollution Modeling and its Application XXII*,
NATO Science for Peace and Security Series C: Environmental Security,
DOI 10.1007/978-94-007-5577-2_90,

90.1 Introduction

Up to some years ago, the conventional approach in weather, climate and air quality modeling was to develop a model, deemed to be the "best", from which to infer causal relationships between the independent and dependent variables. However, the assumed model is usually selected from among several possible competing models, and other plausible models could give different answers to the scientific question at hand, even in the light of the same data. In the last years, the use of model ensembles has become an important component in atmospheric dispersion predictions [4]. However, as the quantities of data/models collected increases, some critical issues concerning the extraction of accurate and essential information arise.

Currently, several basic data/model selection strategies predominate. The most common strategy is *complexity-penalization*. There are many variants of this basic approach, including generalized cross validation, Akaike information criterion, minimum description length principle, Bayesian maximum a posteriori selection and regularization [3]. Another most common strategy is the *hold-out* approach. Again, there are many variants to this basic strategy, e.g., *n*-fold cross validation, leave-one-out testing, bootstrapping, etc. [2].

In this work we propose an alternative strategy to data/model selection, which is based on an information-theoretic approach. In multi-model ensemble modeling, different models are certainly more or less dependent, since they often share, among other features, initial/boundary data, numerical methods, parameterizations and emissions. We present a framework such that models can be partitioned into a tree-structured graph; each branch represents independent classes of models, that is models belonging to the same branch are more inter-dependent than models belonging to different branches.

90.2 Theoretical Framework

Given the predictions from two different models, ξ_k and ξ_l, and assuming that results can be modeled within a probabilistic framework, a formal definition of independence is

$$p_{k,l}\left(\xi_k, \xi_l\right) = p_k\left(\xi_k\right) p_l\left(\xi_l\right) \tag{90.1}$$

In other words, the joint density of model data, $p_{k,l}(\xi_k, \xi_l)$, must factorize into the product of two marginal densities, $p_k(\xi_k)$ and $p_l(\xi_l)$, each depending on only one model [1]. Again, the joint entropy, H, and the Mutual Information, MI, of two continuous random variables, ξ_k and ξ_l, can be defined as

$$H\left(\xi_k, \xi_l\right) = -\int p_{k,l}\left(\xi_k, \xi_l\right) \log p_{k,l}\left(\xi_k, \xi_l\right) d\xi_k d\xi_l \tag{90.2}$$

$$MI\left(\xi_k, \xi_l\right) = \int p_{k,l}\left(\xi_k, \xi_l\right) \log \frac{p_{k,l}\left(\xi_k, \xi_l\right)}{p_k\left(\xi_k\right) p_l\left(\xi_l\right)} d\xi_k d\xi_l \tag{90.3}$$

MI is a measure of independence in the following sense: $MI(\xi_k, \xi_l) = 0$ if and only if ξ_k and ξ_l are independent random variables. On the other hand, if ξ_k and ξ_l are the same, *MI* coincides with the entropy of ξ_k, i.e. all information conveyed by ξ_k is shared with ξ_l. This means that knowing ξ_k exactly determines the value of ξ_l and vice-versa, and ξ_k and ξ_l have the same entropy [1].

A weaker definition of independence is *uncorrelatedness*: model results are said uncorrelated if their Pearson correlation coefficient is zero, i.e. the correlation matrix (in the case of a more than two models) collapse to the identity matrix. It can be shown that independence implies uncorrelation, though the reverse is not always true. Also note that from (90.3) a metric can be derived

$$d_{MI}\left(k, l\right) = 1 - \frac{MI\left(\xi_k, \xi_l\right)}{H\left(\xi_k, \xi_l\right)} \tag{90.4}$$

Given a (pseudo)-distance matrix, i.e. the uncorrelation matrix, or the distance matrix whose elements are given by (90.4), models can be classified using an agglomerative approach. The hierarchical tree clusters uncorrelated/independent models; by this way we can select a few models that can be considered representative of each cluster, until reducing the number of models to a user-selected threshold of "independent" representative models.

90.3 Results

In this section we summarize the results obtained by applying the proposed approach to analyze the multi-model ensemble data of the ETEX-1 experiment (26 different models participating to this exercise). More details are given in Riccio et al. [5].

An agglomerative approach, based on *complete linkage*, is exploited to construct a hierarchical tree, and a representative model, one from each cluster, whose data are closest (in the mean square deviation sense) to the centroid of the cluster it belongs to, is selected. Table 90.1 shows the statistical performance of ensembles made only by 'representative models'; the tag 'Exp1' indicates models selected on the basis of uncorrelation distance, while the tag 'Exp2' models selected on the basis of mutual information. The 'Exp1' subset is made by five models, while the 'Exp2' by four models.

Table 90.1 Root mean square error (RMSE), correlation coefficient (CC), FA2, FA5 and FOEX indexes based on the ensembles made by the subset of Exp1 and Exp2 models

	RMSE	CC	FA2	FA5	FOEX
Exp1	1.04	0.24	21.95	44.44	−1
Exp2	0.87	0.23	27.47	54.85	−7
MM	1.15	0.30	26.43	50.99	13

MM indicates the performance using all ensemble members. FA2 and FA5 give the percentage of model results within a factor of 2 and 5, respectively, of the corresponding measured value, while FOEX is the percentage of modeled concentration values that overestimate (positive) or underestimate (negative) the corresponding measurement. The RMSE dimensions are ng/m^3

Table 90.2 Area of superposition for the selected representative models at different times

Time	m09	m10	m15	m20	m22	m23	m24	m26	MM	Exp1	Exp2
T0+06	1.00	0.41	0.75	0.37	0.89	0.27	0.62	0.42	0.73	0.89	0.57
T0+12	0.60	0.33	0.35	0.26	0.48	0.22	0.57	0.27	0.41	0.48	0.37
T0+18	0.39	0.35	0.24	0.48	0.47	0.33	0.45	0.22	0.41	0.39	0.47
T0+24	0.36	0.35	0.32	0.29	0.45	0.31	0.41	0.21	0.35	0.36	0.43
T0+30	0.37	0.35	0.31	0.24	0.42	0.25	0.65	0.19	0.40	0.41	0.46
T0+36	0.35	0.39	0.29	0.52	0.42	0.27	0.42	0.28	0.43	0.42	0.41
T0+42	0.45	0.36	0.35	0.25	0.53	0.42	0.49	0.07	0.49	0.54	0.56
T0+48	0.58	0.49	0.47	0.09	0.69	0.44	0.65	0.32	0.64	0.69	0.79
T0+54	0.50	0.49	0.25	0.00	0.57	0.40	0.41	0.43	0.60	0.58	0.57
T0+60	0.46	0.48	0.32	0.00	0.64	0.22	0.45	0.61	0.59	0.60	0.60

'MM' indicates the performance of the from the full ensemble; 'Exp1' the performance of the median based on the subset of Exp1 models; 'Exp2' the corresponding performance based on Exp2 models. Only experimental values greater than 0.1 ng/m^3 has been considered, in order to select significant concentrations

Results empirically demonstrated that a few representative models correctly reproduce the same results obtained from the analysis of full ensemble data. Moreover the area of superposition (Table 90.2), i.e. the fraction of model results for which both the modeled and observed concentrations correspond to a value greater than a given threshold, are insensitive to the selection procedure.

Though these results cannot be considered as general, as they have been obtained by the analysis of a single dataset, the positive results demonstrates the feasibility of using theoretically-based information criteria and support the rational behind this approach. We planned to apply this analysis to more extended datasets, e.g. that made available by the recent AQMEII (Air Quality Model Evaluation International Initiative) efforts.

References

1. Cover T, Thomas J (2006) Elements of information theory Wiley series in telecommunications and signal processing, 2nd edn. Wiley-Interscience, New York
2. Efron B (1979) Computers and the theory of statistics. SIAM Rev 21(6):460–480
3. Kaipio J, Somersalo E (2004) Statistical and computational inverse problems (applied mathematical sciences). Springer, New York
4. Kolczynski WC, Stauffer DR, Haupt SE, Deng A (2009) Ensemble variance calibration for representing meteorological uncertainty for atmospheric transport and dispersion modeling. J Appl Meteorol Climatol 48(10):2001–2021. doi:10.1175/2009JAMC2059.1
5. Riccio A, Ciaramella A, Giunta G, Galmarini S, Solazzo E, Potempski S (2012) On the systematic reduction of data complexity in multi-model atmospheric dispersion ensemble modeling. J Geophys Res. doi:10.1029/2011JD016503

Questions and Answers

Questioner Name: S. E. Gryning

Q: How do you take into account uncertainties in your measurements?
A: As you know, measurements are affected by large errors; however the focus of this work is not on error measurements. The main message that we want to convey is that, apart from obvious error measurements, it is possible to systematically highlight model data inter-dependencies and reduce data complexity in an efficient way. Measurements play a minor role in this context, since we are mainly interested in model inter-comparison.

Questioner Name: J. Weil

Q: Since in the ensemble approach it is important to have an outlier model to give a realistic estimate of the variability, NMSE, etc., would it be useful to have a designed "bad" model to include in your ensemble?
A: It is useful and interesting to have many "different models", since the full range of model responses is an added value in ensemble modeling; however the characteristics of a "bad" model depend on the metric used, and a simple answer is not available. Our approach aims at identifying how many classes of different models exist in our ensemble.

Chapter 91
On the Segregation of Chemical Species in a Clear Boundary Layer Over Heterogeneous Surface Conditions

Huug G. Ouwersloot, Jordi Vilà-Guerau de Arellano, Laurens N. Ganzeveld, Chiel C. van Heerwaarden, Maarten C. Krol, and Jos Lelieveld

Abstract The chemical segregation of isoprene has been investigated over heterogeneous surface conditions, and first results are presented and analysed.

Keywords Segregation • Isoprene • Heterogeneous surface

91.1 Introduction

Rural atmospheric chemistry is driven by the exchange of biogenic compounds, dynamic processes, and the diurnal variability of the atmospheric boundary layer (ABL). The influence of ABL dynamics on chemistry is normally not accounted when experimental observations are analysed [2, 7], even though there are numerous effects. One of these processes, the segregation of species due to inefficient turbulent mixing, was not applied to chemistry models and measurements for some time, but has recently been recognized as a possible relevant processto take into account in the observational analyses and models [1, 5, 6]. It is considered as

H.G. Ouwersloot (✉)
Meteorology and Air Quality Section, Wageningen University, Wageningen, The Netherlands

Department of Atmospheric Chemistry, Max Planck Institute for Chemistry, Mainz, Germany
e-mail: huug.ouwersloot@wur.nl

J. Vilà-Guerau de Arellano • C.C. van Heerwaarden • M.C. Krol
Meteorology and Air Quality Section, Wageningen University, Wageningen, The Netherlands

L.N. Ganzeveld
Earth System Sciences Section – Climate Change, Wageningen University, Wageningen, The Netherlands

J. Lelieveld
Department of Atmospheric Chemistry, Max Planck Institute for Chemistry, Mainz, Germany

D.G. Steyn et al. (eds.), *Air Pollution Modeling and its Application XXII*,
NATO Science for Peace and Security Series C: Environmental Security,
DOI 10.1007/978-94-007-5577-2_91,

a potential explanation of large discrepancies between observations and model results of reactive trace gas concentrations over the tropical forest, in particular for isoprene and the hydroxyl radical. However, in order to make observations comply with model results, chemists currently assume ad hoc values of the intensity of segregation that correspond to a substantial decrease in the isoprene-OH reaction rate without considering the physical and chemical processes that govern this effect (e.g., [1]).

This paper summarizes a selection of the results that were published by Ouwersloot et al. [3], who provide answers to the following questions:

- Is the segregation of chemical species important?
  How does this depend on dynamical and chemical conditions?
- Is the chemical species segregation influenced by heterogeneous surface conditions (forest next to savannah)?
  How does this depend on differences in the governing variables?

To investigate these questions, the intensity of segregation needs to be calculated explicitly. It is quantified for Amazonian conditions, using a Large Eddy Simulation model, expanded with a chemistry module. We present a brief overview of the main results after introducing the derivation of the intensity of segregation.

91.2 Formulation of the Intensity of Segregation

We introduce the concept of the intensity of segregation for a chemical in the atmosphere that is produced by the second-order chemical reaction $A + B \xrightarrow{k} C$. For a 3-dimensional field of data, as obtained from Large Eddy Simulations, it satisfies the conservation equation

$$\frac{\partial c_c}{\partial t} + \frac{\partial u_i c_c}{\partial x_i} = R, \tag{91.1}$$

$$R = k \cdot C_A \cdot C_B. \tag{91.2}$$

u_i and x_i are respectively the wind velocity and the coordinate in the i-direction, k is the reaction constant, R is the chemical production rate and c_A, c_B and c_C are the concentrations of respectively the chemicals A, B and C.

Numerical calculations are often performed using spatially averaged values. Every arbitrary variable, φ, can be expressed as

$$\phi = [\phi] + \phi', \tag{91.3}$$

in which the rectangular brackets correspond to a spatial average and the prime corresponds to a deviation therefrom. The spatial average of the production rate is

$$[R] = k \cdot [C_A \cdot C_B] = k \cdot \left([C_A] \cdot [C_B] + \left[C'_A \cdot C'_B\right]\right) \tag{91.4}$$

The physical interpretation of the intensity of segregation is the relative deviation of the total chemical production rate from the production rate due to the mean concentrations, R_{mean},

$$R_{mean} = k \cdot [C_A] \cdot [C_B] \tag{91.5}$$

The intensity of segregation is therefore expressed as

$$I_S \equiv \frac{[R] - R_{mean}}{R_{mean}} = \frac{\left[C'_A \cdot C'_B\right]}{[C_A] \cdot [C_B]}. \tag{96.6}$$

91.3 Relevant Findings for I_S: Homogeneous Versus Heterogeneous Surface Conditions

Due to inefficient turbulent mixing, the intensity of segregation equals −0.07 for the numerical experiment with homogeneous surface conditions (resulting in a decrease in the chemical reaction rate of 7 %). In the case with heterogeneous surface conditions, differences in the energy partitioning over sensible and latent heat flux result in different surface buoyancy fluxes per type of terrain. Due to this difference, mesoscale circulations are induced, which transport chemical species and consequently affect segregation. In Fig. 91.1, it is shown that as a result, isoprene, which is mainly emitted by the forest, has higher concentrations in the upper ABL above the savannah than over the forest. For the cases under study, this altered distribution always leads to a more negative intensity of segregation.

A schematic overview of the different variables that govern I_S, is presented in Fig. 91.2a. In short, I_S is determined by the differences in surface fluxes, the horizontal wind velocity and direction and the chemical conditions in the ABL and free troposphere. In Fig. 91.2b the resulting intensities of segregation are shown as a function of the forcing strengths of these variables. In general, $-0.07 < I_S < -0.20$. For more details, the reader is referred to Ouwersloot et al. [3].

Acknowledgments H.O. gratefully acknowledges financial support by the Max Planck Society for this project. The modelling part of this study was sponsored by the National Computing Facilities Foundation (NCF project SH-060-10) for the use of supercomputer facilities.

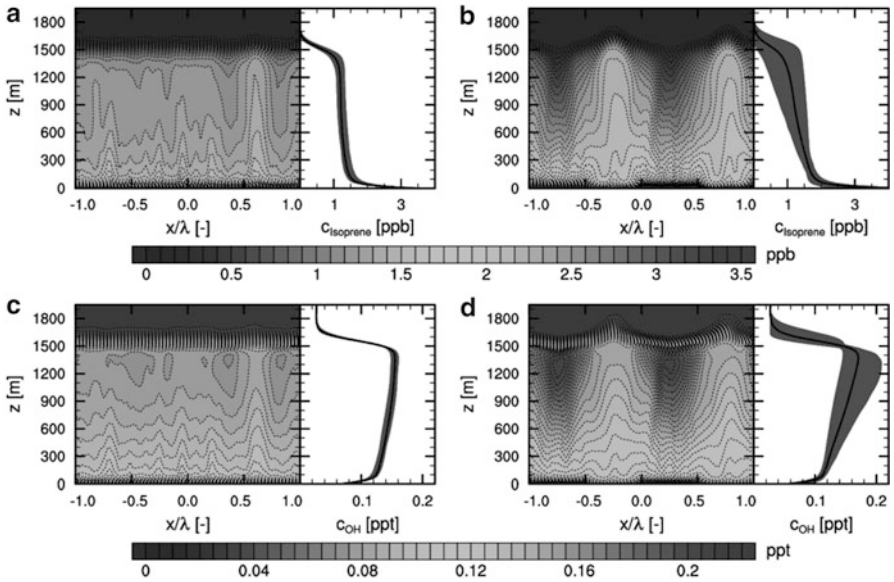

Fig. 91.1 Isoprene (**a**, **b**) and OH (**c**, **d**) concentrations for the homogeneous case (**a**, **c**) and the heterogeneous case (**b**, **d**). Each figure consists of two panels. The first panel shows these variables averaged over the fourth hour of simulated time and the *y*-direction, while the second panel shows an additional average in the *x*-direction. The *grey area* in the second panel shows the variability in the *x*-direction of the temporal and *y* averaged values. The *x*-coordinate is scaled by the length scale of heterogeneity, λ, which is twice the size of a patch. The forest is located at $-1 < \frac{x}{\lambda} < -0.5$ and $0 < \frac{x}{\lambda} < 0.5$. The savannah is located elsewhere

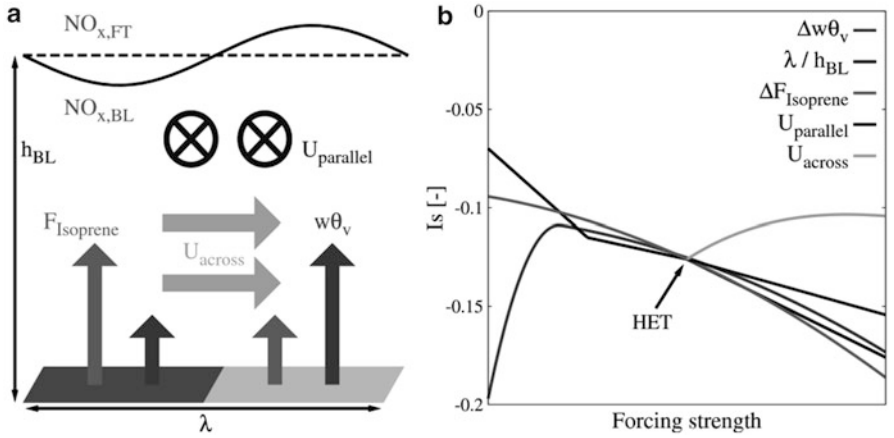

Fig. 91.2 Governing variables which affect the segregation of chemical species (**a**) and the resulting intensity of segregation as a function of the magnitude of those variables (**b**). The governing variables are the **surface buoyancy flux difference**, the **length scale** of heterogeneity, the **isoprene emission difference**, **wind blowing parallel** to the borders between forest and grass and **wind blowing across** those borders. The control numerical experiment with heterogeneous surface forcings, HET, is indicated with an *arrow*. Not shown in panel (**b**) is the impact of $\mathbf{NO_X}$ mixing ratios and their distribution within the boundary layer and free troposphere on I_S

References

1. Butler TM, Taraborrelli D, Brühl C, Fischer H, Harder H, Martinez M, Williams J, Lawrence MG, Lelieveld J (2008) Improved simulation of isoprene oxidation chemistry with the ECHAM5/MESSy chemistry-climate model: lessons from the GABRIEL airborne field campaign. Atmos Chem Phys 8:4529–4546
2. Ganzeveld L, Eerdekens G, Feig G, Fischer H, Harder H, Königstedt R, Kubistin D, Martinez M, Meixner FX, Scheeren HA, Sinha V, Taraborrelli D, Williams J, Vilà-Guerau de Arellano J, Lelieveld J (2008) Surface and boundary layer exchanges of volatile organic compounds, nitrogen oxides and ozone during the Gabriel campaign. Atmos Chem Phys 8:6223–6243
3. Ouwersloot HG, Vilà-Guerau de Arellano J, van Heerwaarden CC, Ganzeveld LN, Krol MC, Lelieveld J (2011) On the segregation of chemical species in a clear boundary layer over heterogeneous land surfaces. Atmos Chem Phys 11:10681–10704
4. Patton EG, Davis KJ, Barth MC, Sullivan PP (2001) Decaying scalars emitted by a forest canopy: a numerical study. Bound-Lay Meteorol 100:91–129
5. Pugh TAM, MacKenzie AR, Hewitt CN, Langford B, Edwards PM, Furneaux KL, Heard DE, Hopkins JR, Jones CE, Karunaharan A, Lee J, Mills G, Misztal P, Moller S, Monks PS, Whalley LK (2010) Simulating atmospheric composition over a South-East Asian tropical rainforest: performance of a chemistry box model. Atmos Chem Phys 10:279–298
6. Pugh TAM, MacKenzie AR, Langford B, Nemitz E, Misztal PK, Hewitt CN (2010) The influence of small-scale variations in isoprene concentrations on atmospheric chemistry over a tropical rainforest. Atmos Chem Phys 11:4121–4134
7. Vilà-Guerau de Arellano J, van den Dries K, Pino D (2009) On inferring isoprene emission surface flux from atmospheric boundary layer concentration measurements. Atmos Chem Phys 9:3629–3640

Questions and Answers

Questioner Name: Jeff Weil

Q: Have you considered putting a canopy into your model and what possible affects it might have on the segregation?
A: In our LES model a representation for the canopy is not included. However, the influence of different roughness lengths is taken into account when representing surface conditions characterized by different properties (savannah versus forest). For the boundary layer averaged quantities this turned out to be a small effect. An interactive canopy model, as presented by Patton et al. [4], could possibly impact our results more, but the effects would in all likelihood be restricted to the surface layer. As we study boundary layer averaged quantities, we did not focus on developing a more accurate canopy model in our LES model. Next to a dynamical effect, the canopy influences the segregation by having different biogenic emissions for each land type and storing and transforming chemical compounds. This results in different surface fluxes for the chemical reactants. The intensity of segregation is studied for different isoprene emission distributions between savannah and forest.

Questioner Name: Golam Sarwar

Q: How much influence it has on ozone?
A: The magnitude of the segregation intensity between e.g. ozone and NO is much smaller than the one between isoprene and OH. For this chemical reaction, the intensity of segregation for the boundary layer, averaged over the 4th hour of simulated time, is equal to 0.7 and 1.4 % for the cases with homogeneous and heterogeneous surface conditions, respectively. Including the contributions of all dynamics and chemical reactions, the difference in the averaged O_3 between the case with homogeneous and the case with heterogeneous surface forcings is only 1.4 % (24.48 ppb vs. 24.14 ppb).

Chapter 92
Response of SIA Concentrations Across Germany to Emission Changes During PM10 Episodes in Spring 2009

Sabine Banzhaf, Martijn Schaap, R. Wichink Kruit, R. Stern, and Peter Builtjes

Abstract The Chemistry Transport Model (CTM) REM-Calgrid (RCG) has been applied to investigate the non-linear relationship between emission changes and modelled SIA ($=SO_4 + NO_3 + NH_4$) concentrations for a high PM10 episode in spring 2009. Emissions were reduced for the model domain only and the model domain including Boundary Conditions. It was found that the effectiveness of emission reductions increases with increasing emission reduction area whereas results were least dependent on the size of emission reduction area for ammonia emission changes.

Keywords Emission scenario • Non-linearity • SIA concentrations • Deposition loads

92.1 Introduction

As precursors of PM10, sulphur and nitrogen compounds influence regional scale tropospheric chemistry and related effects on public health. Related PM10 EU limit values are still exceeded over large parts of Europe indicating a continued need for further implementation of air pollution abatement strategies. Chemistry Transport Models are used to perform emission scenario calculations, which are essential for

S. Banzhaf (✉) • R. Stern
Institute of Meteorology, Freie Universitaet Berlin, Berlin, Germany
e-mail: sabine.banzhaf@met.fu-berlin.de

M. Schaap • R.W. Kruit
TNO, Utrecht, The Netherlands

P. Builtjes
Institute of Meteorology, Freie Universitaet Berlin, Berlin, Germany

TNO, Utrecht, The Netherlands

D.G. Steyn et al. (eds.), *Air Pollution Modeling and its Application XXII*,
NATO Science for Peace and Security Series C: Environmental Security,
DOI 10.1007/978-94-007-5577-2_92,

planning policy actions. Various studies have tried to quantify the impact of emission changes of one pollutant on the concentrations and/or deposition fluxes of the others in Europe (e.g. [4, 7]). Fagerli and Aas [5] analysed trends in nitrogen compounds using long-term measurements and results from the EMEP model at EMEP sites. They found that despite large reductions in NOx emissions only few sites indicate a decline in total nitrate (=sum of NO_3 and HNO_3) in air, which was stated to be connected to SO_2 emission reductions leading to a shift in the equilibrium between nitric acid and ammonium nitrate towards particulate phase. The studies mentioned above investigated the impact of emission changes on long term trends of sulphur and nitrogen compounds. In the present study the CTM RCG has been applied to perform a base case run and emission scenarios for a high PM10 episode on a domain covering Germany. The emissions of PM10 precursors SO_2, NOx and NH_3 have been reduced for both the model domain only and the model domain including Boundary Conditions. The base case run has been evaluated and the non-linear response of modelled SIA levels to emission changes has been investigated.

92.2 Methods and Data

92.2.1 Chemistry Transport Model

The Eulerian grid model RCG simulates air pollution concentrations solving the advection-diffusion equation on a regular lat-lon-grid with variable resolution over Europe [2]. RCG is offline-coupled to the German Weather Service operational NWP model COSMO-EU. RCG was evaluated within many urban and regional applications and within the framework of several European model inter-comparison studies ([9] and references therein). For this investigation a research version of RCG was used as described in Banzhaf et al. [1]. It includes enhanced physical and chemical descriptions of scavenging processes and sulphate production as function of cloud liquid water content and cloud/rain droplet pH.

92.2.2 Investigation Period

The investigation period was 24th March to 28th April in spring 2009. According to German Weather Service the mean temperature over central Europe in April 2009 was up to 4 K higher than the mean of the reference period of 30 years (1961–1990) while precipitation amounts were regionally far under average. This extreme weather was connected to high-pressure systems with rather stable air conditions and low atmospheric mixing. Stable air conditions accompanied with high temperatures lead to high PM10 levels [8]. In April 2009 on 9–12 days the EU limit for daily mean PM10 was exceeded at most stations in the Netherlands and at several stations in Germany.

Table 92.1 Emission scenarios

NH_3 emission change (%)	NOx emission change (%)	SO_2 emission change (%)	Scenario label
0	−20	−50	−NOX-SO2
−40	0	0	−NH3
−40	−20	−50	−NH3-NOX-SO2

92.2.3 Observational Data

For the evaluation of RCG concerning PM10 model results have been compared to daily averages of PM10 at 56 AirBase (http://airbase.eionet.europa.eu/) rural background stations spread over Germany.

92.2.4 Summary of Model Runs

All model runs were performed on a domain covering Germany (47.2 N-55.1 N; 5.4E-15.7E), in the following denoted 'regional domain', with a horizontal resolution of approx. 7×7 km^2 and 20 vertical layers up to 5,000 m. A large scale RCG run covering Europe provided the Boundary Conditions. Emissions for Germany were taken from national inventory (Jörß et al. [6]) combined with the European TNO-MACC data set [3]. Next to the base run three different emission reduction scenarios have been performed (→ Table 92.1). In a first step precursor emissions were only reduced within the regional domain (denoted by RD). In a second step emissions were reduced within the regional and within the large scale run lowering the Boundary Conditions of the relevant precursor (denoted by LD).

92.3 Results and Discussion

92.3.1 Model Performance

Figure 92.1a shows modelled daily mean PM10 concentrations of the base run compared to observations at 56 AirBase stations spread over Germany. The model performs well with a correlation of 0.74 and a reasonable slope and intercept value for linear regression. The corresponding RMSE amounts 9.67 ug/m^3 (observed mean 21.18 ug/m^3). The model tends to overestimate low PM10 values and underestimate the high peaks. The BIAS of +3.36 ug/m^3 indicates a slight overall overestimation of the model. Figure 92.1b shows the PM10 daily means time series at station Westerwald-Herdorf. The model well reproduces the temporal

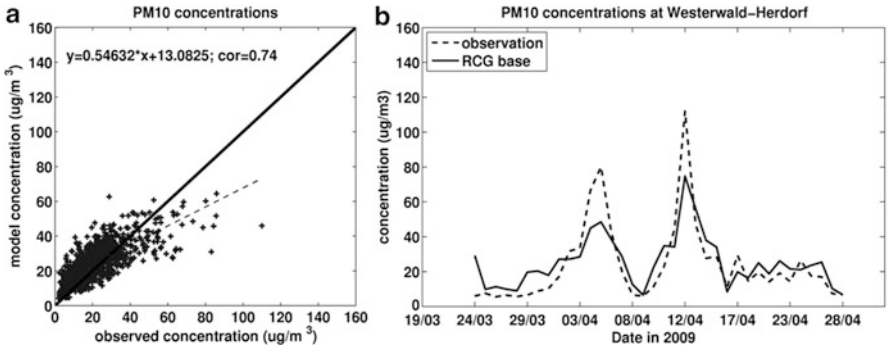

Fig. 92.1 Model daily mean PM10 concentrations compared to observations at (**a**) 56 rural background AirBase stations and (**b**) rural background station Westerwald-Herdorf

devolution of PM10 concentrations for the investigation period. However, as already recognized in the scatter plots the model tends to underestimate peak values and to overestimate low values. Model SIA concentrations have been compared to daily observations at three Dutch stations close to the German border since German SIA observations were not available (not shown here). The corresponding correlation was high with 0.76.

92.3.2 Emission Scenarios

Figure 92.2 shows the regional domain mean SIA concentrations for the base run and emission reduction scenarios (a) within the regional domain only and (b) within the regional domain and the large scale Europe run reducing Boundary Conditions. For all presented emission reduction scenarios all SIA components concentrations decrease compared to the base run. However, the SIA concentrations response to the emission reductions is non-linear. For all scenarios emission reductions are more effective if performed on the large scale run including Boundary Conditions. The -NH3 run is least dependent on the size of emission reduction area. Due to transboundary transport sulphate and ammonium changes only little for the scenarios –NOX-$SO2_{RD}$ and -NH3-NOX-$SO2_{RD}$ although SO_2 is reduced by 50 % while the decrease is significant for the corresponding LD scenarios. Nitrate is only slightly reduced for the –NOX-$SO2_{RD}$ and –NOX-$SO2_{LD}$ runs but is significantly reduced as soon as NH_3 emissions are lowered. However, the reduction of NH_3 increases NOy total deposition fluxes significantly (not shown here). For all RD and LD emission reductions the most effective scenario concerning concentrations and deposition fluxes is lowering emissions of precursors NH_3, NOx and SO_2 simultaneously.

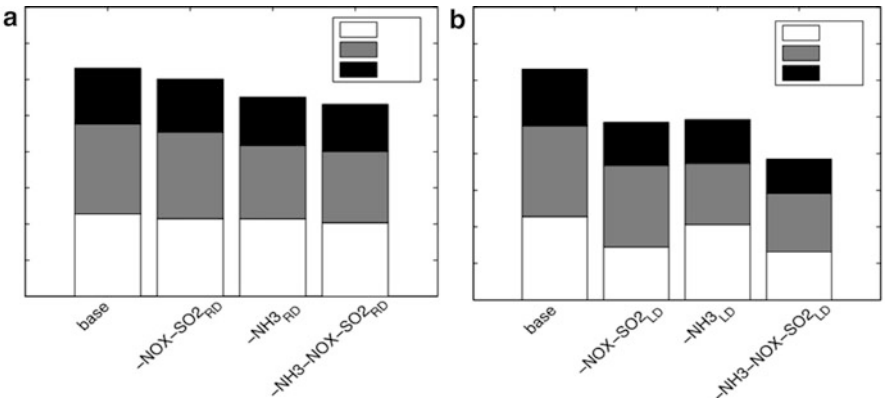

Fig. 92.2 Mean regional domain SIA concentrations for different emission scenarios within (**a**) the regional domain and (**b**) the large scale domain

92.4 Conclusions and Outlook

This study has shown that SIA concentrations respond non-linear to emission reductions of NH_3, SO_2 and NOx. The effectiveness of emission reductions increases with increasing emission reduction area. The results were least dependent on the size of emission reduction area for NH_3 emission changes (-NH3 scenario). However, concentrations and deposition loads of sulphur and nitrogen compounds are connected and emission reductions may have reverse impact. Hence, concentrations and loads on ecosystems should be considered at the same time, as they share the same sources. In a further step the sensitivity of concentrations and deposition loads of sulphur and nitrogen compounds to emission changes for spring 2009 is investigated regarding spatial distribution and temporal devolution.

References

1. Banzhaf S et al (2011) Implementation and evaluation of pH-dependent cloud chemistry and wet deposition in the chemical transport model REM-Calgrid. Atmos Environ. doi:10.1016/j.atmosenv.2011.10.069
2. Beekmann M et al (2007) PM measurement campaign HOVERT in the greater Berlin area: model evaluation with chemically specified particulate matter observations for a 1 year period. Atmos Chem Phys 7:55–68
3. Denier van der Gon H et al (2010) A high resolution European emission data base for the year 2005. UBA-Projekt PAREST. TNO-034-UT-2010e01895_RPT-ML, Utrecht
4. Erisman JW et al (2003) The European perspective on nitrogen emission and deposition. Environ Int 29:311–325
5. Fagerli H, Aas W (2008) Trends of nitrogen in air and precipitation: model results and observations at EMEP sites in Europe, 1980 – 2003. Environ Pollut 154(3):448–461

6. Jörß W, Kugler U, Theloke J (2010) Emissionen im PAREST Referenzszenario 2005–2020. In: Parest-Bericht Mai 2010. Umweltbundesamt, Dessau
7. Lövblad G et al (2004) EMEP assessment part I: European perspective. Norwegian Meteorological InstituteOslo
8. Mues A, Manders A, Schaap M, Kerschbaumer A, Stern R, Builtjes P, Impact of the extreme meteorological conditions during the summer 2003 in Europe on particulate matter concentrations. Atmos Environ 55:377–391
9. Stern R et al (2008) A model inter-comparison study focussing on episodes with elevated PM10 concentrations. Atmos Environ 42:4567–4588

Question and Answers

Questioner Name: Peter Builtjes

Q: How important is the seasonal pattern of NH_3 emissions and do we know that well enough?
A: We do not know the seasonal pattern of NH_3 emissions well enough. NH_3 emissions and the corresponding seasonal pattern are still very uncertain. This is partly the reason why we performed also sensitivity runs with NH_3 emission changes (-60 % to $+40$ %) and analysed the sensitivity of modelled concentrations and deposition fluxes to these changes (not shown here). However, this study was performed over a period of only 6 weeks during springtime. To investigate changes in the seasonal pattern a longer time period would have to be modelled and analysed.

Chapter 93
The Relation of the Planetary Boundary Layer Height to the Vertical Aerosol Distribution in Chemistry Transport Models

Volker Matthias, Armin Aulinger, Johannes Bieser, and Markus Quante

Abstract Simulated meteorological fields, ground values of aerosol concentrations (PM2.5) and aerosol concentration profiles, all calculated within the Air Quality Model Evaluation International Initiative (AQMEII) for the year 2006 for Europe are used to investigate the relation of the height of the planetary boundary layer (PBL) to the modelled aerosol concentrations. It was found that in many cases simulated PBL heights match the observed values at Lindenberg, Germany, quite well at noon and under convective conditions. On the other hand, in winter and at night time, when the atmosphere is more frequently stably stratified, the modelled values underestimate the observed PBL height quite significantly. A strong relationship between the simulated PBL height and the aerosol concentrations at ground was found. While those models which showed good agreement with the observed PBL height typically underestimate PM2.5, too low PBL heights were connected with higher aerosol concentrations close to ground and therefore lower bias. Model biases in PBL height and in PM2.5 concentration at ground were found to be highly anti-correlated.

Keywords Model evaluation • PM2.5 • Vertical profile

93.1 Introduction

The vertical distribution of atmospheric pollutants is of utmost importance for their transport in the planetary boundary layer (PBL) and for their concentration close to ground. Vertical mixing largely determines low level concentrations and is therefore highly relevant for the impact of atmospheric pollutants on humans, animals and ecosystems.

V. Matthias (✉) • A. Aulinger • J. Bieser • M. Quante
Helmholtz-Zentrum Geesthacht, Institute of Coastal Research, Max-Planck-Strasse 1, 21502 Geesthacht, Germany
e-mail: volker.matthias@hzg.de

D.G. Steyn et al. (eds.), *Air Pollution Modeling and its Application XXII*, NATO Science for Peace and Security Series C: Environmental Security,
DOI 10.1007/978-94-007-5577-2_93,

Chemistry transport model (CTM) systems need meteorological fields to calculate transport and transformation of atmospheric pollutants. Many model systems use external fields, e.g. from mesoscale meteorological models which are then fed into the CTMs. It is well known that the PBL height is in many cases not well represented in mesoscale meteorological models. This might in turn lead to significant problems to reliably simulate concentrations of atmospheric pollutants in the PBL.

On the other hand, model deficiencies in correctly simulating the atmospheric aerosol load may be hidden by errors in the PBL height which compensate for them. The Air Quality Model Evaluation International Initiative (AQMEII, [1]) was a great opportunity to investigate these effects for a number of different combinations of mesoscale meteorological and chemistry transport models.

93.2 Methods

The investigations focus on East Germany, where a highly reliable data set with PBL heights was available from the German Weather Service (DWD) for Lindenberg (14.1E, 52.2 N). It considers four radio soundings per day (00, 06, 12 and 18 UT). The derived PBL height is then controlled and verified with other data from wind profilers and sodars. Quality flags are given depending on the agreement between different methods. Ground based aerosol measurements from Melpitz (12.9 E, 51.5N), which is about 120 km south east of Lindenberg, are taken to represent the aerosol levels in East Germany. Nine different model systems for which both, aerosol and meteorological data was stored in the AQMEII data base, were used for the investigation. Daily averaged PM2.5 values for the entire year 2006 were considered. Annual average PBL heights account only for the four launching times per day.

93.3 Results

Deviations between the modelled and observed PBL heights at Lindenberg for nine different model systems show differences for the four launching times (Table 93.1, [3]). Best agreement is achieved at 12 UT while the largest underestimation by the models is seen at 18 UT. At this time, convection is already significantly reduced in many model systems while it is still present the observations.

Observed PM2.5 concentrations are typically underestimated by regional chemistry transport model systems [2]. This is also the case for most model systems participating in the AQMEII. Figure 93.1 shows examples of two time series at Melpitz. Apparently M9 shows higher values than M2 on most of the days and particularly in summer.

Table 93.1 Bias of modelled PBL height at Lindenberg (in m) for nine model systems

	Obs	M1	M2	M3	M4	M5	M7	M8	M9	M10
All	628	30	39	−476	−210	−3	−139	−361	−288	−55
00	363	11	34	−326	−246	22	−113	−317	−293	54
06	366	8	76	−326	−132	32	−126	−313	−276	29
12	1078	167	237	−612	72	33	−264	−280	−150	−170
18	705	−68	−193	−638	−538	−99	−52	−532	−434	−134

Model numbers follow the codes given in [3]. Observations are given at four times in m above ground

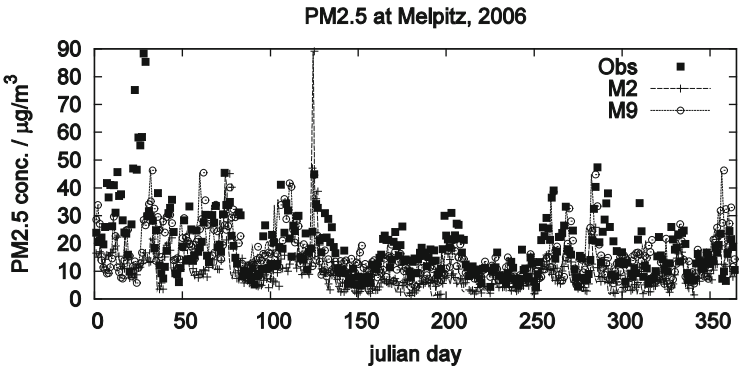

Fig. 93.1 Comparison of observed times series of PM2.5 concentrations at Melpitz to the model results for M2 and M9

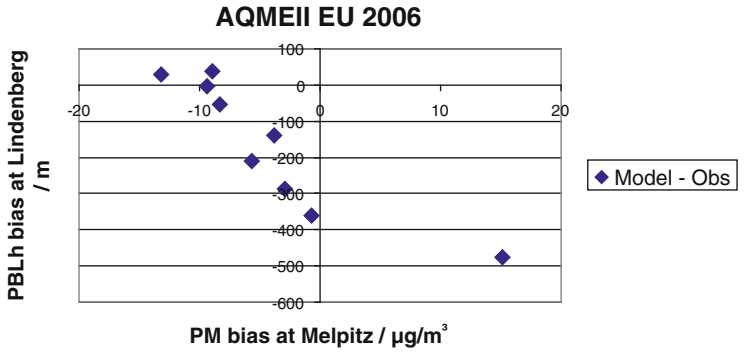

Fig. 93.2 Relationship between annual bias in PBL height and in PM2.5 concentration for nine model systems participating in the AQMEII model intercomparison. The correlation coefficient is −0.89

A comparison between the annual averaged bias of the PM2.5 concentrations at ground and the bias of the PBL height reveals a strong relationship (Fig. 93.2). If the average PBL height is reliably reproduced, like for M1, M2, M5 and M10, the PM2.5 concentration is underestimated by 8 – 13 ug/m^3, while those models

with low bias in the PM2.5 concentrations show a rather strong underestimation of the PBL height. This implies that good agreement in PM2.5 concentrations is only achieved because the vertical mixing of the pollutants is underestimated. Underestimation of PM2.5 in regional models is typical and almost independent of the model system.

Acknowledgments F. Beyrich from the German Weather Service, Meteorologisches Observatorium Lindenberg, is gratefully acknowledged for the observed PBL heights. We thank all AQMEII participants who delivered data for the European domain.

References

1. Galmarini S, Rao ST (2011) The AQMEII two-continent regional Air Quality Model evaluation study: fueling ideas with unprecedented data. Atmos Environ 45(14):2464
2. Solazzo E, Bianconi R, Pirovano G, Matthias V and 29 co-authors (2012) Operational model evaluation for particulate matter in Europe and North America in the context of AQMEII. Atmos Environ 53:75–92. doi:10.1016/j.atmosenv.2012.02.045
3. Vautard R, Moran MD, Solazzo E, Gilliam RC, Matthias V, Bianconi R, Chemel C, Ferreira J, Geyer B, Hansen AB, Jericevic A, Prank M, Segers A, Silver JD, Werhahn J, Wolke R, Rao S, Galmarini S (2012) Evaluation of the meteorological forcing used for the Air Quality Model Evaluation International Initiative (AQMEII) air quality simulations. Atmos Environ., 53:15–37. doi:10.1016/j.atmosenv.2012.10.065

Questions and Answers

Questioner Name: Jordi Vila

Q: Would it be useful to extend the data treatment and classify it according to the PBL prototypes: convective, stable, morning transition and afternoon transition?
A: Yes, this would certainly be useful. Part of this classification is already done by looking at the different starting times of the radiosondes. However one could further classify the data set into stable, neutral and unstable cases. This would give more insight into the reasons why some models underestimate the PBL height even at noon. One problem with the current data set from Lindenberg is that it is too small to give a good statistics if additional separations are made. Therefore I will look into additional data sets from other locations.

Questioner Name: Golam Sarwar

Q: Published articles suggest air quality models have difficulty in predicting clouds accurately. This has influence on sulphate predictions. Any comments?
A: We used profiles of sulphate in PM2.5 to investigate the vertical distribution of atmospheric aerosols in AQMEII. We are well aware of the fact that sulphate

production is influenced by clouds and other meteorological parameters like radiation. Nevertheless we believe it is the most suitable variable that is available in the AQMEII data set to compare vertical profiles of aerosol components. Besides sulphate only PM2.5 is stored in the data set and this variable is even more sensitive to variations in chemistry, emissions (e.g. fire emissions were not considered by all groups) and meteorological conditions.

Chapter 94
Influence of Grid Resolution and Biomass Burning Emissions on Air Quality Simulations: A Sensitivity Study with the Modelling System COSMO-MUSCAT

Ralf Wolke, Wolfram Schroeder, Roland Schroedner, and Eberhard Renner

Abstract Model evaluation studies are essential for determining model performance as well as assessing model deficiencies, and are the focus of the Air Quality Model Evaluation International Initiative (AQMEII). The chemistry-transport model system COSMO-MUSCAT participates in this initiative. In this paper the robustness and variability of the model results against changes in the model setup are analyzed. Special focus is given to the formation of secondary particulate matter and the ability to reproduce unusually high levels of PM10 in Central Europe caused by long-range transported smoke of widespread agricultural burning and forest fires in western Russia. Seven different model configurations are investigated in this study. The COSMO-MUSCAT results are evaluated in comparison with ground-base measurements in Central Europe. The analysis is performed for two selected periods in April/ May and October 2006 which are characterized by elevated concentrations of PM. The model sensitivity is studied against changes in the used grid resolution, the meteorological forcing and the applied aerosol module. Possible reasons for differences in model results will be discussed.

Keywords Chemistry transport modelling • Meteorological forcing • Model assessment and verification • Biomass burning

94.1 Introduction

Health effects due to air pollution and the potential damage from climate change are probably today's most important environmental problems. Of particular interest is the simulation of the origin and fate of particular matter (PM). When chemical

R. Wolke (✉) • W. Schroeder • R. Schroedner • E. Renner
Leibniz Institute for Tropospheric Research (IfT), Permoserstrasse 15, 04303 Leipzig, Germany
e-mail: wolke@tropos.de

D.G. Steyn et al. (eds.), *Air Pollution Modeling and its Application XXII*,
NATO Science for Peace and Security Series C: Environmental Security,
DOI 10.1007/978-94-007-5577-2_94,

processes are taken into account, the uncertainty can become significant for secondary formed PM. The ability to model such complex formation processes are of direct relevance in air quality applications as well as climate modelling. Model evaluation studies are essential for determining model performance as well as assessing model deficiencies, and are the focus of the Air Quality Model Evaluation International Initiative (AQMEII). The chemistry-transport model system COSMO-MUSCAT participates in this initiative.

In this paper the robustness and variability of the model results against changes in the model setup are analyzed. Special focus is given to the formation of secondary particulate matter and the ability to reproduce unusually high levels of PM10 in Central Europe caused by long-range transported smoke of widespread agricultural burning and forest fires in western Russia. Seven different model configurations are investigated in this study. The COSMO-MUSCAT results are evaluated in comparison with ground-base measurements in Central Europe. The analysis is performed for two selected periods in April/ May 2006 and October 2006 which are characterized by elevated concentrations of PM. Both periods were characterized on the one hand, by longer episodes with stable high pressure and moderate winds from the east, and on the other hand, by lows with westerly winds. Additionally, the impact of biomass burning emissions from wildland fires on the particle distribution is investigated for both periods. Furthermore, the sensitivity of the results is studied against the used grid resolution and the meteorological forcing. Here, COSMO is applied with different horizontal grid sizes and, alternatively, forced by reanalysis data with finer resolution.

94.2 The Model System COSMO-MUSCAT

The modelling department of the IfT has developed the multiscale model system COSMO-MUSCAT [10]. It is qualified for process studies as well as the operational forecast of pollutants in local and regional areas [1]. The model system consists of two online-coupled codes. The operational forecast model COSMO is a non-hydrostatic and compressible meteorological model and solves the governing equations on the basis of a terrain-following grid [5]. Driven by the meteorological model, the chemistry transport model MUSCAT treats the atmospheric transport as well as chemical transformations for several gas phase species and particle populations. The transport processes include advection, turbulent diffusion, sedimentation, dry and wet deposition. The modelling system is used for several air quality applications [3, 7].

94.3 Model Setup

One aim of this study is to check the robustness and the sensitivity of the model results against changes in the model setup. COSMO-MUSCAT is applied on uniform horizontal grids with two different grid sizes (approximately 28 and 14 km). The 28 km results are extracted from the annual data of 2006, which are provided for the AQMEII database. Furthermore, a one-way nesting strategy for the COSMO-MUSCAT grids is used. In each of the regions N1 and N2, the meteorological code COSMO works on a uniform grid. The online-coupled MUSCAT uses different resolutions (coarse near the boundaries and finer in the inner regions). This corresponds to a two-way nesting for the chemistry-transport part. In our configuration, the N2 region of interest covers Central Europe. The N2 run is forced by finer meteorological reanalysis data of the DWD provided by COSMO simulations. All these simulations are performed using the mass-based approach for the description of aerosol processes in MUSCAT. Additionally, an extended version of the modal aerosol model M7 [9] is utilized to study the sensitivity of the results against a more detailed aerosol modeling.

94.4 Results and Discussion

Long-term simulations were performed for a spring and an autumn period to study the contribution of secondary aerosol and wild-land fires on the PM concentration in Central Europe, an area that features continental as well as maritime air masses. The influence of different meteorological conditions and model setups on the long-range transport as well as formation of secondary PM is analyzed. We choose the period from the 21st April to the 20th of May 2006 and the month of October 2006 for simulation. The first periods is characterized by unusually high levels of PM10 in the beginning of May caused by long-range transported smoke of widespread agricultural burning and forest fires in western Russia and the Ukraine [6]. Mixtures of pollutants were transported over the whole Europe causing severe degradation of air quality and reaching Great Britain around the 8th of May 2006. High concentrations of several pollutants were observed along the plume pass way. A frontal rain passing over Europe finished the episode.

The model performance was compared for different model configurations (Fig. 94.1). Meteorological processes mainly force the transport and transformation of PM. An appropriate description of these processes is of essential interest in chemistry transport modeling. COSMO-MUSCAT can reproduce the range of PM10 in the first decade of May but overestimates the measured values especially during the period with high concentrations. The finer resolved meteorological simulations calculate lower peaks in the PM concentrations. This different behavior

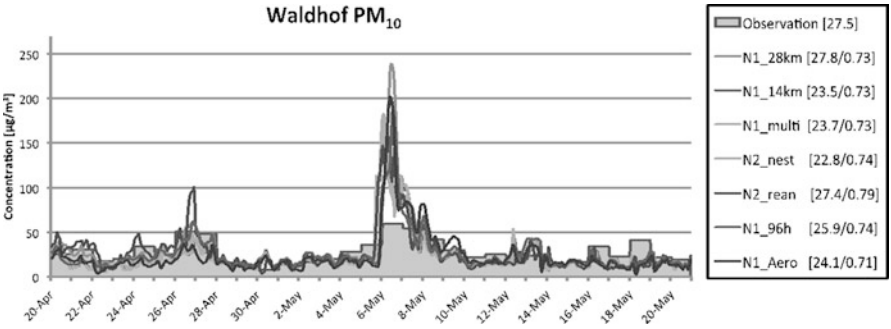

Fig. 94.1 Comparison of measurements and different model configurations for April/ May 2006 for Waldhof: Particulate matter. For quantifying, the mean values and correlation coefficients are given in the legend

seems to be caused mainly by the PBL height modeled by COSMO. The N2 nesting approach and the forcing by COSMO reanalysis data shows the best performance. The coarse horizontal resolution in the N1 (28 km) and N1_96h setups leads to an overestimation of the PM10 burden. Here the runs with 96-h simulation cycles show a slightly better performance than for the setup with shorter cycles. The temporal variations are also captured by all model setups. However The N2 approach tends to produce higher peaks in nitrate and ammonium during the April/May simulation. Significant differences between the N1 runs and the nested N2 approach are observed especially in the end of October

94.5 Conclusions and Outlook

The sensitivity of the simulation results against the grid resolution and the used meteorological forcing data was investigated. The results were compared with a comprehensive set of ground-based measurements at seven selected monitoring stations in Germany. This comparison was performed for concentrations of particulate matter as well as daily mean values of the corresponding compositions. Most of the model configurations are able to capture the PM10 measurements. But PM2.5 is underpredicted significantly in nearly all cases. The simulated ammonia, sulphate and nitrate concentrations show a moderate agreement. The most differences are observed between the mass-based and modal approach for PM10. However, there is a better agreement for PM2.5.

Acknowledgments The ZIH Dresden and the NIC Jülich supported this work. We gratefully acknowledge the AQMEII community and the DWD Offenbach for good cooperation.

References

1. Hinneburg D, Renner E, Wolke R (2009) Formation of secondary inorganic aerosols by power plant emissions exhausted through cooling towers in Saxony. Environ Sci Pollut Res 16:25–35
2. Karl M, Dorn H-P, Holland F, Koppmann R, Poppe D, Rupp L, Schaub A, Wahner A (2006) Product study of the reaction of OH radicals with isoprene in the atmosphere simulation chamber, SAPHIR. J Atmos Chem 55:167–187
3. Renner E, Wolke R (2010) Modelling the formation and atmospheric transport of secondary inorganic aerosols with special attention to regions with high ammonia emissions. Atmos Environ 44:1904–1912
4. Schaap M, van Loon M, ten Brink HM, Dentener FJ, Builtjes PJ (2004) Secondary inorganic aerosol simulations for Europe with special attention to nitrate. J Atmos Chem 4:857–874
5. Schättler U, Doms G, Schraff C (2009) A description of the nonhydrostatic regional COSMO-Model. Part I: Users guide. Deutscher Wetterdienst, Offenbach, 2008. Available from http://www.cosmo-model.org
6. Sofiev M, Vankevich R et al (2009) An operational system for the assimilation of satellite information on wild-land fires for the need so fair quality modelling and forecasting. Atmos Chem Phys Discuss 9:6483–6513
7. Stern R, Builtjes PJH et al (2008) A model intercomparison study focussing on episodes with elevated PM10 concentrations. Atmos Environ 42:4567–4588
8. Stockwell WR, Kirchner F, Kuhn M, Seefeld S (1997) A new mechanism for regional atmospheric chemistry modeling. J Geophys Res 102(D22):25847–25879
9. Vignati E, Wilson J, Stier P (2004) M7: an efficient size-resolved aerosol microphysics module for large-scale aerosol transport models. J Geophys Res 109:D22202. doi:10.1029/2003JD004485
10. Wolke R, Schröder W, Schrödner R, Renner E (2012) Influence of grid resolution and meteorological forcing on simulated European air quality: a sensitivity study with the modeling system COSMO–MUSCAT. Atmos Environ 53:110–130

Questions and Answers

Questioner Name: Golam Sarwar

Q: Most models underpredict sulfate compared to the observed data. Your study shows overprediction. Please elaborate the differences in your model (compared to other models) that may be producing more sulfate than other models.

A: In the applied RACM-MIM2 chemistry [2, 8], sulfuric acid is formed only by the reaction of SO_2 and OH. As model studies reveal, this approach underestimates sulfate levels in Europe especially in winter. Therefore, an additional oxidation pathway in the aqueous phase is parameterized as a first order reaction with a reaction constant depending on the relative humidity and cloud cover [4]. We believe that the meteorological forcing mainly causes the overprediction of sulfate in the annual run with 28 km horizontal grid size. Here the COSMO model generates too much humidity. This was not the case for other model setups. For a more detailed discussion we refer to Wolke et al. [10]. Note that such overprediction of sulfate was not assessed for COSMO-MUSCAT in previous model evaluation studies (e.g., [7]).

Chapter 95
Measurements and Modeling of the Wind Profile Up to 600 meters at a Flat Coastal Site

Ekaterina Batchvarova, Sven-Erik Gryning, Rogier Floors, Claire Vincent, Alfredo Peña, and Torben Mikkelsen

Abstract This study shows long-term ABL wind profile features by comparing long-range wind lidar measurements and the output from a mesoscale model. The study is based on 1-year pulsed lidar (Wind Cube 70) measurements of wind speed and direction from 100 to 600 m with vertical resolution of 50 m and time resolution of 10 min at a coastal site on the West coast of Denmark and WRF ARW (NCAR) simulations for the same period. The model evaluation is performed based on wind speed, wind direction, as well as statistical parameters of the Weibull distribution of the wind speed time series as function of height. It is found that (1) WRF is generally under predicting both the profiles of the measured wind speed, direction and power density, (2) the scatter of observations to model results of the wind speed does not change significantly with height between 100 and 600 m, and (3) the scale (A) and shape (k) parameters of the Weibull distribution above 100 m. The latter signifies that the model suggests a wider distribution in the wind speed compared to measurements.

Keywords Wind lidar • WRF model evaluation • Atmospheric boundary-layer • Wind profile • Weibull distribution of wind • Vertical profiles

E. Batchvarova (✉)
DTU Wind Energy, Risø Campus, Roskilde, Denmark

National Institute of Meteorology and Hydrology, Sofia, Bulgaria
e-mail: ekaterina.batchvarova@meteo.bg

S.-E. Gryning • R. Floors • C. Vincent • A. Peña • T. Mikkelsen
DTU Wind Energy, Risø Campus, Roskilde, Denmark

D.G. Steyn et al. (eds.), *Air Pollution Modeling and its Application XXII*,
NATO Science for Peace and Security Series C: Environmental Security,
DOI 10.1007/978-94-007-5577-2_95,

95.1 Site, Instrumentation and Modeling

The measurements were carried out at the Danish National Test Station of Wind Turbines at Høvsøre, which is located at the western coast of Jutland. Except for the presence of the North Sea to the west, the terrain is flat and homogeneous consisting of grass, various agricultural crops and a few shrubs. Wind speed is measured with cup anemometers at nominal heights of 10, 40, 60, 80, 100, 116.5 m and the wind direction with wind vanes at 10, 60 and 100 m. Data are also available from the 160 m top level at a light tower. For extended height measurements, a pulsed wind lidar (WLS70) has been operating near the meteorological mast between April 2010 and March 2011. The wind lidars Doppler shift are processed into 10-min. average quantities of wind speed and direction. The wind lidar measures from 100 m above the ground and every 50 m up till 1–2 km height dependent on the attainable 10-min averaged Carrier to Noise (CNR) ratio.

Wind profiles were predicted using the WRF ARW model version 3.2 [1]. Data for initial and boundary conditions come from Final Analyses (FNL, Global Final Analysis Data) of the National Center for Environmental Prediction (NCEP, USA) global model. The physical options of model setup include the Noah land surface scheme, the Thompson microphysics scheme and the MYNN PBL scheme. The WRF model calculates the meteorological parameters at 41 vertical levels from the surface to pressure level 100 hPa. Eight of these levels are within the height range of 600 m that is analyzed in this study. Model simulations were performed both in short term forecasts and long term analysis mode. The model is run in analysis mode. It uses the FNL global boundary conditions that are available every 6 h on a one times 1° grid. Two domains with a horizontal grid size of 18 and 6 km respectively are used. The simulations are started every 10 days at 12:00 and after a spin up of 24 h a time series of 10 min simulated meteorological forecast data from 25 to 264 h is generated.

95.2 Results

Figure 95.1(left) shows the profile of the mean wind speed for the period 23 April 2010 to 31 March 2011, based on simultaneous measurements at the meteorological mast and the wind lidar. Good agreement between the wind lidar measurements and the cup anemometer measurements at the overlap heights at 100 and 150/160 m can be observed. Near the ground agreement between the measurements and the WRF modeling analysis is good and above approximately 60 m the model under-predict the mean wind speed. For the wind direction it can be seen in Fig. 95.1 (right) that the WRF analysis produced a smaller wind directional turning than is actually observed.

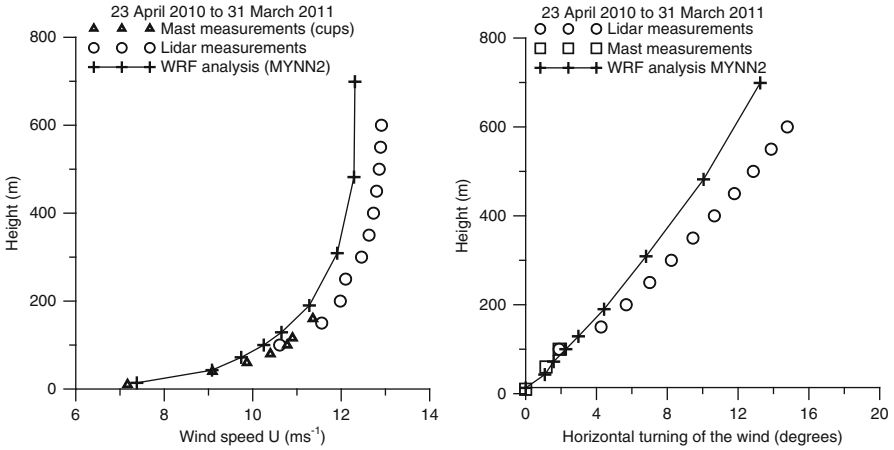

Fig. 95.1 Profiles of wind speed (*left panel*) and wind direction (*right panel*)

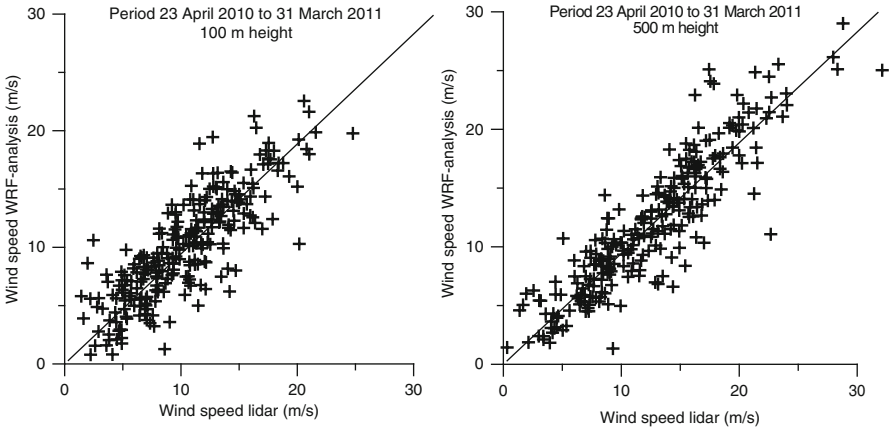

Fig. 95.2 Scatter plots of the measured and the simulated wind speed. Note that only every 60th data point is shown

A scatter plot between the measured and modeled wind speed are shown in Fig. 95.2. The standard error between observations and model values is 2.4 ms^{-1} at 100 m, increasing with height and reaches 2.7 ms^{-1} at 500 m height.

The shape parameter (A) parameter in the Weibull distribution is shown in Fig. 95.3 (left). It can be seen that the A parameter from the WRF simulations are smaller than observed. Also the shape parameter (k) parameter in the Weibull distribution that can be estimated from the WRF simulations is smaller than observed, Fig. 95.2 (right). As expected [2], the shape parameter has a maximum at about 100–200 m height.

Wind power density is an estimate of the effective power of the wind at a particular location. From Fig. 95.4 it can be seen that near the ground there is good

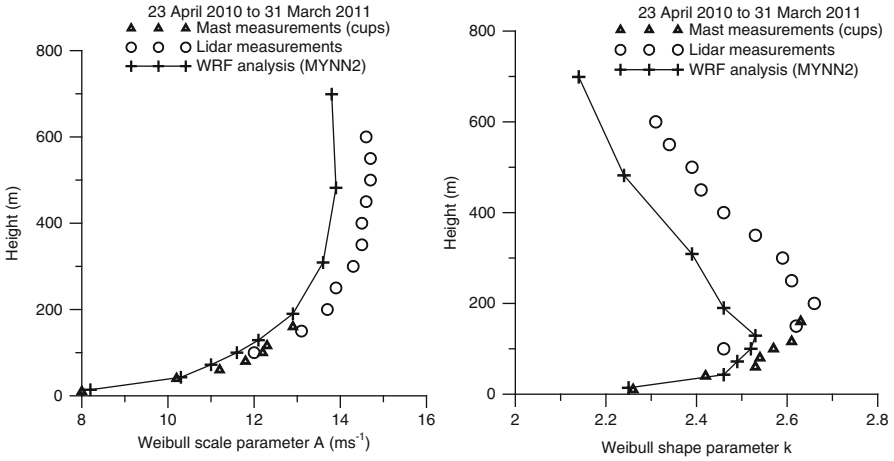

Fig. 95.3 Profiles of the scale (*A*, *left panel*) and shape (*k*, *right panel*) parameter in the Weibull distribution

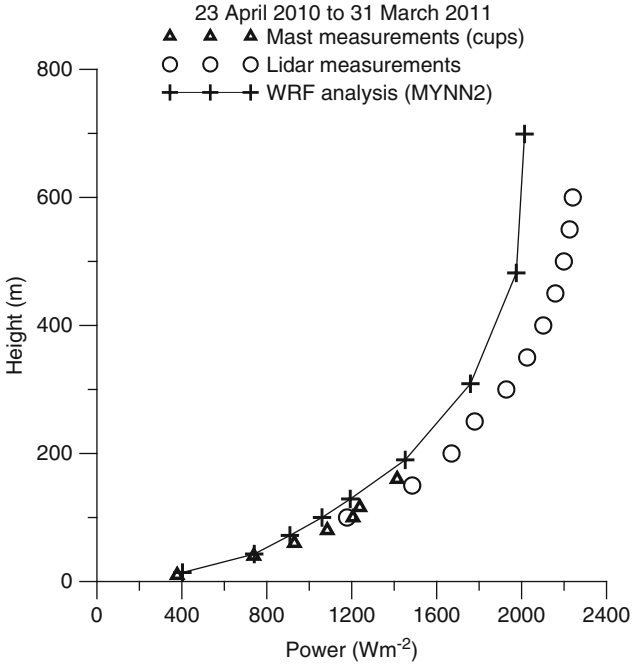

Fig. 95.4 Profiles of the power density modeled by WRF and predicted from measurements of the wind speed

agreement between the power density estimated from the measurements and the model simulations. Beyond 60 m it is found that the simulations underestimate the power density.

95.3 Concluding Remarks

In this study a full year of measurements of the wind profile performed at a coastal site has been analyzed and compared to a number of simulations carried out with the WRF model. In general the WRF model under predicts the wind speed, scale and shape parameters in the Weibull distribution of the long term wind velocity, and the wind power density that can be assessed from the model simulations.

Acknowledgments The study is supported by the Danish Research Agency Strategic Research Council (Sagsnr. 2104-08-0025). C.L. Vincent was supported by the Danish Council for Independent Research (case number 10-093196). The work is related to activities of Sven-Erik Gryning and Ekaterina Batchvarova within the ESSEM COST Actions ES1002 and ES0702.

References

1. Skamarock WC, Klemp JB, Dudhia J, Gill DO, Barker DM, Duda MG, Huang X-Y, Wang W, Powers JGA (2008) Description of the advanced research WRF Version 3, NCAR/TN-475 + STR, 113p
2. Wieringa J (1989) Shapes of annual frequency distributions of wind speed observed on high meteorological masts. Bound-Layer Meteorol 47:85–111

Chapter 96
Investigation, Using CMAQ, of Sensitivity of Air Quality Modelling to Input Ammonia Emissions

P. Sutton, C. Chemel, S. Griffiths, and R.S. Sokhi

Abstract A comparison of the results from two independent CMAQ modelling systems for the same UK 2003 scenario suggests the need for improvement to temporal profiles of the input emissions data used by atmospheric models.

Keywords CMAQ-model • NH3

96.1 Introduction

A recent model evaluation and intercomparison sponsored by the UK Environment Agency has compared the performance of several atmospheric modelling systems to model the same UK 2003 scenario [1]. Two of the participating modelling systems were based on the Community Multi-scale Air Quality modelling system (CMAQ). The two CMAQ modelling systems were setup and operated independently by the Joint Environmental Program (JEP) and the University of Hertfordshire (UH). The difference between these two modelling systems was relatively small; the main differences were:

1. The two modelling systems were based on different versions of CMAQ. The JEP system used CMAQ v4.7; the UH system used CMAQ v4.6.

P. Sutton (✉)
RWE npower, Windmill Hill Business Park, Whitehill Way, Swindon, SN5 6PB UK
e-mail: paul.sutton@rwenpower.com

C. Chemel • R.S. Sokhi
Centre for Atmospheric and Instrumentation Research, University of Hertfordshire, College Lane Campus, Hatfield, Herts, AL10 9AB, UK

S. Griffiths
E.ON New Build and Technology, Ratcliffe-on-Soar, Nottingham NG11 0EE, UK

D.G. Steyn et al. (eds.), *Air Pollution Modeling and its Application XXII*,
NATO Science for Peace and Security Series C: Environmental Security,
DOI 10.1007/978-94-007-5577-2_96,

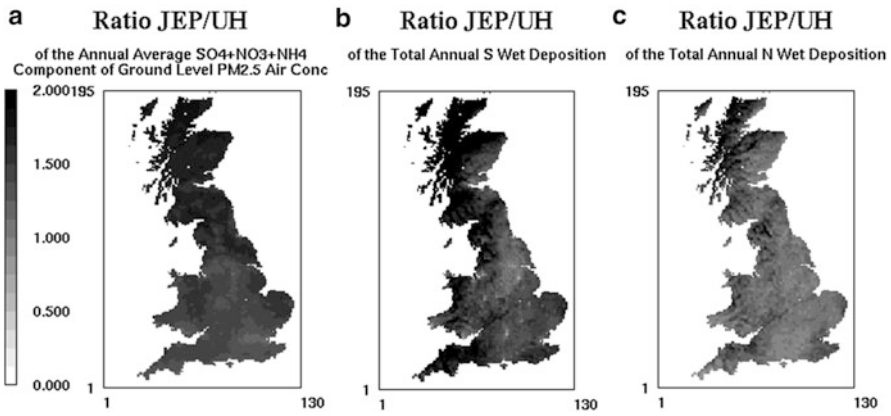

Fig. 96.1 Spatial plots over the UK mainland of the JEP/UH ratio for selected quantities of regulatory interest: (**a**) annual average $SO_4^{2-} + NO_3^- + NH_4^+$ component of ground level $PM_{2.5}$ air concentration, (**b**) total annual S wet deposition, (**c**) total annual N wet deposition

2. The two modelling systems used independently produced temporal profiles for the input emissions data. The total annual emissions at every spatial point on the modelled domain were the same for the two modelling systems.

Despite these apparently small differences, the two modelling systems produced significantly different results for the UK 2003 scenario. Figure 96.1 shows spatial plots over the UK mainland of the ratio of the JEP results to the UH results for selected quantities of regulatory interest. Figure 96.1a shows the ratio for the annual average $SO_4^{2-} + NO_3^- + NH_4^+$ component of ground level $PM_{2.5}$ air concentration. Figure 96.1b shows the ratio for the total annual sulphur (S) wet deposition. Figure 96.1c shows the ratio for the total annual nitrogen (N) wet deposition. All three plots show the ratio increases significantly above 1.0 in some regions of the UK, with values of over 2.0 being reached in North West Scotland.

Foley et al. [2] compared the results produced by CMAQ v4.6 and v4.7 for major air concentration and deposition species. This paper examined in detail the affects of the major scientific upgrades to CMAQ. Changes in the modelled results were found to be insignificant compared to those seen in Fig. 96.1. This suggests that it must be the differences in the temporal profiles for the input emissions data used by the two CMAQ modelling systems which is producing the differences in the results. The general need for improvements of temporal emission profiles is argued in Reis et al. [4]. Figure 96.2a shows a spatial plot over the UK mainland of the JEP/UH ratio for annual average NH_* ($NH_* \equiv NH_3 + NH_4^+$) ground level air concentration. As in the plots in Fig. 96.1, the ratio increases significantly above 1.0 in some regions of the UK, despite the fact that the two modelling systems used identical annual total NH_3 emissions. For comparison, Fig. 96.2b shows a spatial plot over the UK mainland of the JEP/UH ratio for annual average NO_* ($NO_* \equiv HNO_3 + NO_3^-$) ground level air concentration. The ratio is in the range

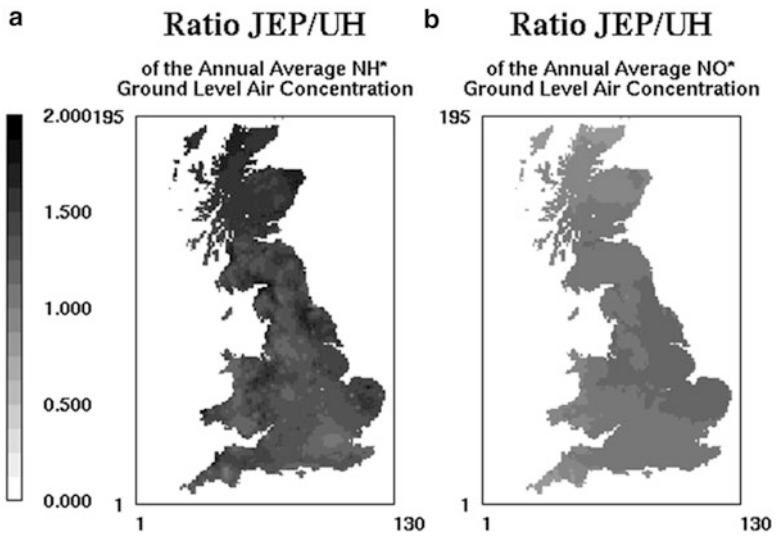

Fig. 96.2 Spatial plots over the UK mainland of the JEP/UH ratio for annual average ground level air concentration: (**a**) shows NH_* ($NH_* \equiv NH_3 + NH_4^+$), (**b**) shows NO_* ($NO_* \equiv HNO_3 + NO_3^-$)

$0.8 \rightarrow 1.2$ over the whole of the UK mainland, which is close to the value of 1.0 which would be expected if the two modelling systems were identical. Pinder et al. [3] found that modelled annual average NH_* ground level air concentration was sensitive to NH_3 emissions temporal profile used. This suggests that the differences in the NH_3 emissions temporal profiles used by the two CMAQ modelling systems may be a prime cause of the differences in the results produced by the two modelling systems. In particular, Pinder et al. [3] shows that the modelled NH_* ground level air concentration produced by a given input NH_3 emission rate varies significantly with the time of year; the modelled NH_* ground level air concentration produced by a given input NH_3 emission rate being significantly higher in the winter/autumn than in the spring/summer.

Figure 96.3 compares the input monthly NH_3 emissions, summed over the whole UK, used by the two modelling systems. The input monthly emissions data for the two modelling systems have significantly different distributions of the annual NH_3 emissions between the winter/autumn and spring/summer months. Using results from Pinder et al. [3], a calculation of the JEP/UH ratio for annual average NH_* ground level air concentration for the different input monthly NH_3 emissions data used by the two CMAQ modelling systems, was found to produce values similar to those shown in Fig. 96.2a.

Different NH_3 and NH_4^+ ground level air concentrations would be expected to result in significantly different HNO_3, NO_3^- and SO_4^{2-} ground level air concentrations and consequently significantly different S and N wet deposition produced by the two CMAQ modelling systems: the proportions of HNO_3 and

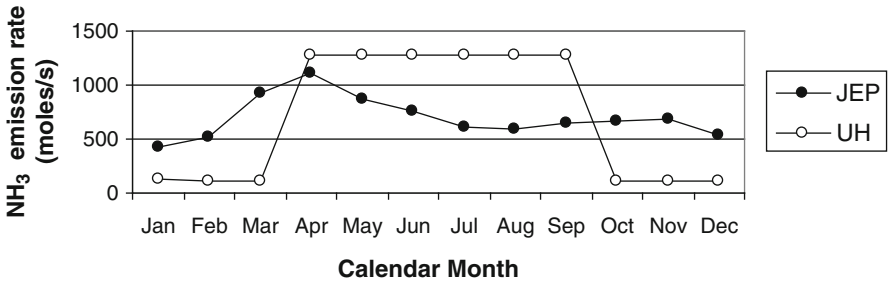

Fig. 96.3 Monthly UK mainland NH_3 emissions rates used by the two CMAQ modelling systems

NO_3^- that NO* air concentrations form depends on the NH_3 air concentration, and the oxidation rate of $SO_2 \rightarrow SO_4^{2-}$ depends on the acidity of liquid water in the atmosphere and therefore on NH_3 air concentration. So the different NH_3 emission temporal profiles used by the two CMAQ modelling systems could generally account for the differences in the results produced by the two systems, shown in Fig. 96.1.

96.2 Implications

1. This analysis suggests that a change in the within-year temporal profile of NH_3 emissions, for fixed annual total emissions, can significantly influence annual average ground level concentrations and deposition rates produced by the models.
2. Improved knowledge of within-year emission profiles, and use of such profiles within modelling systems, is therefore, important to improve the performance of modelling for policy and regulatory purposes.
3. There is a need to make exemplary emissions temporal patterns readily available to the modelling community.

Acknowledgments Part of this work has been supported by the Joint Environmental Programme, which is jointly funded by RWE npower, E.ON UK, Drax Power Ltd, Scottish & Southern Energy, EDF Energy, International Power, Eggborough Ltd and Scottish Power.

References

1. Chemel C, Sokhi RS, Dore AJ, Sutton P, Vincent KJ, Griffiths SJ, Hayman GD, Wright RD, Baggaley M, Hallsworth S, Prain HD, Fisher BEA (2011) Predictions of U.K. regulated power station contributions to regional air pollution and deposition: a model comparison exercise. J Air Waste Manag Assoc 61(11):1236–1245. doi:10.1080/10473289.2011.609756

2. Foley KM, Roselle SJ, Appel KW, Bhave PV, Pleim JE, Otte TL, Mathur R, Sarwar G, Young JO, Gilliam RC, Nolte CG, Kelly JT, Gilliland AB, Bash JO (2010) Incremental testing of the community multiscale air quality (CMAQ) modelling system version 4.7. Geosci Model Dev 3:205–226
3. Pinder RW, Adams PJ, Pandis SN, Gilliland AB (2006) Temporally resolved ammonia emission inventories: current estimates, evaluation tools and measurement needs. J Geophys Res 111:D16310. doi:10.1029/2005JD006603
4. Reis S, Ambelas-Skjoth C, Vieno M, Geels C, Steinle S, Lang M, Sutton MA (2011) Why time and space matters – arguments for the improvement of temporal emission profiles for atmospheric modeling of air pollutant emissions. In: MODSIM2011, 19th international congress on modelling and simulation, Perth, Australia, 11–16 Dec 2011. Canberra, Australia, Modelling and simulation society of Australia and New Zealand, 1817–1823

Chapter 97
A Comparison of Modeled Pollutant Profiles with MOZAIC Aircraft Measurements

Christian Hogrefe, Jim Szykman, Robert Gilliam, Jim Godowitch, Shawn Roselle, Jim Crawford, T. Plessel, Morgan Silverman, J.P. Cammas, A. Volz-Thomas, and S.T. Rao

Abstract In this study, we use measurements performed under the MOZAIC program to evaluate vertical profiles of meteorological parameters, CO, and ozone that were simulated for the year 2006 with several versions of the WRF/CMAQ modeling system. Model updates, including WRF nudging strategies, boundary conditions, lightning NO emissions, and vertical transport were found to affect the simulated profiles. MOZAIC descent/ascent pairs provide a unique dataset to investigate PBL structure and its representation in regional-scale models during afternoon and early evening hours. Other data sources (e.g. ozonesondes, field studies such as DISCOVER-AQ) can be used to complement MOZAIC measurements in evaluating upper air predictions by regional-scale models over various airsheds.

Keywords Model Evaluation • MOZAIC • CMAQ • AQMEII • Ozonesondes

C. Hogrefe (✉) • R. Gilliam • J. Godowitch • S. Roselle • S.T. Rao
U.S. Environmental Protection Agency, Research Triangle Park, Durham, NC, USA
e-mail: hogrefe.christian@epa.gov

J. Szykman
U.S. Environmental Protection c/o NASA Langley Research Center, Hampton, VA, USA

J. Crawford
NASA Langley Research Center, Hampton, VA, USA

T. Plessel
Lockheed Martin, EMVL, National Computing Center, Research Triangle Park, Durham, NC, USA

M. Silverman
Science Systems and Applications Inc, Hampton, VA, USA

J.P. Cammas
Université de Toulouse, Toulouse, France

Centre National de la Recherche Scientifique, Paris, France

A. Volz-Thomas
Forschungszentrum Jülich, Institut für Energie- und Klimaforschung 8, Jülich, Germany

D.G. Steyn et al. (eds.), *Air Pollution Modeling and its Application XXII*,
NATO Science for Peace and Security Series C: Environmental Security,
DOI 10.1007/978-94-007-5577-2_97,

97.1 Introduction

While it is well known that ozone concentrations aloft affect the magnitude and temporal evolution of ground-level ozone concentrations through vertical mixing and entrainment, most comparisons of air quality model predictions with ambient measurements utilize surface data only. In this study, we use aircraft measurements performed under the MOZAIC (Measurements of OZone, water vapor, carbon monoxide and nitrogen oxides by in-service AIrbusairCraft, http://mozaic.aero.obs-mip.fr/web/) program to evaluate vertical profiles of meteorological variables, CO, and ozone simulated for the year 2006 over North America. MOZAIC was started in 1993 as a joint effort involving European scientists, aircraft manufacturers, and airlines and consists of five long-haul aircraft equipped with instruments to measure meteorological variables and chemical species. More than 100 measured profiles were available at each of the following North American airports during 2006: Portland, Oregon (KPDX), Dallas/Fort Worth, Texas (KDFW), Atlanta, Georgia (KATL), and Philadelphia, Pennsylvania (KPHL).

97.2 Database and Methods

Most commercial aircrafts carrying MOZAIC instrumentation arrive from Europe at their North American destination during early to mid afternoon and depart for Europe during mid afternoon to early evening. For Portland, Dallas and Atlanta, inbound flights typically occur around 2–3 pm local time while outbound flights typically occur around 4–5 pm local time. The typical timing of the Philadelphia inbound and outbound flights (3–4 pm and 6–7 pm local time, respectively) allows the analysis of vertical profiles during the evening PBL transition period.

To assess the impact of recent updates to the WRF/CMAQ modeling system on model performance aloft, we compared observed MOZAIC profiles to the following four CMAQ simulations: CMAQ4.7.1-AQMEII,CMAQ4.7.1-Reference, CMAQ5.0-Beta, and CMAQ5.0-Final. The CMAQ4.7.1-AQMEII simulation was described in detail by Appel et al. [1]. The CMAQ4.7.1-Reference simulation was based on CMAQ4.7.1-AQMEII with slight updates to the emission inputs as well as updated boundary condition. It served as a reference case for the development cycle of CMAQ5.0. The CMAQ5.0-Beta simulation incorporated many of the science updates of the CMAQ5.0 release such as NO emissions from lightning and updated treatment of photolysis [2] but used the same meteorological and emission inputs as the CMAQ4.7.1-Reference case. The main changes from the CMAQ5.0-Beta to the CMAQ5.0-Final simulation were the introduction of an additional vertical layer near the ground, the use of a new nudging approach in the WRF simulations used to drive CMAQ, and an updated treatment of vertical advection in CMAQ. As described in Gilliam et al. [3], the new nudging approach incorporates observations from wind speed profiles above the boundary layer to improve the treatment of

overnight pollutant transport. The two WRF simulations are hereafter referred to as WRF_OLD and WRF_NEW. All simulations were performed for January—December 2006 over the continental U.S. at a horizontal grid spacing of 12 km with a model top at 50 mb. The first three simulations used 34 vertical layers with a ~40 m first layer height, while the last simulation used 35 vertical layers with a ~20 m first layer height.

MOZAIC observations and CMAQ simulations were matched using the Remote Sensing Information Gateway (RSIG). RSIG automatically aligns information from various spatial positions and temporal scales into a unified structure. Additional information can be found at http://www.epa.gov/rsig. Unless noted otherwise, the analysis of simulated and observed vertical profiles was performed by averaging over all individual profiles to create annual averages.

97.3 Results and Discussion

The differences in nudging strategies between the WRF_OLD and WRF_NEW simulations caused temperature differences of 0.5 C or less in the PBL and negligible differences above the boundary layer at all four airport locations considered in this study. Most of the temperature differences in the PBL were negative, i.e. the revised nudging strategy led to slightly cooler temperatures. Wind speed values simulated by WRF_NEW are higher by about 0.5 m/s throughout the PBL at all airports compared to WRF_OLD. Both the WRF_OLD and WRF_NEW simulations tend to over predict wind speeds observed by MOZAIC aircraft near the ground and under predict wind speeds observed above ~1.5 km.

Analysis of simulated and MOZAIC-measured CO profiles showed that updated boundary conditions had the largest impact on simulated CO profiles. The CMAQ4.7.1-AQMEII simulations utilizing the boundary conditions derived from GEMS [4] showed closer agreement with observations above the PBL during all seasons at all airports compared to all the other CMAQ simulations that used boundary conditions derived from GEOS-Chem. The better performance of CMAQ using the GEMS-based boundary conditions for CO likely reflects the use of CO data assimilation by GEMS.

Results for ozone show that updated boundary conditions, the updated treatment of photolysis and introduction of lightning NO emissions and the updated treatment of vertical advection, as well as updated meteorological fields, all had a pronounced impact on simulated mid- to upper level ozone, while the impact of these updates tends to be smaller for the lowest 2.5 km. Agreement with observed MOZAIC profiles varied between seasons, different airports and model versions. One common feature during spring and summer at all the airports was that while all the simulations overestimated ozone above 8 km, the overestimation was least pronounced for the CMAQ5.0-Final simulation that utilized an updated vertical advection scheme and the WRF_NEW meteorological fields [2]. The over prediction of ozone above 8 km was also present when comparing CMAQ simulations to ozonesonde

observations at Trinidad Head and Wallops Island during August 2006, though CMAQ5.0-Final was not always the simulation showing closest agreement with observed ozonesonde profiles. Note that in addition to the spatial mismatch between the location of MOZAIC profiles and ozonesonde observations, there also is a temporal mismatch since MOZAIC flights and ozonesonde launches typically do not occur on the same date and at the same time. Analysis of model-to-MOZAIC differences for individual flights showed that model performance in the lower and mid-troposphere is more variable during summer than winter, likely due to more active photochemistry and stronger convective activity.

As mentioned above, the typical timing of the Philadelphia inbound and outbound flights (3–4 pm and 6–7 pm local time, respectively) enables the analysis of vertical profiles during the evening PBL transition period. When computing differences between these ascents and descents, it was found that the MOZAIC observations often show an increase of O_3 and CO concentrations between 4 and 7 pm for altitudes between ~1,000 and ~2,500 m; this effect is not captured by any of the model simulations. Additional analyses using longer time periods, back trajectories and complementary measurements from other platforms are needed to determine the physical and chemical processes causing the observed increases and the reason this phenomenon is not captured by these model simulation. Examples of such additional datasets of interest are the NASA P3 aircraft spirals performed over Maryland during the DISCOVER-AQ campaign in July 2011.

Acknowledgments and Disclaimer Although this work has been reviewed and approved for publication by the U.S. Environmental Protection Agency, it does not reflect the views and policies of the agency. The authors acknowledge the strong support of the European Commission, Airbus, and the Airlines (Lufthansa, Austrian, Air France) who carry free of charge the MOZAIC equipment and perform the maintenance since 1994. MOZAIC is presently funded by INSU-CNRS (France), Meteo-France, and Forschungszentrum (FZJ, Jülich, Germany). The MOZAIC data base is supported by ETHER (CNES and INSU-CNRS).

References

1. Appel KW et al (2012) Examination of the community multiscale air quality (CMAQ) model performance over the North American and European domains. Atmos Environ 53:142–155
2. Pleim J et al (2011) Overview of new features in CMAQv5.0, presentation at the 2011 CMAS conference, October 2011, Chapel Hill, NC. Available online at http://www.cmascenter.org/conference/2011/slides/pleim_overview_new_2011.pptx
3. Gilliam RC et al (2012) Improving the horizontal transport in the lower troposphere with four dimensional data assimilation. Atmos Environ 53:186–201
4. Schere K et al (2012) Trace gas/aerosol concentrations and their impacts on continental-scale AQMEII modelling sub-regions. Atmos Environ 53:38–50

Chapter 98
Validation of Small Scale Prognostic Air Pollution Modeling System in Highly Complex Terrain

Primož Mlakar, Boštjan Grašič, and Marija Zlata Božnar

Abstract In some areas of Slovenia air pollution is still a major problem due to industrial sources, traffic, local domestic heating and complex topography. PM10 pollution is a severe problem as there are many contributors such as industry, domestic heating, traffic and other. PM10 air pollution is a problem in several Slovene cities and industrial regions. In the paper a national research project with the title "Prognostic and diagnostic integrated small scale air pollution modeling system« is described. Such modeling system can significantly contribute to proper understanding of the air pollution in smaller areas with very complex topography. As an example for system development and validation the industrial region Zasavje was chosen which is characterized by highly complex terrain that makes the problem very difficult.

Keywords Lagrangian particle air pollution dispersion model • Validation • Complex terrain • On-line diagnostic and prognostic system • WRF • Short-term forecast • Topographic complexity hlTc

98.1 Introduction and Description

Zasavje region is placed in central part of Slovenia and has severe problems with PM10 air pollution. Zasavje is comprised of Sava river canyon with surrounding very high hills with extremely steep slopes and three valleys perpendicular to

P. Mlakar (✉) • B. Grašič • M.Z. Božnar
MEIS d.o.o, Mali Vrh pri Šmarju 78, SI-1293 Šmarje - Sap, Slovenia
e-mail: primoz.mlakar@meis.si; bostjan.grasic@meis.si; marija.zlata.boznar@meis.si

D.G. Steyn et al. (eds.), *Air Pollution Modeling and its Application XXII*,
NATO Science for Peace and Security Series C: Environmental Security,
DOI 10.1007/978-94-007-5577-2_98,

the canyon, each of them forming almost a basin with a narrow "bottle neck" type connection to the canyon. This colorful topography is hosting three towns, many villages and several industrial facilities from cement to chemical plants, glass factory and thermal power plant all of them contributing to the air pollution which is clearly higher than the limit values in the last decade. These problems are partially regulated by European directive of Integrated Pollution Prevention and Control (IPPC) which requires among other that industrial source's influence to the ambient air is modeled once to obtain the IPPC permit. The future European directives that are now in preparation phase also emphasize the use of air pollution models in on-line mode for informing local community as the state-of-the-art science is enabling this already [5].

In Zasavje region two air quality monitoring networks are operating with several stations measuring basic meteorological and air pollution parameters. Major industrial facilities are placed in the canyon, one of them having 360 m stack. Industrial stacks emissions are perfect case for validation, but only in the cases when and where domestic heating, traffic and other air pollution sources do not interfere [3]. Lagrangian particle model SPRAY (from Arianet srl, Milano) based air pollution modeling system that works in on-line diagnostic and prognostic mode and covers air pollution from several industrial and other sources in the region over highly complex terrain is implemented [6]. In diagnostic mode it is feed with diagnostic meteorological fields produced by SurfPro and Swift [2] using data from several ground level meteorological stations from the valleys and from the hills and in addition profile data produced by implementation of WRF in fine resolution over Slovenia [1]. In prognostic mode also SurfPro and Swift are used as predecessors, but feed only with prognostic data from WRF and this is the point where we are at the edge due to extremely complex topography with the complexity length scale of an $\mathbf{hlTc} = (\mathbf{0.4\ km}, \mathbf{1.5\ km})$ [1]. Presently five industrial sources emissions, domestic heating and traffic are taken into account; all of them are modeled with SPRAY [4].

98.2 Results and Conclusions

For analyze of the modeling system one situation on the 7th of November 2011 has been selected because Thermal power plant Trbovlje (TPPT) has been re-started which caused high emissions of SO2 due to the fact that during the start of TPPT the desulphurization plant is not yet fully operational.

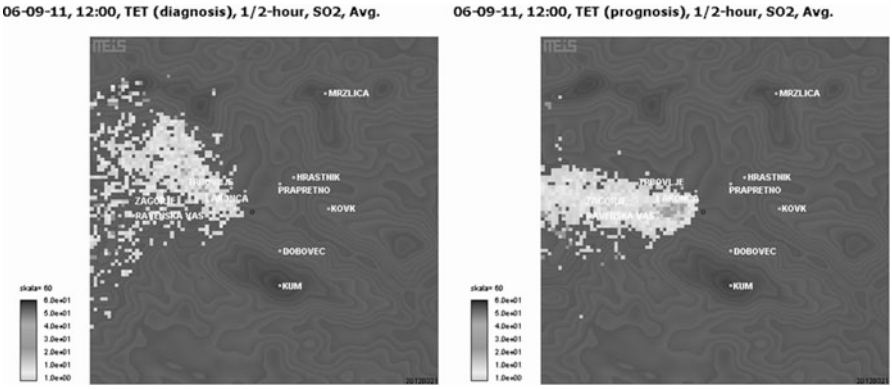

Fig. 98.1 Comparison of diagnostic (*left*) and prognostic (*right*) 2D ground concentrations of SO2 in Zasavje region when peak SO2 concentration was measured on Dobovec station

This situation is presented on the Fig. 98.1 where diagnostic and prognostic ground SO2 concentrations are compared for the same time interval after maximum SO2 concentration has been measured on the Ravenska vas air quality measuring station. Figure 98.2 shows comparison between measured and modeled (diagnostic and prognostic) SO2 ground concentrations. Several other cases detail analysis of results of validation of air pollution diagnosis compared to measured values show that the plume rise is too high. Modeled plume rise is higher than real because "nominal" emission parameters were used in simulation. In reality during the startup of TPPT temperature of emission gases from stack is colder than "nominal" temperature. On the other hand this too high plume rise has been compensated by too strong winds in results of prognosis which show much better results. This conclusion clearly shows that "nominal" emission values are not sufficient enough for this kind of on-line modeling systems because air pollution peaks appear mostly at startups. To improve results in the future real emissions should be used. The modeling system despite of the described problems is performing satisfactory and can be a very good starting tool for understanding of daily mechanisms of the area air pollution. Good understanding of the mechanisms of the air pollution is essential platform for effective air pollution reduction measures.

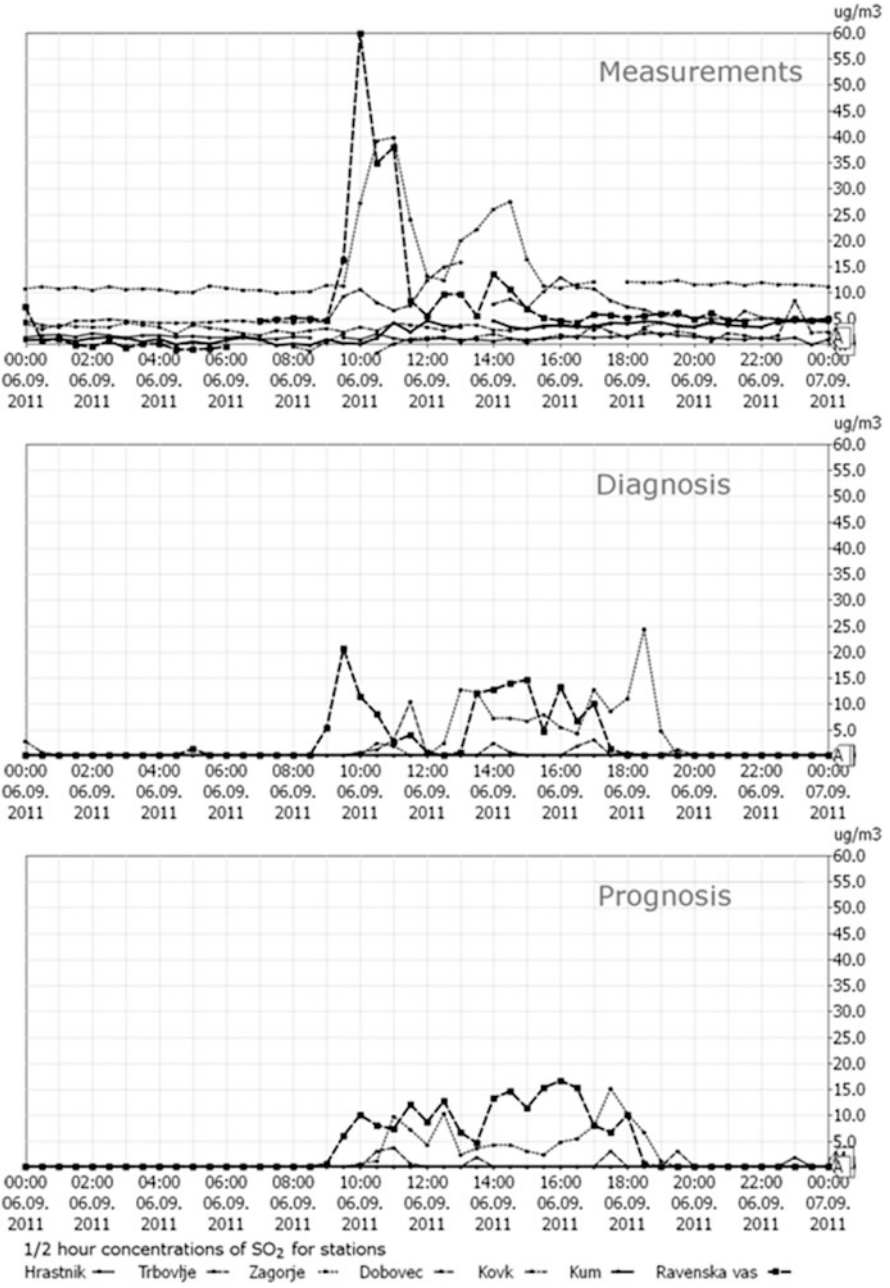

Fig. 98.2 Comparison between measured (*upper*), diagnostic (*middle*) and prognostic SO2 concentrations on locations of several automatic air quality measuring stations in Zasavje region. One color represents one location on all three graphs

Acknowledgements The study was partially financed by the Slovenian Research Agency, Project No. L1-2082 and Project No. L1-4154 (A).

References

1. Božnar MZ, Mlakar P, Grašič B (2011) Short-term fine resolution WRF forecast data validation in complex terrain in Slovenia. In: HARMO 14: Proceedings of the 14th international conference on harmonisation within atmospheric dispersion modelling for regulatory purposes, 2–6 Oct 2011, Kos Island, University of Environmental Technology Laboratory, Department of Mechanical Engineering, University of West Macedonia, Greece, pp 326–330
2. Desiato F, Finardi S, Brusasca G, Morselli MG (1998) TRANSALP 1989 experimental campaign – Part I: Simulation of 3-D flow with diagnostic wind field models. Atmos Environ 32(7):1141–1156
3. Grašič B, Božnar MZ, Mlakar P (2007) Re-evaluation of the Lagrangian particle modelling system on an experimental campaign in complex terrain. Il Nuovo Cimento C 30(6):557–575
4. Grašič B, Mlakar P, Božnar MZ, Vrbinc S (2011) Domestic heating sources identification in complex terrain rural area by local scale diagnostic modeling system. In: HARMO 14: Proceedings of the 14th international conference on harmonisation within atmospheric dispersion modelling for regulatory purposes, 2–6 Oct 2011, Kos Island, University of Environmental Technology Laboratory, Department of Mechanical Engineering, University of West Macedonia, Greece, pp 647–651
5. Mlakar P, Božnar MZ, Grašič B, Tinarelli G (2011) Zasavje canyon regional on-line air pollution modeling system in highly complex terrain as a support to EU directives. In: HARMO 14: Proceedings of the 14th international conference on harmonisation within atmospheric dispersion modelling for regulatory purposes, 2–6 Oct 2011, Kos Island, University of Environmental Technology Laboratory, Department of Mechanical Engineering, University of West Macedonia, Greece, pp 187–191
6. Tinarelli G, Anfossi D, Bider M, Ferrero E, Castelli ST (2000) A new high performance version of the Lagrangian particle dispersion model SPRAY, some case studies. Nato Chal M 23A:499–508

Chapter 99
Study of the Impact of Low vs. High Resolution Meteorology on Air Quality Simulations Using the MINNI Model Over Italy

Massimo D'Isidoro, Mihaela Mircea, Lina Vitali, Irene Cionni, Gino Briganti, Andrea Cappelletti, Sandro Finardi, Giandomenico Pace, Luisella Ciancarella, Giuseppe Cremona, Antonio Piersanti, Gaia Righini, and Gabriele Zanini

Abstract Modelling air quality requires the description of a large number of processes interacting each other. In order to properly model concentrations of atmospheric pollutants it is crucial to have a realistic reproduction of meteorological parameters, which can be critical in areas presenting a complex orography like the Italian peninsula. This work shows an analysis of the results obtained with the national model MINNI at two different horizontal resolutions (20 and 4 km), for a whole year over Italy. Comparisons between modelled and observed temperature and pollutants concentrations are carried out. The prediction of temperature is improved with the increase of model spatial resolution, as it is for pollutants like NO_2 and CO, while the improvement is not always evident for O_3 concentrations. Results are discussed providing an interpretation of the observed features.

Keywords Air quality modelling • High resolution • Italy • MINNI

M. D'Isidoro (✉) • M. Mircea • L. Vitali • I. Cionni • L. Ciancarella • G. Cremona • A. Piersanti G. Righini • G. Zanini
ENEA – Technical Unit Models, Methods and Technologies for the Environmental Assessment, Bologna Research Centre, Via Martiri di Monte Sole 4, 40129 Bologna, Italy
e-mail: massimo.disidoro@enea.it

G. Briganti • A. Cappelletti
ENEA – Technical Unit Models, Methods and Technologies for the Environmental Assessment, Pisa Territorial Office, Pisa, Italy

S. Finardi
Arianet s.r.l., via Gilino 9, 20128 Milan, Italy

G. Pace
ENEA – Technical Unit Environmental and Energy Modeling, Casaccia Research Centre, Rome, Italy

D.G. Steyn et al. (eds.), *Air Pollution Modeling and its Application XXII*,
NATO Science for Peace and Security Series C: Environmental Security,
DOI 10.1007/978-94-007-5577-2_99,

99.1 Introduction

Atmospheric composition modelling requires the description of a large number of processes for describing meteorological conditions and chemical transformations of pollutants. Emitted and transported pollutants are subjected to transformations, enhanced by sunlight (photochemistry), and removal processes (dry and wet deposition), which are closely and non-linearly interlaced with meteorological quantities. Therefore, a good description of meteorology is important to succeed in air quality forecasts. This is supposed to be even more relevant when complex morphology occurs, involving mesoscale features which make local meteorological conditions important. This work shows the effects of improved resolution on a meteorological parameter (temperature) and on some pollutants concentrations (O_3, NO_2 and CO) as given by the Italian national model MINNI (***M****odello* ***I****ntegrato* ***N****azionale a supporto della* ***N****egoziazione* ***I****nternazionale sui temidell'Inquinamento Atmosferico*-National Integrated Model to support the international negotiation on atmospheric pollution, [6]).

99.2 Experimental Setup and Results

Numerical simulations are performed by means of the atmospheric modelling system (AMS) of MINNI project [4]. The main components of AMS are the meteorological model (RAMS) [2] for simulating the meteorological conditions, the Emission Manager (EMMA) for apportioning emission data from the inventories to grid cells and the air quality model (FARM) for simulating the atmospheric chemistry and transport [5]. The chain is completed by pre- and post-processors interfacing the different modules; in particular, the diagnostic meteorological processor SURF*PRO* is used to prepare input meteorological fields for FARM starting from RAMS outputs.

Yearly simulations were carried out for 2005 over Italy at 20 and 4 km horizontal resolution, using the national emission inventory [3] and EMEP emission inventory for the other countries included in the computational domain. ECMWF (European Centre for Medium-Range Weather Forecasts) fields are used as boundary conditions for meteorology within RAMS for the 20 km resolution run. Then, meteorological fields at 4 km resolution are downscaled from the low resolution fields using LAPS [1] by means of WMO surface observations retrieved from ECMWF archives. Concentration fields from EMEP model are adopted for air quality simulations with FARM. Modelling domains (not shown here) comprise the whole Italy at 20 km and northern Italy at 4 km horizontal resolution, the latter being nested inside the former domain. The study has been limited to the northern part of the Italian territory, where independent meteorological surface observations were available for comparison with modelled fields.

Table 99.1 Air quality monitoring stations selected for the study

Site	h(m)	Type	Observed spec.	Site	h(m)	Type	Observed spec.
Bormio	1,230	backgr. urban	O_3, NO_2, CO	Piacenza	59	backgr. urban	O_3, CO
Milano – Lambro	128	backgr. suburban	O_3, NO_2	Reggio Emilia	46	backgr. urban	O_3, NO_2, CO
Trezzod' Adda	205	backgr. suburban	O_3, NO_2, CO	Modena	48	backgr. urban	O_3, NO_2, CO
Varese	421	backgr. suburban	O_3, CO	S. P. Capofiume	4	backgr. rural	O_3
Crema	75	backgr. urban	O_3, NO_2, CO	Ravenna	1	backgr. urban	O_3, CO
Brescia	123	backgr. suburban	O_3, NO_2, CO	Forlì	28	backgr. urban	O_3, CO
Tarvisio	740	backgr. suburban	O_3	Cossato	274	backgr. urban	O_3, NO_2, CO
Udine	92	backgr. rural	O_3, NO_2	Torino – Mandria	338	backgr. rural	O_3, NO_2, CO
M.teS. Pantaleone	67	backgr. suburban	O_3, NO_2, CO	Torino – Lingotto	242	backgr. urban	O_3, NO_2, CO

In order to perform the comparison between modelled and observed data, 18 air quality background monitoring stations, listed in Table 99.1 together with their height (a.s.l.) and the available pollutants, were selected from the BRACE national database (www.brace.sinanet.apat.it/web/struttura.html). Sites locations are showed in Fig. 99.1. Meteorological data were collected at same sites of air quality data. For three air quality stations, surrounding meteorological sites have been used. Hourly observed and simulated temperature (T), mass concentrations of CO, NO_2 and O_3 for whole year 2005 (only period June–August, JJA, was used for O_3) were compared. Aiming to assess if an improvement in meteorology corresponds to an improvement in air quality simulations, only five stations (black ellipses in Fig. 99.1) for which T shows the stronger enhancement in the performance indexes are shown hereafter.

The model's skill was evaluated in terms of correlation and Root Mean Square Error (RMSE). The increase of horizontal resolution from 20 to 4 km causes a general improvement of correlation and RMSE for Tat all locations (not shown here). At the five stations with the stronger enhancement in statistical scores for T (Varese, Brescia, Udine, Monte San Pantaleone and Piacenza), different results, depicted in Fig. 99.2, can be observed for the three considered pollutants: for CO, which is mainly a primary pollutant, the statistical indexes definitely improve at high resolution, with Varese showing smaller differences; for NO_2, both primary and secondary pollutant, correlation is improved(even strongly: Monte San Pantaleone passes from negative to positive correlation) with the exception of Varese, while RMSE experiences a worsening at Udine and Monte San Pantaleone and an

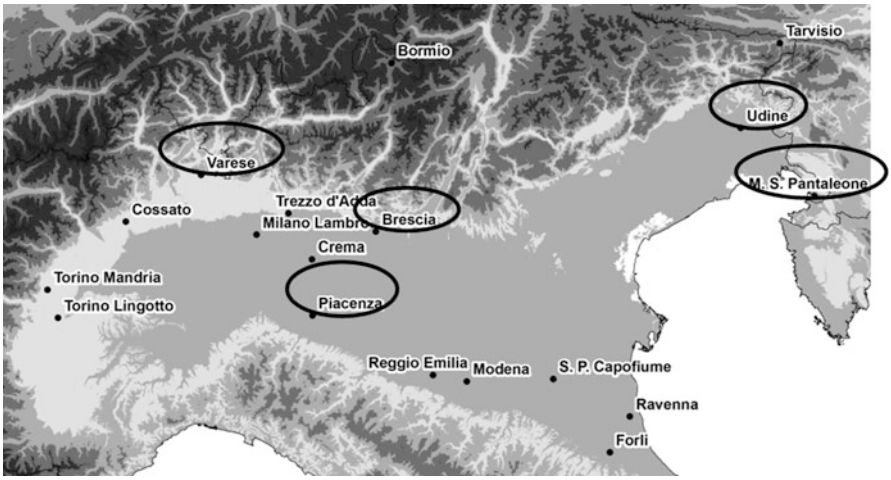

Fig. 99.1 Northern Italy area with the 18 air quality background monitoring stations selected from the BRACE national database. *Black ellipses* indicate locations with better improvement in T indexes passing from 20 to 4 km horizontal resolution

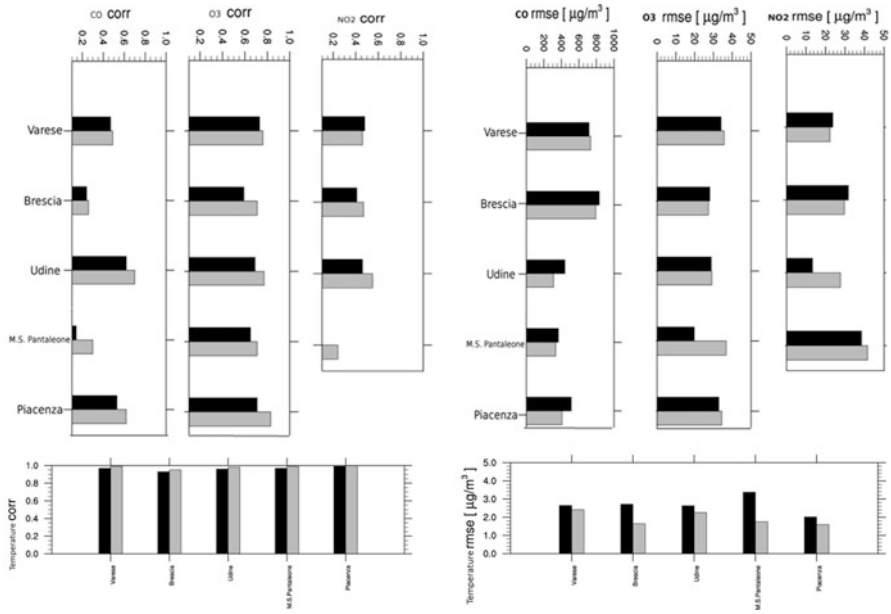

Fig. 99.2 Correlation (*left panel*) and RMSE (*right panel*) at the five selected monitoring sites for T (*bottom*) and CO, O_3 and NO_2 (*top*), respectively. *Black bars* refer to the 20 km resolution simulation; *gray bars* to the 4 km one. NO_2 measurements at Piacenza not available. NO_2 correlation at Monte San Pantaleone is negative for low resolution run. O_3 analysis has been restricted to JJA period

improvement at Varese and Brescia; for O_3, a secondary pollutant, the correlation (only period JJA period is considered) is improved at all the five selected locations, while RMSE remains unchanged, with a worsening at Monte San Pantaleone.

99.3 Conclusions

This work investigates the impact of simulations with high spatial resolution on meteorological and air quality parameters. The study covered the whole year 2005 over Italy by means of the atmospheric modelling system of the MINNI project at 20 and 4 km horizontal resolutions. Statistical indexes such as RMSE and correlation have been computed at 18 monitoring sites located over northern Italy for T, CO, NO_2 and O_3. We found that the increase of horizontal grid resolution from 20 to 4 km determines an improvement of RMSE and correlation for T. At the stations where the stronger temperature statistical Indexes changes are observed, an improvement in air quality correlation index is generally found, whereas the improvement of RMSE is negligible or absent in some cases. In particular, CO definitely shows an improvement in correlation and RMSE; the correlations of NO_2 and O_3 also improve, while RMSE remains unchanged for O_3 and shows a worsening at two sites for NO_2. The differences observed in the statistical scores behaviour for the three gases may be partly explained by the fact that CO is a primary pollutant, less affected by the photochemical processes, while NO_2 is primary and partly secondary but it is also strongly involved in the production of O_3 which is a secondary pollutant. The photochemistry is strongly non linear and only partially governed by temperature. Further investigations will be carried out, extending the statistical analysis to other meteorological parameters such as wind and humidity.

Acknowledgments The MINNI project has been funded by the Italian Ministry for the Environment, the Territory and the Sea and is carried out by ENEA. The authors want to thank also the local environmental agencies ARPA Friuli Venezia Giulia, ARPA Lombardia and ARPA Piemonte which provided meteorological observations. Meteorological data from Emilia Romagna region have been collected from the public database *Dexter* provided by the Emilia Romagna's Idro-Meteorological service ARPA-SIM (http://www.arpa.emr.it/sim/?osservazioni_e_dati/dexter).

References

1. Albers SC, McGinley JA, Birkenheuer DL, Smart JR (1996) The local analysis and prediction system (LAPS): analyses of clouds, precipitation, and temperature. Weather Forecast 11(3):273–287
2. Cotton WR, Pielke RA, Walko RL, Liston GE, Tremback CJ, Jiang H, McAnelly RL, Harrington JY, Nicholls ME, Carrio GG, McFadden JP (2003) RAMS 2001: current status and future directions. Meteorol Atmos Phys 82:5–29
3. ISPRA (2010) http://www.sinanet.isprambiente.it/it/inventaria/disaggregazione_prov2005/

4. Mircea M, Briganti G, Cappelletti A, Vitali L, Pace G, D'Isidoro M, Righini G, Piersanti A, Cremona G, Cionni I, Radice P, Silibello C, Finardi S, Calori G, Ciancarella L, Zanini G (2011) Ozone simulations with atmospheric modelling system of Minni project: a multi-year evaluation over Italy. In: Bartzis J, Syrakos A, Andronopoulos S (eds) The 14th international conference on harmonization within atmospheric dispersion modelling for regulatory purposes, Kos, Greece, pp 52–56
5. Silibello C, Calori G, Brusasca G, Giudici A, Angelino E, Fossati G, Peroni E, Buganza E (2008) Modelling of PM10 concentrations over Milano urban area using two aerosol modules. Environ Modell Softw 23:333–343
6. Zanini G, Pignatelli T, Monforti F, Vialetto G, Vitali L, Brusasca G, Calori G, Finardi S, Radice P, Silibello C (2005) The MINNI Project: an integrated assessment modelling system for policy making. MODSIM 2005 international congress on modelling and simulation. Modelling and Simulation Society of Australia and New Zealand, 2005–2011. ISBN: 0-9758400-2-9

Chapter 100
Scale-Dependent and Seasonal Performance of SILAM Model in Estonia

Riinu Ots, Ardi Loot, and Marko Kaasik

Abstract The SILAM model is running in Finnish Meteorological Institute (FMI) for European air quality forecasts (http://silam.fmi.fi). The 7 km resolution of both TNO-MACC emission grid and Nordic model domain is too coarse for urban and industrial areas. The Estonian modelling domain, operated jointly by the University of Tartu and Estonian Meteorological and Hydrological Institute (http://meteo.physic.ut.ee/silam, resolution 3.3 km) includes the Baltic countries and southern Finland. In this study the database of pollution sources on the territory of Estonia is refined and performance of SILAM with the new database is studied. The new database presents better spatial distribution, differences in yearly emission budgets should be looked into in further studies. Average concentrations of NO_x, SO_2 and particulate matter are reproduced rather well, NO_x underestimated slightly and particulate matter significantly. The new database shows an improvement in hourly and daily correlations, especially for urban stations.

Keywords Air quality forecasts • Model evaluation • Emissions

100.1 Emissions and Model Setup

This study validates air quality forecasts made with SILAM dispersion model (http://silam.fmi.fi), using two different emission databases. Firstly with TNO-MACC emissions (7 km), secondly with a newly composed emission database. Data for the new database was provided by Estonian Centre of Environmental Research and it only concerns the territory of Estonia. All emissions outside Estonia

R. Ots (✉) • A. Loot • M. Kaasik
Institute of Physics, University of Tartu, Tartu, Estonia
e-mail: riinu.ots@ut.ee; marko.kaasik@ut.ee

D.G. Steyn et al. (eds.), *Air Pollution Modeling and its Application XXII*,
NATO Science for Peace and Security Series C: Environmental Security,
DOI 10.1007/978-94-007-5577-2_100,

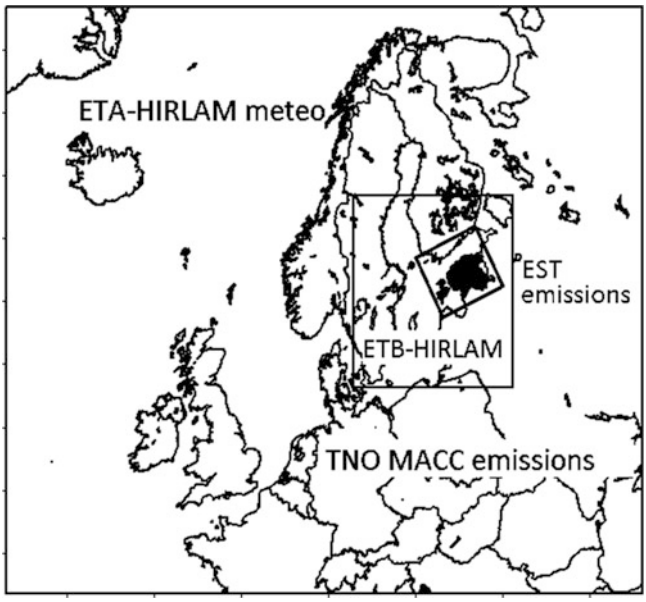

Fig. 100.1 Estonian (*EST*) modelling domain within surrounding HIRLAM meteorological field domains. TNO-MACC emissions are applied outside the borders of Estonia

still originate from TNO-MACC database. The new (further referred EST)emission database includes over 2,000 industrial stacks and other point sources, 5,000 km of streets and roads and domestic heating, based on questionnaire study [1], upscaled for entire country [2]. Emission grid resolution is 0.5 km in urban and 1 km in rural areas.

The SILAM 5.1 applied for these runs, includes formation of secondary aerosol from inorganic gaseous precursors, but no aerosol dynamics (condensation growth, coagulation etc.). Emissions of sea salt aerosol are included. Details see [3].

This study uses two meteodrivers – HIRLAM model run with two different resolutions (ETB-HIRLAM 3.3 km and ETA-HIRLAM 11 km – see Fig. 100.1) in the Estonian Meteorological and Hydrological Institute. 11 km meteodriver is used for boundary conditions (whole Europe, TNO-MACC emissions), 3.3 km for Estonian modelling domain (forecasts with two different emission databases).

100.2 Results and Conclusions

The modelled concentrations through 2011 were validated against measured ones in nine monitoring stations within Estonia: Vilsandi (rural, maritime), Lahemaa and Saarejärve (rural), Tartu and Tallinn-Õismäe (urban background), Tallinn-Liivalaia

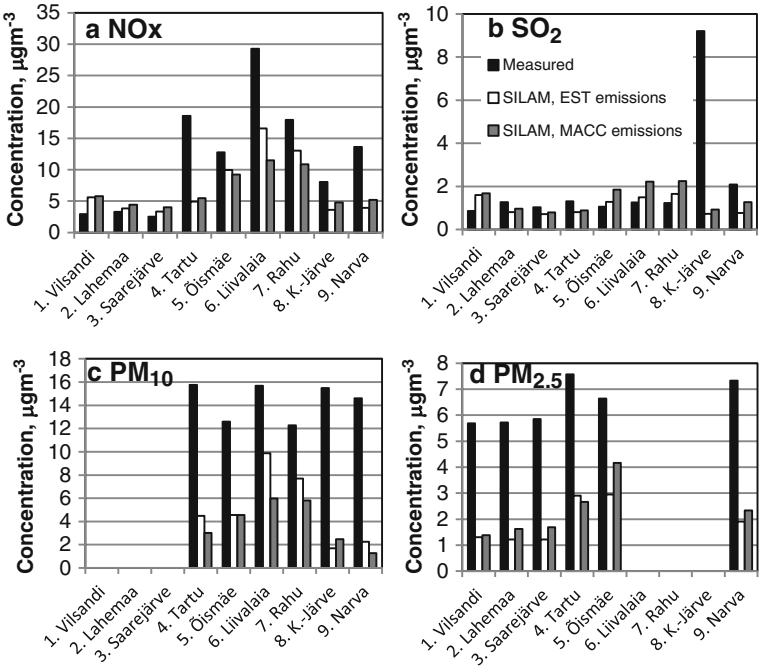

Fig. 100.2 Average measured and modelled concentrations: (**a**) NO_x (sum of NO and NO_2), (**b**) SO_2, (**c**) PM_{10} and (**d**) $PM_{2.5}$. Not all stations measure both $PM_{2.5}$ and PM_{10}

(main street), Tallinn-Rahu, Kohtla-Järve and Narva (urban-industrial). The station-wise average concentrations are given in Fig. 100.2. Tendency of underestimation is evident, except for SO_2 (severe undersetimation in Kohtla-Järve is due to non-resolved local sources). Expected reasons are incomplete PM emission data – no SOA and soil erosion. The differences between runs with MACC and EST database are indecisively small.

The correlations between modelled and measured concentrations (Table 100.1) are slightly, but rather systematically higher for EST database. The latter performs best for urban sites – evidently due to better resolution of small urban areas. Correlations based on daily averaged values are much higher than hourly ones, because the time series include many narrow peaks: missing a peak by a few hours highly damages correlations, but prediction of possible high concentrations for given day, although not perfectly timed, would still constitute a valuable decision-support information.

It is evident that the quality of forecast by SILAM model with developed EST database is sufficient for operational runs, including the urban areas. Fitting this database for fully operational runs is expected within 2012.

Table 100.1 Correlation coefficients between measured and modelled concentrations. Correlations larger than 0.5 are marked in *bold*

Station	PM_{10}	$PM_{2.5}$	SO_2	NO	NO_2	NOx
MACC emissions, hourly values						
Vilsandi		0.50	0.32	0.44	0.48	0.49
Lahemaa		0.32	0.39	0.18	0.33	0.33
Saarejärve		0.42	0.29	0.30	0.33	0.35
Tartu	0.25	0.44	0.39	0.27	0.20	0.29
Õismäe	0.41	0.45	**0.53**	0.45	0.50	**0.58**
Liivalaia	0.24		0.49	**0.53**	0.40	**0.56**
Rahu	0.30		0.46	0.39	0.41	0.48
Kohtla-Järve	0.16		−0.06	0.17	0.25	0.25
Narva	0.22	0.45	0.17	0.17	0.26	0.26
EST emissions, hourly values						
Vilsandi		**0.54**	0.28	0.45	0.48	0.50
Lahemaa		0.36	0.35	0.18	0.34	0.33
Saarejärve		0.44	0.29	0.27	0.30	0.31
Tartu	0.26	0.36	0.44	0.32	0.33	0.41
Õismäe	0.40	0.41	**0.53**	0.46	0.48	**0.56**
Liivalaia	0.33		**0.51**	**0.55**	0.39	**0.54**
Rahu	0.30		**0.52**	0.35	0.42	0.45
Kohtla-Järve	0.15		0.00	0.22	0.26	0.27
Narva	0.22	0.48	0.14	0.21	0.27	0.28
EST emissions, daily averages						
Vilsandi		**0.62**	0.34	**0.53**	**0.62**	**0.63**
Lahemaa		0.45	0.47	0.13	0.40	0.40
Saarejärve		**0.56**	0.44	0.09	0.36	0.37
Tartu	0.48	**0.65**	**0.54**	**0.56**	**0.61**	**0.65**
Õismäe	**0.56**	**0.56**	**0.66**	**0.77**	**0.78**	**0.87**
Liivalaia	0.44		**0.68**	**0.77**	**0.65**	**0.77**
Rahu	0.44		**0.68**	**0.58**	**0.74**	**0.73**
Kohtla-Järve	0.28		0.03	0.49	0.35	0.36
Narva	0.25	**0.58**	0.30	0.47	0.36	0.44

Acknowledgments This study is funded by Estonian National Targeted Financing Project SF0180038s08 and the Estonian Science Foundation, research grant No. 8795. Authors are grateful to Erik Teinamaa from Estonian Centre of Environmental Research for emission data and Mikhail Sofiev and Marje Prank from FMI for valuable advice on SILAM model.

References

1. Kaasik M, Orru H, Tekkel E, Vals P (2007) Situation and tendencies in air quality in a North European medium-sized town. In: Abstracts of the 6th international conference on urban air quality, University of Hertfordshire, Hatfield, 2007, p 212

2. Kesanurm K, Teinemaa E, Kaasik M, Tamm T, Lait T, Orru H (2013) Chapter 8: Country-wide health impact assessment of airborne particulate matter in Estonia. In: Steyn DG, Builtjes PJH, Timmermans RMA (eds) Air pollution modeling and its application XXII. Springer, Dordrecht
3. Sofiev M, Vira J, Prank M, Soares J, Kouznetsov R (2013) Chapter 67: An outlook for integrated modelling of atmospheric composition SILAM v. 5. In: Steyn DG, Builtjes PJH, Timmermans RMA (eds) Air pollution modeling and its application XXII. Springer, Dordrecht

Chapter 101
Validation of WRF Model During O_3 Episodes in an Atlantic Coastal Region

Santiago Saavedra Vázquez, Ángel Rodríguez López, J.A. Souto, and J.J. Casares

Abstract The accurate simulation of PBL dynamics is the most critical aspect of meteorological physics for air quality modeling. In this work, the performance of WRF meteorological model in three different types of high-O_3 episodes (Saavedra S. Characterization of tropospheric ozone episodes in Galicia by applying different simulation techniques and interpretation of field data. Ph. Degree thesis (in Spanish), University of Santiago de Compostela, 2010) in the northwest region of the Iberian Peninsula (IP) is evaluated. Four different planetary boundary layer (PBL) schemes were tested. Surface temperature and wind (speed and direction) simulation results were compared to hourly measurements at 10-m meteorological towers. Following statistics proposed by Emery (Enhanced meteorological modeling and performance evaluation for two Texas ozone episodes. Prepared for the Texas natural resource conservation commission, by ENVIRON international corporation, 2001) for wind speed and temperature, the best model performance is achieved using the Yonsei University (YSU) scheme; Asymmetric Convective Model (ACM2) is more suitable for temperature, and Mellor-Yamada Nakanishi and Niino Level 2.5 PBL (MYNN) are better for wind speed.

Keywords High-ozone episode • WRF model • Validation • PBL parameterization

S. Saavedra • Á. Rodríguez • J.A. Souto (✉) • J.J. Casares
Department of Chemical Engineering, University of Santiago de Compostela, 15782 Santiago de Compostela, Spain
e-mail: ja.souto@usc.es

D.G. Steyn et al. (eds.), *Air Pollution Modeling and its Application XXII*, NATO Science for Peace and Security Series C: Environmental Security,
DOI 10.1007/978-94-007-5577-2_101,

101.1 Introduction

In the last decade the reporting of high ozone concentrations with high pressure conditions is a fairly common phenomenon in the Northwestern Iberian coast during the warm season (March–September), and the population information threshold of current Directive 2008/50/EEC (180 $\mu g/m^3$, hourly) sometimes is close to be exceeded. Three high ozone episodes [9] have been selected for simulation. The first two episodes (9–22 September, 2003 and 14–23 July, 2002) are representative of the most common synoptic weather pattern related to high ozone episodes, "High pressure over the Atlantic Ocean and Europe", and the third episode (16–24 March, 2003) is characteristic of a less frequent synoptic weather pattern ("British-Scandinavian anticyclone"), which leads to lower levels of ozone.

The meteorological model WRF, currently being used to drive regional scale air-quality models, was considered to simulate the meteorological conditions during these episodes. Previous studies have shown that the accurate simulation of PBL dynamics is the most critical aspect of meteorological physics for air quality modeling [1, 2, 4, 6–8, 13]; and surface ozone concentration (SOC) is not an exception: near-surface temperature significantly affects ozone production, surface wind significantly affects dispersion and local transport, and mixing ratio is also related to the ozone dispersion. In this study, four PBL parameterizations were selected for WRF sensitivity testing during three characteristic high ozone episodes in a European coastal Atlantic region.

101.2 Methodology

Selection of air pollution episodes – Three high ozone episodes in the NW coast of Iberian Peninsula (IP) were selected (14–23 July 2002, 16–24 March 2003 and 09–22 September 2003), with hourly maximum SOC exceeding 140 $\mu g/m^3$. July and September ozone episodes show the most common synoptic pressure pattern associated with high ozone episodes in the NW IP, "High pressures over the Atlantic ocean and Europe", whereas March episode was produced under unusual synoptic conditions for ozone episodes, the "Bristish-Scandinavian anticyclone" [9]. Air pollution data from five air quality sites located in this region were considered to identify the episodes [10] and meteorological data from ten surface meteorological stations were considered to analysis the local weather conditions and to validate the WRF model.

WRF simulations – The present study applies the WRF version 3.2 [11], configured with either 29 or 30 vertical layers (depending on the PBL parameterization tested), and three one-way nested domains with horizontal resolutions of 27, 9 and 3 km [3]. Other selected model settings include the Kain-Fritsch cumulus scheme (outer and medium domain), WSM 3-class microphysics scheme, a RRTM long wave and Dudhia shortwave radiation scheme; a five-layer soil model (except with ACM2 Pleim-Xiu PBL scheme, with Pleim-Xiu soil model) was usually applied.

Initial and boundary conditions were provided by NCEP GFS analysis data, at a horizontal resolution of $1° \times 1°$ every 3-h. Elevation and land cover data were provided by the USGS digital terrain model [12]. Four different PBL schemes were tested: Yonsei University scheme (YSU), Mellor-Yamada-Janjic (MYJ), Mellor-Yamada Nakanishi and Niino Level 2.5 PBL (MYNN), and Asymmetric Convective Model (ACM2).

101.3 Results and Concluding Remarks

Comparison between PBL parameterizations – For the present study, meteorological measurements (2-m temperature and 10-m wind speed) at ten meteorological sites in this region were compared to the simulations results. Statistical parameters considered were mean bias (MB), mean absolute gross error (MAGE) and root mean square error (RMSE) [5]. Statistics for every episode and PBL scheme were shown in Tables 101.1 and 101.2.

Considering RMSE and MAGE, the more suitable parameterizations for temperature during these typical high-O_3 episodes are ACM2 and YSU. Unlike temperature, the best results for wind speed are achieved by MYNN scheme, closely followed by YSU scheme. Therefore, YSU PBL scheme can be recommended to simulate high-O_3 episodes in this study area as a compromise between temperature and wind speed performance.

Differences in the July episode statistics respect to the others may be due to the lack of meteorological data during this episode, so less meteorological stations were

Table 101.1 WRF results statistics for 2-m temperature using four different PBL schemes (ACM2, MYJ, MYNN and YSU) during O_3 episodes: mean bias, *MB*, mean absolute gross error, *MAGE* and root mean square error, *RMSE*. Best results for each episode are highlighted

	14-23 July 02			16-24 March 03			9-22 September 03		
PBL	MB	MAGE	RMSE	MB	MAGE	RMSE	MB	MAGE	RMSE
ACM2	***0.238***	***1.643***	***2.238***	0.424	***1.919***	***2.420***	***–0.182***	***1.719***	***2.249***
MYJ	–0.428	1.824	2.411	–1.201	2.276	2.832	–0.982	2.217	2.823
MYNN	–0.819	1.887	2.451	–1.456	2.300	2.860	–1.325	2.263	2.890
YSU	0.679	1.748	2.496	***–0.363***	1.937	2.427	–0.272	1.914	2.516

Table 101.2 WRF results statistics for 10-m wind speed using four different PBL schemes (ACM2, MYJ, MYNN and YSU) during O_3 episodes: mean bias, *MB*, mean absolute gross error, *MAGE* and root mean square error, *RMSE*. Best results for each episode are highlighted

	14-23 July 02			16-24 March 03			9-22 September 03		
PBL	MB	MAGE	RMSE	MB	MAGE	RMSE	MB	MAGE	RMSE
ACM2	–0.499	1.587	2.150	1.055	2.039	2.532	0.328	1.561	1.970
MYJ	***–0.107***	***1.438***	***1.907***	1.273	1.998	2.498	0.638	1.640	2.099
MYNN	–0.722	1.546	2.114	***0.481***	***1.684***	***2.088***	***0.128***	***1.511***	***1.941***
YSU	–0.512	1.484	2.032	0.815	1.789	2.232	0.347	1.551	1.979

used for validation. The comparison of time series (not shown) drives to ACM2 as the best scheme to simulate daily maximum temperatures with clear sky; on the other hand, systematic overestimation of low winds using ACM2 and, also, MYJ schemes, is observed.

101.4 Conclusions

Following the benchmarks proposed by Emery [5], ACM2 is a suitable parameterization related to temperature for all episodes, whereas YSU is only adequate for the March and September episodes, and MYJ for the July episode. MYNN does not satisfy the goals for any period. About wind speed, ACM2, MYNN and YSU meet the benchmark goals for the September episode, and MYJ for the July period.

Acknowledgments The authors acknowledges to As Pontes Power Plant (Endesa) and Meteo-Galicia for providing their observational datasets. PhD Grant of A. Rodríguez ("María Barbeito" Programme) was supported by Xunta de Galicia regional government. This work was developed as part of the project "XIMERE/FUXIMERE" (10MDS009E, Xunta de Galicia), also with support of As Pontes Power Plant.

References

1. Akylas E, Kotroni V, Lagouvardos K (2006) Sensitivity of high-resolution operational weather forecasts to the choice of the planetary boundary layer scheme. Atmos Environ 84:49–57
2. Borge R et al (2008) A comprehensive sensitivity analysis of the WRF model for air quality applications over the Iberian Peninsula. Atmos Environ 42:8560–8574
3. Borrego C et al (2012) The role of transboundary air pollution over Galicia and North Portugal area. 8th international conference on air quality – science and application, Athens, 19–23 Mar 2012
4. De Meij A et al (2009) The impact of MM5 and WRF meteorology over complex terrain on CHIMERE model calculations. Atmos Chem Phys 9:6611–6632
5. Emery CA (2001) Enhanced meteorological modeling and performance evaluation for two Texas ozone episodes. Prepared for the Texas natural resource conservation commission, by ENVIRON International Corporation
6. Lin M, Holloway T, Oki T, Streets DG, Richter A (2009) Multi-scale model analysis of boundary layer ozone over East Asia. Atmos Chem Phys 9:3277–3301
7. Mao Q, Gautney L, Cook T, Jacobs M, Smith S, Kelsoe J (2006) Numerical experiments on MM5-CMAQ sensitivity to various PBL schemes. Atmos Environ 40:3092–3110
8. Perez C et al (2006) Influence of the PBL scheme on high-resolution photochemical simulations in an urban coastal area over the Western Mediterranean. Atmos Environ 40:5274–5297
9. Saavedra S (2010) Characterization of tropospheric ozone episodes in Galicia by applying different simulation techniques and interpretation of field data. Ph. Degree thesis (in Spanish), University of Santiago de Compostela
10. Saavedra S et al (2012) Trends of rural tropospheric ozone at the Northwest of the Iberian Peninsula. Scientific World Journal. doi:10.1100/2012/603034

11. Skamarock WC, Klemp JB (2008) A time-split non-hydrostatic atmospheric model for weather research and forecasting applications. J Comput Phys 227:3465–3485
12. USGS (2008) U.S. Geological Survey, technical report. U.S. Geological Survey. http://www.usgs.gov. Nov 2008
13. Zhang DL, Zheng WZ (2004) Diurnal cycles of surface winds and temperatures as simulated by five boundary layer parameterizations. J Appl Meteor 114:157–169

Chapter 102
Forecasting the Ozone Concentrations with WRF and Artificial Neural Network Based System

Maciej Kryza, Paweł Netzel, Anetta Drzeniecka-Osiadacz, Małgorzata Werner, and Anthony J. Dore

Abstract The WRF model has been used to make forecasts for ozone, using an artificial neural network.

Keywords WRF • Forecasting • Ozone

102.1 Introduction

Ground level ozone (O_3) has serious adverse impacts on human health and ecosystems. Accurate tools that support human and ecosystem protection are necessary. The most often used are complex atmospheric chemistry models [6], driven by off-line meteorology or integrated on-line to allow for two directional effects of atmospheric chemistry and meteorology. These tools need a significant amount of computational effort, but are able to provide information on spatial and temporal information on atmospheric ozone concentrations. Statistical methods, including regression models and artificial neural networks (ANN) are also often applied to provide information on spatial [4] and temporal variability of O_3. ANN were also found to be useful for O_3 forecasting, and were applied to e.g. metropolitan areas by local environmental or health agencies [1–3, 7].

Here we present the preliminary results of the O_3 forecasting system for the city of Wrocław, SW Poland. Two main tools are used to estimate the hourly O_3 for

M. Kryza (✉) • P. Netzel • A. Drzeniecka-Osiadacz • M. Werner
Department of Climatology and Atmosphere Protection, Wrocław University, Wrocław, Poland
e-mail: maciej.kryza@uni.wroc.pl

A.J. Dore
Centre for Ecology and Hydrology, Edinburgh, UK

D.G. Steyn et al. (eds.), *Air Pollution Modeling and its Application XXII*,
NATO Science for Peace and Security Series C: Environmental Security,
DOI 10.1007/978-94-007-5577-2_102,

the next 3 and 24 h – the Weather Research and Forecasting (WRF) meteorological model and ANN. WRF provides the meteorological variables for the next 3 and 24 h, and ANN are applied to forecast the O_3 concentrations.

102.2 Data and Methods

102.2.1 Ozone Measurements and Study Periods

The analysis is based on measured O_3 at an urban background site located in the city of Wrocław, SW Poland. Measurements were collected automatically with a 1 h time resolution. For the analysed period 2005–2009 data completeness was 96 %. No-data periods were removed from the analysis, as well as measurements of O_3 equal to zero. Average O_3 concentration for the years 2005–2009 was 43 $\mu g\ m^{-3}$, with the highest annual value in year 2006 (47 $\mu g\ m^{-3}$). The highest monthly concentration for years 2005–2009 appeared from April to July and exceeded 60 $\mu g\ m^{-3}$. The dataset was divided into a learning (60 % of the 2005–2009 observations) and test subset (TP, 40 %). The period 14.04–10.05.2009 was treated separately as a case study and excluded from the dataset used for ANN setting. The episode was selected because of high concentrations of ground level ozone, exceeding 100 $\mu g\ m^{-3}$ during the day and well represented diurnal cycle.

102.2.2 Meteorological Data

The WRF model provided the meteorological data for ANN with a 3 h time step for the entire 2005–2009 period and 1 h for the selected case study period. The model worked with three one way nested domains [5]. The outer domain covered Europe with a 50 km × 50 km grid resolution. The first nested domain covered the area of Poland with 10 km × 10 km, and the second – SW area of Poland with 2 km × 2 km grid. All the domains were composed of 35 vertical levels, with the top fix at 10 hPa. Newtonian (analysis) nudging was applied. The simulations were driven by the GFS FNL data, available every 6 h.

102.2.3 Neural Network Model

We used the feed forward ANN network with 26 input layer neurons, two hidden layers (the first with 10 and the second with 7 neurons) and the output layer with one neuron. All neurons used the sigmoid transfer function. For the period 10.04–15.05.2009, the hourly meteorological data were used and the ANN provided

O_3 forecasts for the next 3 h (FP 3 h) and 24 h (FP 24 h). For network learning, the following input variables were used: cosine of day number in a year and week, cosine of hour (cos(2*π*hour/24)), sea level pressure (SLP), air temperature(T2), dew point temperature and relative humidity at 2 m, wind speed (WSPD), u and v wind components of wind speed at 10 m and boundary layer height. Additionally, the differences between the current and 3 h back values and 24 h mean SLP, T2 and relative humidity were included in the input layer. The analysis was performed with the Fast Artificial Neural Network library and FANN Tool 1.1 interface.

102.2.4 Evaluation of the WRF and ANN Results

WRF results for the entire period were compared with meteorological measurements of air temperature, sea level pressure and wind speed gathered at Wrocław station. The results were summarised for each year and for the ANN forecasting period. The ANN were evaluated by comparison with hourly O_3 measurements separately for the TP, FP3h and FP24h. Common statistics were used to evaluate the WRF and ANN models, including mean bias (MB), mean absolute error (MAE) and the index of agreement (IOA). For ANN, the fraction of estimated values within a fraction two of the observed value (FAC2) was also provided.

102.3 Results

WRF performance for the entire and ANN forecasting (FP) period is summarised in Table 102.1. There is an improvement in SLP model to measurement agreement after the year 2007. T2 is constantly underestimated, and WSPD overestimated, especially for the forecasting period.

Table 102.1 WRF model performance for each year and forecasting period, Wrocław station

		2005	2006	2007	2008	2009	FP
SLP	MB	1.44	1.58	1.45	0.63	0.55	−0.20
	MAE	1.48	1.61	1.51	0.86	0.83	2.11
	IOA	0.99	0.99	0.99	1.00	1.00	0.92
T2	MB	−2.13	−2.27	−1.96	−1.87	−1.98	−1.89
	MAE	2.98	3.24	3.02	2.71	3.12	2.76
	IOA	0.96	0.96	0.96	0.96	0.96	0.89
WSPD	MB	0.15	0.09	0.12	0.08	0.00	0.65
	MAE	1.01	1.03	1.15	1.12	1.09	1.79
	IOA	0.86	0.85	0.87	0.87	0.84	0.67

Table 102.2 Error statistics of ANN O_3 forecasts (3 and 24 h) for training and forecast period

	MB	MAE	IOA	FAC2 (%)
TP 3 h	−0.69	14.90	0.88	94
TP 24 h	1.09	12.52	0.92	78
FP 3 h	8.36	26.56	0.73	79
FP 24 h	−17.33	25.45	0.68	75

The ANN error statistics are presented in Table 102.2 for test subset (TP) and forecasting period (FP), for 3 and 24 h forecasts. The results are in close agreement with the O_3 measurements for the TP, for both forecasting periods. For the FP, the ANN 3 h results are in reasonably good agreement with the measurements There is a large negative bias for 24 h forecasts, but FAC2 is still above 50 %.

102.4 Summary

We used WRF meteorology as an input to a neural network to predict the hourly ground level O_3 for the next 3 and 24 h. Preliminary results show that the WRF model was able to provide reliable meteorological data, though with significant negative bias for air temperature estimates. ANN were reliable for short 3 h forecasts, but significantly underestimated measured O_3 for 24 h forecasts.

Further steps will include improvements of WRF meteorology – preliminary results show that the MB for T2 can be decreased by changing the model configuration. ANN will be rerun with the improved meteorology, and tested for a larger number of sites. Finally, we will use the WRF-ANN approach for spatial, short term O_3 forecasting and compare the results with atmospheric transport model.

Acknowledgments Calculations have been carried out in Wroclaw Centre for Networking and Supercomputing (http://www.wcss.wroc.pl), grant No. 170. The Voivodeship Inspectorate for Environmental Protection in Wroclaw provided O_3 measurements data.

References

1. Comrie AC (1997) Comparing neural networks and regression models for ozone forecasting. J Air Waste Manag Assoc 47:653–663
2. Corani G (2005) Air quality prediction in Milan: feed-forward neural networks, pruned neural networks and lazy learning. Ecol Model 185:513–529
3. Ibarra-Berastegi G, Elias A, Barona A, Saenz J, Ezcurra A, de Argandona JD (2008) From diagnosis to prognosis for forecasting air pollution using neural networks: air pollution monitoring in Bilbao. Environ Model Softw 23:622–637
4. Pfeiffer H, Baumbach G, Sarachaga-Ruiz L, Kleanthous S, Poulida O, Beyaz E (2009) Neural modelling of the spatial distribution of air pollutants. Atmos Environ 43:3289–3297

5. Skamarock WC, Klemp JB, Dudhia J, Gill DO, Barker DM, Duda MG, Huang X-y, Wang W, Powers JG (2008) A description of the advanced research WRF version 3. National Center for Atmospheric Research, Boulder
6. Vieno M, Dore AJ, Stevenson DS, Doherty R, Heal MR, Reis S, Hallsworth S, Tarrason L, Wind P, Fowler D, Simpson D, Sutton MA (2010) Modelling surface ozone during the 2003 heat-wave in the UK. Atmos Chem Phys 10:7963–7978
7. Yi JS, Prybutok VR (1996) A neural network model forecasting for prediction of daily maximum ozone concentration in an industrialized urban area. Environ Pollut 92:349–357

Chapter 103
An Analytical Model for Contaminant Dispersion Release in the Atmospheric Boundary Layer Considering Time Variable Eddy Diffusivity

Daniela Buske, Marco T. Vilhena, Régis S. Quadros, Bardo Bodmann, and Tiziano Tirabassi

Abstract In this work we present a new model and simulations for more realistic scenarios incorporating in the diffusive model the dependence of the eddy diffusivity profile on the temporal variable. Numerical results and comparison with experimental data are presented.

Keywords Eddy diffusivity • Boundary layer

103.1 Introduction

In the last decade emerged in literature the GILTT approach (Generalized Integral Laplace Transform Technique) [6] whose main feature relies on the analytical solution of transformed GITT (Generalized Integral Transform Technique) solutions by the Laplace Transform technique. This methodology has been largely applied in the topic of simulations of pollutant dispersion in the Atmospheric Boundary Layer (ABL). Recently appeared in literature the three-dimensional GILTT solution (named 3D-GILTT) [2]. The idea of solution is the application of the integral transform in the y-direction and then the resultant two-dimensional problem solution following the previous works. No approximation is made along the solution derivation so that is an exact solution except for the round-off error.

D. Buske (✉) • R.S. Quadros
IFM/DME, Universidade Federal de Pelotas, Pelotas, RS, Brazil
e-mail: danielabuske@pq.cnpq.br; regis.quadros@ufpel.edu.br

M.T. Vilhena • B. Bodmann
PROMEC, Universidade Federal do Rio Grande do Sul, Porto Alegre, RS, Brazil
e-mail: vilhena@pq.cnpq.br; bardo.bodmann@ufrgs.br

T. Tirabassi
Institute ISAC of CNR, Bologna, Italy
e-mail: t.tirabassi@isac.cnr.it

D.G. Steyn et al. (eds.), *Air Pollution Modeling and its Application XXII*,
NATO Science for Peace and Security Series C: Environmental Security,
DOI 10.1007/978-94-007-5577-2_103,

In this work we step forward presenting new simulations for more realistic scenarios incorporating in the diffusive model the dependence of the eddy diffusivity profile on the temporal variable. To reach this goal we consider temporal variation for the eddy diffusivity coefficient in the three-dimensional advection-diffusion equation (ADE). To solve this kind of problem the Decomposition Method is used together with the 3D-GILTT method. Applying the idea of the decomposition method [1] we reduce the ADE with time dependence of eddy diffusivity to a recursive set of diffuse equations. The motivation for such procedure comes from the fact that the resultant recursive problem can be straightly solved by the GILTT method. Simulations and comparisons with experimental data are presented.

103.2 Solution of the Advection-Diffusion Equation

In the sequence we derive the solution of the ADE which is employed to simulate the contaminant concentration in the ABL, considering Fickian closure of turbulence. Indeed, we write the ADE in Cartesian geometry like:

$$\frac{\partial \overline{c}}{\partial t} + \overline{u}\frac{\partial \overline{c}}{\partial x} + \overline{v}\frac{\partial \overline{c}}{\partial y} + \overline{w}\frac{\partial \overline{c}}{\partial z} = \frac{\partial}{\partial x}\left(K_x \frac{\partial \overline{c}}{\partial x}\right) + \frac{\partial}{\partial y}\left(K_y \frac{\partial \overline{c}}{\partial y}\right) + \frac{\partial}{\partial z}\left(K_z \frac{\partial \overline{c}}{\partial z}\right) \tag{103.1}$$

subjected to the usual boundary, initial and source conditions:

$$\begin{aligned} \mathrm{K}\nabla\overline{\mathrm{c}}|_{(0,0,0)} = \mathrm{K}\nabla\overline{\mathrm{c}}|_{(\mathrm{L_x},\mathrm{L_y},\mathrm{h})} = 0;\ c\,(x,\ y,\ z,\ 0) = 0;\ \overline{\mathrm{u}}\mathrm{c}\,(0,\mathrm{y},\mathrm{z},\mathrm{t}) \\ = \mathrm{Q}\delta(\mathrm{x})\delta\,(\mathrm{y}-\mathrm{y_0})\,\delta(\mathrm{z}-\mathrm{H_s}) \end{aligned}$$

where $\overline{c}$ denotes the mean concentration of a passive contaminant (g/m^3), $\overline{u}$, $\overline{v}$ and $\overline{w}$ are the Cartesian components of the mean wind (m/s) in the directions x $(0 < \mathrm{x} < \mathrm{L_x})$, y $(0 < \mathrm{y} < \mathrm{L_y})$ and z $(0 < \mathrm{z} < \mathrm{h})$, K_x, K_y and K_z are the eddy diffusivities. Q is the emission rate (g/s), h the height of the ABL (m), $\mathrm{H_s}$ the height of the source (m), $\mathrm{L_x}$ and $\mathrm{L_y}$ are the limits in the x and y-axis and far away from the source (m) and δ represents the generalized Dirac delta function. The source position is (0, $\mathrm{y_0}$, Hs).

In order to solve the problem (1), we initially apply the integral transform technique in the y variable. For such, we expand the pollutant concentration as:

$$\overline{c}(x,y,z,t) = \sum_{m=0}^{M} \overline{c}_m(x,z,t)Y_m(y) \tag{103.2}$$

where $Y_m(y) = \cos\ (\lambda_m y)$ is a set of orthogonal eigen functions and $\lambda_m = \frac{m\pi}{L_y}$ for $\mathrm{m} = 0,1,2,\ldots$ are the respective eigen values. To determine the unknown coefficient $\overline{c}_m\,(x,z,t)$ for m = 0:M we began substituting Eq. 103.2 in Eq. 103.1 and then

taking moments. We assume that the reference system is aligned with the x-axis. The diffusion component K_x is neglected considering the fact that it is assumed that the advection is dominant in the x-direction. Further, it was also considered that K_y has only dependence on the z-direction. These assumptions lead to:

$$\frac{\partial \overline{c}_m(x,z,t)}{\partial t} + \overline{u}\frac{\partial c_m(x,z,t)}{\partial x} - \frac{\partial}{\partial z}\left(K_z \frac{\partial \overline{c}_m(x,z,t)}{\partial z}\right) + \lambda_m^2 K_y \overline{c}_m(x,z,t) = 0 \tag{103.3}$$

In the example below we demonstrate the closed form procedure for a problem with explicit time dependence of the vertical eddy diffusivity, which is novel in the literature. The solution is generated making use of the decomposition method followed by the Laplace transform that renders the problem a pseudo-stationary one. Further we rewrite the vertical diffusivity as a time average term $\overline{K}_z(z)$ plus a term representing the variations $k_z(z,t)$ around the average for the time interval of the measurement $\left(K_z(z,t) = k_z(z,t) + \overline{K}_z(z)\right)$ and use the asymptotic form of K_y, which is then explored to set-up the structure of the equation that defines the recursive decomposition scheme:

$$\frac{\partial \overline{c}_m}{\partial t} + \overline{u}\frac{\partial \overline{c}_m}{\partial x} - \frac{\partial}{\partial z}\left(\overline{K}_z \frac{\partial \overline{c}_m}{\partial z}\right) + \lambda_m^2 K_y \overline{c}_m = \frac{\partial}{\partial z}\left(k_z \frac{\partial \overline{c}_m}{\partial z}\right) \tag{103.4}$$

According the idea of the Decomposition method, we consider that the solution of Eq. 103.4 has the form:

$$\overline{c}_m(x,z,t) = \sum\nolimits_{j=0}^{J} \overline{c}_{m,j}(x,z,t) \tag{103.5}$$

Upon inserting the expansion (103.5) in Eq. 103.4 one may regroup terms that obey the recursive equations and starts with the time averaged solution for K_z:

$$\frac{\partial \overline{c}_{m,0}}{\partial t} + \overline{u}\frac{\partial \overline{c}_{m,0}}{\partial x} - \frac{\partial}{\partial z}\left(\overline{K}_z \frac{\partial \overline{c}_{m,0}}{\partial z}\right) + \lambda_m^2 K_y \overline{c}_{m,0} = 0 \tag{103.6}$$

The extension to the closed form recursion is then given by

$$\frac{\partial \overline{c}_{m,J}}{\partial t} + \overline{u}\frac{\partial \overline{c}_{m,J}}{\partial x} - \frac{\partial}{\partial z}\left(\overline{K}_z \frac{\partial \overline{c}_{m,J}}{\partial z}\right) + \lambda_m^2 K_y \overline{c}_{m,J} = \frac{\partial}{\partial z}\left(k_z \frac{\partial \overline{c}_{m,J-1}}{\partial z}\right) \tag{103.7}$$

From the construction of the recursion equation system it is evident that other schemes are possible. The specific choice made here allows us to solve the recursion initialization using the procedure described in references [6, 2], where a stationary K_z was assumed. For this reason the time dependence enters as a known source term from the first recursion step on. The first equation of recursive system problems satisfies the boundary conditions of problem (1) meanwhile the remaining equations

satisfy the homogeneous boundary condition. Once the set of problems (7) is solved by the GILTT method, the solution of Eq. 103.1 is well determined. It is important to consider that we may control the accuracy of the results by a proper choice of the number of terms in the series solution summation.

103.3 Turbulent Parameterization

The temporal dependent eddy diffusivity, based on the Taylor statistical diffusion theory and a kinetic energy spectral model, has been derived by Degrazia et al. [3] and can be expressed as an algebraic formulation given by:

$$\frac{K_\alpha}{w_* h} = \frac{0.58 c_i \psi^{2/3} (z/h)^{4/3} X \left[0.55 (z/h)^{2/3} + 1.03 c_i^{1/2} \psi^{1/3} \left(f_m^*\right)_i^{2/3} X\right]}{\left[0.55 (z/h)^{2/3} \left(f_m^*\right)_i^{1/3} + 2.06 c_i^{1/2} \psi^{1/3} \left(f_m^*\right)_i X\right]^2} \tag{103.8}$$

where $\alpha = x, y, z, i = u, v, w, c_i = \alpha_i \, (0.5 \pm 0.05) \, (2\pi\kappa)^{-2/3}, \alpha_i = 1, \frac{4}{3} \; and \; \frac{4}{3}$ for $u, v \; and \; w$ components respectively, $\kappa = 0.4$ is the von Karman constant, $(f_m{}^*)_i$ is the normalized frequency of the spectral peak, h is the top of the convective boundary layer height, w_* is the convective velocity scale, ψ is the non-dimensional molecular dissipation rate function and $X = \frac{x w_*}{\overline{u} h}$ is the non-dimensional time, where $\overline{u}$ is the horizontal mean wind speed. More details on the paper [3].

The wind speed profile used in the simulations was described by a power law. Note that the same procedure adopted for the eddy diffusivity in the derivation of the solution can be applied for the wind profile.

103.4 Application to Experimental Data

In order to show the performance of the present solution of the ADE and the performance of the proposed ABL parameterizations we have applied the model using the well known Copenhagen experimental dataset [4].

We start searching for the suitable number of terms of the series solution to reach results with accuracy of 10^{-4}. For such in Table 103.1 we report the numerical convergence of the results, considering successively one to five terms in the series solutions for experiment 8 of Copenhagen. We promptly observe that the desired accuracy was attained with three terms in the series solution for all distances considered. To perform a statistical comparison between GILTT results and the Copenhagen experiment we consider the statistical indices described by Hanna [5]. So far, from Table 103.2 we readily realize a very good performance of the 3D-GILTT.

Table 103.1 Numerical convergence of the 3D-GILTT model, with time dependence of eddy diffusivity, for the experiment 8 of Copenhagen

Run	Terms decomposition	$\overline{c}\,(x, y, z, t)$ (10^{-7} s·m^{-3})		
8	μ_0	6.38	3.94	1.91
	$\mu_0 + \mu_1$	6.40	4.91	1.91
	$\mu_0 + \mu_1 + \mu_2$	5.99	4.87	1.91
	$\mu_0 + \mu_1 + \mu_2 + \mu_3$	5.97	4.87	1.91
	$\mu_0 + \mu_1 + \mu_2 + \mu_3 + \mu_4$	5.97	4.87	1.91
	$\mu_0 + \mu_1 + \mu_2 + \mu_3 + \mu_4 + \mu_5$	5.97	4.87	1.91

Table 103.2 Statistical comparison between 3D-GILTT model results and the Copenhagen data set, changing the number of terms in Eq. 103.5

Recursion depth	NMSE	COR	FA2	FB	FS
0	0.38	0.83	0.83	0.32	0.59
1	0.16	0.90	1.00	0.11	−0.13
2–5	0.14	0.91	1.00	0.15	−0.07

103.5 Conclusions

In this work we propose an analytical model to predict pollutant dispersion in the ABL considering that the eddy diffusivity coefficient depends on the time and the z spatial variables. Taking into account the analytical feature and fast numerical convergence of the solution, besides the fact that this sort of solution is not found in literature, we are confident to affirm that the proposed model is a promising technique to handle realistic physical problems of pollutant dispersion in the ABL regarding the issue of the fast screening of pollutant concentration distribution from a given source as well the control of critical events related to air quality.

Acknowledgements The authors thank to Brazilian Research Council CNPq and FAPERGS for the partial financial support of this work.

References

1. Adomian G (1988) A review of the decomposition method in applied mathematics. J Math Anal Appl 135:501–544
2. Buske D, Vilhena MT, Segatto CF, Quadros RS (2011) A general analytical solution of the advection-diffusion equation for Fickian closure. In: Integral methods in science and engineering: computational and analytical aspects. Birkäuser, Boston, pp 25–34
3. Degrazia GA, Moreira DM, Campos CRJ, Carvalho JC, Vilhena MT (2002) Comparison between an integral and algebraic formulation for the eddy diffusivity using the Copenhagen experimental dataset. Il NuovoCimento 25C:207–218

4. Gryning SE, Lyck E (1984) Atmospheric dispersion from elevated source in an urban area: comparison between tracer experiments and model calculations. J Appl Meteor 23:651–654
5. Hanna SR, Paine RJ (1989) Hybrid plume dispersion model (HPDM) development and evaluation. J Appl Meteorol 28:206–224
6. Moreira DM, Vilhena MT, Buske D, Tirabassi T (2009) The state-of-art of the GILTT method to simulate pollutant dispersion in the atmosphere. Atmos Res 92:1–17

Chapter 104
A Closed Form Solution for Pollutant Dispersion Simulation in Atmosphere Under Low Wind Conditions

Daniela Buske, Marco T. Vilhena, Bardo Bodmann, Tiziano Tirabassi, and Régis S. Quadros

Abstract The present study proposes a mathematical model for dispersion of contaminants in low winds that takes into account the along-wind diffusion. The solution of the advection-diffusion equation for these conditions is obtained applying the 3D-GILTT method. Numerical results and comparison with experimental data are presented.

Keywords Low wind conditions • Pollutant dispersion

104.1 Introduction

In the last several years, special attention has been paid to the task of searching analytical solutions for the advection-diffusion equation in order to simulate the pollutant dispersion in the Atmospheric Boundary Layer (ABL). Focusing our attention in this direction, in this work we step forward, reporting an analytical solution for the three-dimensional advection-diffusion equation, applying the new 3D-GILTT method (Three-Dimensional Generalized Integral Laplace Transform Technique)

D. Buske (✉) • R.S. Quadros
IFM/DME, Universidade Federal de Pelotas, Pelotas, RS, Brazil
e-mail: danielabuske@pq.cnpq.br; regis.quadros@ufpel.edu.br

M.T. Vilhena • B. Bodmann
Universidade Federal do Rio Grande do Sul, PROMEC, Porto Alegre, RS, Brazil
e-mail: vilhena@pq.cnpq.br; bardo.bodmann@ufrgs.br

T. Tirabassi
Institute ISAC of CNR, Bologna, Italy
e-mail: t.tirabassi@isac.cnr.it

D.G. Steyn et al. (eds.), *Air Pollution Modeling and its Application XXII*,
NATO Science for Peace and Security Series C: Environmental Security,
DOI 10.1007/978-94-007-5577-2_104,

[2], considering the longitudinal diffusion. Furthermore, in the turbulence parameterizations, the eddy diffusivities are functions of distance from the source and represent correctly the near-source diffusion in weak winds [1].

The importance of dispersion modelling in low wind conditions lies in the fact that such conditions occur frequently and are crucial for air pollution episodes. In such conditions, the pollutants are not able to travel far and thus the near-source areas are affected the most. The classical approach based on conventional models, such as Gaussian puff/plume or the K-theory with suitable assumptions, are known to work reasonably well during most meteorological regimes, except for weak and variable wind conditions. This is because (i) down-wind diffusion is neglected with respect to advection (ii) the concentration is inversely proportional to wind speed (iii) the average conditions are stationary and (iv) there is a lack of appropriate estimates of dispersion parameters in low wind conditions. In view of such restrictions, various attempts have been made in literature to explain dispersion in the presence of low wind conditions by relaxing some of the limitations.

104.2 The Closed Form Solution

The advection-diffusion equation of air pollution in atmosphere is essentially a statement of conservation of a suspended material, and it can be written as:

$$\frac{\partial \bar{c}}{\partial t} + \bar{u}\frac{\partial \bar{c}}{\partial x} + \bar{v}\frac{\partial \bar{c}}{\partial y} + \bar{w}\frac{\partial \bar{c}}{\partial z} = \frac{\partial}{\partial x}\left(K_x \frac{\partial \bar{c}}{\partial x}\right) + \frac{\partial}{\partial y}\left(K_y \frac{\partial \bar{c}}{\partial y}\right) + \frac{\partial}{\partial z}\left(K_z \frac{\partial \bar{c}}{\partial z}\right) \tag{104.1}$$

where $\bar{c}$ denotes the mean concentration of a passive contaminant (g/m^3), $\bar{u}$, $\bar{v}$, and $\bar{w}$ are the cartesian components of the mean wind (m/s) in the directions x $(0 < x < L_x)$, y $(0 < y < L_y)$ and z $(0 < z < h)$, K_x, K_y and K_z are the eddy diffusivities. Equation 104.1 is subjected to the usual boundary conditions $\boldsymbol{K}\nabla\bar{c}|_{(0,0,0)} = \boldsymbol{K}\nabla\bar{c}|_{(L_x,L_y,h)} = 0$ and initial and source conditions: $c\,(x, y, z, 0) = 0$; $\bar{u}c\,(0, y, z, t) = Q\delta(x)\delta\,(y - y_0)\,\delta(z - H_s)$, where Q is the emission rate (g/s), h the height of the ABL (m), H_s the height of the source (m), L_x and L_y are the limits in the x and y-axis and far away from the source (m) and δ represents the generalized Dirac delta function. The source position is (0, y_0, H_s).

In order to solve the problem (104.1), we initially apply the integral transform technique in the y variable. For such, we expand the pollutant concentration as:

$$\bar{c}\,(x, y, z, t) = \sum_{m=0}^{M} \bar{c}_m\,(x, z, t)\,Y_m(y) \tag{104.2}$$

where $Y_m(y) = \cos(\lambda_m y)$ is a set of orthogonal eigen functions and $\lambda_m = \frac{m\pi}{L_y}$ for m = 0,1,2,... are the respective eigen values. To determine the unknown coefficient $\bar{c}_m(x,z,t)$ for m = 0: M we began substituting Eq. 104.2 in Eq. 104.1 and then taking moments. This procedure leads to:

$$\frac{\partial \bar{c}_m(x,z,t)}{\partial t} + \bar{u}\frac{\partial \bar{c}_m(x,z,t)}{\partial x} - \frac{\partial}{\partial x}\left(K_x \frac{\partial \bar{c}_m(x,z,t)}{\partial x}\right) - \frac{\partial}{\partial z}\left(K_z \frac{\partial \bar{c}_m(x,z,t)}{\partial z}\right) + \lambda_m^2 K_y \bar{c}_m(x,z,t) = 0$$

The analytical solution of the above two-dimensional problem is obtained by the GILTT (Generalized Integral Laplace Transform Technique) approach [6]. The mean feature of the GILTT method comprehends the steps: solution of an associate Sturm-Liouville problem, expansion of the pollutant concentration in a series in terms of the attained eigen function, replacement of this expansion in the advection-diffusion equation and, finally, taking moments. This procedure leads to a set of second order differential ordinary equations, named the transformed equation. After an order reduction, the transformed problem is solved analytically by the application of the Laplace transform technique without any approximation along its derivation, except the round-off error. In the case $K_x \to 0$, on these assumptions, we obtain the solutions of Buske et al. [2] and Moreira et al. [6].

104.3 Turbulent Parameterization

To represent the near-source diffusion in weak winds the eddy diffusivities should be considered as functions of not only turbulence (e.g., large eddy length and velocity scales), but also of distance from the source [1]. Following this idea, Degrazia et al. [4] proposed for an algebraic formulation for the eddy diffusivities, which takes the form:

$$\frac{K_\alpha}{w_* h} = \frac{0.58 c_i \psi^{2/3} (z/h)^{4/3} X \left[0.55(z/h)^{2/3} + 1.03 c_i^{1/2} \psi^{1/3} \left(f_m^*\right)_i^{2/3} X\right]}{\left[0.55(z/h)^{2/3} \left(f_m^*\right)_i^{1/3} + 2.06 c_i^{1/2} \psi^{1/3} \left(f_m^*\right)_i X\right]^2}$$

where $\alpha = x, y, z, i = u, v, w, c_i = \alpha_i (0.5 \pm 0.05)(2\pi\kappa)^{-2/3}$, $\alpha_i = 1, \frac{4}{3}$ and $\frac{4}{3}$ for u ,v and w components respectively, $\kappa = 0.4$ is the von Karman constant, $\left(f_m^*\right)_i$ is the normalized frequency of the spectral peak, h is the top of the convective boundary layer height, w_* is the convective velocity scale, ψ is the non-dimensional molecular dissipation rate function and $X = \frac{x w_*}{\bar{u} h}$ is the non-dimensional time, where $\bar{u}$ is the horizontal mean wind speed. More details on the paper [4].

The wind speed profile is described by a power law [8].

104.4 Application to Experimental Data

The performance of the 3D-GILTT model was evaluated against experimental ground-level concentration using SF_6 data from dispersion experiments in low wind conditions carried out by the Indian Institute of Technology (IIT Delhi), described in Sharan et al. [9, 10]. The pollutant was released without buoyancy of a height of 1 m and the concentrations of SF_6 were observed near the ground-level (0.5 m). The release rate of SF_6 tracer varied from 30 to 50 ml min^{-1}. The sampling period for each run was 30 min. Wind and temperature measurements were obtained at four levels (2, 4, 15 and 30 m) from a 30 m micrometeorological tower. In all the cases, the wind speed was less than 2 ms^{-1} at the 15 m level. The samplers were located on arcs of 50 m and 100 m radii.

Table 104.1 shows the performance of the new model compared with other models for the unstable experiments of IIT Delhi, using the statistical indices described by Hanna and Paine [5]. While the present approach (3D-GILTT) is based on a genuine three dimensional description an earlier analytical approach called GILTTG uses a Gaussian assumption for the horizontal transverse direction [6]. The ADMM approach [7], solves the two-dimensional advection-diffusion equation by adiscretisation of the ABL in a multilayer domain and also uses a Gaussian assumption for the horizontal transverse direction. The GIADMT [3] is a dimensional extension to the previous work, but again assuming the stepwise approximation for the eddy diffusivity coefficient and wind profile. The model of Arya [1] is obtained by the numerical integration of the Gaussian puff solution using dispersion parameters based on convective similarity scaling. The results obtained with this approach reveal a further under-prediction of concentration. The same happens with the model of Sharan et al. [9]. Better results are obtained by the model of Sharan et al. [10] that is an improvement of the previous one where the friction velocity is used instead of the convective velocity. The statistical indices of Table 104.1 indicate that, compared with other models, a good agreement is obtained between the K-model and observed near ground-level centerline concentrations.

Table 104.1 Statistical comparison between model results

	NMSE	COR	FA2	FB	FS
3D-GILTT	0.14	0.83	0.88	−0.05	−0.04
GILTTG	0.29	0.77	0.81	0.05	−0.25
ADMM	0.35	0.76	0.81	−0.01	−0.33
GIADMT	0.22	0.93	0.88	0.33	0.31
Arya 1995	13.86	0.77	0.00	1.68	1.59
Sharan 1996	7.11	0.76	0.00	1.49	1.32
Sharan 1996	0.37	0.91	0.75	0.45	0.40

104.5 Conclusions

A mathematical model for the dispersion of a pollutant from a continuously emitting near-ground point source in a ABL, with low wind conditions, has been described. Besides advection along the mean wind, the model takes into account the longitudinal diffusion. The closed form analytical solution of the proposed problem is obtained using the 3D-GILTT method. The present model has been evaluated in unstable conditions for concentration distributions. Particularly, the results obtained by the analytical dispersion model agree very well with the experimental concentration data, indicating that the model represents the diffusion process correctly under low wind conditions.

Acknowledgements The authors thank to Brazilian Research Council CNPq and FAPERGS for the partial financial support of this work.

References

1. Arya P (1995) Modeling and parameterization of near-source diffusion in weak winds. J Appl Meteor 34:1112–1122
2. Buske D, Vilhena MT, Segatto CF, Quadros RS (2011) A general analytical solution of the Advection-diffusion equation for Fickian closure. In: Integral methods in science and engineering: computational and analytical aspects. Birkäuser, Boston, pp 25–34
3. Costa CP, Vilhena MT, Tirabassi T (2009) Application of the GIADMT method in pollutant dispersion under low wind conditions (In Portuguese). Ciência e Natura: 17–20
4. Degrazia GA, Moreira DM, Campos CRJ, Carvalho JC, Vilhena MT (2002) Comparison between an integral and algebraic formulation for the eddy diffusivity using the Copenhagen experimental dataset. Il Nuovo Cimento 25C:207–218
5. Hanna SR, Paine RJ (1989) Hybrid plume dispersion model (HPDM) development and evaluation. J Appl Meteorol 28:206–224
6. Moreira DM, Vilhena MT, Buske D, Tirabassi T (2009) The state-of-art of the GILTT method to simulate pollutant dispersion in the atmosphere. Atmos Res 92:1–17
7. Moreira DM, Vilhena MT, Tirabassi T, Costa C, Bodmann B (2006) Simulation of pollutant dispersion in atmosphere by the Laplace transform: the ADMM approach. Water Air Soil Poll 177:411–439
8. Panofsky HA, Dutton JA (1984) Atmospheric turbulence. Wiley, New York
9. Sharan M, Singh MP, Yadav AK (1996) A mathematical model for the atmospheric dispersion in low winds with eddy diffusivities as linear functions of downwind distance. Atmos Environ 30(7):1137–1145
10. Sharan M, Yadav AK, Modani M (2002) Simulation of short-range diffusion experiment in low wind convective conditions. Atmos Environ 36:1901–1906

Chapter 105
Eddy Diffusivity to North Wind Phenomenon in Southern Brazil: Application in an Analytical Dispersion Model

Ivan P. Alves, Gervásio A. Degrazia, Daniela Buske, and Marco T. Vilhena

Abstract In this study, we employed Taylor's statistical diffusion theory, a model that describes observed turbulent spectra and an analytical dispersion model, to investigate turbulent statistical characteristics and diffusive properties associated with the north wind phenomenon in southern Brazil. Numerical results and comparison with the Prairie-Grass experiment are presented.

Keywords Dispersion model • Prairie-Grass experiment

105.1 Introduction

During some winter periods, in a regional scale, in the central regions of south Brazil, occurs a phenomenon known as north wind flow (NWF). It is characterized by a strong and warm wind, originated from north, presenting very low humidity and is associated with frontal meteorological systems. From the fact that this north flow occurs frequently, it is of great importance study the contaminant dispersion due to this characteristic regional wind.

I.P. Alves (✉) • G.A. Degrazia
Departamento de Física, Universidade Federal de Santa Maria, Campus Universitário, Prédio 13 CCNE, 97105-900 Santa Maria RS, Brazil
e-mail: ipmalves@gmail.com; degrazia@ccne.ufsm.br

D. Buske
Departamento de Matemática e Estatística, DME/IFM, Universidade Federal de Pelotas, Campus Universitário, CP 354, 96010-900 Pelotas, RS, Brazil
e-mail: danielabuske@pq.cnpq.br

M.T. Vilhena
Departamento de Engenharia Mecânica, Universidade Federal do Rio Grande do Su, Sarmento Leite, 425, 3° andar, 90046-900 Porto Alegre, RS, Brazil
e-mail: vilhena@pq.cnpq.br

D.G. Steyn et al. (eds.), *Air Pollution Modeling and its Application XXII*,
NATO Science for Peace and Security Series C: Environmental Security,
DOI 10.1007/978-94-007-5577-2_105,

A parameterization for the transport processes in a shear driven atmospheric boundary layer has been established employing turbulent statistical quantities measured during the north wind phenomenon in southern Brazil. The present parameterization is based on the Taylor statistical diffusion theory and a kinetic energy spectral model. Furthermore, for vertical regions in which the wind shear forcing is relevant, the eddy diffusivity derived from the north wind data presents a similar profile to those obtained from the non-extensive statistical mechanics theory.

Finally, a validation for the present parameterization has been accomplished, using an analytical dispersion model. The Prairie Grass data set, which presents high mean wind speed, is simulated. The analysis developed in this study shows that the turbulence parameterization constructed from wind data for north wind flow cases is able to describe the diffusion in a high wind speed, shear-dominated atmospheric boundary layer.

105.2 The Eddy Diffusivity for NWF Phenomenon

From the one-dimensional velocity spectra in neutral conditions (F_i) is possible to obtain the Eulerian turbulent velocity variance $\left(\sigma_i^2\right)$, calculated integrating the turbulent spectra over the whole frequencies domain, and the Lagrangian decorrelation time scale (T_{L_i}), which can be expressed as $T_{Li} = \frac{\beta_i F_i^E(n\to 0)}{4}$.

Following the Taylor diffusion model, the eddy diffusivity is given by the product $K_\alpha = \sigma_i^2 T_{L_i}$. In neutral conditions, the frequency of the spectral peak of the turbulent wind velocities (u, v, w) are represented by [2] $(f_m)_i = (f_m)_{0i}(1 + 0,03a_i f_c z/\mu_{*0})$, where $(f_m)_{0i}$ is the frequency of spectral peak at the surface, f_c is the Coriolis parameter, μ_{*0} the friction velocity at the surface and h is the neutral boundary layer height ($h \pm 0,2\mu_{*0}/|f_c|$) [5]. From the above considerations, results a general asymptotic eddy diffusivity written as:

$$\frac{K_z}{(u_*)_0 h} = \frac{0.1354 C_i^{1/2} \phi_\varepsilon^{1/3} \frac{z}{h}\left(1 - \frac{z}{h}\right)^{0.85}}{(f_m)_{0i}^{4/3}\left[1 + 0.006 a_i \frac{z}{h}\right]^{4/3}} \tag{105.1}$$

where C_i and a_i are constants and ϕ_ε is the non-dimensional dissipation rate function. Using typical values for the NWF ($(f_m)_{0w} = 0.33$, $a_w = 500$, $c_w = 0.36$, $\phi_\varepsilon = 1.1$) we obtain:

$$\frac{K_z}{(u_*)_0^h} = \frac{0.37 \frac{z}{h}\left(1 - \frac{z}{h}\right)^{0.85}}{\left[1 + 3.00 \frac{z}{h}\right]^{4/3}} \tag{105.2}$$

105.3 The Analytical Model

The advection-diffusion equation of air pollution in atmosphere is essentially a statement of conservation of a suspended material, and it can be written as:

$$\frac{\partial \bar{c}}{\partial t} + \bar{u}\frac{\partial \bar{c}}{\partial x} + \bar{v}\frac{\partial \bar{c}}{\partial y} + \bar{w}\frac{\partial \bar{c}}{\partial z} = \frac{\partial}{\partial x}\left(K_x \frac{\partial \bar{c}}{\partial x}\right) + \frac{\partial}{\partial y}\left(K_y \frac{\partial \bar{c}}{\partial y}\right) + \frac{\partial}{\partial z}\left(K_z \frac{\partial \bar{c}}{\partial z}\right) \tag{105.3}$$

where $\bar{u}$, $\bar{v}$, $\bar{w}$, K_x, K_y and K_z are, respectively, mean wind (m/s) and eddy diffusivities profiles (m^2/s) and $\bar{c}$ is the mean concentration of a passive contaminant (g/m^3).

Here, for comparison with experimental data and to use the parameterization obtained for the NWF (Eq. 105.2) we will assume: stationary conditions, crosswind integrated concentrations and, once we have strong winds, that the advection is much higher than the diffusion in the x-direction. The problem (105.3) is subjected to the usual boundary conditions of null flux concentration at the ground and top of the boundary layer as well a source condition represented by a generalized Dirac delta function.

The analytical solution of the proposed problem is obtained by the GILTT (Generalized Integral Laplace Transform Technique) approach [4]. The mean feature of the GILTT method comprehends the steps: solution of an associate Sturm-Liouville problem, expansion of the pollutant concentration in a series in terms of the attained eigenfunction, replacement of this expansion in the advection-diffusion equation and, finally, taking moments. This procedure leads to a set of differential ordinary equations, named the transformed equation. These equations are then solved analytically by the application of the Laplace transform technique without any approximation along its derivation, except the round-off error.

105.4 Numerical Results

Atmospheric conditions associated with the NWF cases are characterized by intense mean wind speeds and, consequently, wind shear forces generate a dominant mechanical turbulence. Therefore, one of the main peculiarities of the present turbulent parameterization is to be able to deal with turbulent dispersion in neutral situations. From these arguments we decided to simulate the classical Prairie Grass tracer dispersion experiments [1] that occurred under high mean wind speed conditions.

In the Prairie-Grass experiment the tracer SO_2 was released without buoyancy at a height of 0.46 m, and collected at a height of 1.5 m at five downwind distances (50, 100, 200, 400 and 800 m) at O'Neill, Nebraska in 1956. The site was quite flat

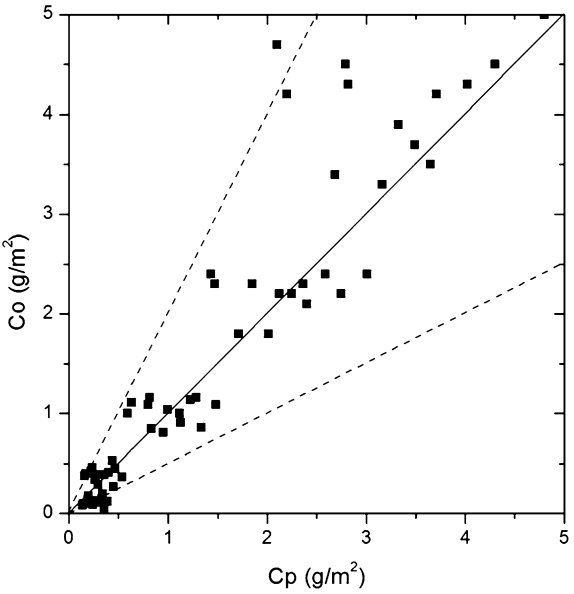

Fig. 105.1 Scatter plot of observed (Co) and predicted (Cp) concentrations for the Prairie-Grass experiment. *Lines* indicate a factor of two (C0/Cp ε [0.5;2])

Table 105.1 Statistical evaluation of the model for the NWF phenomenon

Model	NMSE	COR	FA2	FB	FS
GILTT	0.15	0.93	0.86	0.11	0.18

and much smooth with a roughness length of 0.6 cm. From the Prairie Grass runs we select 13 cases in which the mean wind speed was greater than 6.0 m/s with values of $(u_*)_0 > 0.4$ m/s.

In Fig. 105.1 is shown the scatter diagram of the ground-level observed concentrations at the Prairie-Grass experiment versus the simulated by the GILTT model. Looking at the scatter diagram we realize that the model reproduces satisfactorily the experimental observed concentrations.

Table 105.1 present the statistical indices [3] obtained using the analytical model. The best results are expected to have values near to zero for the indices NMSE, FB and FS, and near to one in the indices COR and FA2. The statistical indices point out that the model, together with the proposed eddy diffusivity for the NWF, reproduces adequately the Prairie-Grass observed concentrations.

105.5 Conclusions

In this work the new turbulent parameterization representing the dispersion condition in a shear dominated PBL occurring during the NWF cases, was evaluated and validated through a comparison with experimental concentration data. Partic-

ularly, the results obtained by the analytical dispersion model, incorporating the parameterization derived from the turbulent statistical characteristics associated to the NWF, agree very well with the experimental concentration data, indicating that the model represents the diffusion process correctly in intense wind speed neutral conditions.

Considering the statistical evaluation and the arguments discussed above the parameterization for the NWF phenomenon allied to the analytical dispersion model is found to be suitable to simulate the diffusion of passive scalars in a intense wind speed neutral ABL.

Acknowledgements The authors thank to Brazilian Research Council CNPq and FAPERGS for the partial financial support of this work.

References

1. Barad M (1958) Project prairie grass: a field program in diffusion. Geophys Res Paper N° 59 (II) TR-58-235 (II) Air Force Cambridge Research Centre USA
2. Degrazia GA, Anfossi D, Campos Velho HF, Ferrero E (2000) Turbulence parameterization for PBL dispersion models in all stability conditions. Atmos Environ 34:3575–3583
3. Hanna SR, Paine RJ (1989) Hybrid plume dispersion model (HPDM) development and evaluation. J Appl Meteorol 28:206–224
4. Moreira DM, Vilhena MT, Buske D, Tirabassi T (2009) The state-of-art of the GILTT method to simulate pollutant dispersion in the atmosphere. Atmos Res 92:1–17
5. Panofsky HA, Dutton JA (1984) Atmospheric turbulence. Wiley, New York

Chapter 106
Air Quality Study of High Ozone Levels in South California

Amela Jeričević, Darko Koračin, Jinhua Jiang, Judith Chow, John Watson, Eric Fujita, and Hiroaki Minoura

Abstract Physical and chemical characteristics within the two distinct meteorological regimes, i.e., convective and stable atmospheric conditions in a complex highly urbanized terrain of the California South Coast Air Basin (CSCAB; the Los Angeles area) were investigated. The Community Multi-scale Air Quality (CMAQ) model was used with a horizontal resolution of 5 km × 5 km to produce the 3D fields of pollutant concentrations. Input meteorological fields were obtained by the MM5 numerical weather prediction model while the input emissions were provided by the Californian Environmental Protection Agency. Modeled meteorological surface parameters and their vertical profiles as well as modeled planetary boundary layer heights (PBL) were compared to the corresponding measurements. The CMAQ simulations of ozone concentrations were compared against the relatively large number of measurements from the CSCAB area. The main goal of the research was to identify the governing atmospheric processes and sources in the coastal area that contributed to the high levels of pollution and to investigate the air quality model's capabilities to simulate the air quality in the complex topography.

Keywords Ozone • Model evaluation

A. Jeričević (✉)
Croatian Meteorological and Hydrological Service, Gric 3, 10000, Zgreb, Croatia
e-mail: jericevic@cirus.dhz.hr

D. Koračin • J. Jiang • J. Chow • J. Watson • E. Fujita
Desert Research Institute, University and Community College System of Nevada, P.O. Box 60220, Reno, NV 89506, USA

H. Minoura
Toyota Motor Engineering & Manufacturing North America, Inc, 1555 Woodridge Ave, Ann Arbor, MI 4810, USA

D.G. Steyn et al. (eds.), *Air Pollution Modeling and its Application XXII*,
NATO Science for Peace and Security Series C: Environmental Security,
DOI 10.1007/978-94-007-5577-2_106,

106.1 Introduction

The California South Coast Air Basin (CSCAB; the Los Angeles area) is known for its air pollution problems, especially for photochemical smog episodes. There has been a considerable amount of studies of air pollution in California (e.g., [1–4]). Frequently observed high levels of pollutants occur due to elevated anthropogenic emissions as well as due to special air circulation patterns which drive the pollutants complex temporal and spatial distribution. In this work an episode of high ozone concentrations that occurred in July 2005 was analyzed. CMAQ model was applied in order to investigate spatial and temporal distribution of pollutants and advantages and limitations as well as recommendations for future work are presented in this paper.

106.2 Results

106.2.1 Ozone Observations in California South Coast Air Basin

Measured hourly ozone concentrations from 21 stations in the domain during July 2005 are used for investigation. Due to specific meteorological conditions spatial and temporal distributions in surface ozone concentrations were not uniform especially during the episode of high ozone concentrations between 15 and 20 July 2005. Areas with different observed ozone levels were identified. Daily distributions of measured and modeled hourly ozone and NO_2 concentrations at different stations in CSCAB domain during July 2005 are shown in Fig. 106.1 Generally the highest ozone concentrations are observed on the stations inland in the eastern part of the Los Angeles (e.g., station 2077 in Fig. 106.1) while the lowest levels are present at coastal stations on the west part (e.g., station 2937 in Fig. 106.1). Medium levels with characteristic urban patterns are visible on four stations situated in the domain centre (e.g., station 2898 and 2160 in Fig. 106.1). For most of the stations measured ozone concentrations are characteristic for urban areas being the highest during the daytime when chemical production of ozone occurs in presence of NOx and sunlight and low nighttime ozone levels resulting from titration with NOx. The ozone July episode was most intensive in the inland stations on the eastern part of the Los Angeles while at coastal stations on the west part ozone levels were low and without high daily variations.

106.2.2 CMAQ Simulations

Surface high pressure system with subsiding air resulting in stable atmospheric conditions was present over the sea and in the coastal area while low pressure areas

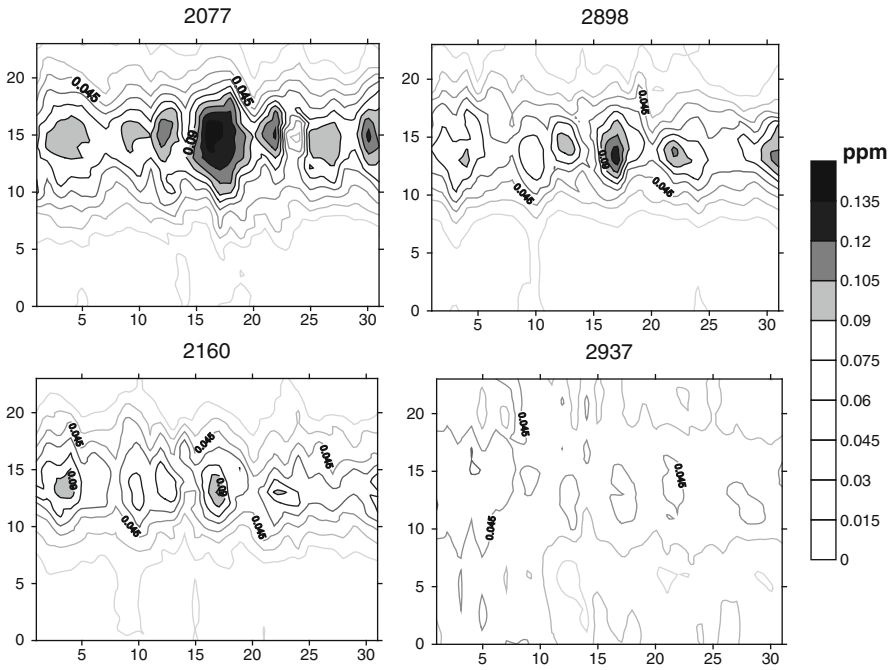

Fig. 106.1 Daily distribution of measured hourly ozone concentrations at different stations in CSCAB (California South Coast Air Basin) domain during July 2005

in the central and eastern part of the domain, where high ozone concentrations were measured, was prevailing during the episode (not shown). Surface wind speeds were generally low, especially during the night, with prevailing west direction. Modeled planetary boundary layer heights (PBL) were uniformly low during the nighttime while during the daytime in the southwest and central part of the domain low PBL values were present and northeast and east parts of the domain had significantly higher PBL values (not shown). Areas with higher daytime PBL height corresponds to the low pressure systems and high measured ozone levels were characterized with unstable, turbulent processes and intensive and mixing in the atmosphere.

Intercomparison of the measured hourly ozone concentrations to the modeled ozone and NO_2 values for different stations in the CSCAB (California South Coast Air Basin) domain are shown in Fig. 106.2 Generally model underestimates measured ozone values but model showed an ability to reproduce daily variations and high correlation factors $\sim$0.7 are found for most of the stations. Also boundary conditions used in CMAQ simulations were provided using profile option. However, a test with different boundary conditions (not shown) using the nesting option into a lower resolution CMAQ run on the larger domain showed a much better agreement with the measurements indicating that significant contribution to the high ozone levels was originating from the larger Californian area.

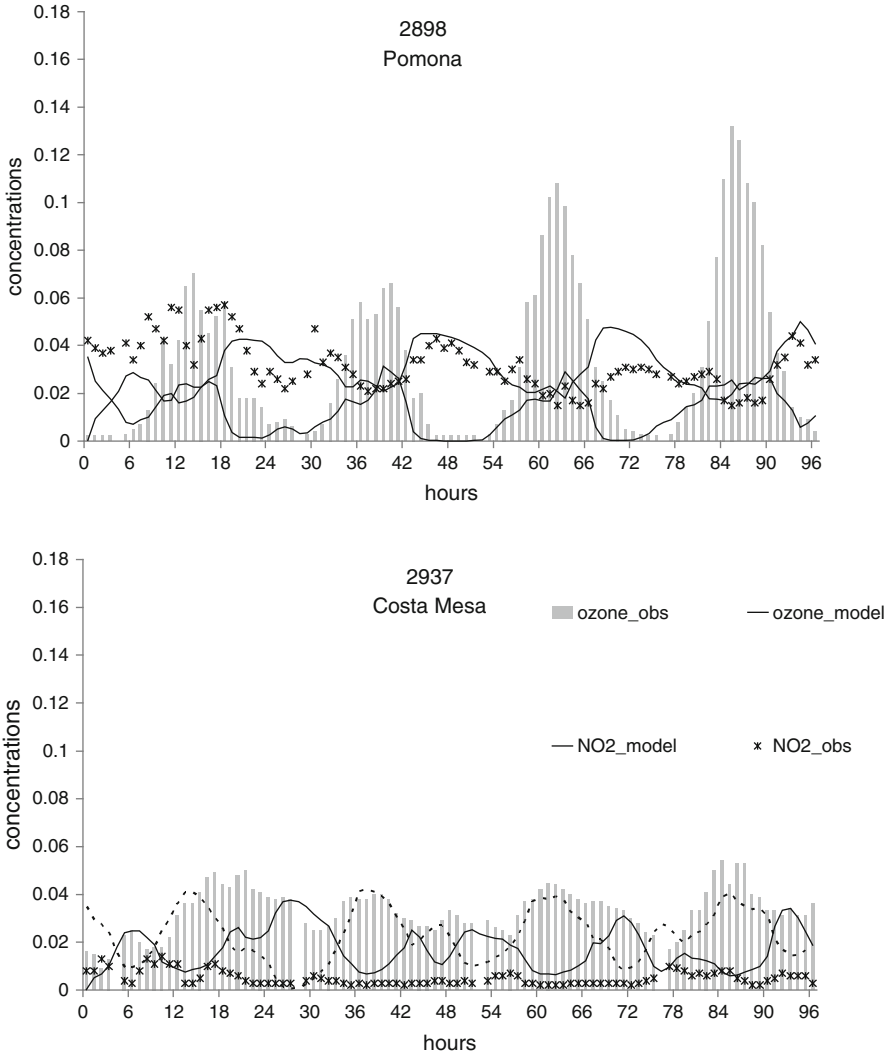

Fig. 106.2 Daily course of measured hourly ozone concentrations (*column*) and NO_2 (*black dot*) values and modeled ozone (*thick black line*) and NO_2 (*thin black line*) values on different stations in the CSCAB (California South Coast Air Basin) domain during 15 and 16 July 2005

106.3 Conclusions

An application of CMAQ air pollution model was conducted on an ozone episode occurred in July 2005. It is found that model was able to reproduce complex physical and chemical phenomena within the two distinct meteorological regimes, i.e., convective and stable atmospheric conditions in a complex highly urbanized

terrain of the California South Coast Air Basin (CSCAB; the Los Angeles area). Due to the fact that the highest ozone levels were found to be related with unstable conditions and high mixing in further work special attention should be given to the investigation of the relationship between the pollutant concentrations and turbulence characteristics in PBL including the investigation of existing vertical diffusion schemes performance in the CMAQ model.

References

1. Blumenthal DL, White WH, Smith TB (1977) Anatomy of a Los Angeles smog episode: pollutant transport in the daytime sea breeze regime. Atm Environ 12:893–907
2. Farber RJ, Huang AA, Bregman LD, Mahoney RL, Eatough DJ, Hansen LD, Blumenthal DL, Keifer WS, Allard DW (1982) The third in the Los Angeles Basin. Sci Total Environ 23:345–360
3. Luria M, Tanner RL, Valente RJ, Bairai ST, Koracin D, Gertler AW (2005) Local and transported pollution over San Diego, California. Atm Environ 39:6765–6776
4. Roth PM, Reynolds SD, Tesche TW, Gutfreund PD, Seigneur C (1983) An appraisal of emissions control requirements in the California South Coast Air Basin. Environ Int 9:549–571

Part VII
Local and Urban Scale Modelling

Chapter 107
Merging the Gap Between Meso and Micro Scales: Enhanced Inflow Boundary Conditions for CFD Modeling of Urban Air Quality

C. Borrego, M. Maché, J.H. Amorim, J.F. Sini, H. Martins, I. Calmet, J. Valente, V. Rodrigues, A.I. Miranda, D. Maro, J.M. Rosant, and C. Pimentel

Abstract Despite the advent of high performance numerical tools, the spatial gap between meso and microscale models is still a challenge in atmospheric modeling. The way boundary conditions are prescribed is crucial for the correct linkage between scales, especially in inhomogeneous canopies, which induce complex airflow dynamics and pollutant concentration patterns. The purpose of this work is to evaluate the sensitivity of microscale modeling results to distinct methods of deriving inflow vertical wind profiles in urban areas. The methodology involves the comparison of three methods for prescribing inflow profiles: (1) Log wind profile based on meteorological observations, (2) the mesoscale model WRF running at 200 m resolution, and (3) the LES model ARPS. The different profiles obtained were fed into the CFD model VADIS. The comparison of results against measured SF_6 concentrations shows that ARPS is capable of accounting for upwind region characteristics, providing more reliable inflow conditions. Moreover, VADIS has provided an enhanced and detailed insight over the 3D wind flow behaviour, accounting for the effects of buildings and trees, and its effect over dispersion.

Keywords CFD-modelling • Vertical wind profiles • Urban areas

C. Borrego (✉) • J.H. Amorim • H. Martins • J. Valente • A.I. Miranda • C. Pimentel
CESAM, Department of Environment and Planning, University of Aveiro, Aveiro, Portugal
e-mail: cborrego@ua.pt

M. Maché • J.F. Sini • I. Calmet
Ecole Centrale de Nantes, LHEEA UMR CNRS 6598, LUNAM Université, Nantes, France

V. Rodrigues • J.M. Rosant
CNRS, LHEEA UMR CNRS 6598, LUNAM Université, Nantes, France

D. Maro
Laboratoire de Radioécologie, Institut de Radioprotection et de Sûreté Nucléaire, Octeville, France

D.G. Steyn et al. (eds.), *Air Pollution Modeling and its Application XXII*,
NATO Science for Peace and Security Series C: Environmental Security,
DOI 10.1007/978-94-007-5577-2_107,

107.1 Introduction

Mesoscale and microscale models, and their applications, have traditionally followed separated approaches. Despite the advent of high performance numerical tools and hardware this spatial gap is still a challenge for the atmospheric modelling community dealing with air pollution issues, wind comfort, energy efficiency, urban planning or climate at the city scale. The way boundary conditions are prescribed to Computational Fluid Dynamics (CFD) is crucial for the correct linkage between scales, especially in inhomogeneous canopies, which induce complex airflow dynamics and pollutant concentration patterns.

107.2 Methodology

This work involves the comparison of three methods for prescribing inflow profiles, which were fed into the CFD model VADIS. The results were compared against data measured in the FluxSAP 2010 campaign. In these experiments, carried out in a district of Nantes (France) in May 2010, 25 releases of SF_6tracer gas were performed [3]. For this paper, one of the releases was selected corresponding to a stationary westerly wind varying from 2.4 to 3.1 $m{\cdot}s^{-1}$ at 21 m high, a quasi neutral atmosphere (MoninObukhov length $L = -300$ m), a release duration of 10 min, at about 1.5 m above ground. The gas concentration was measured using different techniques and in distinct locations.

Method 1: vertical wind profile was derived with the semi-empirical Log-law based on meteorological data measured in a nearby 21 m mast.

Method 2: data was downscaled from the mesoscale WRF model, which was applied to five domains, using the two-way nesting technique for domains 1–4, and one-way nesting between domains 4 and 5: domain 1 (D1) at 27 km resolution covering Western Europe; D2 at 9 km resolution over France; D3 at 3 km resolution over NW France; D4 with 1 km resolution over Nantes; and D5 with 200 m resolution over the study area. The Mellor-Yamada-Janjic scheme was selected for domains 1–4, while for the smallest domain the Large Eddy Simulation (LES) boundary layer, which uses diffusion for vertical mixing, was chosen.

Method 3: a new method was tested in which the vertical profile for temperature and wind obtained with WRF for the first 1,500 m (corresponding to 32 vertical layers) was supplied to the LES model ARPS, in which the canopy is represented by a mean drag force exerted by the buildings [2]. The drag force depends on the sectional drag coefficient $C_d(z)$ and on the frontal area density $a_f(z)$. $C_d(z)$ is parameterized according to plan area density and buildings height. $a_f(z)$ and all needed morphological parameters are calculated from a French urban database (BD Topo) by using a GIS software (OrbisGIS) over cells of $200 \times 200 \times 1$ m^3. The computing resolution of this ARPS run ($20 \times 20 \times 1$ m^3) permits to provide vertical profiles of wind and turbulence inside the canopy.

The three profiles obtained were then fed into the CFD model VADIS [1], in which 3D wind flow was simulated applying a RANS prognostic model with an extended k-ε turbulence closure for the simulation of green canopy, and SF_6 dispersion was tracked applying a Lagrangian approach. Virtual domain was generated using a GIS file, resulting in a total of 101 building blocks. Two hundred and fifty three blocks of trees were defined using satellite imagery. A regular mesh with 1.33×10^6 cells, $3 \times 3 \times 3$ m^3 resolution, was generated. Simulations were performed in steady-state conditions for 10 and 24 min.

107.3 Results and Discussion

VADIS results have been compared with SF_6 measurements carried out by different methods, and in distinct locations in the study area, as shown in Table 107.1.

In general, there is an overestimation of concentrations, which can be associated to the steady state conditions in which the simulations were carried out. However, there is a significant increase on accuracy when using ARPS model. The average relative error is 315 %, 170 % and 105 %, respectively for methods 1, 2 and 3. Figure 107.1 shows a comparison of the computed SF_6 dispersion.

Table 107.1 Geolocation of measuring points and comparison between observed and computed SF_6 concentrations. All values at 1 m above ground

Equipment #	Sampling period (min)	Location		SF_6 concentration ($\mu g \cdot m^{-3}$)			
		Lat	Long	Measured	Meteo.	WRF	ARPS
1	24	47.24570	1.52770	64	138	275	247
2	24	47.24550	1.52743	82	317	306	208
3	24	47.24535	1.52729	95	489	206	166
4	24	47.24519	1.52700	110	393	102	134
5	24	47.24500	1.52672	74	241	48	125
6a	10	47.24535	1.52729	210	910	510	287
6b	24	47.24535	1.52729	109	489	206	166
7a	10	47.24541	1.52745	163	743	599	329
7b	24	47.24541	1.52745	78	461	284	190

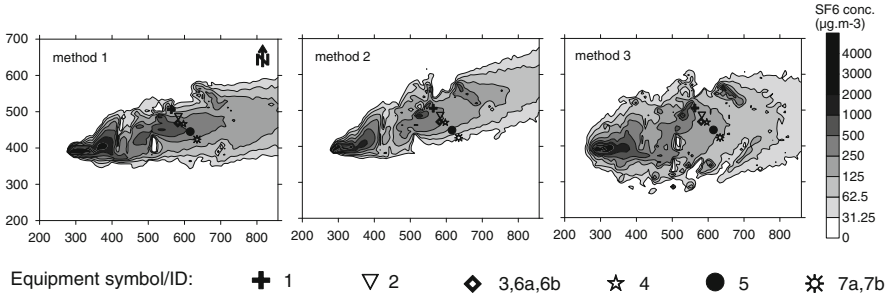

Fig. 107.1 SF_6 concentration fields (1.5 m high) simulated by VADIS. Axis in meters. For simplicity, buildings and trees were not represented

The patterns of SF_6 concentration are significantly distinct for the three methods. Particularly for WRF/ARPS profile (method 3) there is an increase of the overall complexity of the tracer dispersion.

107.4 Conclusions

Three methods for prescribing inflow profiles have been compared: (1) nearby wind measurements, (2) WRF downscaling, and (3) WRF/ARPS approach. This paper shows that inflow conditions are highly dependent on the arrangement of upwind buildings and that micro scale air quality modelling accuracy can be significantly affected by the method used for prescribing inflow vertical profiles. The LES model ARPS has shown to be capable of accounting for upwind region characteristics, providing more reliable inflow conditions than the ones derived directly from observed data or from mesoscale model downscaling techniques. With the input data from WRF/ARPS, VADIS has provided an enhanced and detailed insight over the 3D wind flow behaviour, accounting for the effects of buildings and trees, and its effect over dispersion. This approach appears to be a promising method of describing the real urban canopies and merging the existing gap between meso and micro scales.

Acknowledgements This work was partly funded, in the framework of the Portugal-France Agreement, by FCT under the Pessoa Programme 2010–2011, and by the HPC resources of IDRIS under the allocation 2010010132 made by GENCI. FCT is acknowledged for the Post-Doc grants of J.H. Amorim (SFRH/BPD/48121/2008), H. Martins (SFRH/BPD/66874/2009) and J. Valente (SFRH/BPD/78933/2011), and INSPIRAR project (PTDC/AAC-AMB/103895/2008).

References

1. Borrego C, Tchepel O, Costa AM, Amorim JH, Miranda AI (2003) Emission and dispersion modelling of Lisbon air quality at local scale. Atm Environ 37:5197–5205
2. Maché M, Calmet I, Sini J-F (2010) Analysis of the dynamical interactions between atmosphere and urban canopies of different densities using a drag force approach. In: Proceedings of 13th international conference on Harmonisation within Atmospheric Dispersion Modelling for Regulatory Purposes (HARMO13), Paris, France, 1–4 June 2010, pp 668–672
3. Maro D, Calmet I, Mestayer P, Goriaux M, Hubert D, Connan O, Letellier B, Defenouille P, Rosant JM, Rodrigues V (2011) FluxSAP 2010 experimental campaign over an heterogeneous urban zone, Part 2: Quantification of plume vertical dispersion during a gas tracer experiment using a mast and a small tethered balloon. In: Proceedings 14th international conference on Harmonisation within Atmospheric Dispersion Modelling for Regulatory Purposes (HARMO14), Kos, Greece, 2–6 Oct 2011, pp 438–442

Questions and Answers

Questioner name: M. Sofiev

Q: Could you please show the location of the sites used for the evaluation? Where were they with regard to plume location?
A: The positioning of the equipment relating the emission source and the plume is shown in Fig. 107.1. Please notice that some of the equipment have the same location (i.e., 3 = 6a = 6b and 7a = 7b), the difference relies on the type of measuring method and the acquisition period.

Questioner name: Billaiev M.

Q: What's the order of your difference scheme? Do you have the oscillations of the numerical solution and what do you do with them?
A: VADIS model uses the control volumes/finite differences method for the resolution of the Navier- Stokes equations with Reynolds mean in a stationary flow, at turbulent regime. The discretisation schemes used are, optionally, the exponential or the power law. Under relaxation factors are defined in order to suppress oscillations that would result in divergence. Residuals are monitored until convergence criterion is fulfilled.

Questioner name: Bertrand Carissimo

Q: You have shown that LES + porosity-drag gives better results than the log law or WRF boundary profiles, but have you tried to use a more realistic canopy profile (Mac Donald's type) or the urban parameterization in WRF?
A: Our goal was to use two popular methods for deriving boundary conditions for a CFD model: downscaling from a mesoscale meteorological model and an empirical vertical wind profile. Other methods could be adopted, but these two are definitely among the most frequently applied.

Questioner name: Eduardo Barbaro

Q: How do you account for sub-grid processes specially in the first meters of the ABL?
A: Sub-grid-scale turbulence is parameterized in the model using the standard k-ε model.

Chapter 108
Statistical Variability of Dispersion at Local and Regional Scales: LPDM-LES Model Ensembles and Observations

Jeffrey Weil, Peter Sullivan, Edward Patton, and Chin-Hoh Moeng

Abstract A Lagrangian particle dispersion model (LPDM) driven by velocity fields from large-eddy simulations (LESs) is used to determine the mean and variability of plume dispersion at local and regional scales in a highly convective boundary layer. Comparison of the LPDM-LES results with data from two field experiments shows that they match the observations reasonably well.

Keywords Boundary layer • Dispersion variability • Lagrangian particle model

108.1 Introduction

Statistical variability of dispersion is important for air quality applications at local and regional scales—i.e., from the microscale to the low end of the mesoscale—and is typically greatest in a convective boundary layer (CBL) with light winds. Under these conditions, an elevated plume undergoes significant "meandering" due to the CBL's strong updrafts and downdrafts, which leads to large concentration fluctuations. The fluctuations can be characterized by their root-mean-square (rms) value σ_c or the fluctuation intensity σ_c/C, where C is the ensemble-mean concentration. Observations show that σ_c/C at the surface typically ranges from 1 to 10 and greater for short averaging times (<1 h) and downstream distances (≤ 5 km). Thus, knowledge of the fluctuations is important for predicting the peak concentrations of toxics and evaluating dispersion models.

J. Weil (✉)
CIRES, University of Colorado, Boulder, CO 80309, USA
e-mail: weil@ucar.edu

P. Sullivan • E. Patton • C.-H. Moeng
National Center for Atmospheric Research, Boulder, CO 80307, USA

D.G. Steyn et al. (eds.), *Air Pollution Modeling and its Application XXII*,
NATO Science for Peace and Security Series C: Environmental Security,
DOI 10.1007/978-94-007-5577-2_108,

To determine the statistical variability of dispersion, one needs an ensemble of dispersion realizations collected under the same conditions. In this work, we use a Lagrangian particle dispersion model (LPDM) driven by velocity fields from large-eddy simulations (LES) of the CBL to generate such an ensemble. From the realizations, we calculate the mean, root-mean-square (rms) deviation, and fluctuating fields of dispersion properties including the plume height, dispersion parameters (σ_y, σ_z), and concentrations. The calculations are compared with data from two field experiments.

108.2 Models and Generation of Ensembles

In an LPDM, one tracks passive "particles" in a turbulent flow assuming that the particles behave as fluid elements and move with the local fluid velocity. For a continuous source of strength Q, the concentration is found from the probability density function (PDF), p_1, of the particle position $\boldsymbol{x}_p$, where the boldface symbol denotes a vector. That is, $C = Q \int p_1(\boldsymbol{x}_p, t; \boldsymbol{x}_{os}, t')dt'$, where the integral is over the particle emission time (t') history up to the present time t, and $\boldsymbol{x}_{os}$ is the source location. The $\boldsymbol{x}_p$ is found by integrating $d\boldsymbol{x}_p/dt = \boldsymbol{u}_L(\boldsymbol{x}_{os}, t)$, where $\boldsymbol{u}_L$ is the Lagrangian velocity of a particle released at $\boldsymbol{x}_{os}$. In this "one-particle" Lagrangian model, one follows thousands of particle trajectories to obtain p_1 and the concentration.

Here, we find the $\boldsymbol{u}_L$ from the LES below using the Weil et al. [5] model in which $\boldsymbol{u}_L$ is given by the sum of the LES resolved velocity $\boldsymbol{u}_r$ and a random subfilter-scale (SFS) velocity $\boldsymbol{u}_s$, both obtained at the particle position $\boldsymbol{x}_p$ at time t: $\boldsymbol{u}_L = \boldsymbol{u}_r + \boldsymbol{u}_s$. This approach is similar to that of Lamb [3] except for a more detailed SFS model and a finer spatial resolution (21 m) in the LES.

The LES model used was that of Moeng and Sullivan [4]. It was run for a CBL with a $5 \times 5 \times 2$ km domain and 96^3 grid points, a surface heat flux of 0.24 K ms^{-1}, an average CBL height z_i of 1 km, and a convective velocity scale w_* of 2 ms^{-1}. Other variables were the surface roughness length (0.16 m), the friction velocity u_* (0.31 ms^{-1}), the mean wind speed U over the CBL (3 ms^{-1}), and the Monin-Obukhov length L ($= -9.4$ m). The parameter $-z_i/L$ characterizing the overall bulk stability was 106, which classified the CBL as highly convective.

The LPDM ensemble was generated by releasing passive particles from each of 30 sources at height z_s in a horizontal plane to create 30 "independent" realizations; the sources had separations of 1 km ($= z_i$) and 1.5 km ($= Uz_i/w_*$) in the y and x directions, respectively. For each source, 715 particles were released every 20 s to simulate a continuous plume, and this was carried out for a 28-min averaging period for each of three source heights: $z_s/z_i = 0$, 0.07, and 0.32. The total number of particles released was 60,775 per source and 1.8×10^6 for sources of a given z_s.

108.3 Results

The LPDM realizations, mean values, and variability in dispersion properties are compared with observations from the CONDORS [2] and Prairie Grass [1] experiments. The CONDORS cases selected are those with multiple releases from a given height: a surface source and an elevated source ($z_s/z_i = 0.32$) with ten and five repetitions, respectively. The dispersion properties are shown as a function of the dimensionless downwind distance $X = w_* x/(U z_i)$, which is the ratio of travel time (x/U) to the eddy turnover time (z_i/w_*).

Figure 108.1 compares the LPDM results of scaled plume height z_p/z_i with the CONDORS data for the surface and elevated sources. The realizations overlap well with the measurements and generally reproduce the trend of the data scatterband with X, with the LPDM mean falling in the middle of the scatterband. Such overlap also occurs for the LPDM rms deviation [6]. The above is true with the exception of two "outlier" cases for the surface release [Periods (Pds) 32, 33]. Briggs [2] classified the outliers as "squashed plumes" caused by a persistent mean downdraft velocity as measured on a nearby 300-m tower.

Figure 108.2 presents the dimensionless crosswind-integrated concentration (CWIC), $C^y U z_i/Q$, at the surface as a function of X for the surface source and shows that the LPDM mean is in fair agreement with surface layer similarity (SLS) theory except close to the source, where the model sampling grid is too coarse. For $X > 0.3$, almost all of the data fall within the range of the LPDM realizations (black dots), except for the "squashed plume" cases, and most of the observations fall within the predicted rms error band (for this see [6]). This is encouraging and suggests that the turbulence variability in the LES resolved-velocity field is the principal cause of the CWIC variability.

Weil et al. [6] give more extensive comparisons between the LPDM results and field data. They include modeled realizations of plume height, dispersion parameters, and CWICs, and the statistics derived from them.

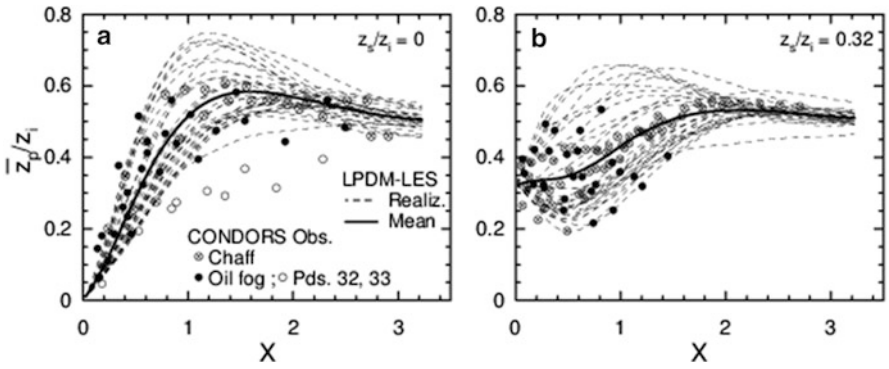

Fig. 108.1 Dimensionless plume height versus dimensionless distance X for LPDM predictions and comparison to the CONDORS data

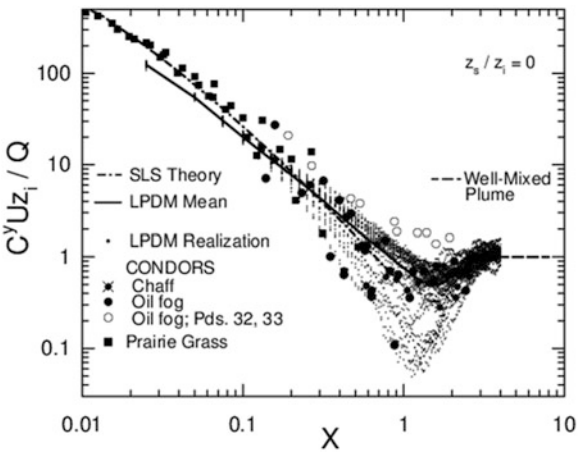

Fig. 108.2 Dimensionless CWIC at the surface as a function of X for a surface source with LPDM results compared with CONDORS and Prairie Grass observations

Acknowledgements This work was sponsored by the U.S. Army Research Office (Grant W911NF-09-0572) and in part by the Defense Threat Reduction Agency.

References

1. Barad ML (1958) Project Prairie Grass. A field program in diffusion. Geophysical Research Paper No. 59, vols I and II. Air Force Cambridge Research Center, Bedford
2. Briggs GA (1993) Plume dispersion in the convective boundary layer. Part II: analyses of CONDORS field experiment data. J Appl Meteor 32:1388–1425
3. Lamb RG (1978) A numerical simulation of dispersion from an elevated point source in the convective planetary boundary layer. Atmos Environ 12:1297–1304
4. Moeng C-H, Sullivan PP (1994) A comparison of shear- and buoyancy-driven planetary boundary layer flows. J Atmos Sci 51:999–1022
5. Weil JC, Sullivan PP, Moeng C-H (2004) The use of large-eddy simulations in Lagrangian particle dispersion models. J Atmos Sci 61:2877–2887
6. Weil JC, Sullivan PP, Patton EG, Moeng C-H (2012) Statistical variability of dispersion in the convective boundary layer: ensembles of simulations and observations. Bound-Layer Meteorol 145:185–210

Question and Answer

Q: Stefano Galmarini: I would recommend for the sake of completeness of the information your simulations provide to produce a Talagrand diagram. It will give you confidence in the convergence of your simulations of the measurement range.
A: Jeffrey Weil: We will consider producing such a diagram in future analysis of the simulations and observations.

Chapter 109
Modelling the Budget of Main Atmospheric Pollutants in Paris Region

Marje Prank, Julius Vira, and Mikhail Sofiev

Abstract The paper evaluates the air pollution budget of Paris by means of multi-domain nested simulations with detailed import-export fluxes delivered by the SILAM model. It is demonstrated that as a grand-total, Paris is a net exporter of nitrogen compounds, several VOCs and primary PM emitted from anthropogenic sources or produced chemically on a short time scale (a few hours). The city is a net importer of NH_3. The budgets of pollutants with long lifetime and high free-troposphere concentrations (CO, O_3) were shown to depend on height.

Keywords SILAM-model • Paris • Budget analysis

109.1 Setup of the Experiment

The experiment was built on a series of nested simulations by SILAM dispersion model (http://silam.fmi.fi/). The domains were set gradually shrinking around Paris (Fig. 109.1) with detailed budget for all pollutants computed for each of them.

CEur: resolution: $0.125 \times 0.065°$, 6 min, 12 layers up to ~8 km.
D4: nested into CEur; resolution: $0.025 \times 0.025°$ (about 3 km), 2 min.
D1-3: nested into D4; resolution same as D4.

Computations were made for 2.–31. July 2009 (**S**) and 15. Jan–15. Feb 2010 (**W**).

Emission: TNO-MEGAPOLI data, high-resolution part for Paris from AirParif.
Chemistry: SILAM heterogeneous chemical mechanism (Acid-Basic) and CB4.
Meteorological input data: IFS ECMWF $0.25 \times 0.25°$ (W); FMI-HIRLAM $0.15 \times 0.15°$ (S Ceur, D4); Enviro-HIRLAM $0.025 \times 0.025°$, (S D1-3).

M. Prank (✉) • J. Vira • M. Sofiev
Finnish Meteorological Institute, Helsinki, Finland
e-mail: marje.prank@fmi.fi

D.G. Steyn et al. (eds.), *Air Pollution Modeling and its Application XXII*,
NATO Science for Peace and Security Series C: Environmental Security,
DOI 10.1007/978-94-007-5577-2_109,

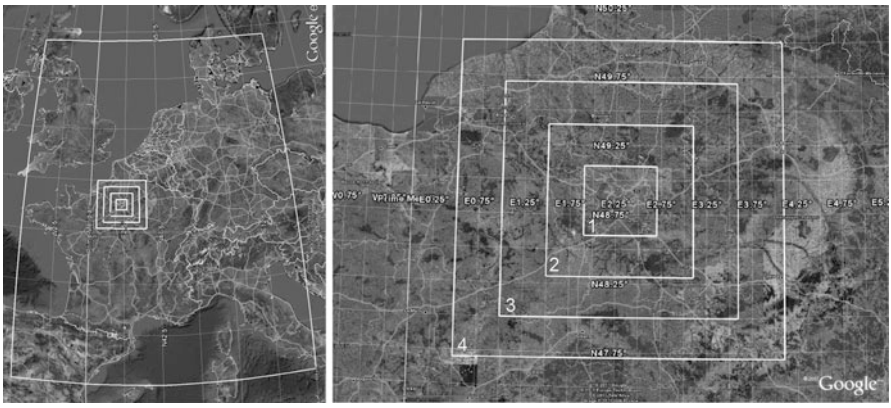

Fig. 109.1 The domains of the SILAM nested simulations (CEur *left*, D1–4 *right*)

109.2 The Total Budget of Atmospheric Pollutants

The main outcome of the study – the pollution budget – is presented in Fig. 109.2

The main exported species are nitrogen compounds, several VOCs and primary PM. The area imports sea salt, NH3 and some short lived species, in some cases SO2. For most species the budget gets closer to neutral further from Paris centre (D1–D4). However, this is not always the case – secondary species are mainly formed already away from the centre and for instance more NH3 is consumed in larger area in winter. CEur domain is a strong exporter of most pollutants.

Intriguingly, O3 and CO show almost neutral budget in all domains, though O3 has a strong sink in the city (reaction with the NO emission) and regional-scale production and thus should be strongly imported by at least the innermost domain, while for CO, the strong direct traffic emission from downtown with only slow large-scale sinks should make it a strongly exported species. However, considering separately in- and outgoing fluxes for each model layer, one sees that the lower layers are behaving as expected. Ozone is imported up to about a kilometer height by all inner domains and CO exported by the innermost domain. CO import in summer by lower layers of D2 and D3 (Fig. 109.3) can be explained by the vertical profiles of species involved in its chemical transformations (HCHO, OH, NO3 radical etc.). The near surface budgets are overshadowed by the thick upper layers.

109.3 Diurnal and Seasonal Variations

Seasonal and diurnal variations of the budget are shown on Fig. 109.4. The emission of some species (C5H8, NH3) varies seasonally; also chemistry is slower in winter, leading to stronger export of primary species and slower production of secondary ones. For O3 and PAN this is enough to turn summertime export to wintertime import.

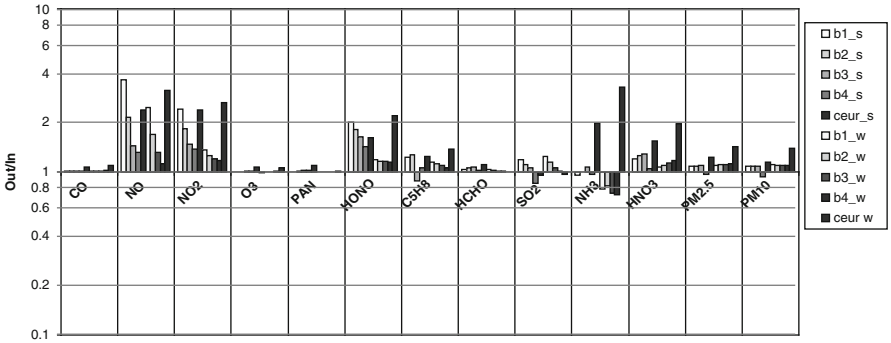

Fig. 109.2 Ratio of outbound and inbound fluxes (out/in) of main pollutants for all domains (D1-4, CEur) for summer (*subscript _s*) and winter (*subscript _w*). Positive values indicate export

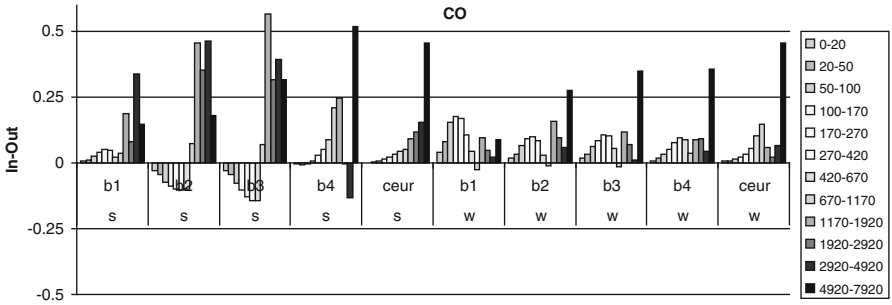

Fig. 109.3 Normalised net flux for model levels (*left* O3, *right* CO)

Expectedly, the agents affected by photolysis and temperature dependent reactions, (e.g. HONO, O3, PAN, NH3, NH4NO3) have different daytime and nighttime behavior. For NO and NO2 the difference is enforced by the diurnal variations of emission.

109.4 Model Performance and Sensitivity Tests

Model results were validated against AirParif observational data (Fig. 109.5). For most pollutants the model performance was found similar for rural, suburban and urban stations, with the exception of NO2 in summer which is clearly better for rural stations. The high resolution computations for the inner domains scored at similar level to the large scale model runs, or in some cases even worse (O3, summer).

One reason for such result is that different meteo data was used for different domains in summer. For winter the same meteo was used for all domains and such differences are not visible there. Meteorology can affect the computations by e.g.

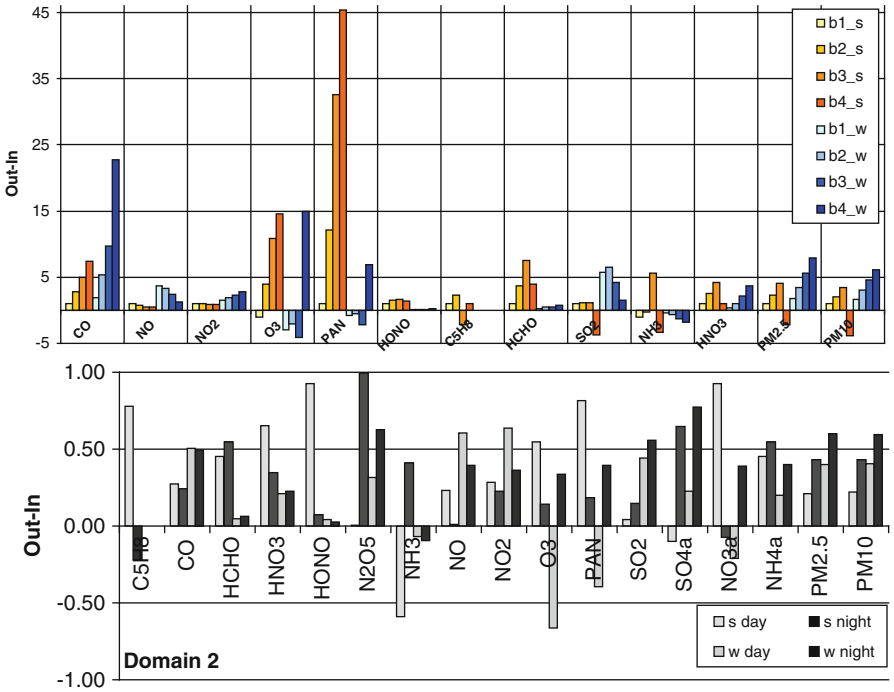

Fig. 109.4 Budgets for summer and winter (*upper*); daytime and nighttime (*lower*)

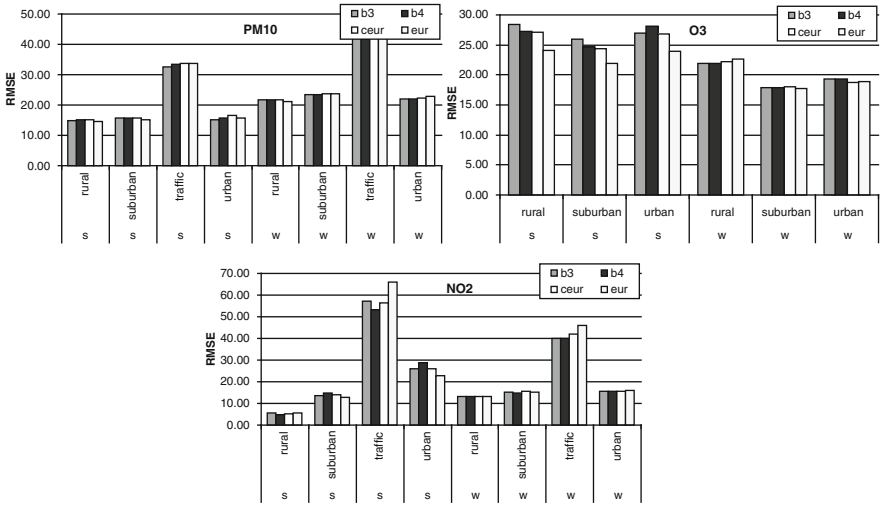

Fig. 109.5 Root mean square error of the modeled concentrations of PM10, O3, NO2

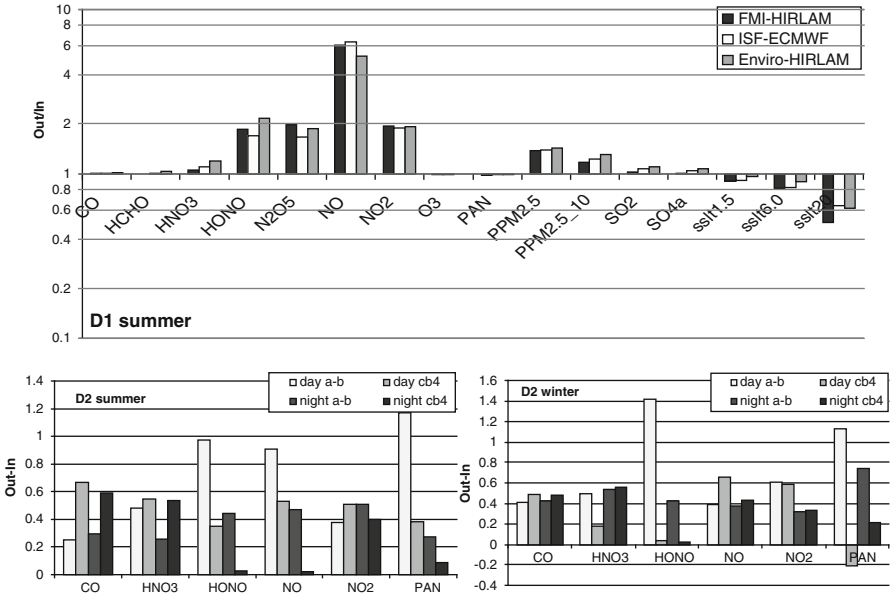

Fig. 109.6 The impact of meteo and chemistry

the wet and dry deposition or vertical fluxes, or chemistry through temperature, humidity etc. The sensitivity of the budget to meteo fields was quantified by repeating the D1 summer computations with IFS ECMWF and FMI-HIRLAM input (Fig. 109.6, up). For most species, the differences were found quite small.

The budgets for common species in CB4 and Acid-basic schemes are shown on Fig. 109.6. The schemes agree well for NO2 budget, though their agreement is not so close for its concentration. The almost neutral budgets of CO and PAN result in uncertain net flux. Large differences were found for species involved in fast transformations (NO, HONO). The differences in HNO3 budget are caused by different reactions present in the schemes – it is terminal species for CB4.

109.5 Summary

Multi-domain nested simulations of SILAM model have quantified the budget of Paris at several different distances from center. NOx, primary PM, anthropogenic VOCs, and their direct chemical derivatives are exported by the city, while NH3 is clearly imported and SOx budget depends on domain and season. The budget for CO and O3 strongly depend on altitude, integral over the column is almost neutral. Seasonal and diurnal variations in emission and chemistry reflected in the budget.

Simulations were performed with two chemical mechanisms and three meteorological inputs to quantify the uncertainties. Regional model performance in large city was found comparable with rural areas; higher resolution not always brought better model performance. Budget proved quite robust regarding the meteo input, the choice of chemistry scheme can strongly affect the results.

Acknowledgments This study was performed within the scope of the FP-7 MEGAPOLI & TRANSPHORM projects.

Questions and Answers

Questioner Name: Nicholas Savage

Q: In comparing resolution you focused on RMSE which can give a double penalty. Did you look at other statistics?
A: We looked at statistics like bias and ratio of standard deviations which should not be affected by this problem. The picture is very similar also for these statistics.

Chapter 110
Estimation of Efficient Height of Buildings for Urban Dispersion Models

Jan Burman

Abstract The purpose of the study was to establish an efficient height for block buildings used as geo-data by simplified urban dispersion models when the buildings in the Real world could have gabled roofs or carry a lot of objects as chimneys, antennas and other things. Assuming that CFD with RANS models can mimic the Real world, comparisons are made on the flow around buildings. Efficient height is defined as the height of a flat roof building when the flow around it most resembles the flow around a building with another shape. The results indicate that the efficient height should be somewhere between just below rooftop height and rooftop height + 5 m. But most of the results indicate that the efficient height should be close to the roof top value.

Keywords Urban dispersion • CFD-RAMS • Building influence

110.1 Background

A common assumption for simplified urban dispersion models is to only consider flat roof buildings. Therefore it is reasonable to derive a dataset that is adjusted to the needs of such a model, e.g. [1]. This includes some simplifications of the geometries but also which is the item here, to make an estimation of an efficient height of the buildings that allows the model to work with flat roof models but the essential flow around the buildings will mimic the flow around a building of the original shape.

J. Burman (✉)
FOI, CBRN Defence and Security, Cementvägen 20, SE-901 82 Umeå, Sweden
e-mail: jan.burman@foi.se

D.G. Steyn et al. (eds.), *Air Pollution Modeling and its Application XXII*,
NATO Science for Peace and Security Series C: Environmental Security,
DOI 10.1007/978-94-007-5577-2_110,

110.2 Methods

The main assumption is that there exists a model that can mimic the flow in the Real world[1] to that extent that results in the model can be transferred to the Real world. Here is assumed that simulating a stationary state of the flow with a RANS (Reynold Averaged Navier Stokes) model is acceptable but it is important to select the turbulence model within the RANS-model according to the scenario. Any turbulence model is tuned to solve a specific type of problems. Flow around bluff bodies and complex geometries are our concern here. The K-eps-model by [2] has shown to have good performance in bluff body flow and is chosen. Here is used the commercial CFD-package PHOENICS [3] which includes the models mentioned. The parameter used for comparison could be any that reflects the effects of the flow as i.e. turbulent viscosity, turbulent kinetic energy or velocity. Simplified dispersion models may rely on a mass conservative approach and thus only calculate velocity and this can be directive. Therefore the wind field velocity may be an appropriate parameter to choose for the comparison. A number of points are selected around the buildings studied and the wind vectors components are used. Of all possible scenarios of flow around buildings only a few are chosen. Primarily the effect of different shapes of the roof is investigated. The chosen types of roofs are: Flat roof, Gabled roof, Rough roof (flat roof with chimneys and ventilation tubes). These are for some scenario combined to two-building cases. The evaluation needs some well defined Statistical Performance Measures, (SPM). A suggestion from [4] is Factor of 2, (F2). The F2 parameter represents the fraction of data that satisfy $0.5 < \psi p/\psi o < 2$, where ψp is the predicted value and ψo is the referent value. For a perfect model F2 equals 1. In this case, the measure is robust, consistent and easy to understand. First a referent dataset with flat roof buildings is compiled and then a comparison dataset is constructed with different configuration. Gabled roof with different elevation and also rough roofs are evaluated.

110.3 Comparison Cases

The configurations studied are gabled roofs with zero and 90° angle to the wind and rough roofs (with chimneys) and combinations of houses to evaluate skimming effects. Wind speed changes are also studied. An example of the combinations is found in Table 110.1.

[1]Real world is referring to the part of the reality that we are interested of and are trying to simulate in the model.

Table 110.1 Description over configuration used for establishing the efficient height

Configuration	Test set	Referent set
(A) Gable roof, side	Square footprint 20 × 20 m^2, gabled roof with side towards the wind, 15–35 m. Wind at 0 m is 2 m/s.	Square footprint 20 × 20 m^2, flat roof with height 15–35 m

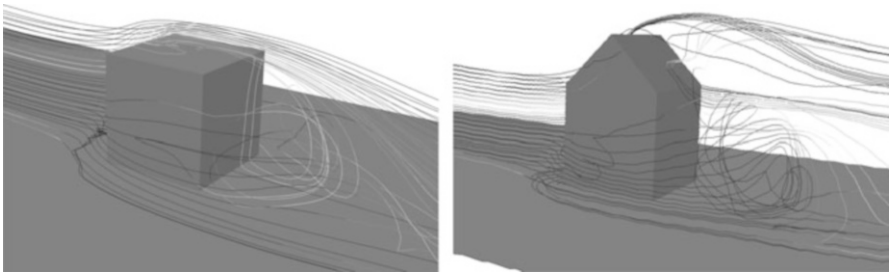

Fig. 110.1 and 110.2 Streamlines around the building types studied. Flat roof (Fig. 110.1) with recirculation on the top and gabled roof top (Fig. 110.2) with elevated flow over the building

110.4 Results

By studying the streamlines around buildings an understanding of the effects from different configurations is facilitated. Figures 110.1 and 110.2 show how the streamlines differ depending on the shape of the roof. The evaluation on efficient height is still based on F2.

The evaluation sheet from Configuration A (cf. Table 110.1) is plotted in Fig. 110.3. The value of F2 is approximately between 0.70 and 0.95 (1.0 means all values are within a factor of 2 from the referent value). Each line represents a certain configuration with a specific height. The maximum value of the line indicates which height a flat roof building should have to give the most similar flow. For instance, a gabled roof with the top at 24 m would have an efficient height represented by a flat roof at about 30 m.

For the Configuration A it is clear that the efficient height overshoots the rooftop height with up to 4–5 m. In other configurations, (not shown here) the overshoot is negligible and the efficient height equals the rooftop.

110.5 Conclusions

The results for the configurations chosen indicate that the efficient height should be somewhere between just below rooftop height and rooftop height + 5 m. But most of the results indicate that the efficient height should be close to the roof top value.

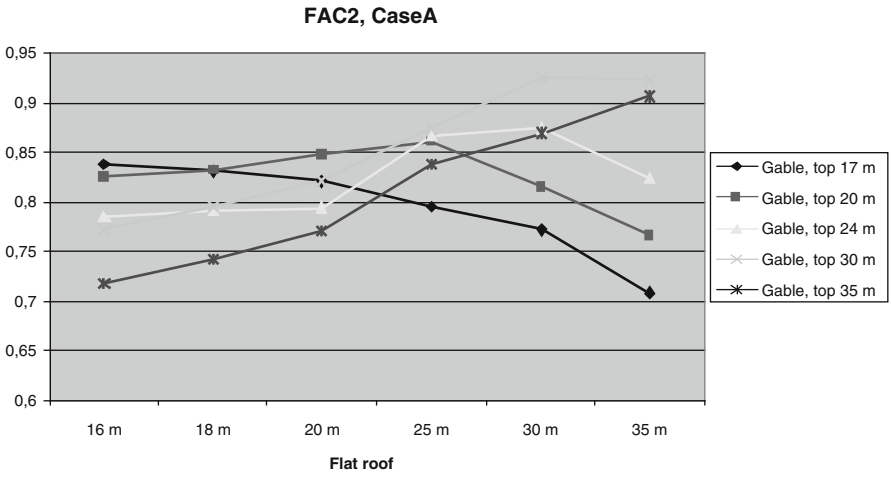

Fig. 110.3 The evaluation sheet show efficient height for configuration A for the tested heights respectively

Considering that a general algorithm calculating an efficient height should include wind direction and distances to buildings close by and that the data set at this stage needs to be processed before wind flow calculation a simplified guideline should be enough. The efficient height of the dataset for building heights produced for a simplified urban dispersion model is:

If the roof is a flat roof: Efficient height = Flat Roof height
If the roof is a rough roof: Efficient height = Flat Roof height
If the roof is a gable roof: Efficient height = Rooftop height at the ridge.

For rough roofs it can be assumed that if bluff bodies are placed on a flat roof as chimneys and antennas they can be neglected as long they are sparsely placed on a flat roof.

References

1. http://www.pdc.dk/Argos/. Accessed 29 Feb 2012
2. Chen YS, Kim SW (1987) Computation of turbulent flows using an extended k-e turbulence closure model. NASA CR-179204
3. http://www.cham.co.uk/. Accessed 29 Feb 2012
4. Jagger SF et al (1998) Definition of parameters for model runs. SMEDIS report 96/14/D

Chapter 111
Combining Models for Assessment of Local Air Quality

Wouter Lefebvre, Bino Maiheu, Jean Vankerkom, Liliane Janssen, Jan Bel, Tim Op't Eyndt, and Stijn Janssen

Abstract Assessing local air quality can be a challenging task. Indeed, local air quality is strongly dependent on local factors but also regional and in some cases even global effects have to be taken into account when assessing local air pollution concentrations. Furthermore, large gradients in pollutant concentrations can be present in the urban environment. In order to assess the local air quality for the city of Antwerp, a combination of an Eulerian dispersion model, a measurement interpolation tool, a Gaussian plume model and a simplified version of the OSPM street canyon model have been coupled to each other, taking into account double counting effects of local emissions. The coupled model which combines the regional, urban and street canyon scale has been applied for the city centre of Antwerp and its harbour. This results in detailed maps with a resolution up to 30 m for four pollutants: PM_{10}, $PM_{2.5}$, EC (elementary carbon) and NO_2. Furthermore, several abatement measures have been assessed in order to improve the urban air quality. It has been shown that local (traffic) measures only have a small effect on total mass PM_{10} and $PM_{2.5}$ concentrations, but exhibit a larger effect on EC and NO_2-concentrations.

Keywords Local air quality • Coupled models

W. Lefebvre (✉) • B. Maiheu • J. Vankerkom • L. Janssen • T. Op't Eyndt • S. Janssen
Vlaams Instituut voor Technologisch Onderzoek (VITO), Boeretang 200, 2400 Mol, Belgium
e-mail: wouter.lefebvre@vito.be

J. Bel
Stad Antwerpen, Stadsontwikkeling, Energie & Milieu, Grote Markt 1, 2000 Antwerpen, Belgium

D.G. Steyn et al. (eds.), *Air Pollution Modeling and its Application XXII*,
NATO Science for Peace and Security Series C: Environmental Security,
DOI 10.1007/978-94-007-5577-2_111,

111.1 Introduction

Modelling of air quality leads to a better understanding of the spatial distribution of air pollution. Furthermore, it is necessary to set up a modelling study if the air quality needs to be assessed in a complete region. However, local air quality is strongly dependent on local factors but also regional and in some cases even global factors have to be taken into account when assessing local air pollution concentrations. Therefore, a chain of different models (ranging from the regional scale to the local and the street canyon scale) has been applied in order to model the air quality for the city of Antwerp, one of the major hotspots in the polluted area of Flanders, Northern Belgium.

111.2 Model Chain and Coupling

An integrated model chain has been setup to assess the air quality, including both regional changes as well as local variation of air pollution. Hereafter the model chain is discussed. The road traffic loads are the input for the MIMOSA4 emission model [7, 9]. The resulting spatially and temporally distributed emissions are used in the bi-gaussian model IFDM [5]. These results are coupled to output of the Eulerian dispersion model AURORA [2, 7, 8] calibrated with the land-use regression model RIO [3, 4]. A mechanism to avoid double counting of the emissions by the different models is applied [6]. The IFDM concentrations related to the local emission sources are first averaged over the grid cells of the regional AURORA model. This local contribution is subtracted from the regional contribution before the concentration pattern of the bi-gaussian plume model is added at high resolution. Finally the output are coupled to results of the OSPM-model [1]. For every receptor point in a street canyon, the concentration due to the road lying in the street canyon is subtracted before adding the OSPM-calculation in order to avoid double counting of emissions. The double counting corrections described above are applied on an hourly basis and result in reliable maps for annual statistics which can be used for compliance checking in the framework of the EU Directive.

111.3 Results and Discussion

The complex model chain briefly presented in Sect. 111.2 is applied for the city of Antwerp. Figure 111.1 shows the NO_2-concentrations as estimated for the year 2015 over the city and its harbor. As an emission projection, a current legislation emission inventory is used. The major roads, the important industries (in the northern part) and the major street canyons are revealed in the NO_2 map. Furthermore, exceedances of the European limit value of 40 $\mu g/m^3$ can be found at several places.

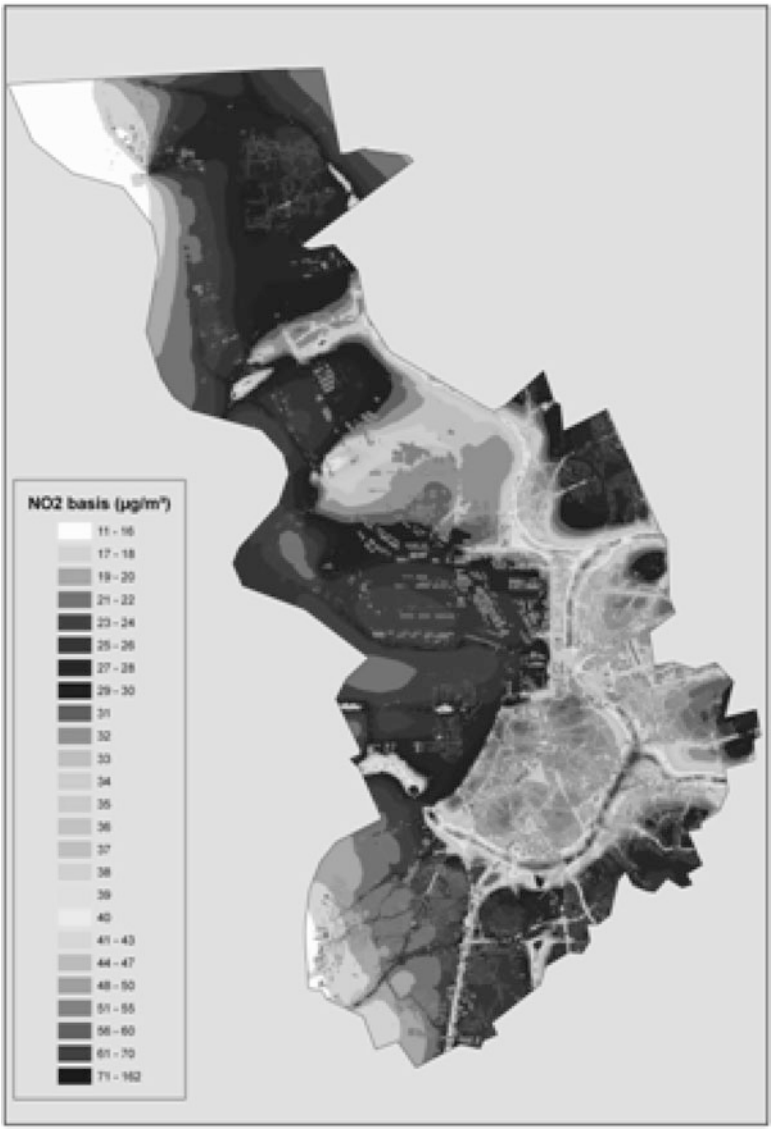

Fig. 111.1 NO_2-concentration for Antwerp (city and harbour) for the year 2015 under a current legislation emission projection

Therefore, it is necessary to take additional measures beyond the current legislation, in order to obtain acceptable air quality levels in the year 2015.

Making use of this air quality map, an number of abatement measures were defined by a local policy makers. The measures were combined in a number of scenarios which were evaluated within the same modeling framework. It has been

shown that local (traffic) measures only have a small effect on total mass PM_{10} and $PM_{2.5}$ concentrations, but exhibit a larger effect on EC and NO_2-concentrations. Based on those results, the most effective and cost efficient action plan was developed for the city of Antwerp.

111.4 Conclusion

A methodology is presented to deal with the multi scale problem in urban air quality. A coupled model chain accounts for the regional, local and street canyon scales and avoids double counting of emissions at the different modeling scales. The framework can be used to assess local air quality up to the street canyon level and can also be used to assess the impact of a set of abatement measures and to define the most effective and cost efficient action plan.

References

1. Berkowicz R, Hertel O, Larsen SE, Sørensen NN, Michelsen JA (1997) Modelling traffic pollution in streets. http://www2.dmu.dk/1_viden/2_Miljoe-ilstand/3_luft/4_spredningsmodeller/5_OSPM/5_description/ModellingTrafficPollution_report.pdf
2. De Ridder K, Lefebre F, Adriaensen S, Arnold U, Beckroege W, Bronner C, Damsgaard O, Dostal I, Dufek J, Hirsch J, IntPanis L, Kotek Z, Ramadier T, Thierry A, Vermoote S, Wania A, Weber C (2008) Simulating the impact of urban sprawl on air quality and population exposure in the German Ruhr area. Part I: reproducing the base state. Atmos Environ 42:7059–7069
3. Hooyberghs J, Mensink C, Dumont G, Fierens F (2006) Spatial interpolation of ambient ozone concentrations from sparse monitoring points in Belgium. J Environ Monit 8:1129–1135. doi:10.1039/b612607n
4. Janssen S, Dumont G, Fierens F, Mensink C (2008) Spatial interpolation of air pollution measurements using CORINE land cover data. Atm Environ 42(20):4884–4903. doi:10.1016/j.atmosenv.2008.02.043
5. Lefebvre W, Fierens F, Trimpeneers E, Janssen S, Van de Vel K, Deutsch F, Viaene P, Vankerkom J, Dumont G, Vanpoucke C, Mensink C, Peelaerts W, Vliegen J (2011) Modeling the effects of a speed limit reduction on traffic-related elemental carbon (EC) concentrations and population exposure to EC. Atmos Environ 45:197–207. doi:10.1016/j.atmosenv.2010.09.026
6. Lefebvre W, Vercauteren J, Schrooten L, Janssen S, Degraeuwe B, Maenhaut W, de Vlieger I, Vankerkom J, Cosemans G, Mensink C, Veldeman N, Deutsch F, Van Looy S, Peelaerts W, Lefebre F (2011) Validation of the MIMOSA-AURORA-IFDM model chain for policy support: modeling concentrations of elemental carbon in Flanders. Atm Environ 45(37):6705–6713. doi:10.1016/j.atmosenv.2011.08.033
7. Mensink C, De Vlieger I, Nys J (2000) An urban transport emission model for the Antwerp area. Atmos Environ 34:4595–4602
8. Van de Vel K et al (2010) Air-quality modelling in the Lake Baikal region. Environ Monit Assess 165:665–674
9. Vankerkom J, De Vlieger I, Schrooten L, Vliegen J, Styns K (2009) Beleidsondersteunend onderzoek: Aanpassingen aan het emissiemodel voor wegtransport MIMOSA. Studie uitgevoerd in opdracht van VMM – MIRA, 2009/TEM/R/084

Chapter 112
Coupling the Town Energy Balance Scheme to the High Resolution LAM ALADIN for Belgium

Rafiq Hamdi, Alex Deckmyn, Daan Degrauwe, Andy Delcloo, and Piet Termonia

Abstract The Town Energy Balance (TEB) single-layer scheme is implemented into a numerical weather prediction model running operationally at ∼4 km resolution. The primary question addressed is the potential use of TEB, at this relatively coarse resolution, in an operational configuration to improve sensible weather performance over Belgium. Simulations with and without TEB are first evaluated against 2 m observations and wind above the urban canopy for 2 months (January and July 2010). The 2 m temperature and 2 m relative humidity improve compared to measurements in urban areas. The comparison of wind speed and wind direction above the urban canopy indicate that the structure of the flow in urban areas is better reproduced with TEB. Results from a 36-h case study during a high heat day (8 July 2010) indicate that even at this coarse resolution, TEB is able to reproduce correctly the intensity of the observed UHI of Brussels.

Keywords Town energy balance • LAM-Aladin

112.1 Introduction

At the Royal Meteorological Institute of Belgium (RMIB), our framework ALARO-0 [1] is a version of the Action de Recherche Petite Echelle Grande Echelle-Aire Limitée Adaptation Dynamique Développement International

R. Hamdi (✉) • A. Deckmyn • D. Degrauwe • A. Delcloo
Royal Meteorological Institute of Belgium, Brussels, Belgium
e-mail: rafiq.hamdi@meteo.be; andy.delcloo@meteo.be

P. Termonia
Royal Meteorological Institute of Belgium, Brussels, Belgium

Department of Physics and Astronomy, Ghent University, Ghent, Belgium

D.G. Steyn et al. (eds.), *Air Pollution Modeling and its Application XXII*,
NATO Science for Peace and Security Series C: Environmental Security,
DOI 10.1007/978-94-007-5577-2_112,

(ARPEGE-ALADIN) operational limited area model with a revised and modular structure of the physical parameterizations. This new version currently allows for the production of consistent and realistic results at resolutions ranging from a few tens of kilometers down to less than 4 km. A version of ∼4 km resolution is operationally used at the RMIB since 2009. However, running ALARO at this high resolution results in more grid points that will represent urban areas for 100 % (see Fig. 1 in Hamdi et al. [2]). In the last few years, several efforts have been made in order to improve the representation of urban surface characteristics with varying levels of sophistication from relatively simplistic bulk approaches to the most sophisticated multi-layer schemes. However, the vast majority of work done with these urban parameterizations has been research oriented with very high resolution runs (1 km or less) for specific urban case studies. Therefore, this study was motivated by the desire to evaluate the performance of the Town Energy Balance (TEB, [3]) single-layer module within the ALARO 4 km resolution in an operational configuration. For this effort, simulations with and without TEB are evaluated over Belgium which is one of the most densely populated countries within Europe with some 330 inhabitants per km^2. Note that the additional resources needed to run ALARO with TEB for our operational domain using the computing resources available at our institute is rather low, the time needed to complete a 36 h forecast is on the order of 0.6 % and the memory increase is about 1.6 %.

112.2 Operational Model Scores

For 2 months (January 2010 and July 2010), a series of simulations is performed, with (ALR-TEB) and without TEB (ALR-OPR), with one simulation of 36 h each day, starting at 0000 UTC (from the operational ALADIN French forecast model analysis).

112.2.1 2 m Temperature

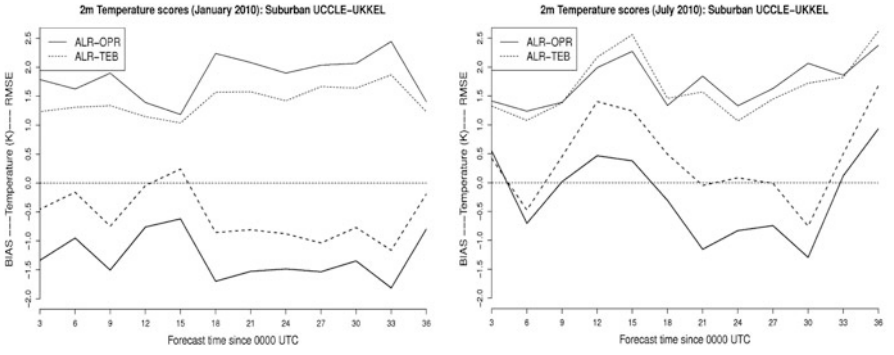

This figure presents the scores obtained for the Uccle station which is situated some 6 km South of the center of Brussels in a suburban area (50.80 N, 04.35 E). During nighttime (which is longer in January than in July), 2 m temperatures are generally cold for both simulations, with and without TEB, compared to observations. However, the average mean bias for Uccle is significantly reduced when using TEB, with an average of −1.39 K for ALR-OPR versus −0.76 K for ALR-TEB during winter and an average of −0.70 K for ALR-OPR versus −0.13 K for ALR-TEB during the summer. Because of radiation trapping effects in street canyon and impermeable surfaces that convert incoming radiation to sensible heat and store it more efficiently than the surrounding rural area, the surface layer in a city is generally warmer than that of its surroundings. This leads to the formation of the so-called urban, heat island (UHI). The effect in ALR-TEB can be attributed to these mechanisms which are not handled with the operational version of ALARO. During daytime, ALR-TEB has a tendency to produce higher maximum temperature especially during the summer. The temperature results correlate with the 2 m relative humidity results (not shown).

112.2.2 30 m Wind

As can be seen, the ALR-TEB run reduces the wind speed over the city due to the urban morphology with an average bias of 0.63 m s^{-1} for ALR-OPR versus 0.31 m s^{-1} for ALR-TEB during winter and an average value of 0.53 m s^{-1} for ALR-OPR versus 0.31 m s^{-1} for ALR-TEB during the summer. There is also significantly less variability with the ALR-TEB run (average RMSE of 1.46 m s^{-1} for ALR-OPR versus 1.18 m s^{-1} for ALR-TEB during winter and an average RMSE of 1.37 m s^{-1} for ALR-OPR versus 1.24 m s^{-1} for ALR-TEB during the summer).

112.3 Model Simulation for a Hot Summer Day (8 July 2010)

The two model simulations are examined in greater detail for the 36-h time period from 0000 UTC 8 July 2010. On this day, an anticyclone covers Belgium and near-record high temperature was observed. The strength of the UHI of Brussels is estimated using the temperature observed at Uccle and at the rural climatological station Brussegem situated in the Northwest, 20 km distant from the centre of Brussels (see Fig. 17 in Hamdi et al. [2]). During the day the UHI reaches its maximum of 1.33 °C at noon which is in agreement with the observed difference in the maximum temperature for this day between Uccle and Brussegem (1.3 °C). This indicates that even at this coarse resolution (∼4 km) ALR-TEB is able to reproduce correctly the intensity of the observed UHI of Brussels. In the afternoon, the cooling process begins with the decrease of solar radiation, including a decrease of the UHI to only 1 °C. However at 1800 UTC, a sudden and strong temperature increase of

the heat island intensity is obvious. Within two hours the UHI intensity reaches about 4.5 °C which is in agreement with the observed difference in the minimum temperature for this day between Uccle and Brussegem (4.2 °C).

References

1. Gerard L, Piriou JM, Brozková R, Geleyn JF, Banciu D (2009) Cloud and precipitation parameterization in a meso-gamma-scale operational weather prediction model. Mon Weather Rev 137:3960–3977
2. Hamdi R, Degrauwe D, Termonia P (2012) Coupling the Town Energy Balance (TEB) scheme to an operational limited area NWP model: evaluation for a highly urbanized area. Weather Forecast 27:323–344. doi:10.1175/WAF-D-11-00064.1
3. Masson V (2000) A physically-based scheme for the urban energy budget in atmospheric models. Bound-Layer Meteorol 94:357–397

Chapter 113
Contribution of Advective and Turbulent Contaminant Transport to the Intersection Ventilation

Libor Kukačka, Štěpán Nosek, Radka Kellnerová, Klára Jurčáková, and Zbyněk Jaňour

Abstract The objective of this experimental study is to determine processes of pollution ventilation above the X-shaped street intersection in an idealised symmetric urban area for several approach flow directions. A unique experimental set-up for simultaneous measurement of the flow velocity and the tracer gas concentration in a high temporal resolution is assembled. Advective and turbulent vertical scalar fluxes are computed from the measured data in a horizontal plane above the street intersection. Vertical turbulent pollution transport was found to be a significant and positive contribution to the total vertical transport of pollutants form the intersection. Prevailing events in vertical scalar and momentum fluxes were determined using quadrant analysis.

Keywords Air pollution • Boundary layer • Wind tunnel modelling • Contaminant transport • Pollution fluxes • Street canyon intersection

L. Kukačka (✉) • R. Kellnerová
Department of Meteorology and Environment Protection, Faculty of Mathematics and Physics, Charles University, Prague, Czech Republic

Institute of Thermomechanics Academy of Sciences of the Czech Republic, Prague, Czech Republic
e-mail: kukacka@it.cas.cz

Š. Nosek • K. Jurčáková • Z. Jaňour
Institute of Thermomechanics Academy of Sciences of the Czech Republic, Prague, Czech Republic

D.G. Steyn et al. (eds.), *Air Pollution Modeling and its Application XXII*,
NATO Science for Peace and Security Series C: Environmental Security,
DOI 10.1007/978-94-007-5577-2_113,

113.1 Introduction

Dispersion of air pollution within urban areas is an important aspect of the environment quality for a significant part of the population. Traffic in street canyons is often a dominant source of pollutants in large cities, see [4]. Improvement of air quality in urban areas is necessary to avoid risk for human health, see [5].

We can define ventilation of built-up areas as a process of changing polluted with a fresh air, which improves the air quality. Street intersections are very important in the redistribution of pollutants between streets and in the air exchanges between streets and the atmosphere. Characteristics of the transport pollution within the street intersection can be found in recent works [2, 3, 8]. We focused on vertical ventilation processes in a complex and highly three-dimensional flow and concentration fields above the idealised street intersection. This study relates to former work published in [6].

113.2 Experimental Set-Up

The experiment was conducted in the open low-speed wind tunnel of Institute of Thermomechanics Academy of Sciences of the Czech Republic in Nový Knín. According to the standard criteria, modelled boundary layer corresponded to a neutrally stratified boundary layer flow above a densely built-up area without much obstacle height variation. The model of an idealised symmetric urban area formed by apartment houses was designed according to common Central European inner-city areas. The model was scaled down to 1:200, the characteristic building height was $H = 120$ mm (24 m in full scale).

The turbulent momentum and mass transport was detected by simultaneous velocity and concentration measurement in a high temporal resolution using two-dimensional optical fibre Laser Doppler Anemometry (LDA) and Fast-response Flame Ionisation Detector (FFID). A point pollution source simulating "pollution hotspot" (the place with higher emission of traffic pollution situated near a junction) was placed at the bottom of the street canyon in front of the studied street intersection.

113.3 Results

The vertical and longitudinal velocity with concentration of tracer gas were simultaneously measured in a horizontal plane at the roof-top level $z = H$ above the studied intersection. Results were obtained for five approach flow directions $\varphi = 0°$, 5°, 15°, 30° and 45°. The dimensionless advective scalar fluxes were computed

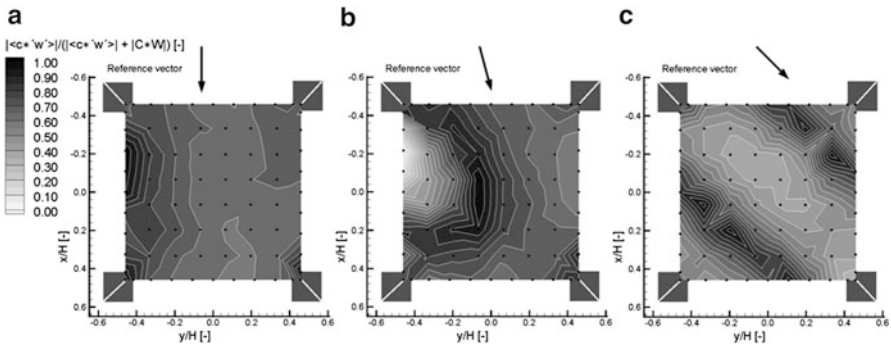

Fig. 113.1 Contribution of the vertical turbulent pollution flux to the total vertical pollution flux at the roof top level above the street intersection (view from the *top*). (**a**) Approach flow $\varphi = 0°$. (**b**) Approach flow $\varphi = 15°$. (**c**) Approach flow $\varphi = 45°$

by C^*W/U_{2H}, where C^* means dimensionless pollutant concentration, W is the mean vertical velocity of the flow and U_{2H} means reference velocity measured at the reference height $z = 2H$, see [1, 3, 7].

Dimensionless vertical turbulent scalar fluxes were computed from synchronised vertical velocity and concentration signals using eddy-correlation method. The turbulent scalar flux is given by $<c^{*\prime}w^{\prime}>/U_{2H}$, where $<>$ is a time average, $c^{*\prime}$and $w^{\prime}$ indicate fluctuations of dimensionless concentration and vertical velocity, respectively (see similar approach in [2]). The positive sign means the flux outwards and the negative sign means the flux inwards the street intersection. A contribution of the turbulent flux to the total flux was computed by $|< c^{*\prime}w^{\prime} >| / (|< c^{*\prime}w^{\prime} > |+| C^*W|)$, see Fig. 113.1.

The quadrant analysis was applied to the velocity and concentration fluctuation time series. We used usual nomenclature published in [9]: "outward interaction" ($x^{\prime} > 0$; $w^{\prime} > 0$), "sweep" ($x^{\prime} > 0$; $w^{\prime} < 0$), "inward interaction" ($x^{\prime} < 0$; $w^{\prime} < 0$), "ejection" ($x^{\prime} < 0$; $w^{\prime} > 0$), where $x^{\prime}$ represents longitudinal velocity fluctuation $u^{\prime}$ or concentration fluctuation $c^{\prime}$. The particular contribution from ith quadrant to the total turbulent flux is given by $S_i =< x^{\prime}w^{\prime}>_i N_i / N_{total}$, where N_i is the number of events in the ith quadrant, number of all measured events is N_{total}. The relative contribution of the prevailing event S_{max} to the total momentum flux is given by $|S_{max}| / \sum |S_i|$ 100 %, see Fig. 113.2.

113.4 Conclusions

Vertical advective and turbulent fluxes of pollution were measured above the modelled X-shaped street intersection in an idealized symmetrical urban area. Determined vertical turbulent flux comprised significant and positive contribution to the ventilation of the area. The quadrant analysis was applied to the synchronized

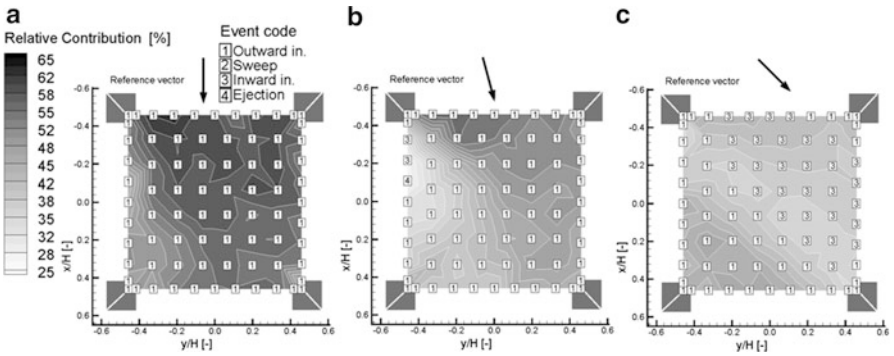

Fig. 113.2 Relative contributions of the dominant event to the total turbulent flux of the passive contaminant at the roof top level above the street intersection (view from the *top*). (**a**) Approach flow $\varphi = 0°$. (**b**) Approach flow $\varphi = 15°$. (**c**) Approach flow $\varphi = 45°$

velocity and concentration signals. In the area of the significant advective pollution transport, sweeps were found to be events with the dominant contribution to the vertical momentum flux. We determined the outward interaction and to a lesser extent inward interaction as a dominant event in the vertical turbulent pollution flux.

Acknowledgments The authors thank the Ministry of Education, Sports and Youth of the Czech Republic (projects AVOZ-20760514 and COST1006 LD 12007), the Czech Science Foundation GACR (project P101/12/1554) and the Charles University in Prague (project GAUK No. 535412) for their financial support.

References

1. Belcher ES (2005) Mixing and transport in urban areas. Philos Trans R Soc A 363:2947–2968
2. Carpentieri M, Hayden P, Robins AG (2012) Wind tunnel measurements of pollutant turbulent fluxes in urban intersections. Atmos Environ 46:669–674
3. Carpentieri M, Robins A (2010) Tracer flux balance at an urban canyon intersection. Bound-Layer Meteorol 135:229–242
4. Fenger J (1999) Urban air quality. Atmos Environ 33:4877–4900
5. Hoek G, Brunekreef B, Verhoeff A, van Wijnen J, Fischer P (2000) Daily mortality and air pollution in the Netherlands. J Air Waste Manage Assoc 50:1380–1389
6. Kukačka L, Kellnerová R, Jurčáková K, Jaňour Z (2012) Chap. Analysis of scalar fluxes and flow within modelled intersection depending on the approach flow direction. In: Steyn DG, Castelli ST (eds) Air pollution modelling and its application XXI. Springer, Dordrecht, pp 113–118
7. Robins A (2008) Dapple (dispersion of air pollution and its penetration into the local environment) experiments and modelling. HPA Chem Hazards Poisons Rep 13:24–28
8. Soulhac L, Garbero V, Salizzoni P, Mejean P, Perkins R (2009) Flow and dispersion in street intersections. Atmos Environ 43:2981–2996
9. Willmath WW, Lu SS (1974) Structure of the Reynolds stress and the occurrence of bursts in the turbulent boundary layer. Adv Geophys 18A:287–314

Chapter 114
Evaluation of a Plume-in-Grid Model for Line Sources with a Multiple Roadway Case Study

Régis Briant and Christian Seigneur

Abstract Eulerian models, which are widely used in air quality modeling are based on a three dimensional grid in which emissions are released. Point sources are mixed in a cell that can be a few kilometers long and therefore in regional scale simulations, the approximation made by the model on the emissions can have a significant impact. Plume-in-grid (PinG) models combine an Eulerian and a plume or puff, typically Gaussian, model aiming at having a better representation of sources within grid cells. Although point sources are convenient to model dispersion from a chimney, line sources are better suited for roadway traffic pollution modeling. Here we present a new PinG model that uses Gaussian line source model embedded within the Eulerian model Polair3D. Emissions are treated as steady-state plumes released from line sources. After a description of the model we present here its application to a case study that includes multiple roadways.

Keywords Plume-In-Grid model • Line source • Polyphemus • Polair3d

114.1 Introduction

Eulerian models, which are widely used in air quality modeling are based on a three dimensional grid in which emissions are released. Point sources are mixed in a cell that can be a few kilometers long and therefore in regional scale simulations, the approximation made by the model on the emissions can have a significant impact. Plume-in-grid (PinG) models combine an Eulerian and a plume or puff, typically Gaussian, model aiming at having a better representation of sources within grid cells. The main purpose is to be able to use Gaussian local precision

R. Briant (✉) • C. Seigneur
CEREA, Joint Research Laboratory, E' cole des Ponts ParisTech/EDF R&D Universite' Paris-Est, Marne la Vallée, France
e-mail: briantr@cerea.enpc.fr; seigneurc@cerea.enpc.fr

D.G. Steyn et al. (eds.), *Air Pollution Modeling and its Application XXII*,
NATO Science for Peace and Security Series C: Environmental Security,
DOI 10.1007/978-94-007-5577-2_114,

at a regional scale. PinG models already exist for point sources (e.g., CMAQ, AMSTERDAM, Polyphemus [4, 5]). They have been used in many studies and have been proven to be efficient. Modeling roadway traffic with point sources would induce a significant increase of the computational burden. Although point sources are convenient to model dispersion from a chimney, line sources are better suited for roadway traffic pollution modeling. Here we present a new PinG model that uses Gaussian line source model embedded within the Eulerian model Polair3D [1]. Emissions are treated as steady-state plumes released from line sources. It required some significant change in the model especially in the way pollutants are transferred from the Gaussian model to the Eulerian model. The model was developed as part of the modeling platform Polyphemus [6]. After a description of the model we present here its application to a case study that includes multiple roadways. Model simulation results are computed with and without the plume-in-grid treatment.

114.2 Model Descriptions

Plume-in-Grid (PinG) models aim at improving the contribution of sources in an Eulerian simulation by using a subgrid-scale treatment with, for example, a Gaussian model. In a PinG model, pollutants are dispersed with a plume or puff model until it can be considered as background pollutants. The plume/puff pollutants are then transferred to the Eulerian model that is running concurrently. Therefore, a PinG model requires a plume or puff model and an Eulerian model. We used here the Polyphemus modeling platform which provides both of them [6]. The Eulerian model is called Polair3D and is relevant up to the continental scale [1]. The Gaussian formulation of the concentration field for a pollutant emitted from a line source presented in [2]. This formulation performs well for all ranges of angles and provides some improvement in terms of accuracy over previous formulations of the Gaussian line source plume model without being too demanding in terms of computational resources. The model used here also includes a Romberg integration to account for the road width. This model was implemented in the Polyphemus modeling platform.

114.3 Gaussian and Eulerian Model Coupling

Existing PinG models use puffs to discretize in time the plume emitted from the source. With the Gaussian plume model presented above a steady state is assumed, therefore, making this discretization of the plume unnecessary. Algorithm 1 explains how the model has been implemented. After the initialization of both models, the time loop is launched. Note that for one iteration of the Eulerian model only one iteration of the Gaussian model is done. Indeed, as stated before, the plume emitted from the source does not need to be discretized with puffs. A Gaussian concentration

from the previous time step is considered as background concentration for the Eulerian model and, therefore, it is added to the current Eulerian concentration before the model iteration. Then, the Gaussian model contribution from each source to each grid cell is computed before the chemistry process can be done. Finally, at the end of the time step, output concentrations are computed at each output receptor location and are saved. The transfer of pollutants from the Gaussian model to the Eulerian model occurs at the beginning of each iteration of the time loop (line 5 of the Algorithm 1). However, pollutants that are to be transferred are computed at the previous iteration during the loop over all sources (lines 7–11 of the Algorithm 1), which computes the contribution of each source to each grid cell. Considering that the total amount of pollutant emitted from a given source during the current time step is: $Q \times L \times l \times \Delta t$, where Q is the emission rate in g m^{-2} s^{-1}, L and l are the width and the length of the source, respectively, and Δt is the time step, we spatially discretize the plume to compute the contribution of the source at several locations in order to know the spatial distribution of the plume. Therefore, we are able to know the contribution of each source to each grid cell.

Algorithm 1 Algorithm of the Plume-In-Grid model using the line source Gaussian plume model.

```
1: -Initialize Eulerian model
2: -Initialize Gaussian model
3: -Read sources information (coordinates and emission rates)
4: for time step 0 to the end do
5:     -Transfer to the Eulerian model Gaussian concentration from the previous time
           step
6:     -Iteration of Eulerian model
7:     for each source do
8:         for each grid cell do
9:             -Compute contribution of the source to the grid cell
10:        end for
11:    end for
12:    -Compute Gaussian chemistry process.
13:    -compute Gaussian contribution at receptor location
14:    return Eulerian concentration + Gaussian contribution at receptor location
15: end for
```

114.4 Results

The model presented above is applied here with a one-day simulation over the Paris region. We used meteorological data computed with the Weather Research and Forecasting model (WRF), boundary conditions from the LMDzT-INCA global model [3] and an emission inventory from the Paris air quality agency (Airparif). We added over 5,000 constant line sources (about 800 km of linear road length) in the

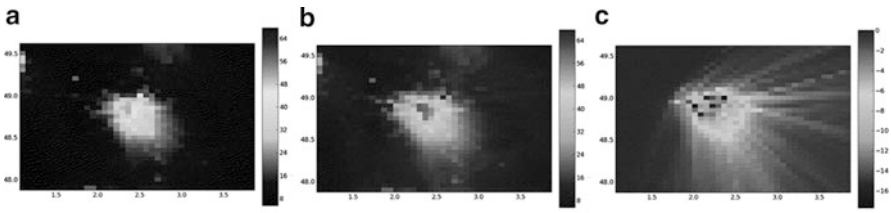

Fig. 114.1 NO_2 concentration over the Paris region simulated with PinG and Polair3D models ($\mu g\ m^{-3}$). (**a**) Polair3D results. (**b**) PinG results. (**c**) Difference: Polair3D – PinG results

Gaussian model to account for traffic emissions. Those emissions were computed with the European model COPERT 3 and were provided by the French technical study and engineering center CETE Nord Picardie. We conducted simulations with both the PinG model and the standard Eulerian model (Polair3D). Line source emissions are considered to be constant grid-based emissions in the Eulerian model. Figure 114.1 shows maps of the NO_2 results obtained with each model and Fig. 114.1 shows the difference map between them. Both models give similar results however, the PinG model gives slightly higher concentrations than Polair3D. This result is due to the use of the Gaussian model in the PinG simulation which computes the contribution of each line source and adds it to background concentration while Polair3D dilutes pollutants immediately in the grid-cell where they are emitted.

114.5 Conclusion

A new Plume-in-Grid model has been developed. It has been tested on a large case study for a one-day simulation. It has shown satisfactory results when compared to the Eulerian model. The next step will be to use this new Plume-in-Grid model for a longer simulation with more complete emission data and to compare results with measurements to evaluate model performance.

Acknowledgments Thank are due to Airparif, the air quality agency of the Paris region for providing us with the emission inventory, to the Laboratoire de Météorologie Dynamique (LMD) for providing us with the LMDzT-INCA outputs, and to the National Centers for Environmental Prediction (NCEP) for providing initial and boundary conditions that we used with the WRF model. Finally, we acknowledge Marie Gadrat and Christine Bugajny of the French technical study and engineering center CETE Nord Picardie who provided us emissions and the associated road network that we used to obtain the above simulation results.

References

1. Boutahar J, Lacour S, Mallet V, Que'lo D, Roustan Y, Sportisse B (2004) Development and validation of a fully modular platform for numerical modelling of air pollution: Polair. Int J Environ Pollut 22:17–28
2. Briant R, Korsakissok I, Seigneur C (2011) An improved line source model for air pollutant dispersion from roadway traffic. Atmos Environ 45:4099–4107
3. Hauglustaine D, Hourdin F, Jourdain L, Filiberti M-A, Walters S, Lamarque J-F, Holland E (2004) Interactive chemistry in the laboratoire de météorologie dynamique general circulation model: description and background tropospheric chemistry evaluation. J Geophys Res 109:D04314
4. Karamchandani P, Vijayaraghavan K, Chen S, BalmoriBronson R, Knipping E (2010) Development and application of a parallelized version of the advanced modeling system for transport, emissions, reactions and deposition of atmospheric matter (Amsterdam): 1. Model performance evaluation and impacts of plumeingrid treatment. Atmos Pollut Res 1:260–270
5. Korsakissok I, Mallet V (2010) Development and application of a reactive plume-ingrid model: evaluation over greater paris. Atmos Chem Phys 10:5091–5134
6. Mallet V, Quélo D, Sportisse B, Ahmed de Biasi M, Debry É, Korsakissok I, Wu L, Roustan Y, Sartelet K, Tombette M, Foudhil H (2007) Technical note: the air quality modeling system Polyphemus. Atmos Chem Phys 7(20):5479–5487

Chapter 115
Risk Analysis and Emergency Forecast of Toxic Substances Local Scale Transport Over Bulgaria

Angelina Brandiyska, Kostadin Ganev, Dimiter S. Syrakov, Maria Prodanova, and Nikolay Miloshev

Abstract The present paper describes the some results of the modelling system for operational response to accidental releases of harmful gases in the atmosphere (as a result of terrorist attack or industrial accident). The system is based on the following models: WRF, used as meteorological pre-processor; SMOKE – the emission pre-processor; CMAQ – the Chemical Transport Model (CTM) of the system. For the needs of the emergency response preparedness mode the risk is defined as probability the national regulatory threshold values for toxic gases to be exceeded. Maps of the risk around potential sources of emergency toxic gas releases are constructed and demonstrated in the present paper. Some examples of the system "operational mode" results are demonstrated as well.

Keywords Risk analysis • Emergency response • Toxic gases

115.1 Introduction

The present work demonstrates results produced by the Bulgarian system for emergency response in case of accidental harmful releases in the atmosphere. The system will supply the authorities, the relevant international organisations and the

A. Brandiyska • K. Ganev • N. Miloshev
National Institute of Geophysics, Geodesy and Geography, Bulgarian Academy of Sciences, Acad. G. Bonchev Str., Bl.3, Sofia 1113, Bulgaria
e-mail: kganev@geophys.bas.bg

D.S. Syrakov (✉) • M. Prodanova
National Institute of Meteorology and Hydrology, Bulgarian Academy of Sciences, 66 Tzarigradsko Chausee, Sofia, 1784, Bulgaria
e-mail: dimiter.syrakov@meteo.bg

D.G. Steyn et al. (eds.), *Air Pollution Modeling and its Application XXII*,
NATO Science for Peace and Security Series C: Environmental Security,
DOI 10.1007/978-94-007-5577-2_115,

public with information, which will help to take proper measures for diminishing the damages. The modelling system is able to assist emergency managers in three stages:

In preparedness mode, "risk analysis" was performed for some selected sites These assessments can be of a direct use for the relevant national bodies for developing strategies for immediate emergency response (for example evacuation of people from the pollution exposed regions, proper assignment of medical teams) in order to minimize the pollution impact on human health. They also give valuable information for optimisation of the air quality monitoring network.

In the operational ("fast decision") mode the system produces fast short-term forecast of the pollutant propagation in local and regional scale, which is governed by the meteorological conditions. This information will help the authority decisions about the immediate measures and activities to be carried out in order to minimize the pollution impact on human health.

The modelling tool used for this study is US EPA Models-3 System: WRF [1], used as meteorological pre-processor, CMAQ [2] – the Chemical Transport Model of the system.; SMOKE [3] – the emission pre-processor. A chlorine chemical mechanism has been added to CMAQ based on [4].

115.2 Examples of Risk Analysis Simulations

The risk may generally be defined as a product of probability (recurrence) of happening of a given event and the impact of this event (in the particular case on human health). The impact should be evaluated by some metrics directly giving the effect of toxic gas on human health – in this case the national regulatory threshold values, so the risk is simply the probability these thresholds to be exceeded.

The industrial site, for which the risk analysis results will be demonstrated is "POLIMERI-DEVNYA" located close to the Black sea. The simulations were carried out for two release times – 2 o'clock and 14 o'clock local time in three nested, covering respectively the regions of South-Eastern Europe, Bulgaria, and the area surrounding the site, downscaling the problem to a horizontal resolution of 1 km around the site. It should be noted that the "regular" emissions are also taken into account not only in the innermost domain, but also in the domain with spatial resolution of 5 km (Bulgaria) thus providing appropriate boundary conditions for the innermost domain.

The simulations were carried out for years 2000–2007 day by day for several hours after the release and thus a large ensemble of simulations was obtained. For each individual run it was checked up where the respective concentration exceeds the regulatory threshold value and so the impact is set equal to 1, and in the points where the concentrations are below the regulatory threshold, the impact value is set equal to zero. Then a simple statistics over this ensemble gives the probability the regulatory threshold to be exceeded – the risk.

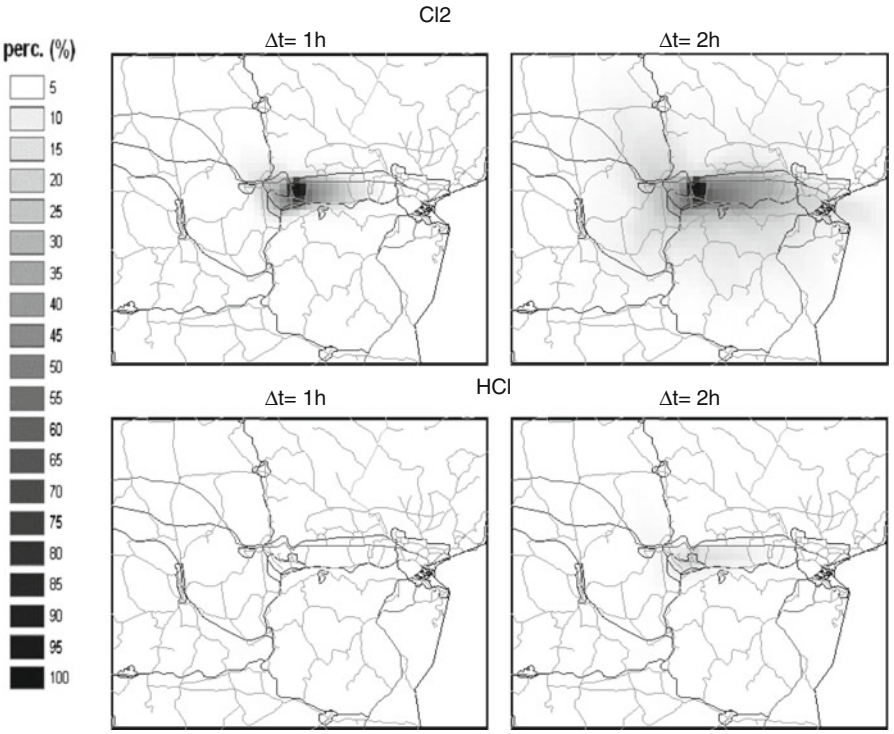

Fig. 115.1 Annual fields of probability surface Cl_2 and HCl concentrations to exceed the threshold value for times $\Delta t = 1$ and 2 h after the release (2 o'clock). The annual risk for HCl pollution for $\Delta t = 1$ h is zero

The probabilities surface concentration fields of Cl_2 (the primary pollutant) and HCl (one of the secondary pollutants) to exceed the respective threshold values are calculated for the four seasons and for the whole year. Due to the limited volume of the paper only the annual risk will be demonstrated here (Fig. 115.1).

There are several things about the probability fields that should be mentioned: The area with non-zero probabilities could cover a big domain around the "POLIMERI-DEVNYA" site. This is another good demonstration why the risk assessment is necessary. It can be seen that significant risk could happen far from the site and with temporal delay. The probability fields are quite different for the different seasons, which yet again demonstrates the importance of the meteorological conditions for the pollution field pattern. The probability field pattern is pretty complex for both Cl_2 and HCl, still a tendency for spreading the pollution in E-W direction could be seen, which reflects the local circulation patterns. In summer, due to the vicinity of the Black Sea, there is a breeze circulation, so during daytime the plume moves inland, while during night time the plume moves towards the sea. The

closest neighbouring cities are under threat – Devnya (large probability during warm daytime conditions) and Varna (during the night or in winter). Some of the roads at certain time could be rather risky, so they should not be used for evacuation of the population. Such roads are both the highway and the T1 road from Devnya to Varna, if the accident happens at night-time or in winter, or the same roads in the opposite direction (Devnya-Shumen) if it happens during daytime in spring and summer. The secondary pollutant concentrations may also exceed the regulatory threshold – for example HCl concentrations are high during spring and summer.

115.3 Examples of the System "Fast Decision" Mode

A specially developed Fortran program, that produces tracer emissions for the 11 locations in the domain of the chemical transport model. The system runs operatively at 00, 06, 12, 18 UTC every day and works in the following way: First, the meteorological input data is downloaded from NCEP and the WRF input files are prepared. Then the meteorological model is run for 15 h, with four nested domains. The first 6 h of the simulation are a spin-up and the next 9 h are processed to become meteorological input for the chemical transport model. Then the CMAQ model is run for 9 h. As an output of the system a series of images are produced, showing the 11 tracer concentrations at 15-min intervals for 9 h. The meteorological simulations are carried out in four nested domains with resolutions 90, 30, 6, 2 km, downscaling from the region of South-Eastern Europe (90 km) to Bulgaria (2 km). The CMAQ simulations are carried out only in the innermost domain.

The main characteristics of the plume propagation, which were outlined by the numerical experiments, carried out so fat are the following:

1. The shape of the plumes and the direction of their movement are governed by the meteorological conditions. Since there are no chemical reactions, the changes in the pollutant concentrations are only due to dispersion and deposition.
2. The local meteorological wind circulation can be very different than the mesoscale and this yet again confirms the need of high resolution. This is especially true for areas with complex terrain, like southern Bulgaria. The breeze circulation at the coast of the Black Sea during the warm months is also important – it can contribute to cleansing the air (when the wind is blowing from the west) or to high pollutant concentrations inland (when the wing is blowing from the east).
3. The simulations show, that if there are strong winds or the thermodynamic conditions are unstable, the surface concentrations drop five times in 2 h, but this is a rare case. In most simulations the concentrations remain high at least 3 h after the release. For some sites in some simulations the toxic plumes remain almost stationary and the surface concentrations remain high for more than 2 h.

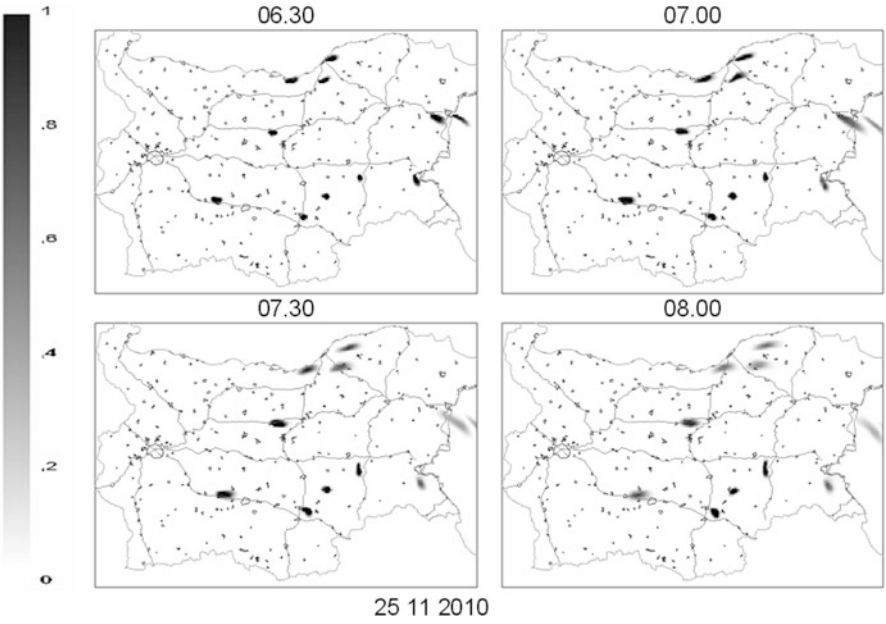

Fig. 115.2 3-houre tracer evolution for a release in 06 o'clock on 25.11.2010

Some of the sites are very close to big cities (Varna, Burgas, Rousse) and major roads or railway lines, so the emergency simulations could be really useful, showing if the plume approaches a region with dense population. Even cities, which are more than 20 km away from the source, can be under threat.

Example of the simulated tracer evolution is shown in Fig. 115.2.

115.4 Conclusions

The work on the risk evaluation and emergency response system is not completed yet. At this stage of the system development, however, it can be concluded that the chosen modelling tools are probably suitable for this particular task and the obtained preliminary results are quite realistic and promising. The shown numerical results very well demonstrate the practical value of the preparedness and fast decision mode of the system.

Acknowledgements The present work is supported by the projects NATO ESP.EAP.SFPP 981393, as well as by the Bulgarian National Science Fund (grants № Д002-161/16.12.2008 and ДЦ -02/1/29.12.2009).

References

1. Byun D, Ching J (1999) Science algorithms of the EPA Models-3 Community Multiscale Air Quality (CMAQ) Modeling system. EPA Report 600/R-99/030, Washington, DC
2. CEP (2003) Sparse Matrix Operator Kernel Emission (SMOKE) modeling system. University of Carolina, Carolina Environmental Programs, Research Triangle Park
3. Shamarock et al. (2007) A description of the Advanced Research WRF Version 2. http://www.mmm.ucar.edu/wrf/users/docs/arw_v2.pdf. Accessed 15 June 2010
4. Tanaka PL, Allen DT, McDonald-Buller EC, Chang S, Kimura Y, Yarwood G, Neece JD (2003) Development of a chlorine mechanism for use in the carbon bond IV chemistry model. J Geophys Res 108:4145

Chapter 116
Coupling WRF and CALMET Models: Validation During Primary Pollutants glc Episodes in an Atlantic Coastal Region

Anel Hernández, Santiago Saavedra, Angel Rodríguez, Jose A. Souto, and Juan J. Casares

Abstract The application of Lagrangian dispersion models, as CALPUFF, at local scales requires as input accurate and very high resolution meteorological fields. In these high resolution applications, the computational cost of numerical weather forecast models, as WRF, recommends the steady-state nesting of a diagnostic model, as CALMET, in order to properly consider the influence of land use and terrain topography over complex terrain domains.

In this work, CALMET diagnostic model is nested to different WRF model simulations over a complex terrain and coastal domain around As Pontes Power Plant during three different periods when some primary pollutants glc peaks were detected. Different horizontal resolutions for the WRF simulations were considered as data input to CALMET. For the meteorological models validation and intercomparison, temperature, wind speed and wind direction statistics were obtained by comparison against measurements from surface meteorological stations located in the domain.

Keywords WRF-CALMET nesting • Meteorological models validation.

A. Hernández
Department of Chemical Engineering, University of Santiago de Compostela, 15782 Santiago de Compostela, Spain

Higher Institute for Applied Science and Technologies (INSTEC), Havana, Cuba

S. Saavedra (✉) • A. Rodríguez • J.A. Souto • J.J. Casares
Department of Chemical Engineering, University of Santiago de Compostela, 15782 Santiago de Compostela, Spain
e-mail: santi.saavedra@usc.es; ja.souto@usc.es

D.G. Steyn et al. (eds.), *Air Pollution Modeling and its Application XXII*,
NATO Science for Peace and Security Series C: Environmental Security,
DOI 10.1007/978-94-007-5577-2_116,

116.1 Introduction

The current development of meteorological and air quality modelling, jointly to the increase of performance computing and environmental databases provided by public institutions, achieved a level that allows the application of models and data input to the now-casting of both steady-state and fugitive atmospheric emissions impact over local domains. Particularly, its application on fugitive emissions supports risks prevention around industrial plants.

However, these applications require accurate and high resolution meteorological fields, which are critical to obtain a good air quality simulation. These fields can be obtained by a diagnostic model, with low computational cost.

CALMET [5] is a flexible diagnostic model that can use high resolution prognostic data from different models (RUC, MM5, WRF) [7]. On the other hand, Weather Research and Forecast model (WRF, [6]) represents one of the state-of-art prognostic models that were applied to produce data input to CALMET [1]. However, comparison of WRF and CALMET results against measurements at different horizontal resolutions is an issue rarely considered, whereas there are several studies comparing MM5 and CALMET [2].

In this work, WRF results at 9×9 and 3×3 km^2 horizontal resolutions were applied as input to CALMET model, in order to obtain high resolution meteorological fields over a complex terrain and coastal domain.

116.2 Methodology

The selected cases for the models validation and intercomparison are located in a 99×99 km^2 centred at As Pontes Power Plant, in the NW of the Iberian Peninsula. This is a complex terrain region were some SO_2 glc peaks were sporadically detected until 2008, due to the SO_2 emissions from that power plant. In this models validation, three different periods were considered: 13–15/July/2005, 1–3/June/2006 and 9–11/July/2006.

WRF simulations were obtained for 27×27, 9×9 and 3×3 km^2 resolution nested domains [4], using GFS-NCEP analysis as initial and boundary conditions. 9×9 and 3×3 km^2 WRF results were applied as input to CALMET simulations over the domain study, to obtain 3×3 km^2 resolution meteorological fields.

Wind and temperature hourly surface measurements from 11 meteorological stations located in the domain study were applied to the models validation. Several statistics [3] were considered, with root mean square error (RMSE) results as the most significant for surface wind and temperature.

116.3 Results and Concluding Remarks

As an example, Table 116.1 shows the RMSE for the simulation results along July 13–15, 2005 period. As expected, CALMET nested to WRF is better than WRF.

Table 116.1 Root mean square error (RMSE) for hourly surface temperature (T), wind speed (WS) and wind direction (WD) results from the following simulations along July 13–15, 2005: WRF9: WRF 9×9 km^2 results

	WRF9			WRF3		
Meteorological station	WS (m/s)	WD (degrees)	T (°C)	WS (m/s)	WD (degrees)	T (°C)
CIS FERROL	1.499	64.517	4.272	1.277	76.107	4.279
FRAGAVELLA	1.649	87.603	3.075	1.447	86.566	2.757
GUITIRIZ	1.489	62.425	3.716	1.615	64.205	3.547
MABEGONDO	1.532	91.236	3.834	1.136	104.717	3.983
MARCO DA CURRA	1.494	71.105	3.718	1.576	72.139	3.651
B-1 MAGDALENA	2.157	81.695	3.303	1.593	71.143	3.163
B-2 LOUSEIRAS	2.166	94.324	2.997	2.158	65.999	2.849
C-9 MOURENCE	1.245	97.791	2.865	1.431	84.589	2.916
F-2 FRAGA REDONDA	1.930	91.746	4.041	1.768	81.702	4.038
G-2 VILANOVA	1.814	103.490	4.117	1.839	90.187	4.427
D1 A MOURELA	1.851	100.474	3.852	1.271	75.691	3.886
All the stations	1.728	86.964	3.646	1.574	80.116	3.635
	CALMET9-3			CALMET3-3		
Meteorological station	WS (m/s)	WD (degrees)	T (°C)	WS (m/s)	WD (degrees)	T (°C)
CIS FERROL	1.435	75.967	3.730	1.398	72.030	3.849
FRAGAVELLA	1.312	105.642	3.094	1.307	107.564	3.009
GUITIRIZ	1.370	57.748	3.378	1.253	65.241	3.431
MABEGONDO	1.266	94.104	3.543	1.090	104.138	3.700
MARCO DA CURRA	1.553	71.687	3.469	1.430	70.242	3.635
B-1 MAGDALENA	1.884	76.805	3.412	1.528	71.851	3.418
B-2 LOUSEIRAS	1.940	62.275	2.743	1.998	65.747	3.027
C-9 MOURENCE	1.637	86.142	3.311	1.254	86.145	3.514
F-2 FRAGA REDONDA	1.599	86.893	4.190	1.430	78.752	4.441
G-2 VILANOVA	2.045	79.612	3.513	2.027	82.362	3.958
D1 A MOURELA	1.619	75.973	3.635	1.225	81.052	3.793
All the stations	1.625	80.199	3.474	1.479	81.692	3.637

WRF3: WRF 3×3 km^2 results. CALMET9-3: CALMET 3×3 km^2 results coupled to WRF9. CALMET3-3: CALMET 3×3 km^2 results coupled to WRF3

For CALMET nested to WRF, it can be observed large differences between the different simulations and, also, between the different sites. Wind direction statistics are quite poor (62–106°), as expected, because of the dominant soft winds along the periods. Better global results in wind speed and temperature RMSE statistics are achieved: from 1.266 to 2.045 ms^{-1} for wind speed, and from 2.743 to 4.190 K for temperature.

Considering site by site for this simulation (Table 116.1), the best adjustment for wind speed was observed at Mabegondo site during the first period; whereas at Louseiras better results for temperature and wind speed were achieved; this is the highest site in the domain study, so the influence of complex terrain is less significant than in the other sites.

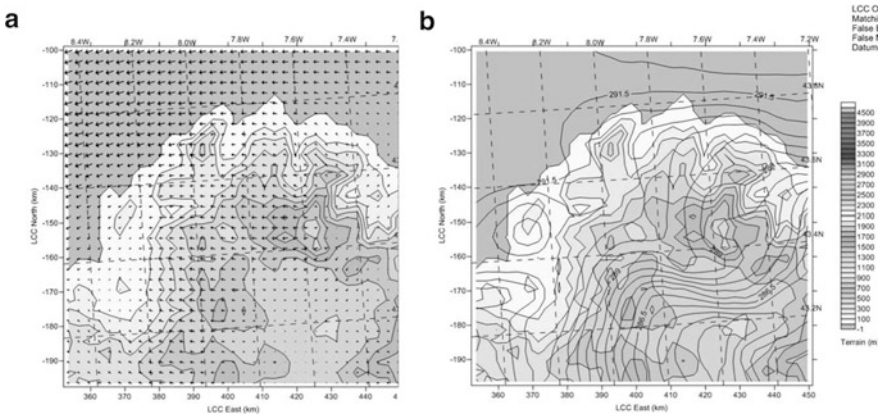

Fig. 116.1 Surface wind field (**a**) and temperature (**b**) from by CALMET simulation (with 9×9 km^2 WRF results input) in the study domain: on July 13th, 2005, at 0600 UTC

Figure 116.1 shows the surface wind field and temperature over the study domain obtained by the best CALMET results on July 13th, 2005 at 0600 UTC. The complexity of the domain due to topographic and coastal effects can be observed.

Acknowledgments Anel Hernández's research stages at the University of Santiago de Compostela were supported by USC-Banco de Santander PhD Programme for Latinoamerican university teachers. Meteorological data provided by MeteoGalicia and As Pontes Power Plant are acknowledged.

References

1. Gualtieri G (2010) Implementing an operational ozone forecasting system based on WRF/CALMET/CALGRID Models: a 5-month case study over Tuscany. Italy Water Air Soil Pollut 209:269–293. doi:10.1007/s11270-009-0197-3
2. Jackson B et al (2006) Comparison of ozone simulations using MM5 and CALMET/MM5 hybrid meteorological fields for the July/August 2000 CCOS episode. Atmos Environ 40:2812–2822
3. Jiménez P et al (2006) Evaluation of MM5-EMICAT2000-CMAQ performance and sensitivity in complex terrain: high-resolution application to the northeastern Iberian Peninsula. Atmos Environ 40:5056–5072
4. Saavedra S et al (2012) Validation of WRF model during both primary and secondary pollutants episodes over an Atlantic coastal region. In: 8th international conference on Air Quality – Science and Application, Athens, 19–23 March 2012
5. Scire JS et al (2000) A user's guide for the CALMET Meteorological Model. Earth Tech, Inc, Concord, MA
6. Skamarock WC et al (2008) A time-split non-hydrostatic atmospheric model for weather research and forecasting applications. J Comput Phys 227:3465–3485
7. Radonjic Z (2005) Coupling NMM Mesoscale weather forecasting model with CALMET/CALPUFF Regulatory Air Dispersion Model. In: A&WMA 98th annual conference and exhibition. Minneapolis, Minnesota, June

Chapter 117
Meteorological Modeling of the PM10 Episode in the Creek Valley of Golden Horn Harbour, Istanbul Under Very Stable Conditions for November 6–9, 2010 Episode

Şeyda Tilev Tanriover, Abdullah Kahraman, Selahattin Incecik, Ali Deniz, Hüseyin Toros, Hafize M. Celebi, Ali Ozturk, and Îsmail Sezen

Abstract This paper presents verification results of numerical simulations of meteorological conditions leading to an air pollution episode on 6–9 November 2010 in Istanbul. WRF-ARW ver 3.3 is run with GFS and ECMWF input. For verification, horizontal wind components and temperature data of nine meteorological stations are used for both simulations. Results indicate that the model is successful in simulating the meteorological conditions with both two different input data, especially with the GFS input, although ECMWF runs had a finer horizontal resolution of 1 km.

Keywords PM10 • Episode • Air quality • Meteorological modelling • WRF

117.1 Introduction

Regional-scale air quality models are designed to simulate air quality in a domain with a horizontal scale of several hundred to several thousand kilometers and a vertical scale of several kilometers. According to the European Environmental

Ş.T. Tanriover (✉) • S. Incecik • A. Deniz • H. Toros • H.M. Celebi • Î. Sezen
Deptartment of Meteorological Engineering, Istanbul Technical University, Istanbul, Turkey
e-mail: tanriovers@itu.edu.tr

A. Kahraman
Deptartment of Meteorological Engineering, Istanbul Technical University, Istanbul, Turkey

Turkish State Meteorological Service, ITU-TSMS Office, Istanbul, Turkey

A. Ozturk
Turkish State Meteorological Service, ITU-TSMS Office, Istanbul, Turkey

D.G. Steyn et al. (eds.), *Air Pollution Modeling and its Application XXII*,
NATO Science for Peace and Security Series C: Environmental Security,
DOI 10.1007/978-94-007-5577-2_117,

Agency air pollution is the environmental factor with the greatest impact on health in Europe and is responsible for the largest burden of environment related diseases [2]. The presence of PM10 is significant due to the associated respiratory health implications in urban areas. Under episodic conditions, PM10 concentrations can considerably exceed air quality standards and WHO limits. The causes of these episodes include various factors, e.g., emissions, local and meso-scale meteorological conditions, and topography. Istanbul is one of the significant mega cities in the world. The city has experienced high PM10 episodes in winter and spring/fall seasons.

Forecasting PM10 concentrations is a challenging issue. First, the meteorological conditions favouring the episodes must be simulated accurately in order to perform a skilful concentration prediction. WRF meteorological model identifies the surface wind fields associated with the highest and lowest air pollutant exposures at most of the sites in Istanbul. This study aims to understand the quality of urban scale modelling using simulations with different initial and boundary conditions.

117.2 Region and Methodology

117.2.1 November 2010 PM10 Episode

The ratio of the days with daily PM10 concentrations exceeding the limit value of 50 $\mu g/m^3$ in some monitoring stations of urban area is varied in between 23 and 60 % of the stations in heating season. The emission sources and local and synoptic meteorological conditions may have been responsible for daily mean concentrations $>50\ \mu g/m^3$ at several ratios of the monitoring sites each year. In order to understand the impact of PM emissions on air quality in creek valley of Golden Horn harbour (Kagıthane), a new air quality station in the region has established since 2009. This part of the city has significantly experienced the higher PM10 concentrations not only heating seasons, but also summer season [1].

The region is exposed to the many industrial facilities and busy urban traffic in this creek valley. Valley topography and industrial and traffic emissions may lead to significant episodic conditions of PM10 in the region.

These episodic conditions lead to high PM10 concentrations ($>300\ \mu g/m^3$ hourly), sometimes reaching to 570 $\mu g/m^3$ in Kagıthane Creek Valley of Istanbul (Fig. 117.1). Figure 117.1 shows the data obtained from Kagıthane station during November 2010 episode over the region. The episode was mainly associated with the influence of a high-pressure system accompanied with thermal inversion in surface layer.

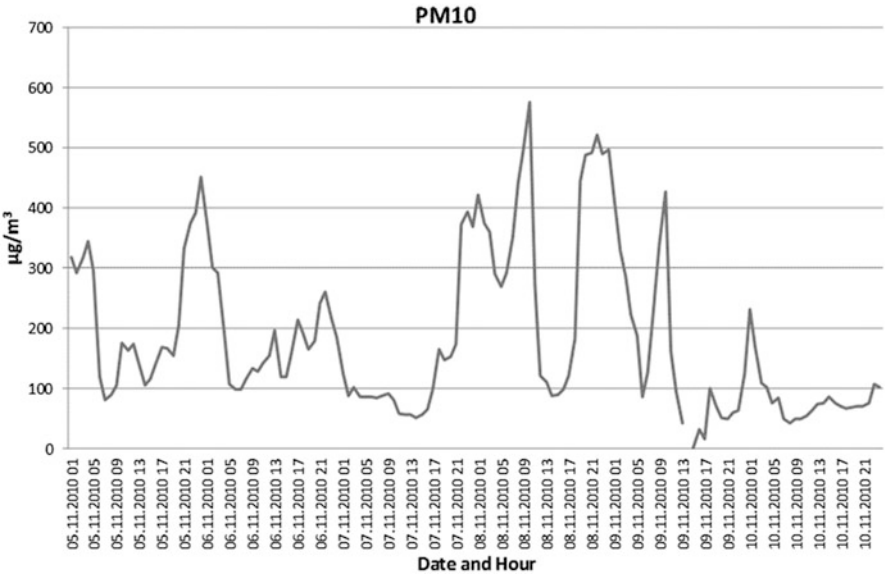

Fig. 117.1 PM10 observations of Kagithane station from 05.11.2010 00UTC to 11.11.2010 00UTC

117.2.2 Numerical Simulation of the Episode

Advanced Research WRF (ARW) modeling system is applied to simulate the episode with ECMWF and GFS input. The model is run with two-way nesting option for domains with 24, 8 and 2.7 km grid intervals for GFS input and 9, 3 and 1 km grid intervals for ECMWF input respectively, both with 44 vertical levels. Simulation period starts on 00UTC, 06 November 2010 and ends on 00UTC, 10 November 2010. The same physical options are used for both experiments, namely RRTMG radiation schemes, Eta similarity surface scheme, WSM6 microphysics, MYJ PBL scheme, NOAH LSM, and KF cumulus parameterization for the outermost domains as well as the second domain of GFS-initiated run. The innermost domains as well as the second domain of the ECMWF-initiated run have no cumulus parameterization.

117.3 Results and Discussions

Simulation results are verified against nine meteorological stations of Turkish Meteorological Service around Istanbul. The statistics for the horizontal wind components and temperature are calculated (Table 117.1). RMSE for u and v are

Table 117.1 Statistical summary of the meteorological parameters for November 2010 episode

Station name	Statistics	U (m/s) ecmwf (1 km)	U (m/s) gfs (2.7 km)	V (m/s) ecmwf (1 km)	V (m/s) gfs (2.7 km)	T (°C) ecmwf (1 km)	T (°C) gfs (2.7 km)
CATALCA	RMSE	5.93	6.41	7.03	5.78	3.48	2.19
	Mean Err.	3.91	5.21	4.9	4.53	0.86	1.05
	σ_m/σ_o	0.52	0.41	0.29	0.55	0.91	0.68
	r	−0.43	−0.05	0.65	0.88	0.23	0.75
	IOA	0.30	0.40	0.56	0.73	0.60	0.81
ISTANBUL BOLGE	RMSE	2.82	3.75	5.53	6.97	2.24	2.18
	Mean Err.	−2.03	−2.69	−4.77	−5.25	−0.83	0.29
	σ_m/σ_o	2.64	2.92	2.92	4.31	0.66	0.64
	r	−0.313	−0.56	0.17	0.08	0.73	0.71
	IOA	0.05	0.02	0.02	0.02	0.80	0.79
IST.UNIV.DENIZ BIL.	RMSE	2.67	1.62	3.57	2.56	2.16	3.35
	Mean Err.	−2.22	−0.31	−2.87	0.52	−0.56	0.02
	σ_m/σ_o	1.03	1.23	2.07	1.99	1.15	1.11
	r	−0.19	−0.02	0.21	0.32	0.80	0.69
	IOA	0.24	0.39	0.28	0.50	0.80	0.73
FLORYA	RMSE	2.41	2.30	3.75	3.81	3.47	2.54
	Mean Err.	0.05	1.52	−2.23	−2.21	−1.73	−0.25
	σ_m/σ_o	1.66	1.06	2.43	2.56	0.31	0.30
	r	−0.03	0.19	−0.04	0.44	0.36	0.77
	IOA	0.32	0.46	0.23	0.46	0.53	0.60
KARTAL	RMSE	3.57	3.58	3.46	4.41	2.93	2.88
	Mean Err.	−1.55	−2.35	−2.66	−3.24	0.03	−0.58
	σ_m/σ_o	3.73	2.89	2.68	3.75	0.80	0.56
	r	−0.06	−0.02	0.03	0.38	0.67	0.71
	IOA	0.23	0.23	0.18	0.30	0.80	0.76

KUMKOY-KILYOS	RMSE	4.41	3.11	2.64	1.89	2.83	2.65
	Mean Err.	−3.78	−2.61	0.41	0.82	0.07	1.56
	σ_m/σ_o	1.29	0.99	0.62	1.01	0.85	0.74
	r	0.04	0.31	−0.16	0.70	0.72	0.86
	IOA	0.32	0.45	0.28	0.81	0.84	0.86
SARIYER-KIRECBURNU	RMSE	2.64	1.39	2.38	2.43	3.03	2.40
	Mean Err.	−1.65	−0.53	−1.73	−2.02	−1.70	0.67
	σ_m/σ_o	2.32	1.62	1.14	1.50	0.76	0.60
	r	−0.23	0.42	−0.08	0.71	0.78	0.87
	IOA	0.02	0.15	0.02	0.15	0.82	0.86
SAMANDIRA-ISTANBUL	RMSE	3.68	2.61	5.15	5.33	4.1	3.97
	Mean Err.	−0.97	−1.29	−3.22	−4.22	−1.33	−1.39
	σ_m/σ_o	2.63	1.84	1.88	2.45	0.55	0.46
	r	−0.33	0.34	−0.54	0.60	0.60	0.80
	IOA	0.07	0.10	0.01	0.06	0.68	0.69
SILE	RMSE	1.97	1.17	1.82	1.97	2.6	2.84
	Mean Err.	−0.97	0.45	−0.59	−1.41	0.82	0.69
	σ_m/σ_o	3.92	2.93	1.45	1.83	0.90	0.83
	r	0.15	0.59	−0.21	0.53	0.8	0.87
	IOA	0.27	0.53	0.27	0.47	0.82	0.85

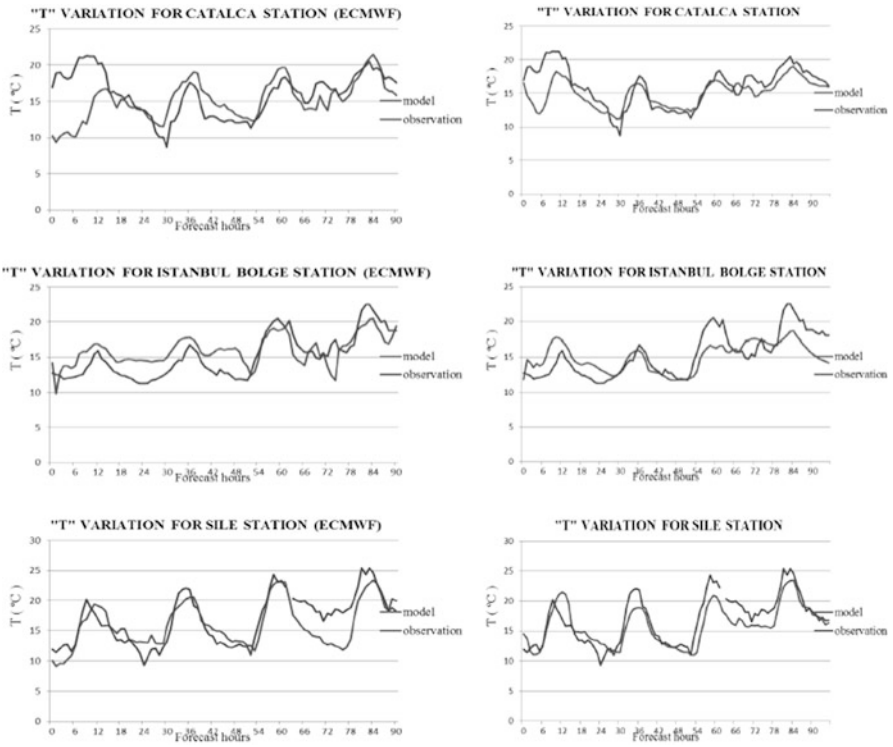

Fig. 117.2 Time series of temperature for November 2010 episode (From 06.11.2010 00Z to 10.11.2010 00Z)

around 2–3 m/s in many stations, in a few like Çatalca show higher values. Mean error values show that the simulations overestimated the wind components for this station, most probably due the high elevation (378 m). The other stations usually have lesser mean error values, being mostly negative. σmodel/σobservation values look acceptable for such simulations. Correlations especially are good for GFS-initiated runs. IOA is also indicating similar results. Temperature statistics also show that GFS-initiated simulations with 2.7 km horizontal grid interval outperform ECMWF-initiated runs with 1 km horizontal grid interval. Time series of temperature (Fig. 117.2), u component of horizontal wind (Fig. 117.3) and v component

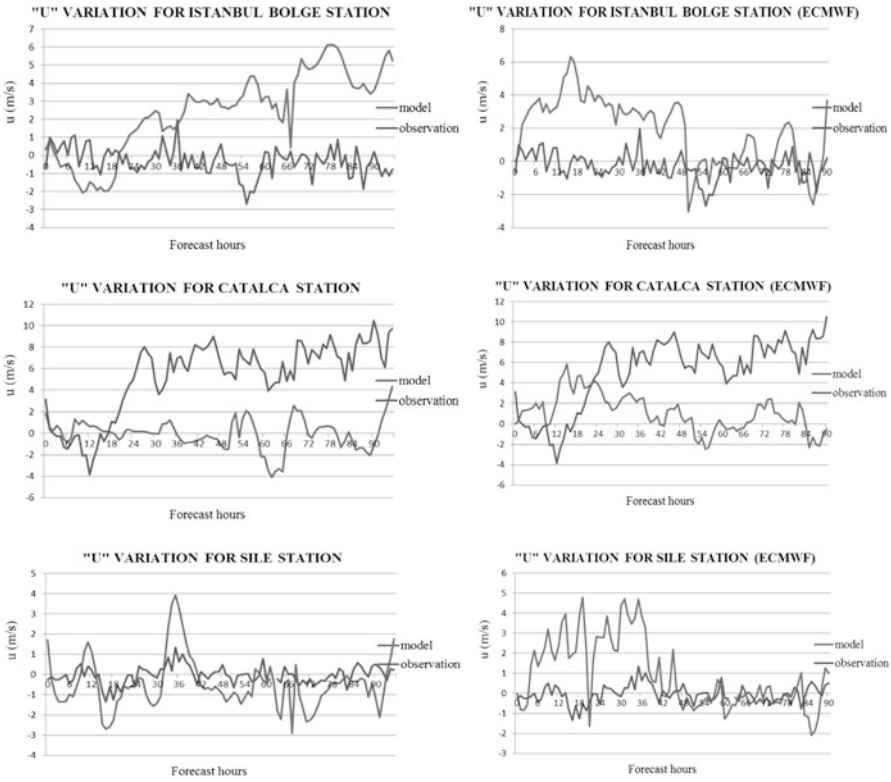

Fig. 117.3 Time series of horizontal wind component u for November 2010 episode (From 06.11.2010 00Z to 10.11.2010 00Z)

of horizontal wind (Fig. 117.4) show that after a spin-up period of approximately 12 h, both simulations have pretty good approximation to observations in three given example stations, namely Çatalca, Goztepe and Şile. Diurnal variation of temperature field is almost perfectly captured for 4 days period of the episode, however, horizontal wind components do have some difference for certain sections of the episode. An application of WRF-Chem for this episode will be a future study.

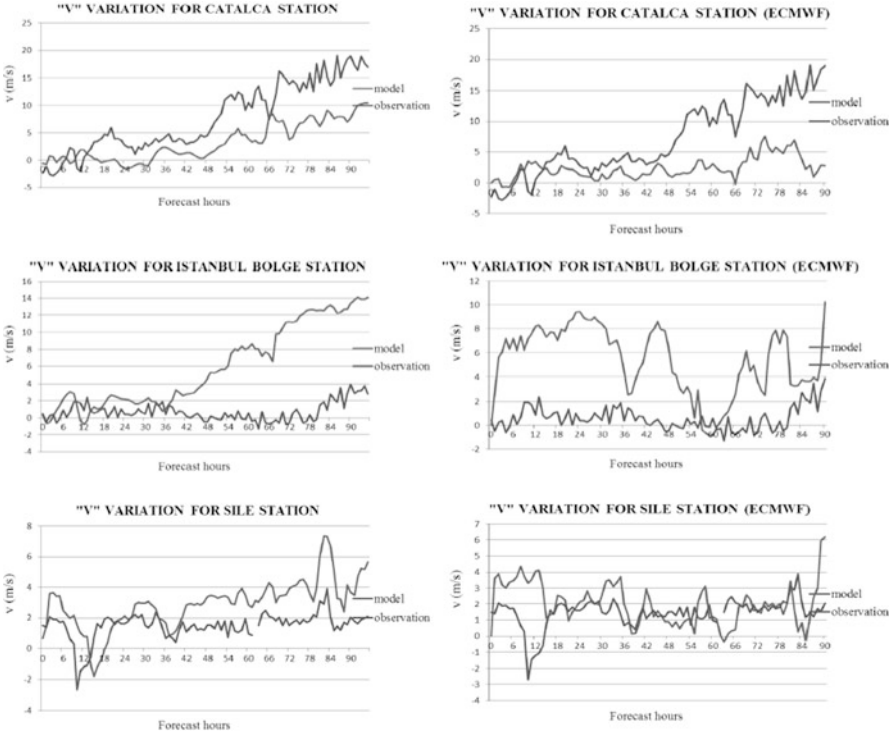

Fig. 117.4 Time series of horizontal wind component v for November 2010 episode (From 06.11.2010 00Z to 10.11.2010 00Z)

Acknowledgements The authors would like to acknowledge the financial support by the Scientific and Technological Research Council of Turkey (TUBITAK, project no:109Y132).

References

1. Deniz A (2009) An investigation of air quality in Kagıthane Creek Valley, TUBITAK, Research Project 109Y132
2. EEA (2005) Environment and Health. European Environment Agency, European Comission, Joint Research Centre, Report 10/2005, 40 pp

Chapter 118
Urban Scale Meteorological and Air Quality Forecast for the Biggest Israeli Cities Jerusalem, Tel Aviv and Haifa: WRF-Chem Model Simulation

Yosef Levitin

Abstract The new version of WRF Modeling System (ver. 3.3) is run on nested domains of resolution 27, 9, 3 and 1 km. The three innermost domains with resolution of 1 km overlap three very different topographical areas with the biggest Israeli cities Jerusalem, Tel-Aviv and Haifa. Namely, Jerusalem is located on the southern spur of the Judean Mountains with the elevation of 700–800 m. The Great Tel Aviv urban area includes Tel Aviv itself and several satellite towns. The urban area lies about 20 km along the Mediterranean shoreline at coastal plain and extends about 10 km inland. Haifa is situated on the slopes of the Carmel range, stretching from the Mediterranean shoreline towards the southeast. The object of study is the high resolution pattern of wind and temperature fields, vertical turbulent structure within and over the urban canopy and the urban heat island (UHI) effect. The simulated by the WRF-ARW model wind field and atmospheric turbulent structure are the base for air pollutants transport and diffusion within urban canopy and outside the city. A coupled WRF-Chem modeling system is applied to analyze the temporal and spatial dynamics of pollutant concentration fields, first of all nitrogen oxides from traffic exhausts. The general goal of the study is to develop an easy-to-use tool for urban air quality forecast, based on the operative short-term weather forecast.

Keywords Urban scale meteorology • Heat island

Y. Levitin (✉)
Israel Meteorological service, P.O. Box 25, Bet Dagan 50250, Israel
e-mail: jlevitin@yahoo.com

D.G. Steyn et al. (eds.), *Air Pollution Modeling and its Application XXII*,
NATO Science for Peace and Security Series C: Environmental Security,
DOI 10.1007/978-94-007-5577-2_118,

118.1 Introduction

It is known from many investigations, both from numerical modeling and field measurements, there are sizeable changes in the surface layer meteorological parameters within urban canopy, by comparison with ones above an open area. First, it understands the urban heat island (UHI) over big cities, with temperature difference between internal urban territory and surrounding rural areas about several degrees, wind speed deceleration and intensification of turbulent mixing within and above urban canopy. The above mentioned features of urban meteorology are able to intensify the air quality problems, first of all transfer and diffusion of motor transport exhausts, i.e. the main pollution source within and around big cities.

The WRF-ARW Modeling System (ver. 3.3) was used for numerical simulation and run on the nested domains of resolution 27, 9, 3 and 1 km. The three innermost domains with 1 km resolution overlap three very different complicated topographical areas where the biggest Israeli cities Jerusalem, Tel-Aviv and Haifa are located.

The Great Tel Aviv urban area includes Tel Aviv itself and several satellite towns. The urban area lies about 20 km along the Mediterranean shoreline at coastal plain and extends about 10 km inland without any meaningful topography features. Mountains to the east limit the coastal plain to width of about 20 km.

Haifa is situated on the slopes of the Carmel ridge, stretching from the Mediterranean shoreline towards the southeast. Complex topography and the Bay of Haifa, shielded on the southwest by the Carmel ridge, often lead to critical situations with air quality.

The Tel Aviv and Haifa climate is Mediterranean; the average daily temperature is of 26 °C during summer and 15 °C during winter; relative humidity is of 69 and 66 % in summer and winter, respectively. The mean global irradiance reaches 27.2 MJ m^{-2} day^{-1} in summer and 9.4 MJ m^{-2} day^{-1} in winter. Precipitation occurs from November to March, mainly in December-February. The summer wind rose reflects the daily sea-land breeze circulation with some influence of the summer trough; in winter the winds caused by different pressure systems play a significant role.

Jerusalem is located on the southern spur of the Judean Mountains with the elevation of 700–800 m. To the west from Jerusalem the Judean Mountains downgrade gradually to the Mediterranean shore; to the east the mountain ridge sharply comes down to the Dead Sea valley with the water surface at 423 m below sea level.

Jerusalem climate is characterized by quite cold, wet winter with an average temperature of 9 °C and relative humidity of 62 % in January. By contrast, summer is dry and warm, with low humidity and average temperature about 24 °C. In summer solar radiation is intense because of the lack of clouds and low humidity, but also because the sun reaches a high angle of 80° above the horizon. The mean global irradiance reaches 29.3 MJ m^{-2} day^{-1} in summer, and 9.9 MJ m^{-2} day^{-1} in winter.

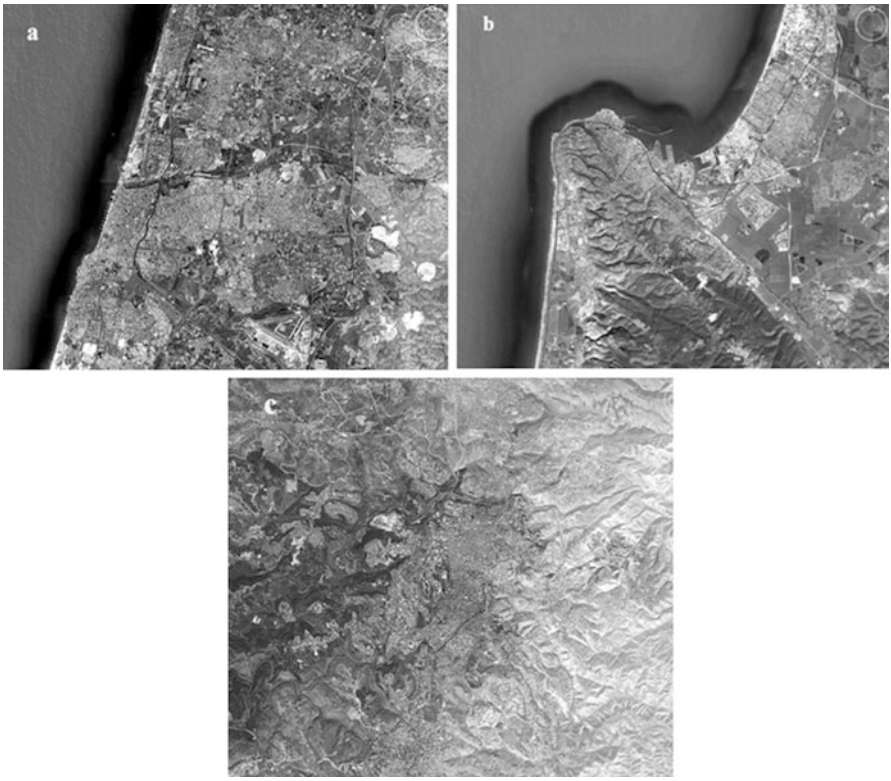

Fig. 118.1 Maps of Tel Aviv (**a**), Haifa (**b**) and Jerusalem (**c**) urban areas

The object of this study is the pattern of temperature, wind and turbulent intensity within and over the urban canopy and the urban heat island (UHI) effect; the general goal of the study is to develop an easy-to-use tool for urban air quality forecast, based on the operative short-term weather forecast.

In the past the UHI effect have been investigated using the WRF mesoscale model coupled with the Noah land surface scheme and Urban Canopy model (UCM) [1–6]. The simulated by the WRF-ARW model wind field and atmospheric turbulent structure with high horizontal grid resolution of 0.5–1 km may be a suitable base for modeling of air pollutants transport and diffusion within urban canopy and outside the city, first of all it concerns traffic exhausts, mainly nitrogen oxides (NO_x) and carbon monoxide (CO).

The WRF-ARW model (version 3.3) was running in a nested mode, involving four domains with spatial grid resolution of 27, 9, 3 and 1 km and with 30 vertical levels. The largest domain runs over the Mediterranean region with size of 3,000 km × 3,000 km. The three finest separate domains with 1 km resolution (30 km × 40 km) involve the Tel Aviv, Haifa and Jerusalem urban areas (Fig. 118.1).

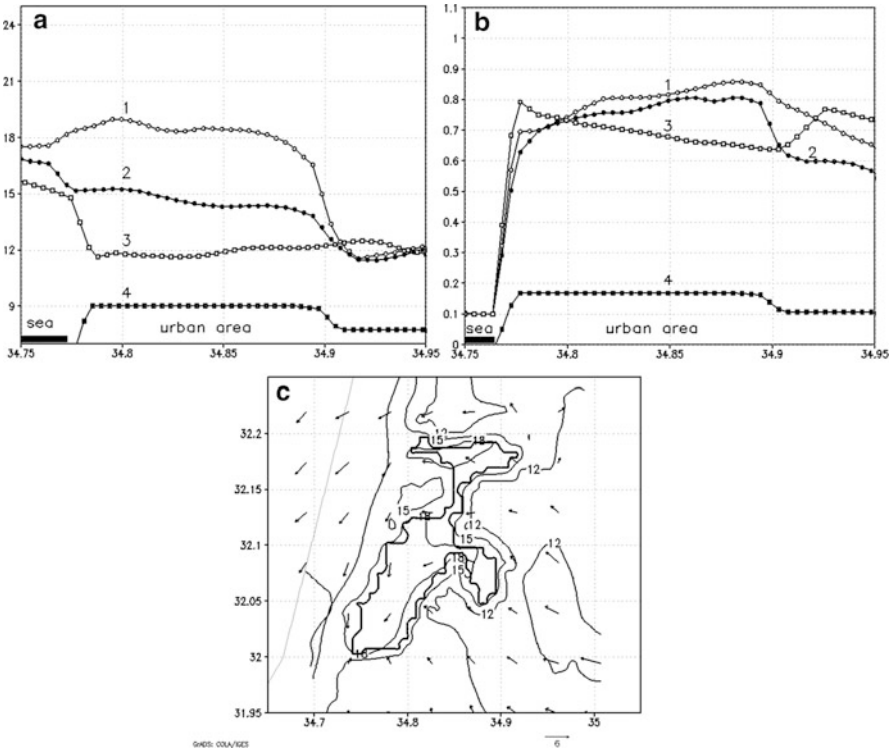

Fig. 118.2 Tel Aviv urban area on 22 January 2011: (**a**) temperature at 2 m, at 20:00 LST; locations of the urban area and sea surface are indicated; (**b**) TKE ($m^2\ s^{-2}$) at 1st and 2nd model levels at 14:00 LST; (**c**) wind (knots) at 10 m and surface temperature isopleths at 20:00 LST. The *thin line* and *bold contour* show the shoreline and the urban area boundary, respectively

The set of physical options includes Mellor-Yamada-Janjic PBL scheme, Ferrier microphysics, Betts-Miller-Janjic cumulus scheme (for domains 1 and 2), RRTM long wave and Dudhia short wave radiation schemes. The anthropogenic heat flux (AH) is assumed by 200 Wm^{-2}; this value fits the upper bound of the energy release within the Tel Aviv conurbation and agrees with the AH used for Taipei [3].

Two days with typical weather conditions, 22 January and 20 June 2011 were used for simulation. The model ran from 00:00 GMT 19 June 2011 and 21 January 2011 with the forecast period of 48 h. The initial and boundary conditions were taken from the global GFS model forecast.

Figures 118.2, 118.3 and 118.4 show modeling results for the Tel Aviv, Haifa and Jerusalem areas on 22 January 2011; namely, 2 m surface temperature (a), turbulent

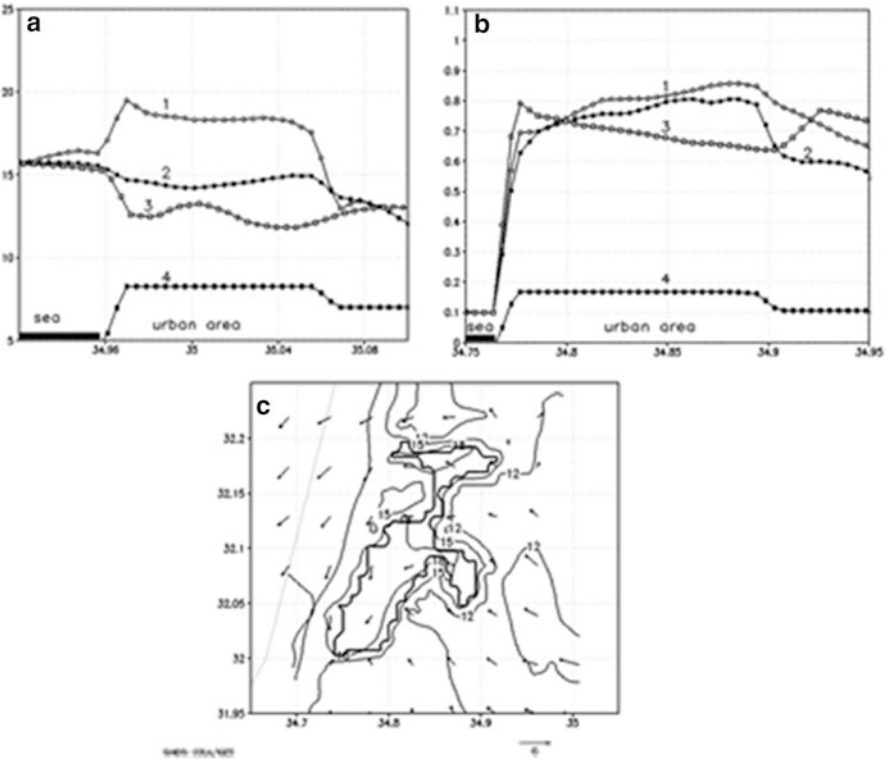

Fig. 118.3 Haifa urban area: the same curves as on Fig. 118.2

kinetic energy (TKE) (b) and 10 m wind field coupled with surface temperature isopleths (c). Figures 118.2a, 118.3a and 118.4a show two temperature curves for two urban land use model, i.e. UCM (1) and 25-category USGS (2), for the cross-section along the west–east longitude across the centre of the cities; the third curve (3) corresponds to the longitude crossed the rural territory outside the cities. The time is 20:00 LST, i.e. the time of the maximum UHI effect. Also shoreline location (for Tel Aviv and Haifa) and schematic profile of land use (4) are shown; the upper flat segment corresponds to the building zone. Figures 118.2b, 118.3b and 118.4b show TKE curves at the 1st (1) and 2nd (2) vertical model levels (about 12 and 29 m over ground) within urban area and at the 1st level over rural surface (3); for the TKE curves the time is 14:00 LST, i.e. the time of the maximum TKE values. Figures 118.2c, 118.3c and 118.4c show 10 m wind field and surface temperature isopleths at 20:00 LST. Here the urban area boundary and the shoreline are also indicated.

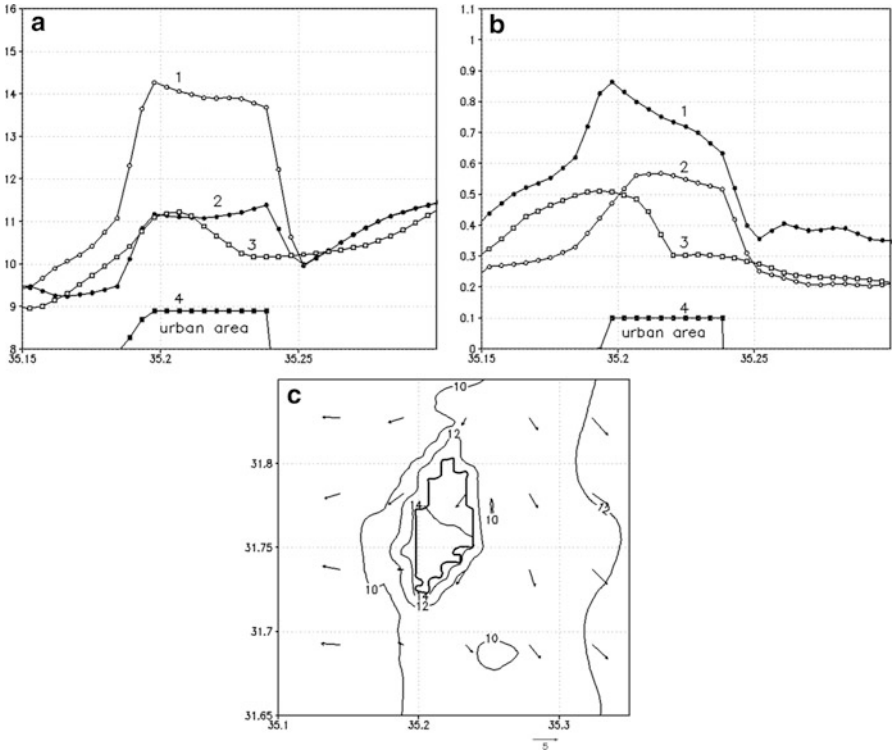

Fig. 118.4 Jerusalem urban area: the same curves as on Fig. 118.2

Figures 118.5, 118.6 and 118.7 show the analogous to Figs. 118.2, 118.3 and 118.4 modeling results for the summer day 20 June 2011, at 21:00 LST for temperature and at 15:00 LST for TKE. In summer surface temperature and TKE increase, whereas the UHI effect (urban–rural temperature difference) reduces, e.g., from 7 in winter to 5° in summer for the Tel Aviv area.

118.2 Summary

Among many factors, the anthropogenic heat flux (AH) plays an important role in UHI intensity. In our study, we use a rough value of 200 Wm^{-2} basing on the upper bound of the energy expenses inventory.

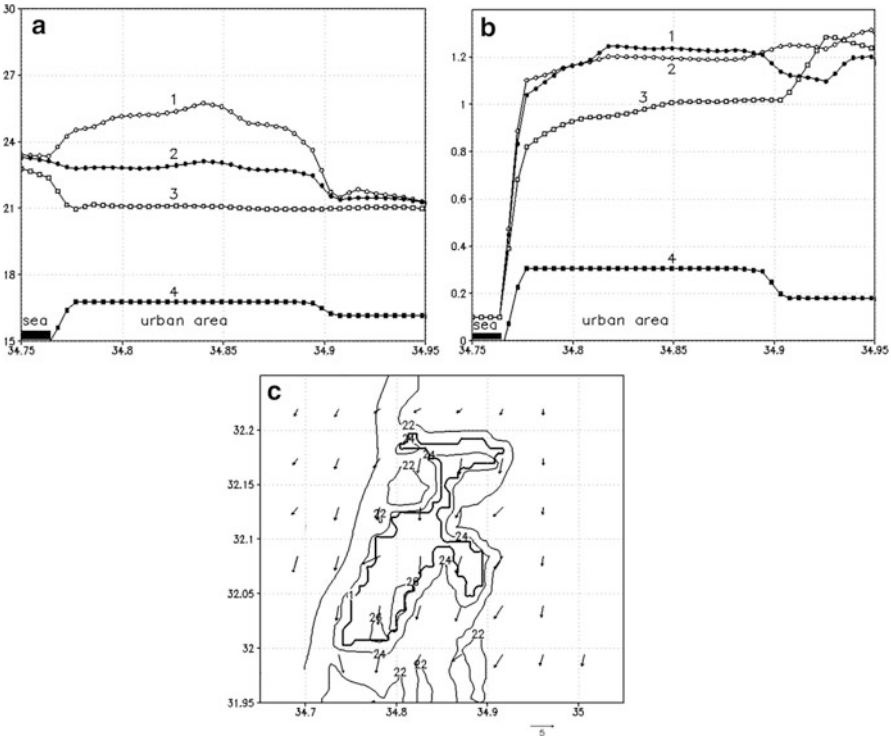

Fig. 118.5 Tel Aviv urban area on 20 June 2011: (**a**) temperature at 2 m, at 21:00 LST; location of the urban area and sea surface are indicated; (**b**) TKE ($m^2\ s^{-2}$) at 1st and 2nd model levels at 15:00 LST; (**c**) wind (knots) at 10 m and surface temperature isopleths at 21:00 LST. The *thin line* and *bold contour* show the shoreline and the urban area boundary, respectively

The predicted intensity of UHI effect, which is an air temperature difference between urban and rural areas, amounts to 7 °C (Tel Aviv) and 3 °C (Jerusalem) in winter and 5 and 3 °C in summer. The UHI appears in the morning, and then its intensity goes down in the middle of the day and then increases again to maximum value in the late evening; in winter the intensity of UHI is higher. Surface air temperatures start with the close values over the sea surface or over open land (Jerusalem) and then diverge along with the airflow movement over urban and rural territory. The heat trace of the city stretches to several kilometers leeward.

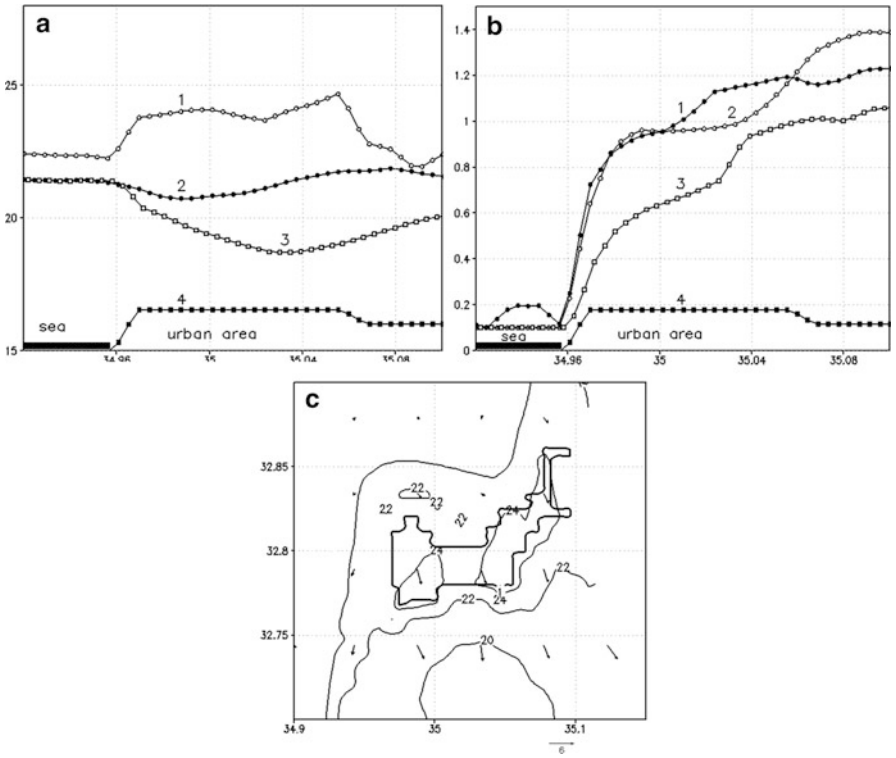

Fig. 118.6 Haifa urban area: the same curves as on Fig. 118.5

TKE values increase on 20–30 % up over urban area compared to rural territory for Tel Aviv, 45–130 % up over the Haifa and 80–130 % up over Jerusalem; it may lead to intensification of pollutants diffusion within urban canopy.

It appears that the high-resolution WRF-ARW model system sufficiently good describes the meteorological features over extended urban areas. On the next stage, it is assumed to use the WRF-ARW-Chem model to analyze transport and diffusion of motor transport pollutants, mainly NO_x and CO, within urban canopy and around big cities.

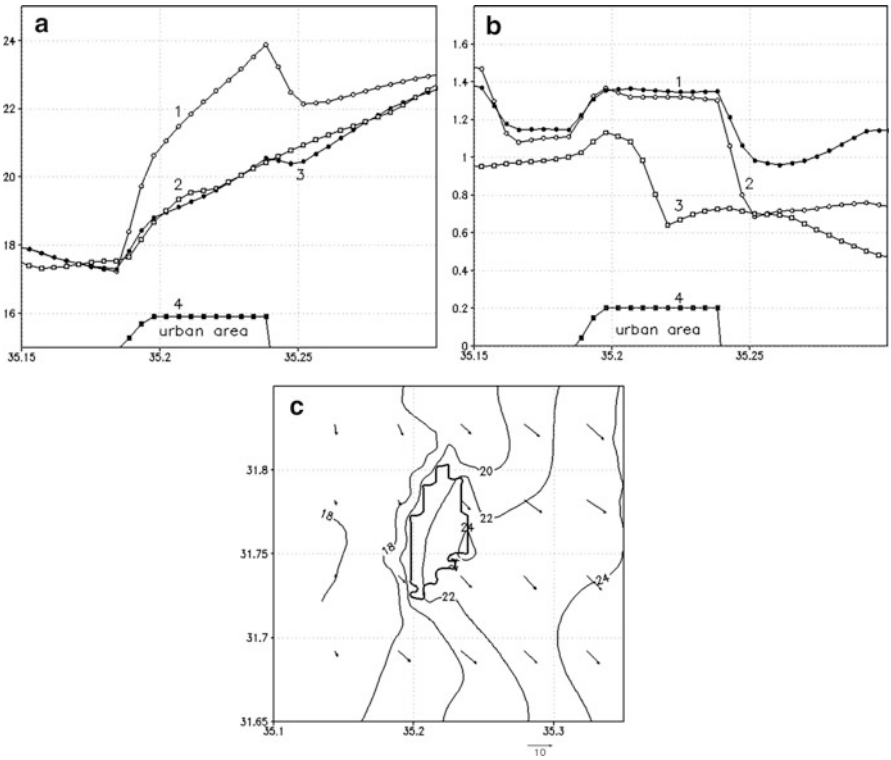

Fig. 118.7 Jerusalem urban area: the same curves as on Fig. 118.5

References

1. Kusaka H, Kondo H et al (2001) A simple single-layer urban canopy model for atmospheric models: comparison with multi-layer and slab models. Bound-Layer Meteorol 101:329–358
2. Ek MB, Mitchell KE, Lin Y et al (2003) Implementation of Noah land surface model advances in the NCEP operational mesoscale Eta model. J Geophys Res 108:8851
3. Lin C-Y, Chen F, Huang JC et al (2008) Urban heat island effect and its impact on boundary layer development and land-sea circulation over northern Taiwan. Atmos Environ 42:5635–5649
4. Skamarock WC, Klemp JB, Dudhia J et al (2005) A description of the advanced research WRF version 2. NCAR Technical Note. National Center for Atmospheric Research, Boulder, CONCAR/TN-468 + STR
5. Tevari M, Chen F, Kusaka H (2006) Implementation and evaluation of a single-layer urban model in WRF/Noah. In: Proceedings of the 7th WRF User's Workshop, June 2006, Boulder, Colorado
6. Tie X, Geng F, Peng L et al (2009) Measurement and modeling of O_3 variability in Shanghai, China: application of the WRF-Chem model. Atmos Environ 43:4289–4302

Chapter 119
Extension to Chemical Products of the CERES Platform Used to Evaluate the Atmospheric Dispersion and Human Health Consequences of Noxious Releases

Luc Patryl, Laurent Deguillaume, Nadine Chaumerliac, Frédéric Tridon, and Patrick Armand

Abstract The CERES platform developed by CEA to assess the atmospheric dispersion and the environmental impact has been coupled with the Model of Multiphase Cloud Chemistry (M2C2) developed by LaMP in order to take account of the chemical reactivity during dispersion. The method used consists to provide lookup tables of the concentration gradient issued by M2C2 to characterize the chemical reactivity in the atmosphere then correct each puff during atmospheric dispersion calculations. A case of NH_3 release is presented and shows that NH_3 concentration in the air is less important taking account of the chemical reactivity, NH_3 undergoing photolysis and oxidation by radicals. Several tests are ongoing to validate the method and improvements have to be done to reduce approximations.

Keywords NH3 • CERES-platform

119.1 Introduction

The CERES platform is an operational computational tool used by CEA to assess the atmospheric dispersion, the environmental impact and the human health consequences from radioactive and chemical accidental or chronic releases [4]. In order to take into account chemical reactivity in the atmosphere, interaction between the dispersion model and the Model of Multiphase Cloud Chemistry (M2C2) developed by the LaMP (Laboratoire de Météorologie Physique) has been performed. Among

L. Patryl (✉) • P. Armand
CEA, DAM, DIF, Arpajon, France
e-mail: luc.patryl@cea.fr

L. Deguillaume • N. Chaumerliac • F. Tridon
Laboratoire de Météorologie Physique, CNRS/Université Blaise Pascal,
24 av. des Landais, BP80026, 63171 Aubière Cedex, France

D.G. Steyn et al. (eds.), *Air Pollution Modeling and its Application XXII*,
NATO Science for Peace and Security Series C: Environmental Security,
DOI 10.1007/978-94-007-5577-2_119,

several possible methods, the one chosen must maintain a moderate computation time in order to provide results very quickly in case of crisis. The purpose of this paper is to present the method used to couple CERES and M2C2 and the results on an academic example of NH_3 release.

119.2 CERES Dispersion Module and M2C2 Description

CERES dispersion module is a physico-mathematical model using a Gaussian puffs model. It assumes that a continuously emitted plume or an instantaneous cloud of pollutant can be simulated by the release of a series of puffs which are carried in a time- and space-varying wind field. The algorithm is based upon Gaussian puff assumptions including a uniform wind. The puffs are assumed to have Gaussian concentration profiles in the vertical and horizontal planes. For a given meteorological conditions and for a puff with small initial dimensions compared to its dimensions at an observation instant, the instantaneous volumetric concentration of a gaseous or particulate species at the point of coordinates (x, y, z), at time t, is calculated by the following equation.

$$C\ (x, y, z, t) = \left(\frac{1}{\sqrt{2\pi}}\right)^3 \frac{Q \cdot D}{\sigma_x \sigma_y \sigma_z} \mathrm{ex}\left[\frac{(x - ut_i)^2}{2\sigma_x^2} - \frac{y^2}{2\sigma_y^2} - \frac{(z-h)^2}{2\sigma_z^2}\right]$$

Where $C\ (x, y, z, t)$ is the instantaneous concentration ($M{\cdot}L^{-3}$) at the point of coordinates x, y and z and at the instant t. $\sigma_x \sigma_y \sigma_z$ are the square root of horizontal, lateral and vertical standard deviations (L). Q is the release quantity (M). D represents the depletion factor to take account of the dry and wet deposition, and the chemical or radioactive decay (1). u is the wind velocity ($L{\cdot}T^{-1}$).

M2C2 (Model of Multiphase Cloud Chemistry) is the result of the coupling between a multiphase explicit chemistry model for gas and aqueous phase [2] and cloud microphysics module at two moments [1]. The chemistry module includes chemical mechanisms detailed especially for HO_x, NO_y, sulfur, methane and COV, chlorine and ammonia in the gas phase. It can also consider a variable photolysis which is calculated by the radiative transfer model TUV developed by Madronich and Flocke [3].

119.3 CERES and M2C2 Coupling

During atmospheric dispersion, each puff is followed in space and time. The quantities of the chemical species as the standard deviations are recorded for each puff and for each time step. The method consists in modifying the quantity of transported species according to chemistry reactivity with the following equation:

$$Q_{puf\ f_c} = \left(Q_{puf\ f} + \frac{dc}{dt} \times \frac{(2\pi)^{\frac{3}{2}} \sigma_{xy}^2 \sigma_z}{2} \Delta t \right)$$

$Q_{puf\ f_c}$ is the new quantity of chemical species ($M{\cdot}L^{-3}$) corrected by the M2C2 concentration gradient $\frac{dc}{dt}$ ($M{\cdot}L^{-3}{\cdot}T^{-1}$) during the internal time step Δt (T). $Q_{puf\ f}$ is the quantity of chemical species ($M{\cdot}L^{-3}$) in the puff before chemical correction.

$\frac{dc}{dt}$ given by M2C2 is computed either "online" at each step time of dispersion model or before dispersion calculations and placed in a "lookup" table. The second way has been chosen for its greater computing efficiency, as the coupling is expected to be used in crisis situations. Before atmospheric dispersion calculations, several simulations have to be performed with M2C2 according to the source term characteristics (species and released quantity). Lookup tables from M2C2 must contain concentrations of species in atmosphere and $\frac{dc}{dt}$ for most possible release concentrations. Once tables performed, according to the concentration at the center of the plume, and for a given time step, $\frac{dc}{dt}$ is chosen and apply to correct the puff quantity. This method involves three hypothesis: (1) each puff is independent from the other ones, (2) there is no chemical correction during the release, (3) inside the puff the reactivity follows the same Gaussian law that the "passive" dispersion. The third point has been checked by calculating, with M2C2, the reactivity at the puff center then by applying a normal law to rebuild the Gaussian puff. Results were successful compared with M2C2 calculations for each concentration inside the Gaussian puff. However some approximations are done when the reactivity of species is strong or when there is a release threshold that leads to several regimes of chemical reactivity.

M2C2 has been adapted to allow high concentrations releases of chemical species. Several tests show that releases must be done in a stable chemical environment and a spin-up of 1 day is necessary before the release.

119.4 Academic Case of Accidental Release of Ammoniac

Figure 119.1 shows the maximum concentration ($mg{\cdot}m^{-3}$) of NH_3 for an accidental release of 100 kg of NH_3 during 30 min. Meteorological situation is unstable with a wind of 3 $m{\cdot}s^{-1}$. Release occurs 36 h after the beginning of the M2C2 simulation in order to have a stable chemical environment which corresponds to a release at 12 h A.M. A "remote" (unpolluted) chemical background has been applied.

If the dispersion is not corrected by chemical reactivity (Fig. 119.1a), the maximum concentration of 0.1 $mg{\cdot}m^{-3}$ is observed beyond 5 km. When the chemical reactivity is taken account, atmospheric concentrations decrease. At 5 km, the maximum concentration is less than 0.1 $mg{\cdot}m^{-3}$. In this case, NH_3 undergoes photolysis and oxidation by the hydroxyl radical (OH) that are maximal at noon.

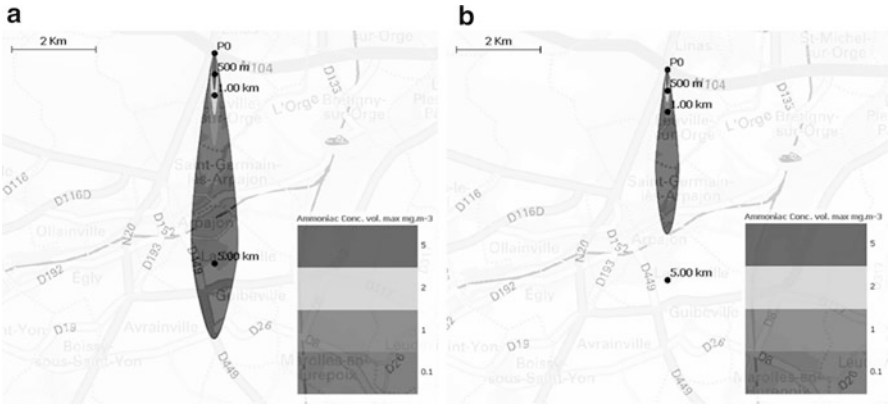

Fig. 119.1 Maximum concentration ($mg \cdot m^{-3}$) for a release of 100 kg of ammonia (**a**) without chemical reactivity, (**b**) with chemical reactivity

It is worth noticing that CERES-M2C2 is able to take into account the products of chemical reactivity that can lead to new species more dangerous for health human than the primary species released.

119.5 Conclusion

The coupling between a puff model dispersion code used by the CEA and the Model of Multiphase Cloud Chemistry (M2C2) developed by the LaMP has been done in order to assess with more accuracy the atmospheric dispersion and the consequences on human health in case of a toxic release. The coupling is based on "lookup table" provided by M2C2. The quantity of species in each puff is corrected according to initial puff concentration and time step. The used method involves computing upstream several academic lookup tables containing puff corrections. With this method, in case of crisis, the calculations are less time consuming even if the search of factors in lookup tables and corrections of each puff at each internal step time slow calculations. The first tests show that the behavior of chemical reactivity on dispersion could be important. Other tests are on-going to validate the method and improvements have to be done to reduce approximations and take into account the chemical reactivity during the release.

References

1. Chaumerliac N, Richard E, Rosset R (1990) Mesoscale modeling of acidity production in orographic clouds and rain. Atmos Environ 24A:1573–1584

2. Deguillaume L, Leriche M, Monod A, Monod A, Chaumerliac N (2004) The role of transition metal ions on HOx radicals in clouds: a numerical evaluation of its impact on multiphase chemistry. Atmos Chem Phys 4(1):95–110
3. Madronich S, Flocke S (1999) The role of solar radiation in atmospheric chemistry. In: Boule P (ed) Handbook of environmental chemistry. Springer, Heidelberg, pp 1–26
4. Monfort M, Patryl L, Armand P (2010) Presentation of the CERES platform used to evaluate the consequences of the emissions or radionuclides in the environment. In: International conference on Radioecology & Environmental Radioactivity – Environment & Nuclear Renaissance, ICRER 2011, Hamilton

Chapter 120
Large Eddy Simulation of Coherent Structures in Street Canyons

Vladimír Fuka and Josef Brechler

Abstract This work presents results of numerical simulation of turbulent flow in a fully developed flow in a series of street canyons. The motivation for this numerical study was an experiment by Kellnerová et al. (Detailed analysis of POD method applied on turbulent flow. In: EPJ web of conferences, vol 25. http://dx.doi.org/10.1051/epjconf/20122501038, 2012). The flow, as well as scalar fluxes, is investigated using proper orthogonal decomposition and spectral analysis. The flow is compared for two shapes of buildings.

Keywords LES • Streetcanyon

120.1 Introduction

The group of Kellnerová et al. [3] performed an experimental investigation of flow in a series of parallel idealized street canyons for two different shapes of buildings. We performed numerical simulation of this flow using our in-house model CLMM (Charles University Large-Eddy Microscale Model). It is a CFD model which employs large-eddy simulation for solution of the Navier–Stokes equations. First numerical results for this problem concerned mainly the velocity flow field (Fuka and Brechler [1]). In this contribution we want to concentrate more on the exchange of scalar quantities between the canyon and the free stream flow.

V. Fuka (✉) • J. Brechler
Department of Meteorology and Environment Protection, Faculty of Mathematics and Physics, Charles University in Prague, V Holešovičkách 2, 180 00 Prague 8, Czech Republic
e-mail: vladimir.fuka@gmail.com

D.G. Steyn et al. (eds.), *Air Pollution Modeling and its Application XXII*,
NATO Science for Peace and Security Series C: Environmental Security,
DOI 10.1007/978-94-007-5577-2_120,

120.2 Numerical Methods

Our simulation software is an LES code developed by the authors. It solves Navier–Stokes equations for incompressible flows and is aimed mainly at flows and pollution dispersion in the atmospheric boundary layer in complex geometry. It uses an orthogonal grid for spatial discretization to keep the code simple and computationally effective. Recently, most of the code was accelerated for graphical processing units using OpenHMPP [5]. Some portions of the code are yet to be accelerated and there is still big room for optimizations.

The time marching scheme is based on the fractional step method for incompressible Navier–Stokes equations. Because of the neutral stratification in the original experiment, no thermal effects were taken into consideration. For the spatial discretization of the (nonlinear) advection terms we use central difference scheme of the second order for momentum, because low numerical diffusion of the method is desirable. For the advection of pollutants this method is not appropriate, because it can lead to numerical instability and negative values can occur. Therefore we use a method with a flux limiter, that preserves positivity (prevents creation of negative values and oscillations) of the solution [2]. The subgrid terms are modeled using an eddy-viscosity model by Vreman [6].

120.3 Boundary Conditions

The layout of the numerical simulation follows closely the original experimental work. The height of buildings is 5 cm and the height and width of the channel is 25 cm. For more details cf. Kellnerová et al. [4]. We chose to preserve the model scale to allow a more direct comparison. We used grid resolution of 1.9 mm.

To achieve a fully developed flow we did not use such a long domain, as in the experiment, but we set up a periodic domain with ten street canyons and cyclic inflow and outflow. We also used the solid wall as an upper boundary condition, as in the experiment, but we also performed a control run with a higher placed free-slip boundary. The effect on the flow inside the canyons was very small, but it was substantial in the free stream.

The total flow through the canyon is governed by a constant horizontal pressure gradient. It is therefore not exactly equal to the measured one.

The reference experiment did not feature any contaminant dispersion. In our computation we tried to set up an idealized experiment to analyze the transport of pollutants. A positive non-dimensional contaminant flux of 1 m^{-2} s^{-1} was defined on the surface of the streets and a negative flux of 0.5 m^{-2} s^{-1} was defined on the top boundary, which has two times larger surface. This way the total amount of passive scalar in the domain remains constant.

120.4 Results

The flow was simulated from initial conditions of constant velocity in the whole domain for 16 s. The last 10 s were used to acquire the statistics.

The average scalar concentrations are in the Figs. 120.1 and 120.2. In the Figs. 120.3 and 120.4 are advective vertical scalar fluxes, i.e. $\phi_a =< w >< c >$, whereas in Figs. 120.5 and 120.6, the average turbulent scalar flux $\phi_t =< w'c' >$, is plotted. The extrema of local values of average turbulent scalar flux are much smaller than of the advective flux and reach the values of 30× to 50× of the value of the horizontally averaged total scalar flux.

In a similar way to the previous studies [1, 4] and to Kellnerová et al. [4] we used the proper orthogonal decomposition (POD) to analyze the main structures in the flow. In this study we applied POD directly to the temporal fields of $\phi = wc$. This way we can see the main types of events that lead to increased or decreased mass exchange within the canyon. The first mode corresponds to events in which there is the most of the upper part of the canyon with enhanced or decreased scalar flux, depending on the sign of the corresponding POD time coefficient. The second mode can be explained as an event with distinct sign of the turbulent part of the scalar flux on both sides of the canyon.

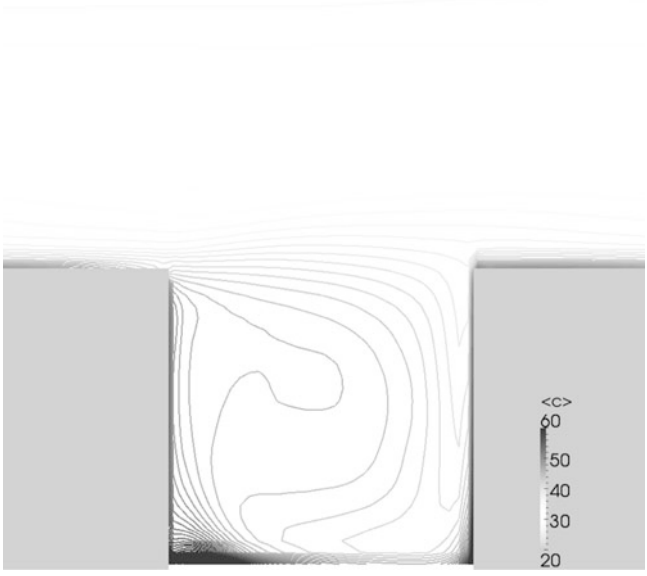

Fig. 120.1 The average concentrations for the flat roofs

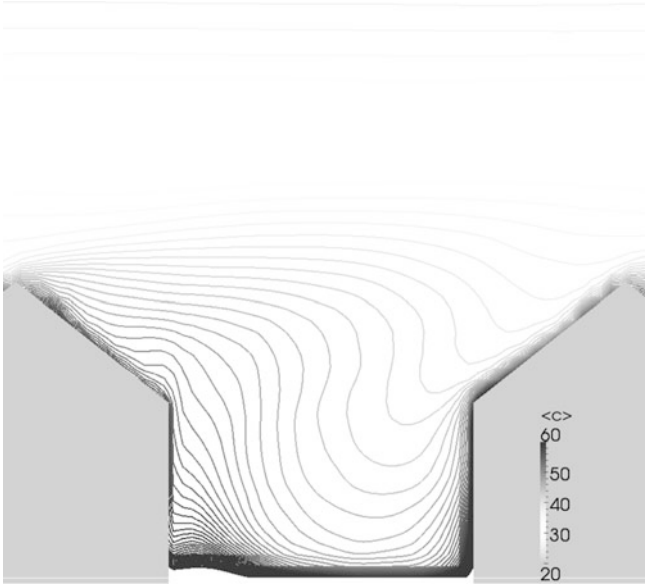

Fig. 120.2 The average concentrations for the pitched roofs

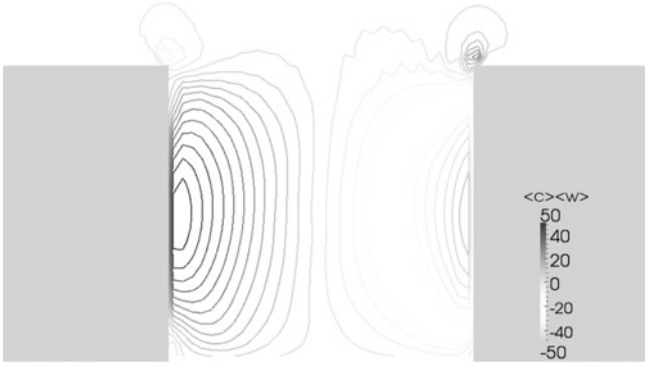

Fig. 120.3 The vertical advective scalar flux for the flat roofs

The results still suffer from a poor resolution, caused partially by the number of parallel canyons that need to be modeled. Otherwise the flow above the canyon would be too correlated due to the cyclic conditions.

There is still a lot to analyze. The important question is the time evolution of the POD modes and their cross correlation and the connection with the velocity POD modes.

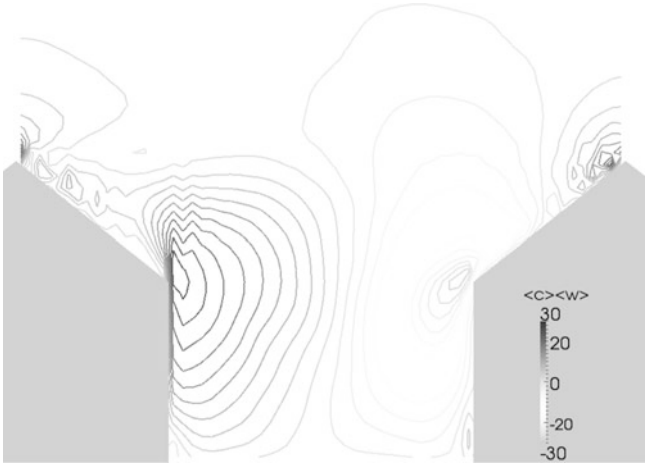

Fig. 120.4 The vertical advective scalar flux the pitched roofs

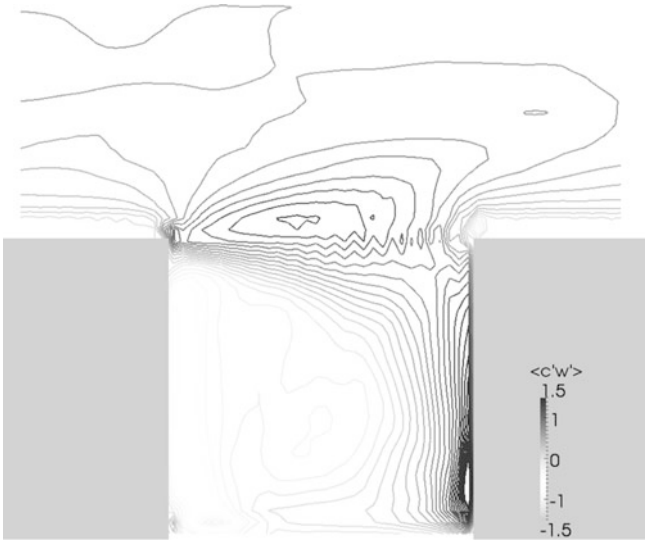

Fig. 120.5 The average vertical turbulent scalar flux for the flat roofs

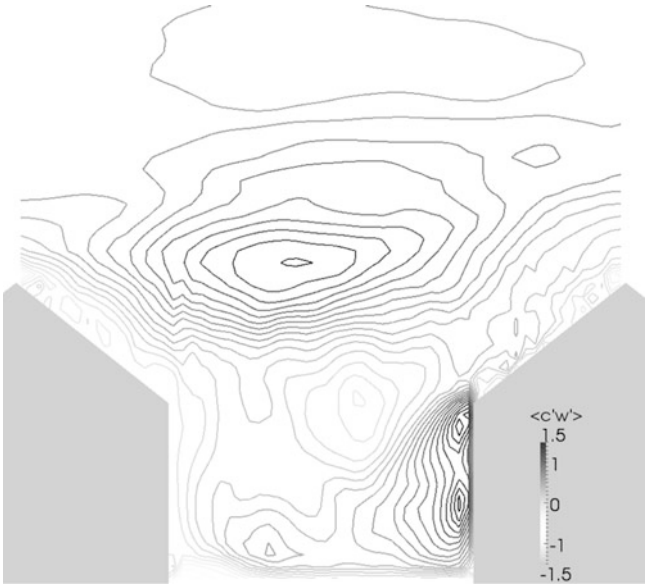

Fig. 120.6 The average vertical turbulent scalar flux the pitched roofs

120.5 Conclusions

We performed a numerical simulation of flow and scalar dispersion in a series of street canyons. The results were also analyzed using proper orthogonal decomposition. In this higher resolution simulation, there are no more any large differences in the average concentrations in canyons with different shapes.

Acknowledgments The work was supported by grant SVV-2010-261308 and by the Czech Ministry of Education, Youth and Sports under the framework of research plan MSM0021620860 and project UHI, No. 3CE292P3, funded by EU, European Regional Development Fund, under Operational Programme Central Europe.

References

1. Fuka V, Brechler J (2012) LES of flow in the street canyon. EPJ Web Conferences 25(01018). doi:10.1051/epjconf/20122501018
2. Hundsdorfer W, Koren B, van Loon M, Verwer JG (1997) A positive finite-difference advection scheme. J Comp Phys 117:35–46
3. Kellnerová R, Kukačka L, Uruba V, Antoš P, Odin J, Jaňour Z (2010) Wavelet and POD Analysis of Turbulent Flow Within Street Canyon. Experimental fluid mechanics 2010. Jičín (Czech Republic)

4. Kellnerová R, Kukačka L, Uruba V, Jurčáková K, Jaňour Z (2012) Detailed analysis of POD method applied on turbulent flow. EPJ web of conferences, vol 25. http://dx.doi.org/10.1051/epjconf/20122501038
5. OpenHMPP Consortium (2011) Concepts directives. http://www.openhmpp.org/
6. Vreman AV (2004) An eddy-viscosity subgrid-scale model for turbulent shear flow: algebraic theory and applications. Phys Fluid 16:3670–3681

Chapter 121
Integration of the Operational Urban Dispersion Model SIRANERISK in the CERES Platform Used to Evaluate Human Health Consequences of Noxious Atmospheric Releases

Luc Patryl, Patrick Armand, Lionel Soulhac, and Guillevic Lamaison

Abstract In order to account for health impact of radioactive, chemical or biological releases in the urban environment, the CERES platform used by CEA has been improved by the coupling with SIRANERIK which is a model dedicated to pollutant dispersion over urban areas in unsteady situations. In case of a crisis, CERES is able to calculate very quickly noxious species concentration and to evaluate health impact of the releases. Thanks to its graphical interface, cartographies are provided as support to decision process.

Keywords CERES-Platform • Urban dispersion model

121.1 Introduction

The CERES platform is an operational computational tool used by CEA to assess atmospheric dispersion, environmental impact and human health consequences of radioactive accidental or chronic releases [2]. In order to answer emergent issues such as accidental or malevolent releases of chemical products or even the dispersion of bioaerosols over urban area, improvements of the CERES platform have been recently carried out. In particular, the coupling between CERES and

L. Patryl (✉) • P. Armand
CEA, DAM, DIF, F-91297 Arpajon, France
e-mail: luc.patryl@cea.fr; patrick.armand@cea.fr

L. Soulhac • G. Lamaison
Laboratoire de Mécanique des Fluides et d'Acoustique, Université de Lyon CNRS, Ecole Centrale de Lyon, INSA Lyon, Université Claude Bernard Lyon I, 36 avenue Guy de Collongue, Ecully, France

D.G. Steyn et al. (eds.), *Air Pollution Modeling and its Application XXII*,
NATO Science for Peace and Security Series C: Environmental Security,
DOI 10.1007/978-94-007-5577-2_121,

the urban dispersion model (SIRANERISK) developed by Laboratory of Fluid Mechanics and Acoustics of Lyon jointly with CEA has been performed [1]. The new version of CERES takes into account urban atmospheric environment with quick response calculations requested by authorities to face crisis situation.

121.2 Main Features of CERES and SIRANERISK

In case of a crisis, the main objective of CERES is to provide, in a first step, atmospheric and dose assessments very quickly. In a second step, CERES allows to improve results by using more realistic and complex input data. A new graphical user interface coupled with geographic information system (GIS) has been developed. At each step of calculation definition, crisis or expert mode can be used. The crisis mode allows to calculate a case very quickly. For example, a very simple definition of the meteorological situation can be done in crisis mode. One direction and one velocity of the wind and the atmospheric stability are the only necessary data to run a case. In the expert mode, atmospheric evolution or three-dimensional fields can be provided. In crisis mode, impact points are set automatically in wind axis. In expert mode, impact points can be set everywhere graphically, manually with geographic coordinates or chosen in a database. Moreover, the three-dimensional implemented viewer provides cartographies as support to decision processes.

SIRANERISK has been coupled to CERES in order to predict the pollutant concentration in the streets of dense European cities. The model is dedicated to pollutant dispersion over urban areas in unsteady situations. It is constituted by the coupling of a Gaussian puff model in the atmosphere over the street level and a specific mass-consistent model that accounts for the dispersion of the pollutants within the urban canopy. The model takes into account the main geometric complexity of urban areas, neglecting the effects of small topological details (such as trees, details of the buildings, etc.). The urban topography is therefore modelled with a network of simple volumes (parallelepipeds) representing each street. Each of these parallelepipedic boxes contains a volume of contaminated air that can be exchanged with the next boxes (through the intersections of the street arrays), or with the atmosphere over the urban canopy. The air flux can therefore be computed in each street canyon, and consequently the mass budget of any pollutant. Therefore, using SIRANERISK requires the map of each urban area in a special form represented by a network of interconnected canyon-streets volumes defined by their length, width and height. It is worth noticing that the comparison of SIRANERISK with wind-tunnel experiments of an urban district and a Lagrangian model gives a good agreement for the mean arrival time of the cloud and the longitudinal spreading of the plume.

Fig. 121.1 Streets network of the town-center at Lyons (France), as represented in SIRANERIK

121.3 Example of a Point Release in Lyons, France

Figure 121.1 shows the schematic two-dimensional urban network of streets in the center of Lyons (France). The domain is about 4×4 km and contains 3,180 streets and 1,902 intersections nodes. At 10 h a.m., a transport accident is supposed to occur with a quick release of 100 kg of chlorine. The meteorological situation is considered as uniform. The wind direction is variable according to time and comes from the South-West (120–150°). The wind velocity is 3 m·s^{-1} and the stability class is B along Pasquill formalism (very unstable). Figure 121.2 shows the instantaneous concentration (μg·m^{-3}) of chlorine in the town-centre of Lyons. For 50 min of physical time simulated, the computation time is about 10 min. In this particular situation, it is worth noticing that chlorine concentration stays below the thresholds prescribed by the French Ecology Ministry.

121.4 Conclusion

The CERES code is now able to predict air concentration and health impact in urban environment by using SIRANERISK developed at Ecole Centrale de Lyon for the atmospheric dispersion. SIRANERISK model combines a Gaussian puff model and a specific mass-consistent model that accounts for the dispersion of the pollutants in

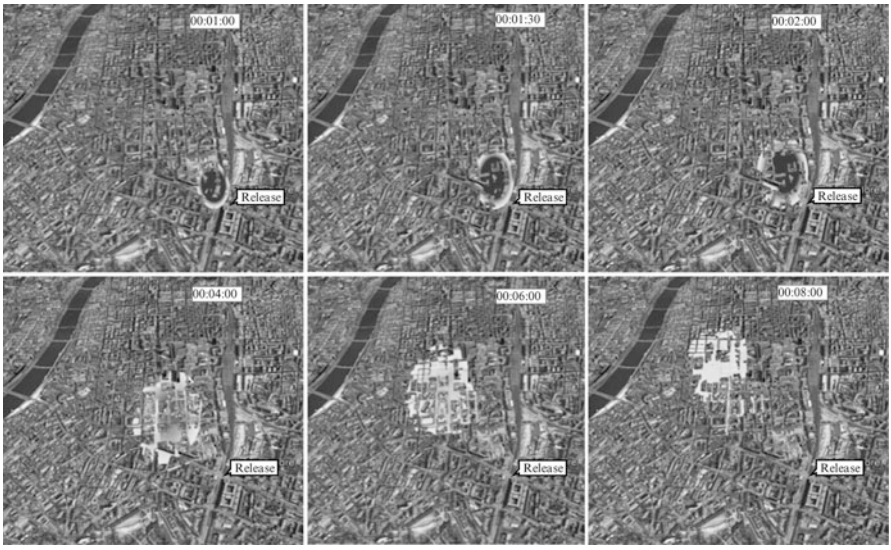

Fig. 121.2 Chlorine instantaneous concentration in the streets of Lyons in case of an accidental release

the urban canopy. Having in a database the description of various large towns, the use of CERES and SIRANERISK is consistent with crisis handling in an urban environment as the computation time for dispersion, is just a few minutes on a multicore laptop.

References

1. Lamaison G, Soulhac L, Armand P (2011) Presentation of SIRANERISK-2.0 – a decision-support oriented computational tool adapted to the dispersion of deleterious RBC agent in the urban atmospheric environment – examples of application. In: 14th international conference on harmonisation within atmospheric dispersion modelling for regulatory purposes. Kos Island, Greece, 2–6 October 2011
2. Monfort M, Patryl L, Armand P, Monfort M, Patryl L, Armand P (2011) Presentation of the CERES platform used to evaluate the consequences of the emissions of pollutants in the environment. Radioprotection 46:S653–S659. doi:10.1051/radiopro/20116668s

Chapter 122
Higher Resolution Modeling of the PM10 Levels Over Istanbul for a Winter Episode

Ulas Im, Kostandinos Markakis, Alper Unal, Tayfun Kindap, Anastasia Poupkou, Selahattin Incecik, Orhan Yenigun, Dimitros Melas, Christina Theodosi, and Nikos Mihalopoulos

Abstract High winter-time PM_{10}, sulfate, nitrate and ammonium levels in Istanbul were investigated using a high resolution WRF/CMAQ mesoscale model system. The results suggested that the system was capable of producing the magnitudes. PM_{10} levels calculated by the model underestimated the observations with an average of 10 % at Bogazici University sampling station, whereas an overestimation of 12 % is calculated for all stations. Base case results together with the sensitivity studies pointed significant contribution of local sources.

Keywords Air quality modeling • Aerosol • Chemical composition • Istanbul • WRF • CMAQ

U. Im • C. Theodosi • N. Mihalopoulos
Environmental Chemical Processes Laboratory, Department of Chemistry, University of Crete, 71003 Heraklion, Greece

K. Markakis • A. Poupkou • D. Melas
Laboratory of Atmospheric Physics, Department of Physics, Aristotle University of Thessaloniki, 54124 Thessaloniki, Greece

A. Unal • T. Kindap
Eurasia Institute of Earth Sciences, Istanbul Technical University, İstanbul, Turkey

S. Incecik (✉)
Department of Meteorology, Istanbul Technical University, İstanbul, Turkey
e-mail: incecik@itu.edu.tr

O. Yenigun
Institute of Environmental Sciences, Bogazici University, 34342 İstanbul, Turkey

D.G. Steyn et al. (eds.), *Air Pollution Modeling and its Application XXII*,
NATO Science for Peace and Security Series C: Environmental Security,
DOI 10.1007/978-94-007-5577-2_122,

122.1 Introduction

Istanbul, a megacity with population well over 12 million, experiences high levels of particulate air pollution. These high particle levels have been investigated through statistical analyses of measurements in a number of studies while sophisticated air quality modeling systems have not been employed sufficiently to investigate these levels. The present study investigates the PM_{10} levels during a wintertime episode in Istanbul and the contributions of the anthropogenic emissions on these levels. Besides the PM_{10} mass concentrations; sulfate, nitrate and ammonium aerosols have also been investigated.

122.2 Materials and Methods

To evaluate the chemical composition of aerosols and identify their sources in Istanbul, PM_{10} samples have been collected at ESC (41.09 N and 29.05 E) for a period between November 2007 and June 2009, where several episodes were identified over the year of 2008 [3]. A 5-day winter episode of high PM_{10} levels, between 13th and 17th of January, 2008, was investigated in this present study where daily PM_{10} levels at the ESC station were above the EU limit value of 50 $\mu g\ m^{-3}$, reaching to 129 $\mu g\ m^{-3}$. Additionally, source apportionment results from Kocak et al. [2] showed that anthropogenic sources accounted for about 90 % of the observed PM_{10}, making the episode suitable for testing the new anthropogenic emission inventory.

The non-hydrostatic, mesoscale Advanced Research Weather Research and Forecasting (WRF-ARW) model, version 3.1 is used as the meteorological model offline-coupled with the US EPA Community Multiscale Air Quality (CMAQ) model, version 4.7 chemistry and transport model (see [1] for details). Three domains have been set up for the modeling system: a mother domain covering Europe on 30 km spatial resolution, the second domain covering the Balkan region on 10 km resolution, and finally, the inner most domain covering the Greater Istanbul Area (GIA) on 2 km resolution. Thirty-seven sigma layers have been used for the vertical resolution of the model.

122.3 Results and Discussions

The highest PM_{10} concentrations were calculated on the coastline surrounding the Bosporus Strait, where most of the population is located (Fig. 122.1a). The temporal variations of model-calculated daily mean PM_{10} concentrations and the individual aerosol species well-agreed with the observations for the ESC station. Correlation factors of 0.83, 0.96, 0.95 and 0.88 for PM10, sulfate, nitrate and ammonium are

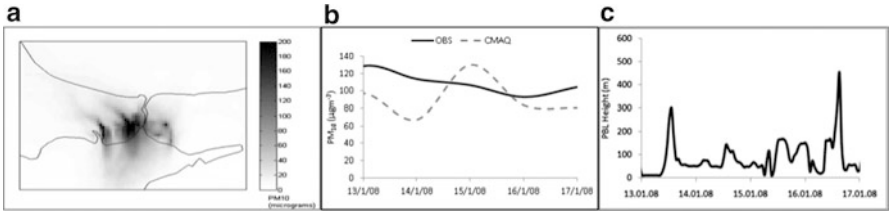

Fig. 122.1 (**a**) Comparison of predicted and observed PM_{10} levels, (**b**) predicted PBL heights and (**c**) spatial distribution of PM_{10} levels in GIA

Table 122.1 Comparison of predicted and observed aerosol levels in GIA

Measures	PM_{10}	SO_4^{2-}	NO_3^-	NH_4^+
Observed mean ($\mu g\ m^{-3}$)	107.1	9.8	6.8	4.1
Model mean/Obs. mean	0.9	0.8	0.3	0.7
Observed STDEV ($\mu g\ m^{-3}$)	15.14	1.08	1.22	1.16
Model STDEV/Obs. STDEV	1.3	1.1	0.5	0.9
BIAS ($\mu g\ m^{-3}$)	−8.9	−2.1	−4.6	−1.28
ABSE ($\mu g\ m^{-3}$)	20.7	2.7	4.6	1.28
RMSE ($\mu g\ m^{-3}$)	24.5	2.9	4.5	1.44
IOA	0.9	0.8	0.5	0.8

calculated, respectively (Table 122.1). PM_{10} concentrations were underestimated on average by 10 % (Fig. 122.1b), whereas sulfate by 23 %, nitrate by 75 % and ammonium by 33 %. The WRF model calculated low PBL heights (Fig. 122.1c), very high cloud fractions (almost equal to 1) and no precipitation throughout the simulation period, which led to excessive amounts of sulfate in-cloud production. This is confirmed by the Integrated Process Rate Analysis (IPR) tool of CMAQ model. IPR results showed that significant amount of sulfate aerosols was produced through emissions and cloud processes, whereas gas-phase production was very limited, which led to very small amount of SOA production.

The underestimated sulfate concentrations can be attributed to the underestimation of coarse mode sulfate that is not associated with ammonium but may be associated with Ca, Mg or Na from soil dust or resuspended dust, which are lacking in our emission inputs (Fig. 122.2). The model calculated 75 % lower nitrate concentrations than the observations, where almost 94 % of the nitrate was in fine mode. This low amount of coarse mode nitrate can be attributed to the emission inputs.

The sensitivity simulations showed that the most significant changes in PM_{10} concentrations at the ESC station were in response to the changes done simultaneously in all emissions. The highest increase of daily PM_{10} concentrations during the episode occurred due to the 10 % increase and decrease in all emissions (± 8.90 %), which was also the case for the inorganic aerosol concentrations.

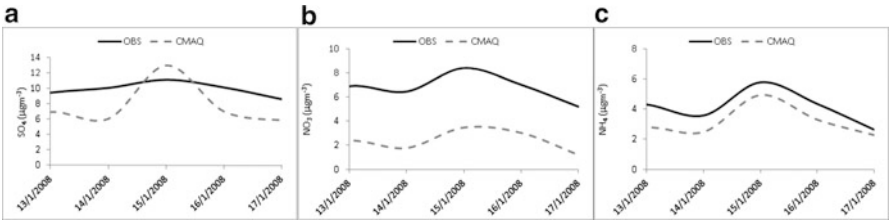

Fig. 122.2 Comparison of predicted and observed (**a**) sulfate, (**b**) nitrate and (**c**) ammonium aerosol levels in GIA

122.4 Conclusions

An offline-coupled WRF/CMAQ high resolution modeling system has been used in order to analyze the observed exceedences in PM_{10}, in conjunction with the aerosol chemical characterization, sulfate, nitrate and ammonium concentrations during a 5-day winter episode of 13–17 January 2008. Istanbul and surrounding areas were used in the innermost domain of the model on 2 km resolution.

The model produced PM_{10} concentrations were comparable with the observations in terms of magnitude. The results point that the emission estimates from traffic and residential coal combustion might be overestimated due to the fact that the overestimations of PM_{10} and sulfate aerosols occurred at regions where these sources are dominant. The Brute force sensitivity simulations showed the highest increase in PM_{10} concentrations occurs in the city center around the coastal area where most of the population is located. PM_{10} concentrations respond most to the simultaneous changes in all emissions. The results show that PM episodes in GIA are largely local-originated, as changes in the primary particulate emissions led to significant responses of the aerosol levels compared to responses to the individual emission changes of the precursors. As a conclusion, the study shows the necessity to develop emission controls strategies that target directly to the primary particulate emissions in the region, more than the gaseous precursor emissions that contribute to the SOA levels.

Acknowledgements The authors would like to acknowledge the financial support by the Scientific and Technological Research Council of Turkey (TUBITAK, COST project no: 105Y005), and the EU funded CITYZEN project for making the aerosol samplings and the analysis possible.

References

1. Im U, Markakis K, Unal A, Kindap T, Poupkou A, Incecik S, Yenigun O, Melas D, Theodosi C, Mihalopoulos N (2010) Study of a winter PM episode in Istanbul using high resolution WRF/CMAQ modeling system. Atmos Environ 44:3085–3094

2. Kocak M, Theodosi C, Zarmpas P, Im U, Bougiatioti A, Yenigun O, Mihalapoulos N (2011) Particulate matter (PM_{10}) in Istanbul: origin, source areas and potential impact on surrounding regions. Atmos Environ 45:6891–6900
3. Theodosi C, Im U, Bougiatioti A, Zarmpas P, Yenigun O, Mihalopoulos N (2010) Aerosol chemical composition over Istanbul. Sci Total Environ 408:2482–2491

Chapter 123
3D Radiative and Convective Modeling of Urban Environment: An Example for the City Center of Toulouse

Yongfeng Qu, Maya Milliez, Luc Musson-Genon, and Bertrand Carissimo

Abstract A three dimensional tool coupling the thermal energy balance of buildings and the modeling of the atmospheric flow in urban areas has been developed. In this work the effects of complexity in real urban geometry on the interaction between airflows and radiation exchanges with different surfaces is tested. The model results are encouraging and give insight into local surface-atmosphere processes, but further and more rigorous testing has to be performed with other datasets.

Keywords Urban energy models • 3D radiative transfer • CFD

123.1 Introduction

Many micrometeorological studies of flow and pollution dispersion assume a neutral atmosphere and most building energy balance models neglect the three-dimensional local variation of the flow and temperature fields. We have developed a three-dimensional (3D) tool coupling thermal energy balance of the buildings and modeling of the atmospheric flow in urban areas. This 3D microscale atmospheric radiative scheme is implemented in the atmospheric module of the 3D open-source Computational Fluid Dynamics (CFD) code *Code_Saturne* adapted to complex geometry. Milliez [3] first evaluated the model with idealized cases, using a constant 3D wind field. Then, Qu et al. [7] have validated the full radiative-convective coupling by comparison with several surface wall temperatures from Mock Urban Setting Test (MUST) field campaign [4, 5]. Furthermore, in order to assess the

Y. Qu (✉) • M. Milliez • L. Musson-Genon • B. Carissimo
CEREA, Teaching and Research Centre in Atmospheric Environment, Joint Laboratory ENPC/EDF R&D, Marne la Vallée/Chatou, France
e-mail: yongfeng.qu@cerea.enpc.fr

D.G. Steyn et al. (eds.), *Air Pollution Modeling and its Application XXII*,
NATO Science for Peace and Security Series C: Environmental Security,
DOI 10.1007/978-94-007-5577-2_123,

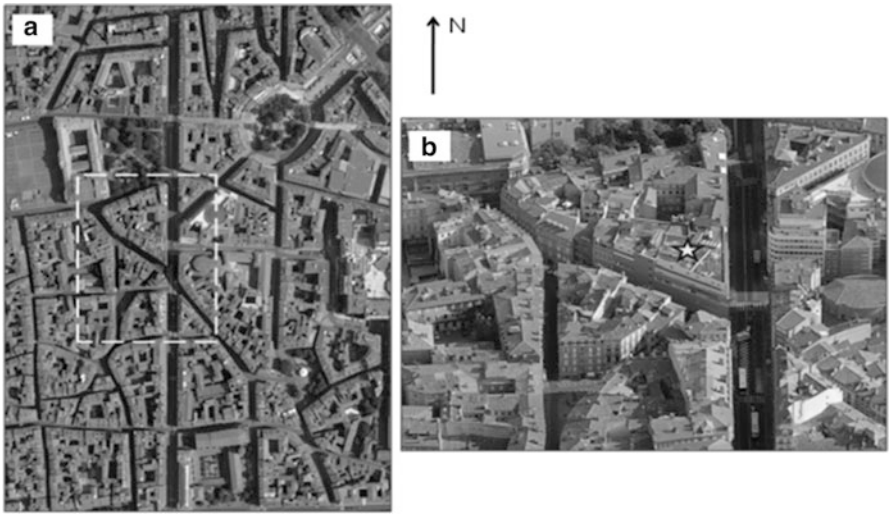

Fig. 123.1 Aerial view of downtown Toulouse, France: (**a**) main study area, from GoogleMaps; (**b**) zoom in the selected area (in a *dashed* contour), from Bing Maps. The north is indicated

thermal impact on the flow fields in different thermal conditions, we extend the work of Qu et al. [7] to lower wind speed and a higher building density than in MUST [8].

In this work, we aim to test the effects of complexity in real urban geometry on the interaction between the airflows and the radiation exchanges with different surfaces. In order to evaluate our model with a large available experimental dataset in a real urban environment, we choose the Canopy and Aerosol Particle Interactions in TOulouse Urban Layer (CAPITOUL) experimental dataset [2]. The campaign is a joint experimental effort in urban climate which took place in the city of Toulouse in southwest of France from 2004 to 2005 [2]. Study of the energetic exchanges between the surface and the atmosphere was one of the objectives. The study area is mainly located in the city center around the corner of the two streets; Alsace-Lorraine and Pomme (yellow contour in Fig. 123.1a, b). In this neighborhood, vegetation is scarce and buildings are around 20 m height [6].

123.2 Model Description

Taking into account the larger scale meteorological conditions and the thermal stratification, the atmospheric module of *Code_Saturne* [1], described in Milliez and Carissimo [4, 5], uses a detailed representation of the surfaces allowing a complex 3D spatial representation of wind speed, turbulence, and temperature. A standard k-ε formulation is used in this work.

Described in detail by Milliez [3], our radiative model takes into account both short- and long-wave radiation. A hybrid method is used in this work to determine the surface temperature [9].

123.3 Results

From the experiment, we selected the day of July 15th 2004. Considering Alsace-Lorraine and Pomme roads as the center of interest in the computational domain (Fig. 123.1), the dimension of the 3D simulation domain is $891 \times 963 \times 200$ m. After a series of geometric optimization with the urban database, described in Qu [9], the volumetric mesh used here is an unstructured grid of about 1.8 M tetrahedral cells (Fig. 123.2).

The base of the meteorological mast was on a roof at 20 m, with the top of the mast at 47.5 m above the road (yellow star in Fig. 123.1b). It provided data including heat fluxes, air temperature, wind speed and direction etc. In our simulations, the wind inlet boundary conditions are determined from measurements. In order to compare the data and fluxes, we set two monitoring points in the computational domain. One is at the same location as the actual sensors on the top of the mast (47.5 m). Another is set on the roof surface where the mast is placed (20 m). As an example, Fig. 123.3 compares the modeled upward global solar flux with the measured one. Compared to the observation, in spite of about 20 W m^{-2} higher values at noon estimated by the model (full line), the agreement between measurement and modeled the outgoing solar flux on mast (dashed line) is very satisfactory.

Several infrared radiometers were set to observe permanently the surface radiation temperatures of the walls and pavement of the three surrounding

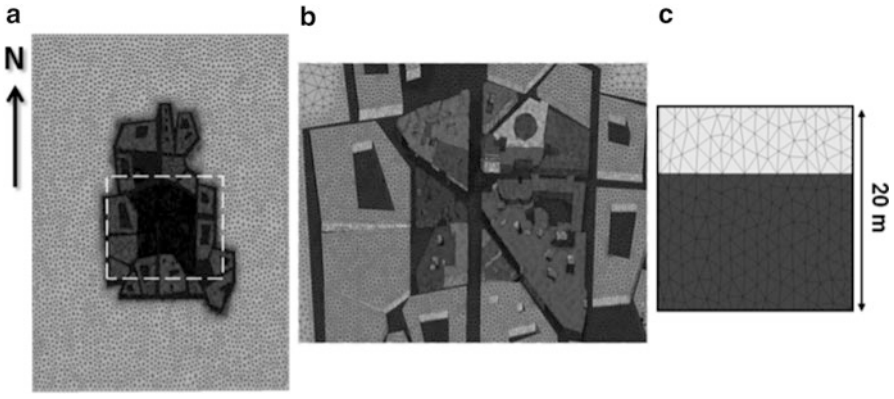

Fig. 123.2 Tetrahedral mesh on the central area: (**a**) whole area; (**b**) zoom in the selected area (**a**) (*dashed* contour); (**c**) zoom in a center building wall. The north is indicated

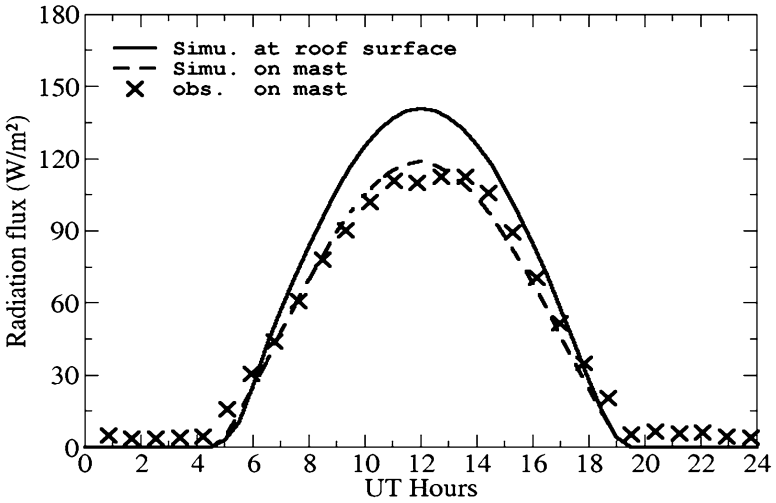

Fig. 123.3 Diurnal variation of outgoing solar flux calculated at roof surface (*full line*), at the mast level (*dashed line*) and measured on the mast (*cross symbol*)

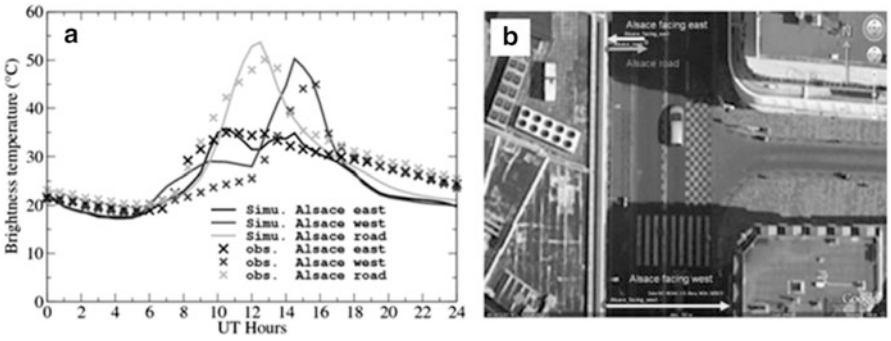

Fig. 123.4 (**a**) Evolution of brightness surface temperature of different positions of the infrared thermometers during a diurnal cycle (*cross symbol*: measurements; *full line*: simulation); (**b**) positions of the infrared thermometers. The north is indicated

streets. Figure 123.4a present the model-observation comparison for the brightness temperature for the faces of the Alsace Street of the diurnal cycle of July 15, 2004. The fixed positions of the infrared radiometers are shown in Fig. 123.4b. Overall, the diurnal evolutions of the brightness surface temperatures at the local positions in the scene are correctly simulated. The bias on the Alsace road (green line in Fig. 123.4a) can be explained by the approximation of the modeled shadow. Indeed, values taken from the selected cell might be quite different from its neighborhood values.

123.4 Conclusions and Perspectives

We have investigated the energy exchanges in a real city with the atmosphere during the CAPITOUL campaign, using new atmospheric radiative and thermal schemes implemented in *Code_Saturne*. A pre-processing is realized including the optimization of the complex geometry and creation of a high quality tetrahedral mesh for this study. It also requires determining the complex thermal parameters which take into account the actual variability of materials in the district. During the same day, the full radiative-dynamics coupling is tested against in situ observation including brightness temperature and heat flux etc. The model results are encouraging and give insight into local surface-atmosphere processes, but further and more rigorous testing has to be performed with other datasets.

References

1. Archambeau F, Mechitoua N, Sakiz M (2003) *Code_Saturne*: a finite volume code for the computation of turbulent incompressible flows-industrial applications. Int J Finite 1:1–62
2. Masson V et al (2008) The Canopy and Aerosol Particles Interactions in TOulouse Urban Layer (CAPITOUL) experiment. Meteorol Atmos Phys 102(3–4):135–157
3. Milliez M (2006) Modélisation micro-météorologique en milieu urbain: dispersion des polluants et prise en compte des effets radiatifs. PhD thesis, Ecole des Ponts ParisTech, 228 pp
4. Milliez M, Carissimo B (2007) Numerical simulations of pollutant dispersion in an idealized urban area, for different meteorological conditions. Bound-Layer Meteorol 122(2):321–342
5. Milliez M, Carissimo B (2008) CFD modelling of concentration fluctuations in an idealized urban area, for different meteorological conditions. Bound-Layer Meteorol 127(2):241–259
6. Pigeon G, Moscicki MA, Voogt JA, Masson V (2008) Simulation of fall and winter surface energy balance over a dense urban area using the TEB scheme. Meteorol Atmos Phys 102(3–4): 159–171
7. Qu Y, Milliez M, Musson-Genon L, Carissimo B (2011) Micrometeorological modeling of radiative and convective effects with a building-resolving code. J Appl Meteorol Climatol 50(8):1713–1724
8. Qu Y, Milliez M, Musson-Genon L, Carissimo B (2012) Numerical study of the thermal effects of buildings on low-speed airflow taking into account 3D atmospheric radiation in urban canopy. J Wind Eng Ind Aerodyn 104–106:474–483
9. Qu Y (2011) Three-dimensional modeling of radiative and convective exchanges in the urban atmosphere. PhD thesis, Ecole des Ponts ParisTech/Université Paris-Est, 168 pp

Chapter 124
Effect of Atmospheric Stability on the Atmospheric Dispersion Conditions Over a Industrial Site Surrounded by Forests

Hanane Zaïdi, Eric Dupont, Maya Milliez, Bertrand Carissimo, and Luc Musson-Genon

Abstract This work investigates the impact of terrain heterogeneity and stability conditions (stable and unstable) on the local turbulence kinetic energy (TKE) around an industrial site using 36 months of data collected at the experimental site SIRTA (Instrumental Site of Atmospheric Research by Remote Sensin). These measurements show that the normalized TKE (TKE/U^2: where U is the wind speed) is highly depended on the upstream complexity of the terrain (presence of forested areas or buildings) whatever the stability conditions (stable, unstable). The highest values of normalized TKE are obtained for unstable thermal stratification for all wind direction sector in the zones located behind the forested areas.

Keywords TKE • CFD • Stability

124.1 Introduction

The atmospheric dispersion of pollutants varies with meteorological conditions and heterogeneities of the terrain. For typical environmental impact studies, we are interested in long term simulations of the atmospheric flow and pollutants dispersion on various industrial sites. In previous studies [2–5], the comparison between numerical results obtained using the CFD code Code_Saturne and measurements obtained over 36 months at the SIRTA site have been presented for neutral condition stability. The results of this comparison show a good agreements between numerical results and measurements.

H. Zaïdi (✉) • E. Dupont • M. Milliez • B. Carissimo • L. Musson-Genon
CEREA, Teaching and Research Centre in Atmospheric Environment, Joint laboratory ENPC-EDF R&D, Marne la Vallee/Chatou, France
e-mail: hanane.externe-zaidi@edf.fr

D.G. Steyn et al. (eds.), *Air Pollution Modeling and its Application XXII*,
NATO Science for Peace and Security Series C: Environmental Security,
DOI 10.1007/978-94-007-5577-2_124,

Fig. 124.1 SIRTA satellite view showing the instrumented zones (Z1, Z4)

In this work, we present the experimental results obtained under stable and unstable stratification over 36 months for all wind direction. The objective is to study the effect of thermal stability and terrain heterogeneities on the wind and TKE.

124.2 Study Site and Instrumentation

The SIRTA (Instrumental Site of Atmospheric Research by Remote Sensing) is an national observational site dedicated to cloud, aerosol and boundary layer research. SIRTA is located in a suburban environment on the campus of the Ecole Polythecnique in Palaiseau, 20 km south of Paris [1]. This site benefits from an important and permanent instrumental set-up including radars, sodars, and masts equipped with sonic anemometers. Two instrumented zones are used in this work (zone 1 and 4, indicated in Fig. 124.1), both located near built-up and forested areas, depending on the wind direction.

124.3 Experimental Results

The experimental data collected at the SIRTA site for 36 months (January 2007–December 2009) are classified according to conditions of thermal stability by calculating the LMO and difference in temperature T between the altitudes 10 and

30 m at the zone4. Then the cases corresponding to every stability classes (stable and unstable) are selected.

For each stability condition, the data used are classified by direction sector of 10°. For each sector, the average ratio of normalized TKE (TKE/U^2: where U is the wind speed) at 10 m in zone 1 and at 10 and 30 m in zone 4 is calculated. The wind direction used for this classification is the direction measured by the sonic anemometer at 30 m in zone4, as it can be considered as weakly affected by the trees. Figure 124.2 shows the normalized TKE obtained for stable and unstable thermal stratification as a function of the wind direction.

The measurements obtained for stable and unstable thermal stratification, for 36 months, show that in zone 1 the production of turbulence is dominated by the dynamical effect of the northern canopy, corresponding to wind direction ranging from 330° to 70°. The lowest values of normalized TKE are founded for wind directions ranging from 90° to 150° and from 220° to 310°, which correspond to open terrain. In zone 4, the highest values of normalized TKE are associated with eastern canopy.

We observe that the normalized TKE obtained in unstable stratification are significantly higher than those obtained in stable stratification for all wind directions in zone 4 at 10 and 30 m. For zone1 at 10 m, the small differences between stable and unstable cases indicates that the TKE is mainly produced by dynamical effects. The largest differences between stable and unstable stratification are observed in zone 4 at 10 m and at 30 m for the wind sectors ranging from 10° to 210°.

124.4 Conclusion

In this study, we present an analysis of stability effects an the inhomogeneous field of TKE around an industrial site surrounded by forest. On the SIRTA site, two instrumented zones provided a 36 months dataset which allowed a comparison of the normalized TKE obtained in the cases of stable and unstable stratification over a long period. These results show that the terrain complexity and thermal stratification (stability condition) has an important impact on the normalized TKE. Hence, in our case, the TKE strongly depends on the rough elements upwind of the measurements mast (close forest, buildings, forest) and on the condition of stability (stable and unstable). Future works will be focused on the long term simulation using a clustering method in order to obtain representative distributions of wind, turbulence and atmospheric dispersion coefficient. The boundary conditions will be obtained from a database of mesoscale model spanning severals years.

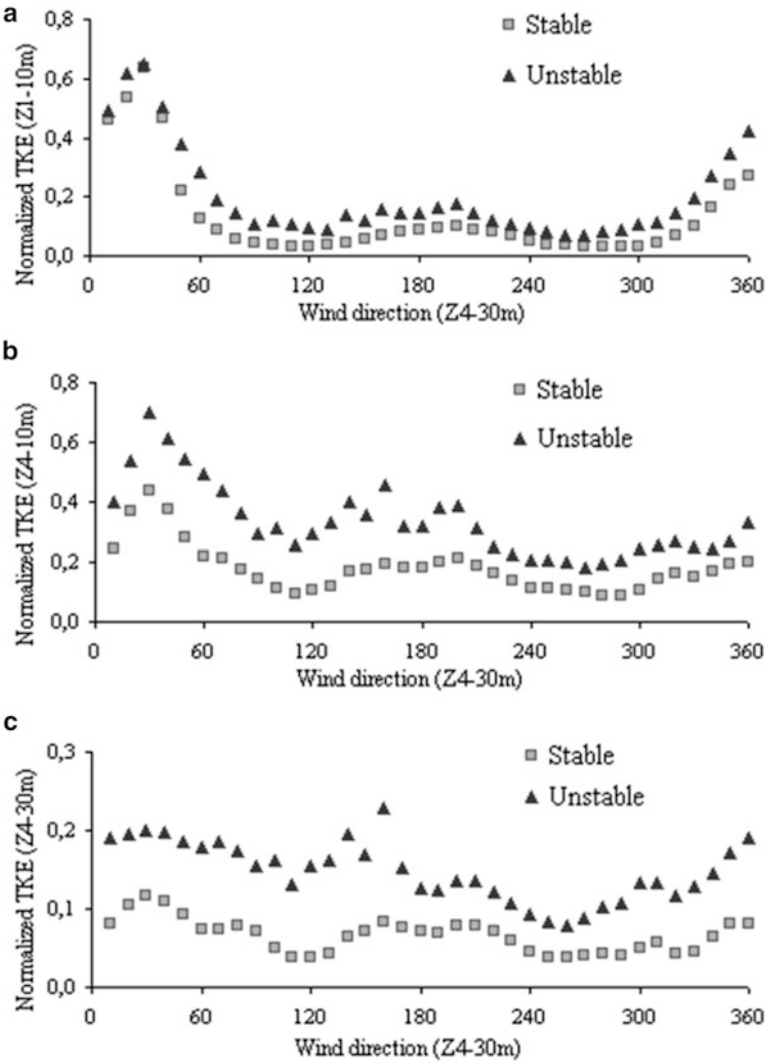

Fig. 124.2 Comparison of the normalized TKE for stable and unstable regimes as a function of wind direction, for zone1 at 10 m (**a**), and zone 4 at 10 m (**b**) and 30 m (**c**)

References

1. Haeffelin M, Barthès L, Bock O, Boitel C, Bony S, Bouniol D, Chepfer H, Chiriaco M, Delanoë J, Drobinski P, Dufresne J, Flamant C, Grall M, Hodzic A, Hourdin F, La- pouge F, Lemaître Y, Mathieu A, Morille Y, Naud C, Noël V, Pelon J, Pietras C, Protat A, Romand B, Scialom G, Vautard R (2005) SIRTA, a ground-based atmospheric observatory for cloud and aerosol research. Ann Geophys 23:253–275

2. Zaïdi H, Dupont E, Milliez M, Carissimo B, Musson-Genon L (2010) Realistic simulation of spatial heterogeneities of wind and turbulence at microscale with an atmospheric CFD code. In: The fifth international symposium on computational wind engineering, 23–27 May, Chapel Hill
3. Zaïdi H, Zhang X, Dupont E, Milliez M, Carissimo B, Musson-Genon L (2010) Comparison between a building resolving micro-meteorological model and measurements at SIRTA. In: International technical meeting on air pollution modelling and its application, 27 Sept – 01 Oct, Torino
4. Zaïdi H, Dupont E, Milliez M, Carissimo B, Musson-Genon L (2011) Numerical simulation of the atmospheric flow over a complex terrain at local scale using Code_Saturne: a comparison of two forest canopy models. In: International conferences on harmonisation within atmospheric dispersion modelling, 3–6 October 2011, Kos Island, Greece
5. Zaïdi H, Dupont E, Milliez M, Carissimo B, Musson-Genon L (2011) Evaluating the two canopy models to reproduce the forested area effects using Code_Saturne. In: 13th international conference on wind engineering, 10–15 July 2011, Amsterdam

Chapter 125
On the Parameterization of Dynamic and Diffusion Processes in the PBL Over Very Rough Surface

Evgeni Syrakov and Kostadin Ganev

Abstract Tree basic parameterization schemes: bulk Richardson number method (Rb-method), PBL resistance laws (RL-method) and combined (Rb-RL)-method are modified and applied to areas with large roughness (urban canopy, forest, buildings, etc.), accounting for a wide range of turbulent PBL urban regimes.

Keywords Diffusion • Process analysis

125.1 Introduction

Let some parameterization schemes at relatively homogeneous (rural) surface be considered at the beginning:

- In this traditional case the bulk Richardson number $Rb = \beta\Delta\theta z_1/{u_1}^2$ (see [11]) is used, where $\Delta\theta = \theta_1 - \theta_0$, $u_1 = u(z = z_1)$, z_1-reference height (a low level in numerical models, or $z_1 = 10$ m, etc.), θ, u – potential temperature and velocity, described in the Monin-Obukhov theory framework. A practically oriented Rb-method when effects, connected with free-flow stability [8], as well as very stable stratification and intermittent turbulence-regime without critical Richardson number (WCR) [9] are considered, was developed in [5–7], which embraces unstable, as well as a wide range of neutral/stable regimes: TN (truly neutral), NS (nocturnal stable), CN (conventional neutral), LS (long-lived stable)

E. Syrakov (✉)
Department of Meteorology and Geophysics, Faculty of Physics, University of Sofia,
J. Baucher str. 5, Sofia 1126, Bulgaria
e-mail: esyrakov@phys.uni-sofia.bg

K. Ganev
National Institute of Geophysics, Geodesy and Geography, Bulgarian Academy of Sciences,
Acad. G. Bonchev Str., Bl.3, Sofia 1113, Bulgaria

D.G. Steyn et al. (eds.), *Air Pollution Modeling and its Application XXII*,
NATO Science for Peace and Security Series C: Environmental Security,
DOI 10.1007/978-94-007-5577-2_125,

and WCR. The dependence of surface fluxes and other parameters for the above listed regimes on the input parameters:

$$Rb, \lambda_u, \lambda_\theta, F_{i0}, \tag{125.1}$$

Is determined in [5, 6], where $\lambda_u = \ln(z_1/z_0)$, $\lambda_\theta = \ln(z_1/z_{0T})$, z_0 and z_{0T} are the aerodynamic and temperature roughness lengths, $F_{i0} = Nz_1/u_1$, N-free-flow Brunt-Väisälla frequency.

- The generalized version of the RL-methods makes it possible the dependence of transfer-interaction characteristics $C_g = u_*/G_0$ – geostrophic drag coefficient, α – the angle of wind full rotation in PBL, μ – internal stability parameter in PBL, etc. on the dimensionless external parameters:

$$Ro, S, Roi, M, \Phi, \Psi, \mu_N, \tag{125.2}$$

to be obtained [5, 7], where $Ro = G_0/fz_0$ – geostrophic drag coefficient, $S = \beta\delta\theta/fG_0$ – external stability parameter, $\delta\theta = \theta_H - \theta_0$ – increment of θ in PBL, $Roi = G_0/fh_i$ – the inversion Rossby parameter, M, Φ – baroclinic parameters (module and angle), Ψ – the angle of terrain slope, $\mu_N = N/f$ – free flow stability parameter.

- The combined (Rb-RL) method, developed by joint and coordinated use of Rb and RL, give the possibility of determining of a set of important links and parameters, for example:

$$f_{ug} = u_{g0}/u_1, \; f_{vg} = v_{g0}/u_1, f_g = G_0/u_1, \; f_\theta = \delta\theta/\Delta\theta, \; \alpha, \tag{125.3}$$

in dependence again to parameters (125.1) and the additional parameter $\check{R}_0 = u_1/fz_0$ [5].

The present work aim is these three parameterization schemes to be applied for urban area.

125.2 Modification of the Parameterization Schemes for Urban Areas

Let start with the Rb-method. The urban roughness sub layer with a height of $z^* \geq (2–5)$ h (for example the lower limit $z^* = 2$ h is used for typical European cities) includes the urban canopy layer (street canyons, buildings and other roughness elements) and the layer above, where the influence of the listed urban heterogeneities with a typical height h can still be felt. When the reference height is chosen to be $z_1 \equiv z^*$, this influence is negligible and so the Monin-Obukhov similarity theory is valid when respective effective parameters are used (see [1]). These parameters are u_*^{eff} (the maximum of Reynolds stress around level z^*), the respective typical value of the heat flux q^{eff} (u_*^{eff} and q^{eff} are unknown quantities, which will be determined

below by implementation of the Rb-method) and the typical roughness parameters z_0^{eff} and z_{0T}^{eff}. The blending height method (see [3]), or simple weighted averaging of the kind $z_0^{\text{eff}} = \sum P_i z_{0i}$, P_i – weighting function, can be used for determining the last for chosen suburban regions with different land use types, while for suburban regions with relatively compact massifs of forest (park) ore buildings with typical height h, simple relations of the kind $z_0^{\text{eff}} = ph$, $p \approx 0.1$ [2] and for displacement height $d = 0.7$ h (see [1]) can be applied. Taking this into account, respective effective Richardson number Rb^{eff} can be introduced, instead of Rb(rural), which characterize in an integral way the urban roughness sub layer:

$$Rb^{\text{eff}} = \beta \Delta\theta e^{\text{ff}} z^* / \left(u^{\text{eff}}\right)^2, \tag{125.4}$$

$$\Delta\theta^{\text{eff}} = \theta^{\text{eff}} - \theta_0^{\text{eff}} = \left(\theta_*^{\text{eff}}/\kappa\right)\left[\lambda_\theta^{\text{eff}} - \Psi_\theta\left(\xi^{\text{eff}}\right)\right],\ \lambda_\theta^{\text{eff}} = \ln\left(\left(z^* - d\right)/z_{0T}^{\text{eff}}\right), \tag{125.5}$$

$$u^{\text{eff}} = \left(u_*^{\text{eff}}/\kappa\right)\left[\lambda_u^{\text{eff}} - \Psi_u\left(\xi^{\text{eff}}\right)\right],\ \lambda_u^{\text{eff}} = \ln\left(\left(z^* - d\right)/z_0^{\text{eff}}\right). \tag{125.6}$$

The following symbols are used in (4–6): $\theta^{\text{eff}} = \theta(z = z^*)$, $\theta_0^{\text{eff}} = \theta(z = z_{0T}^{\text{eff}})$, $u^{\text{eff}} = u(z = z^*)$, $\theta_*^{\text{eff}} = -q^{\text{eff}}/u_*^{\text{eff}}$, $\xi^{\text{eff}} = z^*/L^{\text{eff}}$, $L^{\text{eff}} = -(u_*^{\text{eff}})^3/(\kappa\beta q^{\text{eff}})$, Ψ_u, Ψ_θ are the universal functions in the Monin-Obukhov similarity theory, accounting for the asymptote "−1/3" at free convection (see [5]). The urban roughess layer drag and heat transfer coefficients $(C_d^{\text{eff}})^{1/2} = u_*^{\text{eff}}/u^{\text{eff}}$ and $C_t^{\text{eff}} = \theta_*^{\text{eff}}/\Delta\theta^{\text{eff}}$, in dependence on the modified input parameters (125.1) Rb^{eff}, λ_u^{eff}, $\lambda_\theta^{\text{eff}}$, $F_{i0}^{\text{eff}} = Nz^*/u^{\text{eff}}$, can be obtained on the basis of (125.4), taking into account (125.5) and (125.6), applying respective mathematical procedure (analogous to the conventional case). Results for $N = 0$, $\lambda_u^{\text{eff}} = \lambda_\theta^{\text{eff}}$ are given in Fig. 125.1 for different values of h, $z^* = 30$ m, $d = 0.7$ h, $z_0^{\text{eff}} = 0.1$ h. The curve at $h = 0.15$ corresponds to rural conditions. Significant increase of $(C_d^{\text{eff}})^{1/2}$ and C_t^{eff} with increasing of h (urban conditions).

Let the RL-method be considered. It is known, that above urban regions ($z > z^*$) the Rossby similarity theory is also valid (see [1]). This makes it possible the RL-method to be modified similarly to the Rb-method and thus the dependence of the modified parameters $C_g^{\text{eff}} = u_*^{\text{eff}}/G_0$, α^{eff} and μ^{eff} on the respectively modified external parameters (125.2): $Ro^{\text{eff}} = G_0/fz_0^{\text{eff}}$, $S^{\text{eff}} = \beta\delta\theta^{\text{eff}}/fG_0$, $\delta\theta^{\text{eff}} = \theta_H - \theta_0^{\text{eff}}$, etc. to be obtained.

Combining the modified Rb and RL-methods leads to the modified combined (Rb-RL)-method, making the determination of the modified parameters (125.3): $f_{ug}^{\text{eff}} = u_{g0}/u^{\text{eff}}$, $f_{vg}^{\text{eff}} = v_{g0}/u^{\text{eff}}$, etc. in dependence on the input parameters Rb^{eff}, λ_u^{eff}, $\lambda_\theta^{\text{eff}}$, F_{i0}^{eff} and the additional parameter $\check{R}_0^{\text{eff}} = u^{\text{eff}}/fz_0^{\text{eff}}$ possible.

It can be easily guessed that parameters C_g^{eff}, α^{eff} and μ^{eff} can be obtained by combined implementation of the modified Rb and (Rb-RL)-methods or directly of

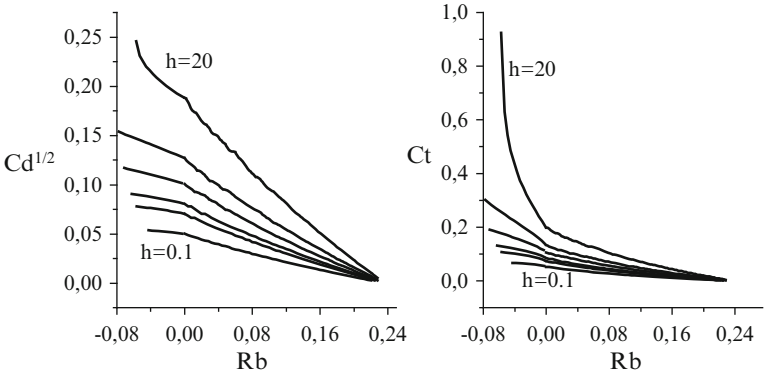

Fig. 125.1 Dependence of drag ($(C_d^{eff})^{1/2}$).and heat (C_t^{eff}) transfer coefficients, integrally characterising the roughness sub layer ($z \leq z^*$) in urban PBL on stratification (Rb^{eff}) and typical urban heterogeneities height h

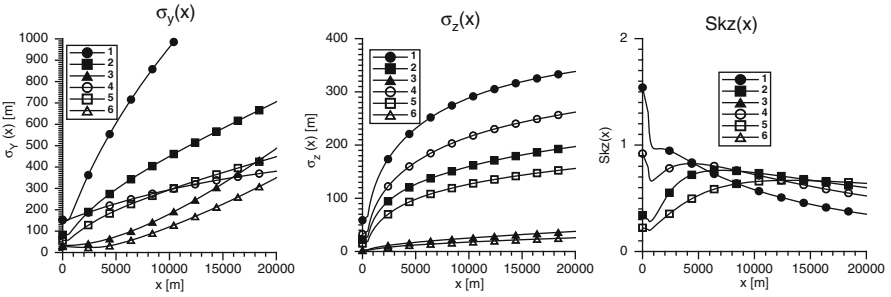

Fig. 125.2 Comparison of plume dispersions $\sigma_y(x)$, $\sigma_z(x)$ and skewness Skz(x) right under the height z^* of the roughness sub layer in urban PBL (cases 1, 2, 3) with the respective rural cases 4, 5 and 6

the RL-method. These parameters are used as an input to a PBL model [4, 5] and on this basis the Plume-MM and Puff-MM models, coordinated with the method of moments, are realized [4]. This makes possible a large set of dynamic and diffusion characteristics of urban PBL ($z \geq z^*$) to be obtained.

Some Plume-MM characteristics: dispersions $\sigma_y(x)$, $\sigma_z(x)$ and skewness Skz(x) right under the height z^* of the roughness sub layer in urban PBL (for input parameters from Fig. 125.1 at $z^* = 30$ m, $h = 15$ m) from a source with height $h_{source} = 150$ m for cases 1 (unstable, $Rb = -0.05$), 2 (neutral, $Rb = 0$), 3 (stable, $Rb = 0.12$) are shown in Fig. 125.2. They are compared with the respective rural cases 4, 5 and 6. It can be seen that the differences are biggest at unstable conditions.

125.3 Conclusions

As a final, practically oriented result, the modified schemes, based on integral parameterization of the urban roughness sub layer ($z < z^*$) makes it possible the basic transfer and dynamic, hence the basic diffusion parameters of urban PBL ($z \geq z^*$) to be obtained for a wide set of turbulent regimes (125.1) and (125.2).

Detailed CFD calculations are usually applied for the urban roughness sub layer ($z < z^*$). Thus the idea of a two-layer urban model is formed. In this case it could be recommended that the basic transfer and dynamic parameters evaluated for $z \geq z^*$ to be used as boundary conditions at $z = z^*$. This will significantly contribute to the detailing and expanding of the CFD modeling in the layer $z < z^*$ by accounting of the whole spectra of turbulent regimes (125.1)/(125.2) in urban PBL ($z \geq z^*$). In conclusion it should be noted that the parameterization schemes can be easily generalized for the case when $z_0/z_{0T} \neq 1$ is a function of the roughness Reynolds number, as well as when z_0 depends on stratification (see [10]).

Acknowledgements The present work is supported by the Bulgarian National Science Fund (grant дц -02/1/29.12.2009).

References

1. Fischer B, Joffre S, Kukkonen J, Pringer M, Rotach M, Schatzmann M (1999) Meteorology applied to urban air pollution problems, Final report COST Action 715, Luxembourg, OPEC
2. Grimond C, Oke T (1999) Aerodynamic properties of urban areas derived from analysis of surface form. J Appl Meteorol 38:1261–1292
3. Gryning S-E, Batchvarova E (2002) Pre-processor for regional-scale fluxes and mixed layer height over inhomogeneous terrain. In: Borego C, Schayers G (eds) Air pollution modeling and its application XV. Kluwer Acad/Plenum Publ, New York
4. Syrakov E, Ganev K (2003) Accounting for effects of wind rotation in the PBL on the plume characteristics. Int J Environ Pollut 20(1–6):154–164
5. Syrakov E (2011) Atmospheric boundary layer: structure, parameterization, interactions. Heron Press, Sofia
6. Syrakov E, Ganev K, Tsankov M, Cholakov E (2011) A comparative analysis of different conventional and none-local stable/neutral pbl regimes and their parameterization in air pollution problems. In: Bardzis J, Syrakos A, Andronopoulos S (eds) Proceedings of 14th international conference on harmonization within atmospheric dispersion modelling for regulatory purposes, Cambridge, pp 390–394
7. Syrakov E, Ganev K, Tsankov M, Cholakov E (2011) Estimation and parameterization of the influence of synoptic conditions on pollution characteristics in the PBL. In: Bardzis J, Syrakos A, Andronopoulos S (eds) Proceedings of the 14th international conference on Harmonization within Atmospheric Dispersion Modelling for Regulatory Purposes, Kos, Greece, pp 250–254
8. Zilitinkevich S, Esau I (2005) Resistance and heat/mass transfer laws for neutral and stable planetary boundary layers: old theory advanced and re-evaluated. Q J R Meteorol Soc 131:1863–1892

9. Zilitinkevich S, Elperin S, Kleeorin N, Rogachevski I (2007) Energy and flux budget turbulence closure model for the stably stratified flows. Part I: Steady-state homogeneous regimes. Bound Layer Meteorol 125:167–192
10. Zilitinkevich S, Mammarella I, Baklanov A, Joffre S (2009) The effect of stratification on aerodynamic roughness length. In: Baklanov A, Grimmond G, Alexander M, Athanassiadou M (eds) Meteorological and air quality models for urban areas. Springer, Berlin
11. van den Hurk B, Holstag M (1999) On the bulk parameterization of surface fluxes for various conditions and parameter ranges. Bound Layer Meteorol 92:119–134

Chapter 126
A Methodology for Modeling Environmental Effects of Pollutants Dispersion Generated by Explosions

David Sidilkover, Shlomi Shitrit, Tamir Reisin, and Shlomi Pistinner

Abstract Dispersion of liquid or solid aerosol pollutants via an explosive device is a multiple scale process. We model the blast wave propagation with a BKW equation of state using a modification to the hydrodynamic tool box OpenFOAM. (OPENFOAM® is a registered trade mark of OpenCFD Limited, the producer of the OpenFOAM software.) We proceed into a BKW modified Boussinesq phase using the standard k-ε model for turbulent dispersion. The agreement of the detonation product cloud top final height of the computation and field observation is to within $10 \div 20$ %.

Keywords OpenFoam • Explosion • Detonation products

126.1 Introduction

In this work we concentrate on the dispersion of detonation products (DP) only (for reasons demonstrated in [1]). When an improvised radiological dispersive device is explosively driven, the risk is determined to a great extent by the dynamics of the detonation products. When the toxicant mass is considerably smaller than the DP mass, the toxicant concentration, at least at the initial stages, is mainly determined by the DP dispersion dynamic properties.

DP dispersion in the atmosphere differs from common passive scalar assumption that underlies standard dispersion models. The difference lies in the fact that the DP gas has high density and temperature, which makes the pollutant (the DP) an

D. Sidilkover (✉) • T. Reisin • S. Pistinner
Soreq NRC, Yavne 81800, Israel
e-mail: david.sidilkover@gmail.com

S. Shitrit
Rafael Ltd., Haifa, Israel

D.G. Steyn et al. (eds.), *Air Pollution Modeling and its Application XXII*,
NATO Science for Peace and Security Series C: Environmental Security,
DOI 10.1007/978-94-007-5577-2_126,

active, rather than passive scalar, i.e. a heavy gas dispersion model is required. Furthermore, if interaction of the explosion generated blast waves with various obstacles is important in shaping the DP spatial form, then the model must include the blast wave dynamics or the compressible modeling of the DP.

To model such a scenario the equation of state of the DP must be considered explicitly, at least at the initial blast wave stages [2]. Furthermore, the equation of continuity momentum and energy must be solved self consistently with the equation governing the pollutant dispersion. This paper is arranged as follows: Sect. 126.2 describes the equations which govern our simulations, in Sect. 126.3 we portray the numerical implementation. We compare our results with field measurements [3] in Sect. 126.4 and present the conclusions in Sect. 126.5.

126.2 Governing Equations

The equations which govern the entire process are the hydrodynamic conservation equation. The continuity equation for the mixture of air and DP ρ reads:

$$\frac{\partial \rho}{\partial t} + \nabla \cdot \left(\rho \vec{V}\right) = 0 \tag{126.1}$$

where the continuity equation for the detonation products must fraction α_m reads:

$$\frac{\partial \left(\rho \alpha_{\mathrm{m}}\right)}{\partial \mathrm{t}} + \nabla \cdot \left(\rho \vec{\mathrm{V}} \alpha_{\mathrm{m}}\right) = \nabla \cdot \left[\kappa_M \nabla (\rho \alpha_m\right] \tag{126.2}$$

The air DP mixture momentum and energy conservation is governed by:

$$\frac{\partial \left(\rho \vec{\mathrm{V}}\right)}{\partial \mathrm{t}} + \nabla \cdot \left(\rho \vec{\mathrm{V}} \vec{\mathrm{V}}\right) = -\nabla \mathrm{P} + \rho \mathrm{g} + \nabla \cdot \left(\mu_{MoM} \nabla \vec{\mathrm{V}}\right) \tag{126.3}$$

$$\frac{\partial \left(\rho \mathrm{E}\right)}{\partial \mathrm{t}} + \nabla \cdot \left(\rho \vec{\mathrm{V}} \mathrm{h}\right) = \nabla \cdot \left(\kappa_E \nabla \overline{T}\right) \tag{126.4}$$

where $\vec{V}$, P, h and E, are the velocity, pressure, enthalpy and specific energy respectively. The other symbols κ_M, μ_{MoM}, κ_E, denote the turbulent mass momentum and energy diffusion coefficient respectively. Their computation procedure is a standard one and due to page limitation is not discussed here.

We turn now to the equation of state (EOS) which are used in the conjunction with Eqs. (126.3) and (126.4). Using the Dalton law of gaseous mixture, the EOS is:

$$\left(\frac{P}{\rho R_{air} T}\right)_T = 1 + \alpha_m \left[\frac{M_{BKW}}{M_{air}} F(x) - 1\right] \equiv G(x) \tag{126.5}$$

Note that for $\alpha_m = 0$ we obtain the air EOS and for $\alpha_m = 1$ we obtain the DP EOS. The value of $f(x)$ is a quantity calibrated for each type of explosive DP and is given by:

$$f(x) = xe^{\beta x}, \qquad x = \frac{\rho\kappa k}{M_{BKW}(T+\theta)^{\alpha}} \tag{126.6}$$

where κ, k, θ, and β are the DP calibration constants and all other symbols have their usual meaning. Page limit precludes us from providing details with regard to the turbulent transport coefficients and the governing equations of the standard k-ε model.

126.3 Details on Numerical Implementation

The numerical tool used in this study is OpenFOAM (http://www.openfoam.com). This numerical toolbox is being maintained and developed by OpenCFD Ltd. (now subsidiary of SGI Corp.) and distributed through OpenFOAM Foundation. From this tool box we chose two different solvers, each for the dominant physical process. When the pressure is high and the velocity field can become supersonic we use the solver rhoCentralFOAM (v 1.7) based upon the Kurganov-Tadmor scheme [4] and treat Equation (5) explicitly. At this stage the transport term in Eqs. (126.1, 126.2, 126.3 and 126.4), and thus turbulence, are ignored. Only the Euler equation, and a set of two continuity equations supplemented by an adiabatice energy equation, are considered. When the pressure effects become negligible compared to the turbulent stresses, and the transport is dominated by turbulent process we use buoyantBoussinseqPisoFoam (v 1.6), with the standard k-ε model. Thus, Eq. (126.1) reduces to: $\nabla \cdot V = 0$. The DP continuity equation is Eq. (126.2) explicitly. The momentum equation is the incompressible Boussinesq Navier–Stokes equation, and the energy equation is Eq. (126.4).

The initial conditions to the first stage are a homogenous sphere at rest which conserves the mass and the energy of the explosive. This homogenous radius is chosen such that its pressure does not exceed 500 Bars (Over which rhoCentral-FOAM may become numerically unstable). Thus, we set in the region of the DP $\alpha_m = 1$, we calculate the density and the energy via $\rho = 3(4\pi)^{-1} M R^{-3}$, and $e = 3(4\pi)^{-1} E(M) R^{-3}$, where the energy of the explosive is measured in mass of an equivalent TNT charge mass. Once the density and internal energy are available we iterate the temperature in Eqs. (126.5) and (126.6) (cf. [4]) to obtain the initial pressure. The boundary conditions are reflecting on rigid walls. The final results of the Euler compressible calculation are fed as initial conditions to the turbulent Boussinesq Navier–Stokes equation solver.

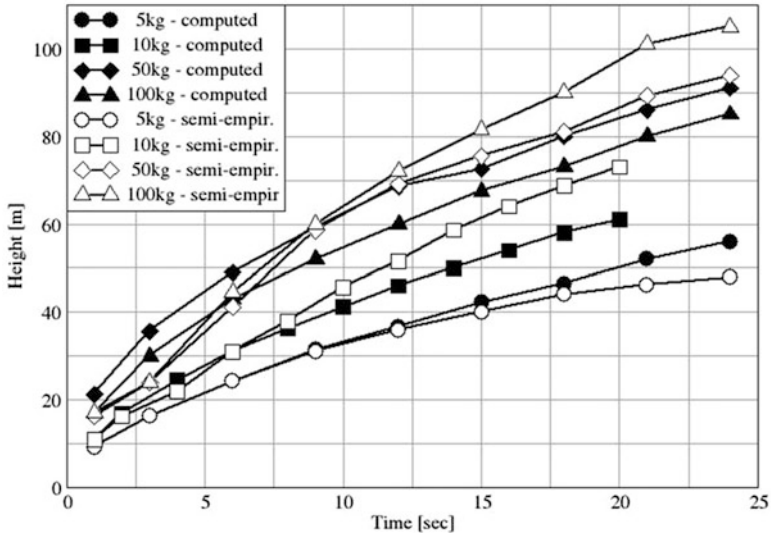

Fig. 126.1 A comparison between OpenFOAM calculation procedure and the fit formula provided in [3] for a TNT charge of 5, 10, 50 and 100 kg

126.4 Results

We have compared the results of the procedure discussed in Sect. 126.3 to field observations. As explained above the verification can be done in two stages. Here we focus on the second stage. For this purpose we use the results provided in [3]. This comparison is illustrated in Fig. 126.1. As can be seen the agreement is very good.

126.5 Conclusions and Discussion

We have demonstrated that the methodology of modeling presented here using OpenFOAM provides reasonable agreement with the observational results provided in [3]. That said the results shown in Fig. 126.1 are obtained only after meticulous initialization of the second stage of the calculation depicted in Sect.126.3. First, one must verify that the wind initial conditions are set consistently with the turbulence. To that goal we use a wind power law which is consistent with the law of wall boundary conditions that are implemented in OpenFOAM.

The cloud final height is mainly sensitive to the final radius of the DP after the blast wave has propagated, and the atmospheric initial mixing length (which in this case is roughly 15 cm).

References

1. Gold VM, Baker EL, Poulos WJ, Fuchs BE (2006) PFRAG modeling of explosive fragmentation munitious performance. Int J Impact Eng 33:294–304
2. Clutter KJ, Mathis JM, Stahl MW (2007) Modeling environmental effects in the simulation of explosion events. Int J Impact Eng 34:973–989
3. Yaar I, Sharon A (2008) Calibration of cloud rise model for RDD scenario. NATO Sci Secur Ser B Phys Biophys 3:193–205. http://www.nucleonica.net/wiki/images/7/76/ITRAC2_Sharon.pdf
4. Kurganov A, Tadmor ESL (2000) New high-resolution central schemes for nonlinear conservation laws and convection-diffusion equations. J Comput Phys 160:214–282

Chapter 127
An Extended Street Canyon Model for Pollutant Concentrations in Street Canyons with Detached Houses and Specified Traffic Lane Width

J.J. Erbrink, Esther Kokmeijer, and Joost J. de Wolff

Abstract A street canyon model has been used to calculated concentrations of NO2 in a specific situation with detached houses and a specific traffic lane width.

Keywords Street canyon • Traffic emissions • NO_2 • OSPM • STACKS

127.1 Introduction

In urban environments relatively high concentrations of NO_2 and PM_{10} may occur in street canyons. To identify locations that exceed the EU-limit values and to predict the effect of potential reduction measures, a reliable model is essential. The Danish OSPM model for street canyons [1] is based on the formation of a recirculation zone. The OSPM model calculates the concentrations of pollutants using a combination of a plume model for the direct contribution and a box model for the contribution of the recirculation zone. The (basics of the) OSPM model is widely used and successfully applied. The formulation of the OSPM model is implemented in STACKS [2] and further extended.

127.2 Street Canyon Model in STACKS

The OSPM model is suitable for busy streets with relative high buildings with respect to the width of the street. The original OSPM model assumes that (1) buildings form a continuous wall and (2) emissions are uniformly distributed across the

J.J. Erbrink (✉) • E. Kokmeijer • J.J. de Wolff
KEMA, Arnhem, The Netherlands
e-mail: hans.erbrink@dnvkema.com

D.G. Steyn et al. (eds.), *Air Pollution Modeling and its Application XXII*,
NATO Science for Peace and Security Series C: Environmental Security,
DOI 10.1007/978-94-007-5577-2_127,

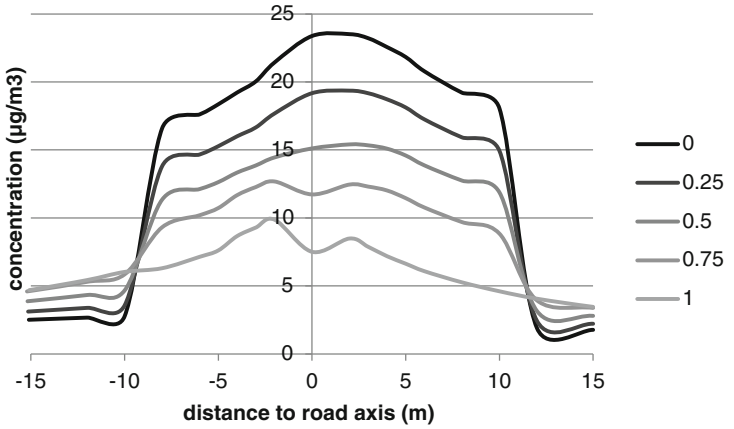

Fig. 127.1 Annual averaged concentration in a street canyon (width 20 m) for different ventilation factors (from 0 to 1)

canyon width. However, often there are open spaces between the buildings, e.g. in suburban roads with detached houses. In reality the emissions only occur over a limited part of the canyon i.e. the width of the traffic lanes. Limiting the emission to the traffic lanes will result in lower calculated concentrations near buildings, especially in wider streets and higher concentrations nearby the road. In order to extend the applicability of the model to a greater variety of canyon parameters the formulation was extended with respect to these assumptions.

127.3 Ventilation Factor

The space between buildings is implemented in the model with a ventilation factor (the fraction open space in between the buildings) i.e. a ventilation factor of 0 stands for a real street canyon and 1 for a street without buildings. The effect of the ventilation factor was studied using CFD calculations. Based on that study the transition is modeled as a linear relation with the fraction open space (Fig. 127.1).

127.4 Limiting the Emissions to the Traffic Lanes

The OSPM model calculates the concentrations of pollutants using a combination of a plume model and a box model. To limit the emissions to the traffic lanes, adaptations were needed in the calculation of the concentration from box as well as the direct plume. The concentrations in the recirculation zone in the OSPM

model are based on that part of the canyon width that is in the recirculation zone. The changes for this part comprise the calculation of the contribution based on the fraction of the traffic lanes in the recirculation zone. The contribution of the plume in the original OSPM is calculated by integration of the direct plume along the wind path at street level. Here the adjustment concerns the reduction of the integration path to the path length over the traffic lanes.

127.5 Results

The extended model has been validated with the measured data from a street canyon in Rotterdam. For this street hourly measurements (from a location 2 m next to the traffic lanes) were available from July 2010 to May 2011. Figure 127.2 shows the measured and calculated data as moving average over 1 week.

The agreement between measured and calculated concentrations is very well especially in wintertime (3,000–5,000 h). The slightly higher concentrations in the first 1,000 h can well be explained by the summer holidays: the traffic intensity will have been lower than the nominal intensity that was used in the calculations.

The calculated concentrations are highly dependent on the wind direction. Therefore the concentrations were analyzed as function of the wind direction as well. As is shown in Fig. 127.3, again a good agreement has been found between measured and calculated concentrations. A good agreement in the shape between measured and calculated data in this figure gives confidence in the basic assumptions of the model.

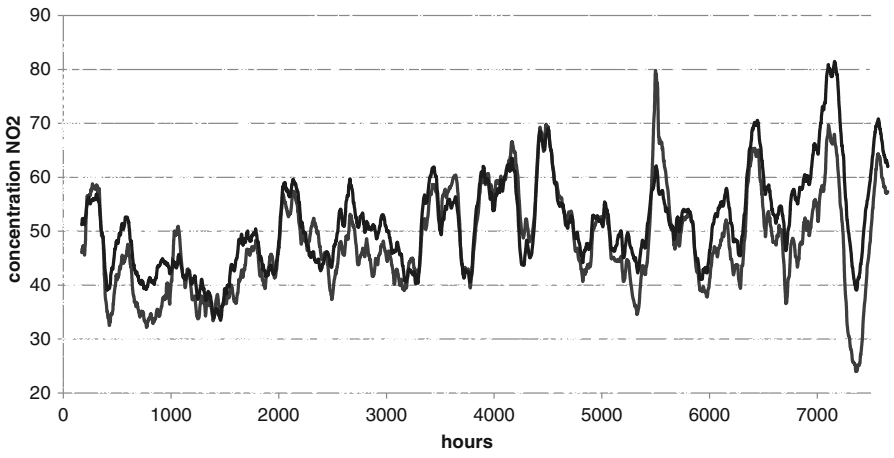

Fig. 127.2 Measured and calculated NO2 concentrations ($\mu g/m^3$) in a street canyon in Rotterdam (Moving average over 1 week)

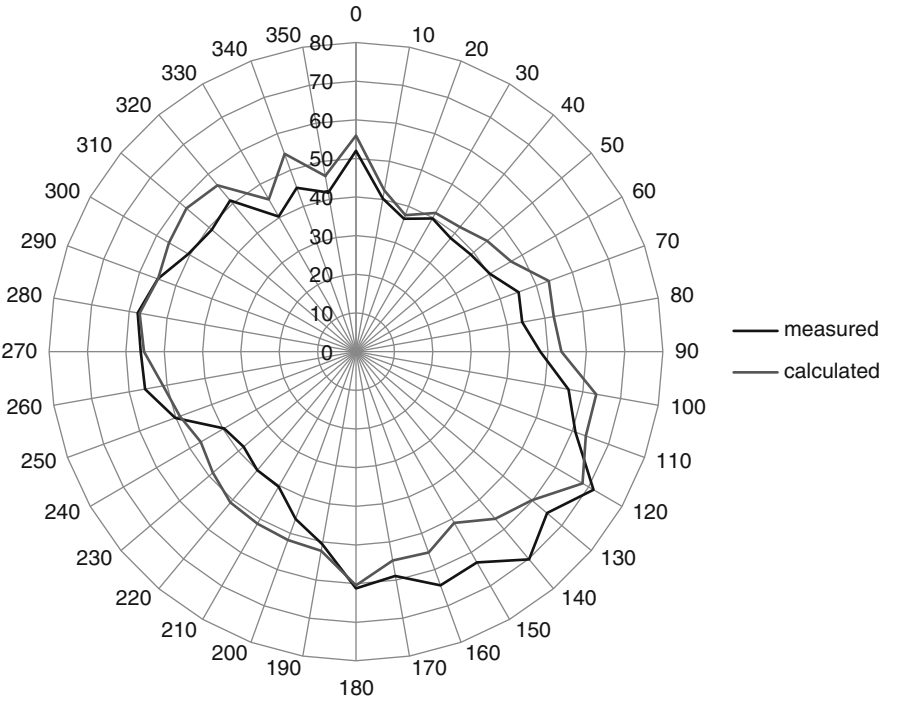

Fig. 127.3 Measured and calculated concentrations as function of the wind direction

127.6 Conclusions

The Street canyon model in STACKS (based on OSPM) is extended with two parameters: the ventilation factor (amount of open space between buildings) and the width of the traffic lanes. The resulting model is successfully validated to a busy street in Rotterdam. With the presented adaptations the model is applicable for canyons with a greater variety of parameters.

References

1. Berkowicz R, Hertel O, Larsen SE, Sørenssen NN, Nielsen M (1997) Modelling traffic pollution in streets. Ministry of Environment and Energy and National Environmental Research Institute, Roskilde
2. Erbrink (1995) Turbulent diffusion from tall stacks. The use of advanced boundary layer meteorological parameters in the Gaussian dispersion model "STACKS". PhD thesis, Free University, Amsterdam, April 1995, 228 pp

Chapter 128
Enhanced Dispersion from Tall Stacks Near Modern Wind Mills

J.J. Erbrink and Luc Verhees

Abstract An investigation has been performed on the increased dispersion of a plume from a tall stack in the vicinity of a wind turbine.

Keywords Dispersion model • Wind mill obstruction • STACKS • Air pollution

128.1 Introduction

Dispersion modeling of emissions from tall stacks is often done with regulatory models, based on the Gaussian plume concept. When the plumes of tall stacks are influenced by the turbulence of nearby wind mills, the concentration pattern can be very different due to the enhanced turbulence of the wake of the wind mill and the reduced wind speed. In the Netherlands wind energy is strongly encouraged by different governmental programs. Therefore at a few places wind mills and stacks from incinerators or power stations are planned very close to each other. From a sketch of the situation it can easily be concluded that there will be a significant plume-wind mill interaction. In the Dutch regulatory model STACKS we combined a wind mill wake-model with the Gaussian plume model.

128.2 The Model

The wake model is parameterized by the same wind and turbulence parameters as is done with the plume dispersion parameters. This makes it easy to adapt the plume dimensions and dispersion for the wake dimensions and turbulence intensity.

J.J. Erbrink (✉) • L. Verhees
DNV KEMA, Arnhem, The Netherlands
e-mail: hans.erbrink@kema.com

D.G. Steyn et al. (eds.), *Air Pollution Modeling and its Application XXII*,
NATO Science for Peace and Security Series C: Environmental Security,
DOI 10.1007/978-94-007-5577-2_128, © Springer Science+Business Media Dordrecht 2014

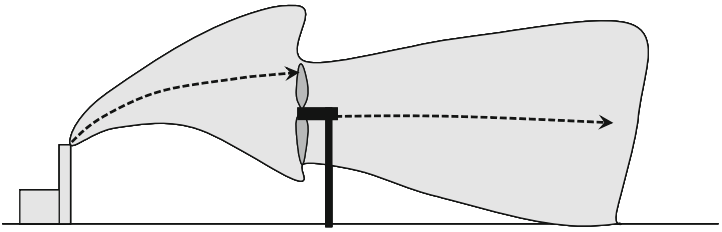

Fig. 128.1 Upwind plume trapped into the wake of a wind mill

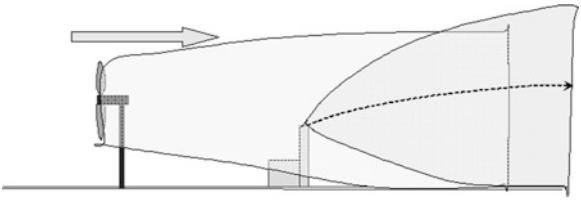

Fig. 128.2 Downwind plume is emitted into the wake of a wind will

This can be done under the condition that the stacks height and turbine axe height do not differ too much. We distinguish two situations: the plume is upwind or downwind from the wind mill, see Figs. 128.1 and 128.2. In order to model conservatively, we assume the upwind plume to be trapped in total into the wake when the plume axes is lower than the top of the wind turbine. When the plume is downwind, we assume plume dispersion takes place with a lower wind speed in the wake and with higher turbulence. The parameterization of plume dispersion is based on turbulence parameters σ_v and σ_w and time scale T_l (see [1]). In the wake turbulence intensities are increased, while the length scale is decreased.

The dimensions of the wake are derived from Taylor [2] and Vermeer [3], velocity deficit). The formulations:

$\frac{\Delta V}{V_{hub}} = \Delta_s \left(\frac{x_s}{x}\right)^n$: wind velocity deficit behind the wind turbine.

$\Delta_s = 1 - (1 - C_T)^{\frac{1}{2}}$: the initial wind deficit, function of thrust coefficient C_T

$\frac{X_s}{D} = 0.97\left(\frac{m+1}{8}\right)^{\frac{1}{2}} \left\{ \left(\frac{u'_a}{0.51}\right)^2 + \left(\frac{0.22(m-1)^2}{m^2 - 4m + 1}\right)^2 \right\}^{-\frac{1}{2}}$: the wake length x_s

$m = (1 - C_T)^{-\frac{1}{2}}$ the axial induction factor

$b = \left(\frac{3,56\, c_T}{8\Delta_s(1 - \Delta_s)}\right)^{0,5}$ the width of the wake (b)

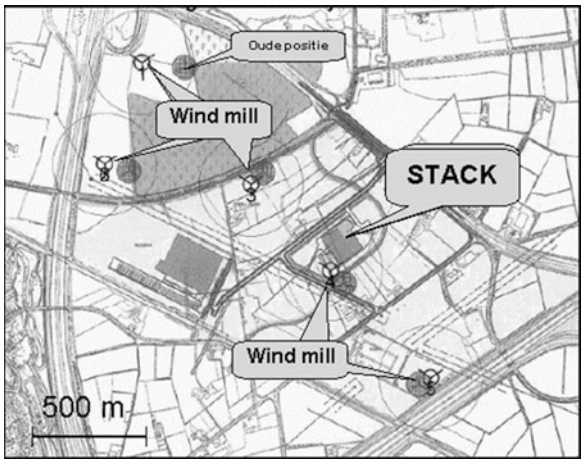

Fig. 128.3 Position of the stack and the wind turbines

The added turbulence as a function of distance x from the turbine:

$$\Delta I = 1,31\, {c_T}^{0,71} {I_a}^{0,68} (x/x_S)^{-0,96}$$

I_a being ambient turbulence intensity (σ_w/u).
ΔV velocity difference at the turbine height compared to undisturbed situation
V_{hub} wind speed at the height of the turbine axes.
D wind turbine diameter
X distance to the wind turbine
X_s wake length
Δ_s Initial velocity deficit depending on the trust coefficient
n relaxation constant. $n \approx 1$

With given trust coefficients, the width of the wake and the generated extra turbulence can be calculated and added tot the atmospheric turbulence $\sigma^2_{w\_total} = \sigma^2_{wa} + \sigma^2_{w\_turbine}$ with adopted time scale $Tl = 0.15b - 0.08$ in the wake. These parameters are used to calculate the values of σ_y and σ_z. The plume height is calculated using the reduced wind speed in the wake in the down wind case; in the up wind case plume rise is fully neglected (plume height = stacks height).

128.3 Model Results

We carried out dispersion calculations for a 90 m stack height and turbine height of 105 m; meteorology of 1995–2004 (10 year hourly data). The positions of the stack and wind turbines are indicated in (Fig. 128.3). In the calculations the two nearest turbines are included into the calculations: there are 4 wind directions with a significant effect: two upwind and two down wind directions. From the results

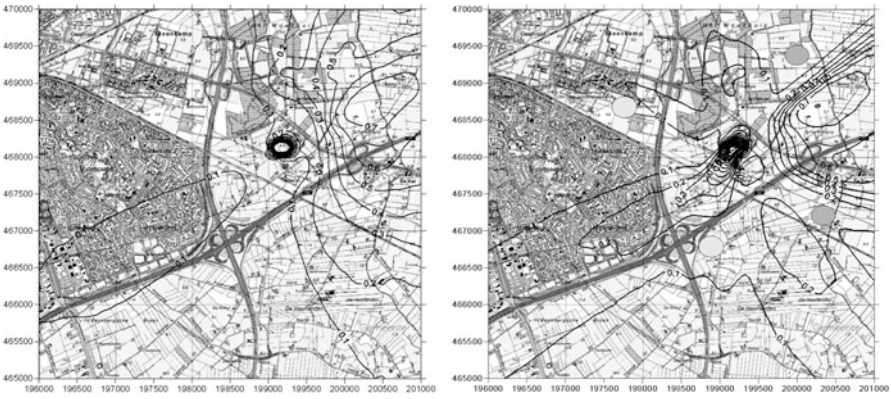

Fig. 128.4 Calculated 98-percentages of a 90 m stack. *Left*: without wind turbines, *right* with wind turbines. *Grey* and *light grey* spots: respectively lower and higher concentrations due to the upwind and downwind wind turbine effects

(Fig. 128.4) it can be seen for the upwind situation, that the plume will undergo significant downwash resulting in higher concentrations closer to the stack. This is especially the case for odor, since limit values for odor are set by taking the higher percentiles. In Fig. 128.4 the 98-percentiles are given for with and without turbine included dispersion.

For the downwind situation (plume is emitted into the wake) there is no strong down wash due to the enhanced plume rise in the lower wind speed regime; in this case the concentrations may be even lower (grey spot). In the plume down wash wind directions (light grey spots) concentrations are significantly higher.

References

1. Erbrink (1995) Turbulent diffusion from tall stacks. The use of advanced boundary layer meteorological parameters in the Gaussian dispersion model “STACKS”. PhD thesis, Free University, Amsterdam, April 1995, 228 pp
2. Taylor GJ (1993) Development of an improved eddy viscosity model of a wind turbine wake. Report prepared by TNO, CEC project JOUR-0087, June 1993
3. Vermeer LJ et al (2003) Wind turbine wake aerodynamics. Prog Aerospace Sci 39:467–510, Pergamon

Chapter 129
Crisis Management Modeling and Simulation Laboratory

Oscar Björnham, Jan Burman, Oskar Parmhed, and Christer Fureby

Abstract Transports of substances to or from Seveso classified facilities are always a dangerous link in today's industrial societies. Despite the risk of serious accidents, it is common that these transports use routes that pass through densely populated urban areas. We present a computational concept employing a multi-model simulation platform that allows for simulation of diverse scenarios. This platform allows us to simulate severe incidents in a city including leakage from either a stationary or moving transport vehicle, dispersion of the released substance, and finally the injury panorama of the affected population. Different scenarios of leakage are studied in combination with various environmental conditions regarding parameters such as wind strength and direction. The dispersion model utilizes a synthetic 3D model of the city in which the wind driven convective fields spread the released substance. In this model, a large number of virtual habitants are allowed to walk on the streets following individual paths while obeying a set of predetermined rules of behaviour. Each individual accumulates an individual dose of the agent by inhaling the harmful substance and is subject to injury scaling from no harm at all to lethal injury. The total expected injury panorama of the population in the city, for the current scenario, is finally obtained from the statistics of the synthetic actors that represent the real population.

Keywords Crowd simulation • Urban modelling • Multi-model • Crisis management

O. Björnham (✉) • J. Burman
Swedish Defence Research Agency, Cementvägen 20, 90621 Umeå, Sweden
e-mail: oscar.bjornham@foi.se; jan.burman@foi.se

O. Parmhed • C. Fureby
Grindsjön Research Center, Swedish Defence Research Agency, 147 25 Tumba, Sweden
e-mail: oskar.parmhed@foi.se; christer.fureby@foi.se

D.G. Steyn et al. (eds.), *Air Pollution Modeling and its Application XXII*,
NATO Science for Peace and Security Series C: Environmental Security,
DOI 10.1007/978-94-007-5577-2_129,

129.1 Concept

The laboratory (Fig. 129.1) is scenario oriented where many predetermined parameters will have a strong impact on the resulting injury panorama. Major scenario properties are; the geometry of the urban environment, the wind profile, the source, the dispersion (driven by the wind profile), the population with regards to the sheer number of people but also their behavior, and finally when and how the initial detection of the extraordinary emission is reported. All these properties are regarded as *prerequisites* of the scenario. When the first indications of an emission are received, or unusual injuries among the present habitants occur, users of the *Management System* may start to perform actions. These actions may include different forms of emergency responses, embarring or evacuating areas, place sensors at strategic positions and of course locate and obviate the source. The scenario is managed in real time which makes the laboratory an excellent training environment for assessment of potential outcomes of hazard situations as well as for handling extraordinary events.

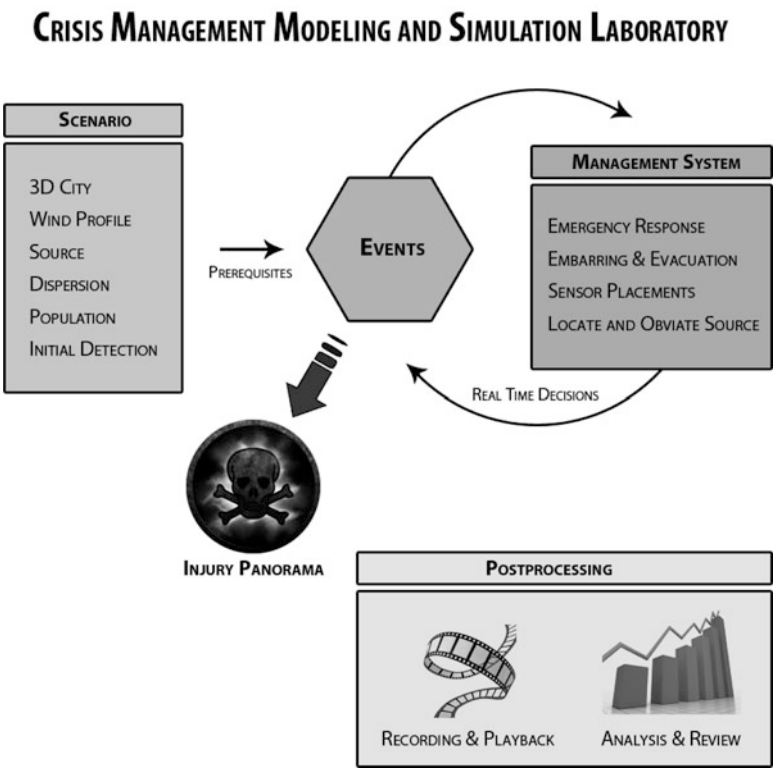

Fig. 129.1 A schematic layout of the concept of the simulation laboratory

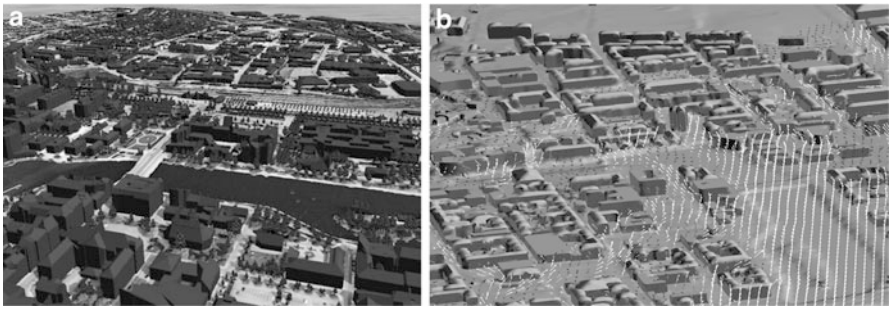

Fig. 129.2 Panel *A* shows the geometric representation of Norrköping. Panel *B* presents the calculated wind field in the city at a selected height where *white arrows* represent the strongest wind speeds

129.2 Geometry, Wind and Dispersion

The city of Norrköping, Sweden, has been scanned from a helicopter by a laser system called TopEye producing height information with a resolution of ∼2.5 dm in the vertical direction. The data is stored in GeoTIFF format and allows for high resolved reconstruction of the topography of the city. It is of interest to distinguish between different types of objects (for instance if an object is a house or a couple of trees) which can be done by combining the topography data with other datasources which results in a good representation of the city and is illustrated in panel A in the figure below [1].

A toxic chemical substance is suddenly released somewhere in the city. The substance is then dispersed in the air effectively by the turbulent wind profile created in the complex urban environment. The wind profile is calculated by CFD simulations using LES methods [2], see Fig. 129.2 panel B.

129.3 Management System

The user may interact with the cause of events in real time in areas such as emergency response, embarring and evacuating areas and eliminating the source. Depending on the scenario the source might be obvious but also more difficult to locate. In the latter case it might be necessary to place sensors at strategic positions in the city but also to understand how the collected measurement data should be interpreted to achieve the best possible understanding of where the source most likely is located.

129.4 Injury Panorama

The emitted substances in these scenarios give rise to different levels of injuries depending on the *toxic load* a person experiences. The toxic load, *TL*, is a nonlinear accumulation of inhaled toxic substance and can be written

$$TL = \int C^n (r, t, v)\, dt$$

where C is the inhaled concentration that depends on the position r, the time t, and v which is the respiratory minute volume. The dimensionless exponent n that gives rise to the nonlinearity depends strongly on the substance and is normally larger than or equal to unity. Given the toxic load, an injury level may be predicted from a statistical point of view [3].

To estimate the distribution of toxic load of the entire population, individual behavior must be considered. A crowd simulation module that generates the behavior of an arbitrarily sized population, based on statistical distributions, at an individual level is therefore included in the laboratory. This means that every person in the simulation has its own properties (such as age, gender, but also relations to other persons) and geographic goals they travel towards (Fig. 129.3).

The behavior of the population may also be affected by its toxic intake. This is a very important factor since people can be expected to try to escape an obvious dangerous area. This may lead to that people start running instead of walking which will decrease the time they are exposed to the toxic substance. However, a running person inhales a considerable larger volume air, and thereby more toxic substance, per second. The crowd simulation is an important factor in this type of modeling to obtain an injury panorama which is the most interesting result of such a scenario.

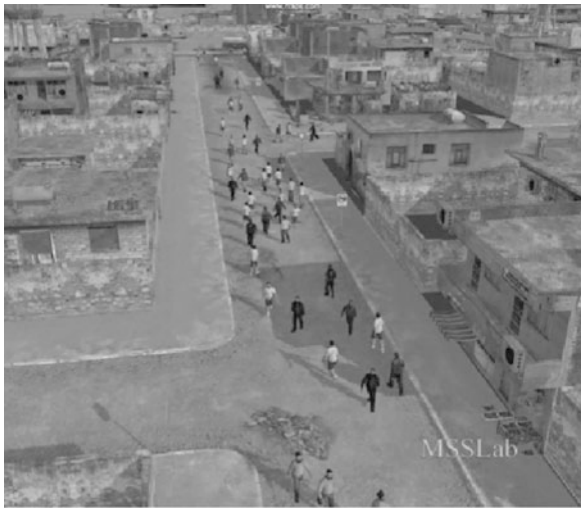

Fig. 129.3 Illustration of virtual habitants walking on a street

References

1. Tolt G, Persson Å, Landgård J, Söderman U (2006) Segmentation and classification of airbourne laser scanner data for ground and building detection. In: SPIE Defense and Security symposium, vol 6214, Laser radar technology and applications XI, April 2006
2. Fureby C (2008) Towards the use of large eddy simulation in engineering. Prog Aerospace Sci 44(6):381–396
3. Finney DJ (1971) Probit analysis, 3rd edn. Cambridge University Press, Cambridge

Index

D.G. Steyn et al. (eds.), *Air Pollution Modeling and its Application XXII*,
NATO Science for Peace and Security Series C: Environmental Security,
DOI 10.1007/978-94-007-5577-2, © Springer Science+Business Media Dordrecht 2014